LBL-31854
CONF-9106323
UC-411

Applications of Circularly Polarized Photons at the ALS with a Bend Magnet Source

Report of the Workshop

Lawrence Berkeley Laboratory
June 10–11, 1991

Lawrence Berkeley Laboratory
University of California
Berkeley, California 94720

February 1992

Prepared for the U.S. Department of Energy under Contract No. DE-AC03-76SF00098

DISCLAIMER

Applications of Circularly Polarized Photons at the ALS with a Bend Magnet Source

Report of the Workshop

Lawrence Berkeley Laboratory
June 10–11, 1991

Local Organizing Committee:
S. Cramer
A.J. Hunt
A. Jackson
K.J. Kim
B.M. Kincaid
M.F. Maestre
J.N. Marx
D.R. Nygen
P.N. Ross
A.S. Schlachter
J. Stöhr
M. Wong

Lawrence Berkeley Laboratory
University of California
Berkeley, California 94720

February 1992

This work was supported by the Director, Office of Energy Research, Office of Basic Energy Sciences, Materials Sciences Division, of the U.S. Department of Energy under Contract No. DE-AC03-76SF00098

Contents

Applications of Circularly Polarized Photons at the ALS with a Bend Magnet Source

Monday & Tuesday
June 10–11, 1991
at
Lawrence Berkeley Laboratory

The purpose of this workshop is to focus attention on, and to stimulate the scientific exploitation of, the natural polarization properties of bend-magnet synchrotron radiation at the ALS - for research in biology, materials science, physics, and chemistry.

Topics include:
- The Advanced Light Source
- Magnetic Circular Dichroism and Diffferential Scattering on Biomolecules
- Tests of Fundamental Symmetries
- High T_c Superconductivity
- Photoemission from Magnetic and Non-magnetic Solids
- Studies of Highly Correlated Systems
- Instrumentation for Photon Transport and Polarization Measurements

Invited speakers:

M. Blume	(BNL)	M. McClain	(Wayne State)
C.T. Chen	(AT&T Bell Labs)	M.F. Maestre	(LBL)
E.D. Commins	(U. C. Berkeley)	J.N. Marx	(LBL)
S. Cramer	(U.C. Davis)	G. Sawatzky	(Groningen)
E. Gluskin	(APS)	G. Schütz	(Munich)
K.J. Kim	(LBL)	P.A. Snyder	(Florida Atlantic)
J. Kirschner	(Berlin)	E.A. Stern	(U. Washington)
J. Kortright	(LBL)	A. Zettl	(U.C. Berkeley)
R. Laughlin	(Stanford)		

Local organizing committee: S. Cramer, A.J. Hunt, A. Jackson, K.J. Kim, B. M. Kincaid, M.F. Maestre, J.N. Marx, D.R. Nygren, P.N. Ross, A.S. Schlachter, J. Stöhr, and M. Wong

For further information, contact:

Fred Schlachter
Lawrence Berkeley Laboratory
MS 46-161
Berkeley, CA 94720
Tel: (415) 486-4892
Fax: (415) 486-4873
e-Mail: Fred@LBL

Mervyn Wong
Lawrence Berkeley Laboratory
MS 50A-2129
Berkeley, CA 94720
Tel: (415) 486-4534
Fax: (415) 486-5401
e-Mail: MWong@LBL

Applications of Circularly Polarized Photons
at the ALS with a Bend Magnet Source

Lawrence Berkeley Laboratory
Building 66 Auditorium
June 10-11, 1991

SUNDAY EVENING JUNE 9

5 - 7 pm	Registration	(Shattuck Hotel Lobby)

MONDAY MORNING JUNE 10

7:45 am	Registration	(Building 66 Auditorium)
SESSION I	**A.S. Schlachter,** Chair	(Lawrence Berkeley Laboratory)
8:30 am	**D.S. Chemla**	(Lawrence Berkeley Laboratory)
	Welcome Remarks *Can We Transpose Visible, Nonlinear Optics to X-rays?*	
8:45 am	**B.M. Kincaid**	(Lawrence Berkeley Laboratory)
	The Advanced Light Source	
9:15 am	**K.J. Kim**	(Lawrence Berkeley Laboratory)
	Exploiting the Polarized Nature of Synchrotron Radiation Beams	
9:45 am	**Coffee Break**	
SESSION II	**M.R. Howells, Chair**	(Lawrence Berkeley Laboratory)
10:15 am	**C.T. Chen**	(AT&T Bell Laboratories)
	Dragon Beamline and MCD Measurements at NSLS	
10:45 am	**S.P. Cramer**	(U. C. Davis)
	A Split-Coil Superconducting Magnet for Soft X-ray MCD Experiments on Paramagnetic Samples	
11:05 am	**E. Gluskin**	(Argonne National Laboratory)
	Instrumentation and Preliminary Results of Polarization Measurements of Undulator Radiation in the Soft X-ray Region	
11:25 am	**J.M. Kortright**	(Lawrence Berkeley Laboratory)
	Soft X-ray Phase Retardation Using Multilayer Optics	
11:45 am	**Lunch**	

MONDAY AFTERNOON JUNE 10

SESSION III **S.P. Cramer,** Chair (U. C. Davis)

1.30 pm **P.A. Snyder** (Florida Atlantic University)

Magnetic and Natural Circular Dichroism Measurements in the Vacuum Ultraviolet Region with Synchrotron Radiation

2.10 pm **W.M. McClain** (Wayne State University)

Measurement of the Whole Mueller Scattering Matrix Using a Polarization Modulated Light Source

2.50 pm **M.F. Maestre** (Lawrence Berkeley Laboratory)

Recent Advances in Polarization Spectroscopy: Perspectives for Extension to the Soft X-ray region

3.30 pm **Tour of the Advanced Light Source**

5.00 pm **Reception** (Building 66)

TUESDAY MORNING JUNE 11

SESSION IV **P.N. Ross, Chair** (Lawrence Berkeley Laboratory)

8.30 am **E.A. Stern** (University of Washington)

Simple Physics behind Magneto-Optics in the Soft X-ray Regime

9.05 am **A. Zettl** (U. C. Berkeley)

Using Photons to Determine the Electronic Structure of Oxide Superconductors

9.40 am **M. Blume** (Brookhaven National Laboratory)

Magnetic Scattering, Anomalous Dispersion, Circular Dichroism, and All That

10.15 am **Coffee Break**

10.45 am **E.D. Commins** (U. C. Berkeley)

Can ALS Photons be Used to Study Fundamental Symmetries in Atomic Physics?

11.20 am **R.B. Laughlin** (Stanford University)

Possible P,T Violations in High-T_c Superconductors

11.55 am **Lunch**

TUESDAY AFTERNOON JUNE 11

SESSION V **J. Stöhr, Chair** (IBM, Almaden)

1.30 pm **G. Schütz** (Technische Universität München)

Absorption and Bragg Scattering of Circularly Polarized "Hard" X-rays in Ferro(i)magnetic Materials

2.20 pm **J. Kirschner** (Freie Universität Berlin)

Photoemission with Circularly Polarized Synchrotron Radiation from Magnetic and Non-Magnetic Solids

3.10 pm **Coffee Break**

3.40 pm **G.A. Sawatzky** (University of Groningen)

Applications of Polarized X-ray Absorption to the Study of Highly Correlated Systems

4.30 pm **Panel Discussion:** J. Stöhr (IBM, Alamaden), Moderator

Panelists: **M. Blume, K.J. Kim, J. Kirschner, R.B. Laughlin, M.F. Maestre, G.A. Sawatzky, G. Schütz, A. Zettl**

Scientific Opportunities with Circularly Polarized XUV Synchrotron Radiation

5.30 pm **Adjourn**

APPLICATIONS OF CIRCULARLY POLARIZED PHOTONS AT THE ALS WITH A BEND MAGNET SOURCE
June 10-11, 1991

David T. Attwood
Ctr. for X-Ray Optics
Lawrence Berkeley Laboratory
1 Cyclotron Road
Berkeley, CA 94720
(415) 486-4463

Sofie Bjorling
Chemistry/Thimann Labs.
University of California, Santa Cruz
Santa Cruz, CA 95064

Martin Blume
Bldg. 460
Brookhaven National Laboratory
Upton, NY 11973
(516) 282-3735

Roger G. Carr
Stanford Synchrotron Radiation Lab.
Stanford University
P. O. Box 4349, Bin 69
Stanford, CA 94309
(415) 926-3965

Daniel S. Chemla
Bldg. B-66
Lawrence Berkeley Laboratory
1 Cyclotron Road
Berkeley, CA 94720
(415) 486-4999

Chien-Te Chen
AT&T Bell Laboratories
600 Mountain Avenue
Murray Hill, NJ 07974-2070
(908) 582-6030

Eugene D. Commins
Department of Physics
University of California, Berkeley
257 Birge
Berkeley, CA 94720
(415) 642-2321

Stephen P. Cramer
University of California, Davis
Davis, CA

Glen H. Dahlbacka
Brobeck Division
Maxwell Laboratories, Inc.
4905 Central Avenue
Richmond, CA 94804-5803
(415) 524-8664

Daniel Dessau
SEL Receiving
Stanford University
Stanford, CA 94305
(415) 723-3209

Silvia Di Fonzo
ITSE - CNR
Via Salaria Km 29.300 CP 10
00016, Ro

Chuck Fadley
Lawrence Berkeley Laboratory
1 Cyclotron Road
Berkeley, CA 94720

Aaron Friedman
Brookhaven National Laboratory
Building 725C
Upton, NY 11973
(516) 282-5076

Efim Gluskin
APS/Bldg. 360
Argonne National Laboratory
9700 South Cass Avenue
Argonne, IL 60439
(708) 972-4788

Jeff A. Guckert
Department of Chemistry
Stanford University
Box B6, Mudd Bldg.
Stanford, CA 94305
(415) 723-0041

Phil Heimann
Lawrence Berkeley Laboratory
1 Cyclotron Road
Berkeley, CA 94720
(415) 486-7628

Malcolm R. Howells
Bldg. 46-161
Lawrence Berkeley Laboratory
1 Cyclotron Road
Berkeley, CA 94720
(415) 486-4949

Wolfgang Hubner
University of California, Berkeley
Berkeley, CA 94720
(415) 642-1031

APPLICATIONS OF CIRCULARLY POLARIZED PHOTONS AT THE ALS WITH A BEND MAGNET SOURCE

June 10-11, 1991

Patricia G. Hull
Department of Physics
Tennessee State University
3500 John A. Merritt Blvd.
Nashville, TN 37209-1561
(615) 251-1570

Arlon J. Hunt
Bldg. 90-2024
Lawrence Berkeley Laboratory
1 Cyclotron Road
Berkeley, CA 94720
(415) 486-5370

Zahid Hussain
Bldg. 2-300
Lawrence Berkeley Laboratory
1 Cyclotron Road
Berkeley, CA 94720
(415) 486-7591

Yves U. Idzerda
Code 6345
Naval Research Laboratory
Department of the Navy
Washington, D.C 20375-5000
(202) 767-3603

Alan Jackson
Bldg. 80-101
Lawrence Berkeley Laboratory
1 Cyclotron Road
Berkeley, CA 94720
(415) 486-6752

Roderich Keller
Bldg. 80-101
Lawrence Berkeley Laboratory
1 Cyclotron Road
Berkeley, CA 94720
(415) 486-5223

Kwang-je Kim
Lawrence Berkeley Laboratory
1 Cyclotron Road
Berkeley, CA 94720
(415) 486-7224

Brian M. Kincaid
Bldg. 2-400
Lawrence Berkeley Laboratory
1 Cyclotron Road
Berkeley, CA 94720
(415) 486-4810

Jurgen Kirschner
Freie Universitat Berlin
Institut for Experimentalphysik
Arnimallee 14
D-1000 Berlin Ger

David S. Kliger
Chemistry/Thimann Labs.
University of California, Santa Cruz
Santa Cruz, CA 95064

Jeffrey B. Kortright
Center for X-Ray Optics
Lawrence Berkeley Laboratory
1 Cyclotron Road
Berkeley, CA 94720
(415) 486-5960

Robert Laughlin
Physics Department
Stanford University
Stanford, CA 94305
(415) 723-4563

James W. Lewis
Chemistry/Thimann Labs.
University of California, Santa Cruz
Santa Cruz, CA 95064
(408) 459-4007

Steve Lidia
Lawrence Berkeley Laboratory
1 Cyclotron Road
Berkeley, CA 94720

Robley J. Light
NSF
DIR-Room 312
Washington, DC 20550

Ingolf Lindau
Stanford University
SEL
Stanford, CA 94305
(415) 723-1052

Marcos F. Maestre
Bldg. 70A-3307
Lawrence Berkeley Laboratory
1 Cyclotron Road
Berkeley, CA 94720

Jay N. Marx
Bldg. 46-161
Lawrence Berkeley Laboratory
1 Cyclotron Road
Berkeley, CA 94720
(415) 486-5244

APPLICATIONS OF CIRCULARLY POLARIZED PHOTONS AT THE ALS WITH A BEND MAGNET SOURCE
June 10-11, 1991

William McClain
Chemistry
Wayne State University
Detroit, MI 48202
(313) 577-2689

Wayne R. McKinney
Bldg. 2-400
Lawrence Berkeley Laboratory
1 Cyclotron Road
Berkeley, CA 94720
(415) 486-4395

Soren Moller
Chemistry/Thimann Labs.
University of California, Santa Cruz
Santa Cruz, CA 95064

Richard Mowat
Physics Department
North Carolina State University
P. O. Box 8202
Raleigh, NC 27695-8202
(919) 737-7914

David R. Nygren
Bldg. 50B-6208
Lawrence Berkeley Laboratory
1 Cyclotron Road
Berkeley, CA 94720
(415) 486-7162

Don O'Connor
Chemistry/Thimann Labs.
University of California, Santa Cruz
Santa Cruz, CA 95064

Douglas A. Ortendahl
Radiologic Imaging Lab.
University of Calif., San Francisco
San Francisco, CA

Sarah Paquette
Chemistry/Thimann Labs.
University of California, Santa Cruz
Santa Cruz, CA 95064

Piero A. Pianetta
Stanford Synchrotron Radiation Lab.
Stanford University
P. O. Box 4349, Bin 69
Stanford, CA 94309-0210
(415) 926-3484

Tommaso Prosperi
Consiglio Nazionale delle Ricerche
Area della Ricerca di Roma
Via Salaria Km 29.300 - C.P.10
00016, Ro
0039-6-90020317

Mohan Ramanatha
Bldg. 223, MSD
Argonne National Laboratory
9700 S. Cass Avenue
Argonne, IL 60439

Art Robinson
Bldg. 46-161
Lawrence Berkeley Laboratory
1 Cyclotron Road
Berkeley, CA 94720

Daniel B. Roitman
Dow Chemical Company
Central Research
2800 Mitchell Drive
Walnut Creek, CA 94598

Philip N. Ross
Bldg. 2-100
Lawrence Berkeley Laboratory
1 Cyclotron Road
Berkeley, CA 94720
(415) 486-6226

Ed M. Rowe
Synchrotron Radiation Center
3731 Schneider Drive
Stoughton, WI 53589-3097
(608) 873-6651

Michael Rowen
Stanford Synchrotron Radiation Lab.
Stanford University
P. O. Box 4349, Bin 99
Stanford, CA 94309
(415) 926-3487

Mahesh G. Samant
IBM Almaden Research Center
650 Harry Road
San Jose, CA 95120

George A. Sawatzky
University of Groningen
Materials Science Centre
Nijemborgh 18
Groningen, The
31-50-634975

APPLICATIONS OF CIRCULARLY POLARIZED PHOTONS AT THE ALS WITH A BEND MAGNET SOURCE
June 10-11, 1991

Alfred S. Schlachter
Bldg. 46-161
Lawrence Berkeley Laboratory
1 Cyclotron Road
Berkeley, CA 94720
(415) 486-4892

Gisela Schutz
Technische Universitat Munchen
E12
James-Franck-Strasse
Garching, 8046 Ger
49-89-3209-2435

Zhixun Shen
Electrical Engineering Department
Stanford University
Stanford Electronics Laboratories
Stanford, CA 94305
(415) 725-8254

Patricia A. Snyder
Department of Chemistry
Florida Atlantic University
P. O. Box 3091
Boca Raton, FL 33731
(407) 367-3339

George Srajer
Argonne National Laboratory
9700 S. Cass Avenue, 360
Argonne, IL 60439
(708) 972-3267

Edward A. Stern
Physics Department, FM-15
University of Washington
Seattle, WA 98195
(206) 543-2023

Joachim Stohr
K32/802
IBM Almaden Research Center
650 Harry Road
San Jose, CA 95120-6099

James G. Tobin
Mail Stop L-268
Lawrence Livermore National Lab.
P. O. Box 808
Livermore, CA 94550
(415) 422-7247

Stacie Wallace-Williams
Chemistry/Thimann Labs.
University of California, Santa Cruz
Santa Cruz, CA 95064

Tony Warwick
Bldg. 46-161
Lawrence Berkeley Laboratory
1 Cyclotron Road
Berkeley, CA 94720
(415) 486-5819

Mervyn Wong
Bldg. 50A-2129
Lawrence Berkeley Laboratory
1 Cyclotron Road
Berkeley, CA 94720
(415) 486-4534

Peter Y. Yu
Department of Physics
University of California, Berkeley
Birge Hall
Berkeley, CA 94720
(415) 641-8087

Alex Zettl
Department of Physics
University of California, Berkeley
363 Birge Hall
Berkeley, CA 94720

Chian Fan Zhang
Chemistry/Thimann Labs.
University of California, Santa Cruz
Santa Cruz, CA 95064

Preface

Introduction

A two-day workshop on "Applications of Circularly Polarized Photons at the ALS with a Bend-Magnet Source" was held at Lawrence Berkeley Laboratory on June 10 and June 11, 1991. The workshop addressed the dramatic increase in scientific interest in the use of the polarization properties of synchrotron radiation. The use of circular polarization to probe spin-dependent properties of magnetic solids and thin films, for example, is a subject not only of academic interest to solid-state physicists and materials scientists but also of considerable economic importance to the magnetic materials industry. Moreover, turning transitions on and off by varying the polarization is a powerful means of ascertaining state or band symmetry.

Synchrotron radiation is naturally polarized. When observed in the plane of the electron-beam orbit, radiation from a bend magnet is linearly polarized with the *E*-vector in the orbit plane. Out of the plane, the radiation intensity decreases, but is elliptically polarized: the *E*-vector has horizontal and vertical components that are 90° out of phase. The observation angle above or below the orbit plane determines the sense and degree of circular polarization, with large angles producing essentially 100% circular polarization, albeit with low intensity. The scaling of circular polarization and intensity with angle depends on the ratio of the photon energy to the critical photon energy.

The Advanced Light Source (ALS), a third-generation synchrotron light source optimized for the generation of high-brightness soft x-ray and ultraviolet radiation, is now nearing completion at Lawrence Berkeley Laboratory in California. Operations are scheduled to begin at this facility in 1993. It is one of several third-generation sources planned or under construction for the production of XUV radiation (Elettra in Trieste, Italy; the Pohang Light Source, Korea; and Bessy II in Berlin) or hard x-rays (ESRF in Grenoble, France; the Advanced Photon Source, Argonne National Laboratory; and SPring-8 at Harima Garden Science City, Kobe, Japan).

The ALS features a storage ring with a very low emittance (less than 10 nanometer-radians) and long straight sections (typically 5 meters) for the accommodation of insertion devices (undulators and wigglers). The low emittance of the storage ring also makes bend magnets highly desirable sources of light with superior brightness—well suited to experiments with circularly polarized photons. ALS bend-magnet beamlines, with a critical photon energy of 1.56 keV at the nominal storage-ring operating energy of 1.5 GeV, will provide high flux at photon energies up to about 6 keV.

Summary

The workshop emphasized XUV applications of circularly polarized photons: C. T. Chen (AT&T Bell Laboratories) reviewed recent experiments that showed large magnetic circular dichroism (MCD) signals in the core-level spectroscopy of magnetic materials, providing a practical tool for investigating the local electronic structure of ferromagnetic materials and chemically specific magnetic moments in a wide range of systems. S. Cramer (U.C. Davis) described opportunities and an apparatus for the site-specific spectroscopy of small concentrations of paramagnetic metal atoms and clusters in protein molecules by means of MCD measurements with florescence detection. P.A. Snyder (Florida Atlantic University) surveyed chemical and biochemical vacuum-ultraviolet applications of the MCD of molecules in magnetic fields and of natural circular dichroism and circular intensity differential scattering (CIDS) of chiral molecules. M. Maestre (LBL) showed early results of the angular dependence of ultraviolet and soft x-ray CIDS that indicated a high sensitivity to structural features of biological structures and suggested the technique could be used to study the higher-order structure of chromosomes. A. Zettl (U.C. Berkeley) illustrated the uses of angle-resolved photoelectron spectroscopy (PES) to map the electronic band structure of high-T_c oxide superconductors and of high-resolution PES to measure the superconducting energy gap. J. Kirschner (Freie Universität Berlin) gave a broad review of MCD in core-level PES and in valence-band PES of magnetic materials to probe magnetic moments and to investigate magnetic effects on electronic structure, respectively. Kirschner also discussed spin-resolved PES of nonmagnetic materials with circularly polarized photons. And G.A. Sawatzky (University of Groningen) took a similarly broad look at the use of core-level absorption spectroscopy with linearly and circularly polarized photons to obtain high-resolution (millivolts) fingerprints of the electronic structure of highly correlated systems that contain transition-metal and/or rare-earth ions.

K-J Kim (LBL) presented an overview of sources of polarized synchrotron radiation and a theoretical framework for characterizing it. This includes the coherency matrix and the Stokes vectors that describe partially polarized radiation and the Mueller matrix that relates the Stokes vectors before and after a generalized scattering event. W.M. McClain (Wayne State University) described an instrument and techniques for determining all the elements of the Mueller scattering matrix as a function of scattering angle. These techniques are applicable when the wavelength is comparable to the size of the scattering particle and hence should be extremely useful in the XUV spectral region. E. Stern (University of Washington) reviewed the roles of the exchange and spin-orbit interactions in the dielectric constant (matrix) as a means for understanding element-specific, local magnetic properties in ferro-, antiferro-, and ferrimagnetic materials, including disordered and complex, multicomponent systems. And M. Blume (Brookhaven National Laboratory) worked through the theory for describing transmission and small-angle scattering of circularly polarized photons passing through matter with a matrix index of refraction, including the case of photon energy near an absorption edge.

In the area of future uses for synchrotron radiation, D. Chemla (LBL) looked forward to the exploitation of the spatial coherence and pulsed time structure of undulator radiation in the XUV spectral region for nonlinear optical processes analogous to those that have become so widely practiced at longer wavelengths by means of lasers. He emphasized experiments requiring two beams, such as pump-probe, time-resolved wave mixing, and multiphoton techniques. E. Commins (U.C. Berkeley) concluded that the prospects were not good for XUV to replace visible laser photons as a tool to study fundamental symmetries in atomic physics, specifically parity nonconservation in atoms, which could provide constraints on extensions of existing quantum field theories of elementary particles (i.e., beyond the Standard Model). R. Laughlin (Stanford University) speculated on the possibility of parity and time-reversal symmetry violations in high-Tc superconductors. Such symmetry violations could support a novel theory of these materials that has direct parallels with elementary particle theories and could therefore provide an insight on what is beyond the Standard Model.

E. Gluskin (APS, Argonne) described instrumentation for and summarized preliminary results of spectral and polarization measurements on a prototype Advanced Photon Source undulator that is now in operation at the National Synchrotron Light Source. He also compared the measured properties with calculated values. J. Kortright (LBL) reported on early attempts to achieve phase retardation (the difference in phase change of two polarization components) by passing XUV radiation through free-standing transmission Mo/Si multilayer optics. This is a possible means of converting linearly polarized bend-magnet radiation into circularly polarized radiation. G. Schütz (Technische Universität München) described techniques for measuring magnetic absorption (the spin-dependent part of the absorption coefficient) and Bragg scattering on ferro- and ferrimagnetic materials with circularly polarized hard x rays. Schütz gave a comprehensive overview of experiments of this type and suggested that some lessons from these experiments could be extrapolated to the soft x-ray regime.

B. Kincaid (LBL) reviewed the status of the ALS construction project and emphasized ALS features contributing to high spectral brightness. A tour of the partially completed facility was conducted, allowing those attending to see for themselves the advanced state of the project. The workshop concluded with a panel discussion on how to exploit near-term and future scientific opportunities with circularly polarized XUV synchrotron radiation. The discussion was chaired by J. Stöhr (IBM). To provide a framework for subsequent discussion, he divided the science into three general areas—magnetic materials and phenomena, molecules and macromolecules, and fundamental symmetries of matter—and noted that there were two relevant photon-energy regimes—ultraviolet for probing valence band phenomena and soft x-ray for core-level effects. The panel was asked to consider what kinds of experimental facilities could initially service needs in these areas, to balance the roles of advanced insertion devices and XUV optics in developing future sources of circularly polarized synchrotron radiation, to distinguish carefully

between experiments requiring high brightness and high flux, and to search for truly unique opportunities for the use of circularly polarized photons.

Although the workshop focused on circularly polarized synchrotron radiation from bend magnets, the development of advanced insertion devices designed specifically to produce high-brightness, energy-tunable, circularly polarized XUV radiation will provide new opportunities for research. Some of the many possible types of insertion devices with these capabilities include the asymmetric wiggler, the helical undulator, the elliptical wiggler, and the crossed undulator. At the ALS, at least one straight section is being reserved for an advanced insertion device of a type yet to be determined. Studies now under way will lead to a decision that is sure to emphasize high brightness.

Can We Transpose Visible, Nonlinear Optics to X-Rays?

D.S. Chemla

Lawrence Berkeley Laboratory

CAN WE TRANSPOSE VISIBLE NONLINEAR-OPTICS TO X-RAYS ???

DANIEL CHEMLA
MATERIAL SCIENCES DIVISION LBL
PHYSICS DEPARTMENT UC BERKELEY

EXAMPLES OF NONLINEAR OPTICAL PROCESSES REQUIRING LIGHT SOURCES WITH PROPERTIES SIMILAR TO THAT OF THE ALS:

BROAD CONTINUUM
HIGH BRIGHTNESS
PHOTON PULSES

TWO BEAM CONFIGURATION:

1) NARROW PUMP / CONTINUUM PROBE EXPERIMENTS

2) CIRCULARLY POLARIZED PUMP / PROBE EXPERIMENTS

3) TIME RESOLVED WAVE MIXING

4) TWO BEAM MULTI-PHOTON PROCESSES

Principle of Experiments

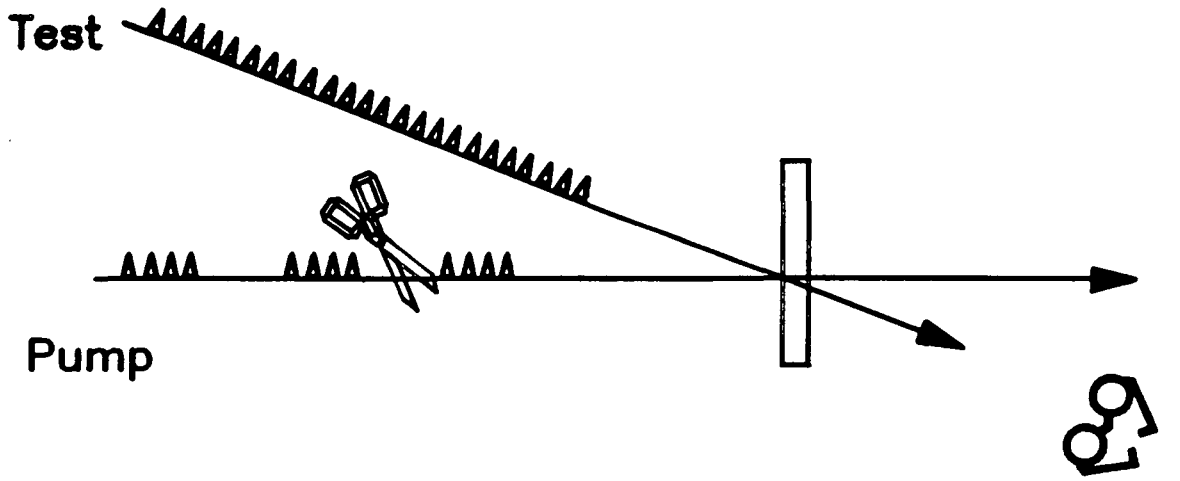

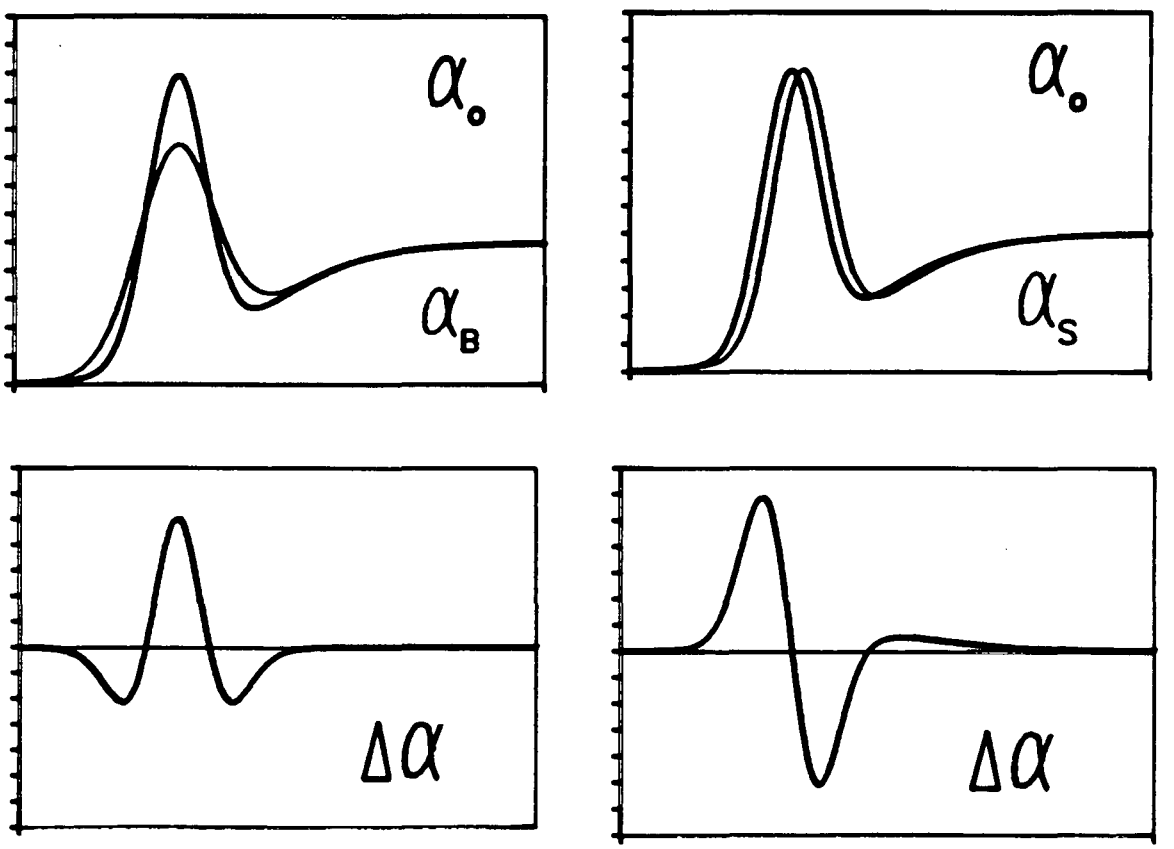

SPECTRUM OF 100fs CONTINUUM & ABSORPTION SPECTRUM OF PIN-QW

PIN-QW SAMPLE 50 PERIODS OF 74Å QW + 60Å BARRIERS

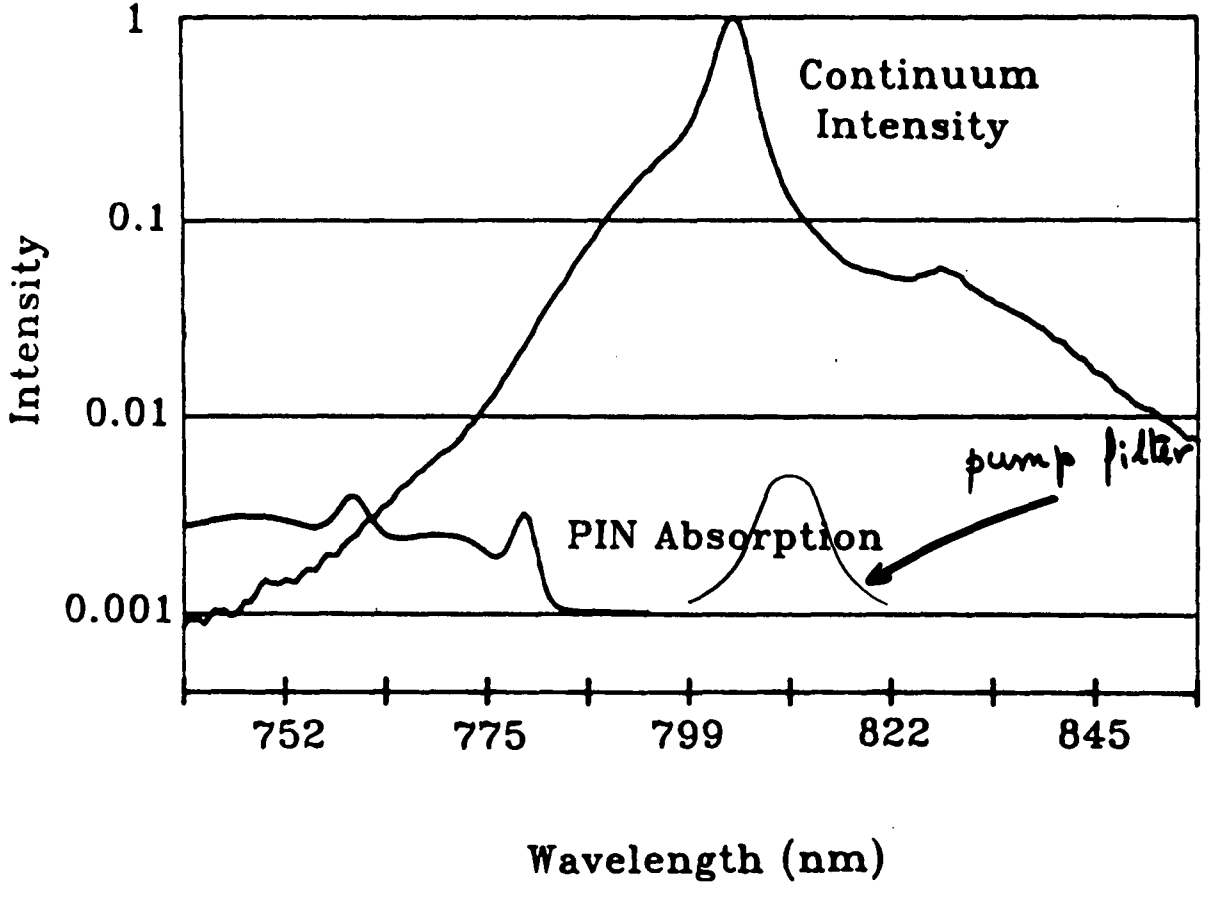

at $T \simeq 35\,K$

$0 \leq E_g - \omega_p \leq 150\,meV$

$0 \leq I_p \leq 1\,TW/cm^2$

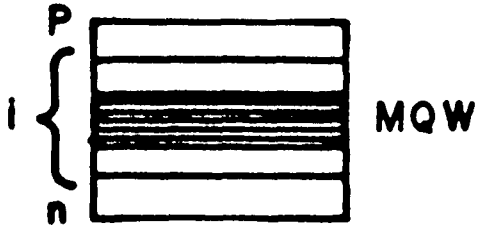

COMBINED EFFECTS OF VIRTUAL POPULATIONS AND TWO PHOTON–INDUCED REAL POPULATIONS

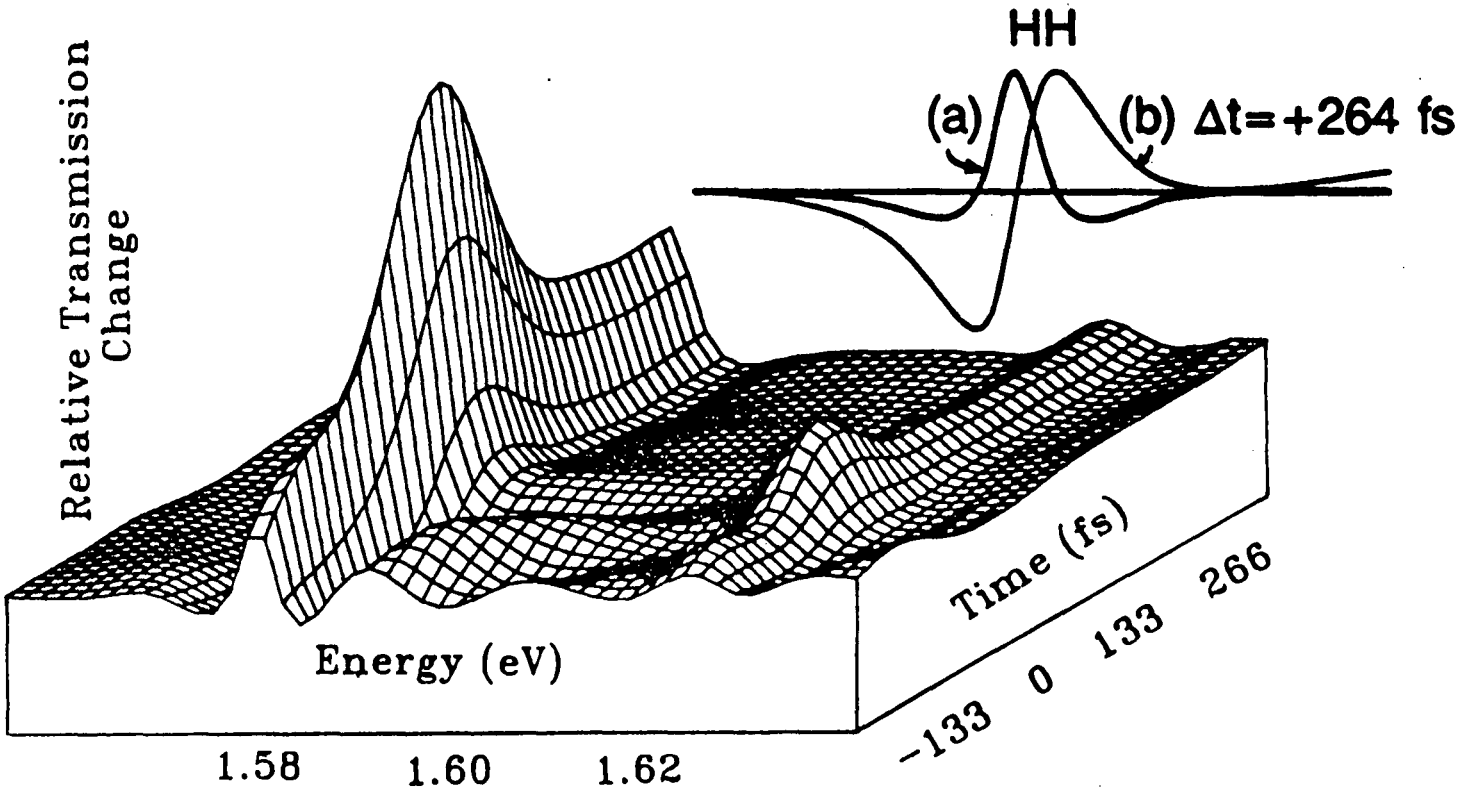

Experimental Differential Transmission Spectrum

Large detuning (80 meV), High excitation (10 GW/cm^2)

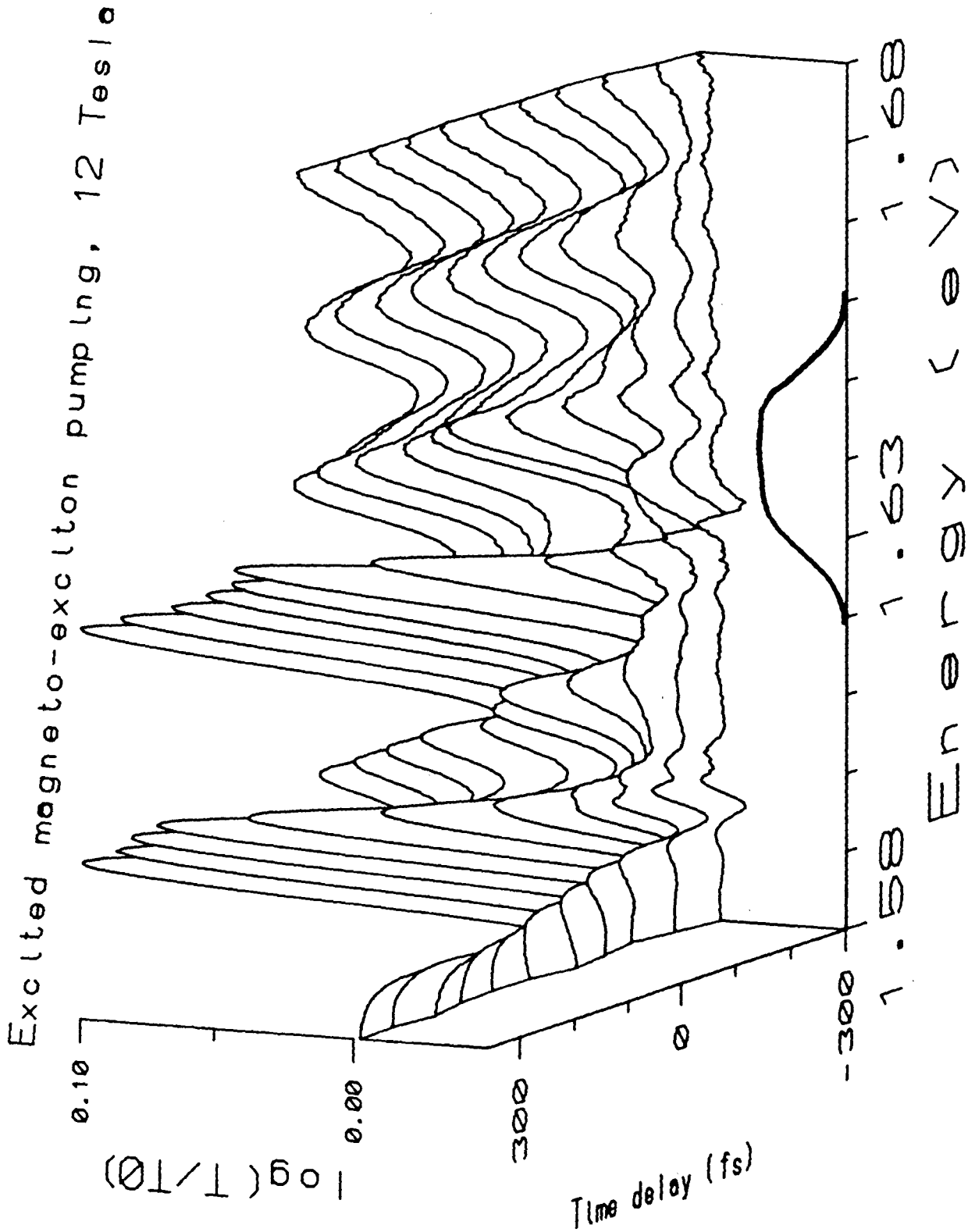
Excited magneto-exciton pumping, 12 Tesla
log(T/T0)
0.10
0.00
300
0
-300
Time delay (fs)
1.58
1.63
1.68
Energy (eV)

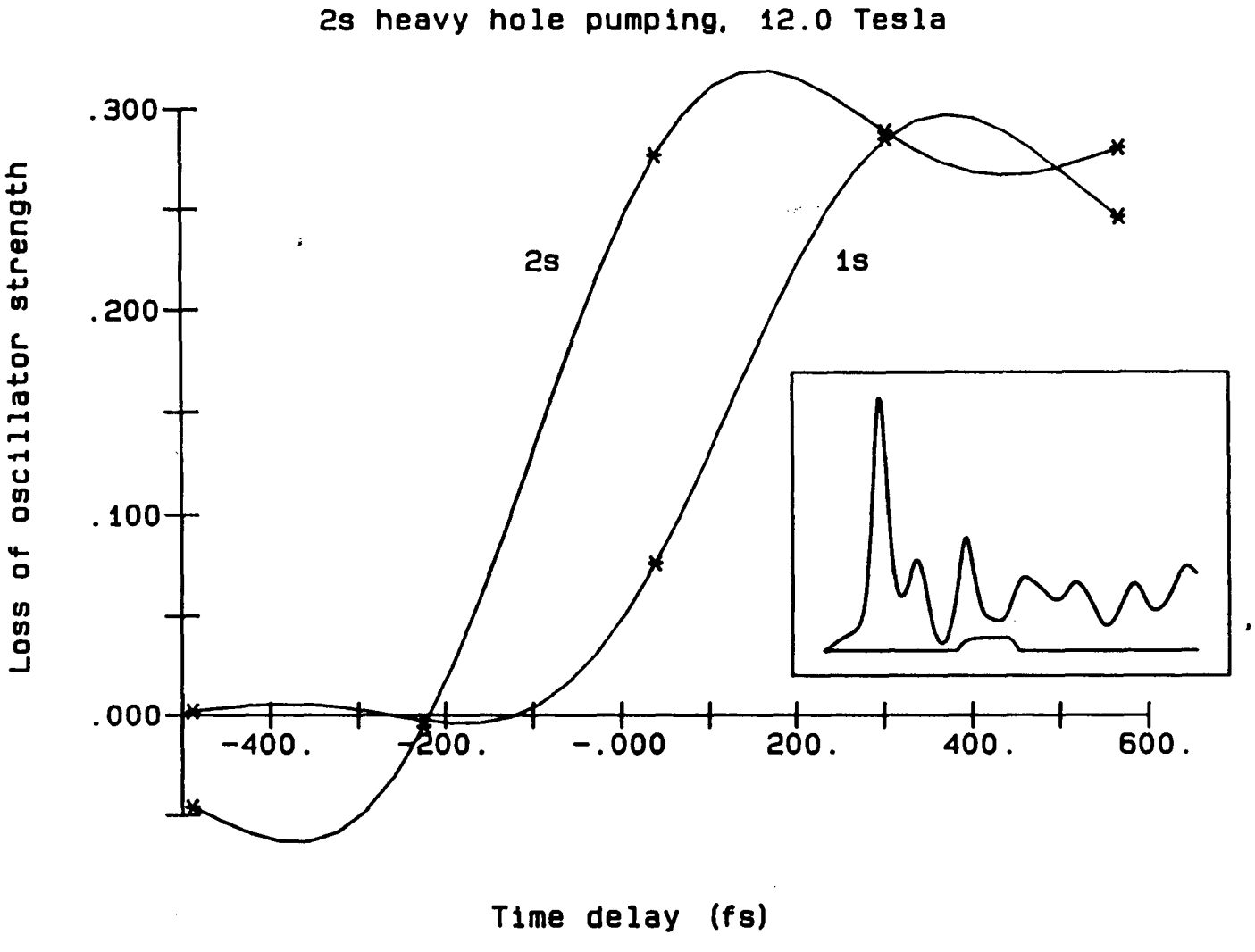
2s heavy hole pumping, 12.0 Tesla
Loss of oscillator strength
.300
.200
.100
.000
-400.
-200.
-.000
200.
400.
600.
2s
1s
Time delay (fs)

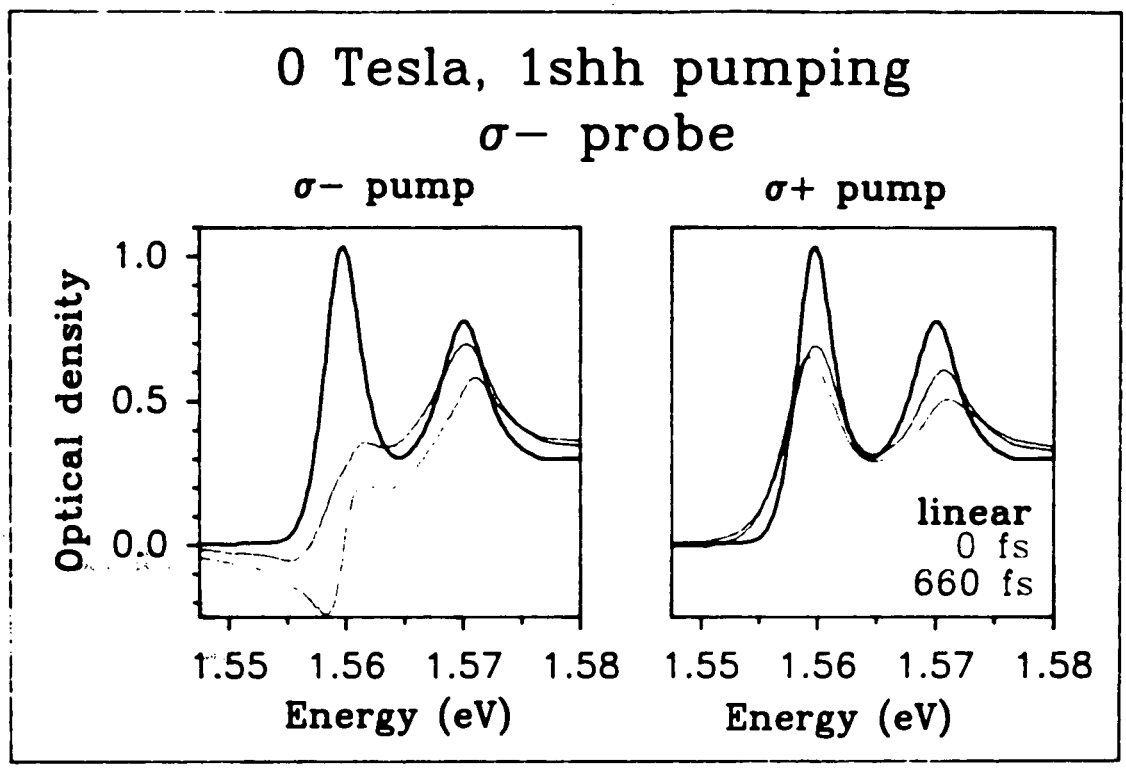
0 Tesla, 1shh pumping
σ− probe
σ− pump
σ+ pump
Optical density
1.0
0.5
0.0
linear
0 fs
660 fs
1.55 1.56 1.57 1.58
Energy (eV)
1.55 1.56 1.57 1.58
Energy (eV)

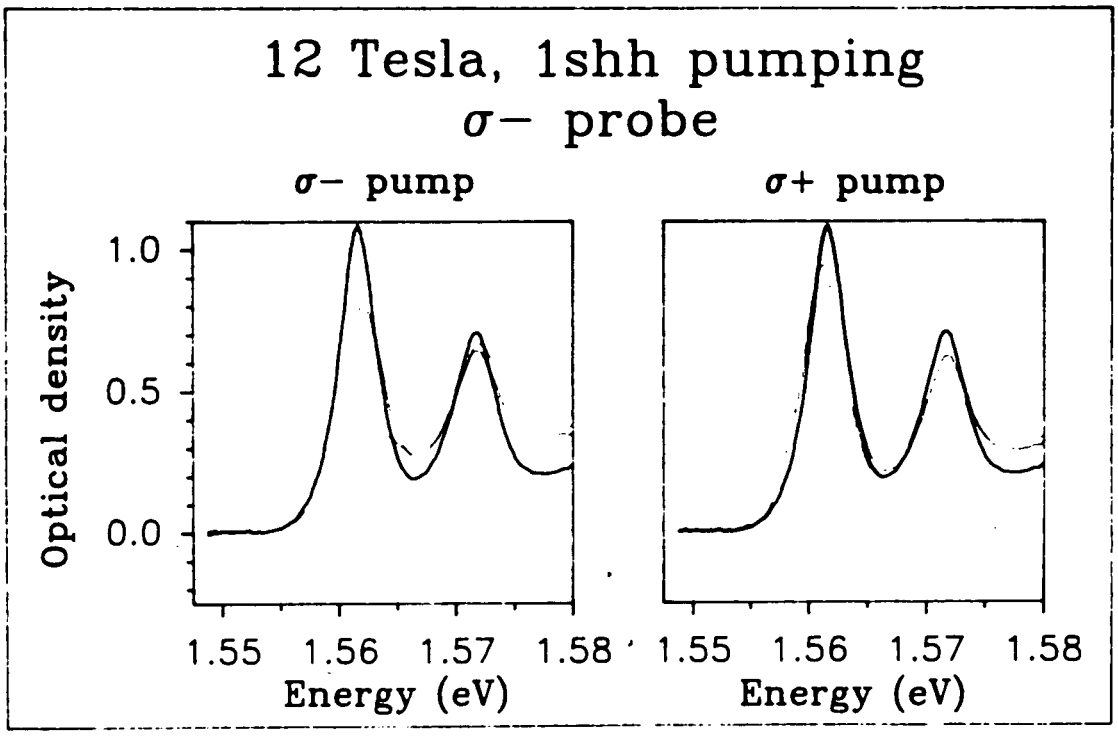
12 Tesla, 1shh pumping
σ− probe
σ− pump
σ+ pump
Optical density
1.0
0.5
0.0
1.55 1.56 1.57 1.58
Energy (eV)
1.55 1.56 1.57 1.58
Energy (eV)

17jan0t

Measurement of Polarization Dephasing by Time Resolved Four Wave Mixing

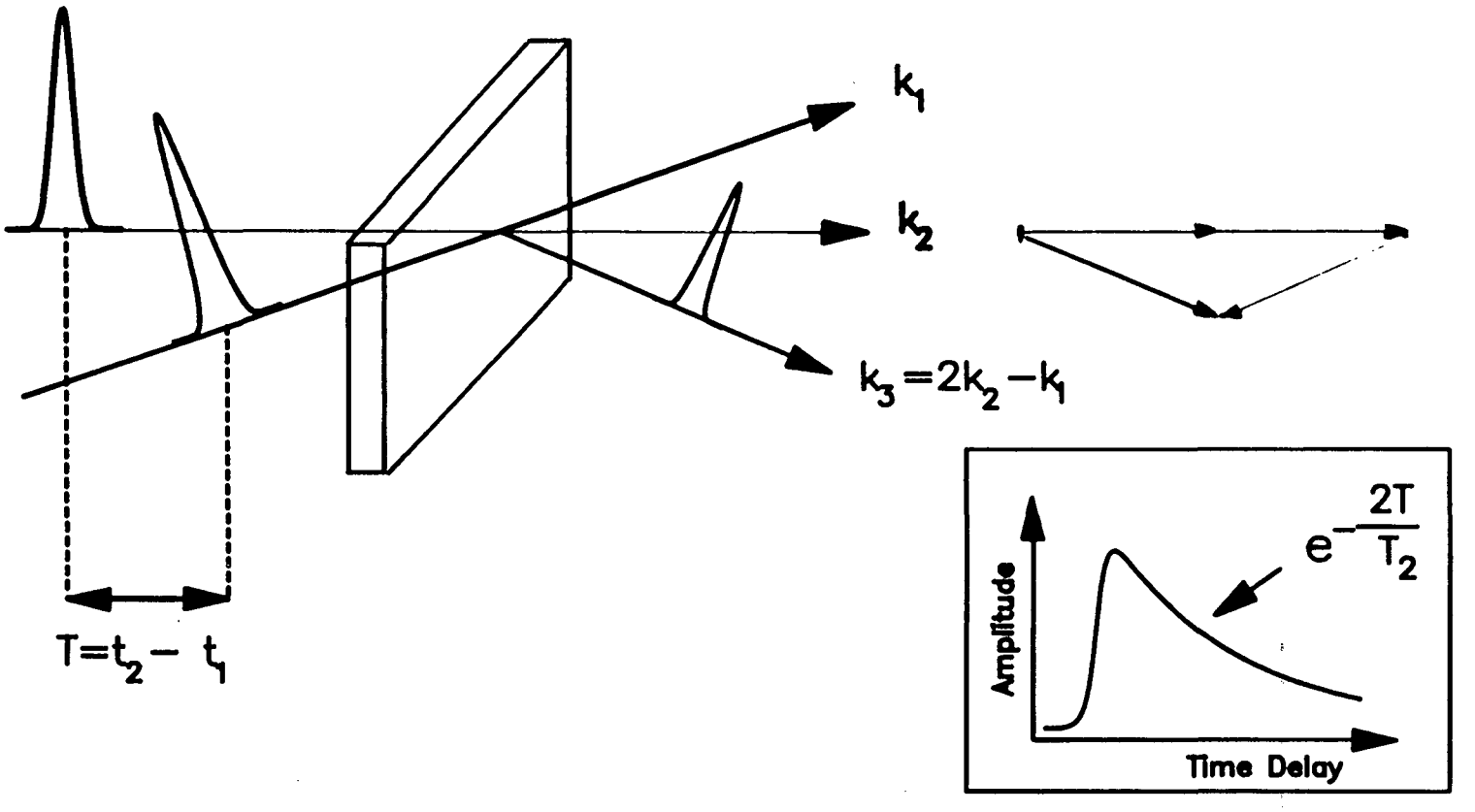

Interpretation Based on Two Level System Model
(T. Yajima, Y. Taira J. Phys. Soc. Jpn. 47, 1620 1979)

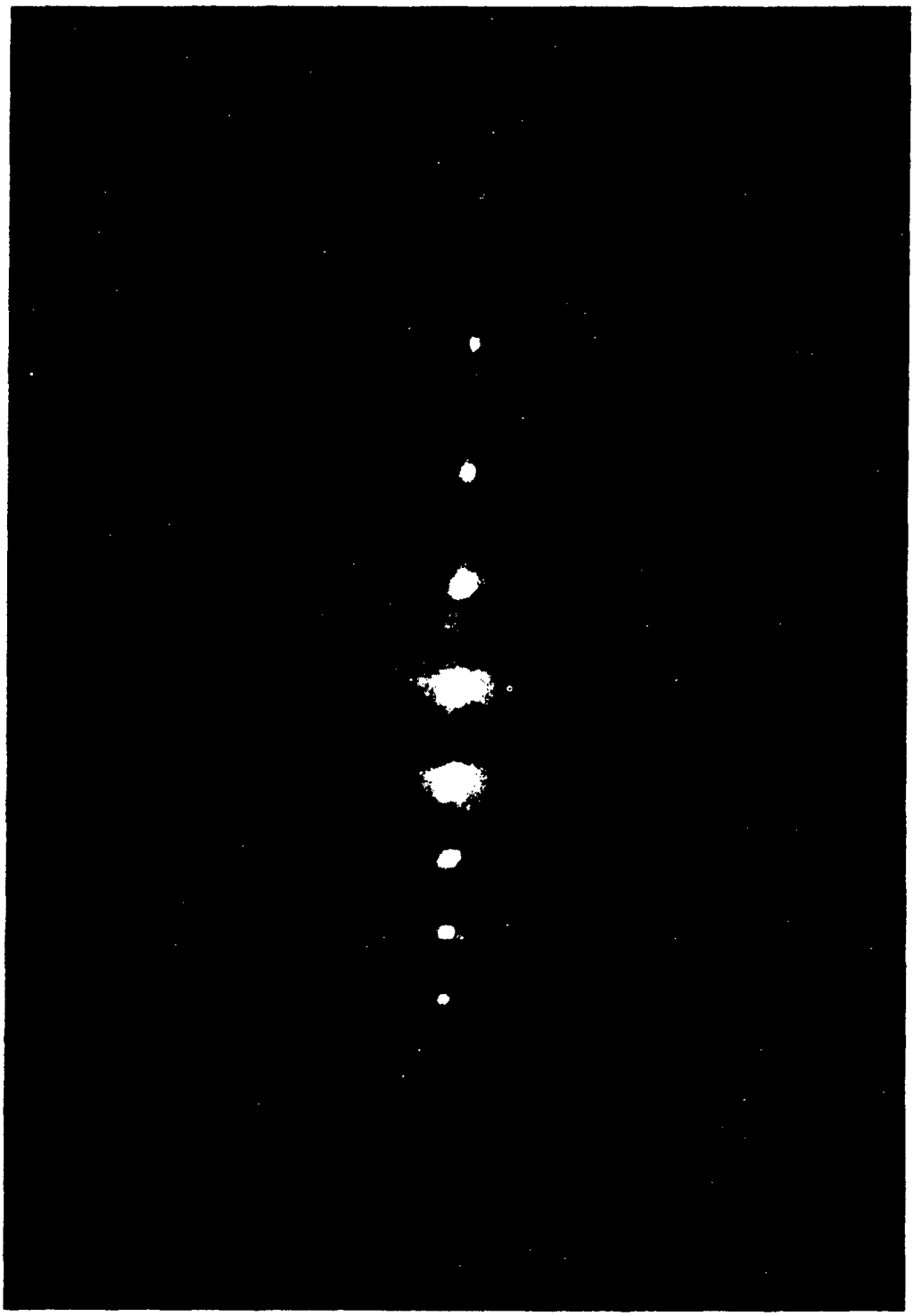

Photograph of the track of the beams originating from multiple scatterings. The two bright spots are the tracks of the pump and the test beams. The other spots correspond to beams scattered in the direction: $k_N^+ = k_p + N(k_p - k_t)$ and $k_N^- = k_t + N(k_t - k_p)$ the nth-order scattering corresponds to a (2N+2)-photon process.

DOUBLE EXCITON–BIEXCITON RESONANCE

OBSERVATION OF 5th ORDER PROCESSES IN MULTIPLE SCATTERING

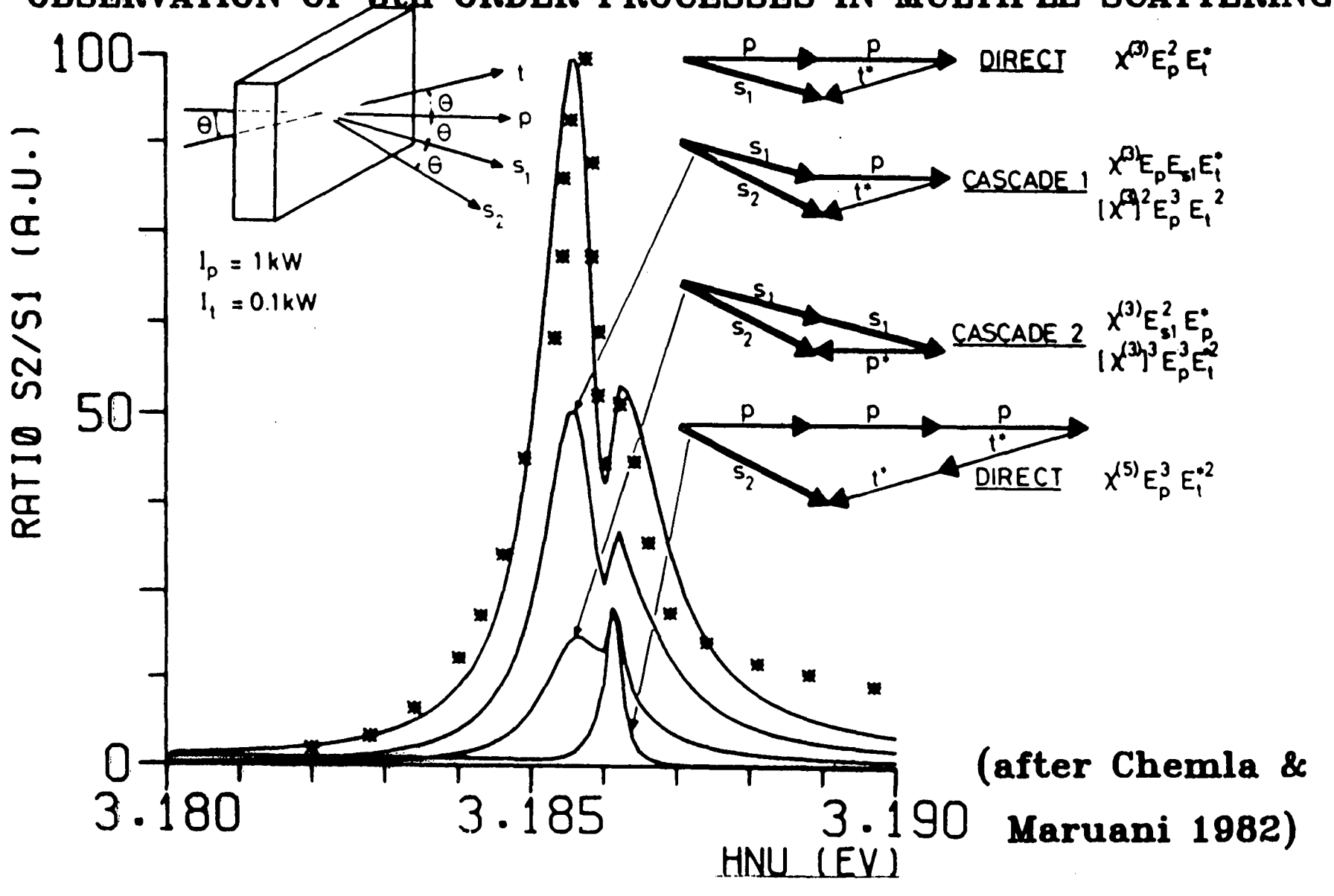

(after Chemla & Maruani 1982)

CONCLUSION

ALREADY MANY OPPORTUNITIES WITH THE ALS AS IT SHALL BE IN 93

OTHER CHALLENGES:

EXPLOITING THE COHERENT PROPERTIES OF ALS

ps-TIME RESOLUTION BY PULSE COMPRESSION

The Advanced Light Source

B.M. Kincaid

Lawrence Berkeley Laboratory

The Advanced Light Source

The Advanced Light Source is the first of the new generation of synchrotron radiation sources to be built. Expected to produce beam for scientific users in the spring of 1993, it is a 1.5 GeV electron storage ring targeted for the VUV and soft x-ray part of the spectrum and optimized for low emittance and high-brightness undulator beamlines. Of the 12 long straight sections in the storage ring, 10 are available for insertion devices. Four such devices are being built as part of the ALS construction project. In addition, there are 48 bend magnet ports, 24 of them able to provide high-brightness synchrotron radiation. Several participating research teams (PRTs) have been approved for both insertion device and bending magnet beamlines. These PRTs represent a wide range of scientific interests in materials, chemistry, structural biology, and physics.

The small electron beam emittance, combined with the tightly focused and collimated electron beam source in the bend magnets, makes the ALS bend magnet beams ideal sources of circularly polarized VUV and soft x-ray light. Work has been started on a future crossed-undulator insertion device that will produce a high-intensity beam with variable polarization.

What is the Advanced Light Source (ALS)?

- National user facility
- Provides UV and soft x-ray beams of unprecedented brightness
  - Broadly tunable with narrow spectral features
  - Partially coherent
  - 30 psec time structure
- Utilized by researchers from industry, academic, and national laboratory communities
  - Technology (e.g., projection lithography)
  - Materials and surface science
  - Atomic and molecular physics
  - Chemistry
  - Life sciences
- Construction project began in late 1986
- Begin operations in spring 1993
- Construction cost — $99.5 million

Advanced Light Source
Project Organization

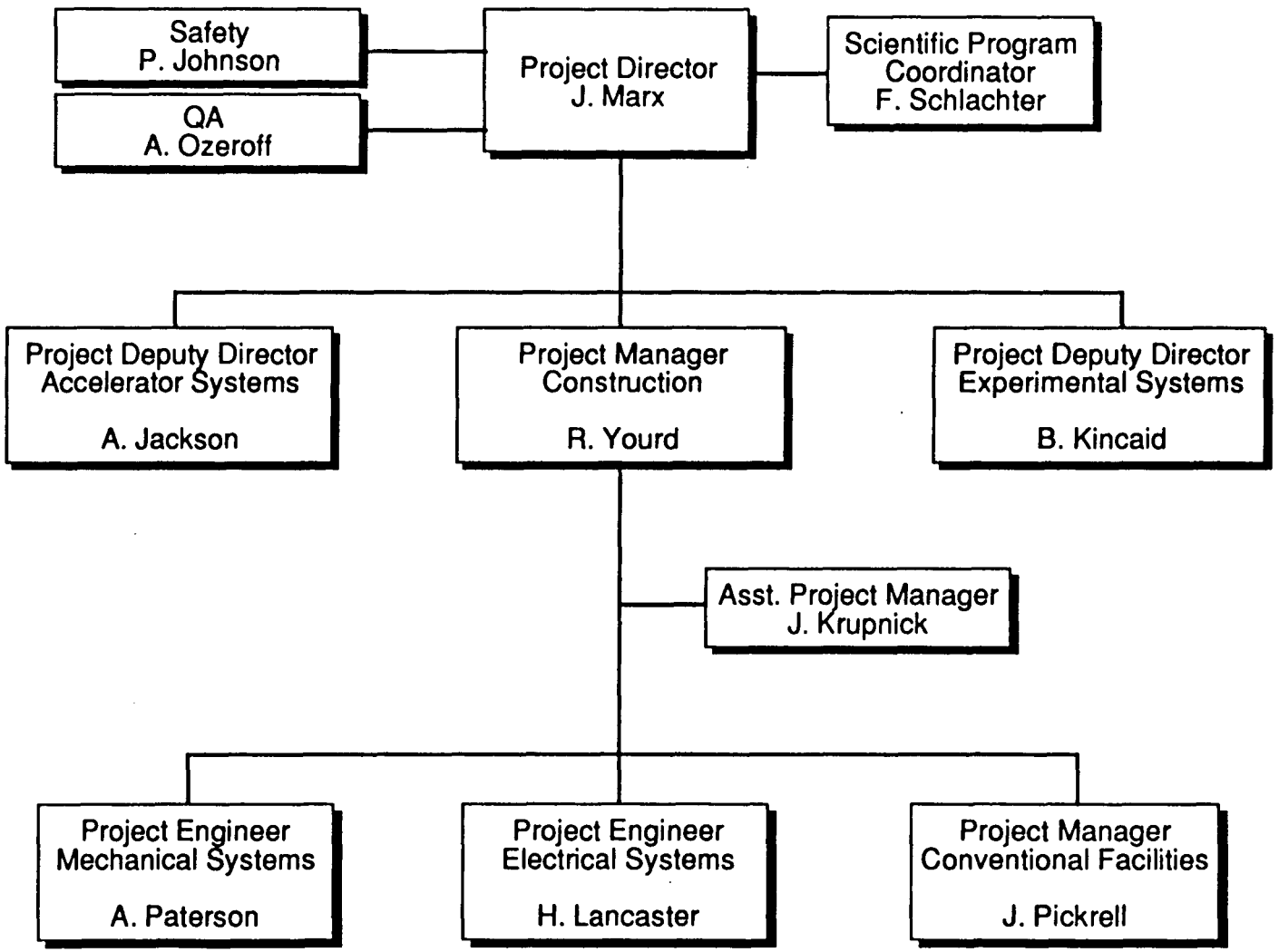

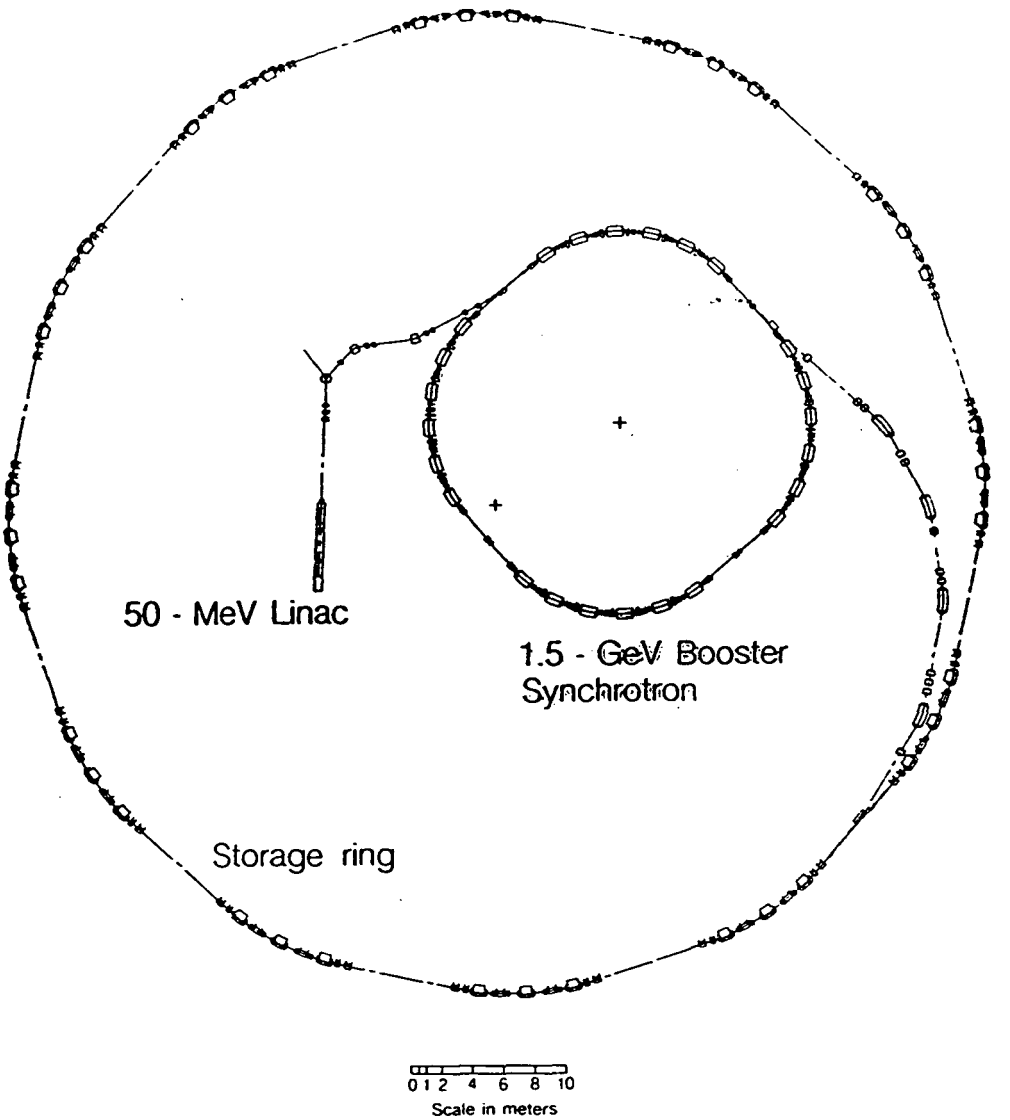

Fig. 2-1. Layout of the ALS accelerator complex showing the placement of the 50-MeV electron linear accelerator, the 1.5-GeV booster synchrotron, and the storage ring.

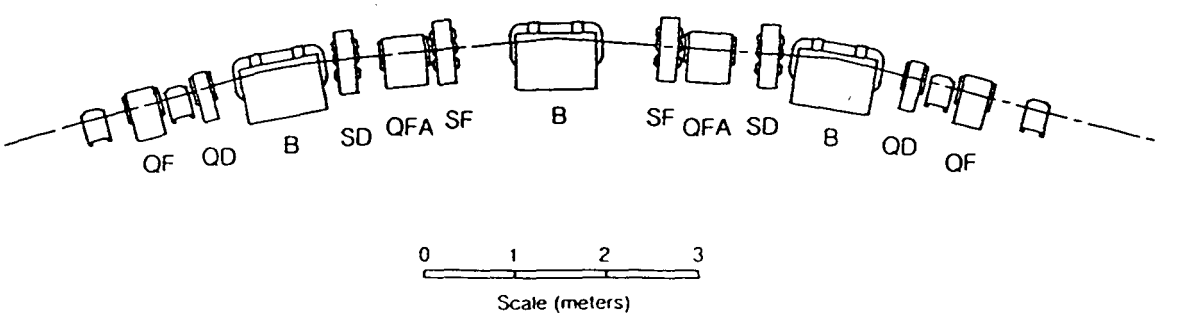

Fig. 2-2. One superperiod of the ALS triple-bend achromat lattice contains three combined-function (bending and focusing) magnets (B), six quadrupole focusing magnets (QF and QD), and four sextupole magnets (SF and SD).

Major Specifications for Accelerator Systems

- **Injector**
  - Linac — 50 MeV
  - Booster — 1.5 GeV, 1 Hz
- **Storage Ring Optimum Energy** — 1.5 GeV
- **Maximum Current (multibunch mode)** — 400 mA
- **Maximum Current (single bunch mode)** — 7.6 mA
- **Horizontal Emittance** — $< 10^{-8}$ m-rad
- **Straight Sections** — 12
- **Time Structure (2 sigma)** — 20–50 psec
- **Lifetime** — > 6 hours
- **High Position and Angular Stability**
- **Minimum Longitudinal Jitter**
- **Flexible Modes of Operation**
  - variable energy 1.0 to 1.9 GeV
  - variety of operating modes: multibunch, few-bunch, single-bunch

Experimental Systems Scope

- Construction Project

  Four insertion devices

  Two I. D. beamlines

  One bend magnet front end system

  Storage ring diagnostic beamline

- R&D

  SSRL beamline VI used as ALS prototype

  Deformable mirror optics

  Undulator technology, advanced magnetic measurements

  Precision optical metrology for SR optics

  High stability photon beam position monitoring and feedback systems

- User interactions

ALS PHOTON BEAM CAPABILITIES

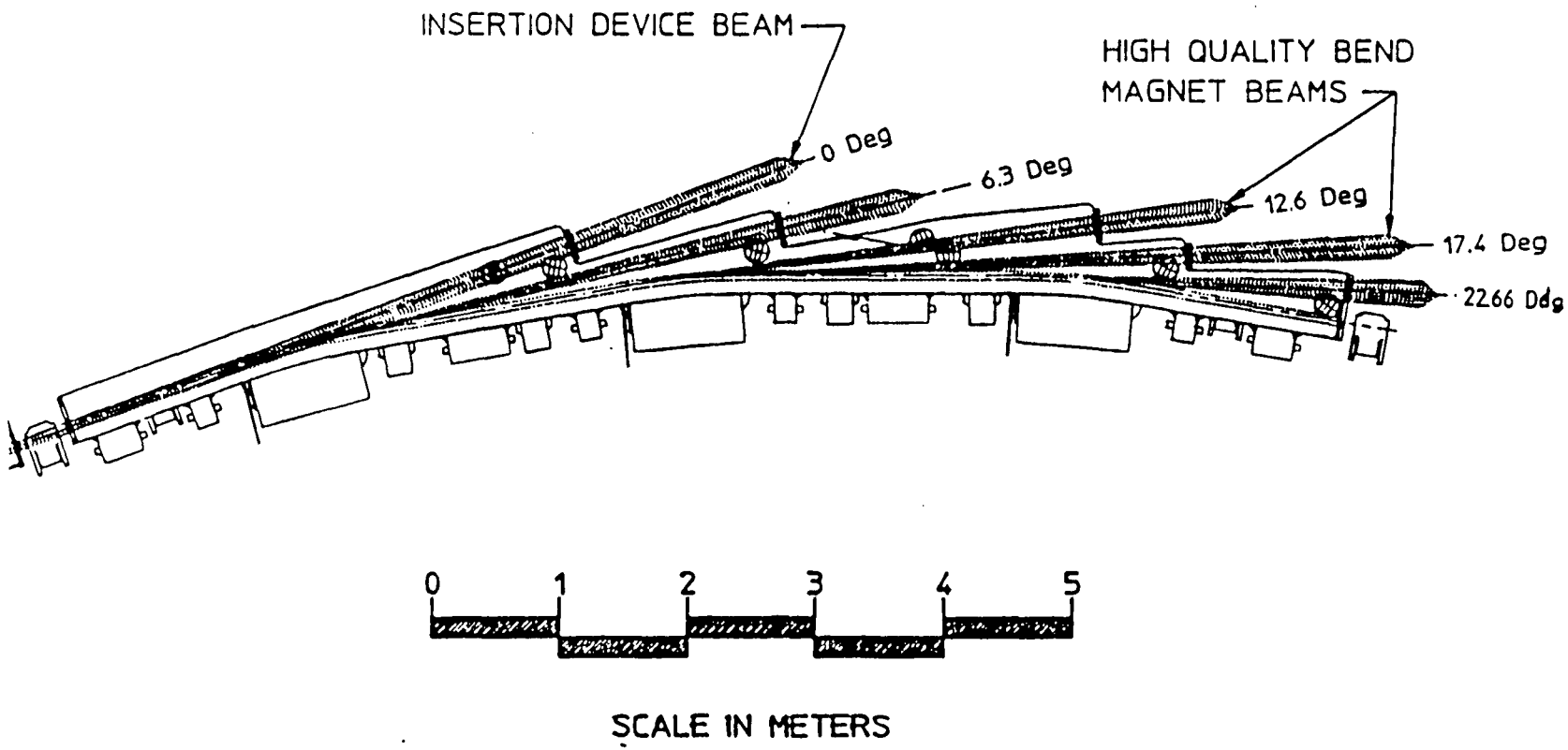

Evolution of Synchrotron Radiation

Todays
Synchrotrons:

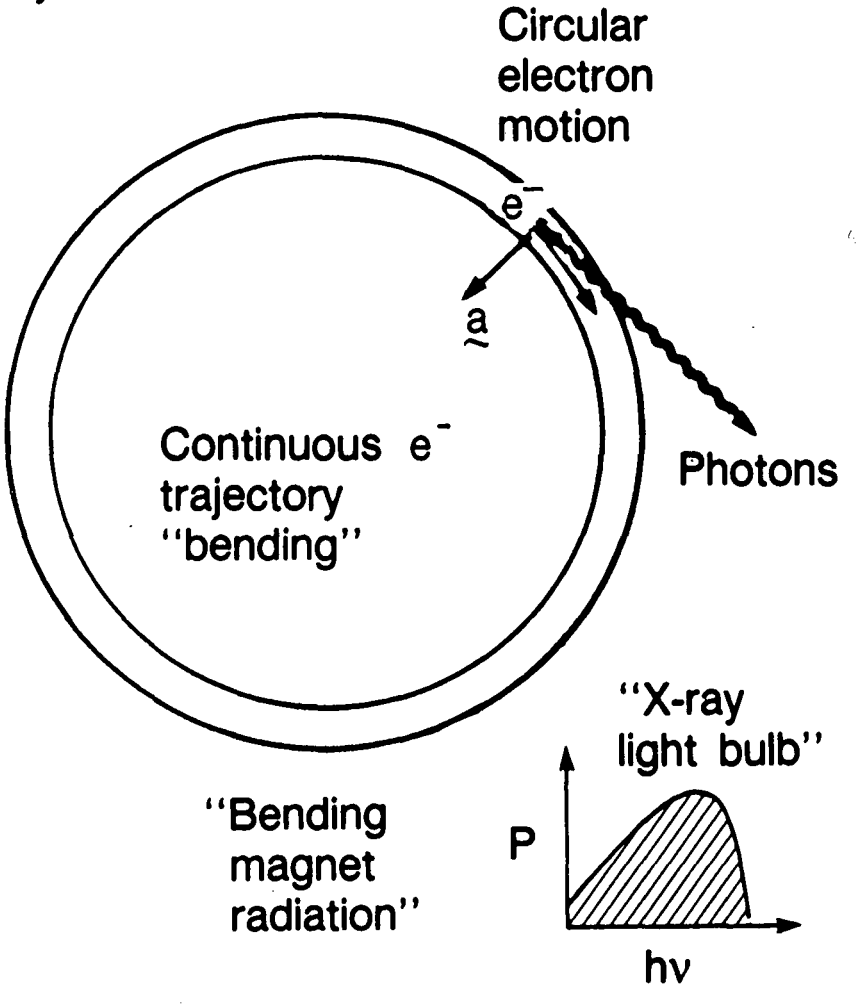

Tomorrows
Synchrotrons:

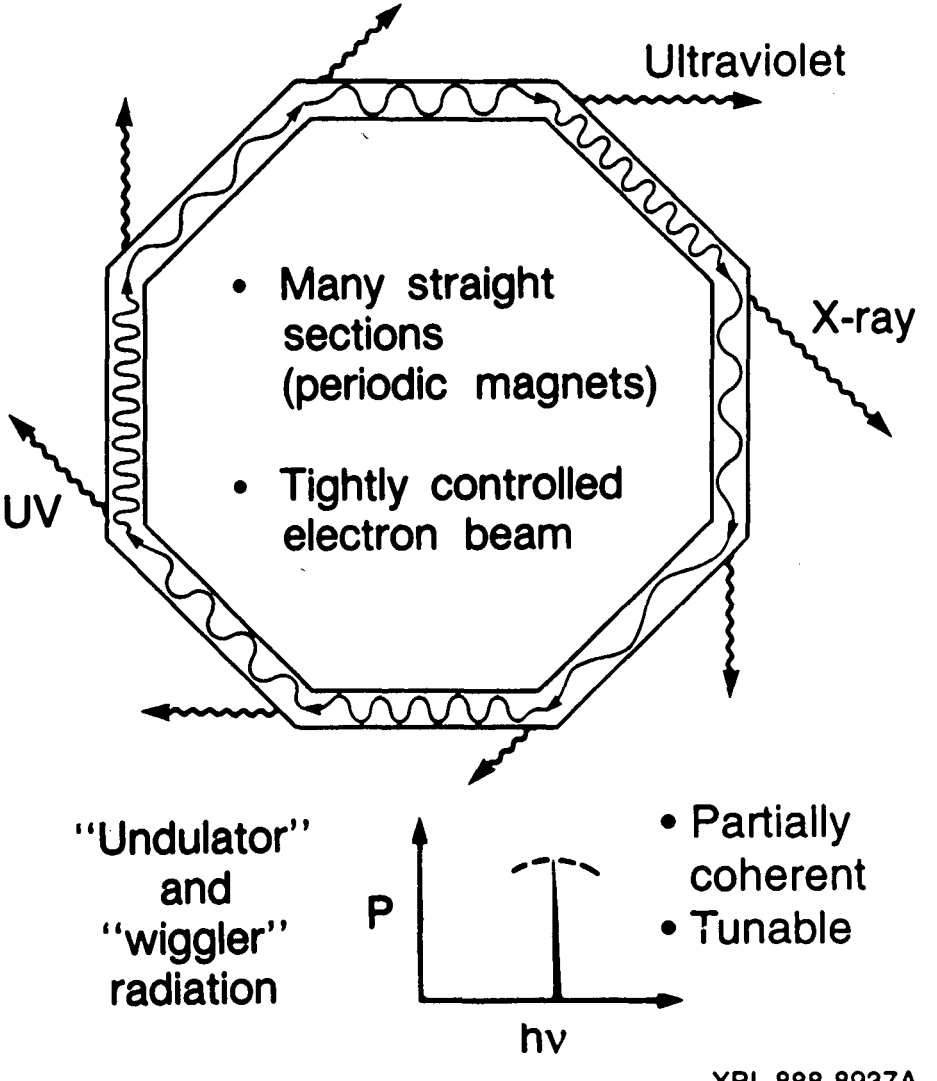

XBL 888-8937A


V=C

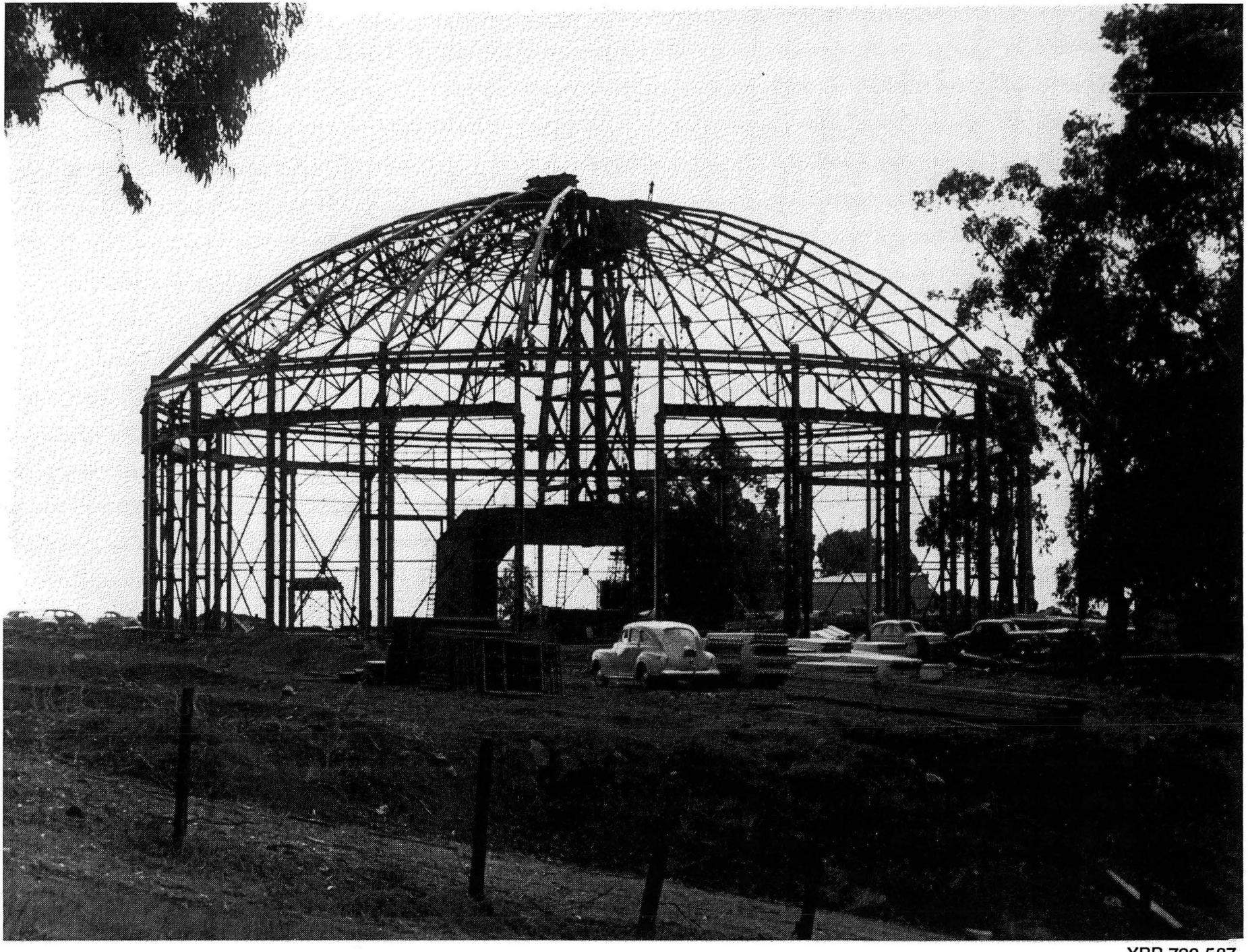

XBB 732-587

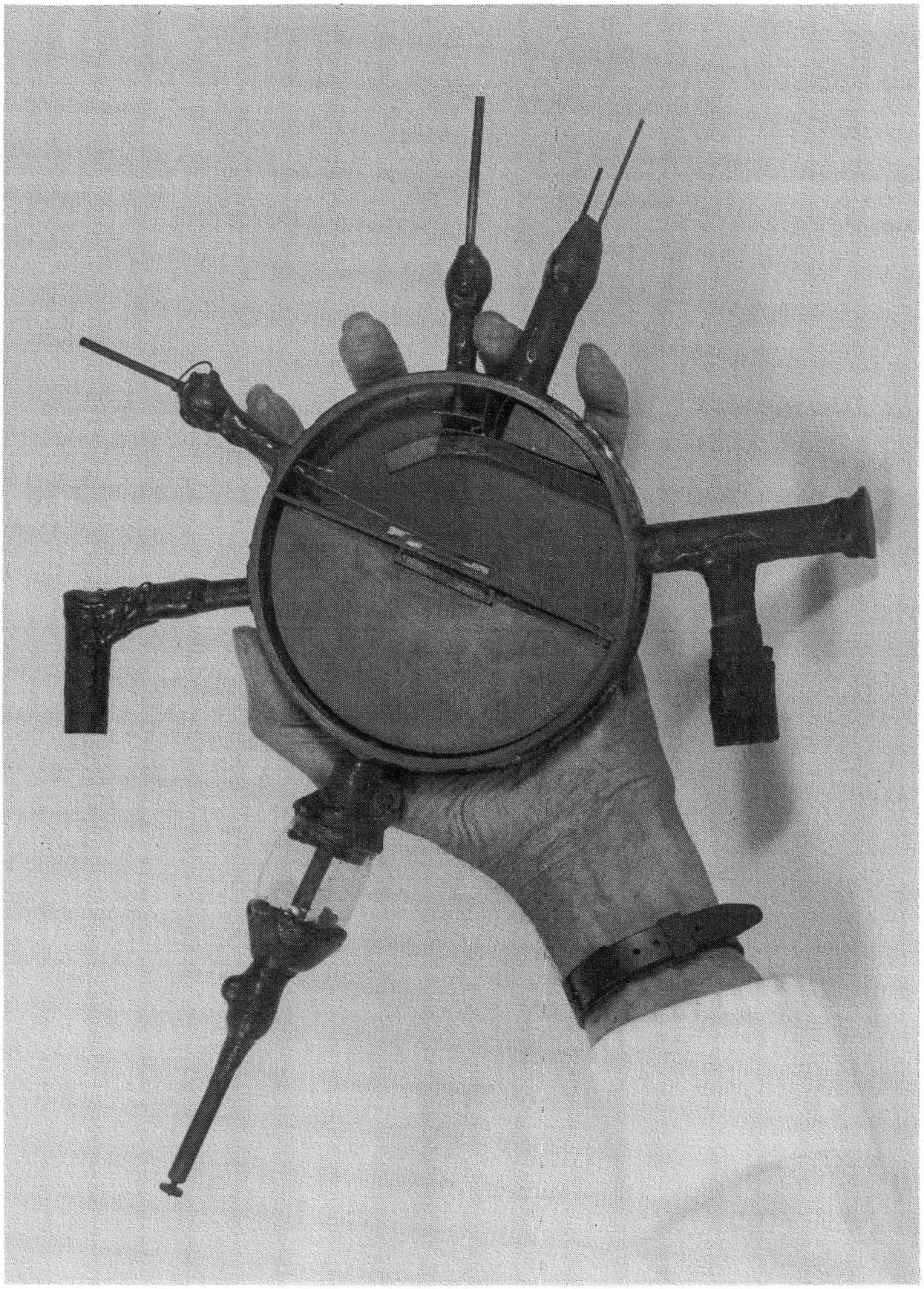

XBC 901-176

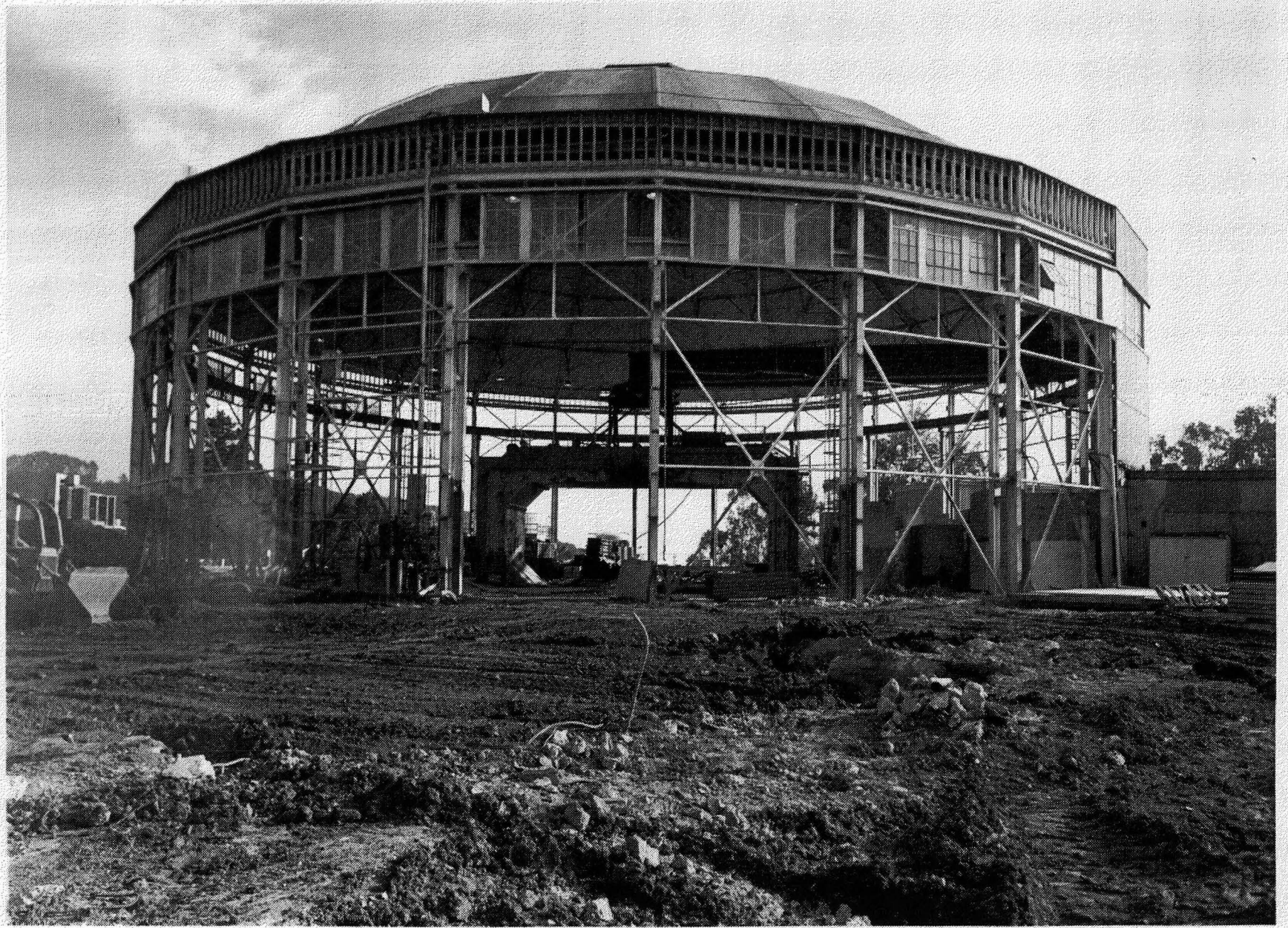

XBB 892-1015

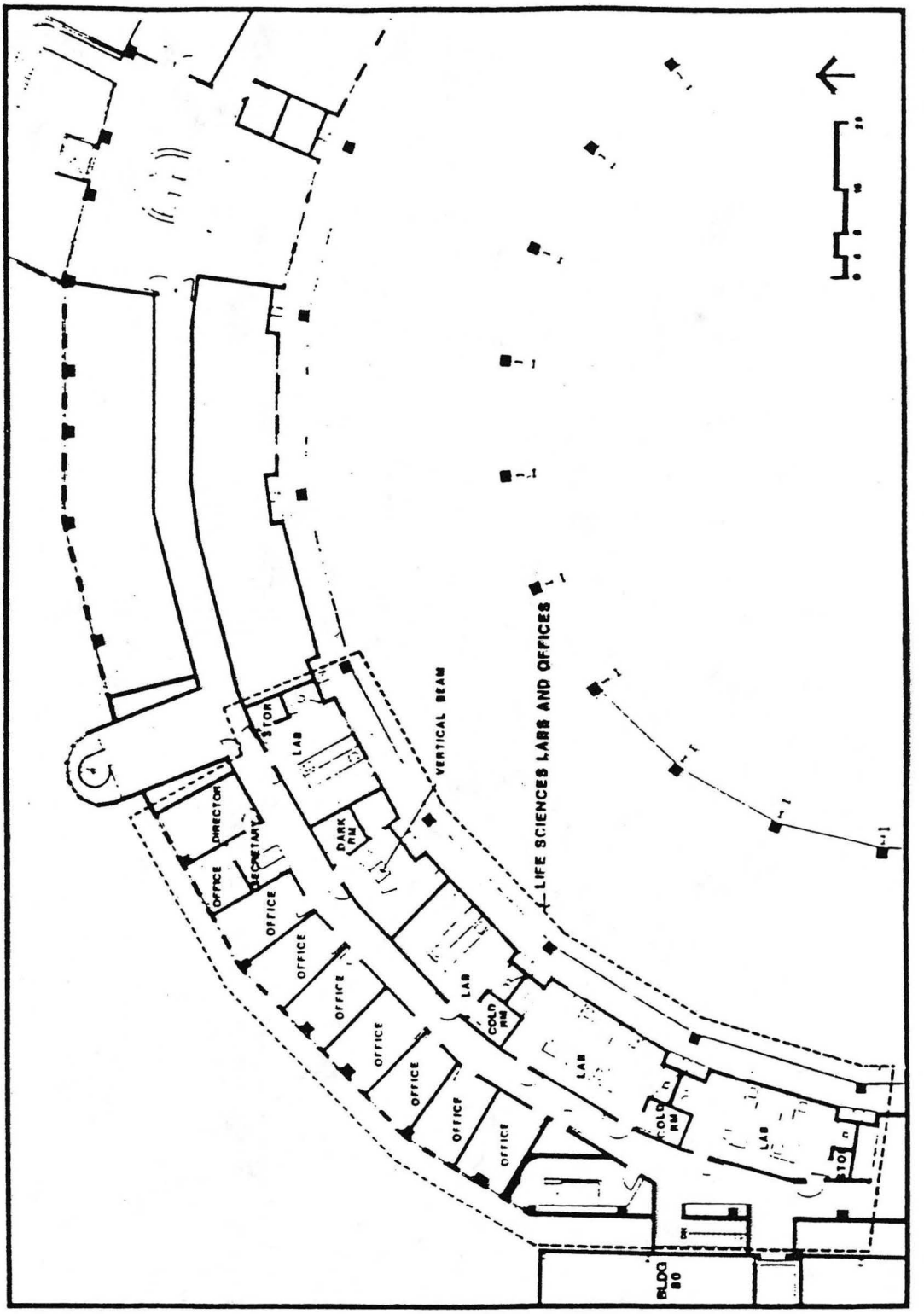

LAWRENCE BERKELEY LABORATORY
UNIVERSITY OF CALIFORNIA

ALS LIFE SCIENCES CENTER

ALS BUILDING - PARTIAL MEZZANINE PLAN

C-3

TABLE II: Comparison of Approximate Heat Flux Levels in Various Physical Processes

Process of Component	Approx. Heat Flux (w/mm^2)
Meteor re-entry	100 to 500 ← APS
Fusion reactor components	0.05 to 80
Sun's surface	60
Commercial plasma jet	20
Interior of rocket nozzle	10 ← ALS
Fission reactor cores	1 to 2

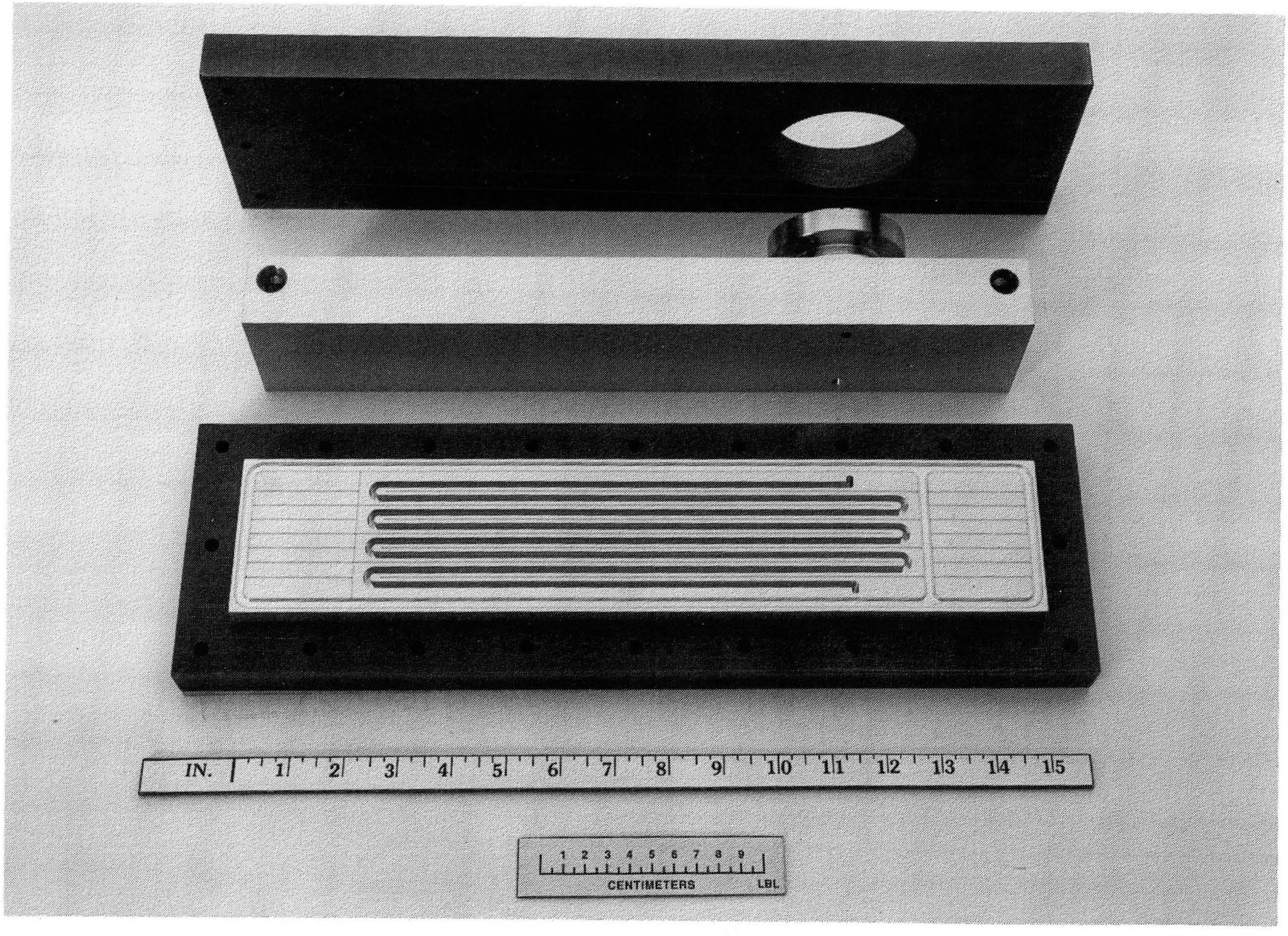

CBB 909-7882

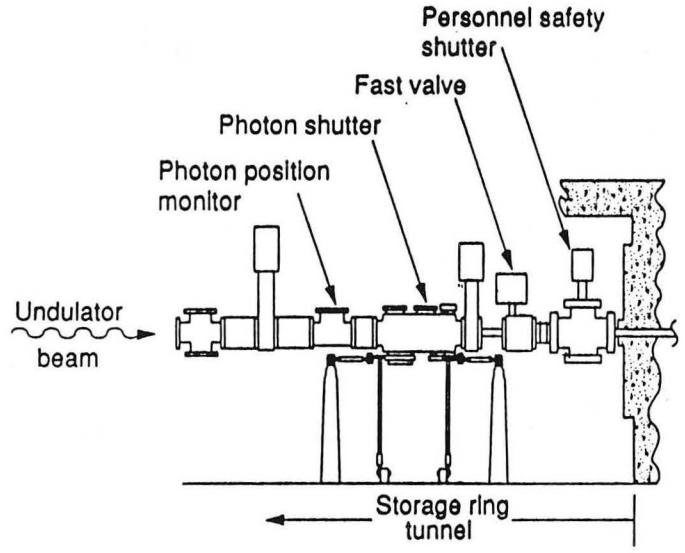

Spherical Grating Monochromator Beam Line for a 8 cm Period Undulator at the ALS

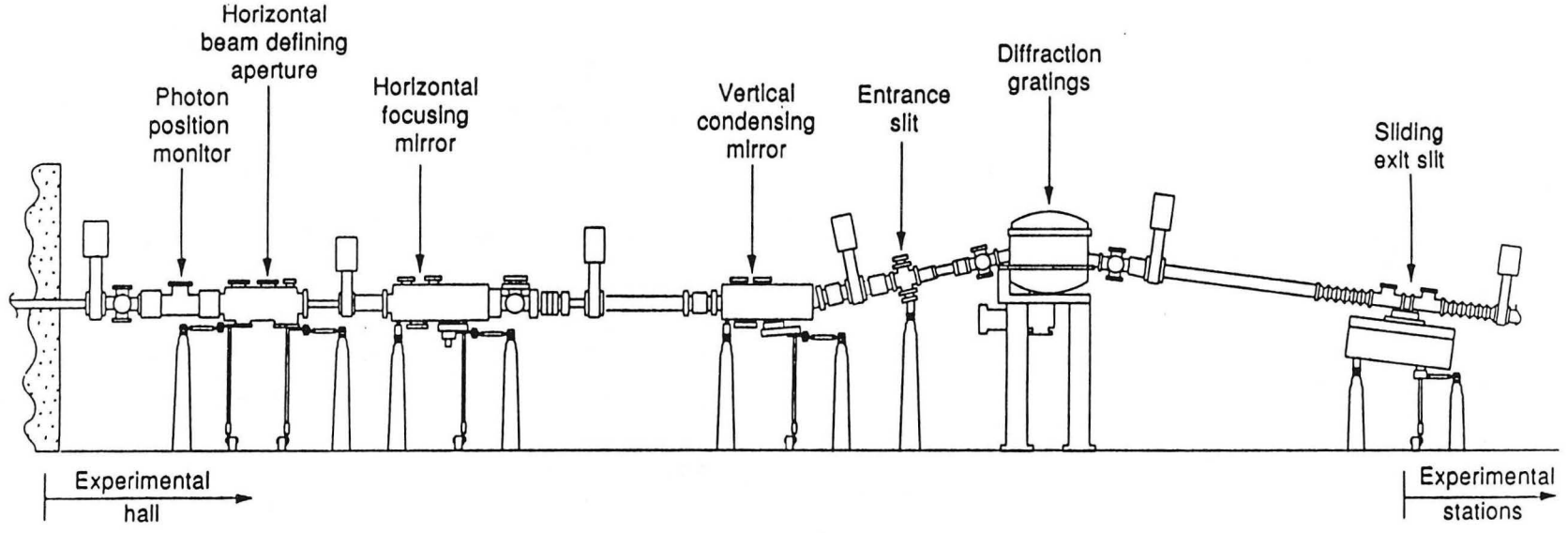

XBL909-6746

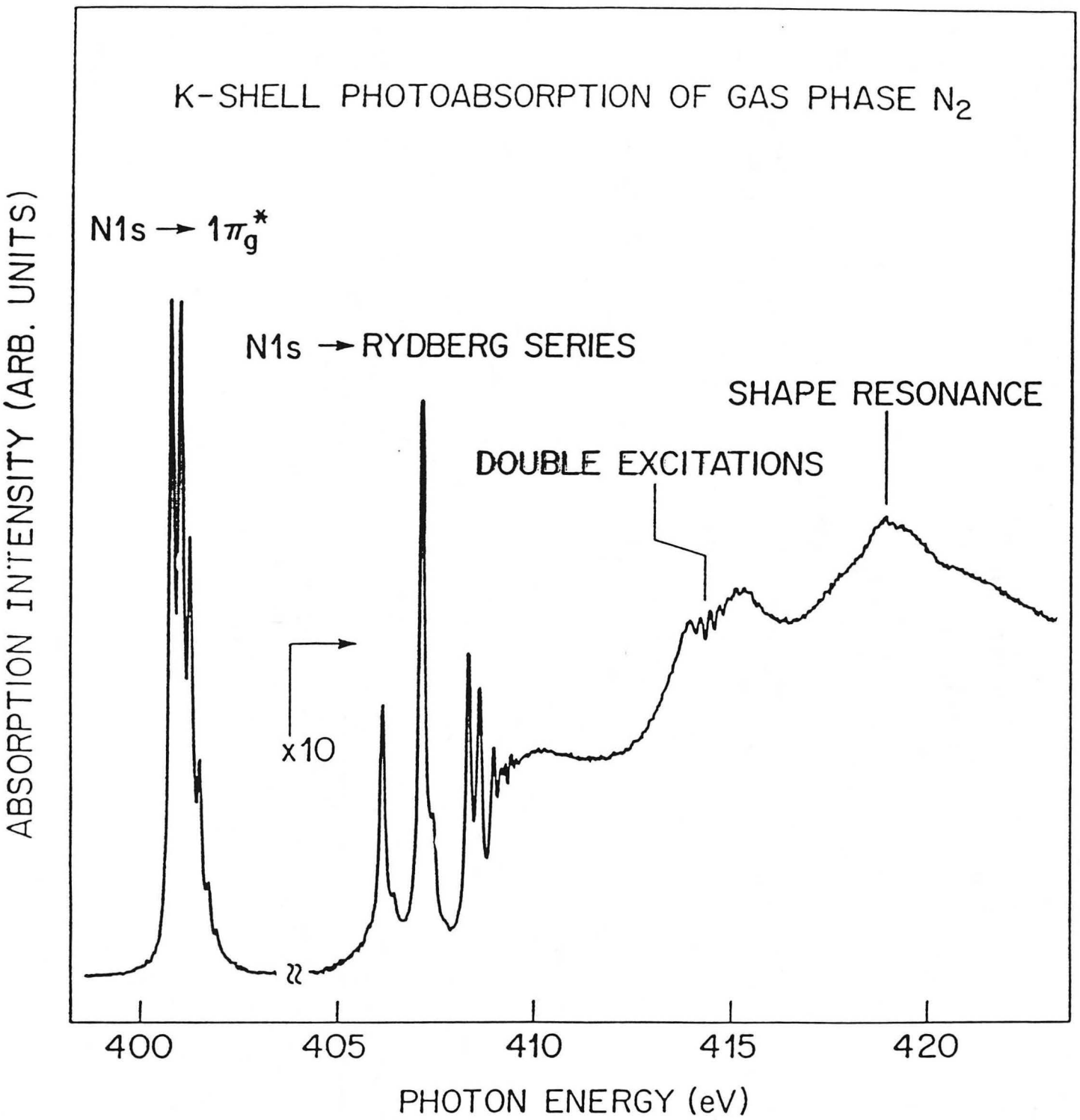
K-SHELL PHOTOABSORPTION OF GAS PHASE N_2
N1s → $1\pi_g^*$
N1s → RYDBERG SERIES
SHAPE RESONANCE
DOUBLE EXCITATIONS
x10
ABSORPTION INTENSITY (ARB. UNITS)
400
405
410
415
420
PHOTON ENERGY (eV)

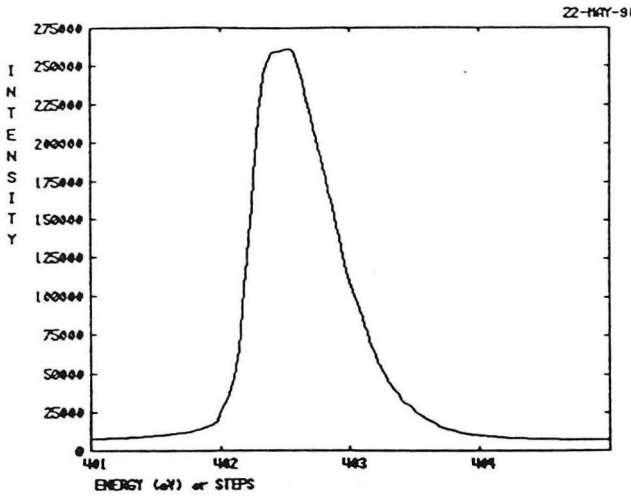

100 μ slits

File name	Chan.,	Offset,	Gain,	Shift,	Line,	File no.,	Attr.
10.BIN	1	0.0000E+00	1.0000E+00	0.0000E+00	1	1	

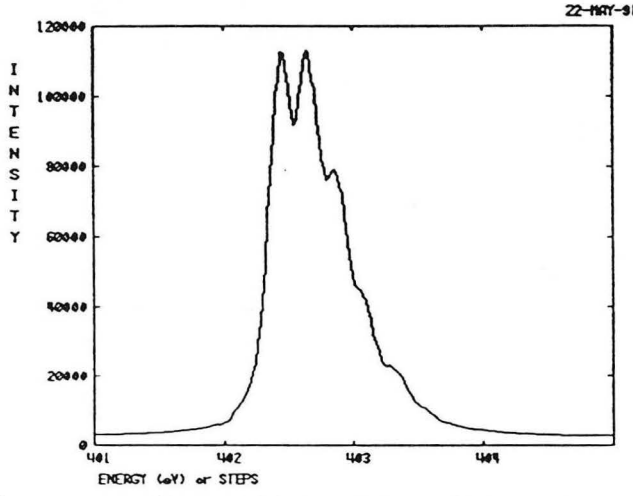

30 μ

File name	Chan.,	Offset,	Gain,	Shift,	Line,	File no.,	Attr.
9.BIN	1	0.0000E+00	1.0000E+00	0.0000E+00	1	1	

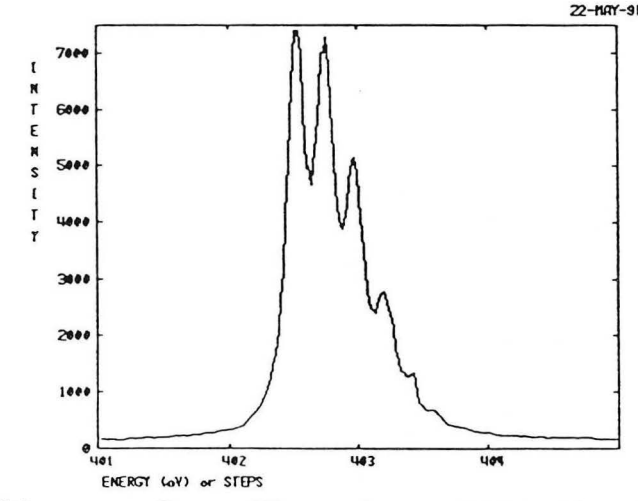

10 μ

File name	Chan.,	Offset,	Gain,	Shift,	Line,	File no.,	Attr.
6.BIN	1	0.0000E+00	1.0000E+00	0.0000E+00	1	1	

Advanced Light Source

Commissioning Schedule

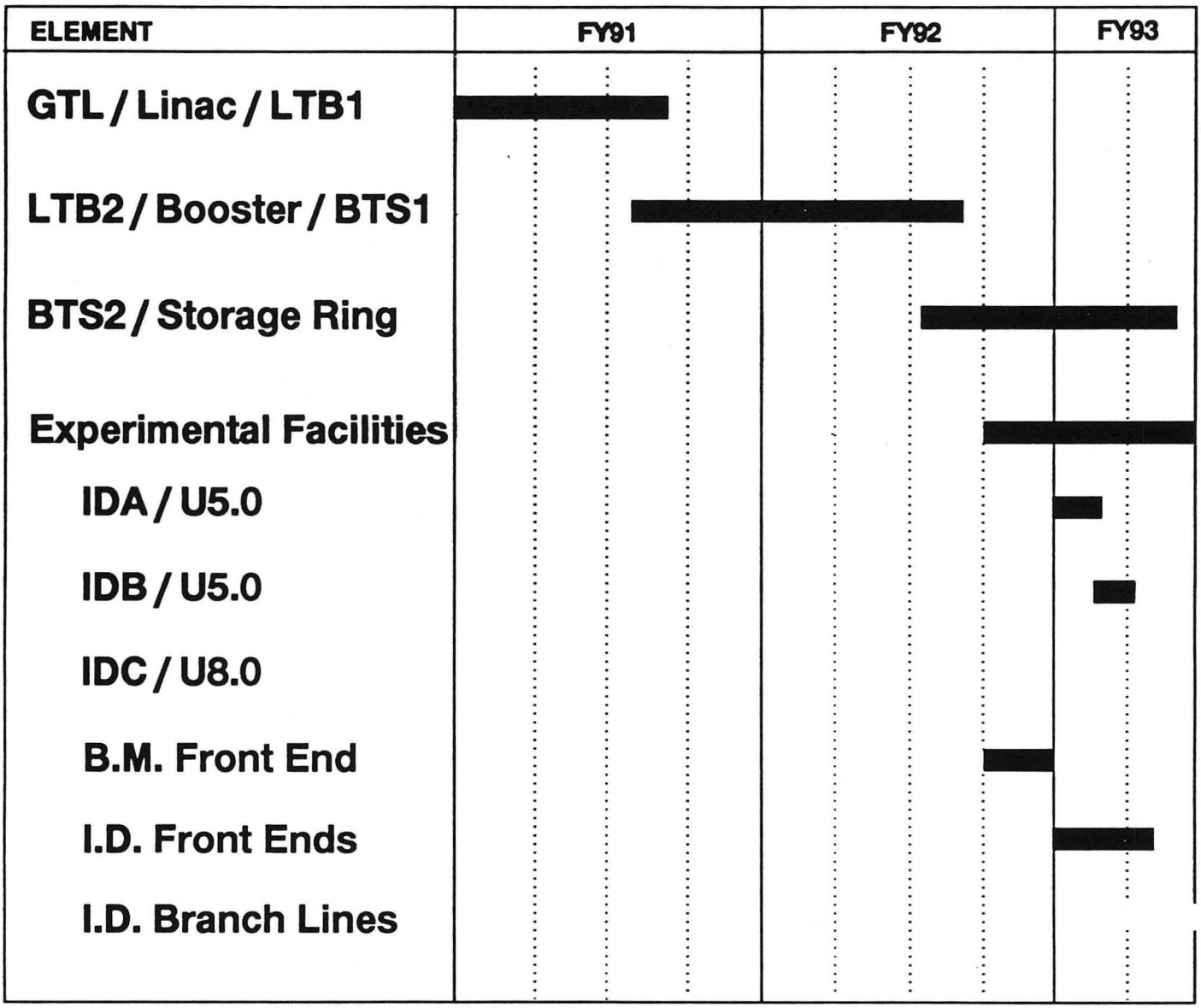

Project Completion: 3/31/93

Exploiting the Polarized Nature of Synchrotron Radiation

K.J. Kim

Lawrence Berkeley Laboratory

Exploiting the Polarized Nature of Synchrotron Radiation

Kwang-Je Kim
Accelerator & Fusion Research Division
Lawrence Berkeley Laboratory
University of California
Berkeley, CA 94720

Paper Presented at the Workshop on Application of Circularly
Polarized Photons at ALS with a Bend Magnet Source
Lawrence Berkeley Laboratory
June 10-11, 1991

This work was supported by the director, Office of Energy Research, Office of Basic Energy Sciences, Materials Sciences Division, of the U.S. Department of Energy under Contract No. DE-AC03-76F00098.

Exploiting the Polarized Nature of Synchrotron Radiation

Kwang-Je Kim

Synchrotron radiation is inherently highly polarized, and this fact makes synchrotron radiation useful for probing the directional and/or helical nature of the matter via polarization sensitive experiment. Here we summarize briefly the nature of the polarization experiments and the polarization characteristics of synchrotron radiation.

1. Experiment with partially polarized radiation

Partially polarized radiation is characterized by the Stoke's vector $\mathbf{S} = (S_0, S_1, S_2, S_3)$, where S_0 is the total intensity, S_1, S_2 are respectively the partial intensities polarized linearly along the x-direction (the propagation direction is assumed to be in the z-direction) and along the direction 45° from the x-direction in the x-y plane, and S_3 is the partial intensity with circular polarization [1]. The quantities $(P_1, P_2, P_3) = (S_1/S_0, S_2/S_0, S_3/S_0)$ are some times referred to as the degree of the polarization in the respective directions. In general, $P_1^2 + P_2^2 + P_3^2 \leq 1$.

A general light scattering experiment can be thought of as a study of the transformation of the Stoke's vector from the initial value S to the final value S';

$$\mathbf{S}' = \mathbf{MS}$$

Here M is a 4x4 matrix known as the Mueller matrix, which is the properties of the sample. An experiment leading to a determination of every element M_{ij} of the Mueller matrix (there are ten independent elements [2]) may be termed as the "complete" experiment. An example of the simpler experiment is to measure the final intensity

$$S_0' = M_{00}S_0 + M_{01}S_1 + M_{01}S_2 + M_{02}S_3$$

The element M_{03} represents the helical characteristics of the sample, and can be determined by measuring the final intensities $S'_{0\pm}$ corresponding to the incident radiation of opposite helicities, $S_3 = \pm P_3 S_0$. This type of experiment is called the circular intensity differential scattering (CIDS).

These discussions show that a determination of the Mueller matrix requires, in general, the ability to modulate the polarization [3]. In particular, to determine the helical properties it is necessary to have circularly polarized light which can be modulated between opposite helicities. Synchrotron radiation provides such capabilities in wavelength regions not available with conventional lasers.

2. Polarization Characteristics of Bending Magnet Sources.

The radiation from a bending magnet is of the form

$$\begin{pmatrix} E_x \\ E_y \end{pmatrix} \alpha \begin{pmatrix} K_{2/3}(\eta) \\ \dfrac{i\gamma\psi}{\sqrt{1+(\gamma\psi)^2}} K_{1/3}(\eta) \end{pmatrix},$$

where E_x (E_y) is the field amplitude in the horizontal (vertical) direction, γ is the electron's kinetic energy in unit of the rest energy, ψ is the vertical angle, K's are the modified Bessel functions, and $\eta = \left(\frac{\omega}{2\omega_c}\right)\left(1+(\gamma\psi)^2\right)^{3/2}$, ω = radiation frequency and ω_c = the critical frequency. We see from this that,when $\psi \neq 0$, the vertical component is non-vanishing and is 90° out of phase with respect to the horizontal axis. This implies that the radiation is elliptically polarized, the ratio between the minor and the major axis of the polarization ellipse being given by $r = E_y/iE_x$. The corresponding Stoke's vector is

$$P_1 = \frac{1 - r^2}{1 + r^2},\ P_2 = 0,\ P_3 = \frac{2r}{1 + r^2}$$

The fact that $P_2 = 0$ implies that the polarization ellipse lies along the horizontal direction. The sign of r, and hence P_3, can be reversed by reversing the sign of ψ. Therefore the circular polarization can be modulated by collecting the radiation alternately from above and below with respect to the orbit plane. However, the sign of the linear polarization P_1 can not be reversed since $0 \leq r^2 < 1$.

Figure (1) shows the polarization and flux characteristics of the ALS bending magnet. The PRT A018 is a proposal to exploit the polarized nature of the ALS bending magnet radiation using the double-headed Dragon monochrometer developed by C. T. Chen [4]. The beam line will provide a powerful tool for the study of the magnetism in condensed matter physics as well as the biological samples.

3. Special devices for enhanced polarization capabilities

Recently, several novel types of synchrotron radiation sources have been developed for higher flux and for more versatile polarization control. Table 1 gives an overview of such devices. The devices are classified according to the usual classification scheme; bending magnet, wigglers and undulators. In the following, these devices are discussed briefly, referring to the literature [5] for more details.

Each device in the Table has different merits. Thus the wiggler type of the devices will produce intense flux of elliptically polarized radiation over a broad spectral range. However, in wiggler type devices, the direction of the linear component of the polarization can not be modulated, being fixed in the horizontal direction. This could be a drawback for some experiments aiming for a complete determination of the Mueller matrix.

The undulator type of devices will provide higher brightness (in a small phase space area). The spectrum is concentrated in narrow peaks, but the peaks can be tuned by changing the magnet

gaps. The undulator devices can be further classified into two groups; those based on the helical field (helical undulators) and the crossed undulator based on the interference principle. A clever scheme for a helical undulator due to P. Elleaume (referred to the planar-helical undulator in Table 1) is to separate the magnet producing the vertical and the horizontal field on two different (top and bottom) jaws, making it possible to accommodate a conventional flat vacuum chamber.

Some of the helical undulators (Tilt-pole undulator, Cross-overlapped undulator and Planar-helical undulator) have the capability of modulating the polarization by mechanical motion. The Stoke's vector for these devices and the crossed undulator is of the form

$$P_1 = 0, \qquad P_2 = P \cos \alpha, \qquad P_3 = P \sin \alpha.$$

Here P is the degree of the polarization and α is the polarization phase determined by the relative position of the magnets in the case of helical undulators and by the modulator current level in the case of the crossed undulator. Note that the sign of either P_2 or P_3 can be reversed by changing α; thus both the linear and the circular polarization can be modulated. Helical undulators produce a high degree of polarization ($P \sim 1$). For a crossed undulator, there is some reduction in the degree of polarization P due to the angular smearing from the electron beam emittance and the opening angle of the pinhole. However, it turns out that the crossed undulator produces a significant amount of polarization even at very high photon energies where the angular effect is expected to be maximum. Figure 2 shows the performance of the crossed undulator in the limiting case of the vanishing photon wavelength and a large angular opening, assuming that N is large and that the effect of the modulator section can be neglected.

The crossed undulator can be operated at higher harmonics in contrast to the helical undulators. This is an important feature to reach high photon energies with low energy electron machines. Also, the polarization of the crossed undulators can be modulated electromagnetically by modulating the current in the modulator magnet between two planar undulators, while the modulation is mechanical for the helical undulators.

References:

[1] M. Born and E. Wolf, "Principles of Optics", Pergamon Press, Oxford, 1980

[2] H.C. Van de Hulst, "Light Scattering by Small Particles", Dover Publications, New York, 1981

[3] For further discussions see the articles in "Applications of Circularly Polarized Radiation Using Synchrotron and Ordinary Sources", F. Allen and C. Bustamente, eds, Plenum Press, New York, 1985

[4] C.T. Chen,

[5] K-J. Kim, "Survey of Synchrotron Radiation Devices Producing Circular and Variable Polarizations", in SPIE proc. Vol.1345, "Advanced X-ray/EUV Radiation Sources and Applications" page 116 (1990)

P. Elleaume, "New Developments on the Generation of Arbitrary Polarized Radiation from Insertion Devices: in Proceedings of 1991 Particle Accelerator Conference.

Insertion Devices for Variable Polarization

- **Bending Magnet**
  Off plane observation($\psi \neq 0$). *BESSY, SRC, ..*

- **Wiggler**
  Asymetric wiggler (Goulon, Elleaume, Rauox), *HASYLAB, LURE,..*
  Elliptical wiggler (Yamamoto, Kinoshita), *KEK*

- **Undulator**
  Devices based on helical field:

  Helical U..bifilar windindgs(Madey),
  permanent magnet(Halbach)
  Tilt-pole U(Halbach)
  Cross-overlapped U(Onuki),*ETL*
  Planar-helical U(Elleaume),*ESRF*
  Modified planar-helical U(Diviacco, Walker), *Elettra*

  Device based on interference effect:

  Crossed U(Moissev,Nikitin, Fedorov), (Kim) *BESSY, SRC*

Issues:
Modulation versatility(mechanical, electrical, not possible)
Vacuum chamber constraints(achievable K)
Sensitivity to electron beam emittance
Effect on electron trajectory
Use of harmonics

Table 1

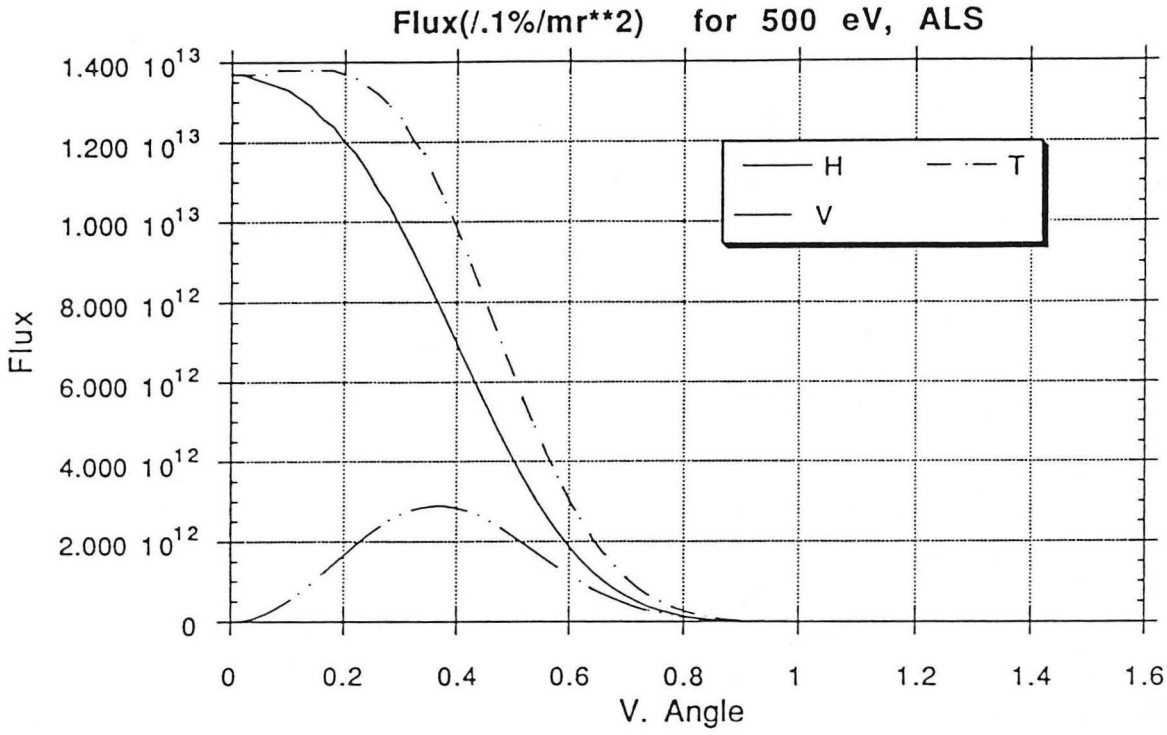
Flux(/.1%/mr**2) for 500 eV, ALS
Flux
1.400 10^13
1.200 10^13
1.000 10^13
8.000 10^12
6.000 10^12
4.000 10^12
2.000 10^12
0
H
T
V
0
0.2
0.4
0.6
0.8
1
1.2
1.4
1.6
V. Angle

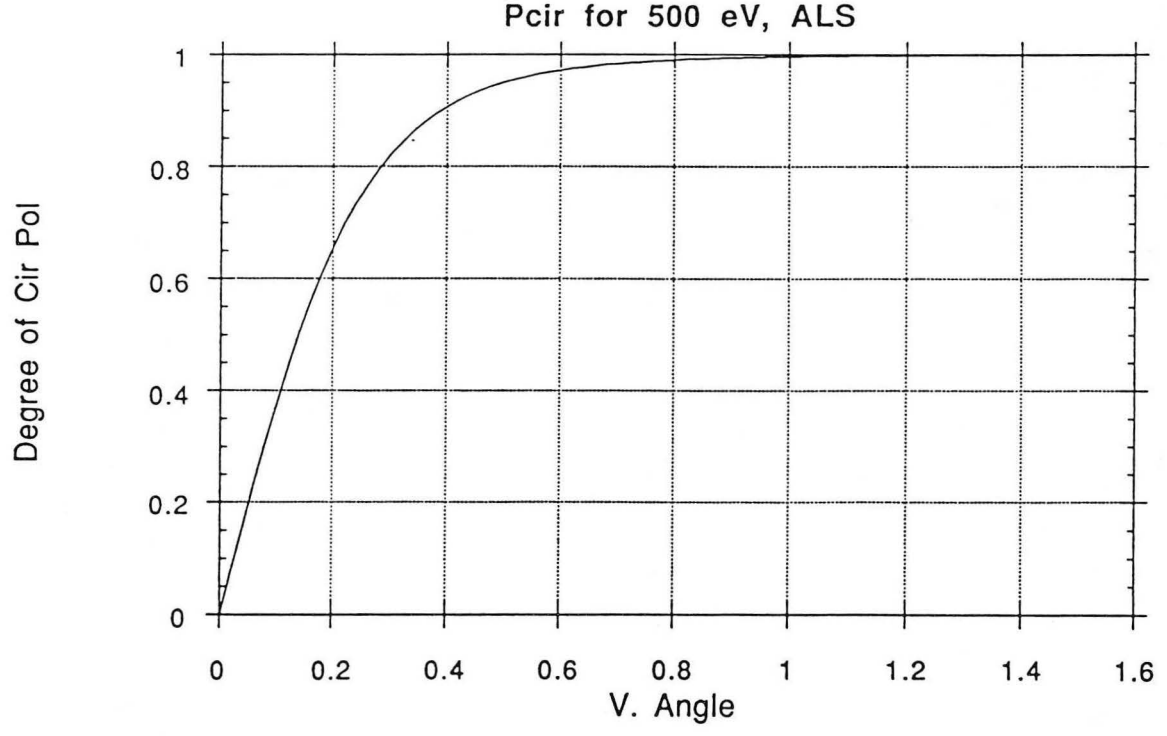
Pcir for 500 eV, ALS
Degree of Cir Pol
1
0.8
0.6
0.4
0.2
0
0
0.2
0.4
0.6
0.8
1
1.2
1.4
1.6
V. Angle

Fig. 1

Crossed Undulator(N+N) Performance in the Short Wavelength Limit

(angular opening >> $(\lambda/L)^{1/2}$)

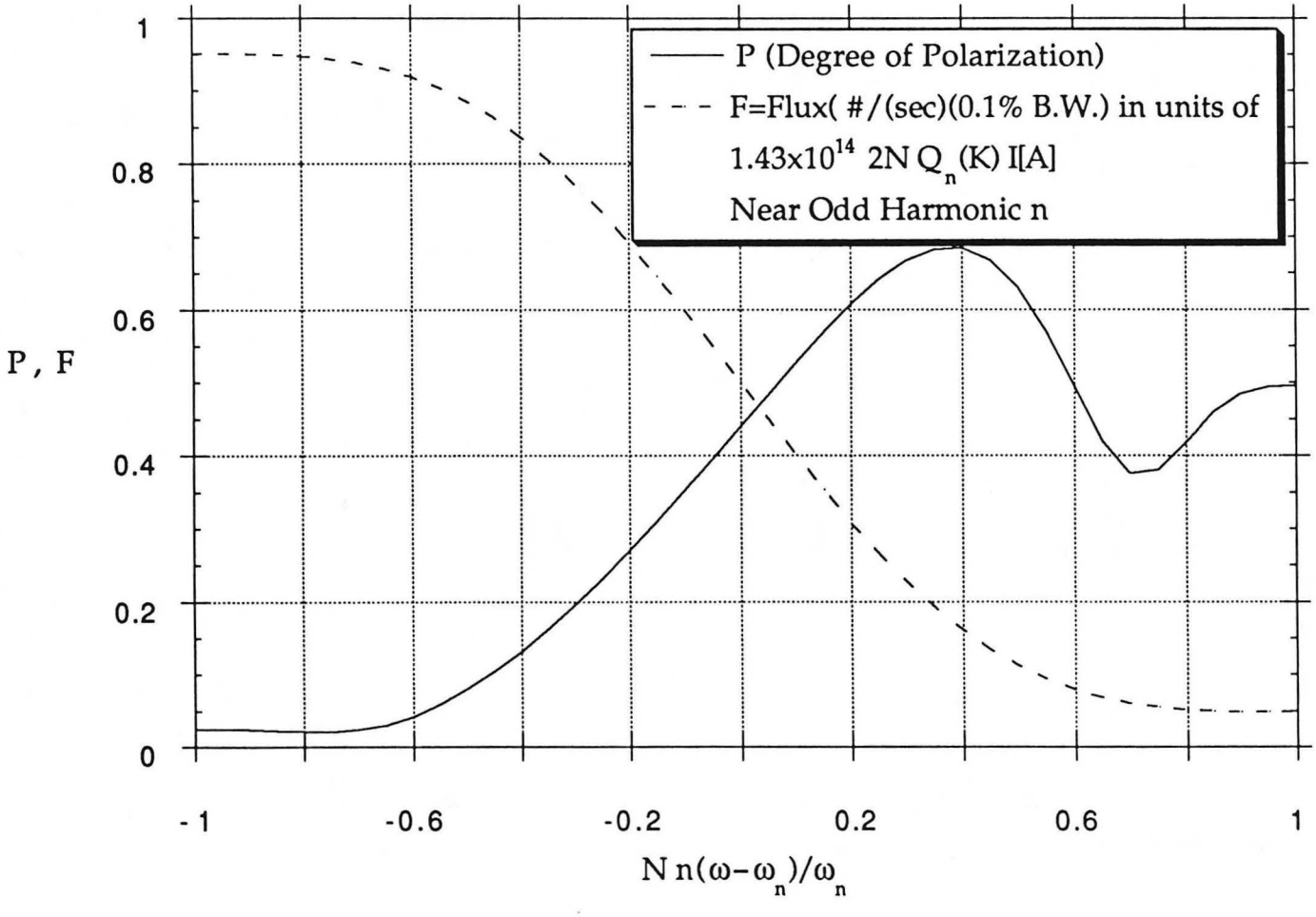

Fig. 2

June 10, 91

Exploiting the Polarized Nature of Synchrotron Radiation

KWANG-JE KIM, LBL

- Polarized Light
- Experiments
- Polarizatin & Flux of Bending magnet Rad.
- Special S.R. Devices for Polarization

(Completely) Polarized Light

$$\underset{\sim}{E} = Re\left\{ e^{i(\omega t - kz)} [a_1 e^{i\delta_1}, a_2 e^{i\delta_2}] \right\}$$

polarization ellipse

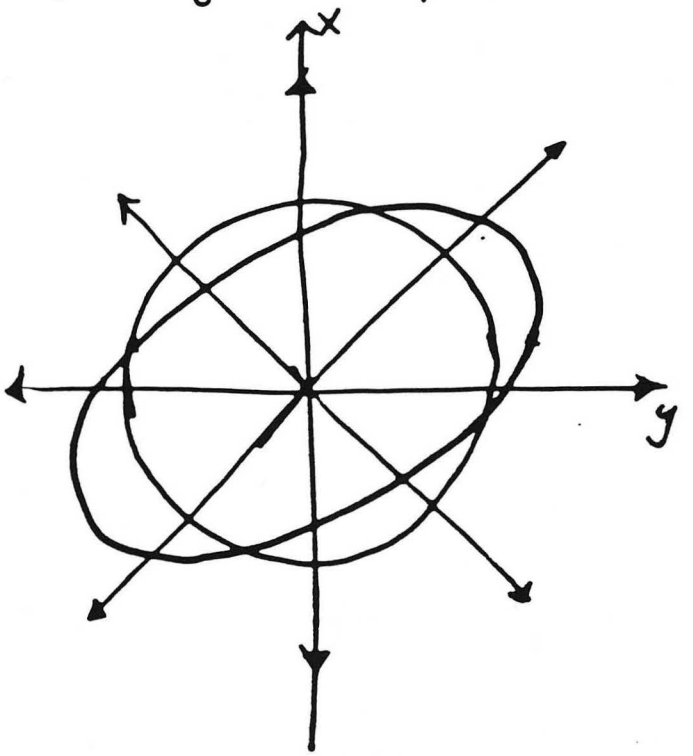

$\underset{\sim}{e}(\lambda)$

$\underset{\sim}{e}(1) = (1, 0)$

$\underset{\sim}{e}(2) = (0, 1)$

$\underset{\sim}{e}(45°) = \frac{1}{\sqrt{2}}(1, 1)$

$\underset{\sim}{e}(135°) = \frac{1}{\sqrt{2}}(1, -1)$

$\underset{\sim}{e}(+) = \frac{1}{\sqrt{2}}(1, i)$

$\underset{\sim}{e}(-) = \frac{1}{\sqrt{2}}(1, -i)$

Partially Polarized Light

- The components E_x, E_y are stochastic; Introduce the average of the quadratic quantities $E_i E_j^*$.

Coherency matrix

$$\mathbb{J} = \begin{pmatrix} \langle E_x E_x^* \rangle , \langle E_x E_y^* \rangle \\ \langle E_y E_x^* \rangle , \langle E_y E_y^* \rangle \end{pmatrix} = \begin{pmatrix} J_{xx} , J_{xy} \\ J_{yx} , J_{yy} \end{pmatrix}$$

$\mathbb{J}$ is the density matrix

$$J_{ij} = \sum_{\lambda=1,2} P_\lambda E_i(\lambda) E_j^*(\lambda) = \langle \cdot | \Sigma P_\lambda | \lambda \rangle \langle \lambda | j \rangle$$

A) Unpolarized light

$$\langle |E_x^2| \rangle = \langle |E_y|^2 \rangle = \frac{I}{2}$$

$$\langle E_x E_y^* \rangle = 0 \qquad \text{(no coherence)}$$

$$\therefore \quad \mathbb{J} = \frac{I}{2} \begin{pmatrix} 1 & 0 \\ 0 & 1 \end{pmatrix}$$

B) Partially polarized Light can be decomposed into two parts:

$$\mathbb{J} = \frac{I_0}{2}\begin{pmatrix} 1 & 0 \\ 0 & 1 \end{pmatrix} + \begin{pmatrix} a_x a_x^* & a_x a_y^* \\ a_y a_x^* & a_y a_y^* \end{pmatrix}$$

Polarized Intensity $I_p = |a_x|^2 + |a_y|^2$ $\quad A$

Total intensity $I_T = I_0 + I_p$

Degree of polarization

$$P = \frac{I_p}{I_T} = \sqrt{1 - \frac{4(\mathrm{Det}(\mathbb{J}))}{(\mathrm{Tr}(\mathbb{J}))^2}}$$

The A-matrix determines the polarization ellipse

$(a_x, a_y) = (1, 0)$

$$A = \begin{pmatrix} 1 & 0 \\ 0 & 0 \end{pmatrix}$$ linear along x

$(a_x, a_y) = \frac{1}{\sqrt{2}}(1, 1)$ $\begin{pmatrix} 1 & 1 \\ 1 & 1 \end{pmatrix}$ linear along x+5°

$(a_x, a_y) = \frac{1}{\sqrt{2}}(1, i)$ circular

$$\begin{pmatrix} 1 & i \\ -i & 0 \end{pmatrix}$$

Stokes Vector

An equivalent set to $\{J_{ij}\}$ is

$S_0 = J_{xx} + J_{yy}$ = total intensity

$S_1 = J_{xx} - J_{yy}$ = difference of x-polarizer & y-polarizer

$S_2 = J_{xy} + J_{yx}$ = difference of 45°-polarizer & 135°-pol.

$= 2|E_x E_y| \cos\delta$

$S_3 = i(J_{xy} - J_{yx}) = 2|E_x E_y| \sin\delta$ = difference of left circular polarizer & right circular pol.

$P = \frac{\sqrt{S_1^2 + S_2^2 + S_3^2}}{S_0} \leq 1$: degree of polarization

$P_3 =$ degree of circular pol.

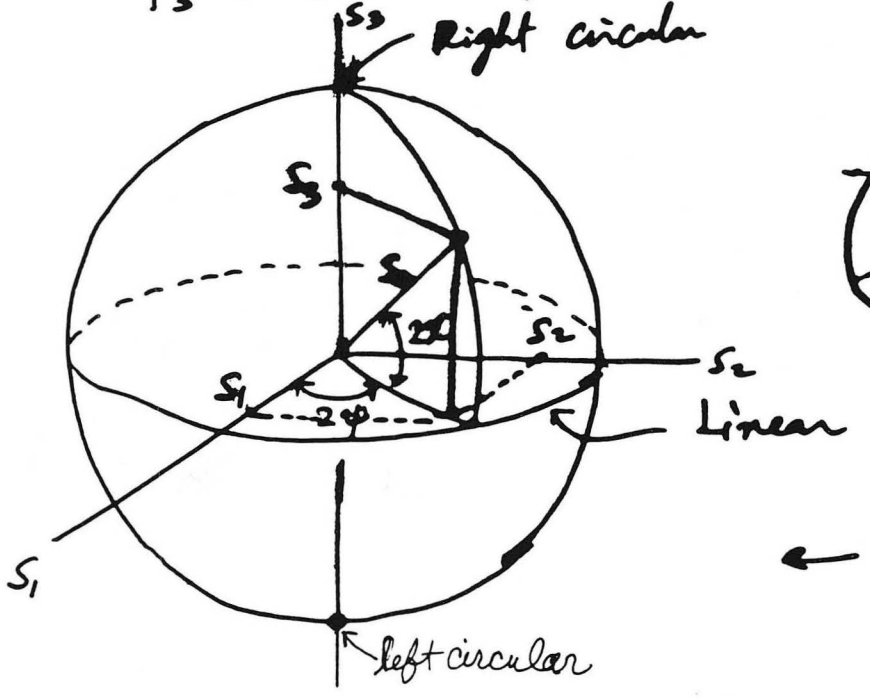

← Poincaré Sphere

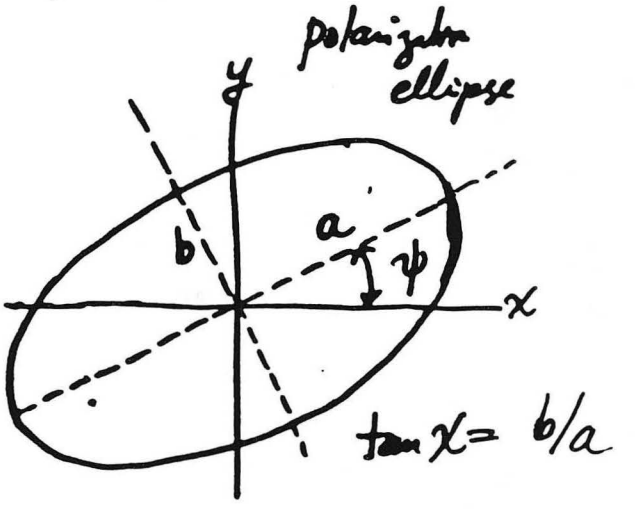

Example

(A) Bending magnet Radiation

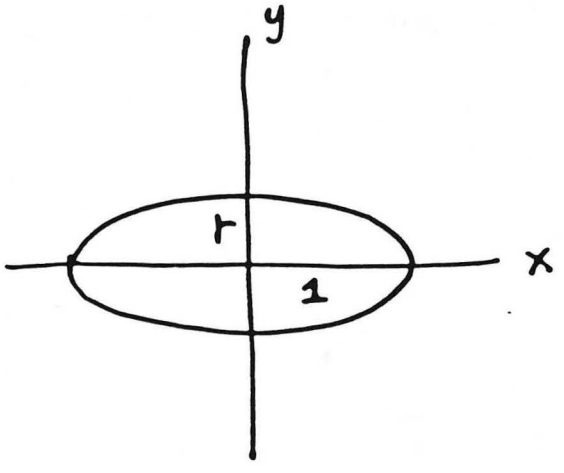

$$E = E_0 (1, ir)$$

$$J = \begin{pmatrix} 1 & ir \\ -ir & r^2 \end{pmatrix}$$

$$\frac{S}{S_0} = \frac{((1-r^2), 0, 2r)}{1+r^2}$$

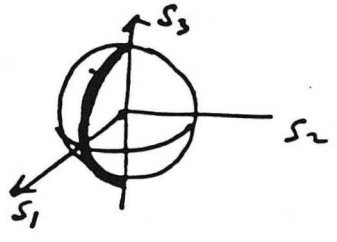

(B) Crossed undulator

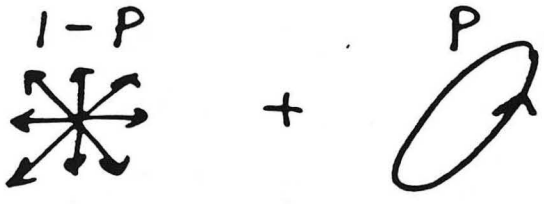

$$J = \frac{1-P}{2} \begin{pmatrix} 1 & 0 \\ 0 & 1 \end{pmatrix} + \frac{P}{2} \begin{pmatrix} 1 & e^{i\alpha} \\ e^{-i\alpha} & 1 \end{pmatrix}$$

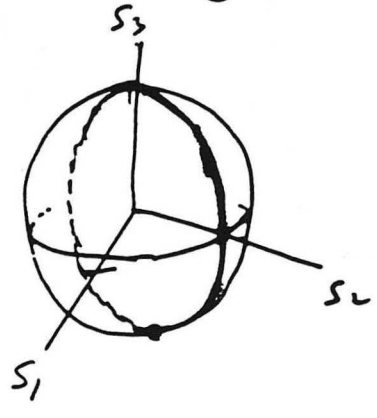

$$\frac{S}{S_0} = (0, P\cos\alpha, P\sin\alpha)$$

Polarization Experiment

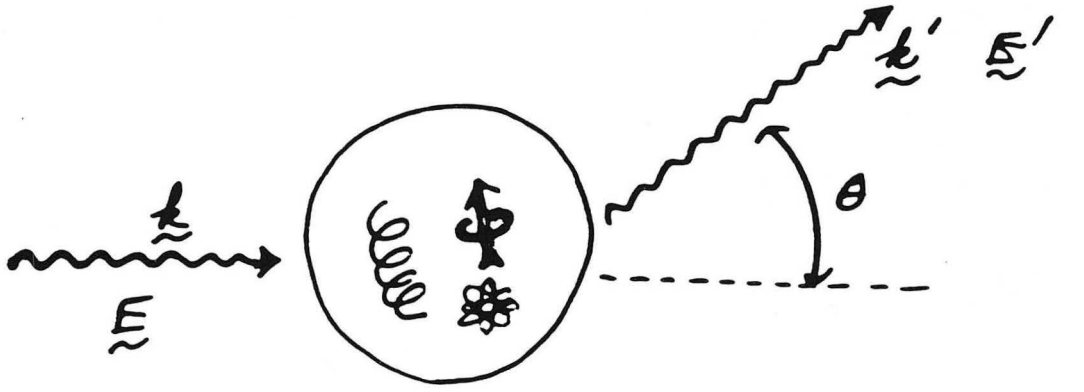

$$E_i' = \frac{e^{i(\omega t - kr)}}{ikr} \tilde{S}_{ij}(\underset{\sim}{k}, \underset{\sim}{k}', \cdots) E_j$$

Thus $$J_{ij}' \equiv \langle E_i' E_j'^{*} \rangle = \frac{1}{(kr)^2} \left(\tilde{S} J \tilde{S}^{+} \right)_{ij}$$

or for Stokes parameter

$$\begin{pmatrix} S_0' \\ S_1' \\ S_2' \\ S_3' \end{pmatrix} = \mathcal{M} \begin{pmatrix} S_0 \\ S_1 \\ S_2 \\ S_3 \end{pmatrix}$$

Complete experiment; determine $\mathcal{M}$ experimentally & compare with theory.

A more restricted Experiment

Total scattered intensity

$$S_0' = \sum_j |E_j'|^2 = M_{00} S_0 + M_{01} S_1 + M_{02} S_2 + M_{03} S_3$$

For rotationally symmetric sample

$$M_{01} = M_{02} = 0$$

$\therefore$

$$S_0' = F S_0 + M S_3$$

M contains information on helicity

The ratio M/F can be determined by

Circular Intensity Differential Scattering (CIDS)

$$CIDS \equiv \frac{S_0'(S_3 = P S_0) - S_0'(S_3 = -P S_0)}{S_0'(\text{total})}$$

$$\equiv \frac{MP}{F}$$

- For better S/N, larger P_3 (degree of cir. pol)
- As long as P_3 is the same, it doesn't matter whether elliptically polarized or partially circularly polarized.
- Figure of merits; $P_3 \cdot S_0$

Polarization of Bending Magnet Radiation

$$\begin{pmatrix} E_x \\ E_y \end{pmatrix} = e^{i\Phi} \begin{pmatrix} K_{2/3}(\eta) \\ \dfrac{i\gamma\psi}{\sqrt{1+(\gamma\psi)^2}} K_{1/3}(\eta) \end{pmatrix}$$

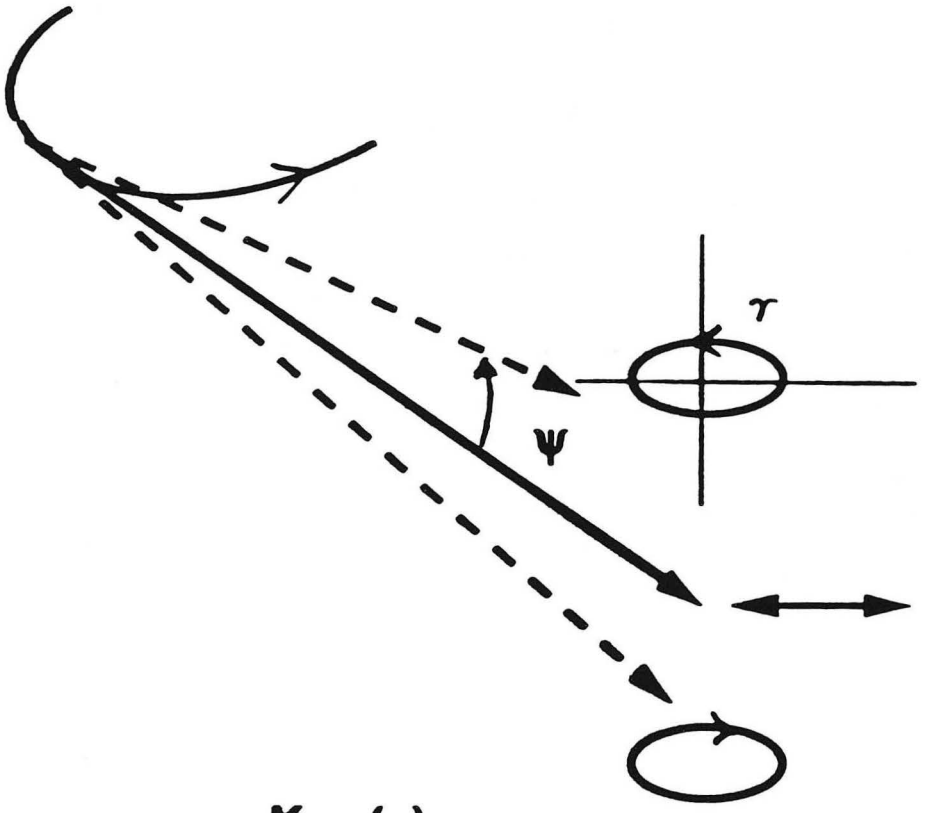

$$r = \frac{\gamma\psi}{\sqrt{1+(\gamma\psi)^2}} \frac{K_{1/3}(\eta)}{K_{2/3}(\eta)}$$

$$P_3 = \frac{2r}{1+r^2}$$

A018 PARTICIPATING RESEARCH TEAM

AT&T Bell Laboratories

C.T. Chen
F. Sette

Florida Atlantic University

P.A. Snyder

Lawrence Berkeley Laboratory

M.R. Howells
A.J. Hunt
K.J. Kim*
B.M. Kincaid
M.F. Maestre
D.R. Nygren*
M. Wong+

University of Washington

E.A. Stern

---

* *Consultant*
\+ *Spokesperson*

(a) DOUBLE HEADED DRAGON (TOP VIEW)

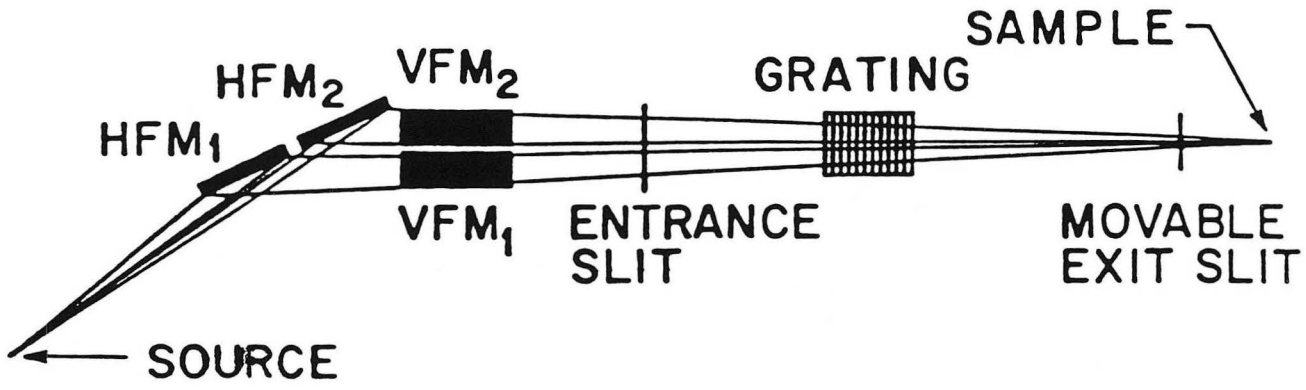

(b) CIRCULAR POLARIZATION (SIDE VIEW)

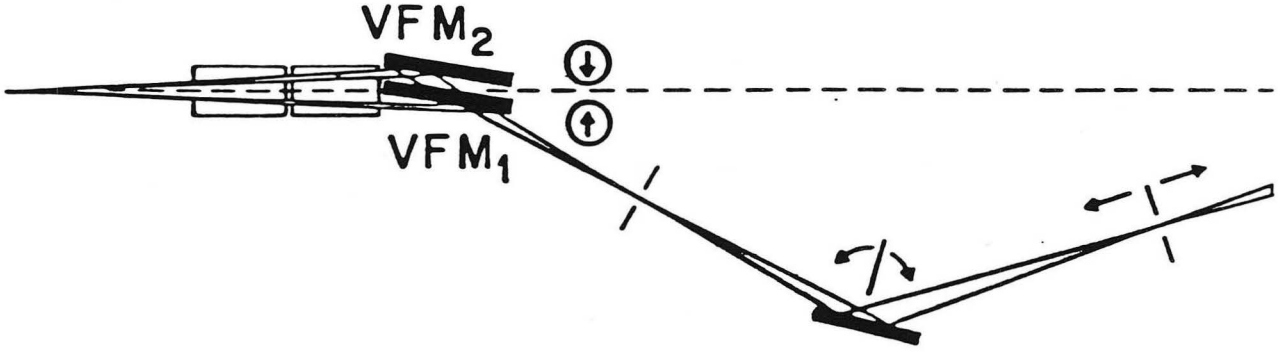

(c) LINEAR POLARIZATION (SIDE VIEW)

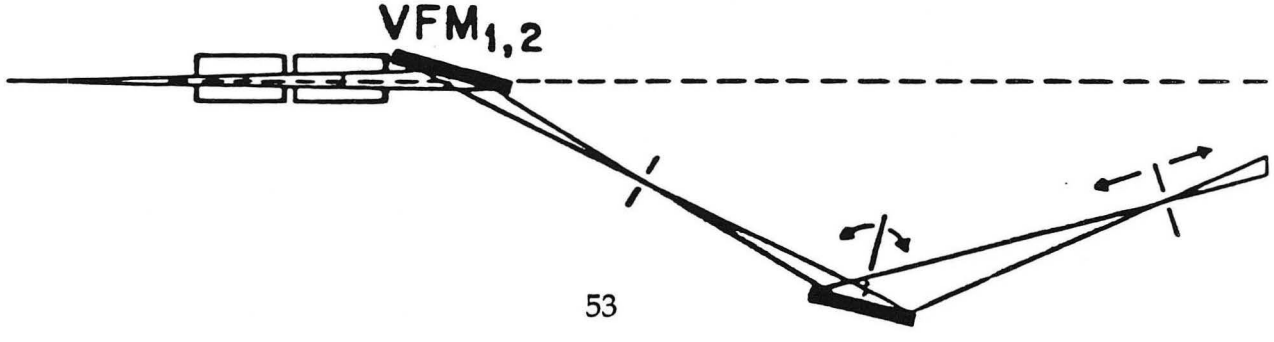

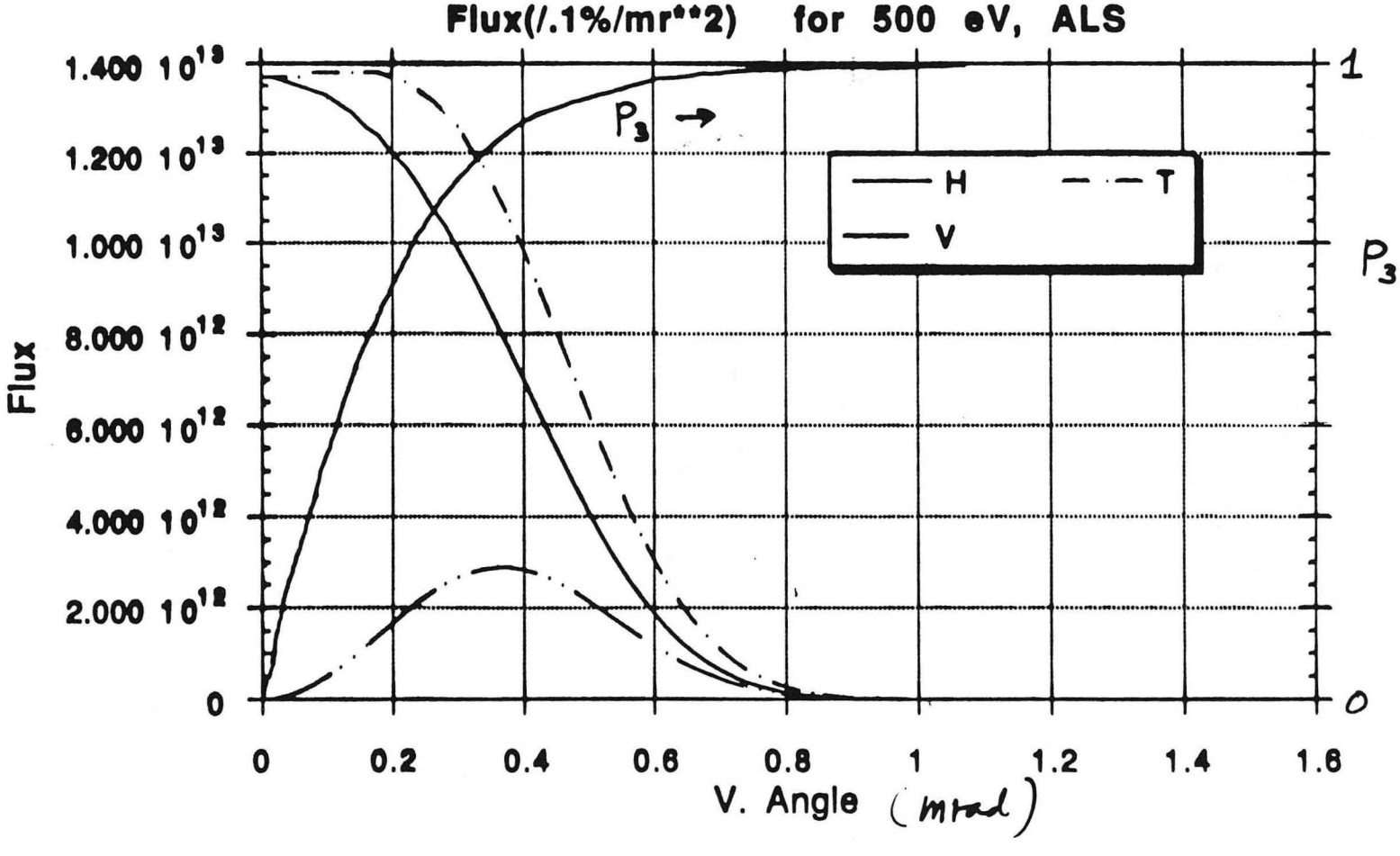
Flux(/.1%/mr**2) for 500 eV, ALS
1.400 10^13
1.200 10^13
1.000 10^13
8.000 10^12
6.000 10^12
4.000 10^12
2.000 10^12
0
Flux
P3 →
H
V
T
1
P3
0
0
0.2
0.4
0.6
0.8
1
1.2
1.4
1.6
V. Angle (mrad)

Insertion Devices for Variable Polarization

- **Bending Magnet**
  Off plane observation($\psi \neq 0$). *BESSY, SRC, ..*

- **Wiggler**
  Asymetric wiggler (Goulon, Elleaume, Rauox), *HASYLAB, LURE,..*
  Elliptical wiggler (Yamamoto, Kinoshita), *KEK*

- **Undulator**
  Devices based on helical field:

    Helical U..bifilar windindgs(Madey),
    permanent magnet(Halbach)
    Tilt-pole U(Halbach)
    Cross-overlapped U(Onuki),*ETL*
    Planar-helical U(Elleaume),*ESRF*
    Modified planar-helical U(Diviacco, Walker), *Elettra*

  Device based on interference effect:

    Crossed U(Moissev,Nikitin, Fedorov), (Kim) *BESSY, SRC*

Issues:

- Modulation versatility(mechanical, electrical, not possible)
- Vacuum chamber constraints(achievable K)
- Sensitivity to electron beam emittance
- Effect on electron trajectory
- Use of harmonics

Variably Polarized Radiation can be Generated with Crossed Undulators in Low Emittance Storage Rings

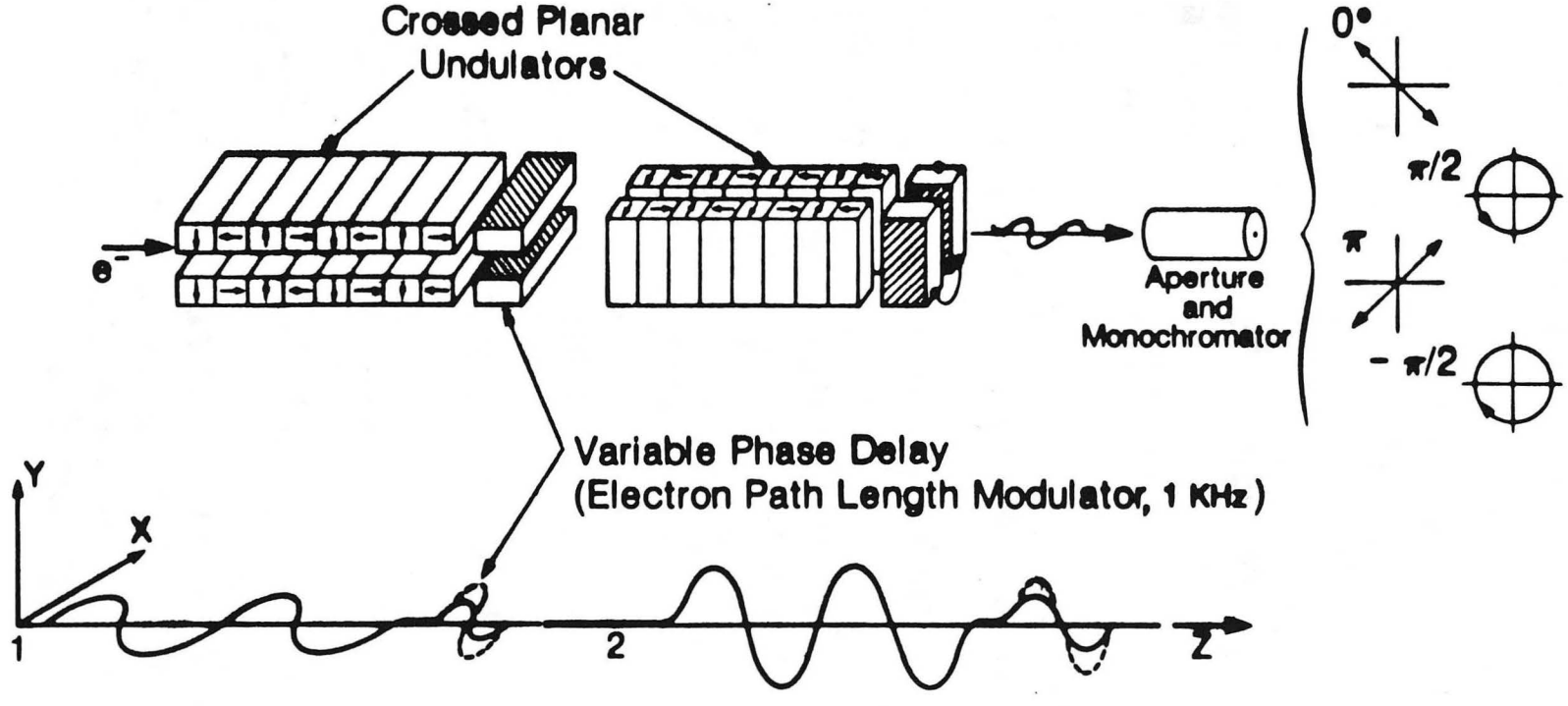

XBL 8311-4539-A

Crossed Undulator Performance

- Modulation of the polarization is achieved electromagnetically (rather than mechanically).

  ----→ fast modulation (1 kHz)

- Unlike helical undulators, operation at higher harmonics is possible for higher photon energies.

- As the device is based on the interference, the degree of polarization is sensitive to the electron beam angular divergence. The expected degree of polarization for typical next generation storage rings is

  $\geq$ 90 % for $\varepsilon \leq$ 10 eV

  $\geq$ 50 % for 100 eV $\leq \varepsilon \leq$ 500 eV

  $\geq$ 30 % for $\varepsilon \geq$ 10 keV

ESRF	
E = 6 Gev	I = 100 mA
β_x = 13 m	β_z = 30 m
$\varepsilon_x = 7\ 10^{-10}$ m	$\varepsilon_z = 7\ 10^{-9}$ m

CROSSED UNDULATOR	
$B_x = B_z = 0.5$ T	$\lambda_0 = 30$ mm
$N_x = N_z = 26.5$	K = 1.4
Dispersive Section	
$B_z = 0.7\sqrt{2}$ T	$\lambda_0 = 70$ mm

Slit $1*1$ mm^2 @ 30 m

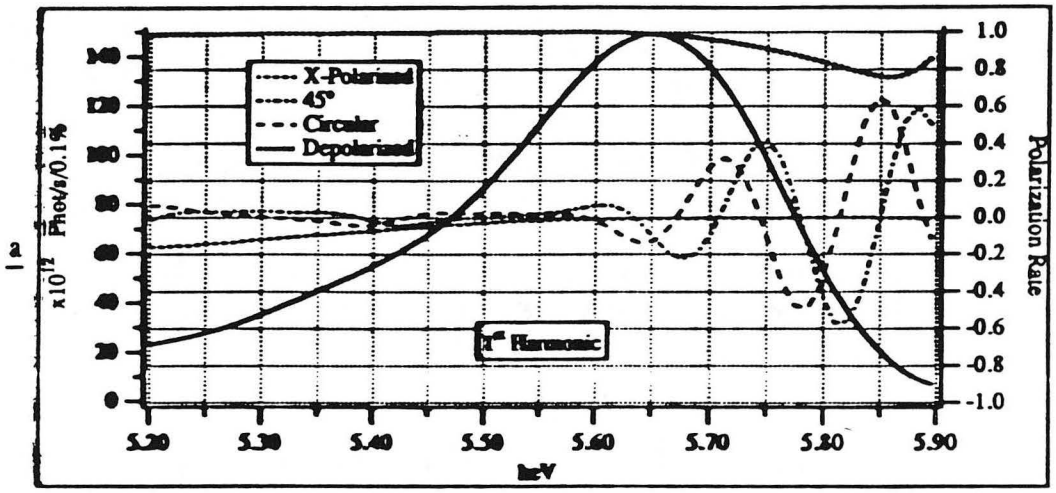

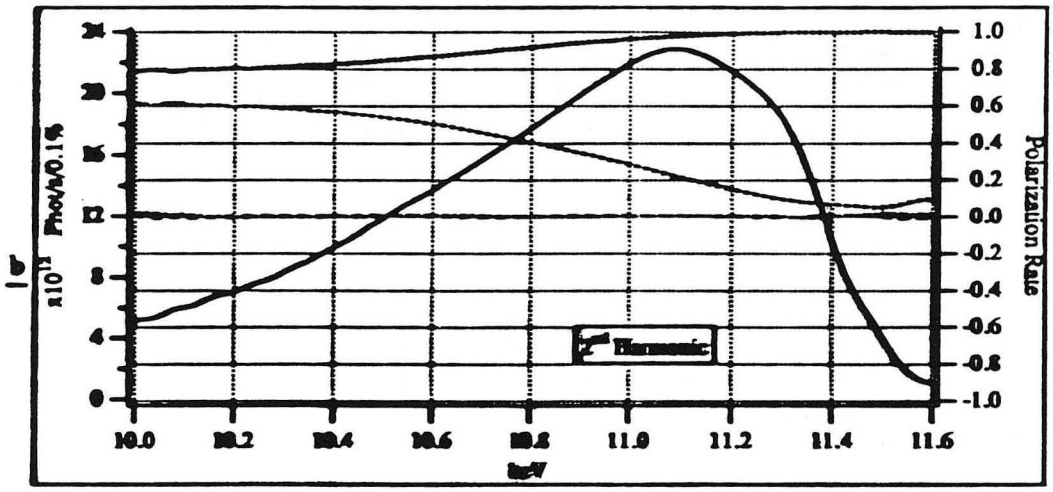

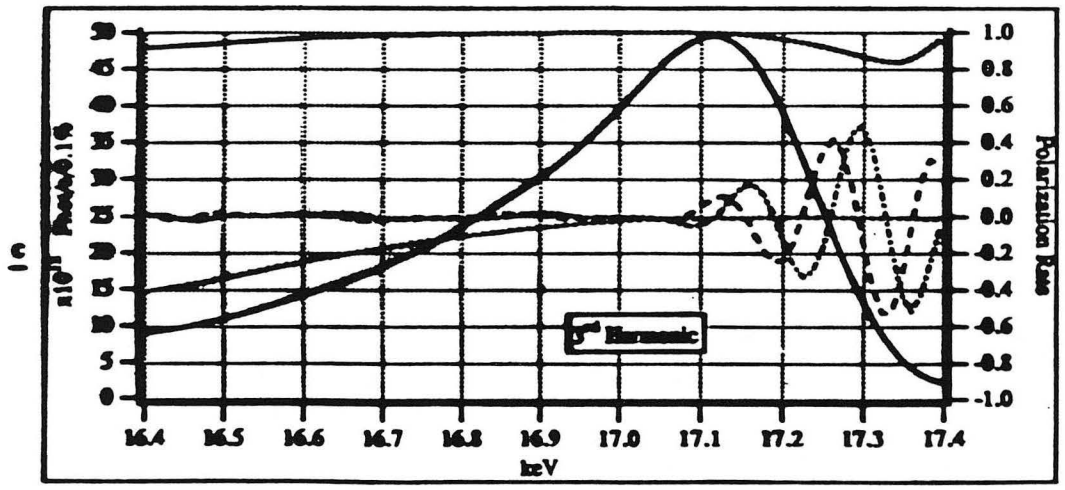

SXMCD Measurements with a Dragon

C.T. Chen

AT&T Bell Laboratories

SXMCD Measurements with a Dragon*

C. T. Chen

AT&T Bell Laboratories, Murray Hill, New Jersey

June 10, 1991

- **Motivation: why MCD in soft-x-ray region?**
- **Dragon beamline and experimental setup**
- **Fe, Co, Ni and relativistic tight-binding calculation**
- **Transition metal and rare earth compounds**
- **Ultrathin Ni films on Cu(001)**
- **Conclusion and outlook**

* *In collaboration with F. Sette, L. H. Tjeng, P. Rudolf, G. Meigs, Y. Ma, S. Modesti, N. V. Smith (Bell Labs) and Y. U. Idzerda (NRL)*

Motivation

- **Visible light magnetic circular dichroism (MCD) or MOKE has been widely utilized in magnetism research**
  Neither element nor site specific; Requires JDOS!
- **Prediction of Ni (3p→3d) MCD** --- *Erskine & Stern (1975)*
- **Observation of magnetic x-ray dichroism (MXD) effect using linear polarized soft-x-rays** --- *van der Laan et. al. (1986)*
- **Observation of MCD effect using circularly polarized hard-x-rays** --- *Schütz et. al. (1987)*
- **Great demand for soft-x-ray MCD (SXMCD)**
  - **Dipole permitted 2p→3d and 3d→4f transitions of 3d TM and 4f RE elements** --- $\langle \vec{m} \rangle$ *and large* $\Delta I/I$
  - **Investigate the local electronic structure of ferromagnetic systems** --- *SDDOS, exchange splitting, spin-orbit and Zeeman effects*
  - **Probe element and site specific magnetic moments in wide spectrum of magnetic samples** --- *thin films, multi-layers, compounds, disorder and impurity systems*

$$\sigma_{\pm}(h\nu) \propto \sum_i \sum_f |\langle f|\vec{A}_{\pm}\cdot\vec{p}|i\rangle|^2 \delta(h\nu - (E_f - E_i))$$

$$\vec{A}_{\pm} = \hat{\epsilon}_{\pm} e^{i\vec{k}\cdot\vec{r}}$$

3d transition metals

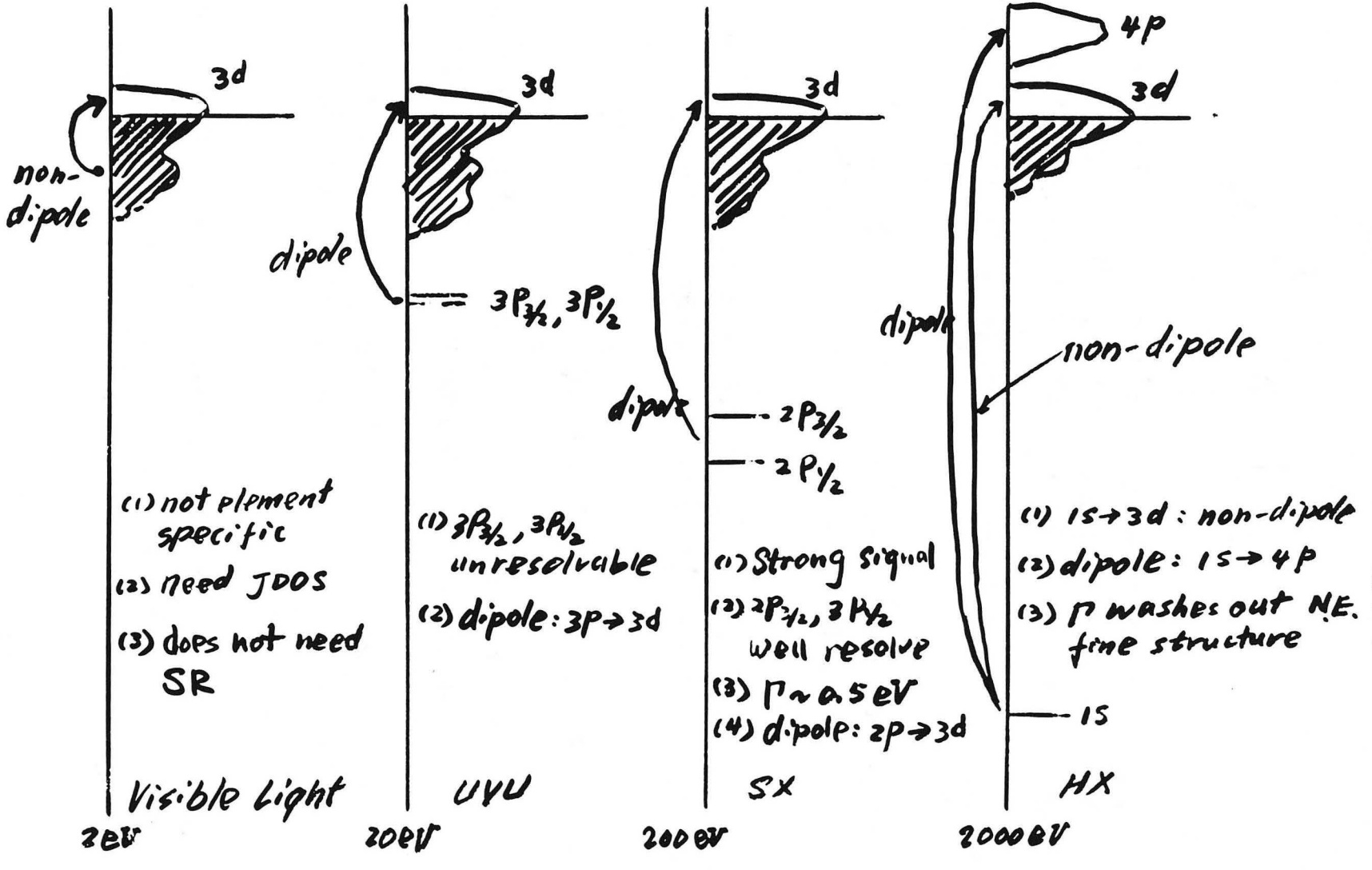

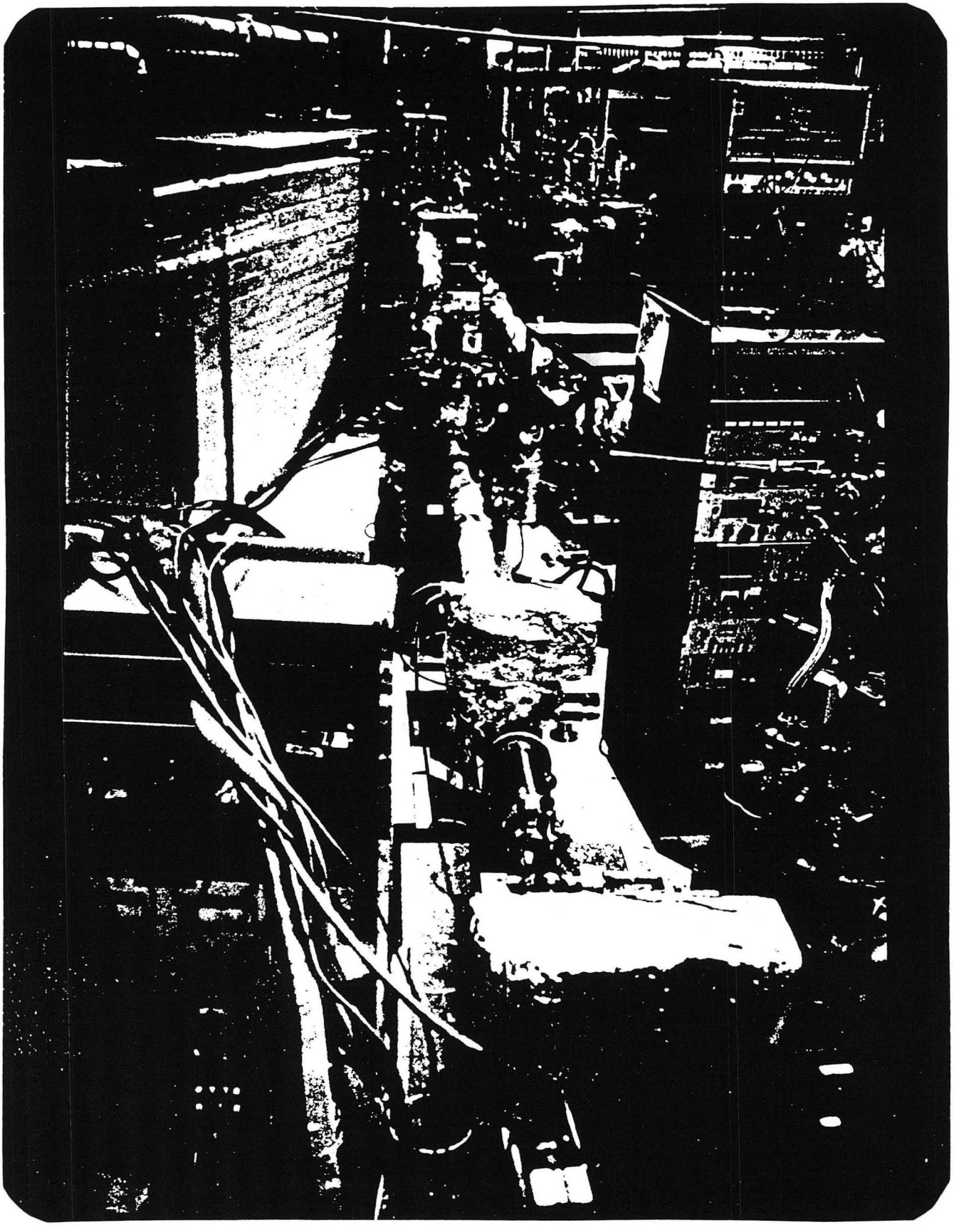

a) DRAGON BEAMLINE SET-UP (SIDE VIEW)

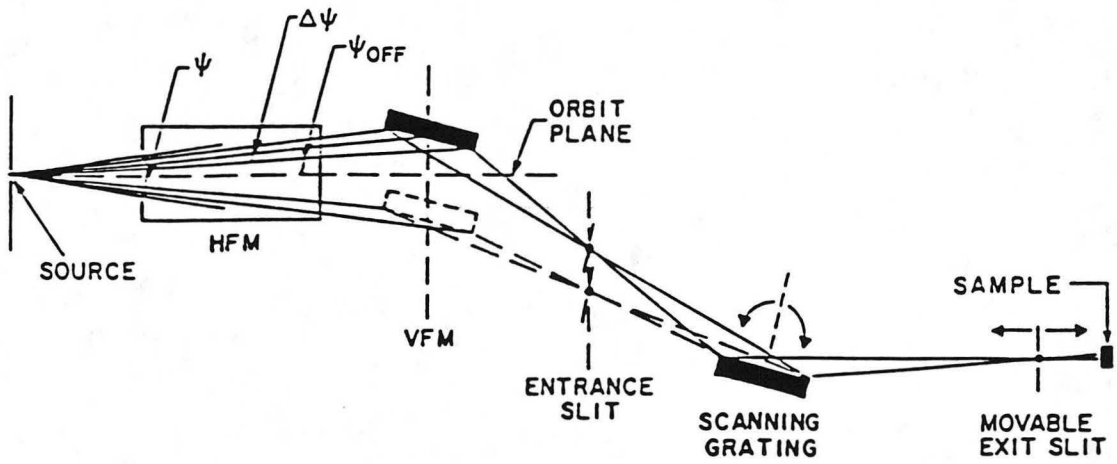

b) END STATION SET-UP

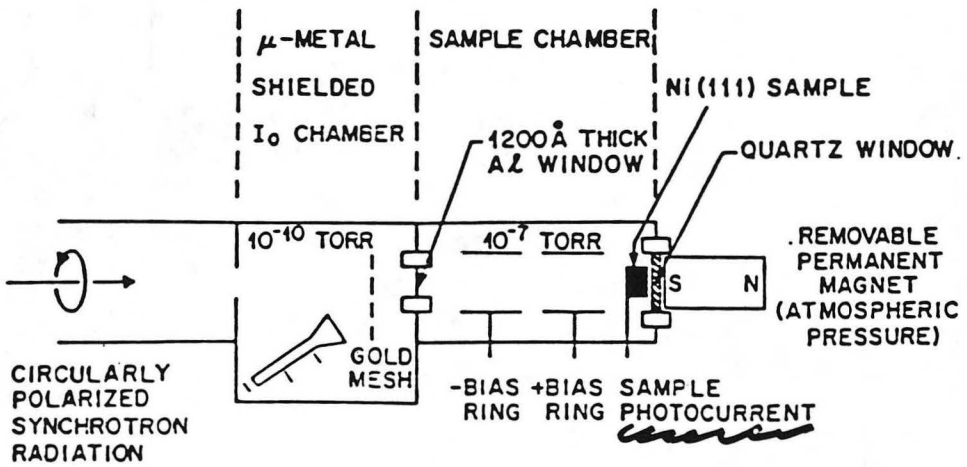

(a) DOUBLE HEADED DRAGON (TOP VIEW)

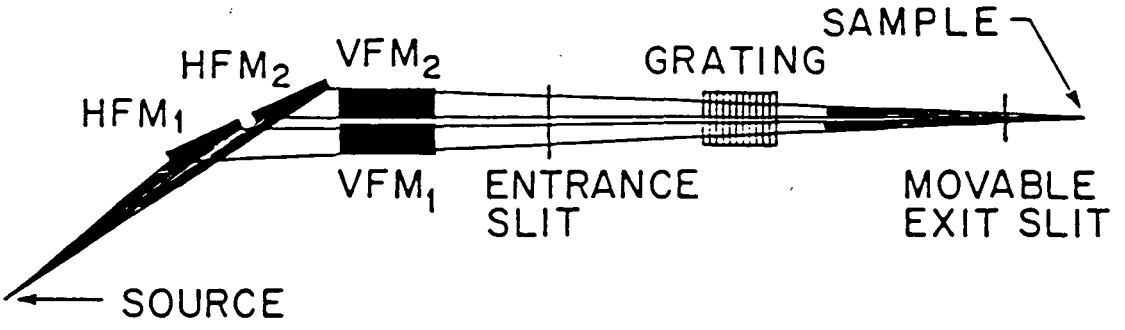

(b) CIRCULAR POLARIZATION (SIDE VIEW)

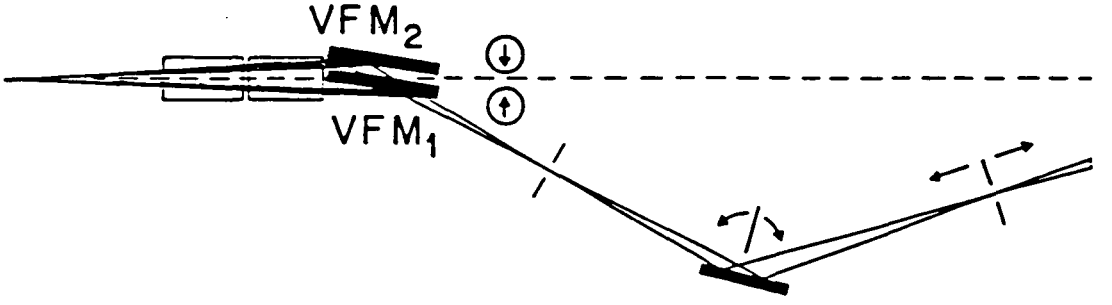

(c) LINEAR POLARIZATION (SIDE VIEW)

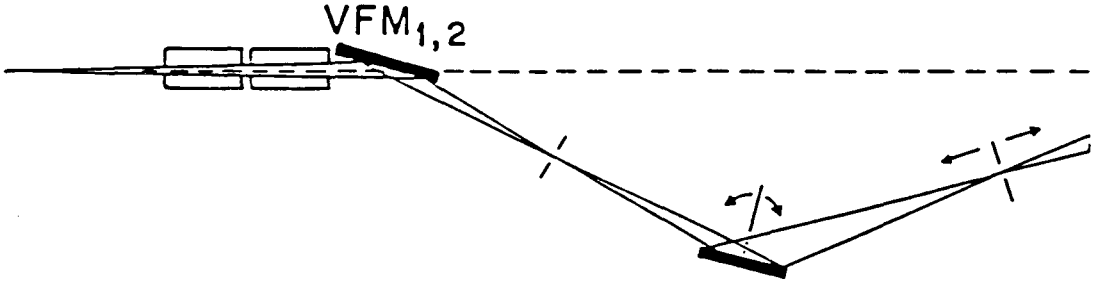

Ni $L_{2,3}$ Edges XAS + MCD

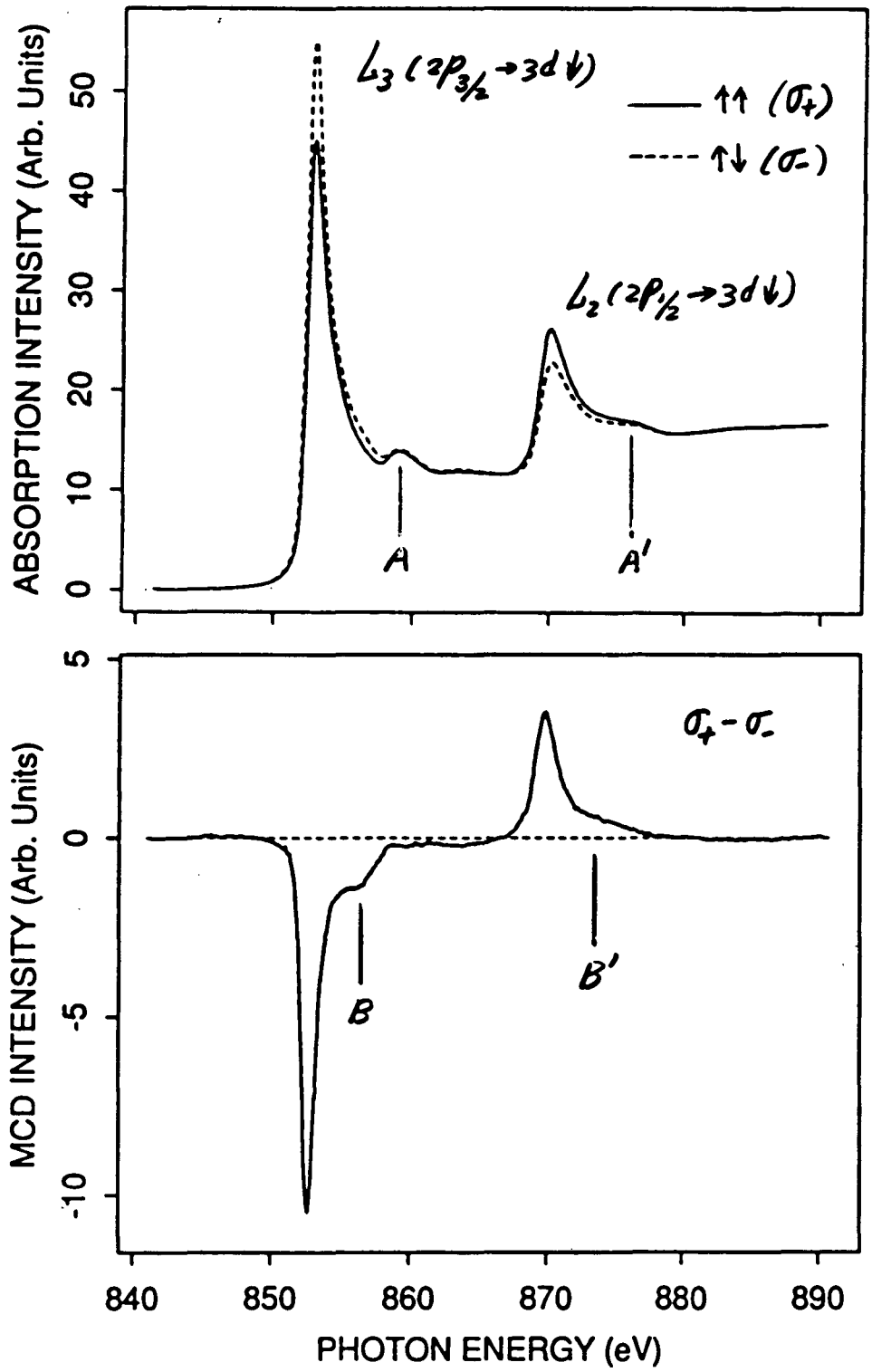

XAS $\equiv$
$\sigma_+ + \sigma_-$

$L_3 : L_2 \approx 2.6$

MCD $\equiv$
$\sigma_+ - \sigma_-$

$L_3 : L_2 \approx -1.6$

Comparison to Calculations

- **Compare to exchange-split-valence-band-model**
  Erskine and Stern (1975)

	Theory	Expt.
$XAS(L_3) / XAS(L_2)$	2	2.55±0.10
$MCD(L_3)/MCD(L_2)$	-1	-1.60±0.10
$MCD(L_3)/XAS(L_3)$	25%	12.5%±2.5%
$MCD(L_2)/XAS(L_2)$	50%	20.0%±4.0%

where: $XAS = \sigma_+ + \sigma_-$
$MCD = \sigma_+ - \sigma_-$

- **The simple model predicts strong Ni core-level MCD effect, it is unable, however, to explain the observed intensity ratios and fine structures.**

- **To make the calculated XAS and MCD ratios different from 2 and -1 respectively, the population of 3d states with opposite m_l must be different.**
  The orbital magnetic moment is nonzero!

- **Perform a relativistic tight binding calculation:**
  Slator-Koster + spin-orbit interaction + cir. dipole transition

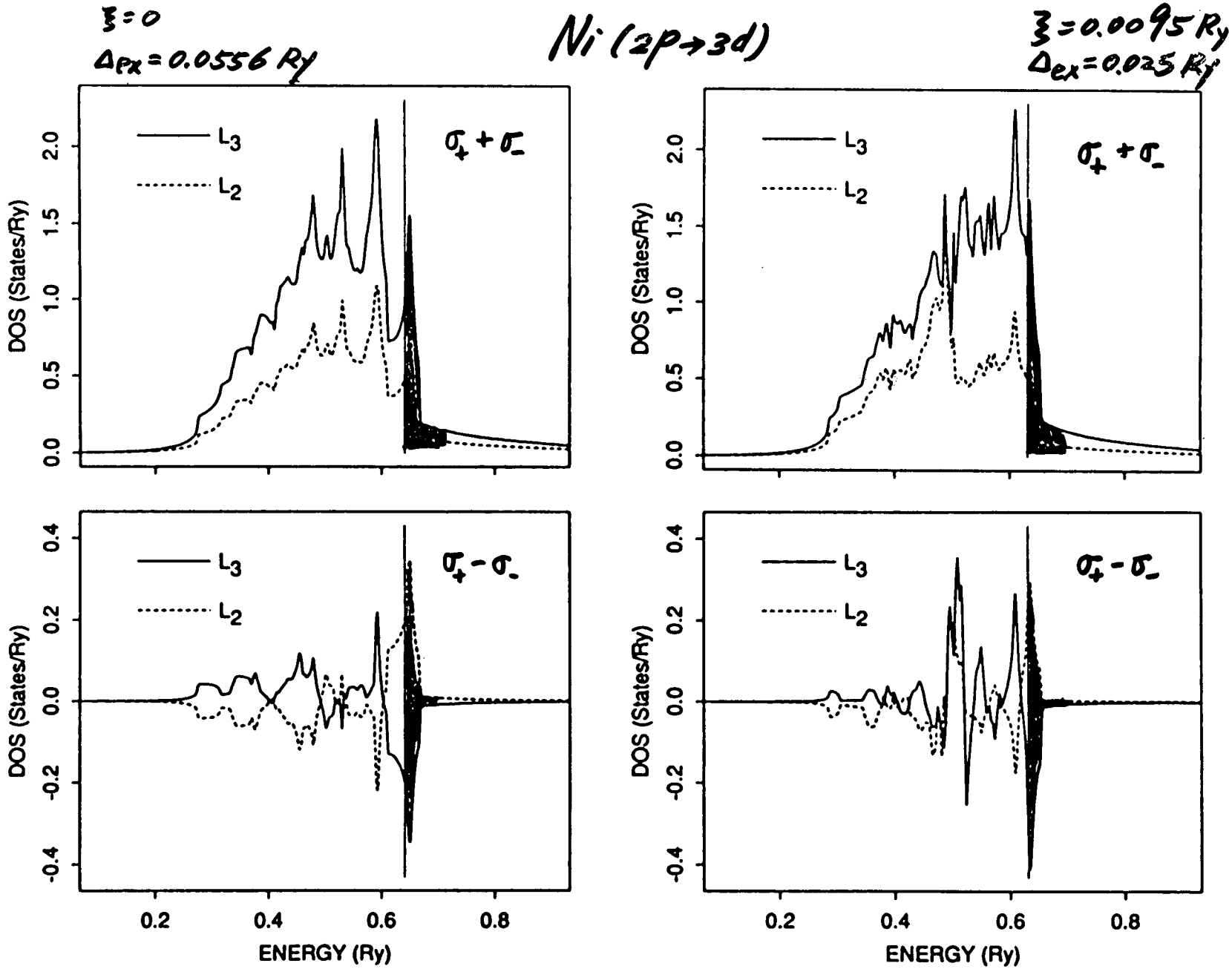
ξ = 0
Δpx = 0.0556 Ry
Ni (2p→3d)
ξ = 0.0095 Ry
Δex = 0.025 Ry
L3
L2
σ+ + σ-
σ+ - σ-
DOS (States/Ry)
ENERGY (Ry)
0.0
0.5
1.0
1.5
2.0
-0.4
-0.2
0.2
0.4
0.6
0.8

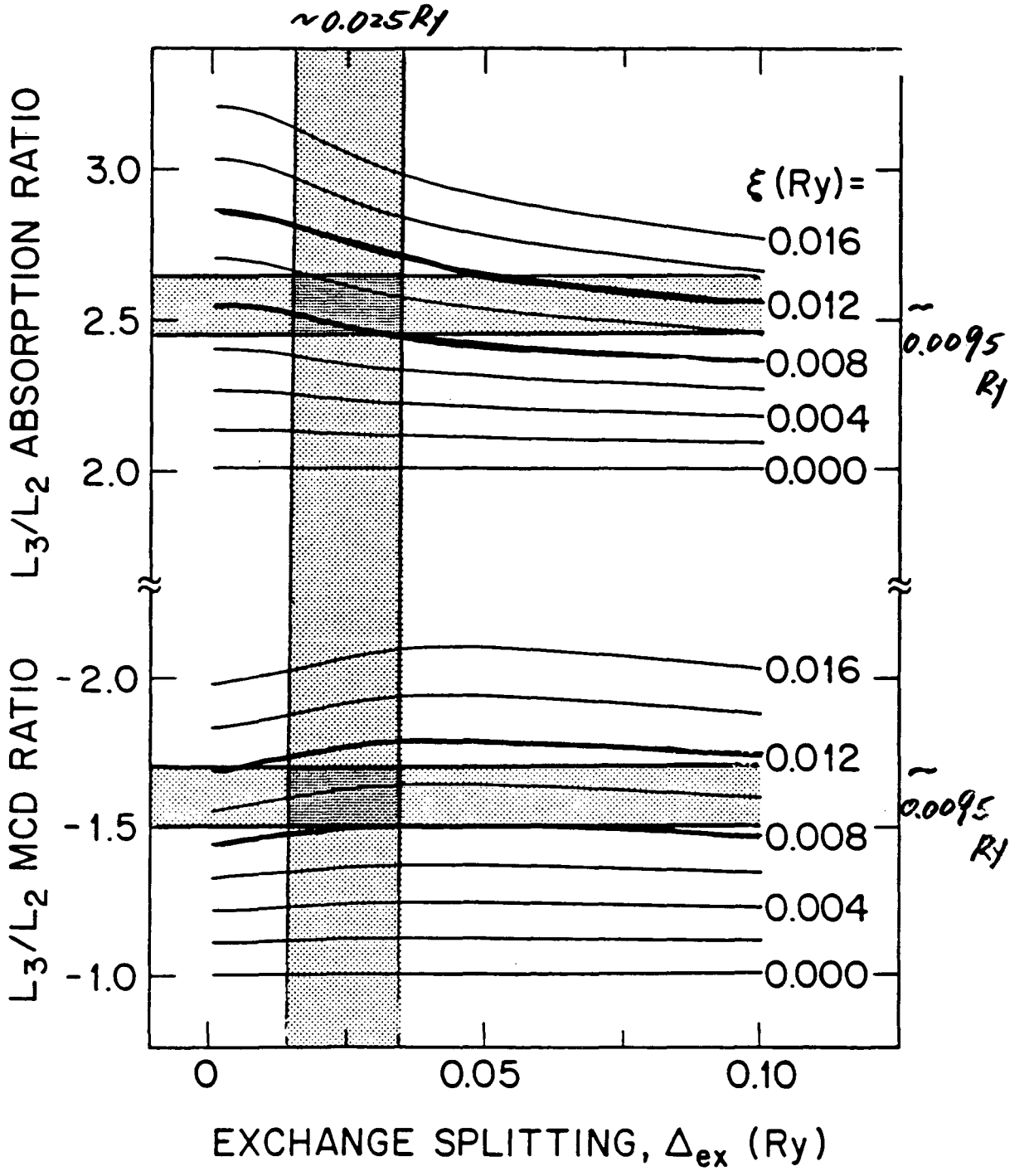
~0.025Ry
3.0
2.5
2.0
-2.0
-1.5
-1.0
L_3/L_2 ABSORPTION RATIO
L_3/L_2 MCD RATIO
ξ (Ry) =
0.016
0.012
0.008
0.004
0.000
0.016
0.012
0.008
0.004
0.000
~ 0.0095 Ry
~ 0.0095 Ry
0
0.05
0.10
EXCHANGE SPLITTING, Δ_{ex} (Ry)

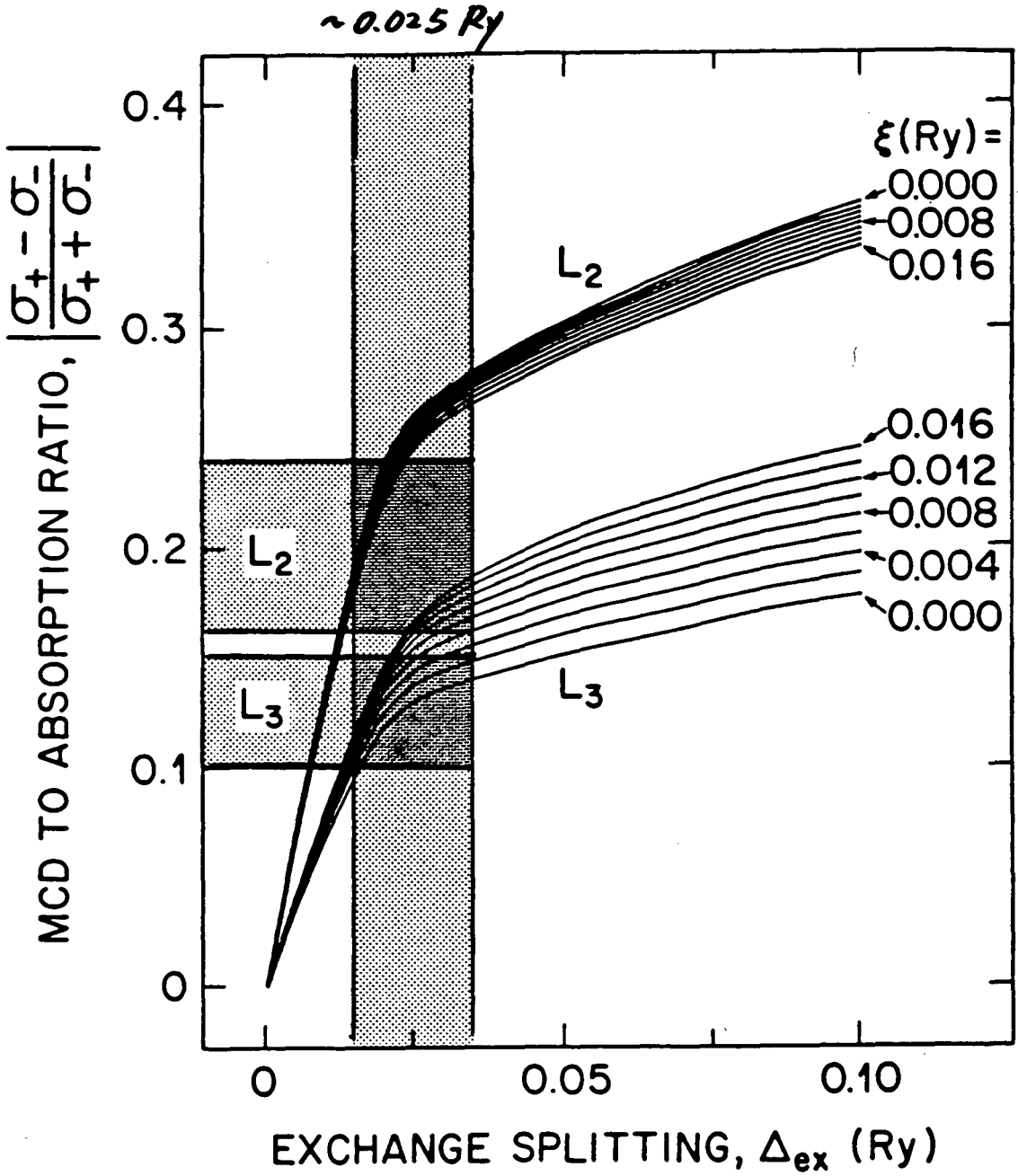
~0.025 Ry
0.4
0.3
0.2
0.1
0
ξ(Ry) =
0.000
0.008
0.016
0.016
0.012
0.008
0.004
0.000
L2
L2
L3
L3
0
0.05
0.10
MCD TO ABSORPTION RATIO, |σ+ − σ−| / |σ+ + σ−|
EXCHANGE SPLITTING, Δex (Ry)

$\xi = 0.0095\,Ry$ > atomic (0.0055) band (0.0067)

$\Delta ex = 0.025\,Ry$ < band (~0.05)

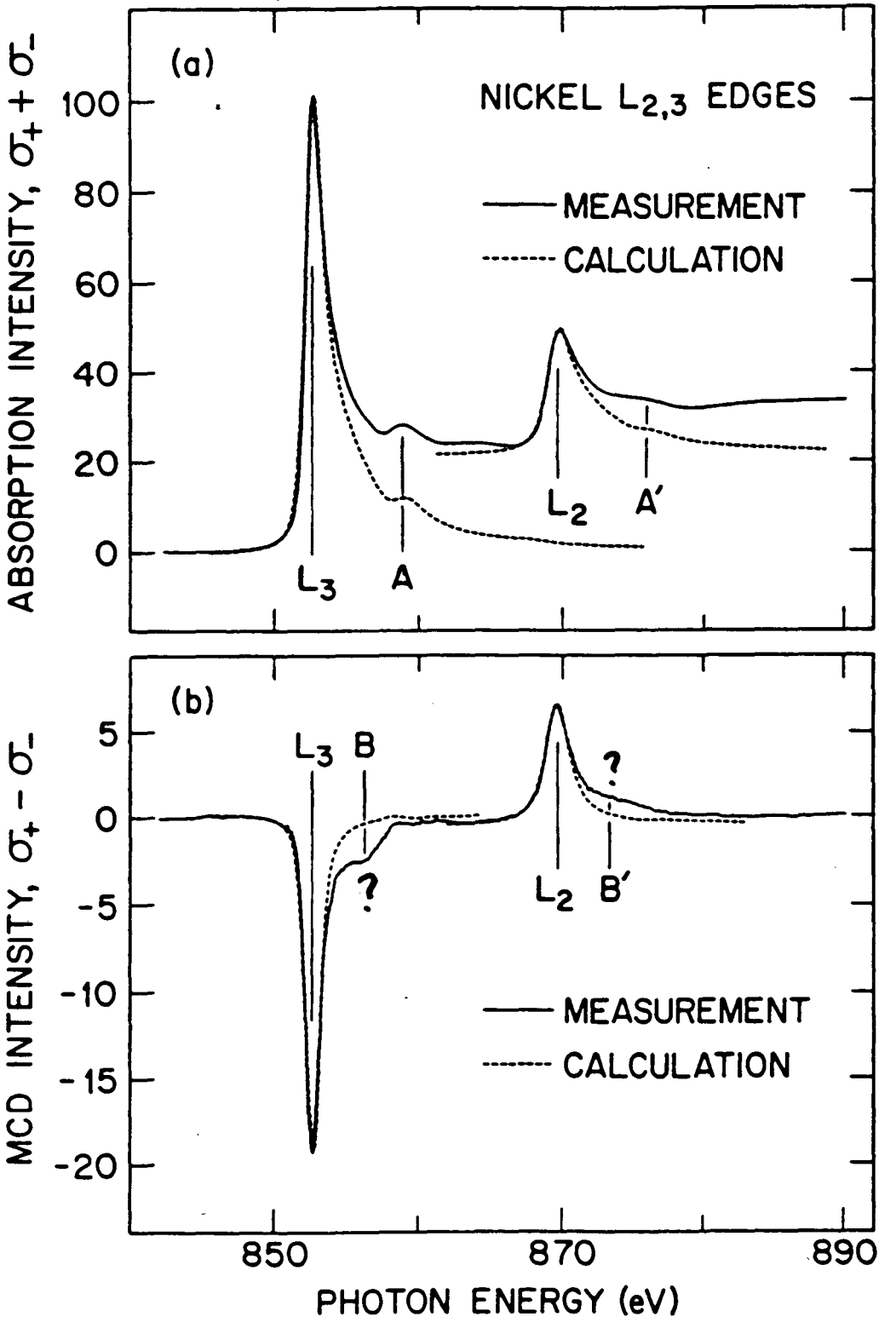

$\xi = 0$

$\Delta_{ex} = 0.125\,Ry$

Fe ($2p \rightarrow 3d$)

$\xi = 0.1\,Ry$

$\Delta_{ex} = 0.125\,Ry$

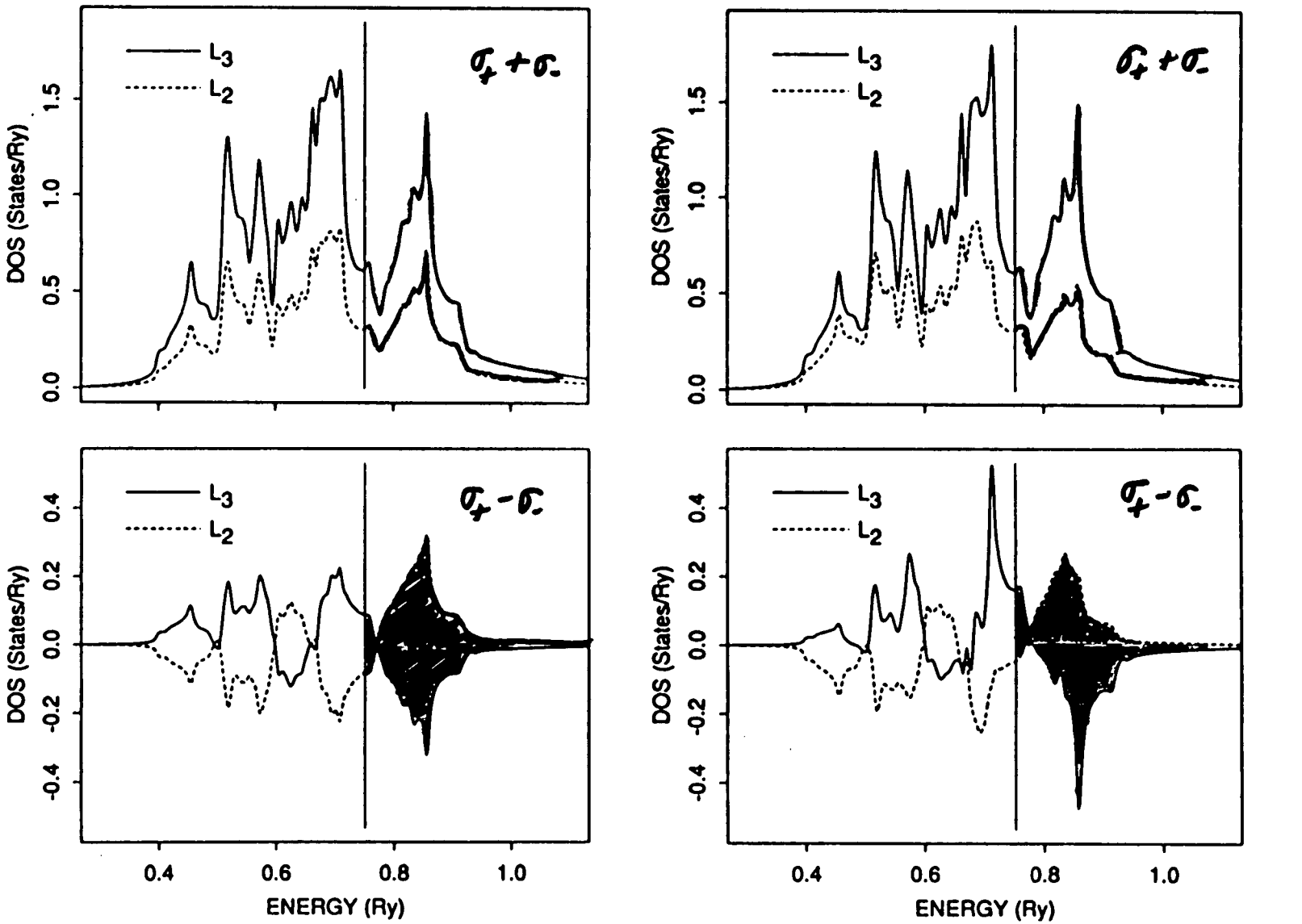

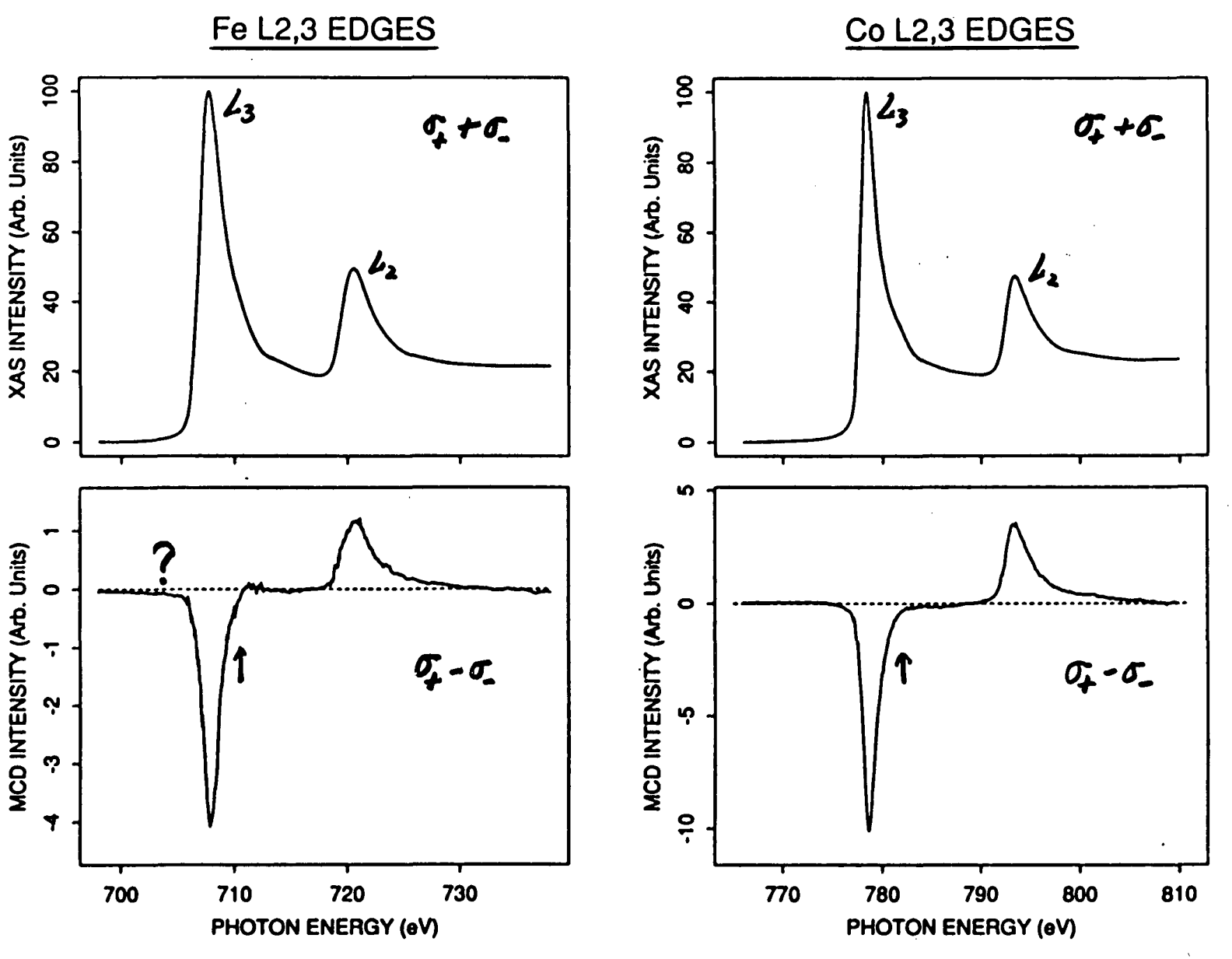
Fe L2,3 EDGES
Co L2,3 EDGES
XAS INTENSITY (Arb. Units)
MCD INTENSITY (Arb. Units)
PHOTON ENERGY (eV)
L3
L2
σ+ + σ-
σ+ - σ-
?
0
20
40
60
80
100
-4
-3
-2
-1
0
1
-10
-5
0
5
700
710
720
730
770
780
790
800
810

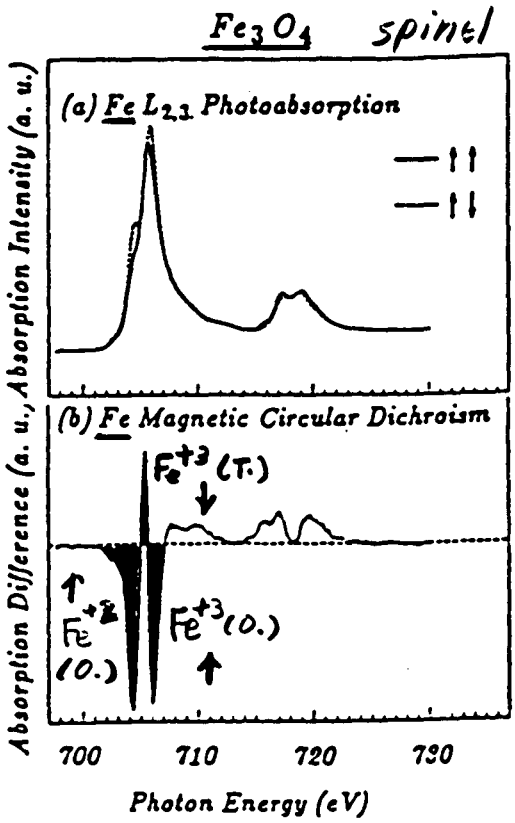

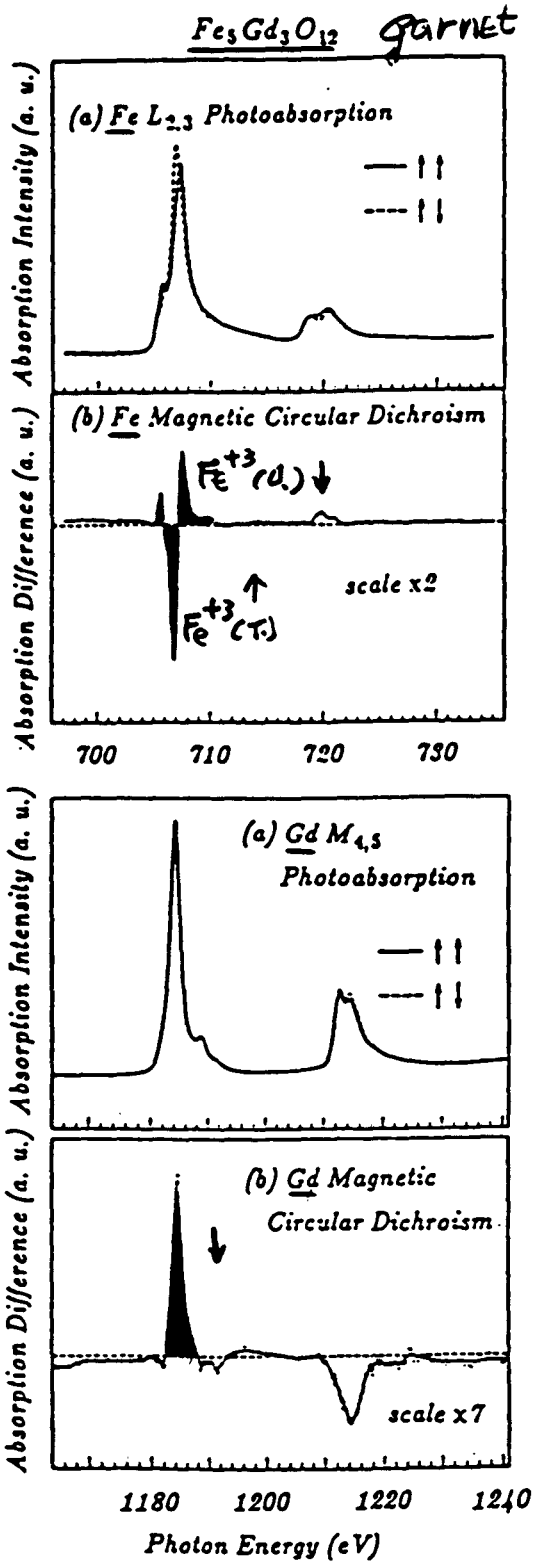

Fe_3O_4 (spinal)

1 Fe^{+3} octa. ↑

1 Fe^{+2} octa. ↑

1 Fe^{+3} Tetra. ↓

$Fe_5Gd_3O_{12}$ (garnet)

3 Fe^{+3} Tetra. ↑

2 Fe^{+2} Octa. ↓

3 Gd^{+3} ↓

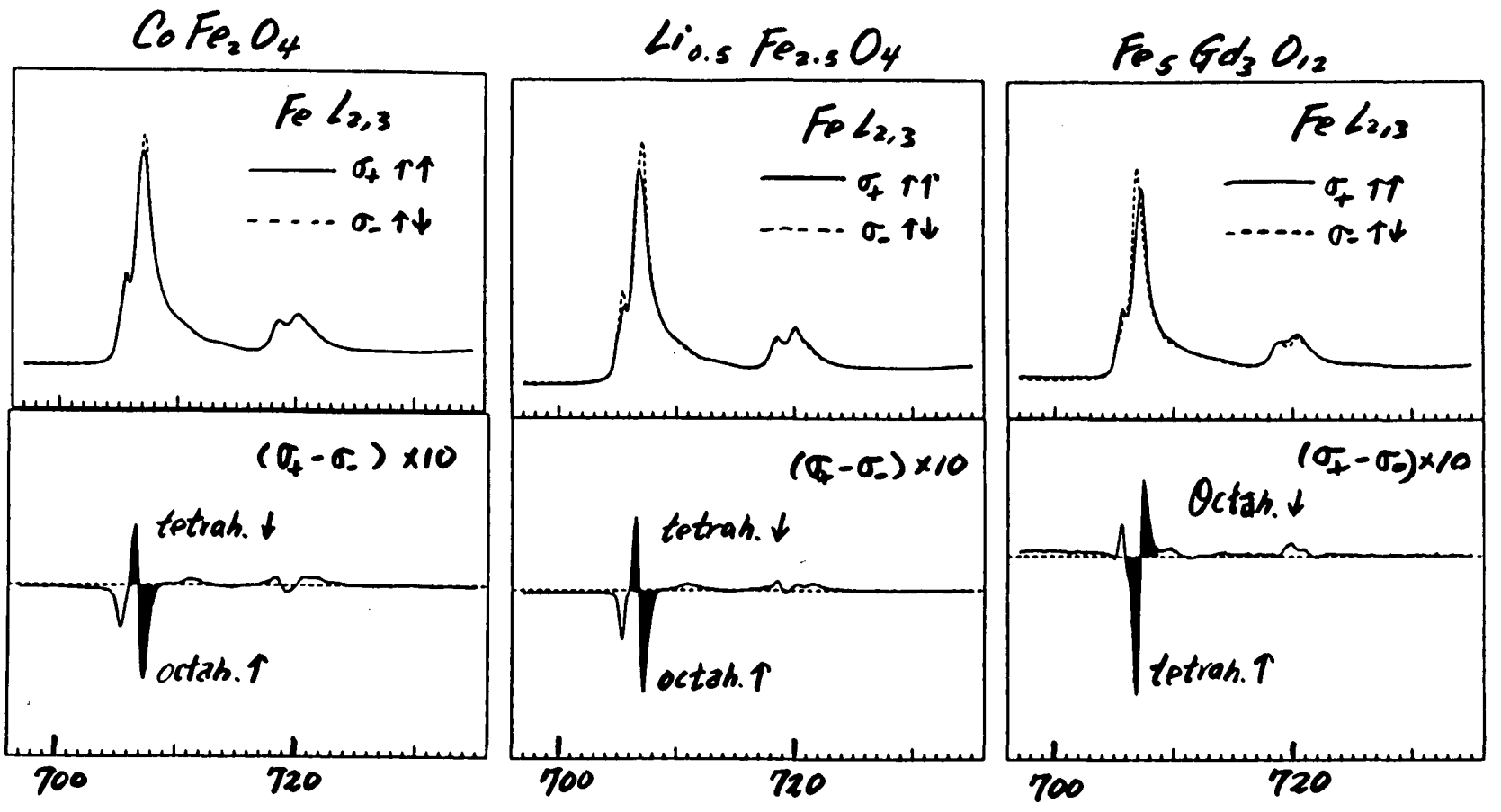

1.0 octah. ↑ Fe^{3+} $5\mu_B$ 1.0 tetrah. ↓ Fe^{3+} $5\mu_B$

1.5 Octah. ↑ Fe^{3+} $7.5\mu_B$ 1.0 tetrah. ↓ Fe^{3+} $5\mu_B$

3.0 tetrah. ↑ Fe^{3+} $15\mu_B$ 2.0 Octah. ↓ Fe^{3+} $10\mu_B$

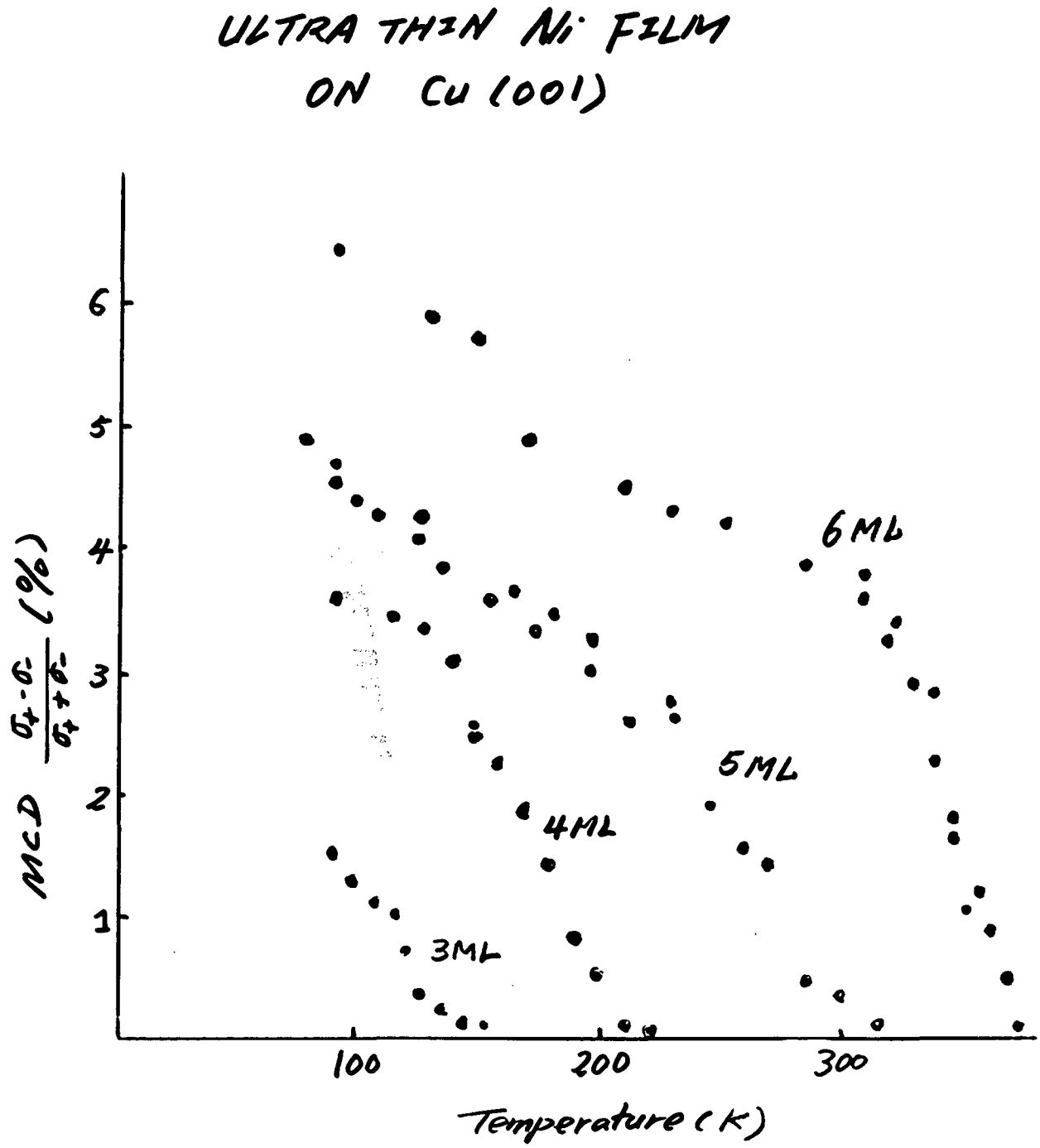
ULTRA THIN Ni FILM
ON Cu (001)
MCD $\frac{\sigma_+ - \sigma_-}{\sigma_+ + \sigma_-}$ (%)
6
5
4
3
2
1
6ML
5ML
4ML
3ML
100
200
300
Temperature (K)

C. A. Ballentine et al.

App. Phys. A49, 459 (1989)

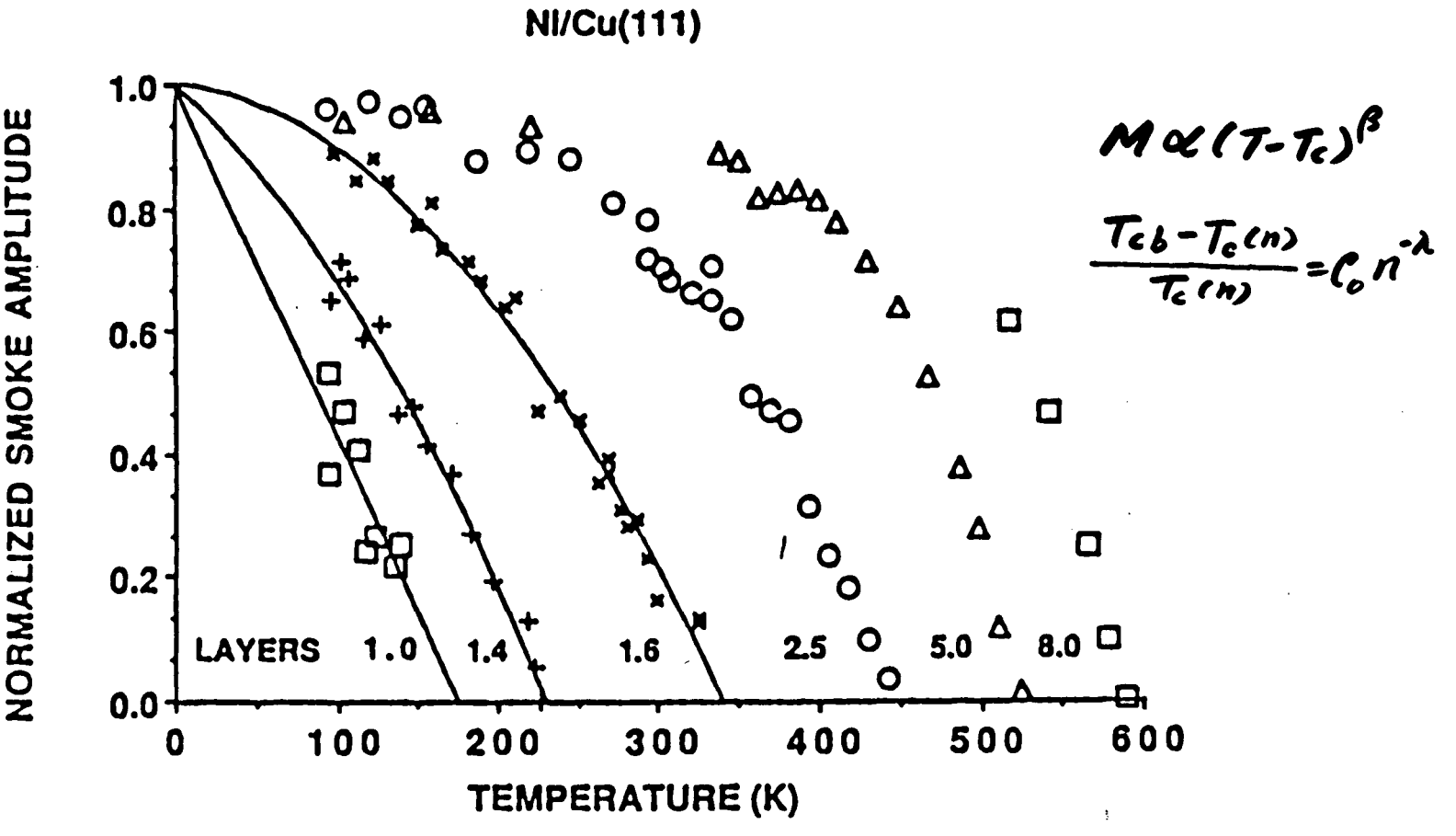

Temperature and thickness dependent magnetization of epitaxial Ni layers on Cu(111). Note the striking dependence of Curie temperature on film thickness

Conclusion

- **The feasibility of circularly polarized radiation in the soft-x-ray region** *(150 - 1500 eV)*

- **Observation of strong MCD effects at the $L_{2,3}$ edges of Fe, Co and Ni** --- *dipole-permitted transitions to final states of magnetism importance ($2p \rightarrow 3d$ of TM and $3d \rightarrow 4f$ of RE)*

- **A new vantage point from which to examine core-hole and valence-valence correlation effects** --- *SDDOS, exchange splitting, L-S coupling and MCD fine structures*

Outlook

- **SXMCD as a practical tool for probing chemical specific magnetic moments of wide range of samples**
  --- *surfaces, thin films, multi-layers, alloys, compounds, disorder, impurity and paramagnetic systems*

- **The Double-headed Dragon**

A Split-Coil Superconducting Magnet for Soft X-Ray MCD Experiments on Paramagnetic Samples

S.P. Cramer

University of California, Davis

Abstract

S. P. Cramer

X-ray magnetic circular dichroism of metals in proteins is an attractive new technique. It offers the potential for site specific spectroscopy (since it will only sense paramagnetic species). The relative spin orientations of metals in clusters can also be determined. We plan to build a 6 Tesla magnet with split coils and a cold UHV bore to conduct XMCD experiments. Samples will be maintained at 2 Kelvin with a pumped helium cryostat. Fluorescence detection will be used to examine dilute metals in enzymes such as nitrogenase, hydrogenase, and photosystem II.

Applications of Circular Polarization

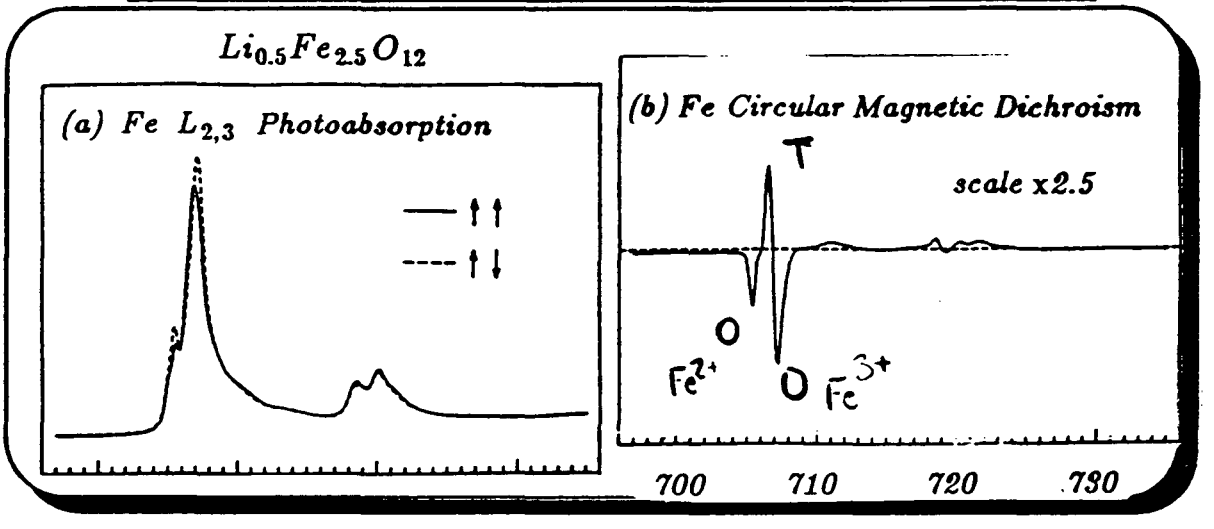

Chem. Sci. Rev.

X-Ray Magnetic Circular Dichroism

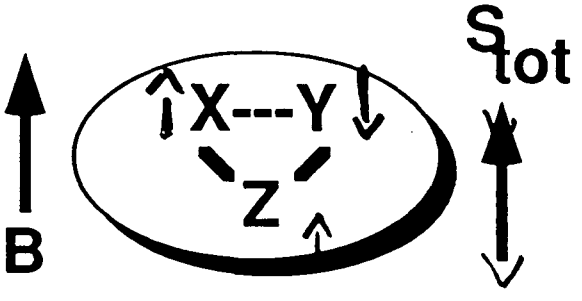

- resolution of spin-coupled atoms

- orientation of individual spins

BIOINORGANIC XMCD

APPLICATIONS

(1) 'SHARPEN' L-EDGE SPECTRA

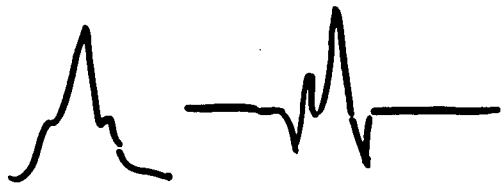

(2) UNTANGLE MIXTURES

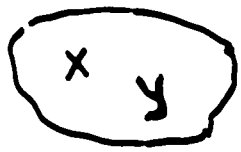

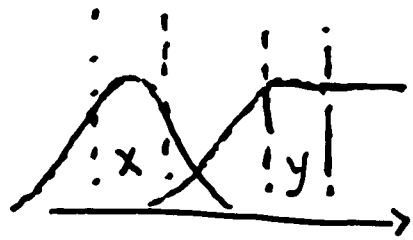

(3) RELATIVE SPIN ORIENTATIONS

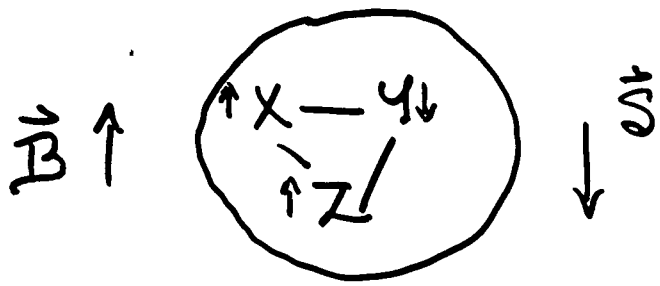

MANY ENZYMES CONTAIN PARAMAGNETIC METAL CLUSTERS

NITROGENASE $N_2 \longrightarrow 2NH_3$

Fe, Mo

HYDROGENASE $H_2 \rightleftharpoons 2H^+ + 2e^-$

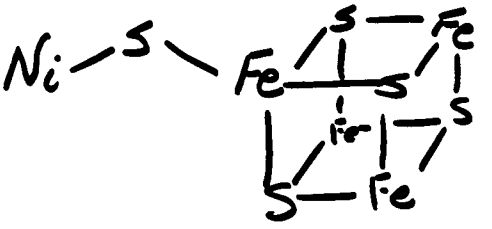

PHOTOSYSTEM II $2H_2O \xrightarrow{4h\nu} O_2 + 4H^+ + 4e^-$

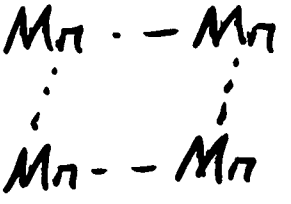

CYTOCHROME OXIDASE $O_2 \longrightarrow 2H_2O$

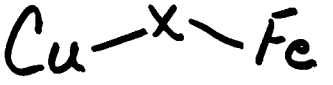

A Mixed Valence Application

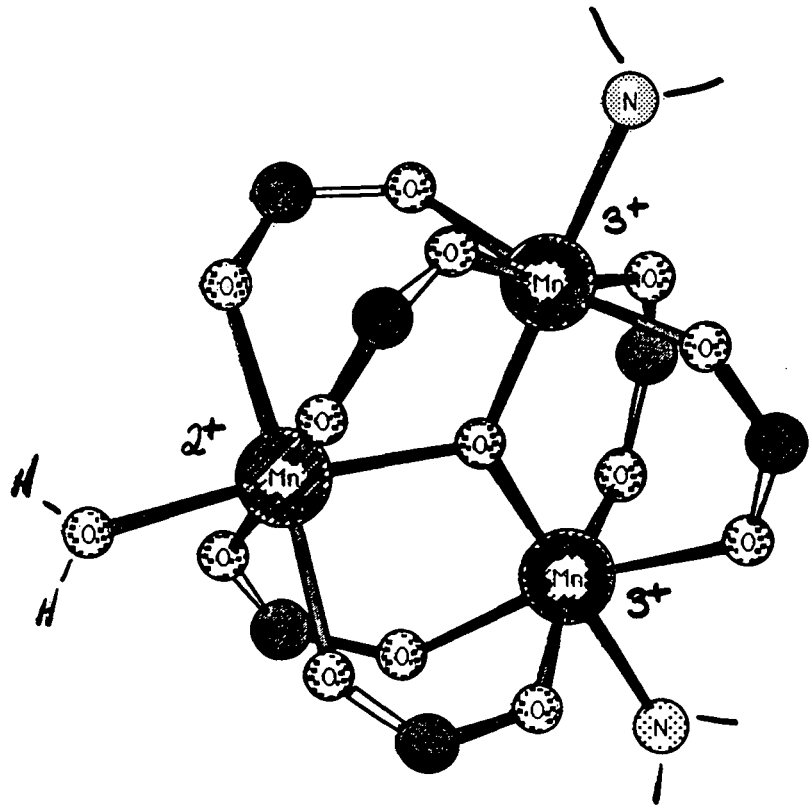

- aquo complex shows expansion at water site [Mn(II)]
- all pyridine complex yields symmetric crystal structure at room temperature
- is complex Mn(II), Mn(III), Mn(III) or delocalized?

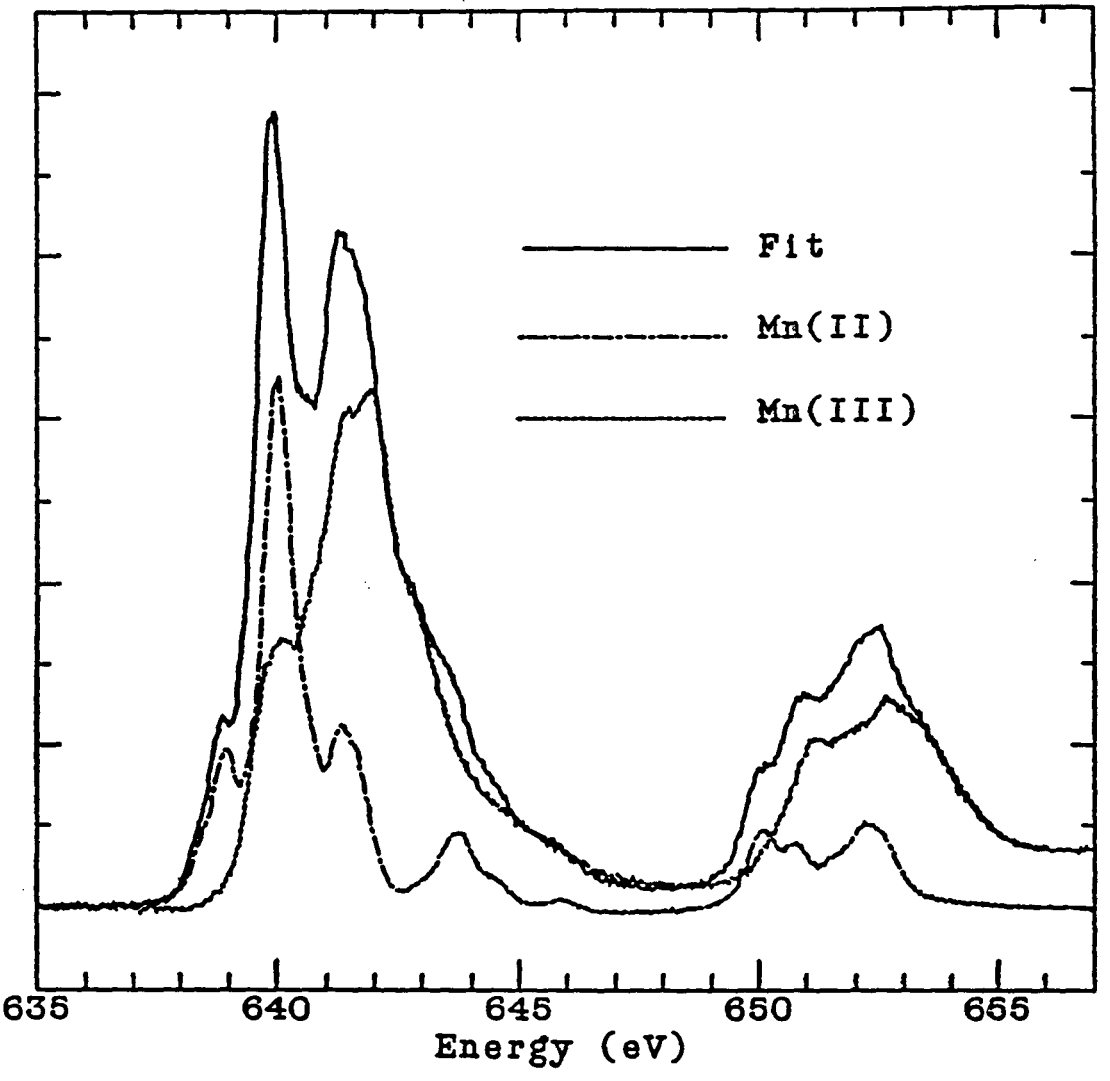
Fit
Mn(II)
Mn(III)
635
640
645
650
655
Energy (eV)

Nitrogenase

$N_2+8e^-+8H^++nMgATP \rightarrow 2NH_3 + H_2+nMgADP$

- 220,000 m.w. protein
- ~28 Fe & 2 Mo(or V)
- first crystallized early '80's

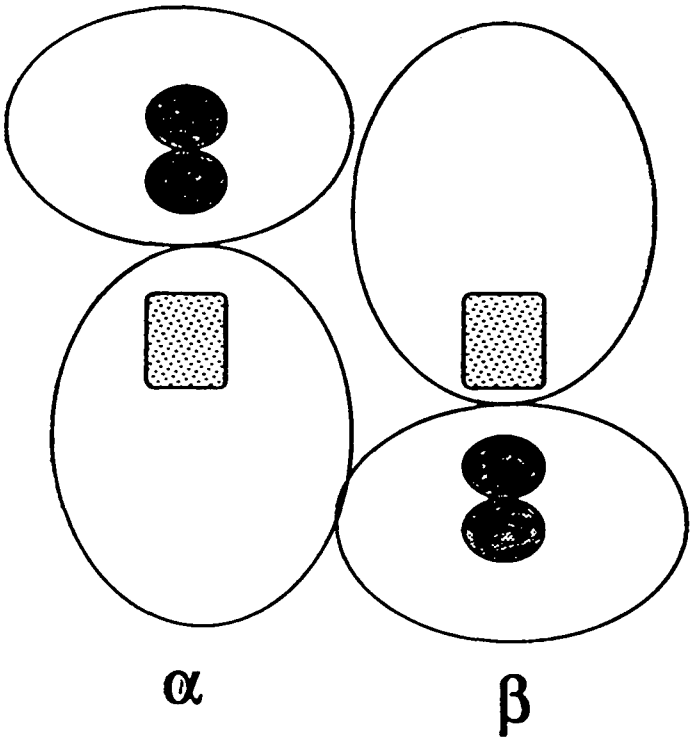

Fe-Mo cofactor

~1 Mo(V), ~6Fe, S

P-clusters

8 Fe (tot)

at least 14 different Fe

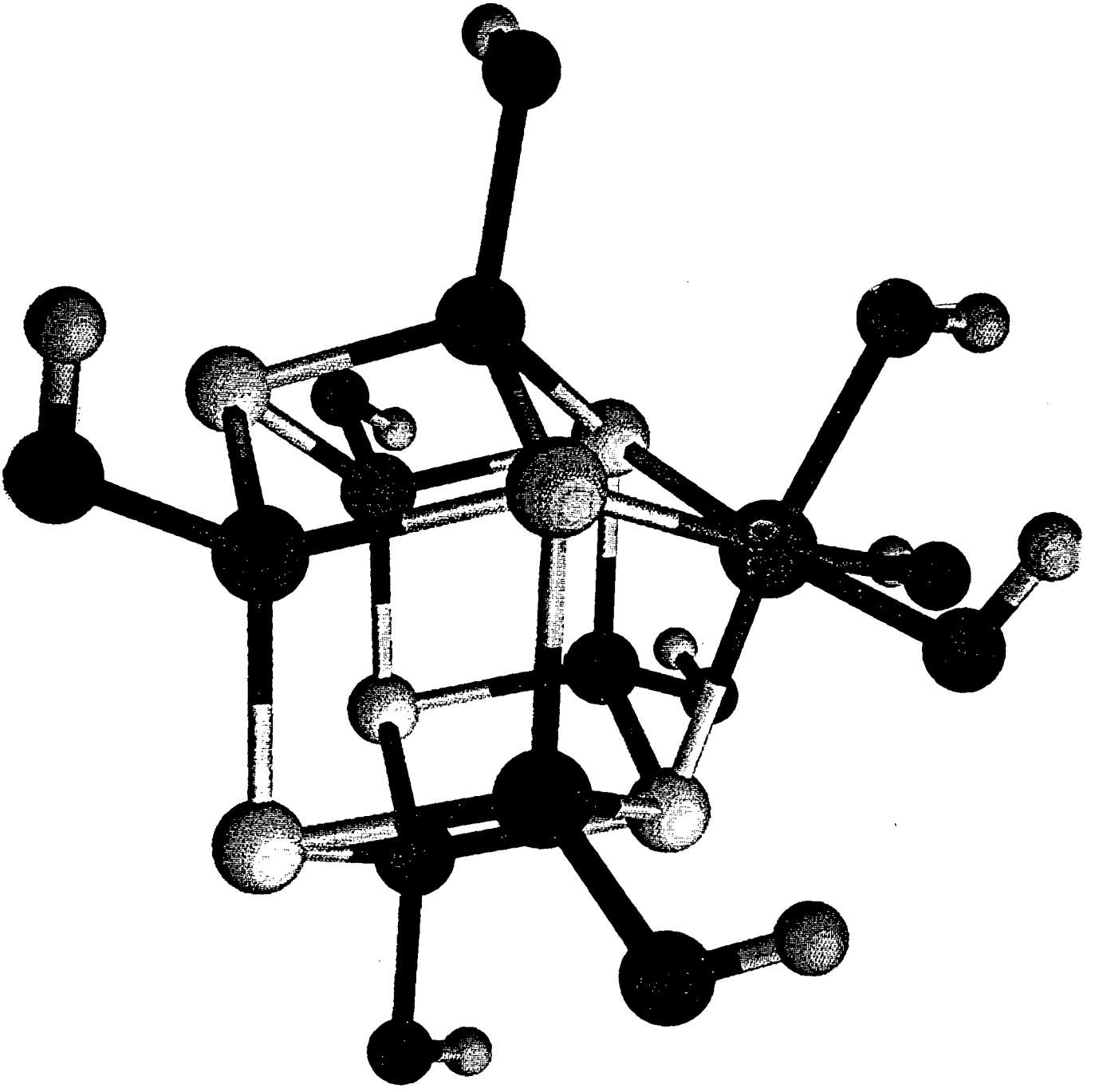

Troubles for Proteins

$$I_F = I_0 \cdot \underbrace{5x10^{-3}}_{F_{Mn}} \cdot \underbrace{5x10^{-3}}_{\omega} \cdot \underbrace{5x10^{-1}}_{escape} \cdot \underbrace{.5x10^{-1}}_{\Omega} \cdot \underbrace{5x10^{-1}}_{window} \sim 1x10^{-6} \cdot I_0$$

- Path Length - - 8000 Angstroms for manganese L
- Diluteness - - 0.5 % absorption by Mn
- Diluteness requires fluorescence detection for background rejection
- Fluorescence yields are low - ~0.5 %
- Limited collection solid angle
- Possible fluorescence absorption by ice buildup and windows
- Possible radiation damage

INTERESTING SAMPLES FREQUENTLY

~100 ppm or less

Problem-Solving

- sensitive Ge array detector
- focussed beam and glancing incidence geometry
- eliminate windows (beamline, chamber, sample, and detector)
- 4K cryostat operation to reduce sample damage
- filters to remove oxygen fluorescence

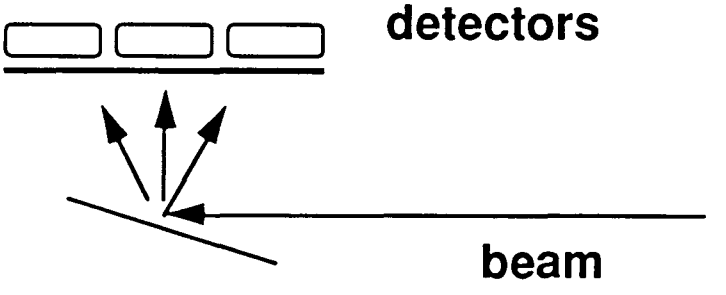

Low Energy Ge Detector Resolution

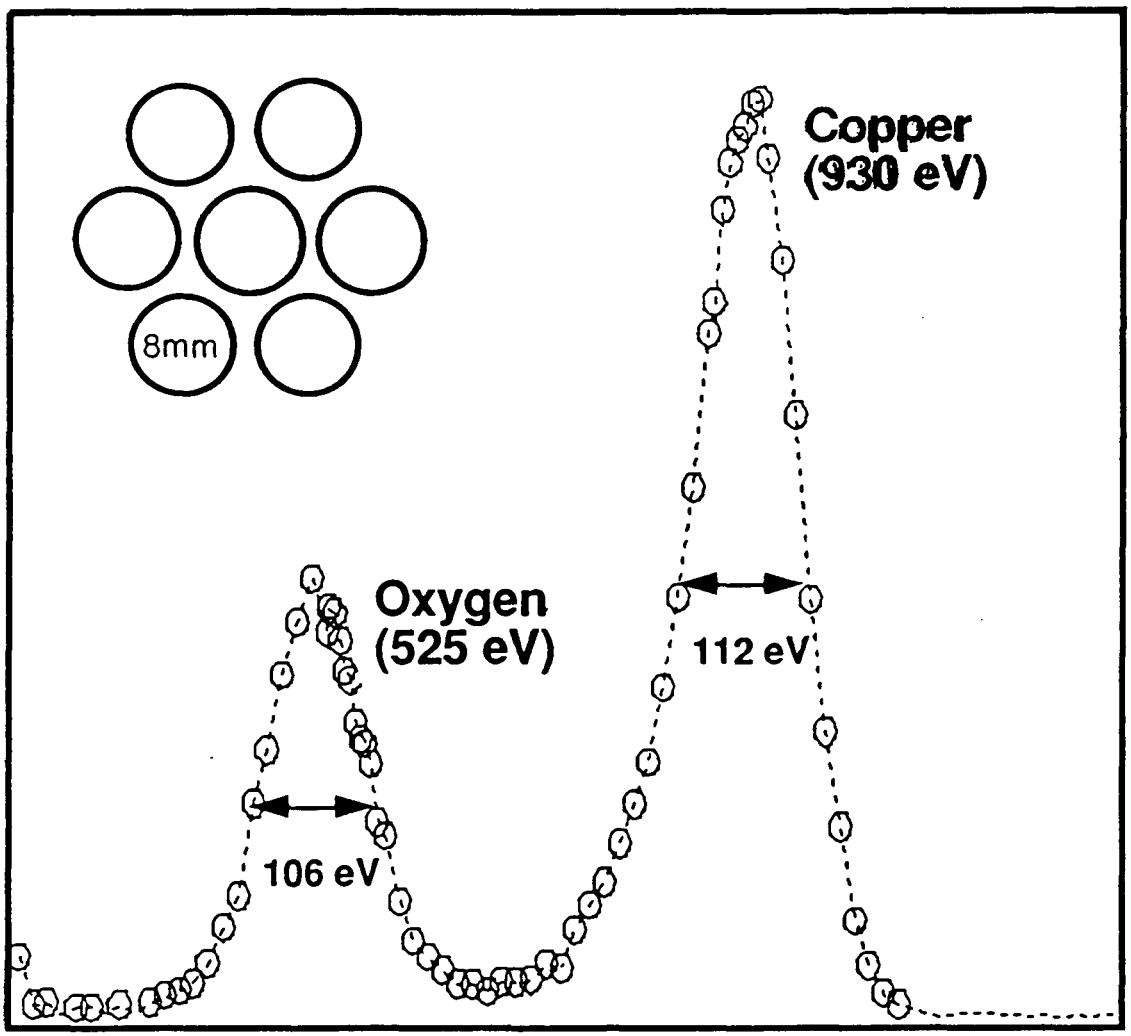

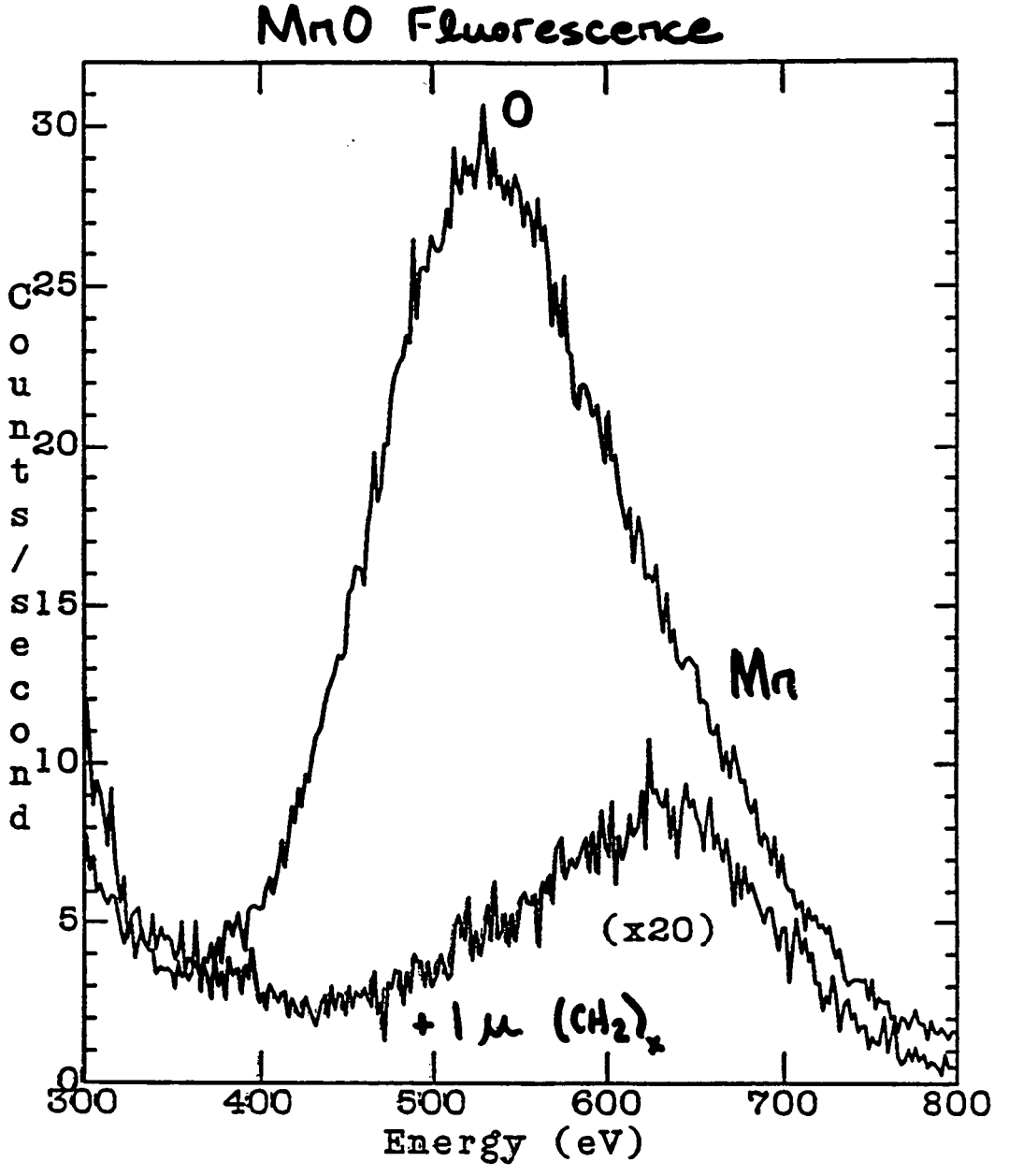
MnO Fluorescence
O
Mn
(x20)
+ 1 μ (CH2)x
Counts/second
Energy (eV)
0
5
10
15
20
25
30
300
400
500
600
700
800

Detector Plans

100 Element Si Array Detector - Electronics and Controls

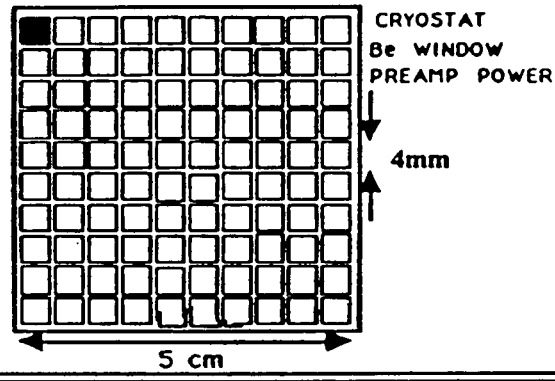

- **ALS device will emphasize high resolution (~100 eV) for soft x-rays**
- **UHV compatible**
- **prototype being built at NSLS with Instrumentation Division and Canberra**
- **joint electronics/software development with BNL and SSRL**

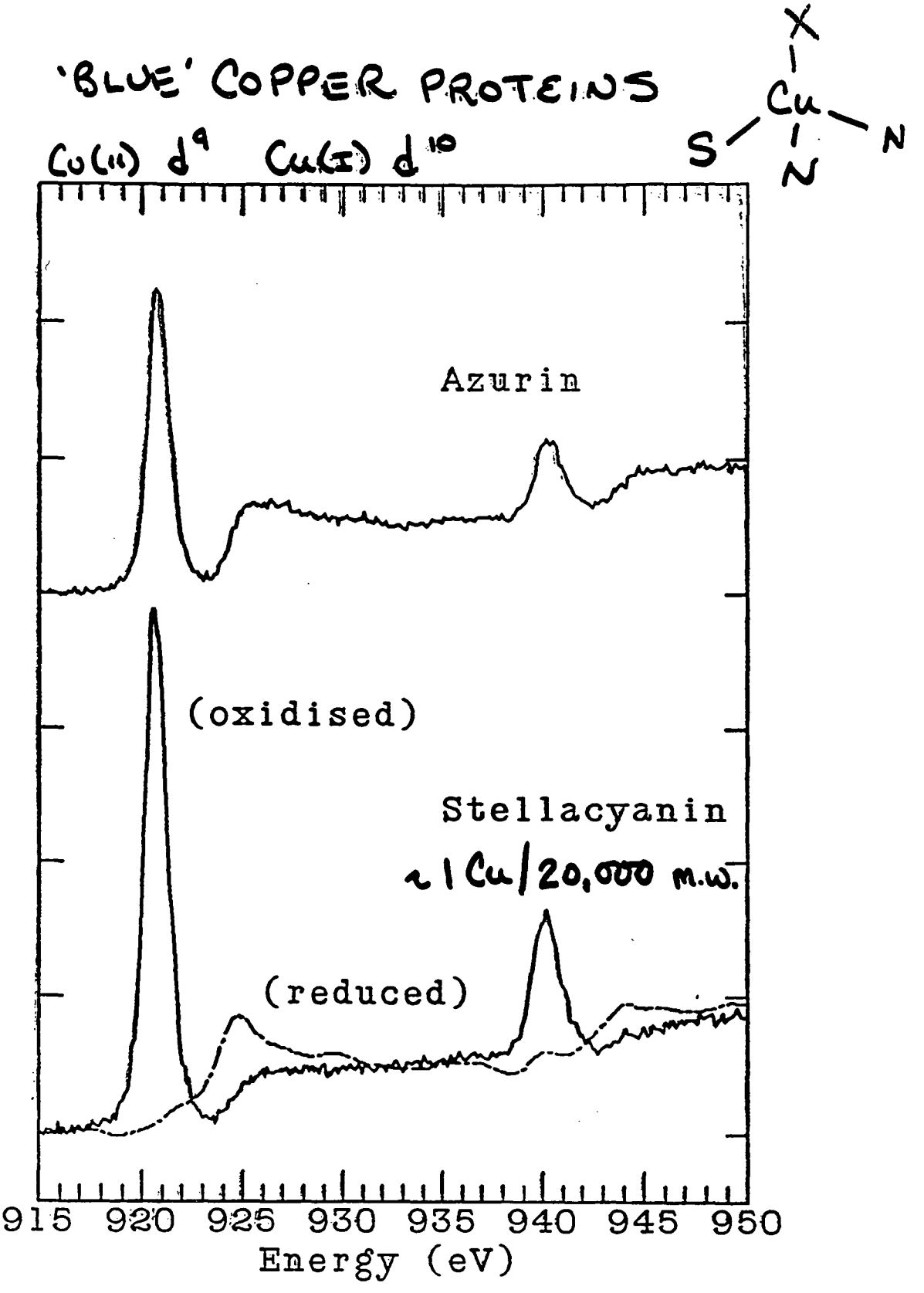
'BLUE' COPPER PROTEINS
Cu(II) d⁹ Cu(I) d¹⁰
X
Cu
S
N
N
Azurin
(oxidised)
Stellacyanin
≈ 1 Cu/20,000 m.w.
(reduced)
915 920 925 930 935 940 945 950
Energy (eV)

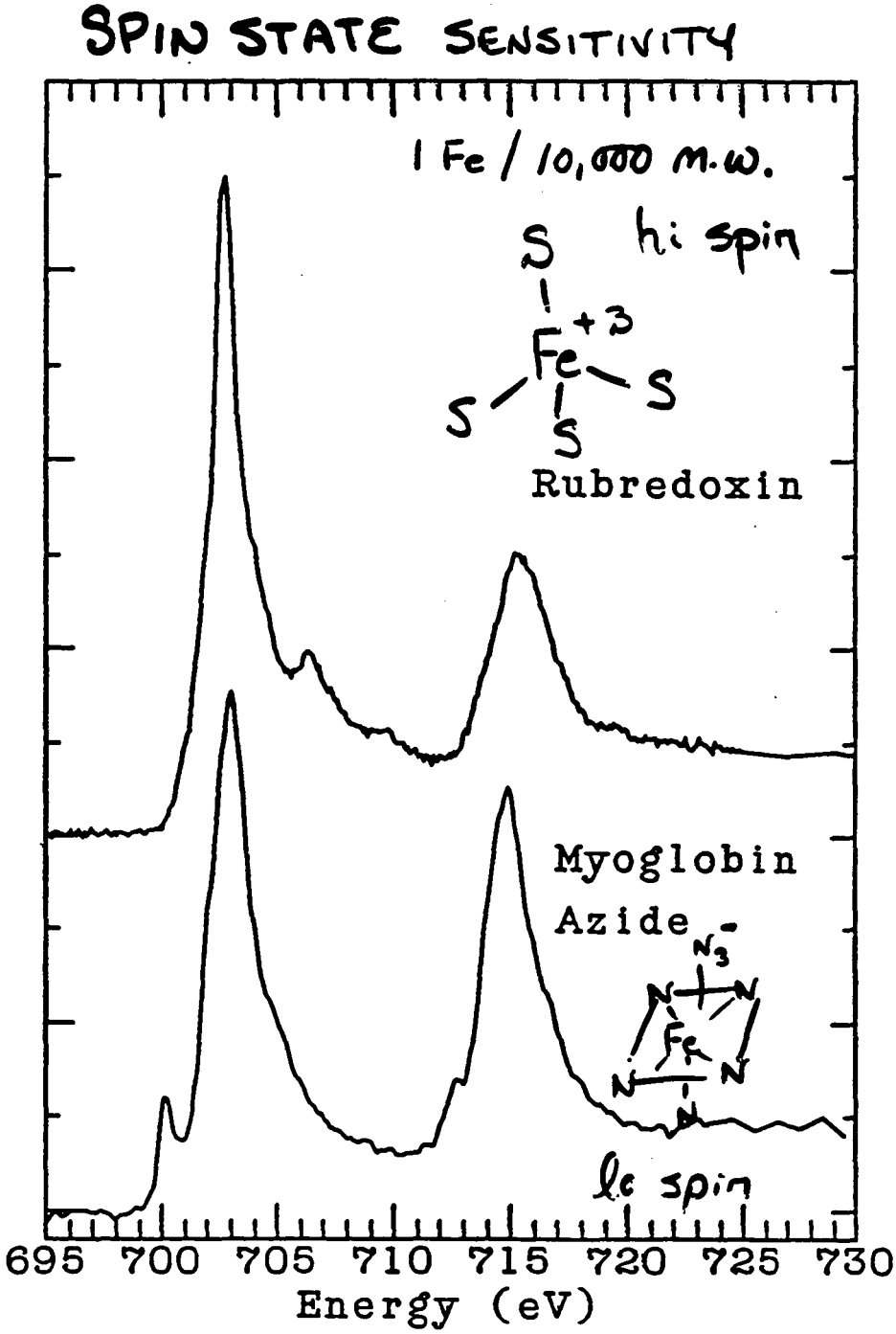
SPIN STATE SENSITIVITY
1 Fe / 10,000 m.w.
hi spin
+3
Fe
S
S
S
S
Rubredoxin
Myoglobin
Azide
N_3^-
Fe
lo spin
695 700 705 710 715 720 725 730
Energy (eV)

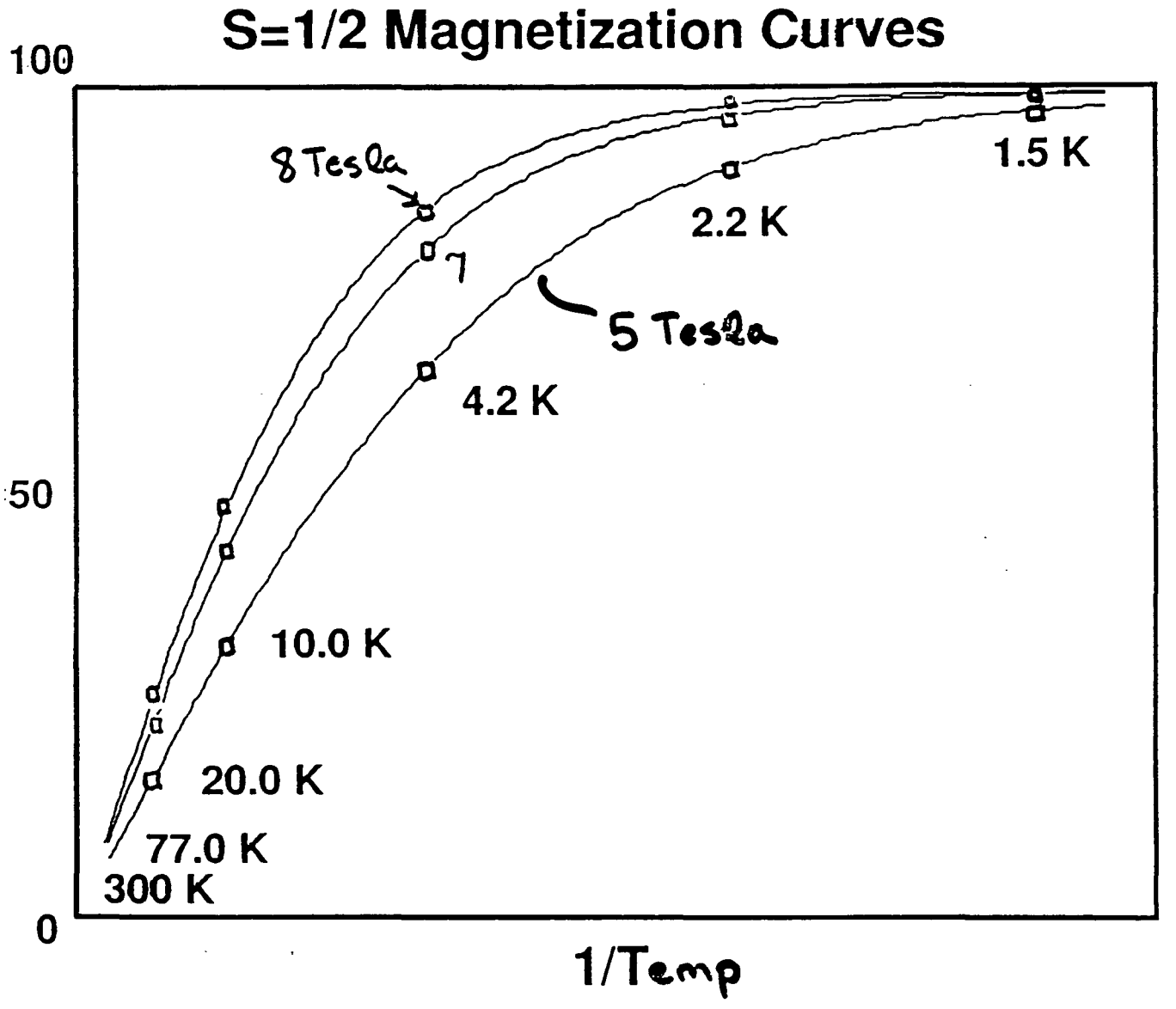

- field dependence → g-values
- T dependence → excited states

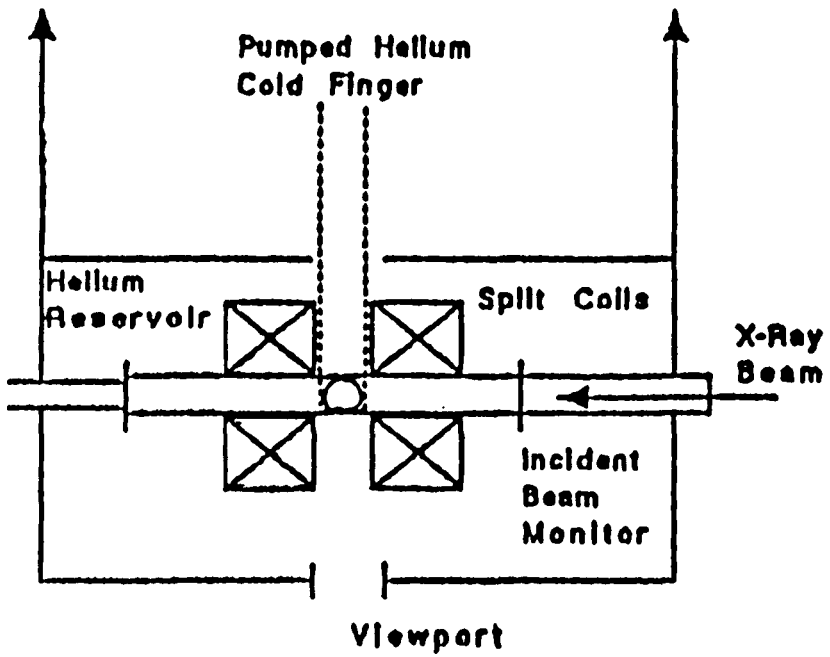

ELEVATION

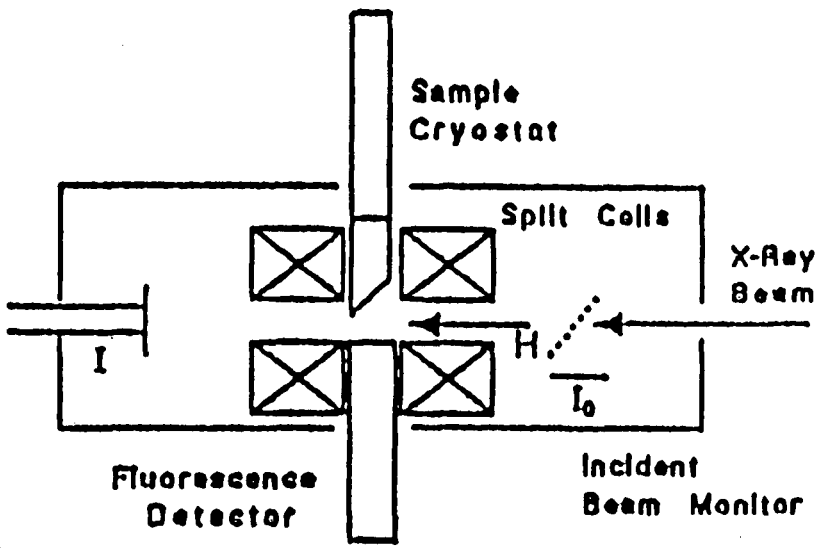

PLAN

PLANS < 2 Kelvin

≥ 6 Tesla

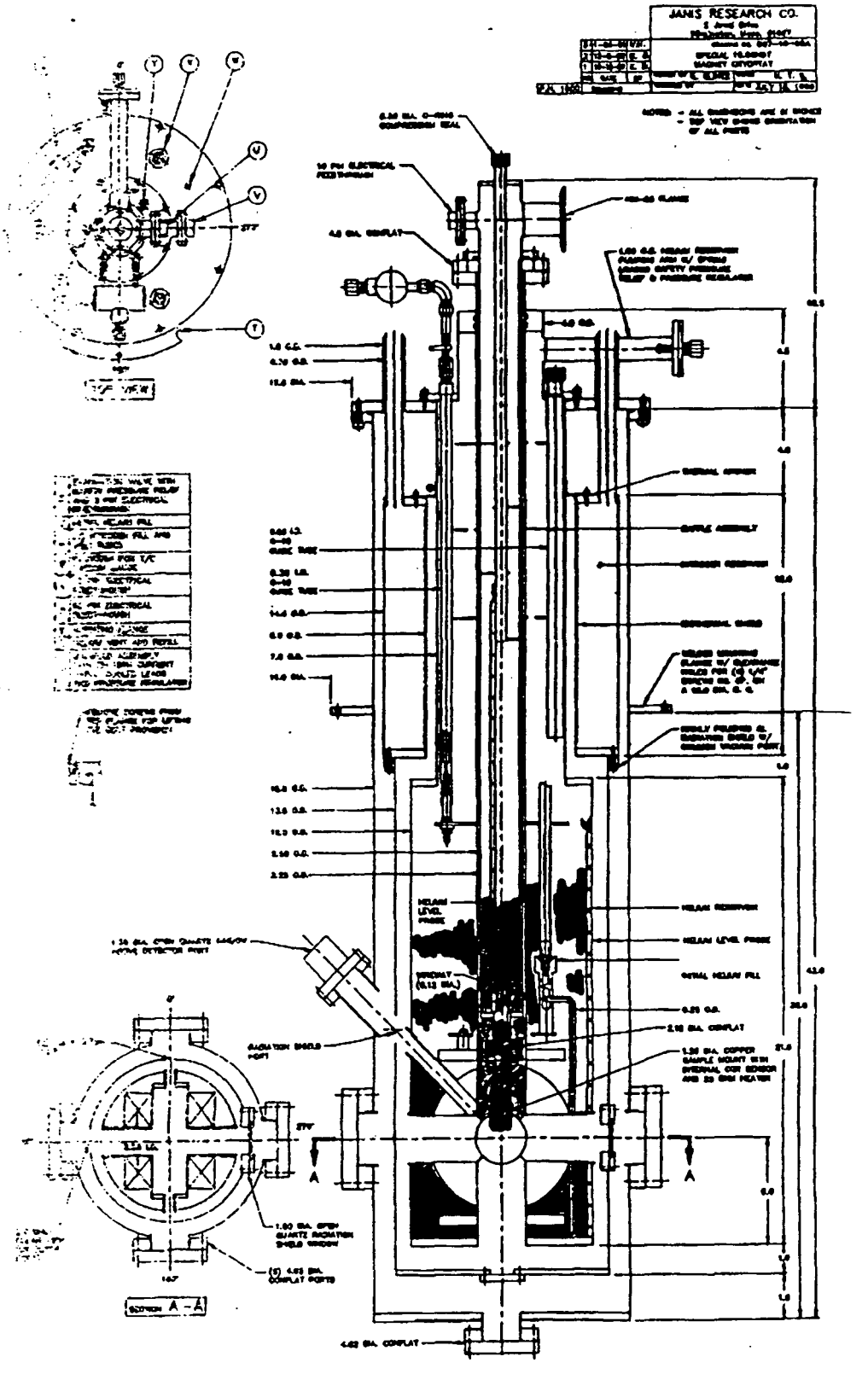
JANIS RESEARCH CO.
SECTION A - A

WHAT WE NEED

1. MORE FLUX
2. FASTER DETECTORS
3. INTERPRETATION SOFTWARE

Instrumentation and Preliminary Results of Polarization Measurements of Undulator Radiation in the Soft X-Ray Region

E. Gluskin

Argonne National Laboratory

Instrumentation and Preliminary Results of Polarization Measurements of Undulator Radiation in the Soft X-Ray Region

E.Gluskin, APS Argonne National Lab

This work is sponsored by U.S. Department of Energy,
BES-Materials Sciences under Contract W-31-109-ENG-38

List of Co-Authors:

S.D.Bader J.E.Mattson P.J.Viccaro	Argonne National Laboratory
T.W.Barbee,Jr	Lawrence Livermore Nat. Lab.
N.Brookes	Brookhaven National Laboratory
A.Pitas	Baker Manufact. Co., WI
R.Watts	Nat. Inst. of Standards&Technology

Efficient use of the radiation from new generation synchrotron radiation sources requires development of instrumentation for the complete characterization of various radiation properties. At present, very little instrumentation is available to measure polarization in the energy region between 100-1000 ev.

One approach based on the multilayer usage as a polarizer for the soft x-ray wavelength region is discussed in this talk.

OUTLINE

- spectral and polarization properties of undulator radiation: calculations;

- instrumentation for measurements of these properties:
  monochromator, polarimeter;
  polarizers characterization;

- experimental results: spectral and polarization data for APS-NSLS U5 undulator radiation;

- discussion and conclusion.

U5 Undulator and Experimental Set-up Parameters

Undulator period: λ_u = 7.5 cm

Number of periods: N = 27

Deflection parameter: K = 2.30

Distance
Undulator - Pinhole: 5.4 m
Pinhole - Polarimeter: 1.7 m

$$\lambda = \frac{\lambda_u}{2n\gamma^2}\left(1 + \frac{K^2}{2} + \gamma^2\theta^2\right)$$

λ - radiation wavelength

γ - relativistic factor

θ - observation angle

For $\gamma = 1.5 \cdot 10^3$ and $\gamma \cdot \theta = 1$ beam size at pinhole: 3.6 mm

U5 Undulator: No emittance case (30 s CPU on VAX).
Flux on-axis through a 1mm x 1mm pinhole at 5.4 m from the source.

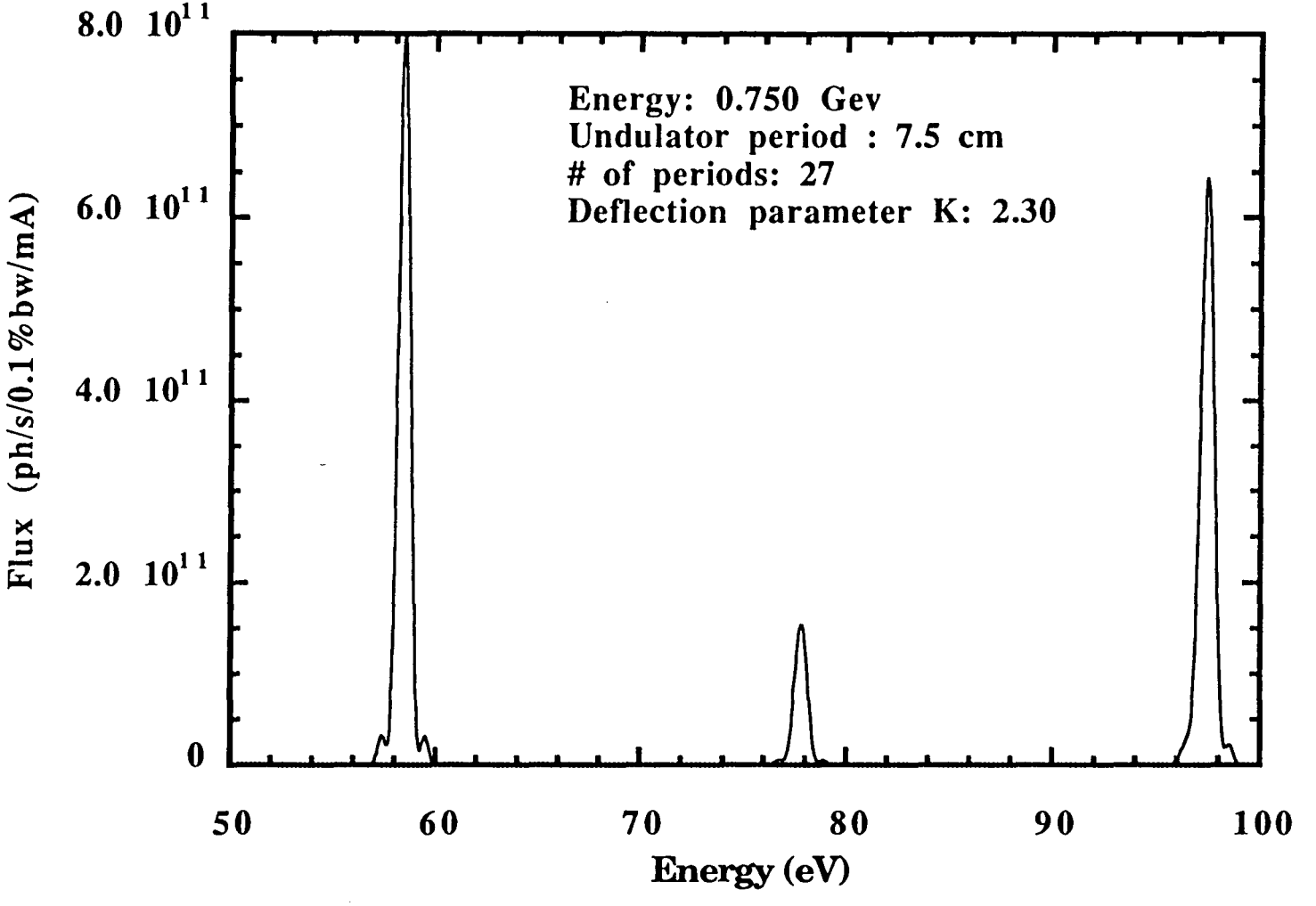

Ref: Roger J. Dejus, The Advanced Photon Source, ANL.
R.P. Walker, Rev. Sci. Instr. 60 (7), July 1989.
S.Krinsky et.al. in Handbook on Synchrotron Radiation, vol 1. (1983), pp. 146-158.

U5 Undulator: Emittance included (2 min CPU on VAX).
Flux on-axis through a 1mm x 1mm pinhole at 5.4 m from the source.

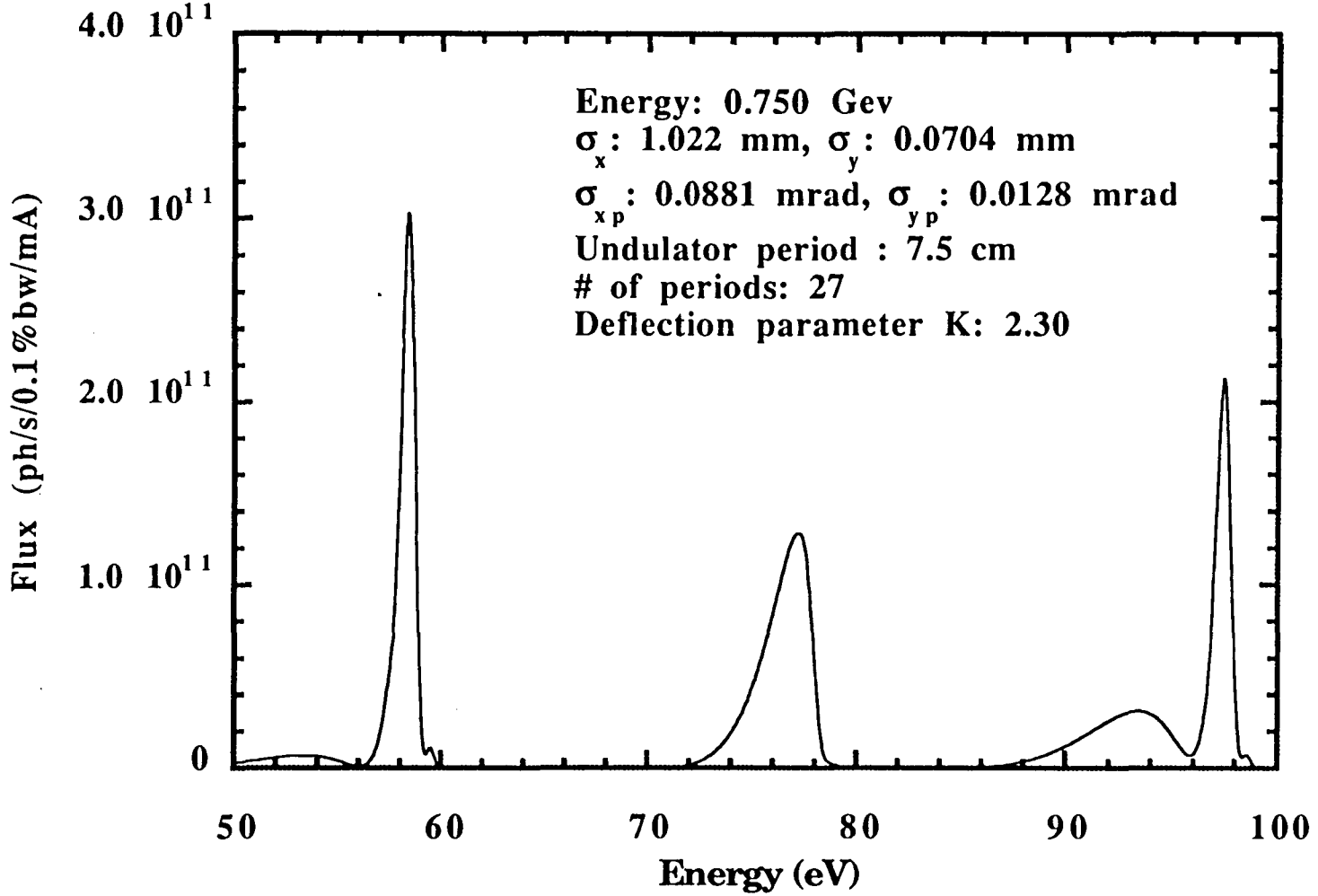

Ref: Roger J. Dejus, The Advanced Photon Source, ANL.
R.P. Walker, Rev. Sci. Instr. 60 (7), July 1989.
S.Krinsky et.al. in Handbook on Synchrotron Radiation, vol 1. (1983), pp. 146-158.

1-st harmonic

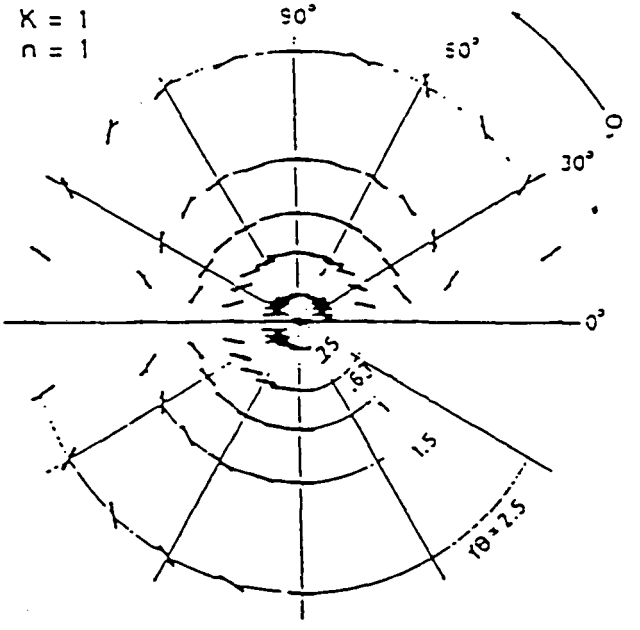

2-nd harmonic

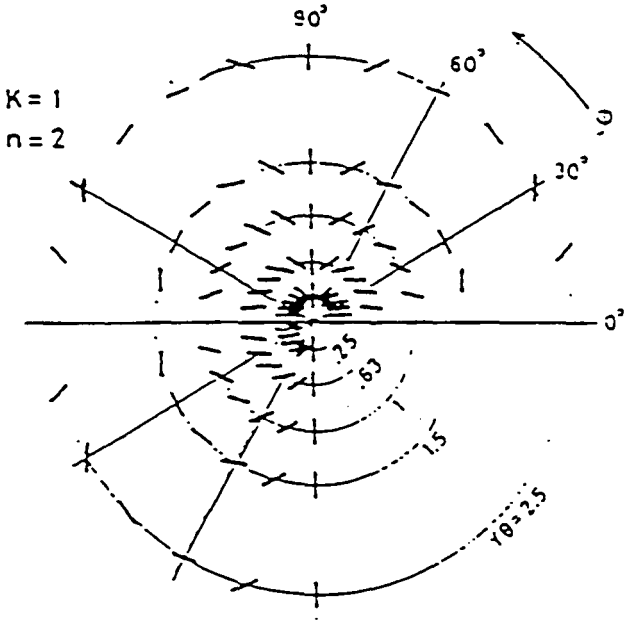

H.Kitamura, Jap. J. of Appl. Phys., vol. 19, No.4, 1980, p. L185

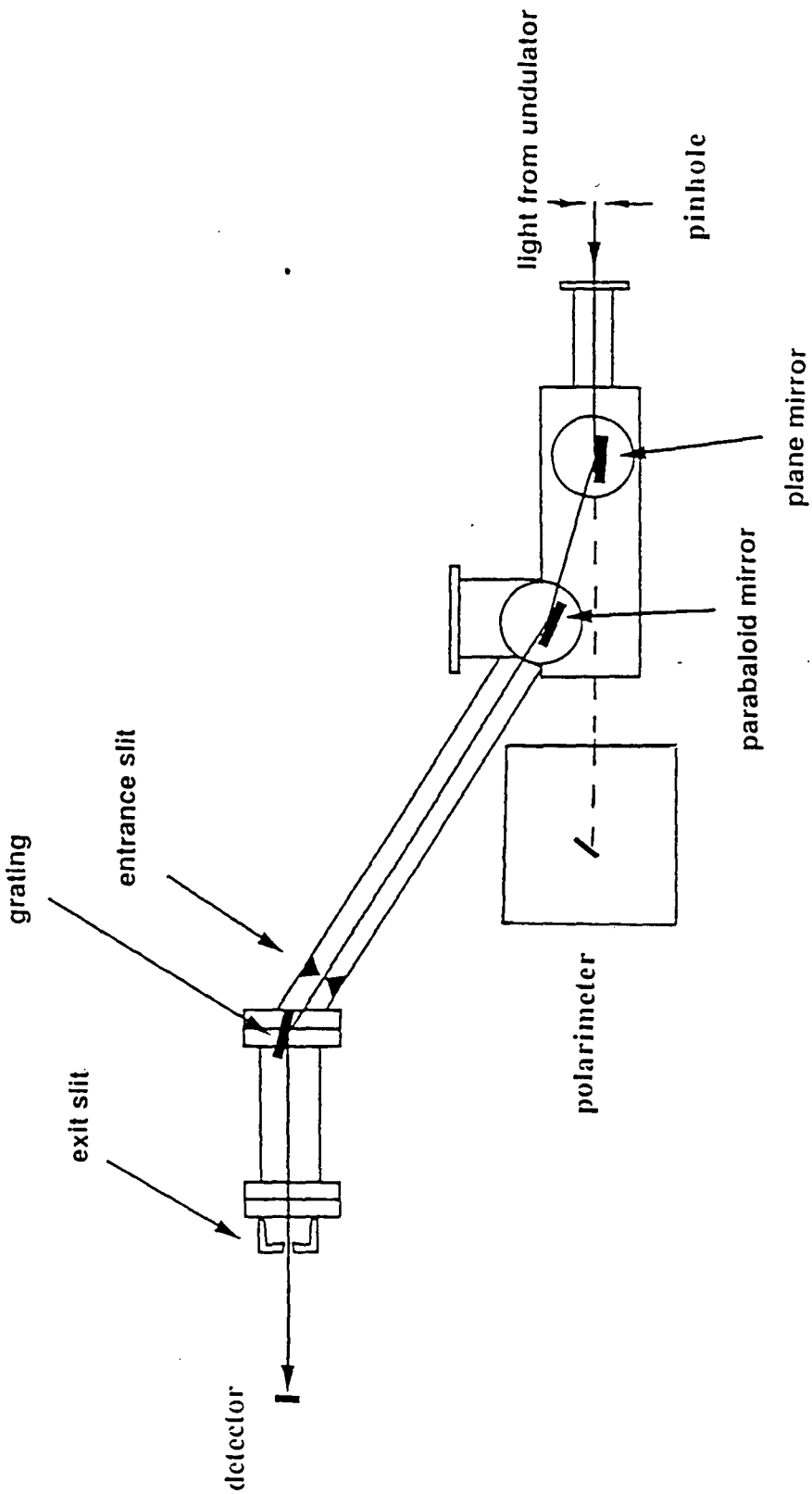
light from undulator
pinhole
plane mirror
parabaloid mirror
polarimeter
grating
entrance slit
exit slit
detector

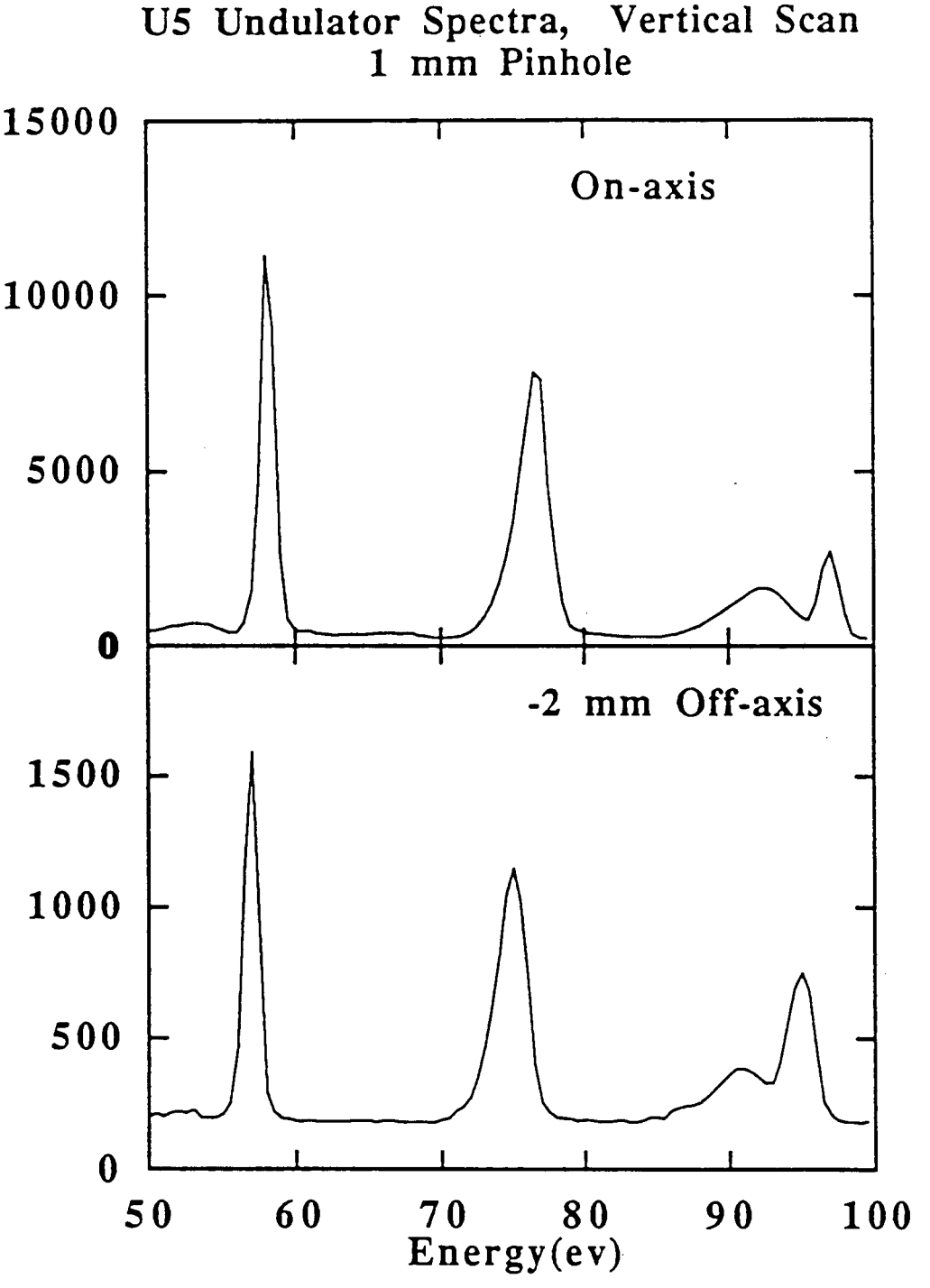
U5 Undulator Spectra, Vertical Scan
1 mm Pinhole
15000
10000
5000
0
On-axis
-2 mm Off-axis
1500
1000
500
0
50
60
70
80
90
100
Energy(ev)

U5 Undulator Spectra, Horizontal Scan
1 mm Pinhole

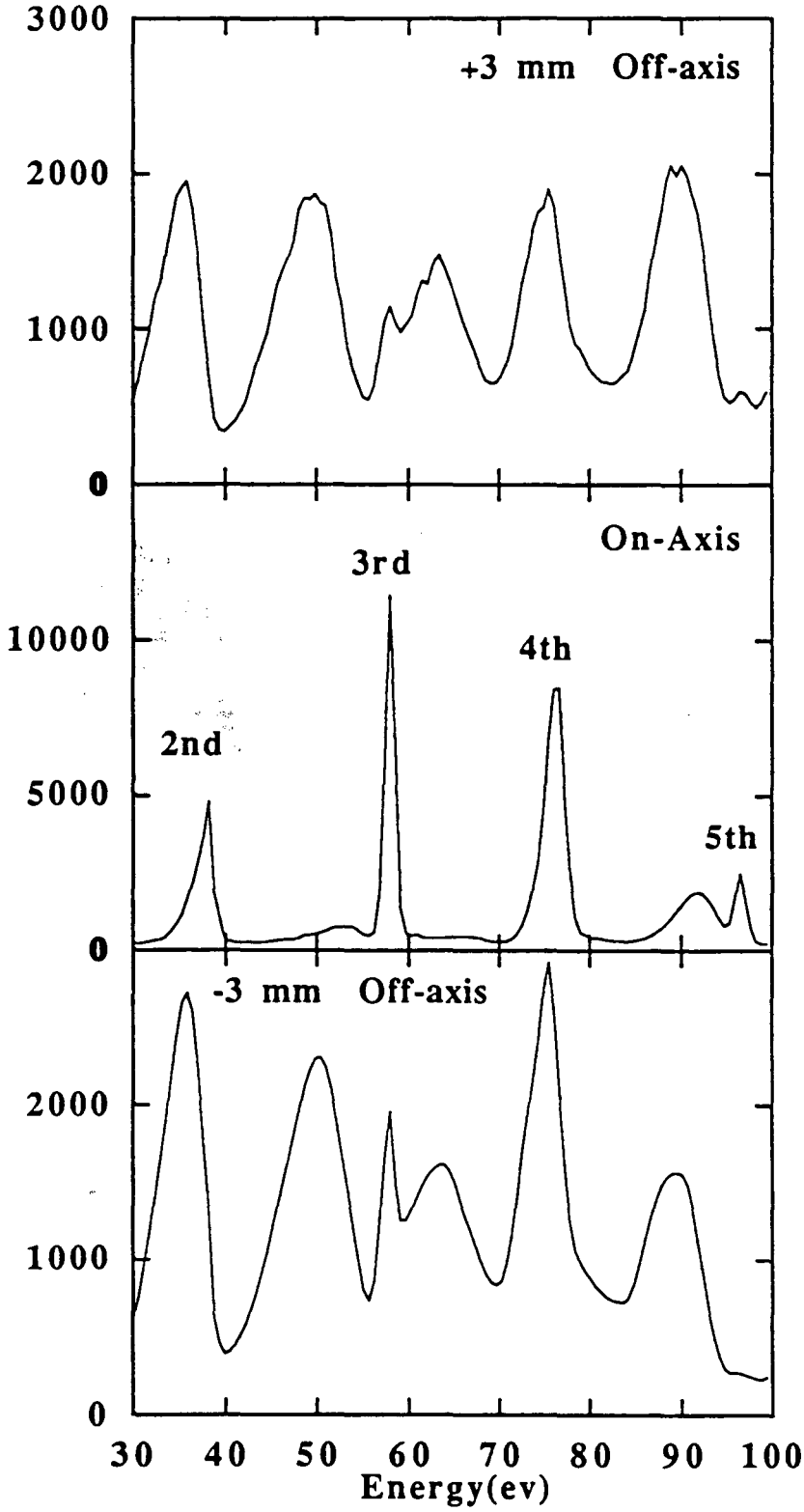

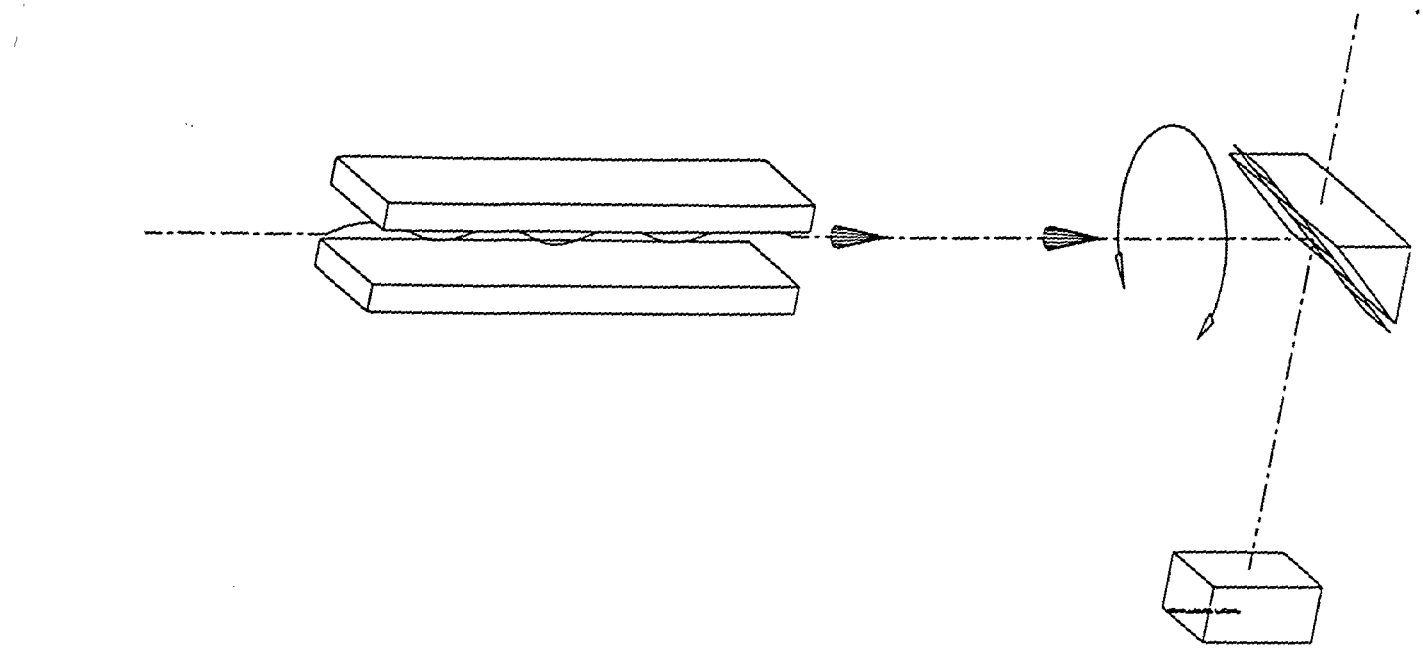

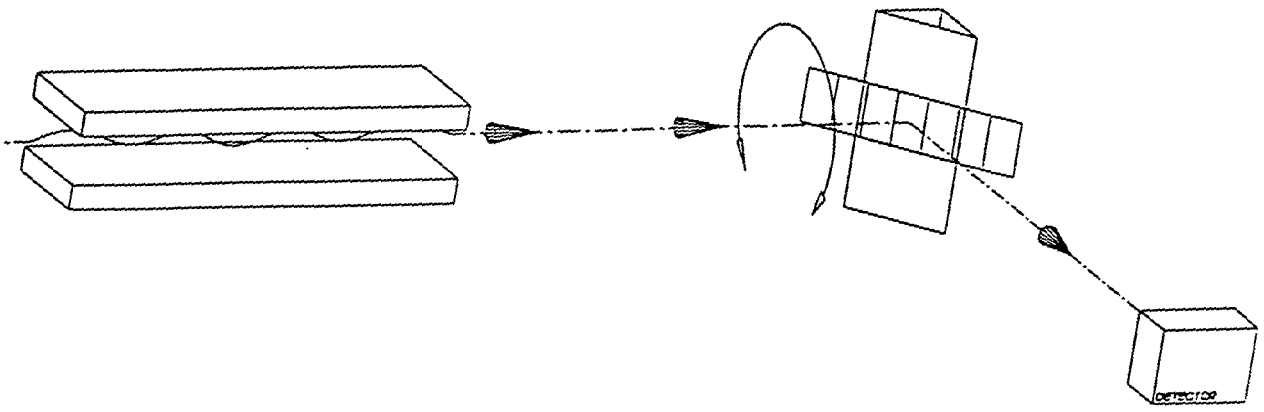
DETECTOR

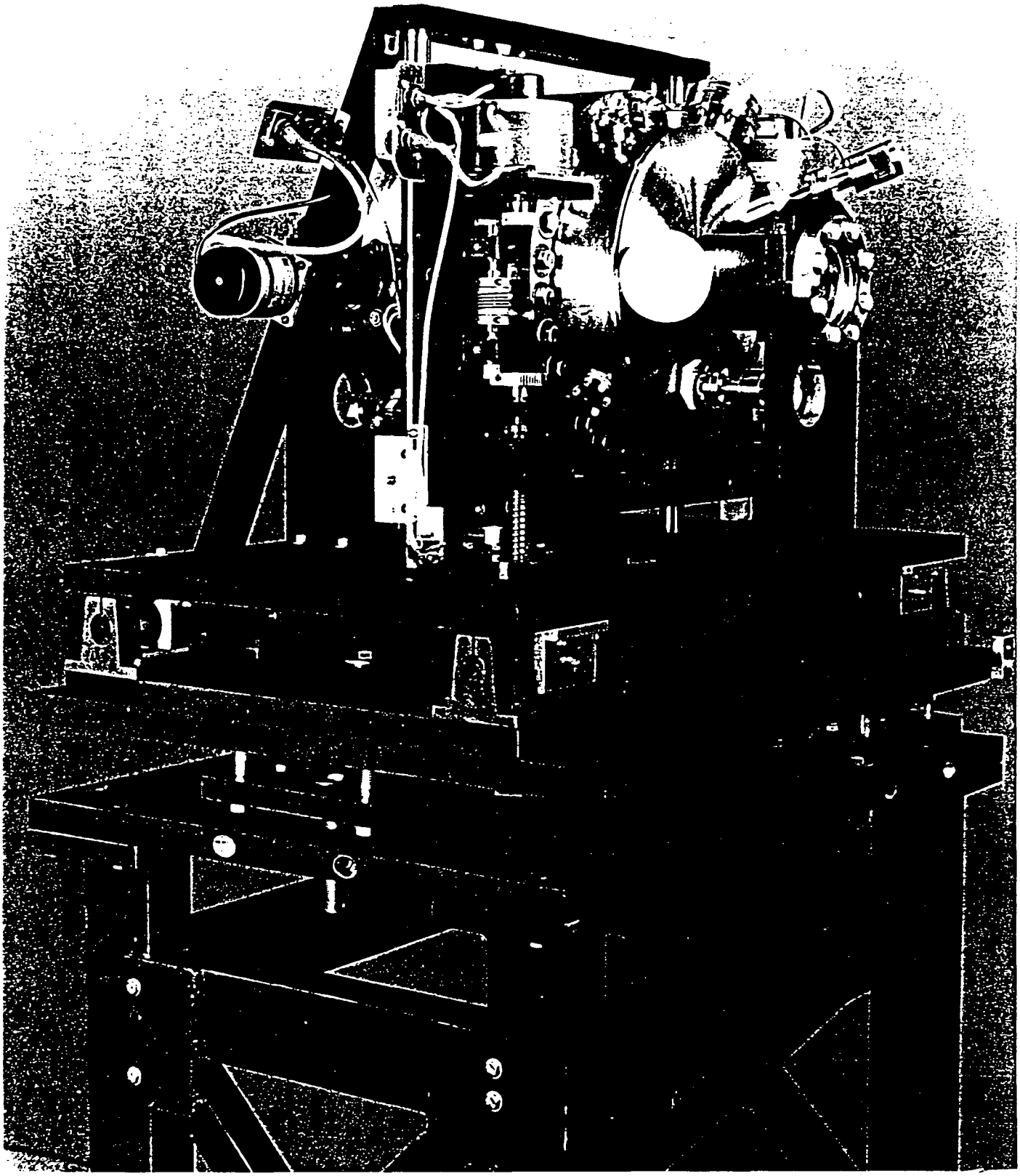

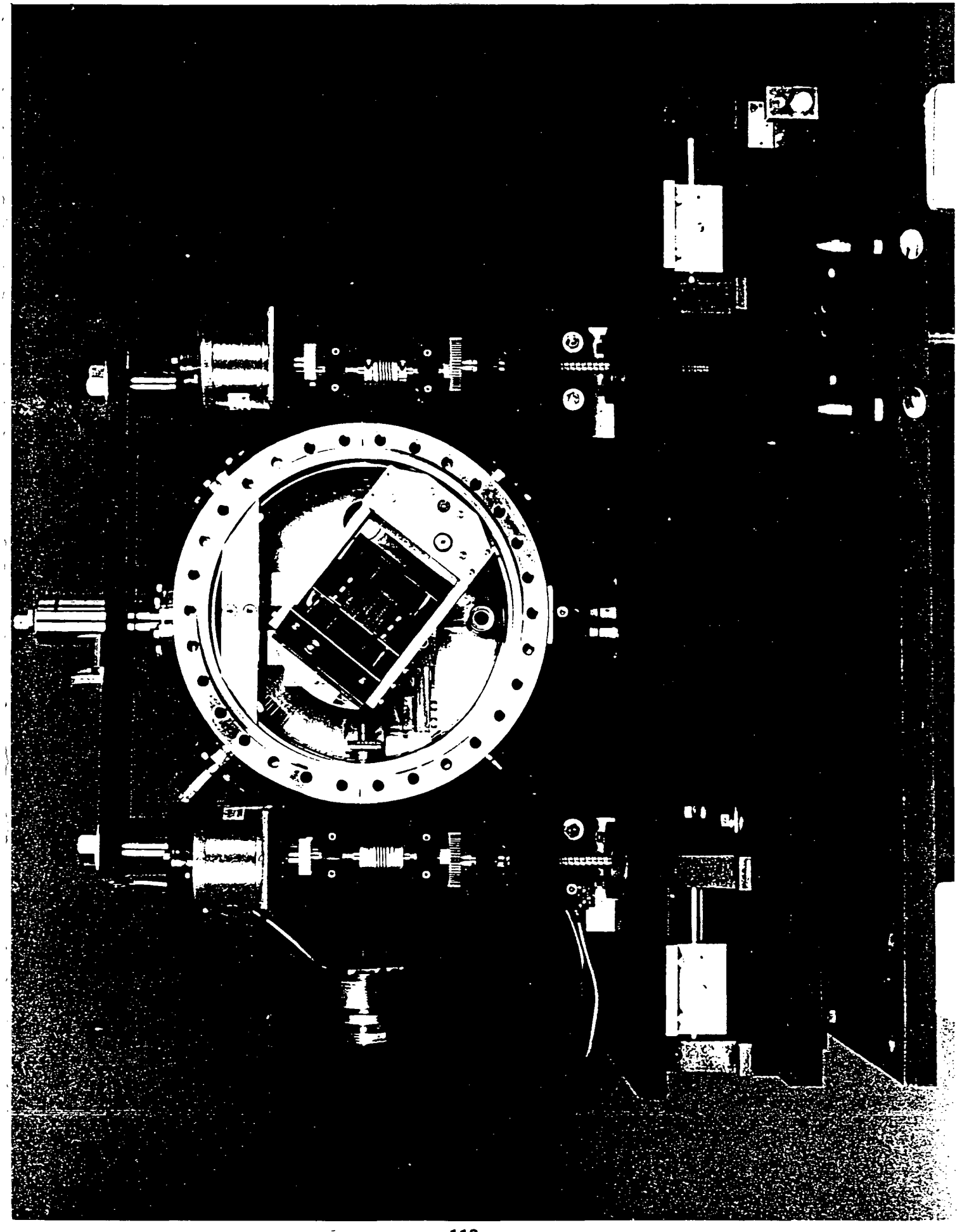

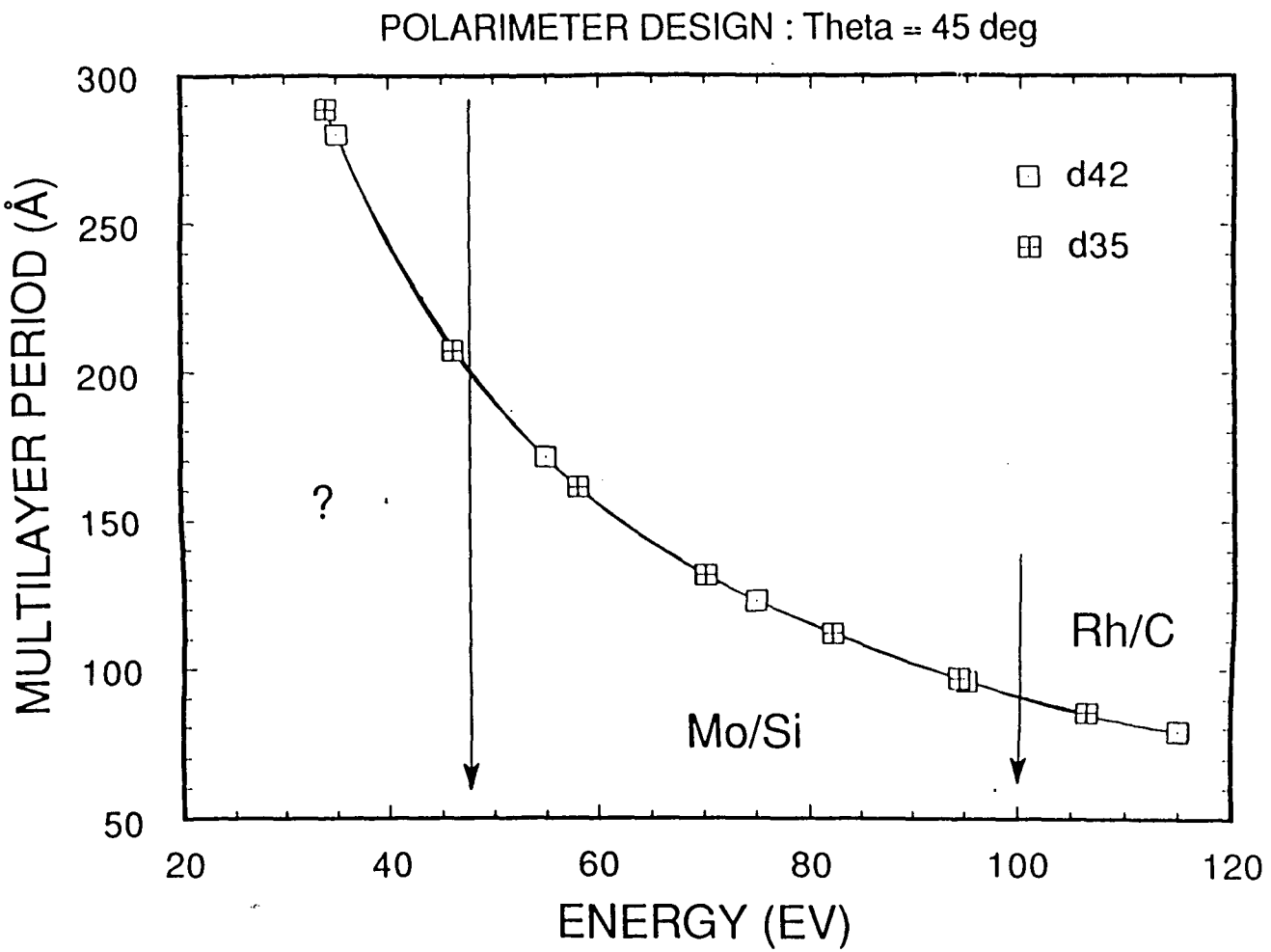
POLARIMETER DESIGN : Theta = 45 deg
MULTILAYER PERIOD (Å)
300
250
200
150
100
50
20
40
60
80
100
120
ENERGY (EV)
d42
d35
?
Mo/Si
Rh/C

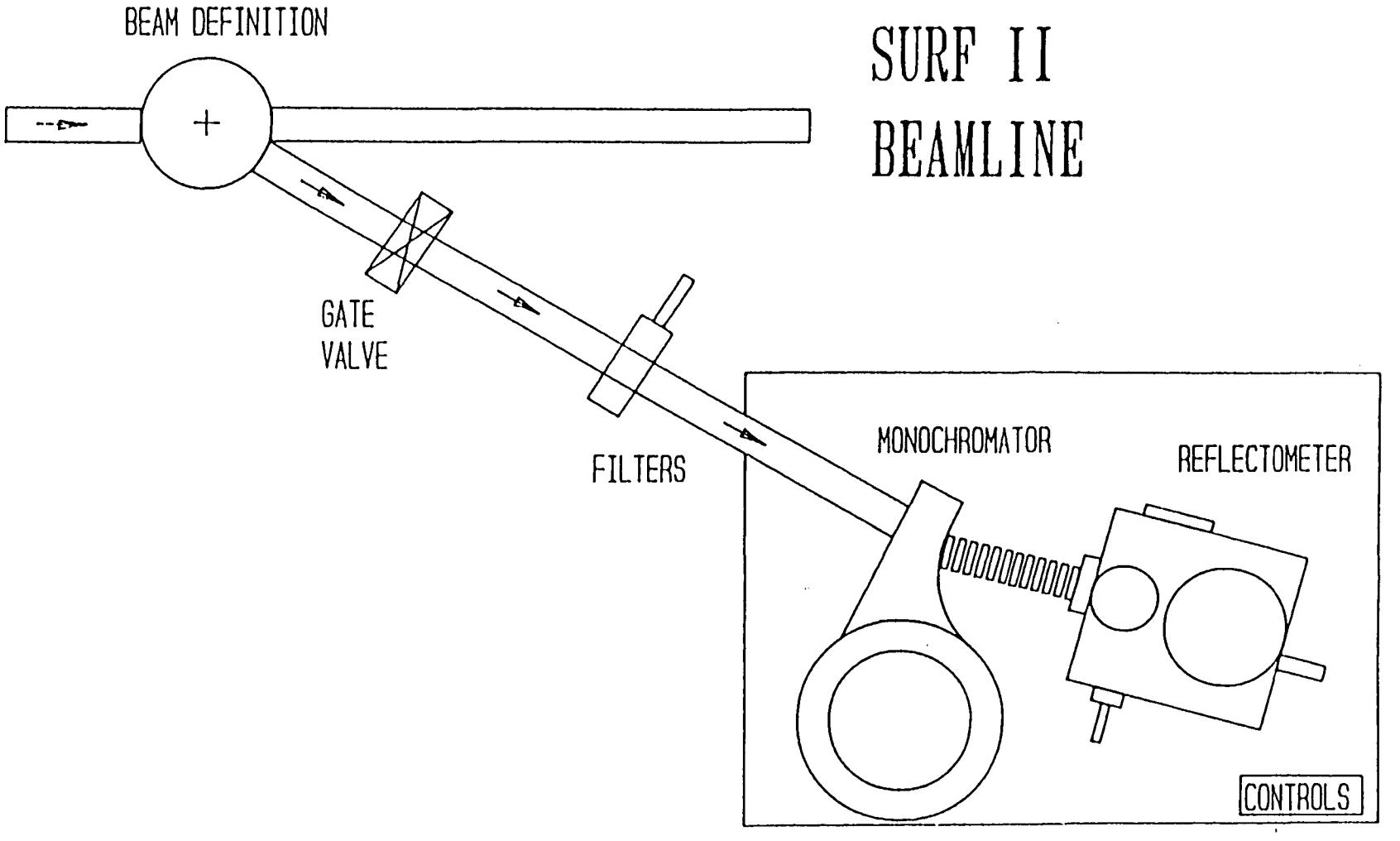
BEAM DEFINITION
SURF II
BEAMLINE
GATE
VALVE
FILTERS
MONOCHROMATOR
REFLECTOMETER
CONTROLS

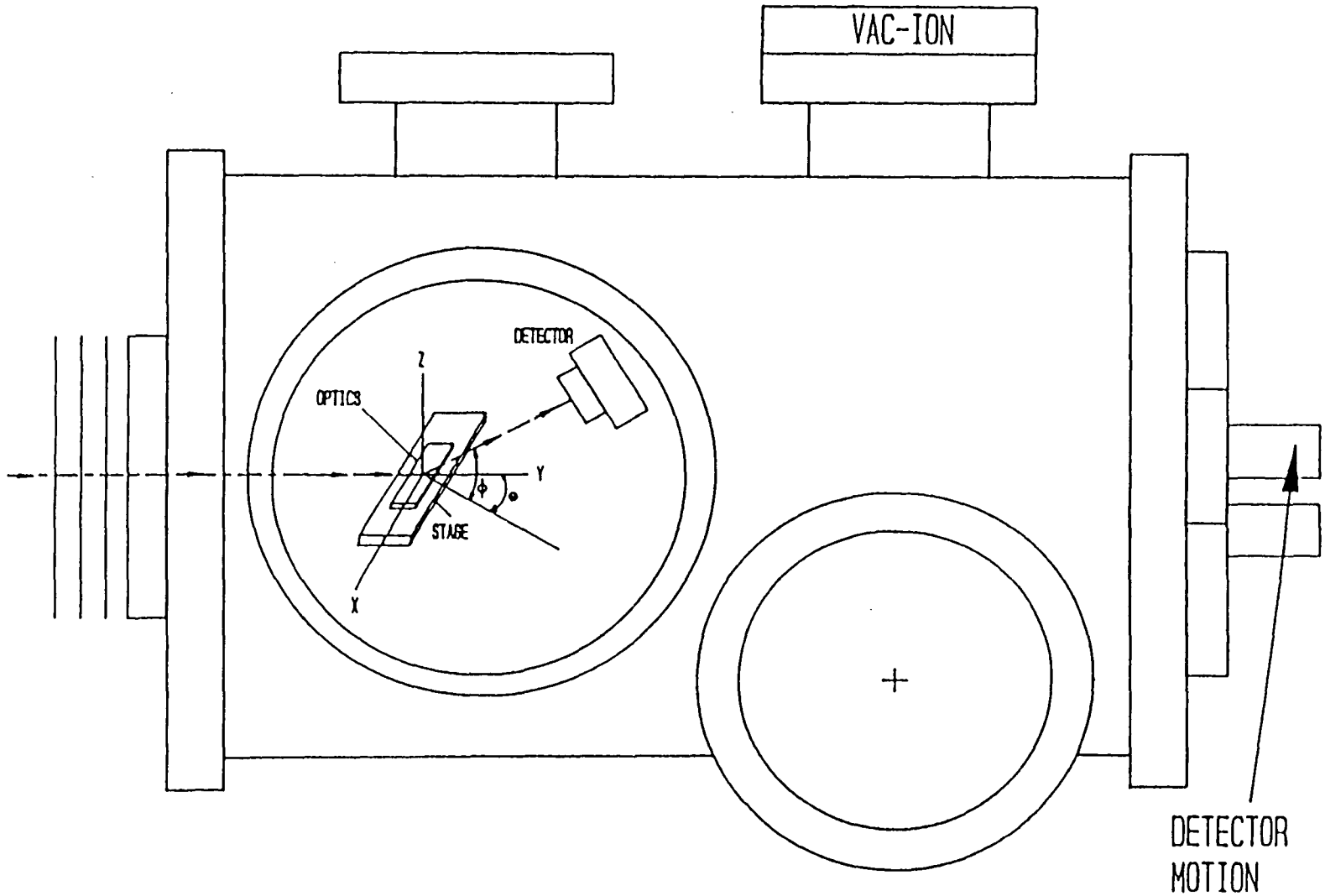

REFLECTOMETER

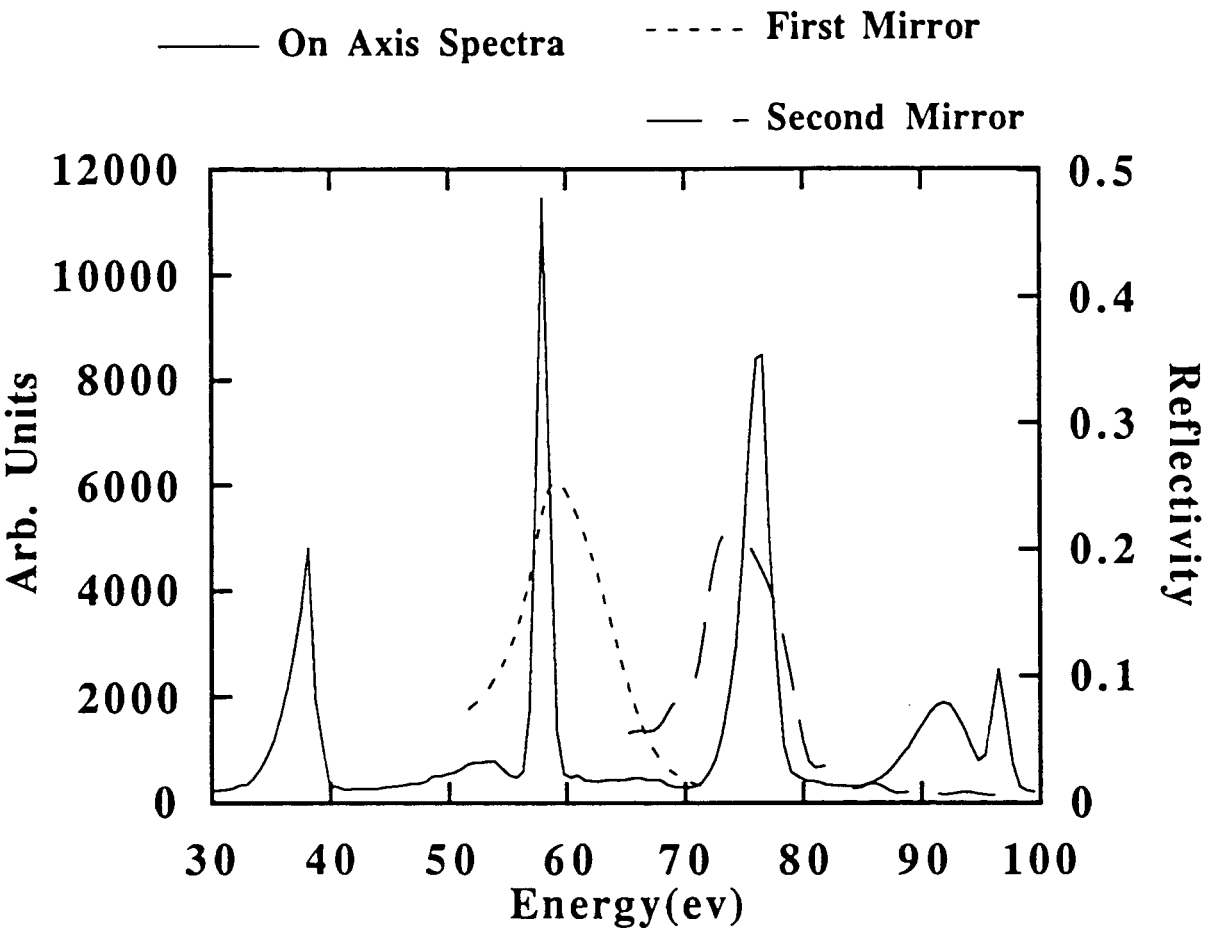
On Axis Spectra
First Mirror
Second Mirror
12000
10000
8000
6000
4000
2000
0
Arb. Units
0.5
0.4
0.3
0.2
0.1
0
Reflectivity
30
40
50
60
70
80
90
100
Energy(ev)

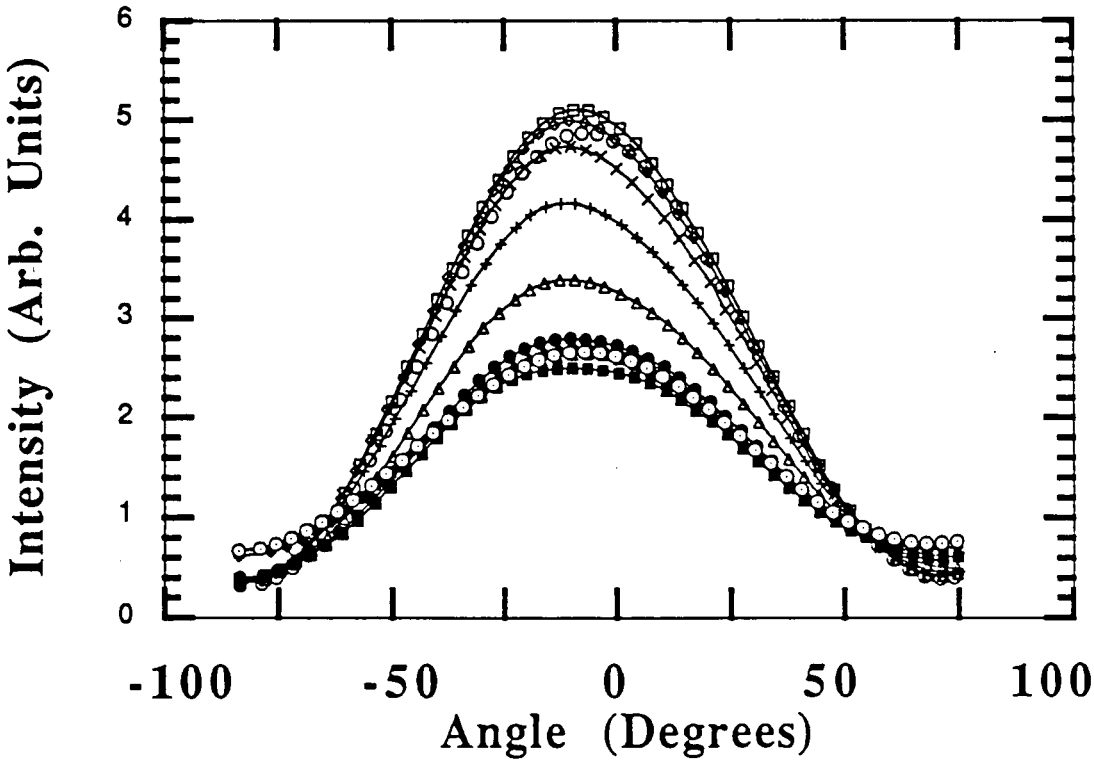
Intensity (Arb. Units)
6
5
4
3
2
1
0
-100
-50
0
50
100
Angle (Degrees)

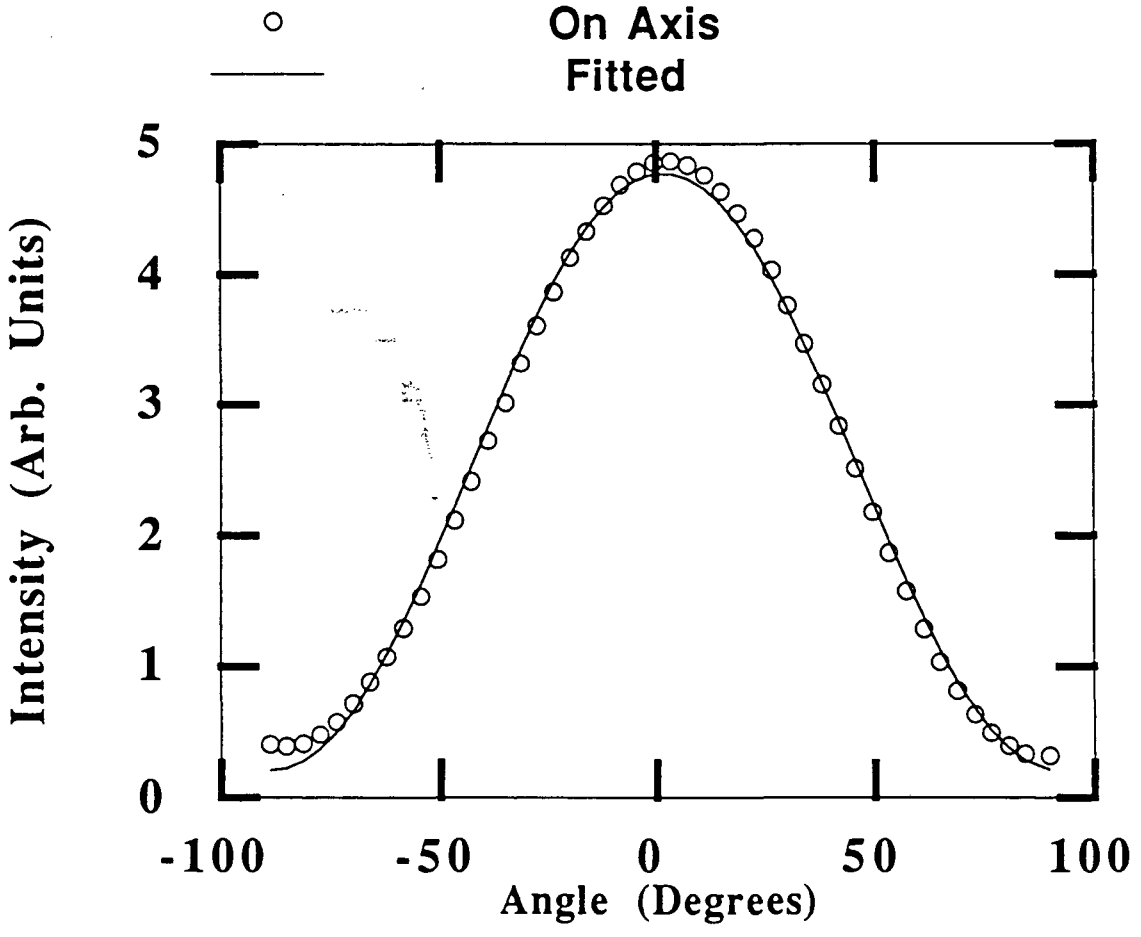
On Axis
Fitted
Intensity (Arb. Units)
5
4
3
2
1
0
-100
-50
0
50
100
Angle (Degrees)

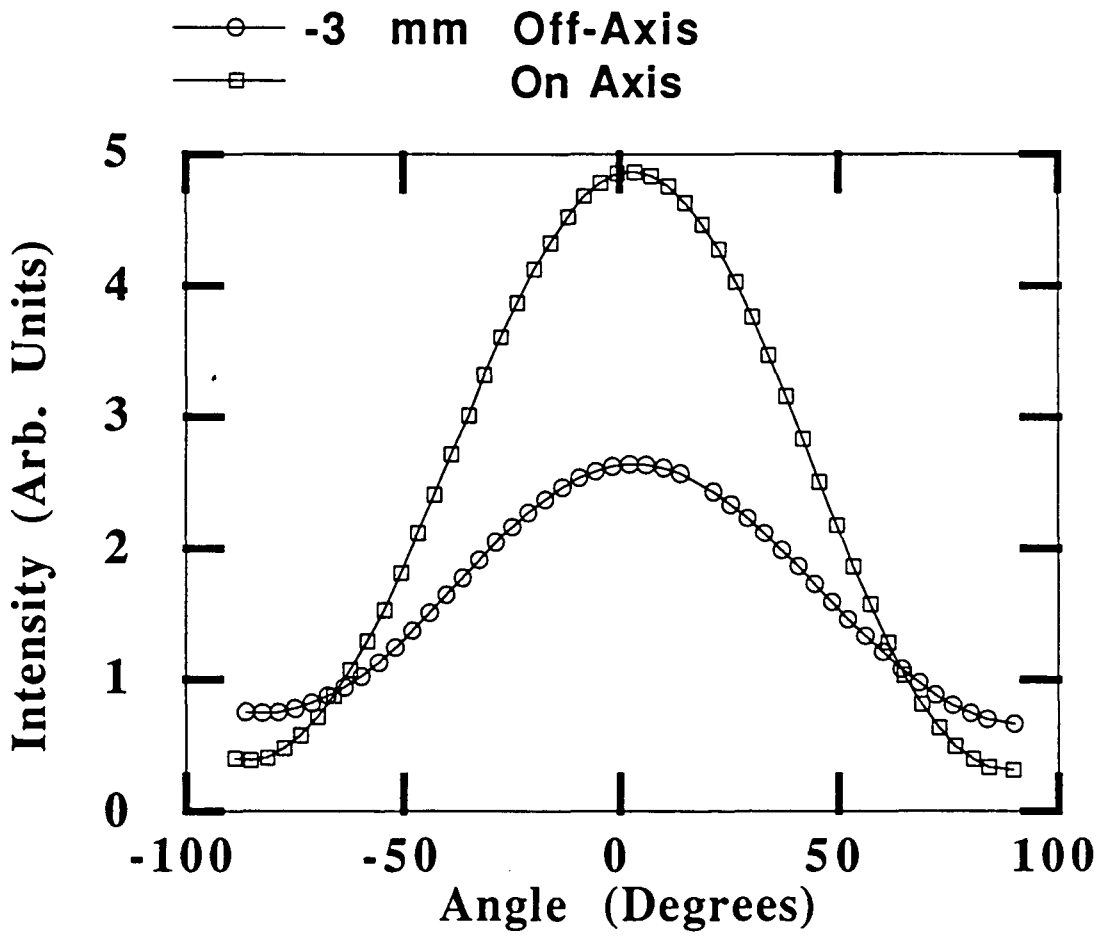
-3 mm Off-Axis
On Axis
Intensity (Arb. Units)
5
4
3
2
1
0
-100
-50
0
50
100
Angle (Degrees)

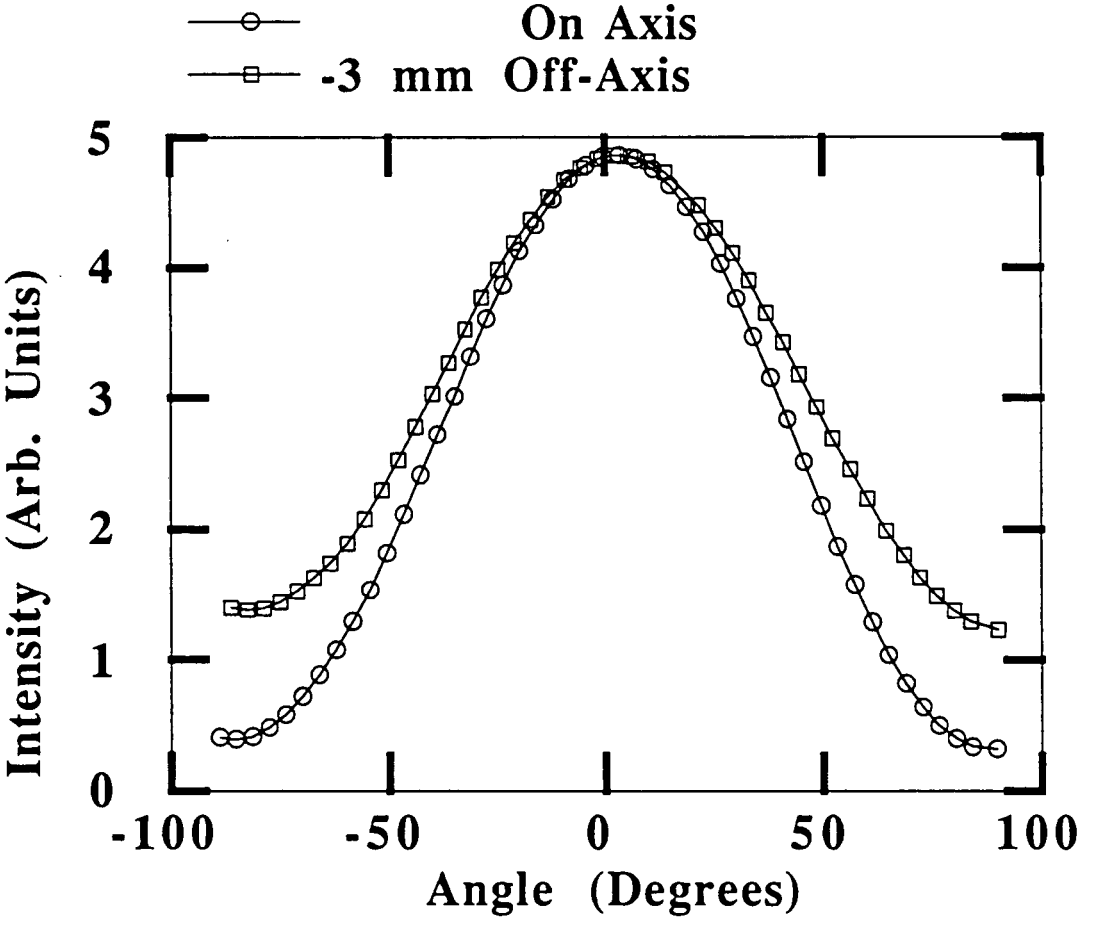
On Axis
-3 mm Off-Axis
Intensity (Arb. Units)
0
1
2
3
4
5
-100
-50
0
50
100
Angle (Degrees)

Soft X-Ray Phase Retardation Using Multilayer Optics

J.B. Kortright

Lawrence Berkeley Laboratory

Soft X-ray Phase Retardation Using Multilayer Optics

Jeffrey B. Kortright
Center for X-ray Optics
Lawrence Berkeley Laboratory

Optical elements having specific polarization properties, such as linear polarizers and quarter-wave plates, are required to fully characterize and exploit the polarization of photon beams. In addition, such optical elements can be used to generate beams with specific polarization states, and to modulate those states, thus easing the demands on complex and expensive sources capable of polarization control. The realization of such optics for the soft x-ray region, especially phase retarders, is an area of ongoing research.

The polarization dependence of Thompson (charge) scattering, together with the enhanced reflectance of multilayers, provide several useful phenomena which can be used to control the polarization of extreme ultraviolet and soft x-ray beams. Linear polarizers result by adjusting conditions so that the multilayer Bragg reflectance peak is very close to 45° (total scattering angle 90°), so that the component of the radiation field with electric vector in the scattering plane is extinguished by its extremely small reflectance at this angle. Such linear polarizers have been investigated by various groups and can produce beams with a high degree of linear polarization.

Phase retardation, or the difference in phase change of two components on interaction with a sample or optic, can be obtained using either the reflected or transmitted beam after interaction with a multilayer,[1] as in Figure 1. Calculations, illustrated in Figure 2, show that a beam with $h\nu \approx 100$ eV transmitted through an ideal free-standing multilayer can experience phase retardations approaching 90°. Recent experiments confirm these predictions by measuring large phase retardations on transmission through free-standing Mo/Si multilayers at $h\nu = 98$ eV.[2] These free-standing structures

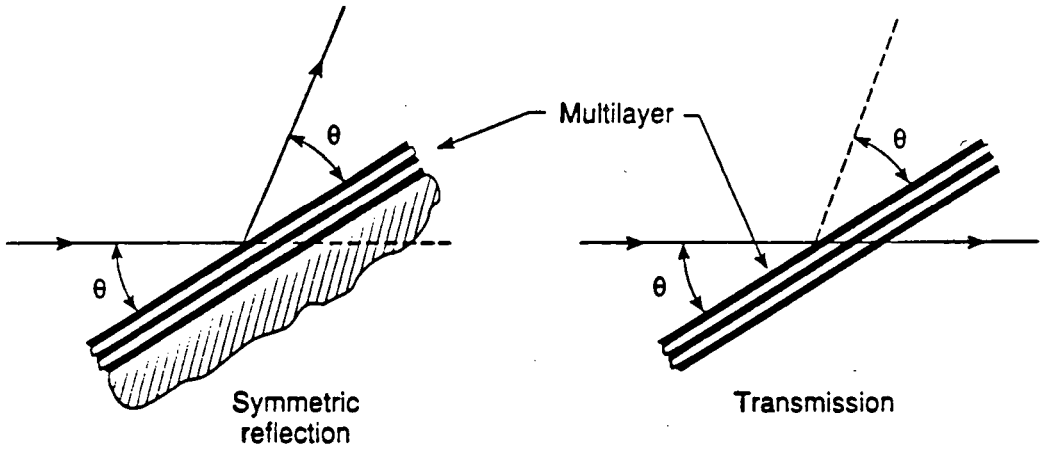

Figure 1. Multilayer x-ray interference coatings offer different possibilities to obtain phase retardation in both reflection and transmission geometries [from ref. 1].

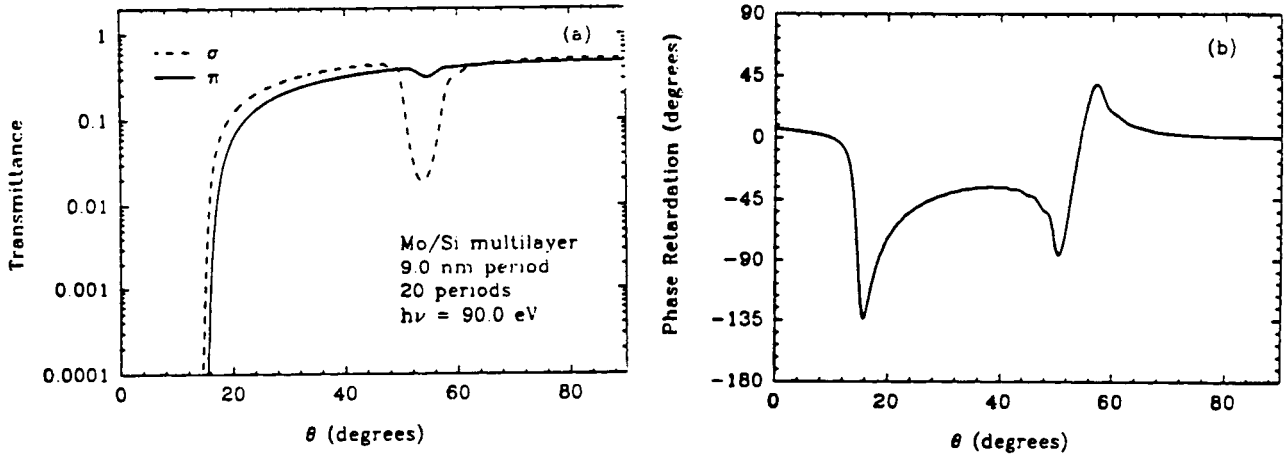

Figure 2. Calculated transmitted intensity for σ and π components through a Mo/Si multilayer is in (a). The phase retardation, or difference in phase for the two components on transmission is is (b).

are not ideal, however, and there is room for improved sample preparation techniques, which may lead to improved performance of transmission multilayer phase retarders. Other experiments are investigating the reflection multilayer case for phase retardation.[3]

As $h\nu$ increases above 100 eV into the soft x-ray, the magnitude of phase retardation obtainable with transmission multilayers decreases as the optical constants of materials decrease and since multilayers having smaller periods are less ideal. The high energy limit of multilayer phase retarders is not established at this point. For a range from less than 300 eV to at least 3000 eV there

are ro demonstrated optical techniques to obtain significant values of phase retardation.

This work was supported by the Director, Office of Energy Research, Office of Basic Energy Sciences, Materials Sciences Division, of the U.S. Department of Energy under Contract No. AC03-76SF00098.

References

1. J.B. Kortright and J.H. Underwood, NIM, **A291**, 272 (1990).

2. J.B. Kortright, M. Yamamoto, M. Yanagihara, H. Kimura and T. Namioka, to be published.

3. M. Yamamoto, M. Yanahihara, H. Kimura, T. Maehara, H. Nomura, and T. Namioka, to be published in the proceedings of SRI 91.

Soft X-ray Phase Retardation

Using Multilayer Optics

Jeffrey B. Kortright
Center for X-ray Optics
Lawrence Berkeley Laboratory

Polarization control with soft x-ray optics?

linear polarizer

phase retarder (e.g., ¼-wave plate)

⇒ considerable experimental capabilities

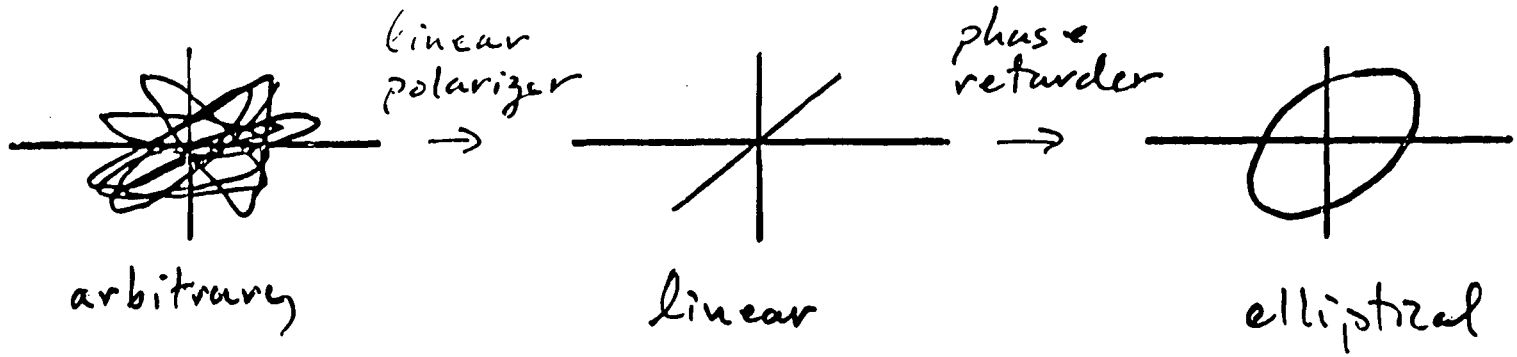

Overview of talk:

- simple physics underlying soft x-ray polarization phenomena presented here
- theoretical examples of what ideal total reflection and multilayer mirrors can do
- early experimental results of soft x-ray phase retardation with multilayers
- summary and prospects for future

Polarization dependence of Thompson (charge) scattering provides basis for polarization control with optics.

---

electrons

$$I_e \propto \begin{cases} |e^2/mc^2|^2, & \sigma \\ |e^2/mc^2|^2 \cos^2 2\theta, & \pi \end{cases}$$

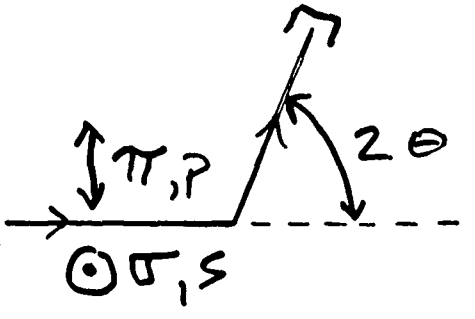

atoms

$I_{atom} \propto I_e \cdot f$, atomic scattering factor $f(\omega,q) = f_o(q) + f'(\omega) + if''(\omega)$

solids (elemental)

$$\hat{n}(\omega) = 1 - \delta(\omega) - i\beta(\omega)$$

$$\delta(\omega) = (N\lambda^2 I_e/2\pi)\cdot[f_o(q) + f'(\omega)]$$

$$\beta(\omega) = (N\lambda^2 I_e/2\pi)\cdot f''(\omega)$$

(N = # density)

Total reflection mirrors

offer little promise as phase retarders in soft x-ray.

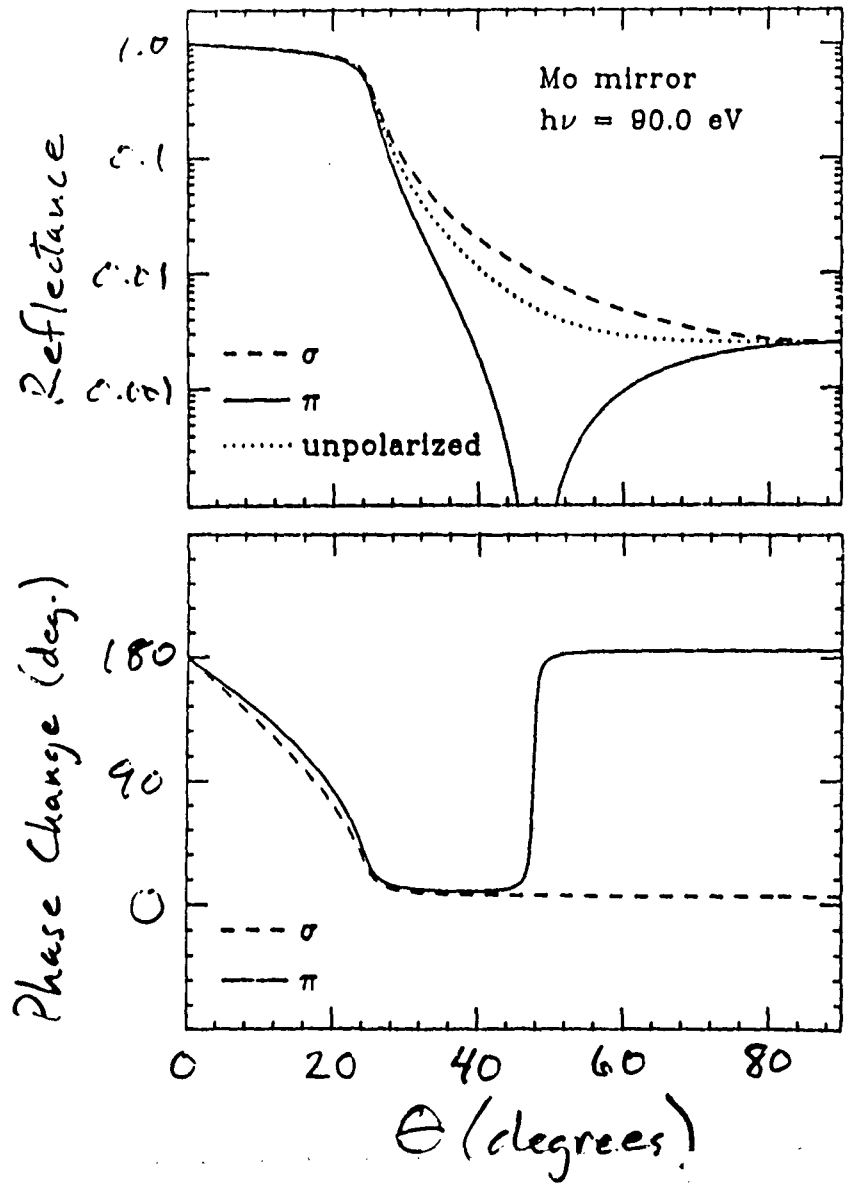

Phase Retardation =

σ phase change − π phase change

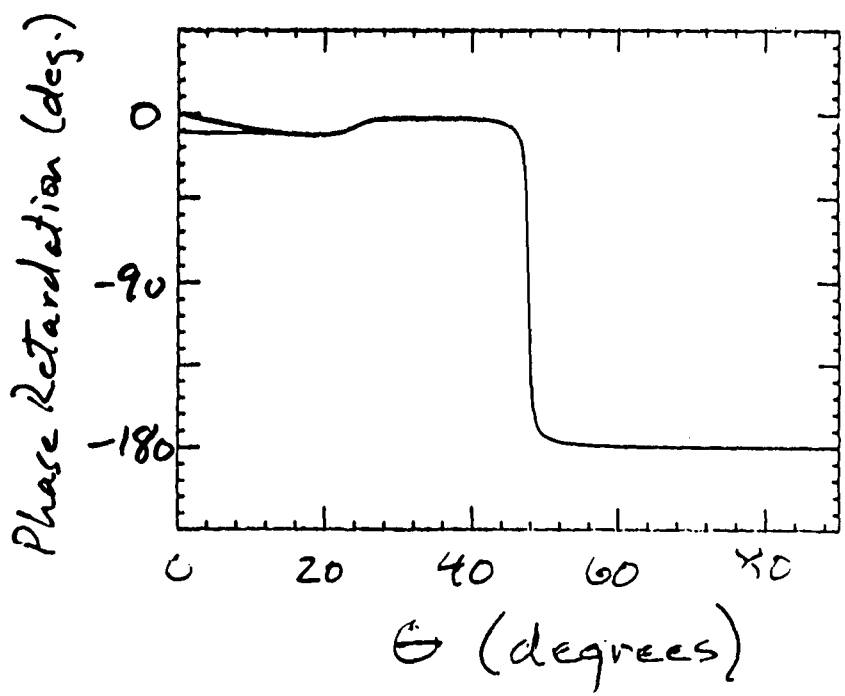

Multilayer mirrors provide increased reflectance,
and additional phase retardation effects.

J.B. Kortright and J.H. Underwood, NIM, A291, 272 (1990)

$\lambda = 2d \sin\theta$, d = multilayer period

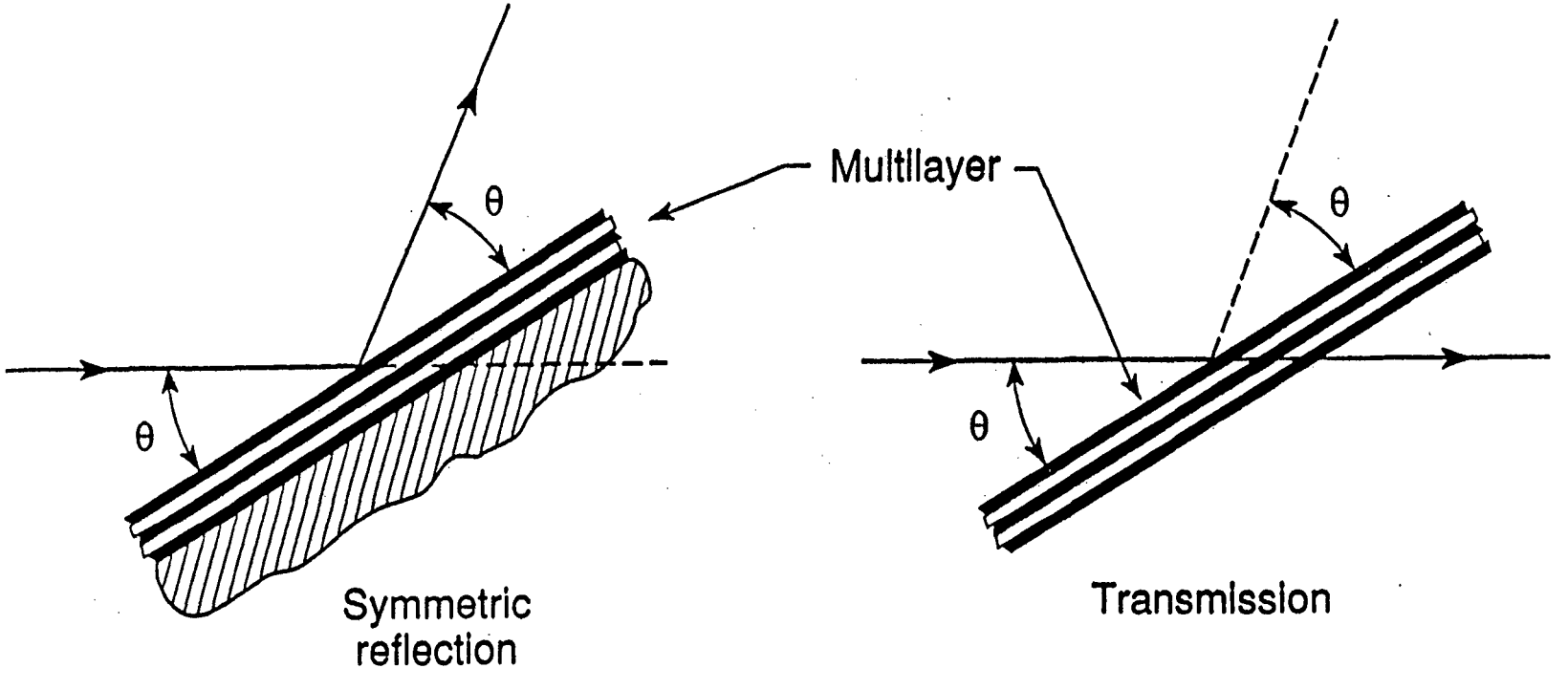

Mo/Si Multilayer Mirrors for $h\nu \leq 100$ eV

T.D. Nguyen, R. Gronsky, J.B. Kortright (CXRO/NCEM)

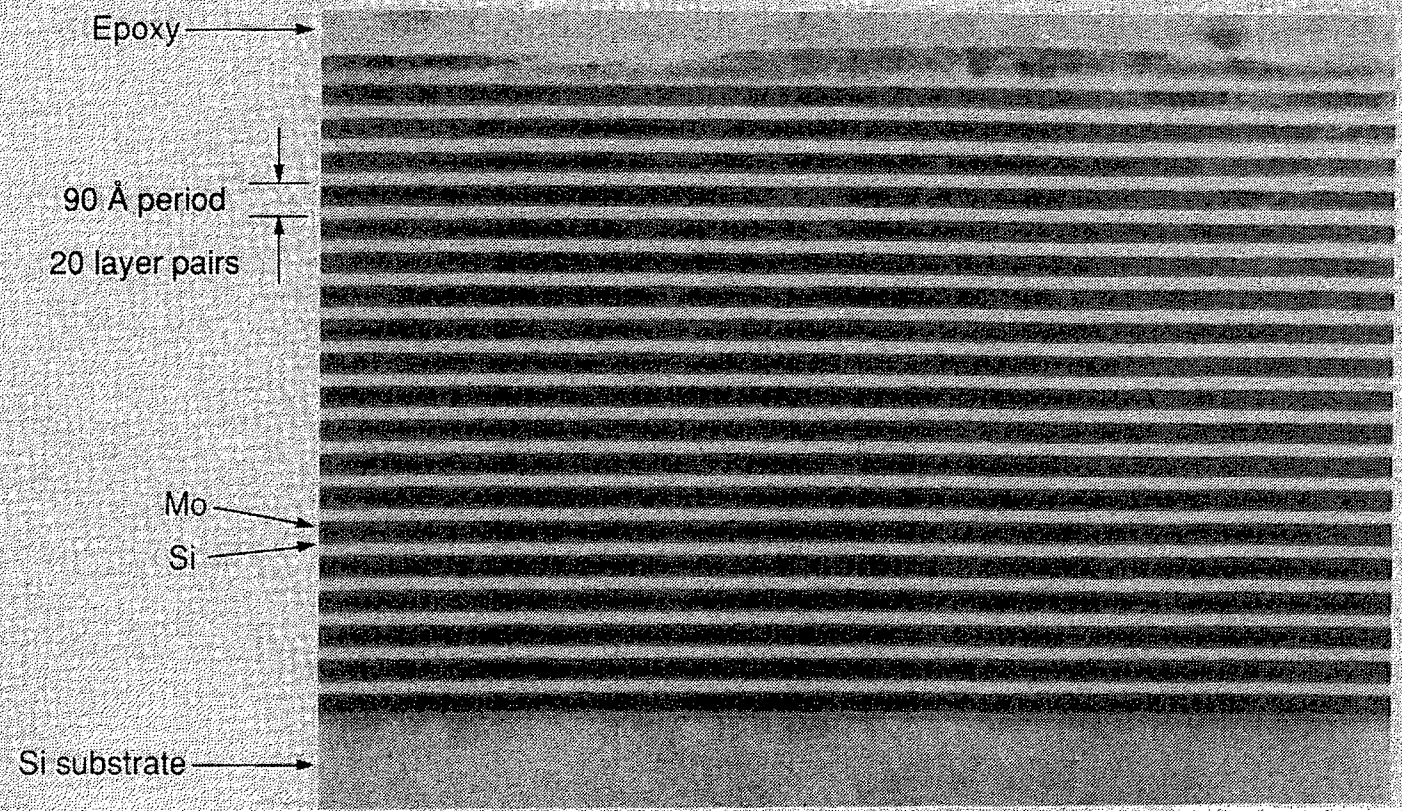

JEOL 200 CX — high resolution TEM — bright field image

XBB 8911-9902

Reflection multilayer case: phase change across Bragg peak, and different response for σ and π when $\theta \approx 45°$, predict phase retardation.

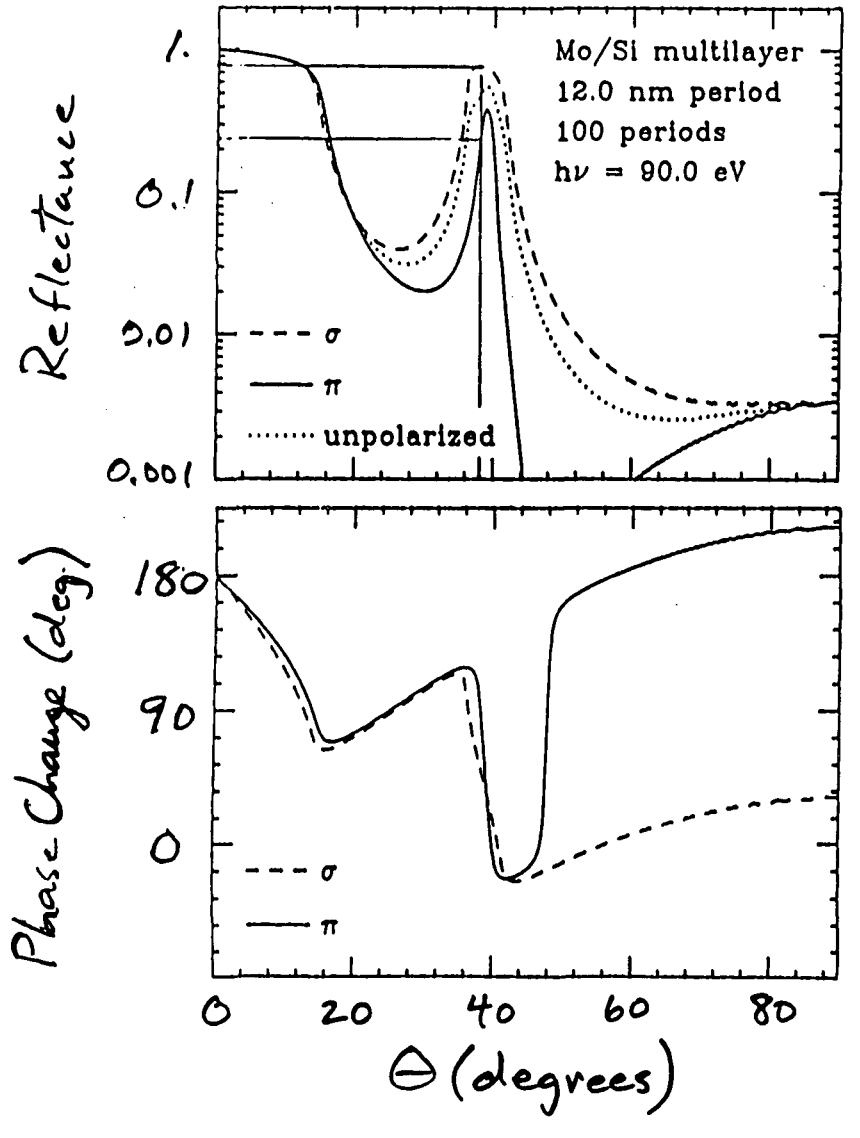

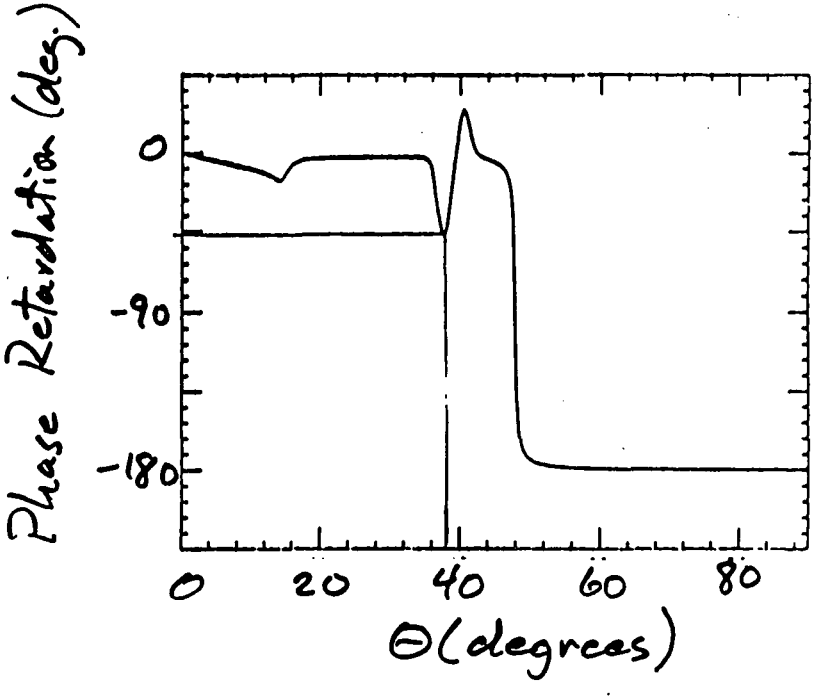

Transmission multilayer case: σ and π components experience different effective refractive index when $\theta \approx 45°$ (standing waves). Large retardation predicted.

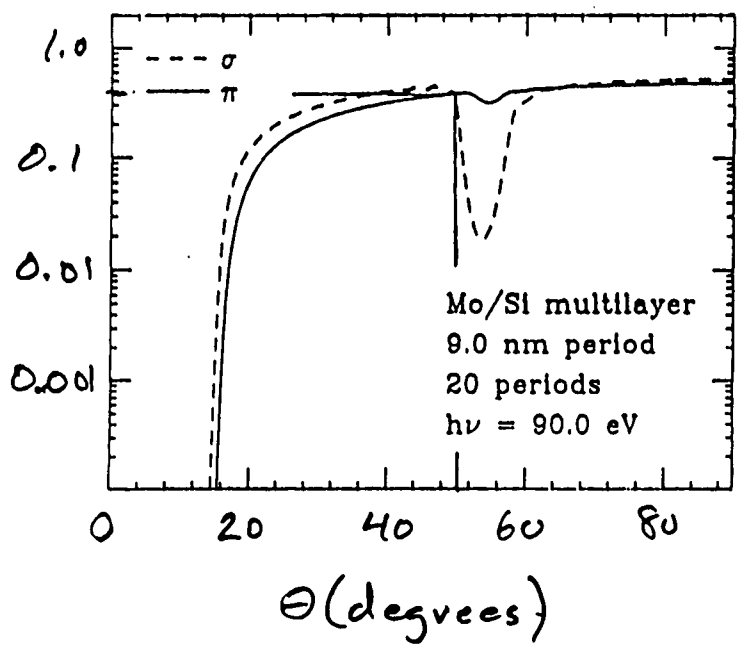

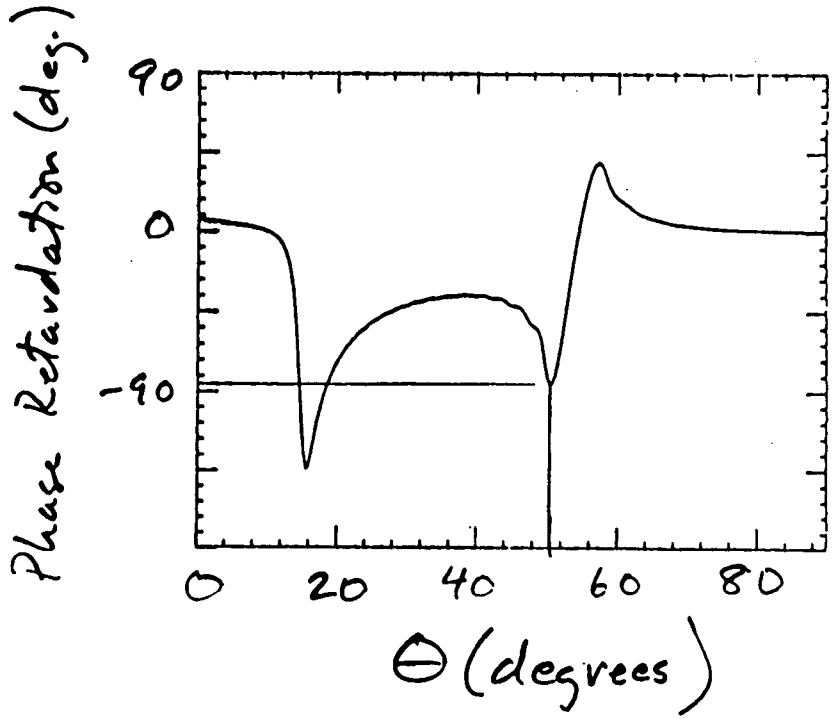

Measurement of phase retardation of transmission sample uses two linear polarizers.

---

collaborators M. Yamamoto, M. Yanagihara, H. Kimura and T. Namioka
Tohoku University, Sendai, JAPAN

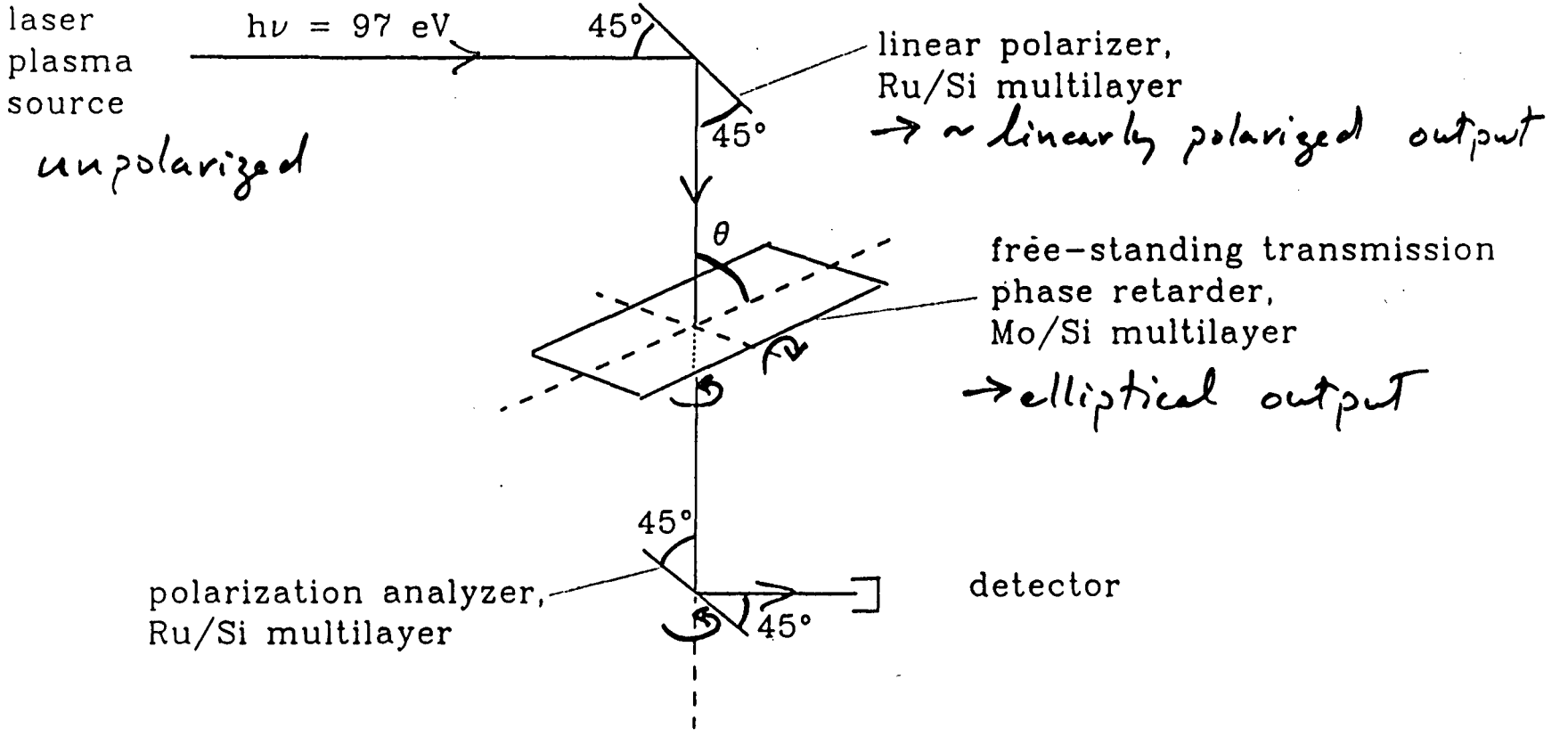

Conclusions from first transmission multilayer phase retarder measurements

- Calculations predict larger phase retardation for transmission than for reflection.
- Free-standing transmission multilayers can be made, but are not perfect.
- Measured 50° retardation, compared to 75° predicted for ideal structure. $T \simeq .25$
- Further study warranted.

Other considerations of transmission multilayer phase retarders

- Modulation of polarization is possible (e.g., left ↔ right).

- Multilayer phase retarders are chromatic.

  Tunability of order of multilayer bandwidth (1 - 10%)

- Difficulties obtaining significant retardation to shorter λ:
  - optical constants $\propto \lambda^2$, less contrast
  - multilayers are less ideal as d decreases ($d \approx \lambda/2\sin(45°)$)

- Durability of free-standing transmission structures

Summary and future directions: Optics offer significant capabilities

Optical elements

- linear polarizers exist
- linear phase retarders with significant retardation appear feasible
- ⇒ can think of extending traditional optical techniques into EUV/soft x-ray

Applications

- analyze polarization state of synchrotron beam, or signal from sample
- generate beams with specific polarization properties of use in experimentation

BEND MAGNET - convert linear part to elliptical

Chemistry, Chemical Physics, and Biochemistry

P.A. Snyder

Florida Atlantic University

CHEMISTRY, CHEMICAL PHYSICS, AND BIOCHEMISTRY

Patricia Ann Snyder

A source of modulated circularly polarized synchrotron radiation is needed in a number of areas of research in chemistry and biochemistry. In general, these types of experiments entail the measurement of small differences in large numbers with the result that modulation techniques are necessary unless the signal is unusually large. To date, there have been two approaches to synchrotron radiation research that requires variable polarization. The first is to convert the linear polarization of synchrotron radiation to modulated circular polarization through the use of a modulated quarter wave retarder.[1] (Beamline and monochromator design are important for obtaining linear polarization.) This approach (pioneered by P.A. Snyder) has been used very successfully to study natural and magnetic circular dichroism with synchrotron radiation.[1–6] It is a modification of methods pioneered by workers using conventional sources in the vacuum ultraviolet;[7–15] however, the use of synchrotron radiation allows measurements to be made to higher energies and with better resolution. Since the initial measurements, a number of other investigations have used this approach with synchrotron radiation,[16–23] but were limited to wavelengths longer than 125 nm because the quarter wave modulator is constructed of calcium fluoride.

The second approach is to use out-of-plane polarization of synchrotron radiation. As you go out of plane, the radiation becomes elliptically and then circularly polarized. Unfortunately, as you go out of plane, the intensity decreases, and large horizontal acceptances are needed for the monochromator. (Fifty milliradians has been used.) In addition, the ability to modulate becomes more difficult. However, this method has the advantage that it is not limited by the transmission of calcium fluoride. It has been used successfully by Heinzman *et al.* for spin-resolved photoelectron studies,[24,25] but an attempt to use it for natural circular dichroism measurements in the vacuum ultraviolet region was unsuccessful.[26] Recently, however, the use of this approach was demonstrated for photoelectron studies of carbon monoxide adsorbed on a Pd (111) surface.[27] The signal was predicted and observed to be relatively large.

A source of modulated circularly polarized radiation at high energies could be used for development of the following areas of research in chemistry, chemical physics, and biochemistry:

1. Magnetic circular dichroism measurements

    a. Study of electronic structure
    b. Study of interactions
    c. Magnetic circular dichroism near absorption edges

d. Analytical uses
e. Comparison with theory
f. Perhaps information about predissociation
g. Understanding photochemistry
h. Studies of electronic structure changes as one goes from gas, to matrix, to solid

2. Natural circular dichroism measurements

   a. Study of electronic structure
   b. Conformational information
   c. Kinetic studies
   d. Comparison with theory
   e. Two-photon circular dichroism
   f. Circular dichroism near absorption edges
   g. Interactions between molecules

3. Circular intensity differential scattering (structural information on chiral objects)

4. Fluorescence circular dichroism measurements

   a. Interactions
   b. Fluorescence of metal in a chiral environment

5. Linear and circular differential imaging (microscopic image without staining or destructive treatments)

6. Stereochemical photosynthesis.

At this time, my particular interests are circular intensity differential scattering (CIDS) experiments and magnetic and natural circular dichroism measurements near absorption edges. The CIDS measurements are being made in conjunction with M. Maestre and C. Bustamante, pioneers in CIDS measurements in the visible region.[28] In fact, we will be carrying out feasibility experiments at the Synchrotron Radiation Center, University of Wisconsin–Madison, using my vacuum chamber, electronics, and computerized data collection system for vacuum ultraviolet magnetic and natural circular dichroism measurements. A CIDS attachment that fits into my vacuum chamber with a computer-controlled photomultiplier will be supplied by Dr. Maestre. In March 1991, CIDS feasibility experiments were carried out at Aladdin by M. Maestre, E. Rowe, R. Hansen, and P. Snyder. The results of these experiments will be presented by M. Maestre at this workshop (Applications of Circularly Polarized Photons at the ALS with a Bend Magnet Source).

The investigation of natural and magnetic circular dichroism

measurements in energy ranges not previously available will allow comparison of experiment with theory and allow investigation of electronic structure in a totally different way. Clearly, the statements that certain effects in the lower energy range are due to higher energy transitions will finally be tested. Some investigators have already carried out exploratory circular dichroism (or optical rotation) measurements.[29–37] It is clear that the opportunities for investigations with modulated circularly polarized light at high energles are indeed exciting.

References:

1. Patricia Ann Snyder, "Vacuum Ultraviolet Natural and Magnetic Circular Dichroism with Conventional Sources and Synchrotron Radiation," *Photochemistry and Photobiology* **44**, 237 (1986).

2. Patricia Ann Snyder and Ednor M. Rowe, "The First Use of Synchrotron Radiation for Vacuum Ultraviolet Circular Dichroism Measurements," *Nucl. Instrum. Methods* **172**, 345 (1980).

3. Patricia Ann Snyder, "Status of Natural and Magnetic Circular Dichroism Instrumentation Using Synchrotron Radiation," *Nucl. Instrum. Methods* **222**, 364 (1984).

4. P.A. Snyder, P.A. Lund, P.N. Schatz, and E.M. Rowe, "Magnetic Circular Dichroism of the Rydberg Transitions in Benzene," *Chem. Phys. Lett.* **82**, 546 (1981).

5. P.A. Snyder, P.N. Schatz, and E.M. Rowe, "Natural and Magnetic Vacuum Ultraviolet Circular Dichroism Measurements at the Synchrotron Radiation Center, University of Wisconsin-Madison," in *Applications of Circularly Polarized Radiation Using Synchrotron and Ordinary Sources*, edited by F. Allen and C. Bustamante (Plenum Press, New York, 1985), p. 43.

6. Patricia Ann Snyder, "High Resolution Circular Dichroism Spectroscopy in the Vacuum Ultraviolet, 1988, Technical Digest Series (Optical Society of America) **4**, 121 (1988).

7. W.C. Johnson, Jr., "A Circular Dichroism Spectrometer in the Vacuum Ultraviolet," *Rev. Sci. Instrum.* **42**, 1283 (1971).

8. O. Schnepp, S. Allen, and E.F. Pearson, "The Measurement of Circular Dichroism in the Vacuum Ultraviolet," *Rev. Sci. Instrum.* **41**, 1136 (1970).

9. G.S. Pysh "Optical Activity in the Vacuum Ultraviolet," *Ann. Rev.*

Biophys. Bioengr. **5**, 63 (1976).

10. S. Brahms, J. Brahms, G. Spach, and A. Brack, "Identifications of B-tums and Unordered Conformations in Polypeptide Chains by Vacuum Ultraviolet Circular Dichroism," *Proc. Nat. Acad. Sci. USA* **74**, 3208 (1977).

11. A.F. Drake and S.F. Mason, "The Absorption and Circular Dichroism of Chiral Olefins," *Tetrahedron* **33**, 104 (1977).

12. A.J. Duben and C.A. Bush, "Vacuum Ultraviolet Circular Dichroism Spectrometer and Its Application to N-acetylamino Saccharides," *Anal. Chem.* **52**, 635 (1980).

13. J.D. Scott, W.S. Phelps, G.L. Findley, and S.P. McGlynn, "Molecular Rydberg Transitions Magnetic Circular Dichroism of Methyl Iodide," *J. Chem. Phys.* **68**, 4673 (1978).

14. S.D. Allen, M.G. Mason, 0. Schnepp, and P.J. Stephens, "Magnetic Circular Dichroism Spectrum of Benzene and Toluene and Magnetic Moment," *Chem. Phys. Lett.* **30**, 140 (1975).

15. A. Gedanken and M. Levy, "New Instrument for Circular Dichroism in the Vacuum Ultraviolet," *Rev. Sci. Instrum.* **48**, 1661 (1977).

16. J.C. Sutherland, K.P. Griffin, P.C. Keck, and P.Z. Takacs, "Simultaneous Measurement for Absorption and Circular Dichroism in a Synchrotron Spectrometer," *Nucl. Instrum. Methods* **195**, 375 (1982).

17. J.C. Sutherland, K.P. Griffin, and P.Z. Takacs, "Versatile Spectrometer for Experiments Using Synchrotron Radiation at Wavelengths Greater Than 100 nm," *Nucl. Instrum. Methods* **172**, 195 (1980).

18. J. Hormes, A. Klein, W. Krebs, W. Lasser, and J. Schiller, "A System for Measuring MCD Spectra for Low Temperature Samples with Synchrotron Radiation in the VUV Region," *Nucl. Instrum. Methods* **208**, 849 (1983).

19. B. Alexa, M.A. Berg, J.P. Connerade, W.R.S. Garton, J. Hormes, and T.A. Stavrakas, *Nucl. Instrum. Methods* **208**, 841 (1983).

20. J.P. Connerade, *J. Phys. B* **16**, 399 (1983).

21. J.P. Connerade, W.R.S. Garton, M.A. Bag, J. Hormes, T.A. Stavrakas, and B. Alexa, *J. Phys. (Paris)* **43**, Coll. C2, 317 (1982).

22. P.N. Schatz, J.L. Rose, T.C. VanCott, M.E. Boyle, and B.E. Williamson, Synchrotron Radiation Center Users Group Meeting **64** (1987).

23. M.A. Wickramaaratchi, E.T. Premuzic, M. Lin, and P.A. Snyder, "Circular Dichroism Spectroscopy Using Vacuum Ultraviolet Synchrotron Radiation From U9A Beamline: Instrument and Future Applications," NSLS Report, Brookhaven National Laboratory Report No. 37619 (1986).

24. U. Heinzman, B. Osterheld, and F. Schafers, "Measurements and Calculation of the Circular Polarization of the Wavelength Range from 40 to 100 nm," *Nucl. Instrum. Methods* **195**, 395 (1982).

25. U. Heinzman, I. Schafers, K. Thimm, A. Wolcke, and J. Kessler, "Polarized Photoelectrons Produced at Xenon Atoms by Circulatory Polarized Synchrotron Radiation," *J. Phys. B* **12**, 679 (1979).

26. J. Schiller and J. Hormes, "Using the Circulatory Polarized Components of Synchrotron Radiation for Circular Dichroism Measurements Between 400 and 3500 Å," *Nucl. Instrum. Methods* **A246**, 772 (1986).

27. C. Westphal, J. Bransmann, M. Getzlaff, and G. Schonhense, "Circular Dichroism in the Angular Distribution of Photoelectrons from Oriented CO Molecules," *Phys. Rev. Lett.* **63**, 151 (1989).

28. I. Tinoco, W. Mickols, W.F. Maestre, and C. Bustamante, "Absorption Scattering and Imaging of Biomolecular Structures with Polarized Light," *Ann. Rev. Biophys. Chem.* **16**, 319 (1987).

29. T. Koide, T. Shidara, H. Fukutani, K. Yamaguchi, A. Fujimori, and S. Kimura (submitted to *Phys. Rev. Lett.*).

30. G. Schutz, W. Wagner, W. Wilhelm, P. Kienle, R. Zeller, R. Frahm, and G. Meterlik, *Phys. Rev. Lett.* **58**, 737 (1987).

31. F. Schutz, R. Frahm, P. Mautner, R. Wienke, W. Wagner, W. Wilhelm, and P. Kienle, *Phys. Rev. Lett.* **62**, 2620 (1989).

32. G. Schutz, M. Knulle, R. Wienke, W. Wilhelm, W. Wagner, P. Kienle, and R. Frahm, *Z. Phys.* **B73**, 67 (1988).

33. G. Schutz, R. Wienke, W. Wilhelm, W. Wagner, P. Kienle, R. Zeller, and R. Frahm, *Z. Phys.* **B75**, 495 (1989).

34. S.P. Collins, M.J. Cooper, A. Brahmia, D. Laundy, and T. Pikanen, *J. Phys. Condens. Matter* **1**, 323 (1989).

35. C.T. Chen, F. Sette, Y. Ma, and S. Modesti, *Phys. Rev. B* **42**, 7262 (1990).

36. L. Baumgarten, C.M. Schneider, H. Petersen, F. Schafers, and J. Kirschner, *Phys. Rev. Lett.* **65**, 492 (1990).

37. C. Kao, J.B. Hasting, E.D. Johnson, D.P. Siddons, G.C. Smith, and G A. Prinz, *Phys. Rev. Lett.* **65**, 373 (1990).

Complete Polarization Studies of Light Scattering by Particles Near Wavelength Size: Theory, Model Calculations, and Experiments

W.M. McClain

Wayne State University

Complete Polarization Studies of Light Scattering by Particles Near Wavelength Size: Theory, Model Calculations, and Experiments

W. M. McClain
Wayne State University, Detroit, Michigan, 48202

Orientationally random ensembles of particles larger than several tenths of a wave in size alter the polarization of scattered light in a way that is never seen in small particle scattering. The multipole expansion of all electromagnetic properties about a single point within the particle fails to account for observed phenomena in such large particles; in particular, the Mueller scattering matrix [1] elements M_{13}, M_{23}, M_{43}, and their transposes are always predicted by multipole expansion theories to be exactly zero, even when very high multipoles are included. But in reality, these properties are nonzero and easily measureable for particles near wavelength size; they may be 25% or more of M_{11}, the total scattered intensity. Their measurement involves the use of both circularly and diagonally polarized photons.

The mechanism by which these elements achieve nonzero values is revealed by a dipole array model of the particle. A particle of any shape is modeled as a lattice of point polarizabilities filling the volume of the particle. The polarizability on each lattice point responds only as a dipole to the total local electric field (the sum of the incident wave plus the dipole fields of all the other points in the array). When the radiation at the detector is summed up over all the points of the array, the particle as a whole emits its scattered light by means of electric and magnetic dipoles, quadrupoles, octupoles, etc., up to multipoles so high they have no names.

The key thing in modeling M_{13}, M_{23}, M_{43}, and their transposes is to include the *retarded* part of the dipole-dipole interaction in the model. The dipole-dipole interaction appears most simply in the formula

$$E_i^{(a)} = T_{ij}^{(ab)} p_j^{(b)}$$

where $E_i^{(a)}$ is the electric field in direction i at point (a) due to oscillating polarization $p_j^{(b)}$ in direction j at point (b), and where $T_{ij}^{(ab)}$ is the interaction tensor, given by [2]

$$T_{ij}^{(ab)} = \left(r^{(ab)}\right)^{-3} \exp\left[i\, k\, r^{(ab)}\right] \times$$
$$\left[\left(1 - i\, k\, r^{(ab)}\right)\left(3u_i^{(ab)}u_j^{(ab)} - \delta_{ij}\right) + \left(k\, r^{(ab)}\right)^2\left(\delta_{ij} - u_i^{(ab)}u_j^{(ab)}\right)\right].$$

Here $r^{(ab)}$ is the distance between lattice points a and b, and $u^{(ab)}$ is a unit vector pointing from a toward b, and k is 2π divided by wavelength λ. The static part is obtained by setting $k = 0$; the "retarded" part is everything else; it accounts properly for delays in the interactions caused by the finite speed of light. The main point here is that even the static part of $T_{ij}^{(ab)}$ is incapable of producing nonzero orientation averaged values in M_{13}, M_{23}, M_{43}, and their transposes; only the retarded part is effective. We therefore call these six Mueller elements the "retardation elements".

After averaging over all orientations of the model particle, the Mueller scattering matrix may be expanded in powers of wavelength λ and particle diameter d [3]. The asymptotic behavior at long wavelength is given by

$$\langle M \rangle_{orientation} \approx \frac{1}{\lambda^4}\begin{bmatrix} 1 & 1 & (d/\lambda)^4 & (d/\lambda) \\ 1 & 1 & (d/\lambda)^4 & (d/\lambda) \\ (d/\lambda)^4 & (d/\lambda)^4 & 1 & (d/\lambda)^5 \\ (d/\lambda) & (d/\lambda) & (d/\lambda)^5 & 1 \end{bmatrix}$$

Two facts are immediately apparent from this result. First, the retardation elements are hypersensitive to particle diameter, going like d^4 or d^5; and second, their intensity goes like the eighth or ninth power of $1/\lambda$. This is why these Mueller elements are never observable when (d/λ) is near 10^{-3}, as for molecules of normal size scattering visible light. Even for protein molecules scattering UV light, this ratio is no more than 10^{-2}. Clearly, if these effects are ever to be seen in molecules of ordinary size, or even in enzymes, it must be with synchrotron wavelengths.

A third important fact has emerged from modeling studies [4]: The dependence of the retardation elements on scattering angle is hypersensitive to particle shape as well as to particle size. Here we begin to envision scattering of ALS wavelengths by enzymes in order to follow very subtle shape changes as a function of time, upon introduction of a substrate or prosthetic molecule into an aqueous solution of enzyme. Such studies would be complementary to NMR studies of these systems, since the NMR responds to very local interactions, while retarded scattering studies would respond best to overall shape changes.

We have constructed an instrument to measure the whole Mueller scattering matrix as a function of scattering angle; the light source is a He-Ne laser, and there are two rotatable retardation plates in the incidence arm and a similar pair in the detection arm. These four rotatable retardation plates (with two positions each) provide sixteen different polarization experiments at each scattering angle.

A similar experiment could be set up using synchrotron radiation if we had available an undulator with complete polarization control, as described at this conference by K. J. Kim [5], and the retarder plates described by J. B. Kortright [6]. It is not necessary that such elements be perfect; imperfect elements are just as useful as perfect ones, provided we know the Stokes parameters of the undulator light and the Mueller matrices of retarders.

Fig. 1 shows our measured Mueller matrix for tobacco mosaic virus (TMV) suspended in water. TMV is a rigid rod 3000 Å long and 180 Å in diameter. The light is 6328 Å in air, or 4758 Å in water, so the maximum d/λ is

about 3000 / 4758 = 0.63. Each virus consists of thousands of identical proteins stacked helically around an RNA core, and much care has been taken to assure that we have only whole, unbroken viruses in our sample. The water is conductivity water, to minimize virus aggregation, and the concentration of virus is as low as possible, about $2x10^{12}$ particles per cm^3.

The dipole Mueller elements (11, 12, 21, 22, 33, and 44) of Fig. 1 show roughly the expected uninteresting behaviour. The nondipole lements 34 and 43 are easily measureable and do not at all resemble the $\sin^2(\theta)$ longwave angular behaviour of this element, indicating that we are well out of the longwave asymptotic regime. But it is in the helicity quadrants (upper right and lower left quadrants) that we find the most interesting feature. Three of the helicity elements in each quadrant show nothing, but elements 23 (in the upper helicity quadrant) and 32 (in the lower helicity quadrant) are quite definitely nonzero. These signals may be due to the helical character of this virus. Note in particular that elements 14 and 41, often measured as helicity indicators, are useless in this case.

At the concentration we used, each 300 nm rod virus has on average an 800 nm cube to itself. This weakens, but probably does not entirely prevent, nematic alignment of the viruses. Fluctuating alignment domains may be the reason we see so much noise in the forward part of the 23 and 32 curves. We know that the retardation elements are also hypersensitive to partial alignment of particles [7].

Crude models (50 subunits or fewer) give crude fits to the general shape of all the dipole elements and of 23 and 34 and their transposes. But the weakness of 13 is not predicted, and we have no explanation for it as of now. More elaborate modeling is under way.

These results show interesting new phenomena are to be seen in elements of the Mueller matrix that have so far been little exploited. It should be possible to extend these experiments into the size range of proteins using the polarization modulated undulator and the shortwave retarders described at this conference.

Tobacco Mosaic Virus in Water, d/L=18nm/300nm, λ=633nm

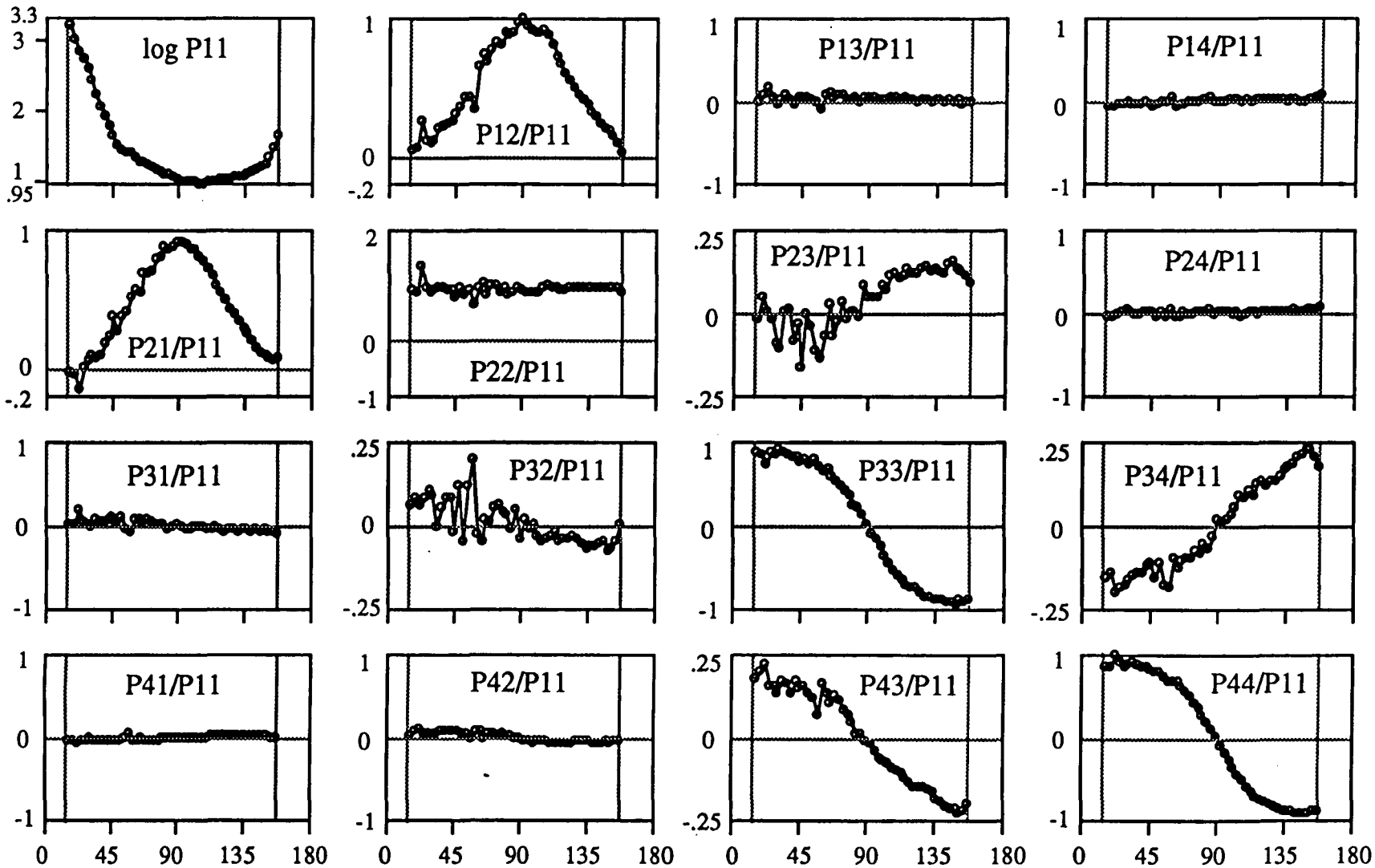

References

1. The Mueller matrix is defined in the contribution by K.J. Kim in this report. We number the Mueller indices (and the Stokes parameters) 1 to 4 rather than 0 to 3, but the order is the same.
2. J.D. Jackson, *Classical Electrodynamics*, 2nd ed. Wiley, New York, (1975), section 9.2.
3. (a) *Longwave Properties of the Mueller Scattering Matrix for Particles of Arbitrary Shape. I. Dependence on Wavelength and Scattering Angle*
Yaoming Shi and W. M. McClain, J. Chem. Phys. **93**, 5605-5615 (1990)
(b)*Longwave Properties of the Mueller Scattering Matrix for Particles of Arbitrary Shape. II. Molecular parameters and Perrin symmetries*
Yaoming Shi, W. M. McClain, and Duan Tian, J. Chem. Phys. **94**, 4726-4740 (1991)
4. W. M. McClain and W. A. Ghoul, J. Chem. Phys. **84**, 6609-6622 (1986)
5. K. J. Kim, this conference report.
6. J. B. Kortright, this conference report.
7. (a)*Nondipole light scattering by partially oriented ensembles. I. Numerical calculations and symmetries*
Duan Tian and W. M. McClain, J. Chem. Phys. **90**, 4783-4794 (1989)
(b)*Nondipole light scattering by partially oriented ensembles. II. Analytic algorithm.*
Duan Tian and W. M. McClain, J. Chem. Phys. **90**, 6956-6964 (1989)
(c)*Nondipole light scattering by partially oriented ensembles. III. The Müller pattern for achiral macromolecules*
Duan Tian and W. M. McClain, J. Chem Phys. **91**, 4435-4439 (1989).

Circular Intensity Differential Scattering (CIDS) Measurements in the Soft X-Ray Region of the Spectrum (~16 eV to 500 eV)

M.F. Maestre,[*] C. Bustamante,[†] P. Snyder,[§] E. Rowe,[‡] and R. Hansen[‡]

[*]Lawrence Berkeley Laboratory
[†]University of Oregon
[§]Florida Atlantic University
[‡]Synchrotron Radiation Center, Wisconsin

CIRCULAR INTENSITY DIFFERENTIAL SCATTERING (CIDS) MEASUREMENTS IN THE SOFT X-RAY REGION OF THE SPECTRUM (~16 TO 500 eV).

M.F. Maestre,* C. Bustamante,† P. Snyder,§ E. Rowe,‡ and R. Hansen‡

*Lawrence Berkeley Laboratory, Berkeley
†Chemistry Dept., University of Oregon
§Chemistry Dept., Florida Atlantic University
‡Synchrotron Radiation Center (SRC), Wisconsin

Summary

We propose the use of recently developed techniques of circular intensity differential scattering (CIDS), as extended to the soft x-ray region of the spectrum (16 to 500 eV), to study the higher-order organization of the eukaryotic chromosome. CIDS is the difference in scattering power of an object when illuminated by right circularly polarized electromagnetic radiation versus left circularly polarized electromagnetic radiation of arbitrary wavelength. CIDS has been shown to be a very sensitive measure of the helical organization of the scattering object, e.g., the eukaryotic chromosome. Preliminary results of measurements of samples of bacteriophages and octopus sperm done at SRC show the technique to be very sensitive to the dimensional parameters of the particles interrogated by circularly polarized light.

I. CIDS studies at shorter wavelengths (200 to 392 eV). The scaling law for CIDS.

We have performed a series of computations to estimate the feasibility of detecting CIDS in the soft x-ray region. This requires a knowledge of the magnitudes of the atomic polarizability at these high frequencies as well as their intrinsic anisotropies. The latter are not known because systematic studies of polarized x-ray diffraction using synchrotron sources have started only recently (Templeton & Templeton, 1982).

The strategy in these computations has been as follows:

1) Assume that the intrinsic atomic polarizability is perfectly spherically symmetric, allow polarizable groups to couple to each other to generate

some degree of anisotropy, and then proceed to calculate the CIDS for randomly oriented scatterers.

2) Carry out a series of computations assuming some degree of anisotropy to establish the minimum anisotropy in the atomic polarizability required to observe the CIDS signal.

In all the cases studied, we found that scheme (l) gives CIDS values much too small to be measured with the polarization methods used at present. Thus, intergroup coupling mechanisms are not enough to generate the necessary anisotropy to yield CIDS values in the region of 100 eV or at higher energies.

To carry out strategy (2), we have chosen a very simplified model for performing the computations. The chiral scatterer is modeled as a hypothetical carbon helix formed by arranging carbon atoms in a chiral fashion. In the computations, the pitch, radius, number of groups per turn and number of turns of the helix are variable, as are the polarizability anisotropies. The wavelength of the incident light was chosen to be 31.6 Å. This choice corresponds to the desire for using wavelengths between the oxygen absorption K-edge (24 Å, 511 eV) and the carbon K-edge (43Å, 280 eV), corresponding also to the spectral window in which x-ray absorption by water is minimal. The computations have been carried out within the first Born approximation for an ensemble of helical scatterers randomly oriented in a medium. Given the crudeness of the model, no attempt has been made to take into account the scattering background of the suspending solvent, although, because of its non-chiral structure, such background is expected to subtract away in calculating the CIDS ratio of the two incident circular polarizations. At x-ray frequencies, the electrons involved in the scattering process are the single-atomic-core electrons, whose binding energies are high enough to interact with the high-energy photons. The polarizabilities for the carbon atoms were calculated from the formula:

$$\alpha = \frac{\lambda^2 e^2}{4\pi^2 mc^2}(f_1 + if_2)$$

where λ and c are the wavelength and the speed of light in vacuum, respectively, e and m are the charge and mass of the electrons, and f_1 and f_2 are the atomic scattering factors (Henke *et al.*, 1982). We have found that the maximum CIDS depends strongly on the polarizability anisotropy according to:

$$\text{CIDS} \ \alpha \ \ (\text{polarizability anisotropy})^{\mu}$$

where μ is the scaling parameter. Figure l(a) shows this behavior obtained through computer simulations for a collection of randomly oriented helices with a pitch of 31.6 Å and a radius of 20 Å. These dimensions were chosen so as to maximize the CIDS values. The curves correspond to different numbers of helical turns but the same values for pitch and radius. Notice that, in general, the magnitude of the signal increases with increasing value of the polarizability anisotropy as well with the number of turns in the helix. The value of μ for these computer simulations was 2. The area inscribed in the inner quadrant corresponds to the range of polarizability anisotropies too small to render the measurement of CIDS feasible. Notice that for λ = 31.6 Å (40 eV), measurable values of CIDS (greater than 10^{-4}) can be obtained only for atomic polarizabilities above 1/1000, i.e., for cases in which the values of the polarizabilities along the axes differ by at least one part per thousand. These anisotropies, while certainly common in the visible range of the spectrum involving the outer electronic shells, are unlikely in the soft x-ray regions. The meaning of the scaling relationship is that the exponent μ is quite independent of the details of the calculation such as the number of turns of the helices. More importantly, μ is also independent of the pitch and the radius of the helix as long as the ratio of these helical parameters to the wavelength of light is maintained, i.e., as long as they are scaled proportionately. This is depicted in Figure l(b), where a plot similar to that of Fig. 1(a) is shown for λ = 252 Å (49 eV), P = 252 Å, and R = 140 Å. Notice that again the slope is independent of the number of turns of the helices and, in all cases, is also equal to 2. Here it is seen that values of anisotropies greater or equal to 1% are necessary to detect CIDS signals. At these intermediate energies, however, these anisotropies are not so unlikely, and the detection of optical activity effects might be possible. Figure 2 shows an example of CIDS patterns calculated for carbon helices at an incident wavelength of 31.6 Å. The two patterns are mirror images of each other and correspond to the two enantiomers of the model. The polarizabilities had a geometrical anisotropy of 6%, well above that needed for detection.

II. CIDS measurements in the 3000 to 2000 Å wavelength region of bacteriophages, sperm cells, and polystryrene spheres at the Synchrotron Radiation Center, Wisconsin.

CIDS measurements of the following samples—extended to the UV region—were carried out using the Aluminum Seya monochromator at the SRC :

1) T4 and T7 bacteriophages, particles approximately 800 Å and 500 Å in diameter.

2) The helical sperm of the Mediterranean octopus *Eledone cirrhosa*, a structure that has a lefthanded helical superstructure with a pitch of about 0.65 mμ and a length of about 43 mμ.

3) Polystyrene spheres 5.85, 0.45, and 0.19 mμ in diameter.

The results showed that both the *Eledone cirrhosa* and the T7 bacteriophage had differential scattering structure that varied with wavelength in the 3000 to 2000 Å range. T4 phage showed little change in its CIDS. Unexpectedly, the most structure was shown by the differential scattering of the polystyrene spheres. As shown in the three graphs of the CIDS of 0.45-mμ-diameter spheres, the scattering lobes are rich in structure (both positive and negative lobes) and show a strong dependence on the ratio of wavelength to the diameter of the sphere. At present, there is no theoretical explanation for this surprising behavior of the CIDS signal when the measurements are done at wavelengths of dimensions corresponding to those of the scattering object.

III. Conclusions

The differential scattering of circularly polarized and linearly polarized light can occur at any wavelength. No absorption bands or edges are required. In particular, the angular dependence of CIDS provides structural information about chiral organization. Experimental results for this new method have been obtained on bacteriophages, helical sperm cells from an octopus, cholesteric liquid crystals, and spinach chloroplasts. Recent measurements in the UV region of the spectrum have indicated the extreme sensitivity of the measurement to dimensional parameters not necessarily reflecting helical organization.

References

Bustamante, C., M.F. Maestre, and I. Tinoco, Jr., "Circular intensity differential scattering of light by helical structures," I. "Theory," *J. Chem. Phys.* **73**, 4273 (1980); II. "Applications," *J. Chem. Phys.* **73**, 6046 (1980); III. "A general polarizability tensor and anomalous scattering," *J. Chem. Phys.* **74**, 4839 (1980); IV. "Randomly oriented species," *J. Chem. Phys.* **76**, 3440 (1980); V. "Circular differential scattering can be an important part of the circular dichroism of macromolecules," *Proc. Nat. Acad. Sci. USA* **80**, 3568 (1983).

Henke, B. L. et al., *Atomic Data and Nuclear Data Tables*, Vol. 27 (1982), pp. 1–144 .

Keller, D., C. Bustamante, M.F. Maestre, and I. Tinoco, Jr., "Imaging of optically active biological structures using circularly polarized light," *Proc. Nat. Acad. Sci. USA* **82**, 401 (1985).

Kim, K. J., "A crossed undulator system for a variable polarization synchrotron radiation source," in *Applications of Polarized Radiation*, edited by F.S. Allen and C. Bustamante (Plenum, New York, 1985), pp. 21-33.

Tinoco, Jr., I., C. Bustamante, and M.F. Maestre, "The optical activity of nucleic acids and their aggregates," *Ann. Rev. Biophys. and Bioeng.* **9**, 104 (1980).

Figure Legends

Figure 1(a): Log-log plots of maximum CIDS (scattering angle = 180 degrees) vs. polarizability anisotropy. Each line corresponds to a different number of helical turns with all other variables constant. The incident wavelength is 31.6 Å.

Figure l(b): Log-log plots of the maximum CIDS at (scattering angle = 180 degrees) with incident wavelength of 252 Å.

Figure 2: Calculated CIDS for a suspension of hypothetical carbon helices illuminated with circularly polarized radiation of λ = 31.6 Å. The mirror image curves are produced by identical structures but with opposite handedness. The helix pitch is 31.6 Å (solid line, righthanded).

Figure 3: Plot of the CIDS signal (1 volt = 27% differential scattering) of 0.45-mμ-diameter spheres as a function of the scattering angle 0 degrees corresponding to the forward direction of scattering, i.e., parallel to the light

beam. This scattering plot was measured at a wavelength of 2300 Å.

Figure 4: CIDS of the above 0.45-mμ spheres, measured at 2267.8 Å. The differential scattering envelope is showing positive scattering lobes. By the time that the wavelength reaches 2210 Å, the pattern inverts and becomes wholly positive.

Figure 5: CIDS of 0.45-mμ-diameter spheres at λ = 2210 Å. The differential scattering pattern is positive, and the number of lobes has been reduced. The critical wavelength at which the CIDS pattern was mostly symmetrical about the zero line was determined to be at 2267.8 Å, approximately half the nominal size of the diameter of the sphere.

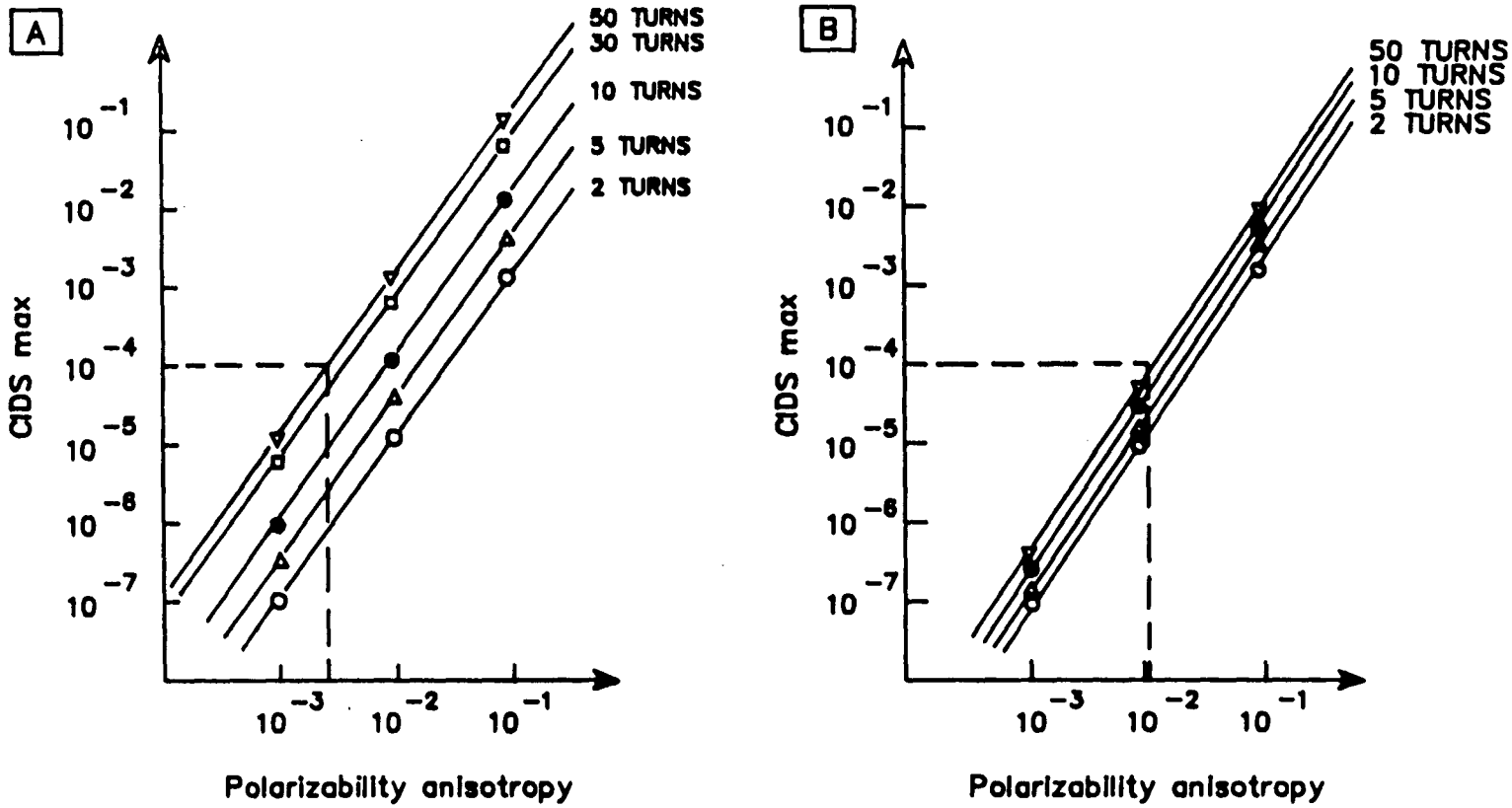

Log–Log plots of maximum CIDS (at $\theta = 180°$) *vs* polarizability anisotropy. Each line corresponds to a different number of helical turns with all other variables constant. (a) The incident wavelength is 31.6 Å, (b) the incident wavelength is 252 Å.

Figure 1

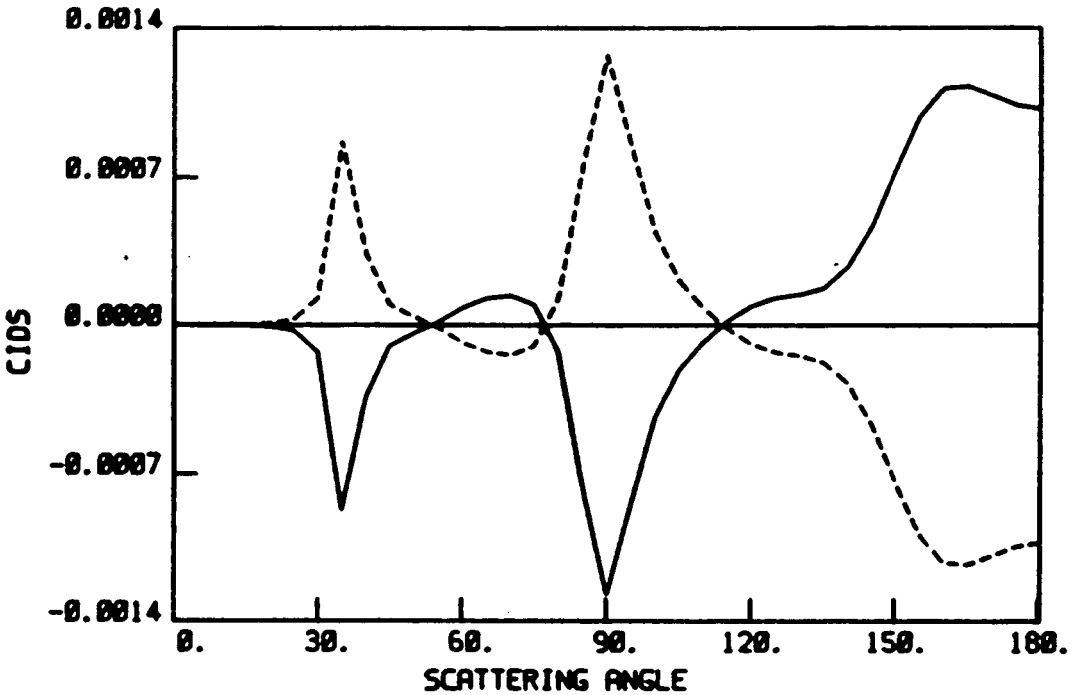
0.0014
0.0007
0.0000
-0.0007
-0.0014
CIDS
0.
30.
60.
90.
120.
150.
180.
SCATTERING ANGLE
XBL 899-3259

Figure 2

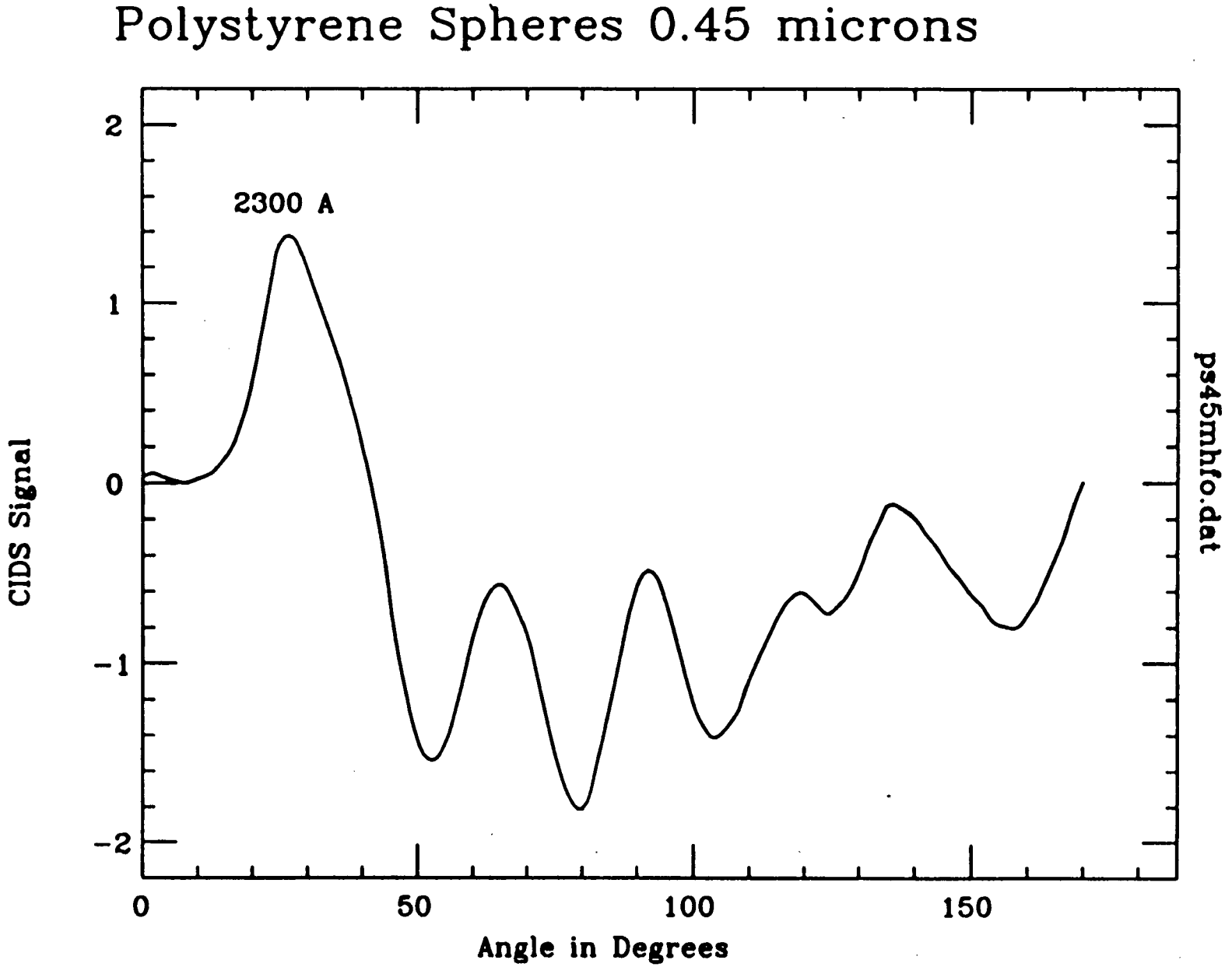
Polystyrene Spheres 0.45 microns
2300 A
CIDS Signal
Angle in Degrees
ps45mhfo.dat
2
1
0
-1
-2
0
50
100
150

Figure 3

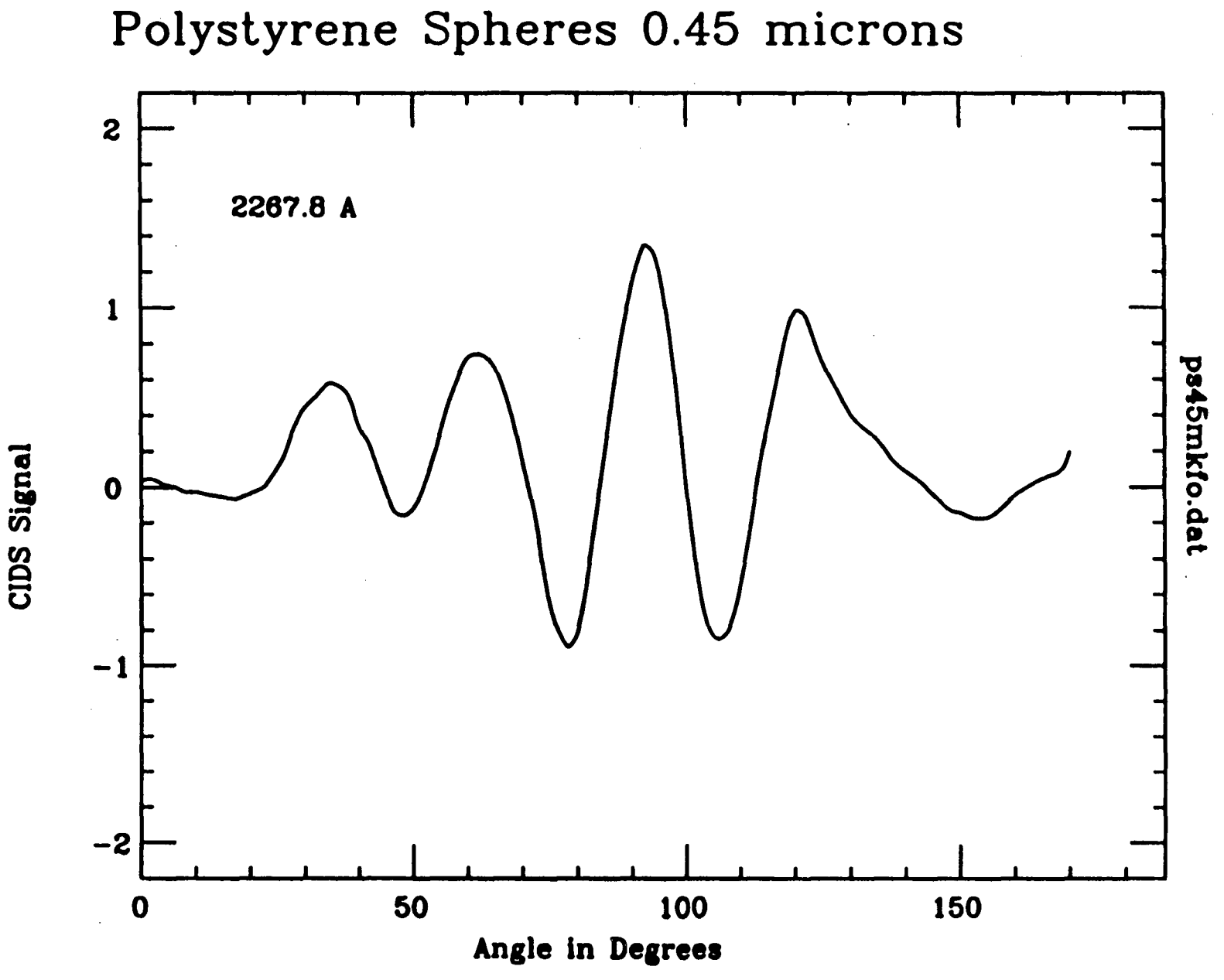
Polystyrene Spheres 0.45 microns
2267.8 A
CIDS Signal
Angle in Degrees
ps45mkfo.dat
2
1
0
-1
-2
0
50
100
150

Figure 4

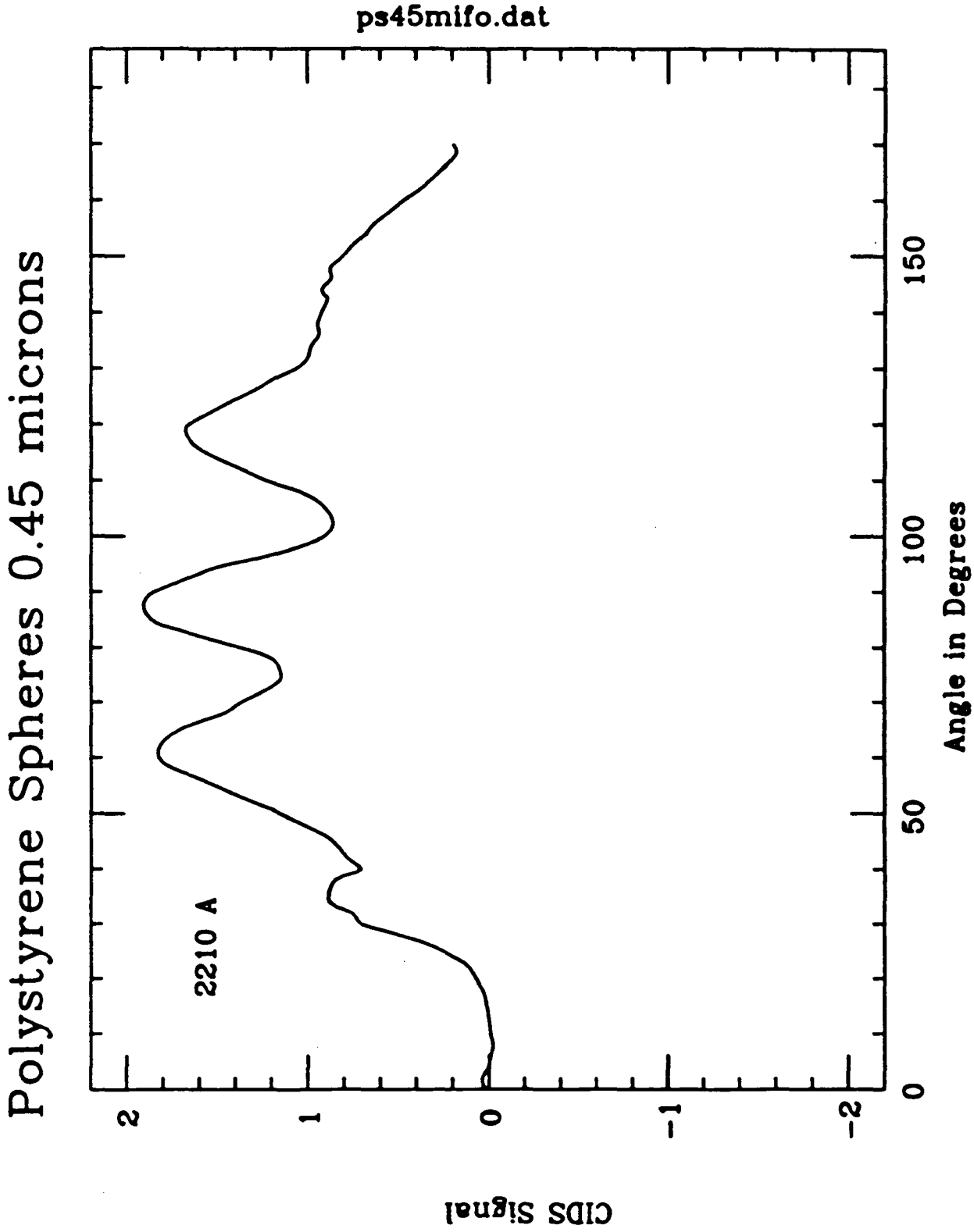
ps45mifo.dat
Polystyrene Spheres 0.45 microns
2210 A
CIDS Signal
2
1
0
-1
-2
0
50
100
150
Angle in Degrees

Simple Physics behind Magneto-Optics in the Soft X-Ray Regime

E.A. Stern

University of Washington

Magnetism Studies with the ALS

E.A. Stern

Using circularly polarized radiation opens the possibility of studying magnetism in ferri- and ferromagnetic materials. The exciting aspect of using the ALS is that one can study the local magnetic properties in disordered and complicated materials. The information that can be obtained from such measurements is the exchange and open-orbit interaction in the empty states above the Fermi energy. The ability to obtain information on these states is due to the fact that the initial state is a core level with well known properties; thus, the experimental result depends only on the final-state properties, which can be inferred from the measurement.

The element specificity of this information is a strength of the ALS that permits the study of disordered materials with many types of atoms. Such detailed studies will provide experimental evidence to help in understanding the fundamental properties of disordered and surface magnets and to test theoretical calculations.

Simple Physics behind magneto-optics in the soft x-ray Regime

E.A. Stern

I. Introduction:

In assessing what are useful experiments to do it is helpful to have simple physical ideas which can be used to estimate what information can be obtained from a given measurement.

Will present the basic physics in magneto-optics, i.e., samples which contain macro magnetic moments due to spin. Ferromagnetism anti-, ferri-magnetism. (not paramagnetism)

The basic physical phenomena are:

exchange and spin-orbit interaction

(X) (S.O)

X is a combination of electrostatics and the Pauli exclusion principle. ↑↑ have an exchange hole which is absent with ↓↑.

S.O. is relativistic effect. Moving electron in electrostatic potential senses a magnetic field $\frac{\vec{v}}{c} \times \vec{E}$ which couples to the magnetic moment of its spin.

II E+M relation

To emphasize physics will consider simplest case. Optical isotropic medium when $M = 0$. Interaction with E.M. waves dominated by

$$\varepsilon(0,\omega) = \begin{pmatrix} \varepsilon_0(\omega) & 0 & 0 \\ 0 & \varepsilon_0(\omega) & 0 \\ 0 & 0 & \varepsilon_0(\omega) \end{pmatrix}$$

$\vec{q} \simeq 0$, forward scattering

Consider first ferro, or ferri-magnetism. $M \neq 0$. Neglect effect of H-field except to align M.

$$\varepsilon(\omega) = \begin{pmatrix} \varepsilon_{xx} & \varepsilon_{xy} & 0 \\ -\varepsilon_{xy} & \varepsilon_{xx} & 0 \\ 0 & 0 & \varepsilon_{zz} \end{pmatrix}$$

$$\varepsilon_{xx} = \varepsilon_0 + M^2 \Delta\varepsilon_{xx}(M^2)$$

$$\varepsilon_{zz} = \varepsilon_0 + M^2 \Delta\varepsilon_{zz}(M^2)$$

$$\varepsilon_{xy} = M\,\varepsilon_1(M^2)$$

$\varepsilon_{xx}, \varepsilon_{zz}$ even in M

ε_{xy} odd in M

In practice effect of M weak so need to include only to 1st order

$$\varepsilon(\omega) = \begin{pmatrix} \varepsilon_0(\omega) & M\varepsilon_1(\omega) & 0 \\ -M\varepsilon_1(\omega) & \varepsilon_0(\omega) & 0 \\ 0 & 0 & \varepsilon_0(\omega) \end{pmatrix}$$

All magneto-optics in ε_{xy} or ε_1

Both ε_0 and ε_1 complex

$\varepsilon_R = \varepsilon^+ = \varepsilon_{xx} + i\,\varepsilon_{xy}$

$\varepsilon_L = \varepsilon^- = \varepsilon_{xx} - i\,\varepsilon_{xy}$

$\frac{\varepsilon_R + \varepsilon_L}{2} = \varepsilon_{xx}$, absorptive part is $\mathrm{Im}\,\varepsilon_{xx}$

$\frac{\varepsilon_R - \varepsilon_L}{2} = i\,\varepsilon_{xy}$, absorptive part is $\mathrm{Re}\,\varepsilon_{xy}$

Both ε_{xy} and ε_{xx} satisfy Kramers–Kronig relations so need to know only absorptive part

III Physics

To sense magneto-optic effect need to distinguish between RH and LH, chirality

Strongest optical coupling is electric dipole which couples only to currents (orbital angular momentum) and not spins (M).

Physics of coupling between M (spin) and EM wave is spin-orbit coupling

We consider absorption by transition from core to unfilled states above E_F. Since initial state well characterized, have hope to determine properties of final states.

Two S.O. states

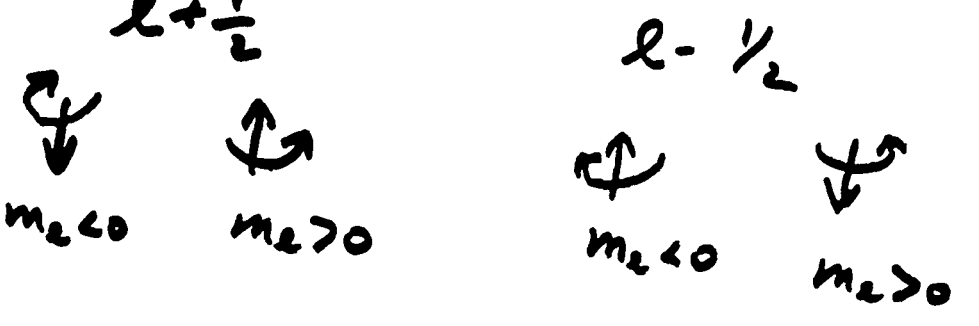

S.O. coupling: $\zeta(r)\,\vec{L}\cdot\vec{S}$

$$\zeta(r) = \frac{1}{2m^2c^2}\frac{1}{r}\frac{dV}{dr} > 0$$

$\ell+\frac{1}{2}$ higher energy than $\ell-\frac{1}{2}$

$\ell+1/2$ has RH chirality
$\ell-1/2$ has LH chirality

From Fermi Golden Rule

$$\mathrm{Re}\,\varepsilon_{xy} \propto \sum_{\alpha,\beta} |\pi^{+}_{\alpha\beta}|^2 \delta(\omega - \omega^{+}_{\alpha\beta}) - |\pi^{-}_{\alpha\beta}|^2 \delta(\omega -$$

S.O alone cannot make $\varepsilon_{xy} \neq 0$

That's because

Ψ and Ψ have same energy

$l + \frac{1}{2}$

similarly for $l - \frac{1}{2}$

so both spins are equally occupied

and $|\pi^{+}_{\alpha\beta\downarrow}|^2 = |\pi^{-}_{\alpha\beta\downarrow}|^2$

and $\omega^{+}_{\alpha\beta\uparrow} = \omega^{-}_{\alpha\beta\downarrow}$

and $\varepsilon_{xy} = 0$

Add exchange: $\omega^{+}_{\alpha\beta\uparrow} \neq \omega^{-}_{\alpha\beta\downarrow}$

and $\varepsilon_{xy} \neq 0$.

Conversely exchange alone cannot produce $\varepsilon_{xy} \neq 0$ because

$$\left(\Pi^{+}_{\alpha p \uparrow}\right)^2 = \left|\Pi^{-}_{\alpha p \uparrow}\right|^2$$

Need both S.O + X.

IV Simple model

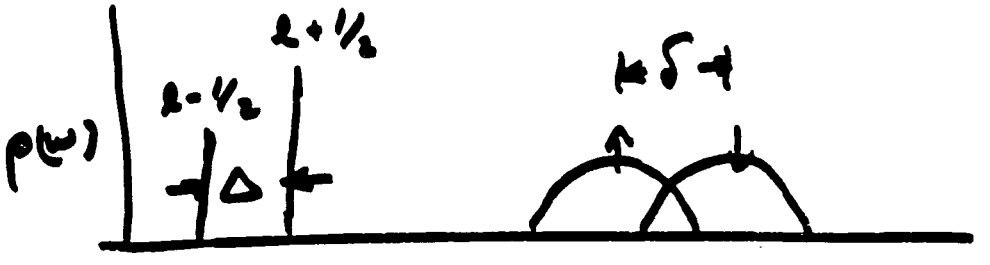

ω

Δ = S.O. splitting $\approx$ 2 eV

δ = X splitting $\approx$ 1 eV

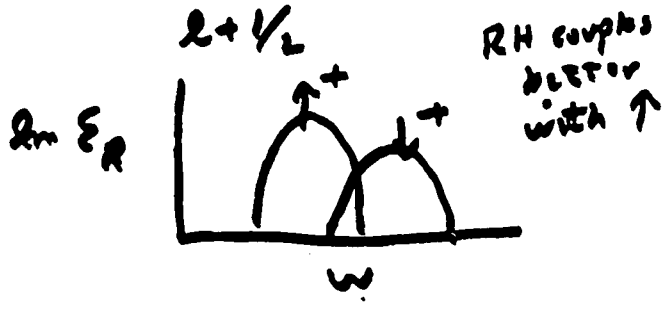

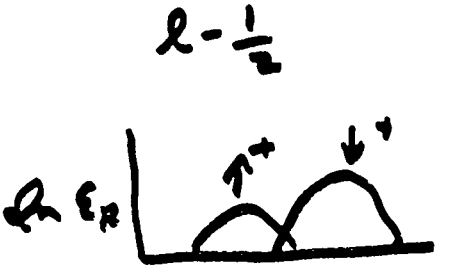

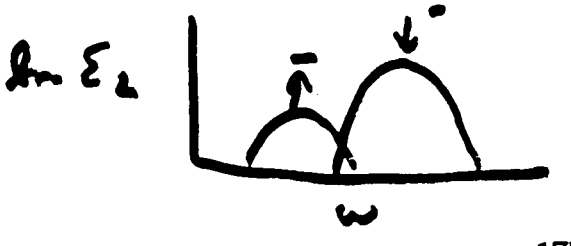

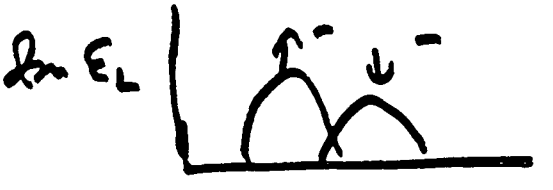

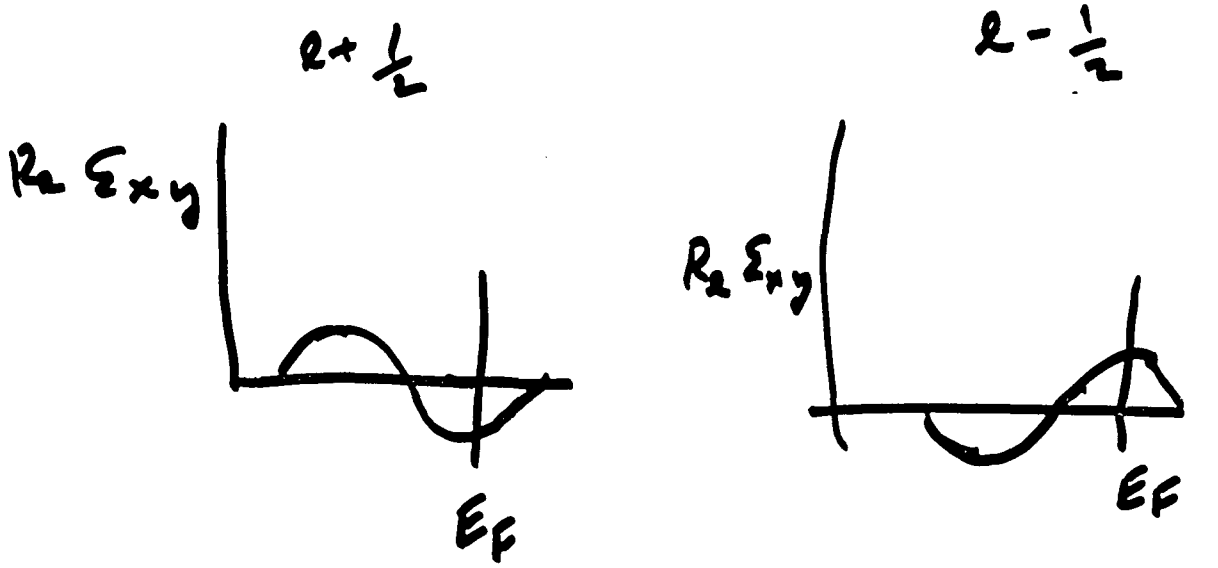

$\Delta \simeq 2eV$

smeared by core hole lifetime ~ 1eV

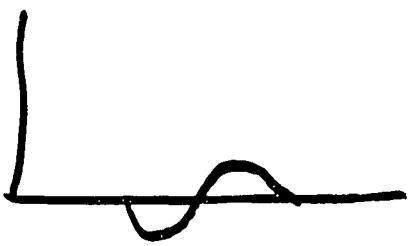

No spin-dependent XAFS in soft-x-ray region. Need to sense spectra 100's eV past edge. Both $\ell+\frac{1}{2}$ and $\ell-\frac{1}{2}$ contribute and tend to

cancel. Need hard x-rays where $\Delta \simeq 100$'s eV.

Conclusion: No spin dependent XAFS in ALS. Obtain information about states above E_F, exchange & s.o. However, resolution limited to ≈ 1 eV. Advantage: atom specific. Disordered systems, surfaces. For Ni obtain ground state magnetic properties. For almost empty band obtain final state magnetic properties. Mixture in between.

Relation to magnetic scattering. ferri magnetism ↑ cancels ↓ Get around this by clever idea of Blum Scatter. so $\vec{q} = \vec{k} - \vec{k}'$

However, not useful for ALS since $\vec{q}$ too small.

Using Photons to Determine the Electronic Structure of Oxide Supeconductors

A. Zettl

Lawrence Berkeley Laboratory
and
Physics Department, University of California, Berkeley

Outline

Introduction to Oxide Superconductors

Photoemission Spectroscopy
- High resolution
- Angular resolved
- Circular polarization

Superconductors and the ALS

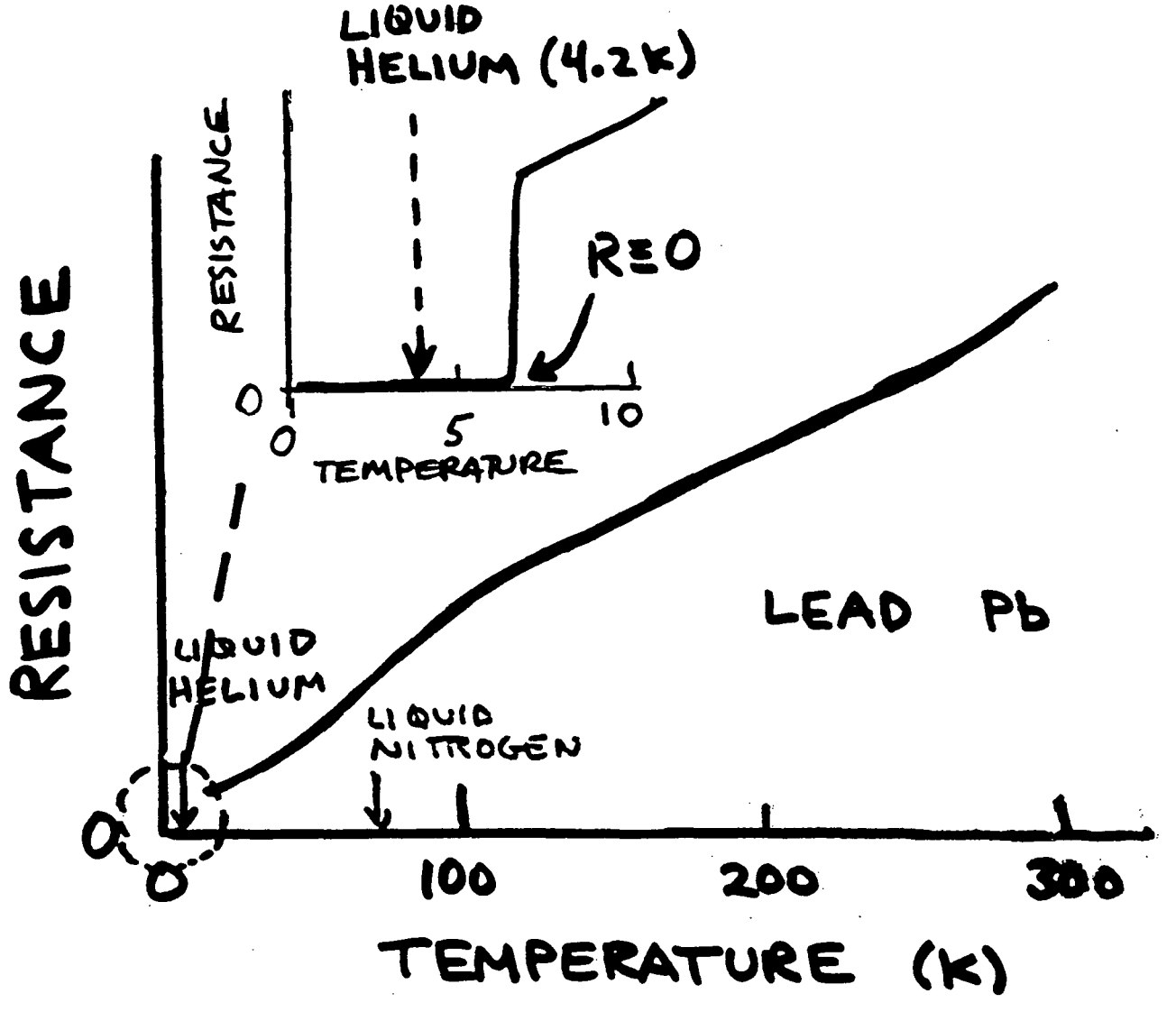
LIQUID
HELIUM (4.2K)
RESISTANCE
R=0
0
0
5
10
TEMPERATURE
RESISTANCE
LEAD Pb
LIQUID
HELIUM
LIQUID
NITROGEN
0
100
200
300
TEMPERATURE (K)

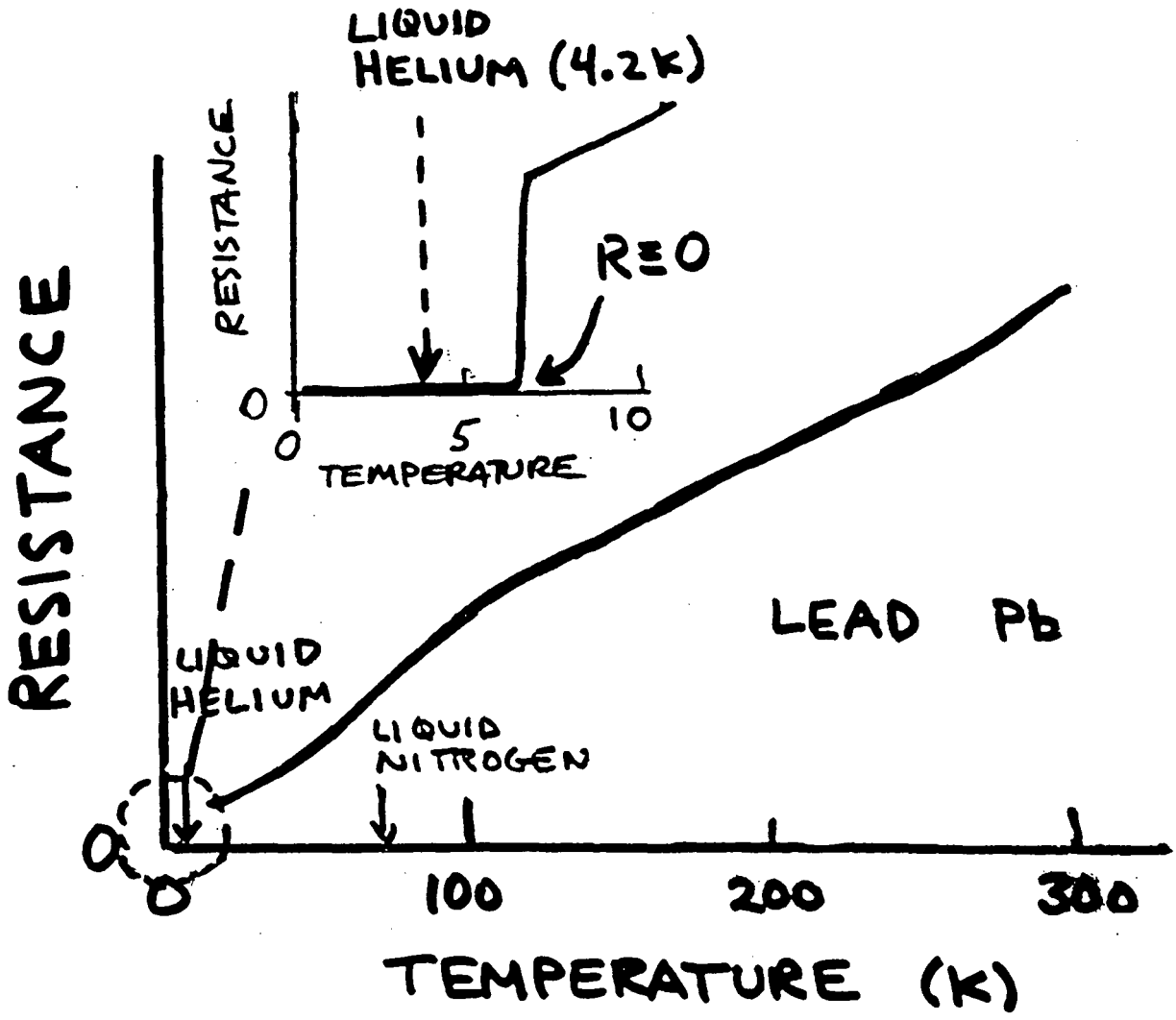
LIQUID
HELIUM (4.2K)
RESISTANCE
R=0
0
0
5
10
TEMPERATURE
RESISTANCE
LIQUID
HELIUM
LIQUID
NITROGEN
LEAD Pb
0
0
100
200
300
TEMPERATURE (K)

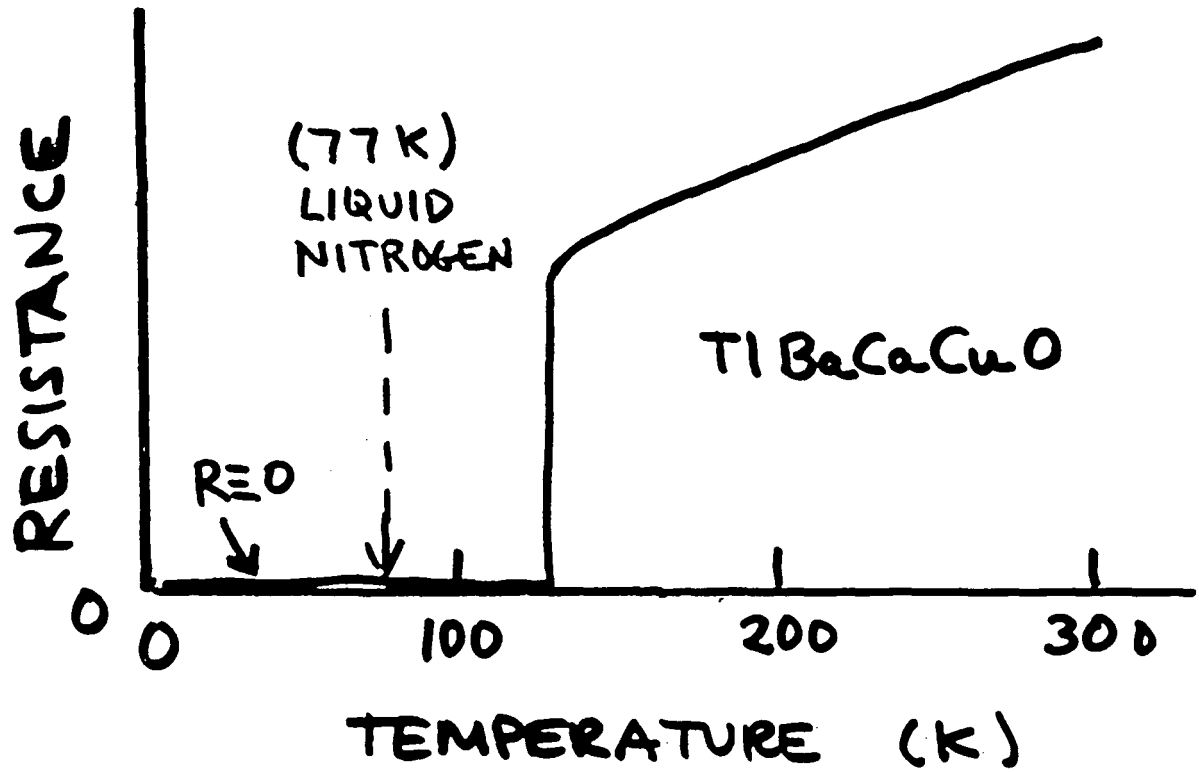
RESISTANCE
(77K)
LIQUID
NITROGEN
R=0
TlBaCaCuO
0
0
100
200
300
TEMPERATURE (K)

DEVELOPMENTS IN SUPERCONDUCTIVITY

THEORY	DATE	EXPERIMENT
NO THEORY	1911	SUPERCONDUCTIVITY DISCOVERED $T_c \approx 4.2$ K
LONDON EQNS.	1930	MEISSNER EFFECT
	1950	ISOTOPE EFFECT
BCS THEORY		
SUPERCONDUCTIVITY: "MOST WELL-UNDERSTOOD PROBLEM IN SOLID STATE PHYSICS"	1960	TYPE II MATERIALS, JOSEPHSON EFFECTS
	1970	$T_c \approx 23$ K
HIGH-T_c THEORY ?	1986	$T_c \approx 30$ K
	1987	$T_c \approx 90$ K
	1988	$T_c = 125$ K
		Cu-OXIDES

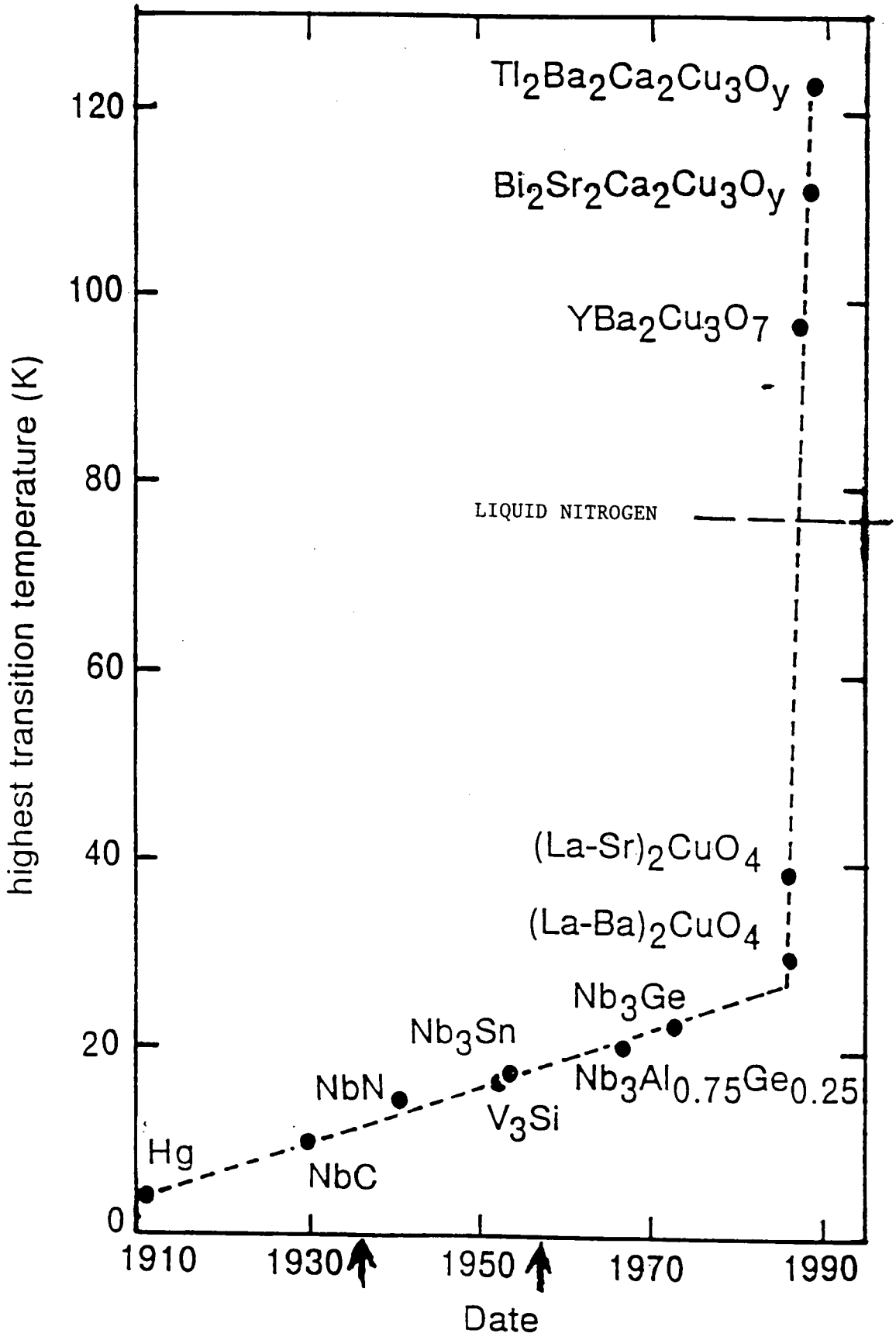
highest transition temperature (K)
120
100
80
60
40
20
0
1910
1930
1950
1970
1990
Date
$Tl_2Ba_2Ca_2Cu_3O_y$
$Bi_2Sr_2Ca_2Cu_3O_y$
$YBa_2Cu_3O_7$
LIQUID NITROGEN
$(La\text{-}Sr)_2CuO_4$
$(La\text{-}Ba)_2CuO_4$
Nb_3Ge
Nb_3Sn
$Nb_3Al_{0.75}Ge_{0.25}$
NbN
V_3Si
Hg
NbC

$YBa_2Cu_3O_7$

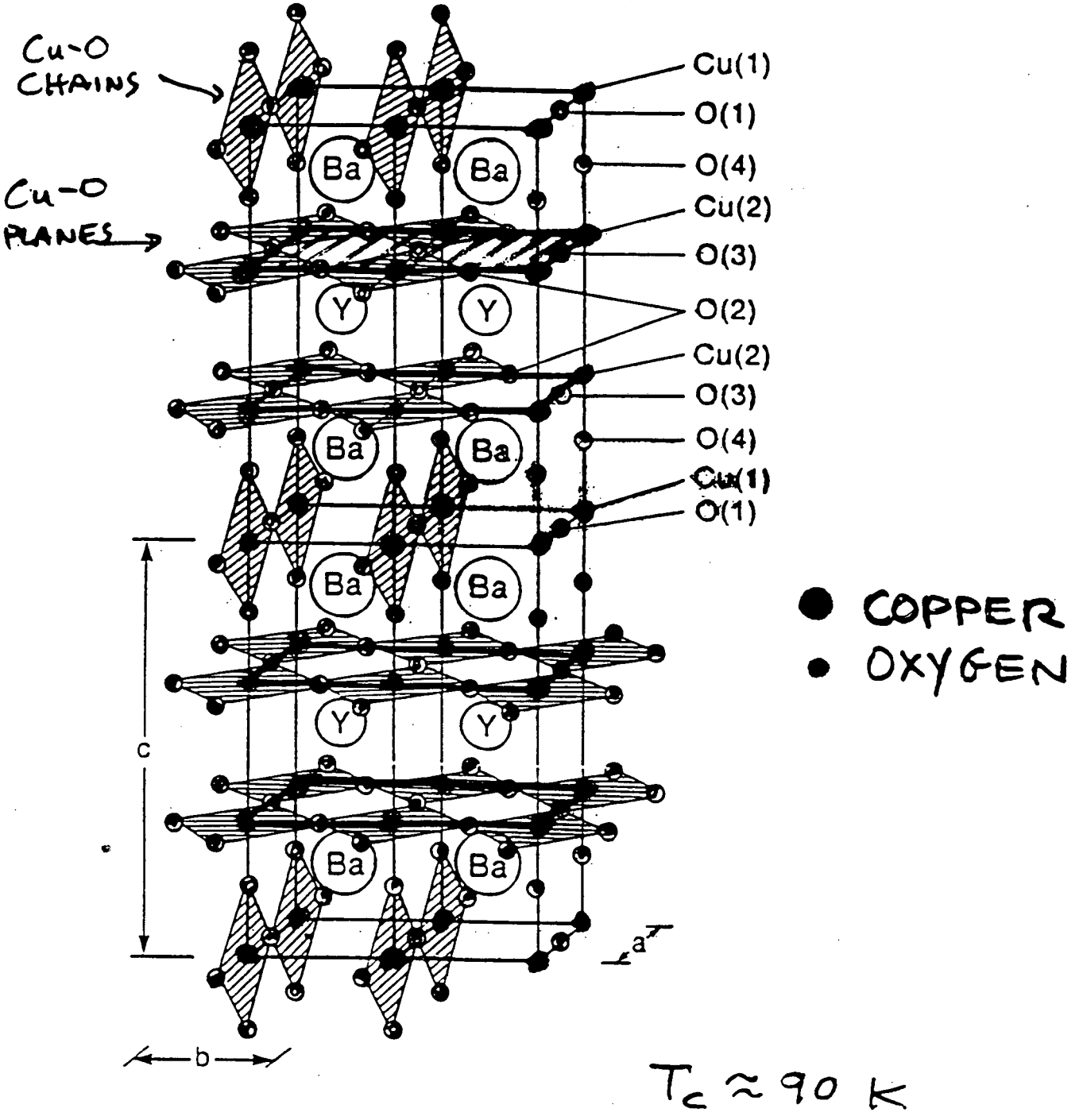

Four unit cells of $YBa_2Cu_3O_7$ showing the copper-oxygen conducting planes (horizontal) and ribbons together with the positions of the atoms. The orthorhombic cell, containing one formula unit, has dimensions a = 3.8863(1)Å, b = 3.8231(1)Å, c = 11.6809(2)Å .

MODELS FOR THE SUPERCONDUCTIVITY

① BCS (ELECTRON-PHONON, OR OTHER BOSON) COOPER PAIRS
CHARGE = 2e

② RESONATING VALENCE BOND (ANDERSON)
NEAREST NEIGHBOR ELECTRON-ELECTRON INTERACTION. PAIRING DUE TO RESONATING BONDS. MIGHT HAVE CHARGE OF BOSON = e, (BUT MOVE IN PAIRS ?)

③ 2-D PLASMONS (KRESIN, RUVALDS)
PAIRING MEDIATED BY PLASMONS
2-D NATURE OF MATERIAL IMPORTANT

④ EXITONIC MECHANISMS (ALLENDER, BRAY, BARDEEN)

$e^- - e^-$ PAIRING MEDIATED BY EXITONIC MECHANISM (e^- - HOLE PAIRS)

MAGNONS
BIPOLARONS
DEMONS
SUPEREXCHANGE
SPINONS
ACOUSTIC PLASMONS
HOLE SUPERCONDUCTIVITY
ANYONS

HIGH - T_c

DO WE HAVE AN ELECTRON PAIRING MECHANISM ?

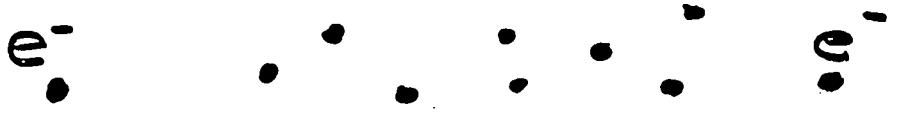

FAR APART (BCS)

$e^- e^-$ CLOSE (BOSON-LIKE)

EXPERIMENTAL TEST FOR PAIRS :

A)

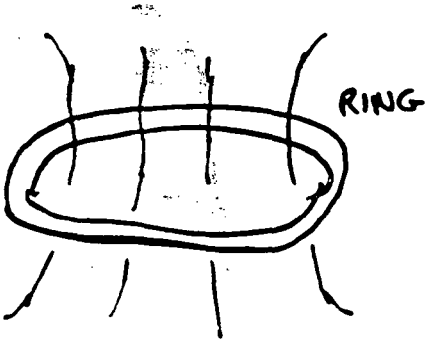

FLUX QUANTIZATION

$\Phi_0 = \frac{2\pi\hbar c}{q}$ $q=2e$?

B) PROTON INTERFERENCE WITH "JOSEPHSON" JUNCTION

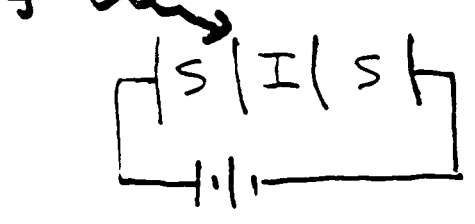

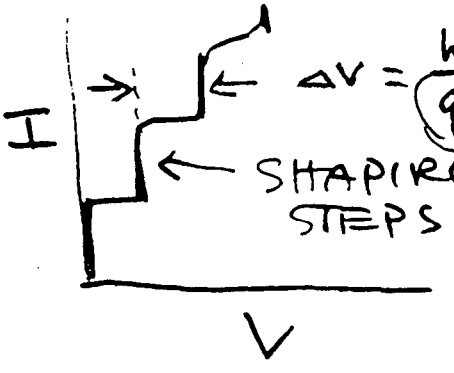

$q=2e$?

EXPERIMENTAL RESULTS:

FLUX QUANTIZATION: $q = 2e$

SHAPIRO STEPS: $q = 2e$

$\Rightarrow$ WE HAVE A

PAIRING MECHANISM

BARDEEN COOPER SCHRIEFFER (BCS) THEORY: (1957)

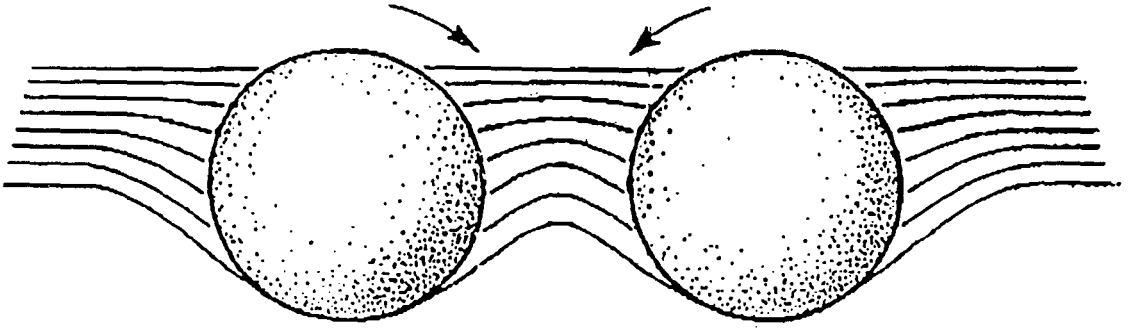

BCS THEORY: ELECTRON - ELECTRON ATTRACTION (CAN BE MEDIATED BY PHONON)

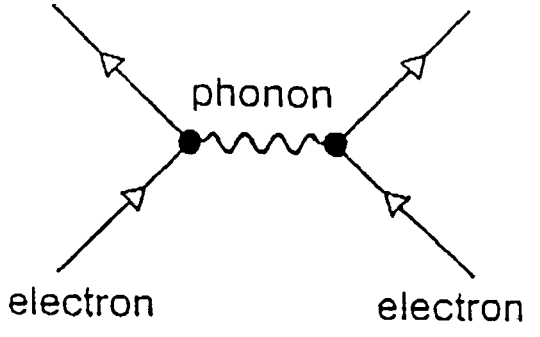

FROM MODEL:

$T_c = \omega e^{-\frac{1}{\lambda - \mu}}$ TRANSITION TEMP.

$2\Delta = 3.5 K_B T_c$ ENERGY GAP OR "PAIRING ENERGY"

WHAT ABOUT BINDING ENERGY OF

ELECTRON PAIRS?

BCS THEORY PREDICTS

BINDING ENERGY $(=2\Delta) = \underbrace{3.5k_B}_{\text{CONSTANT}} T_c$

(ENERGY GAP
IN DENSITY OF STATES)

HOW CAN ONE MEASURE 2Δ ?

ENERGY GAP IN EXCITATION SPECTRUM

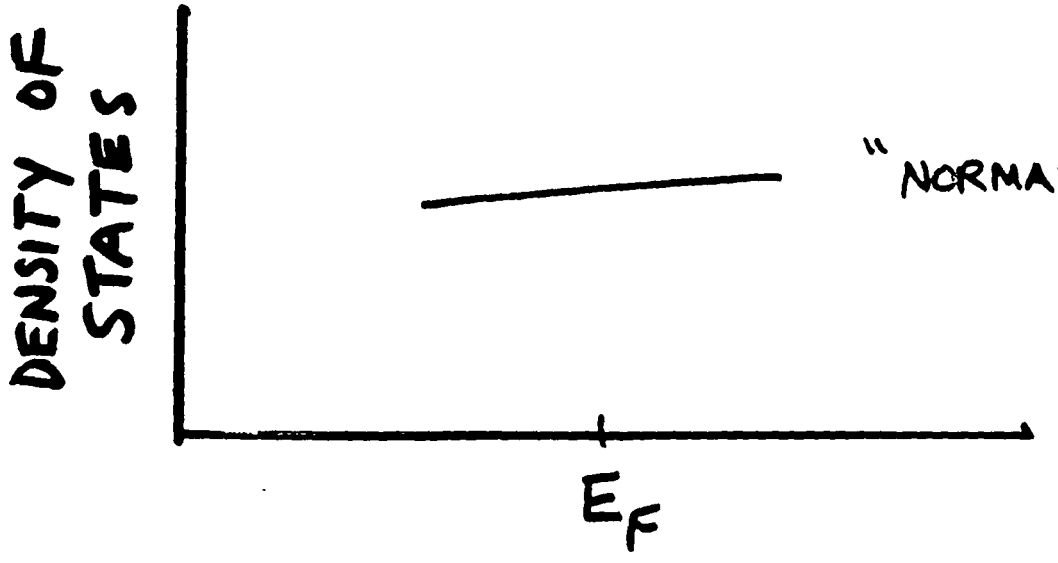

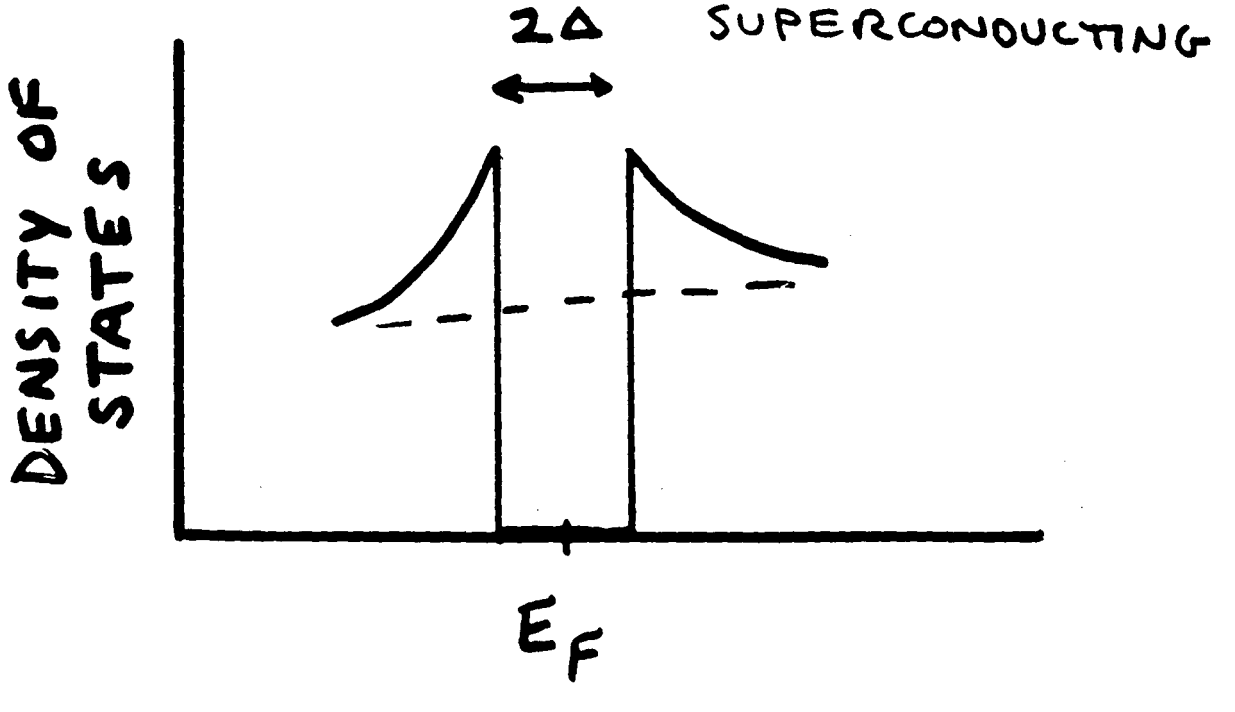

METHODS TO DETERMINE 2Δ:

IF $\Delta = 3.5 k_B T_c$, $T_c \approx 100K$

$\Rightarrow \Delta \approx 35 meV$

$\approx 280 cm^{-1}$ (FIR)

CAN USE (FOR CONVENTIONAL SC's)

1) FIR ABSORPTION

2) TUNNELING SPECTROSCOPY

3) SPECIFIC HEAT

4) ULTRASONIC ATTENUATION

5) <u>PHOTOEMISSION</u> ?

PHOTOEMISSION

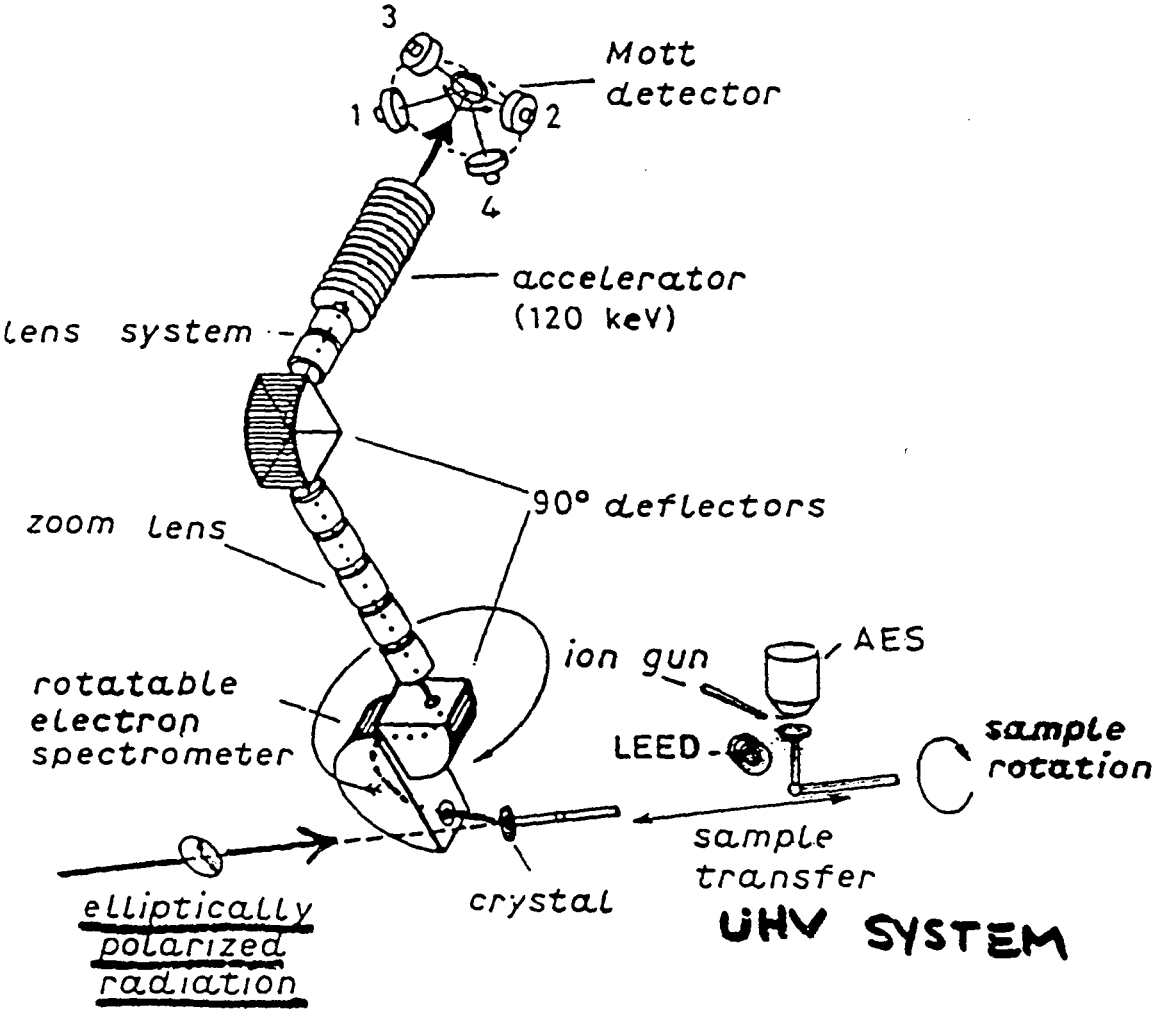

ENERGY, ANGLE, SPIN RESOLVED

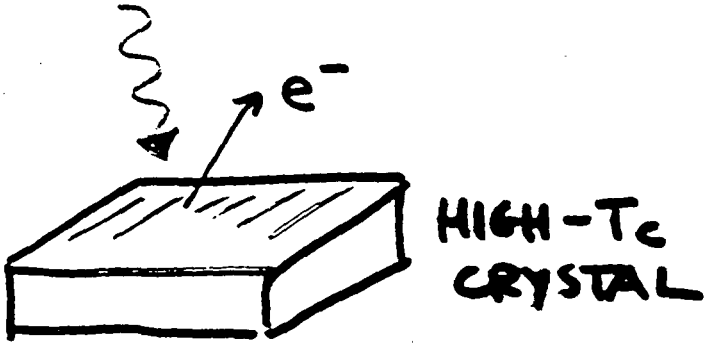

$YBa_2Cu_3O_7$ POLYCRYST.

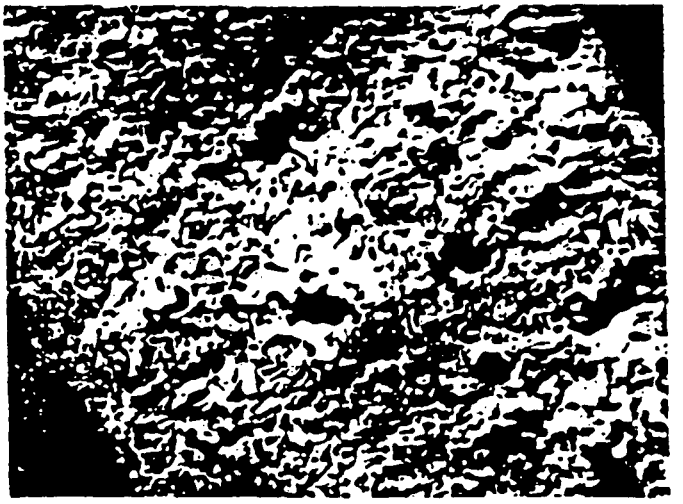

Single Crystals — $YBa_2Cu_3O_7$

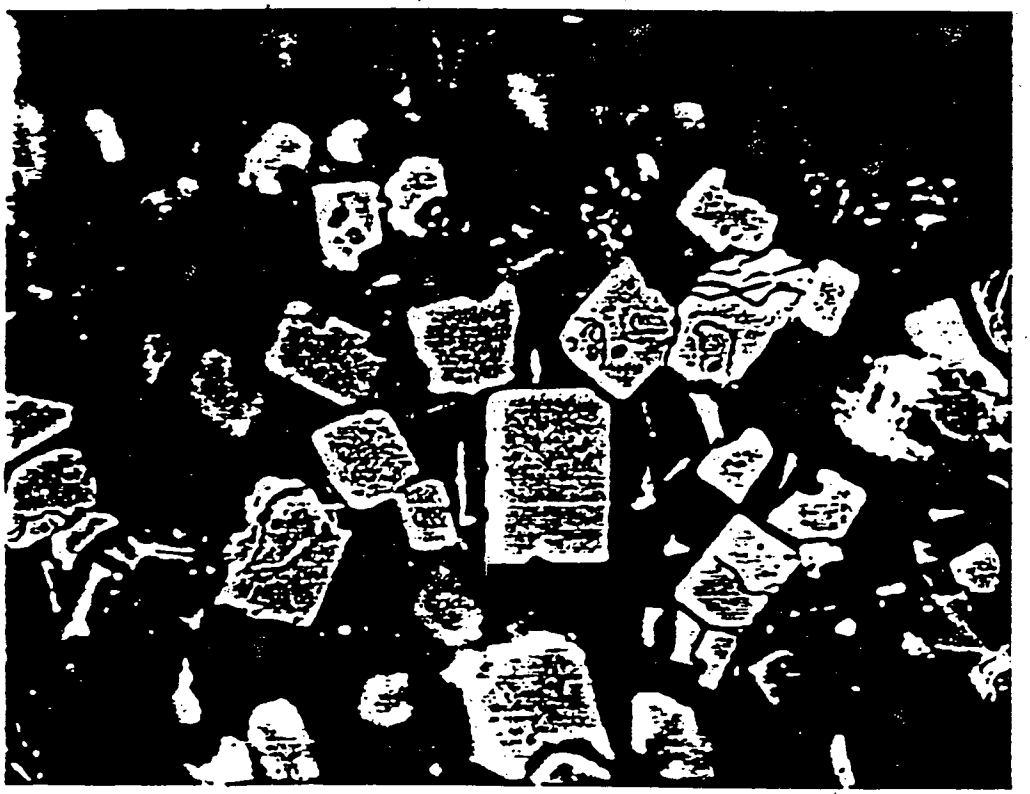

40x lens (.25 mm) 8/3/87 CK

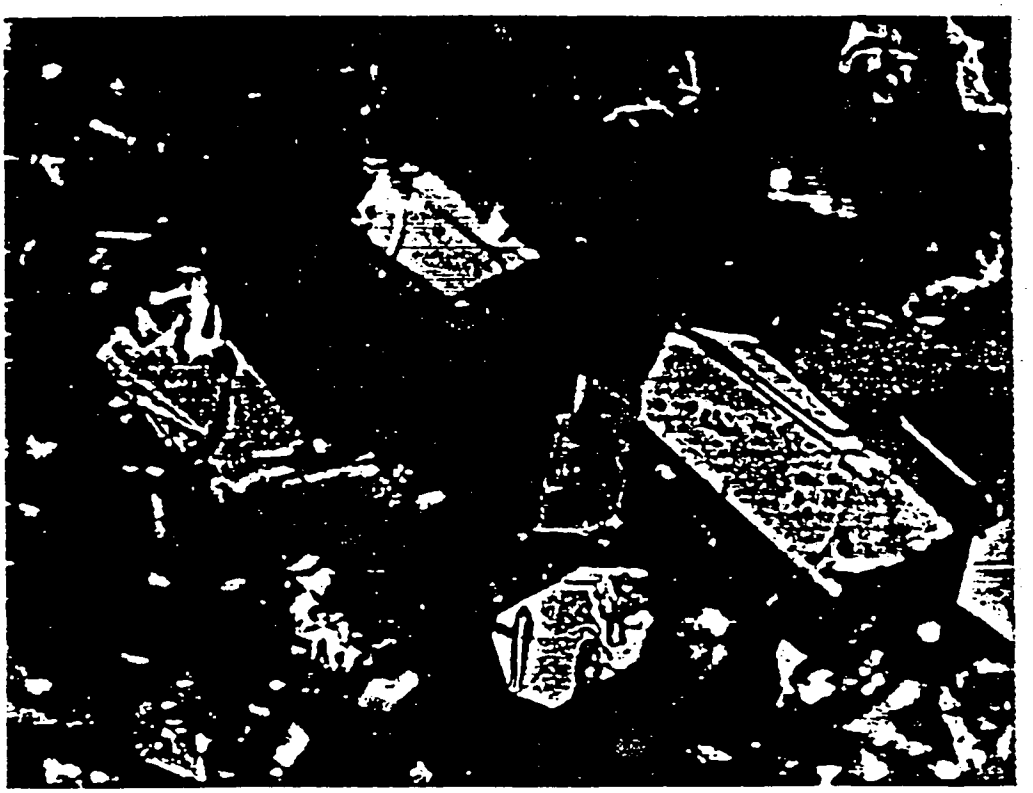

40x lens (.25 mm) 7/28/87 CK

Usual Results

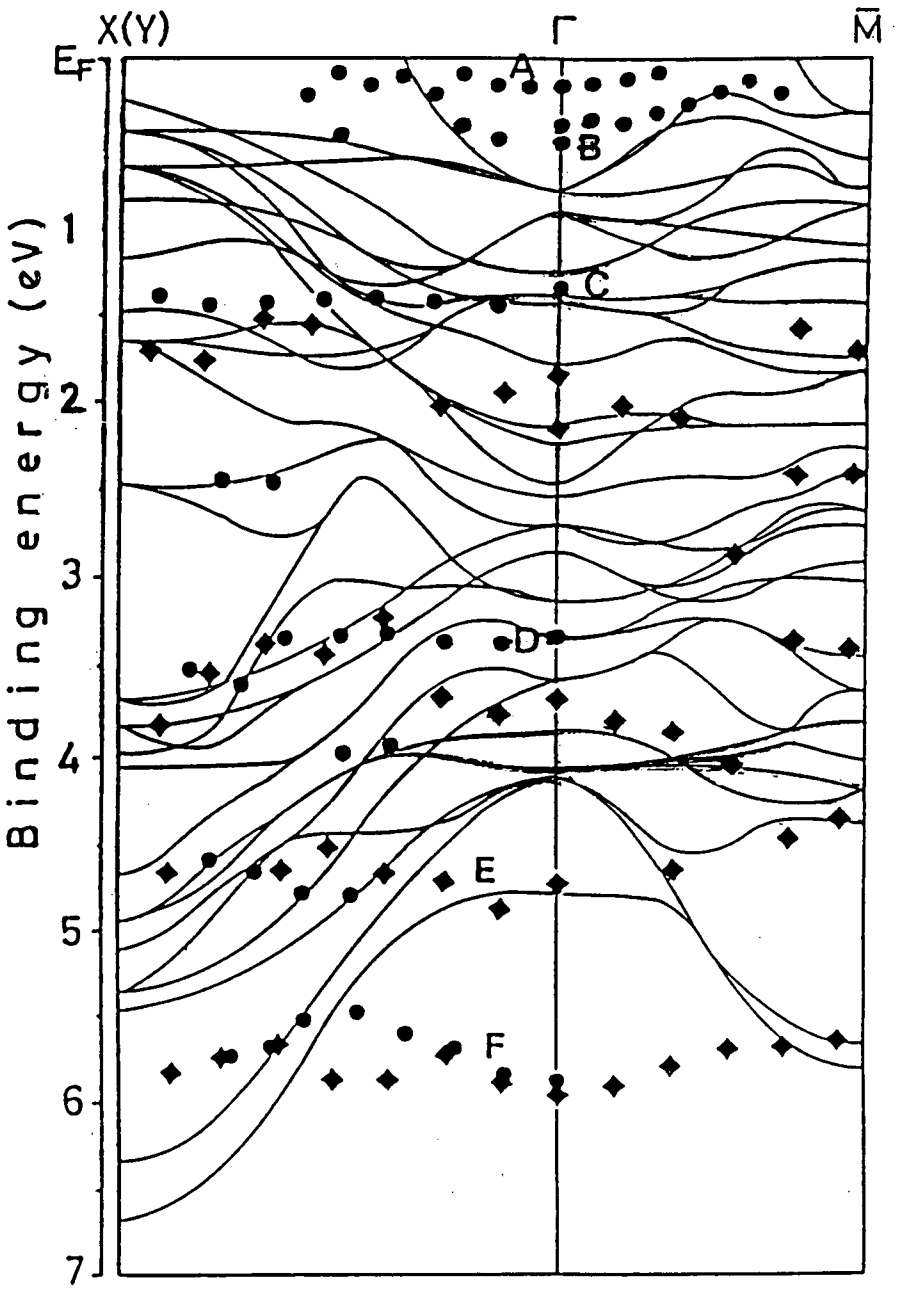

Band structure of $Bi_2Sr_2CaCu_2O_8$ determined by the angle-resolved photoemission with $h\omega = 18$ eV (circles) and 40 eV (squares). Note that the experimental results with $h\omega = 18$ eV are shown only for the ΓX direction in the high-binding energy region. A band structure calculation (Katayama-Yoshida et al.) is shown by thin, solid lines for comparison.

200 meV Resolution

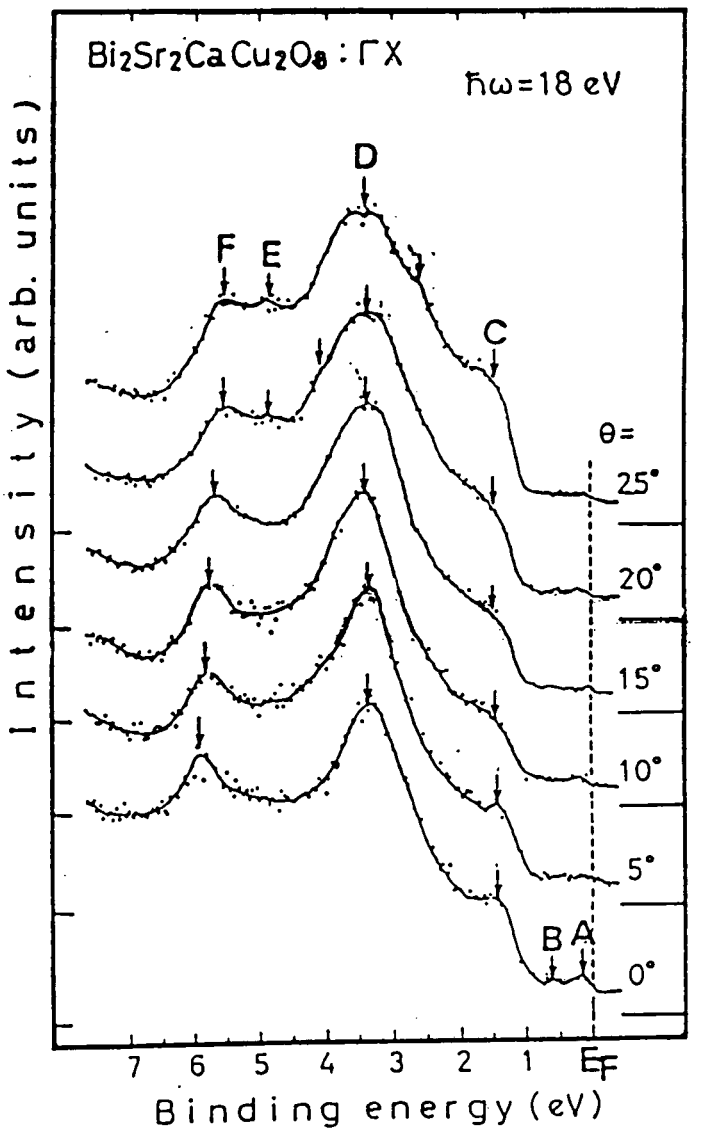

Angle-resolved photoemission spectra of $Bi_2Sr_2CaCu_2O_8$ measured in the direction of ΓX using hω = 18 eV. Polar angle referred to the surface normal is indicated on each spectrum. (Katayama-Yoshida et al.)

TO OBSERVE ENERGY GAP STRUCTURE:

NEED GOOD RESOLUTION !

THIS STUDY:

U-U PHOTOEMISSION ($\hbar\omega = 21.2$ eV, 40.8 eV)

RESOLUTION = 20 meV

MATERIAL: SINGLE CRYSTAL

$Bi_2Sr_2CaCu_2O_8$

$T_c \approx 88$ K

TEMPERATURES: $T = 105$ K

$T = 15$ K

Imer, Petroff, Zettl, et al., PRL

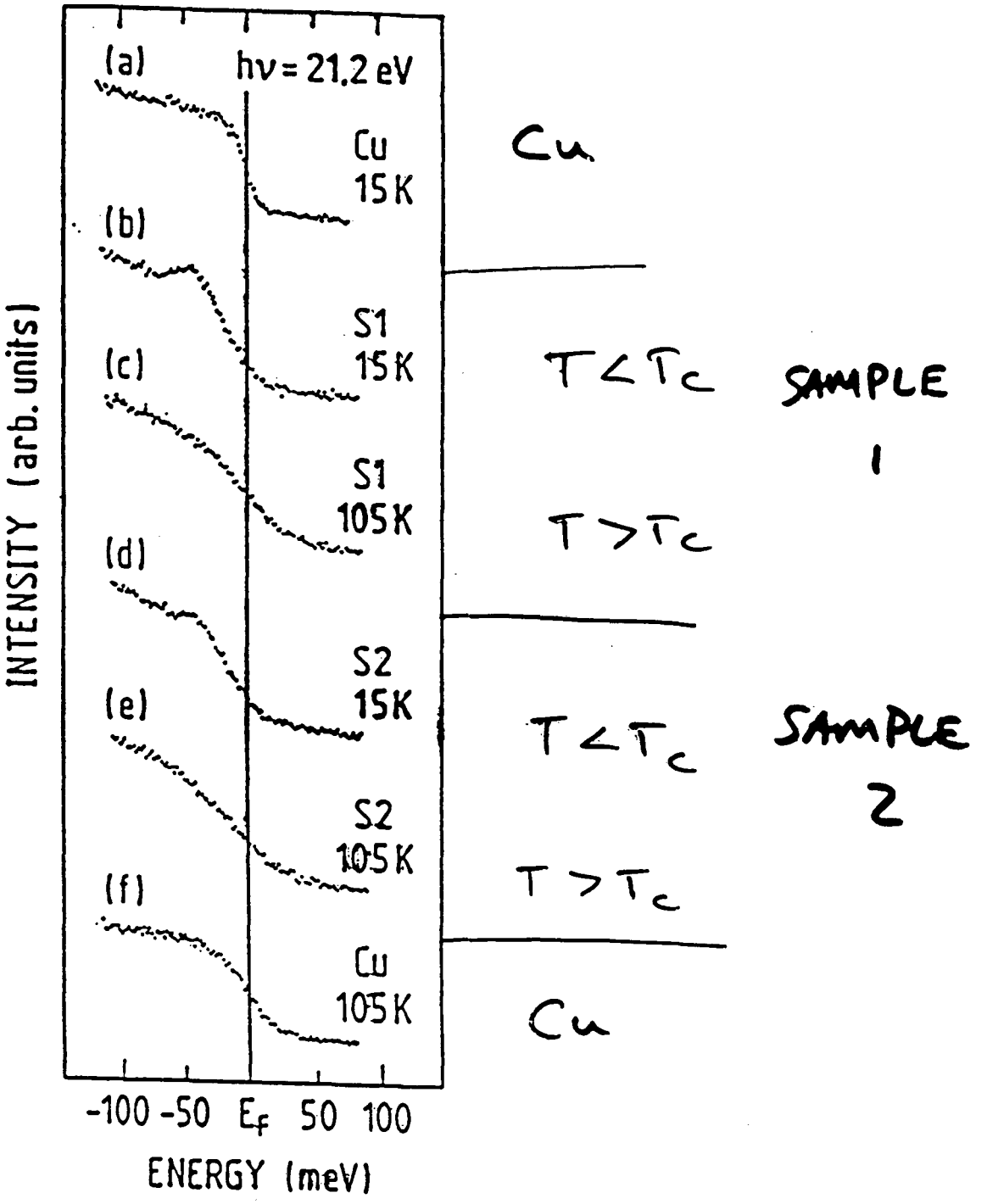

Photoemission spectra of Bi-Sr-Ca-Cu-O samples (S1, S2) in the normal state [(c) and (e)] and the superconducting state [(b) and (d)]. Reference spectra of Cu [(a) and (f)] recorded under identical conditions. Note that the 200 meV energy range of these spectra corresponds to two data points around E_F in the wide energy range spectrum of the preceding figure.

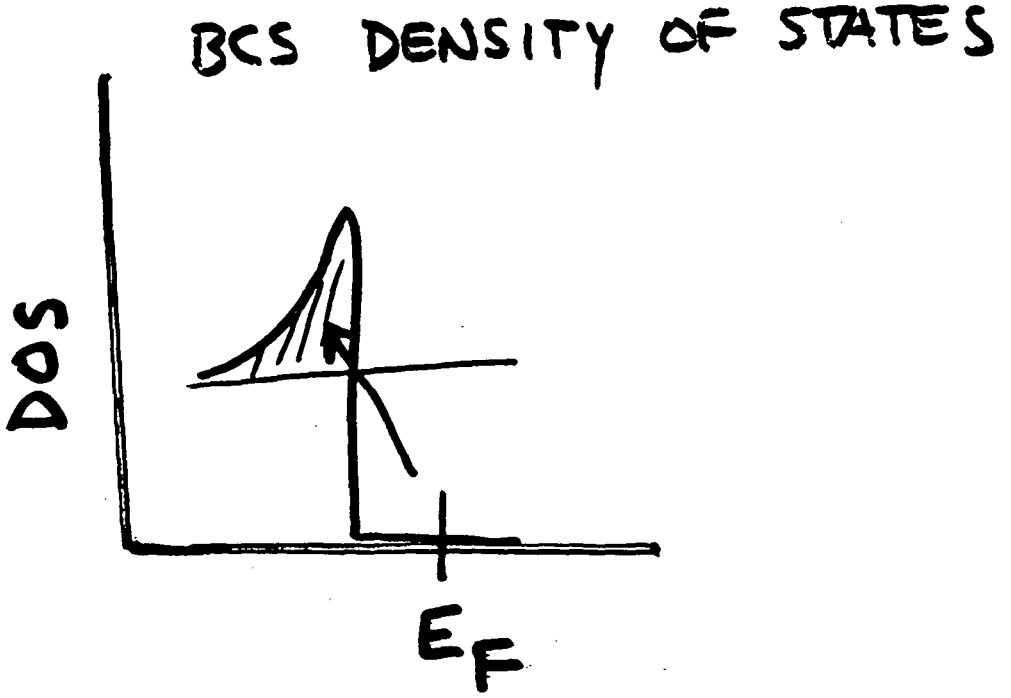
BCS DENSITY OF STATES
DOS
E_F

Photoemission

Petroff, Zettl, et al., PRL

FIT:

Convolute DOS with 20 meV Gaussian (resol) and Fermi FN.

User 2Δ as fitting parameter.

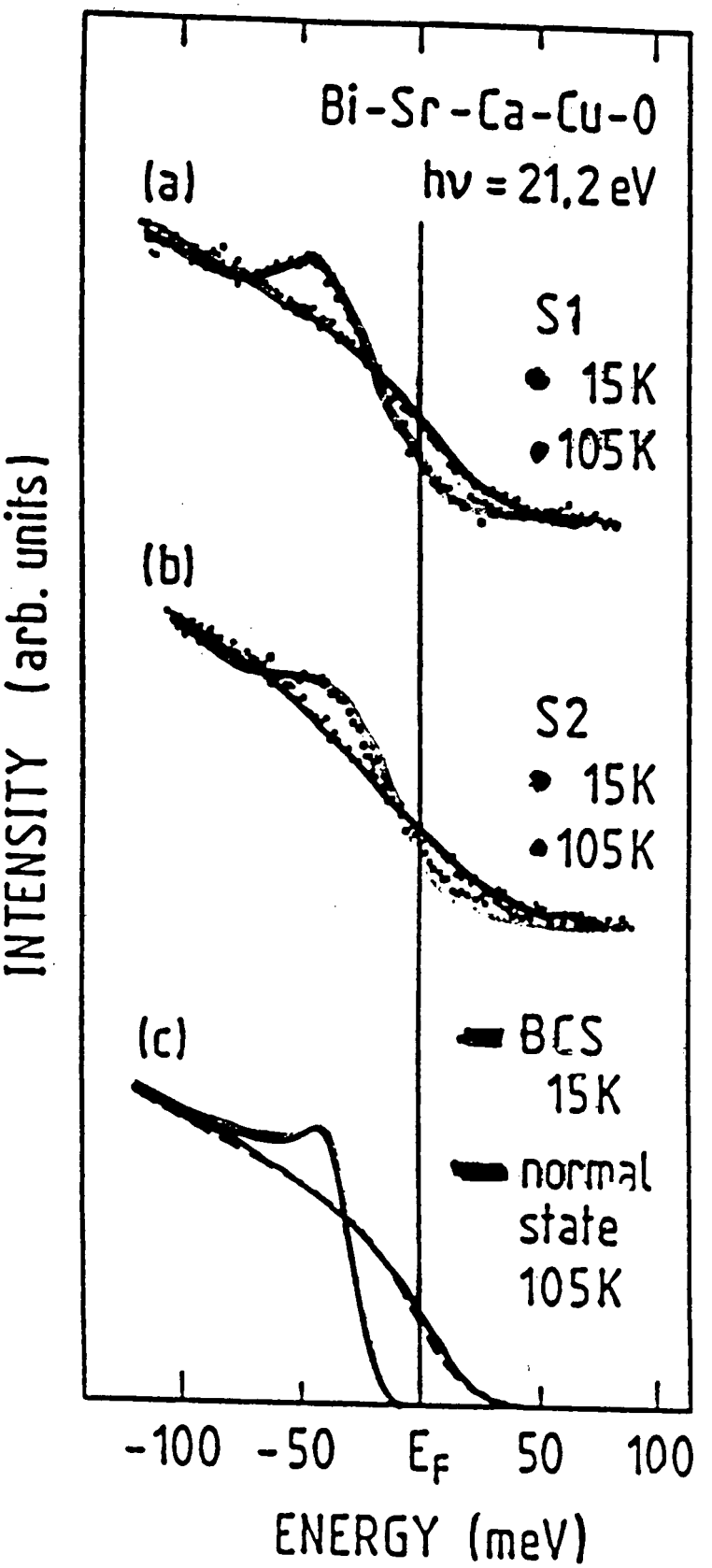

Exp.

Exp.

"Theory"
$2\Delta_0/K_BT_C$
$\approx 6.5 - 9$

We observed the gap as expected from BCS theory.

However, gap size:

Predicted: $\boxed{2\Delta = 3.5\ K_B T_C}$

Measured: $\boxed{2\Delta = 8\ K_B T_C}$

The gap size is over twice that expected from conventional theory.

ADDITIONAL PHOTOEMISSION POSSIBILITIES:

1) ANGULAR RESOLVED

CAN PROBE DIFFERENT CRYSTAL DIRECTIONS

2) PHOTON POLARIZATION

SPIN ORBIT COUPLING, OTHER POLARIZATION-DEPENDENT EXCITATION, TRANSPORT, TRANSMISSION PHENOMENA

Pristine Host Material

BSCCO 2212

a = b = 5.4 Å

c = 30.8 Å

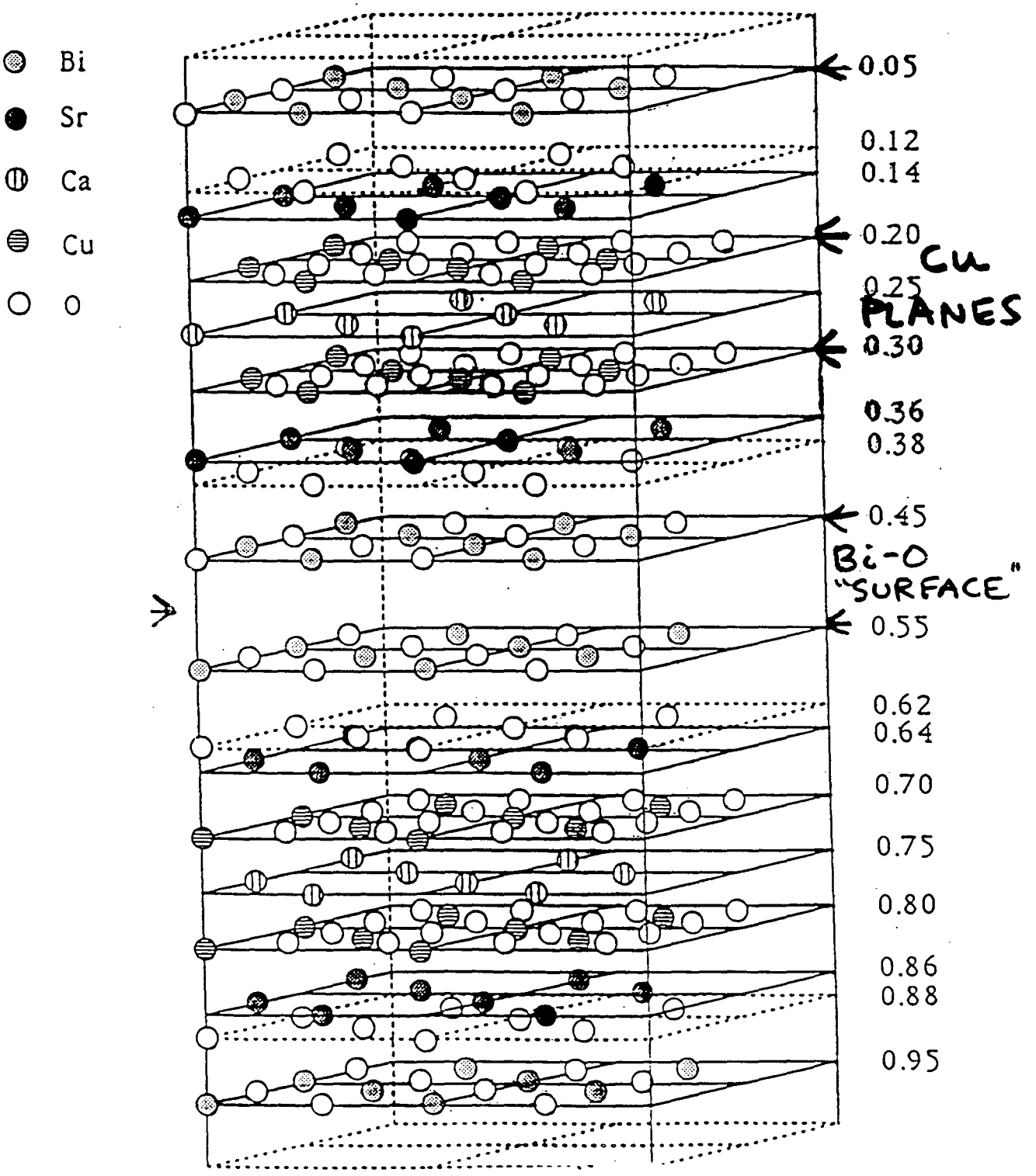

B.O. Wells et al.

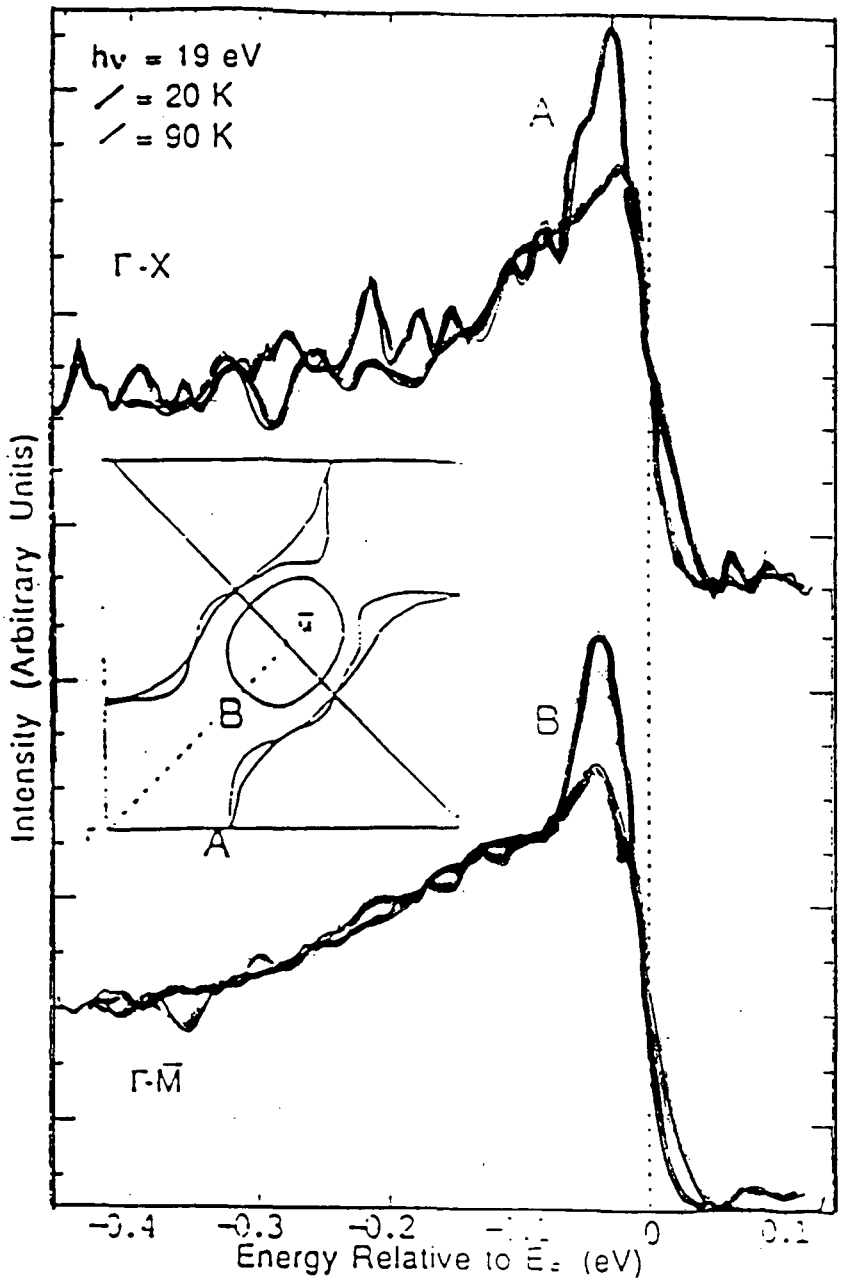

— SUPER-CONDUCTING

— NORMAL

Cu-O PLANES

Bi-O LAYERS

Photoemission spectra showing the opening of a superconductiong gap along both the Γ-X and the Γ-M directions in k space for the 12-atm-O_2-annealed sample.

$2\Delta/K_BT_C$ Cu-O Planes

$2\Delta/K_BT_C$ Bi-O Planes : Larger!

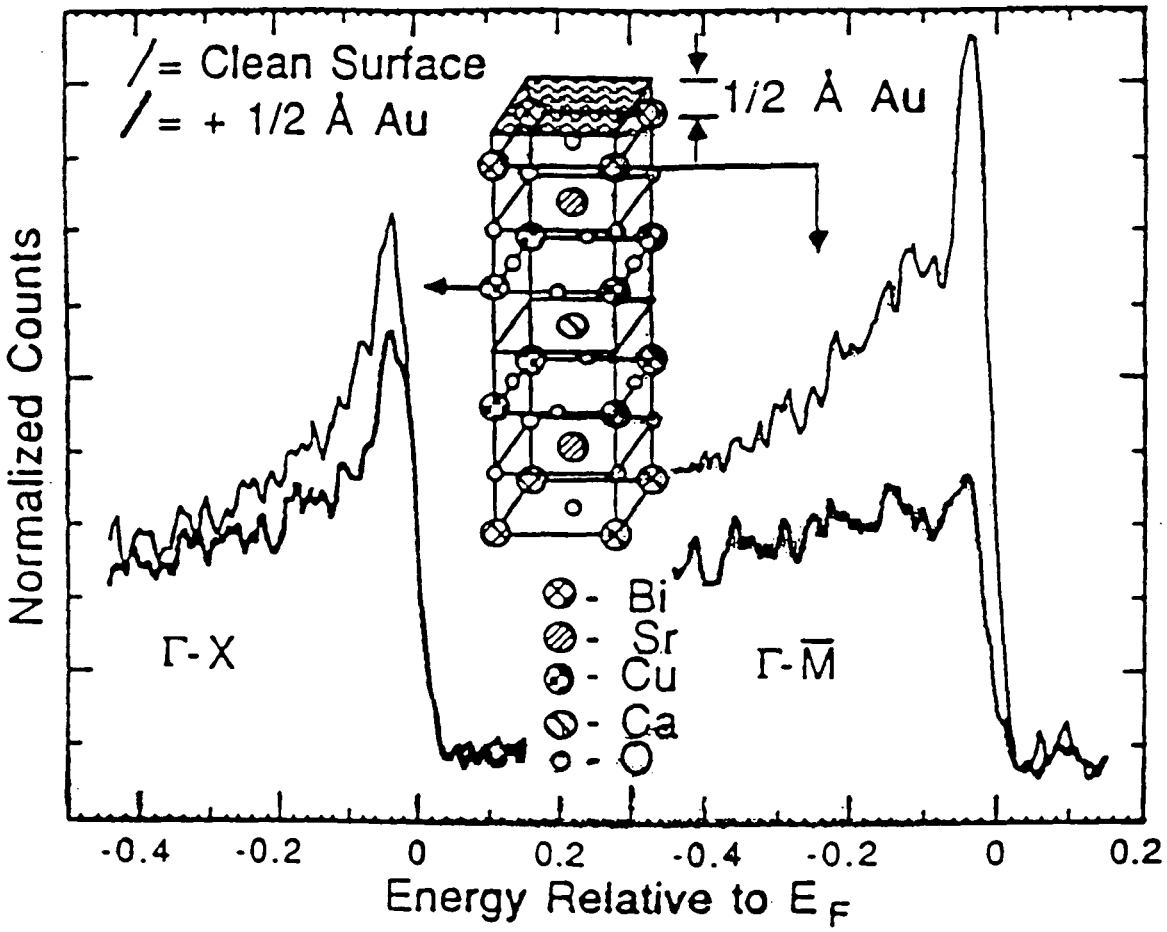

Photoemission spectra of the states at the Fermi level along both the Γ-*X* and the Γ-*M* directions before and after deposition of $\frac{1}{2}$ Å of Au. Spectra were taken at 20 K with 19-eV photons and are normalized to incident photon flux. Inset: A schematic representation of the experiment. The actual Au overlayer is not continuous but consists mostly of isolated Au atoms. Arrows indicate the layers from which we believe each feature originates.

D.S. DESSAU ET.AL.

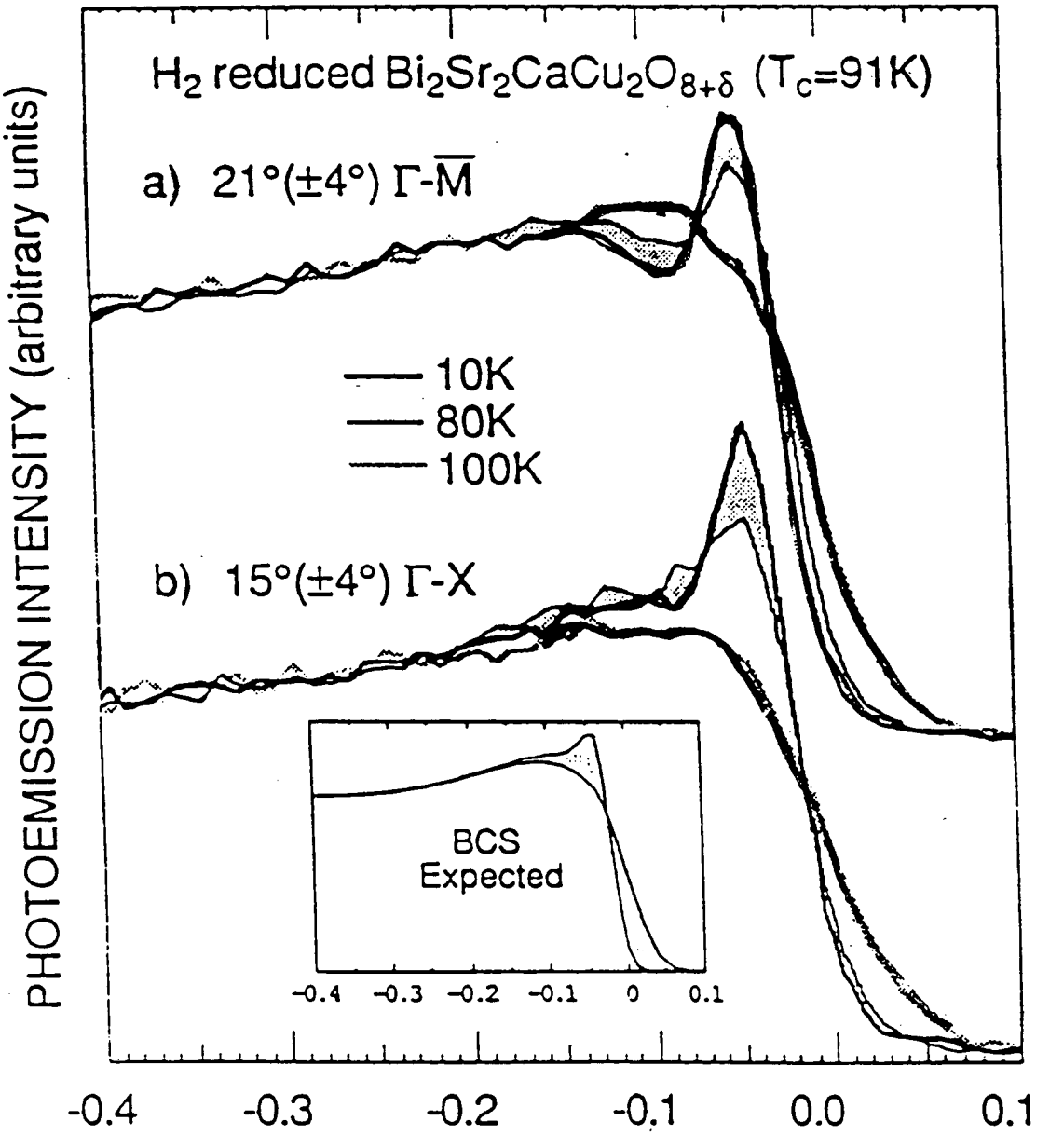

ANOMALOUS SPECTRAL WEIGHT TRANSFER (NON-BCS-LIKE)

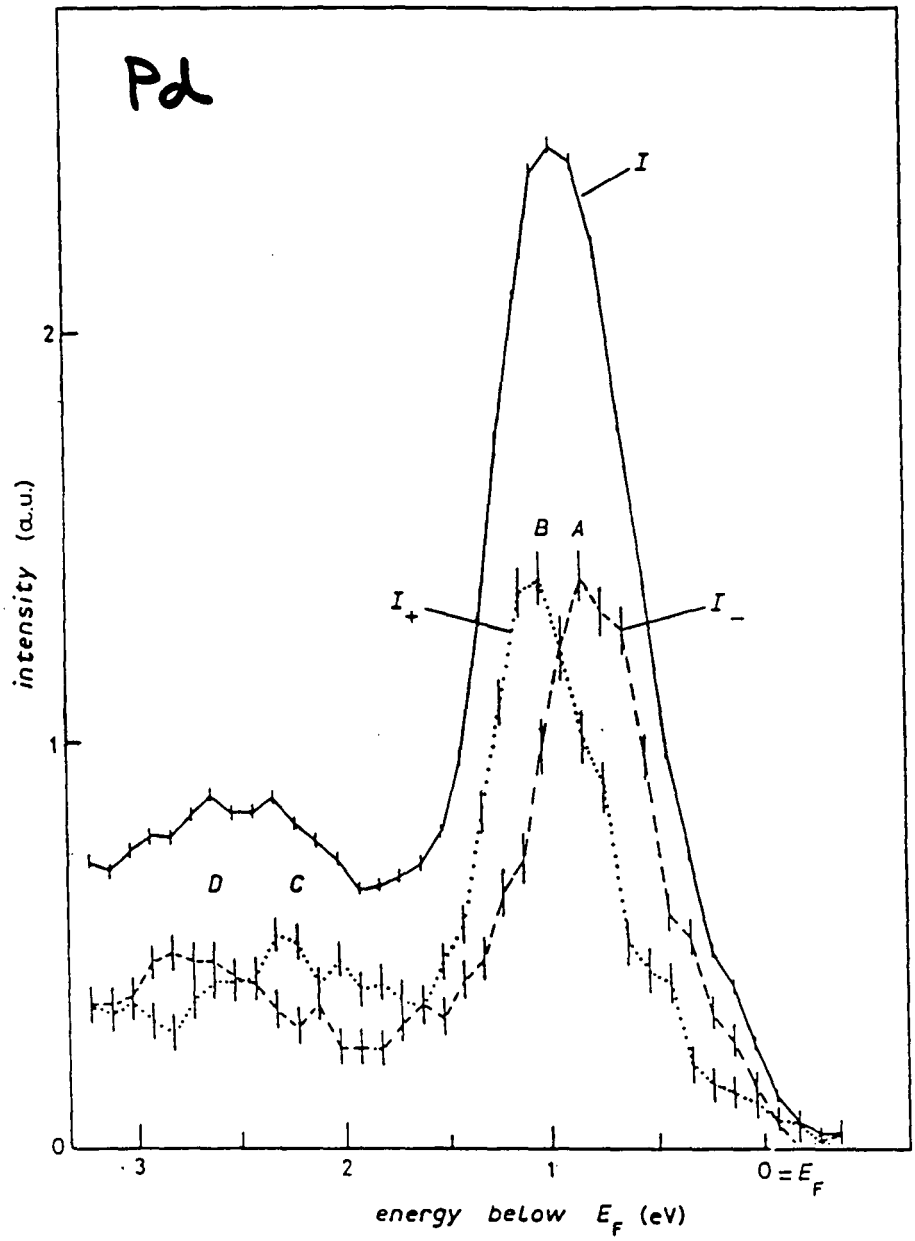

Photoelectron spectra from Pd(111) for circularly polarized synchrotron radiation at $h\nu = 16\,\mathrm{eV}$. The solid line is the photoelectron intensity I at normal photoemission, which is separated into the partial intensities I_+ and I_- by means of the spin polarization P [19].

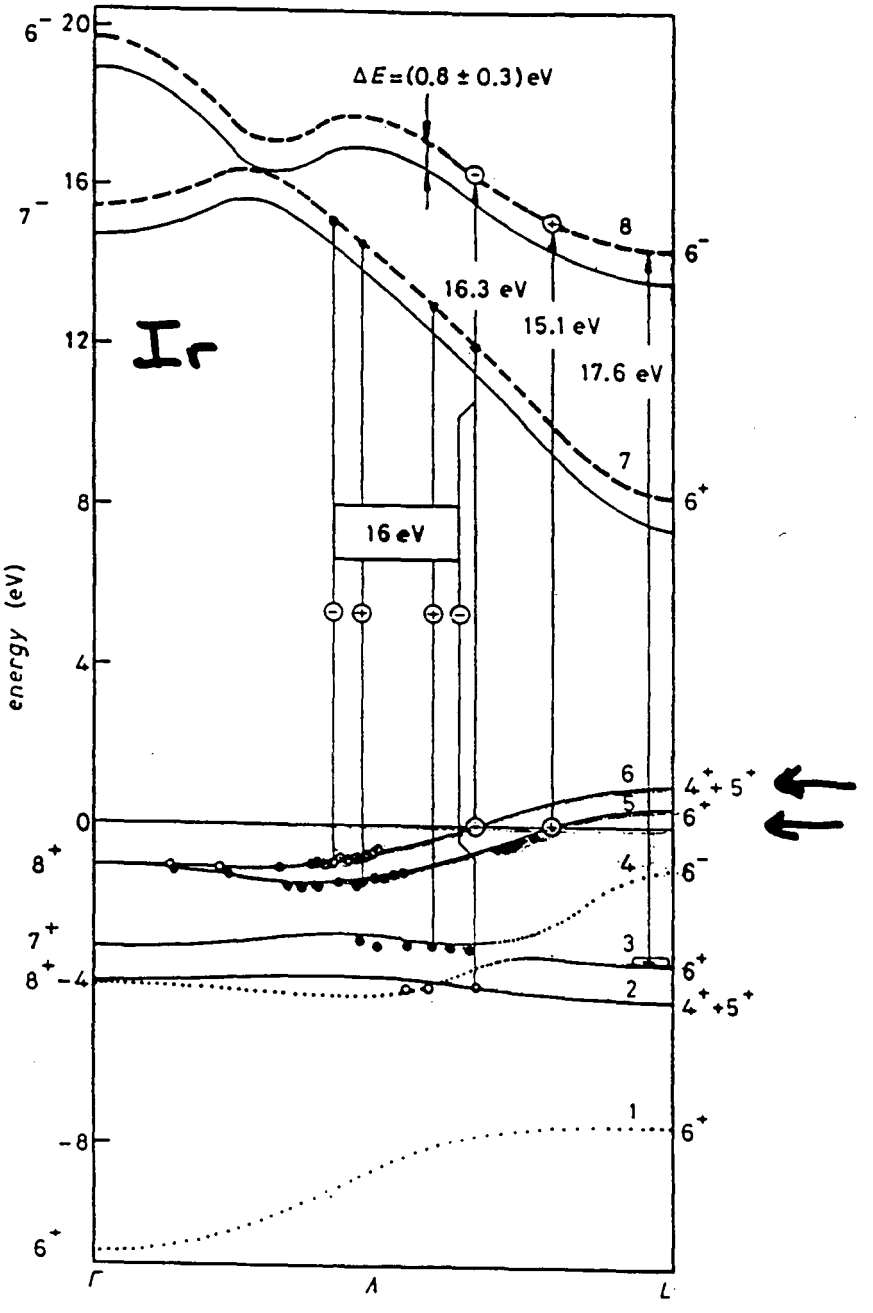

Symmetry-resolved band mapping of Ir(111)[17] in comparison with the calculated band structure[36]. The mapping points have been obtained from the spin-resolved partial photoelectron spectra. Bands with full symbols yield positive polarized electrons and correspond to Δ_6 symmetry, while bands with open symbols (negative polarization) are characterized by Δ_{4+5}. The calculated band structure has to be corrected by a 0.8 eV broader band gap (difference between dashed and full band curves) in order to map the uppermost band between 15.1 and 16.3 eV photon energy well.

CAN RESOLVE DIFFERENT BANDS WITH SPIN ANALYSIS

UNUSUAL PAIR STATES MAY LEAD TO MANY SURPRISES IN SPIN-RESOLVED PHOTOEMISSION.

(NOT YET PERFORMED)

ALS: GOOD SOURCE OF PHOTONS FOR PHOTOEMISSION (CIRCULAR POLAR.)

PHOTOEMISSION IN SUPERCONDUCTORS:

NEW FIELD (EXPERIMENTAL + THEORETICAL)

NOTE: GAP STRUCTURE IN CONVENTIONAL SUPERCONDUCTORS HAS NOT BEEN INVESTIGATED VIA PHOTOEMISSION!

Magnetic Scattering, Anomalous Dispersion, and Circular Dichroism

M. Blume

Brookhaven National Laboratory

MAGNETIC SCATTERING, ANOMALOUS DISPERSION, AND CIRCULAR DICHROISM

M. Blume

Brookhaven National Laboratory
Upton, NY 11973

Circular polarization is of importance in probing properties of matter that are either not time-reversal invariant (magnetism) or not parity conserving (chirality). This talk includes a discussion of transmission and small-angle scattering experiments (i.e., those below a Bragg cutoff that would be appropriate for an ALS bending magnet). Such experiments include absorption as a function of polarization, change of polarization as a function of transmission, and small-angle scattering about a surface reflection as a function of polarization. The latter experiment might be used to study "magnetic roughness" of surfaces, for example.

Also discussed are the intensity and final polarization of radiation transmitted through matter with a matrix index of refraction. It is pointed out that there are phenomena in which rotation of polarization and absorption do not commute. The calculation of the index of refraction near absorption edges is described, and symmetry arguments are used to give explicit forms for the indices. These phenomena may also be of use in providing polarization and analysis for soft x rays.

$$(\nabla^2 + n^2 k^2)\psi = 0$$

$$\psi(z) = e^{ink z}\psi(0) \qquad \psi = E_x, E_y$$

$$I(z) = |\psi(z)|^2 = |e^{ink z}|^2 |\psi(0)|^2$$

$$= I(0)\, e^{-2n'' k z} \qquad n = n' + in''$$

For polarized radiation

n is a 2×2 matrix, and

$$|\psi\rangle = \begin{pmatrix} E_x \\ E_y \end{pmatrix} \quad \left[|\psi\rangle = \sqrt{I_0}\begin{pmatrix} 1 \\ 0 \end{pmatrix} \text{ for linear pol., etc} \right]$$

$$I(z) = \langle \psi(z) | \psi(z) \rangle = \langle \psi | e^{-in^\dagger k z} e^{ink z} | \psi \rangle$$

$$\left[= e^{-2n'' k z} \text{ only if } [n', n''] = 0 ! \right]$$

$$\overline{I(z)} = \sum_{mm'} \langle m|\overline{|\psi\rangle\langle\psi|}|m'\rangle \langle m'|e^{-in'kz} e^{ink z}|$$

$$\overline{|\psi\rangle\langle\psi|} = \text{2x2 matrix}$$

$$= I_0 \cdot \tfrac{1}{2}\left(1 + \underline{P}\cdot\underline{\sigma}\right)$$

$$\equiv I_0 \cdot \rho$$

$$\overline{I(z)} = \sum_{mm'} \langle m|\rho|m'\rangle\langle m'|e^{-in'kz} e^{ink z}|n \times I(0)$$

$$\boxed{I(z) = tr\left(e^{ink z}\, \rho\, e^{-in'kz}\right)\cdot I(0)}$$

$$\boxed{\underline{P}' I(z) = tr\left(\underline{\sigma}\, e^{ink z}\, \rho\, e^{-in'kz}\right)\cdot I(0)}$$

$\underline{P}$ = Poincaré - Stokes vector.

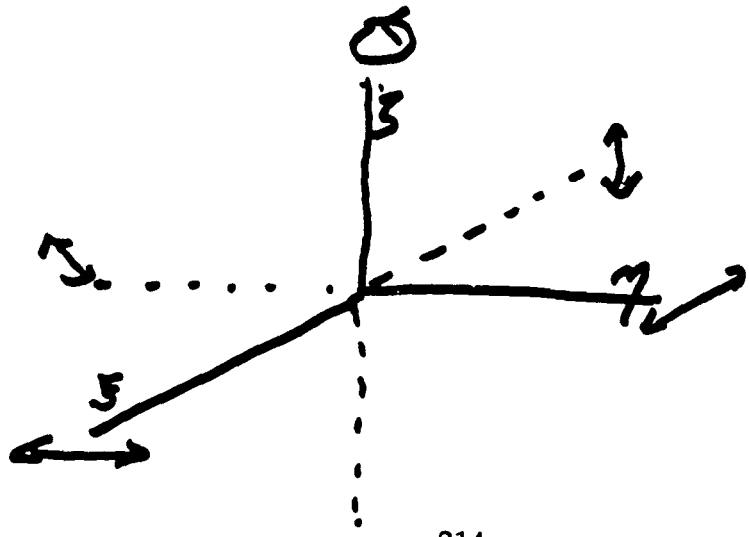

$$nkz = a + \underline{b}\cdot\underline{\sigma}$$

$$a = \tfrac{1}{2} kz\,(n_{++} + n_{--})$$

$$b_\xi = \tfrac{1}{2} kz\,(n_{+-} + n_{-+})$$

$$b_\eta = \tfrac{1}{2} i\, kz\,(n_{+-} - n_{-+})$$

$$b_\zeta = \tfrac{1}{2}(n_{++} - n_{--})$$

e^{inkz} represents a <u>rotation</u> of the Poincaré vector about the $\underline{b}$ axis.

$$\frac{I(z)}{I(0)} = e^{i(a-a^*)}\Big\{\cos b^*\cos b + (\hat{b}^*\cdot\hat{b})\sin b^*\sin b$$

$$- i\,\hat{b}^*\cdot\underline{P}\sin b^*\cos b + i\,\hat{b}\cdot\underline{P}\sin b\cos b^*$$

$$+ i\,\underline{P}\cdot(\hat{b}^*\times\hat{b})\sin b^*\sin b\Big\}$$

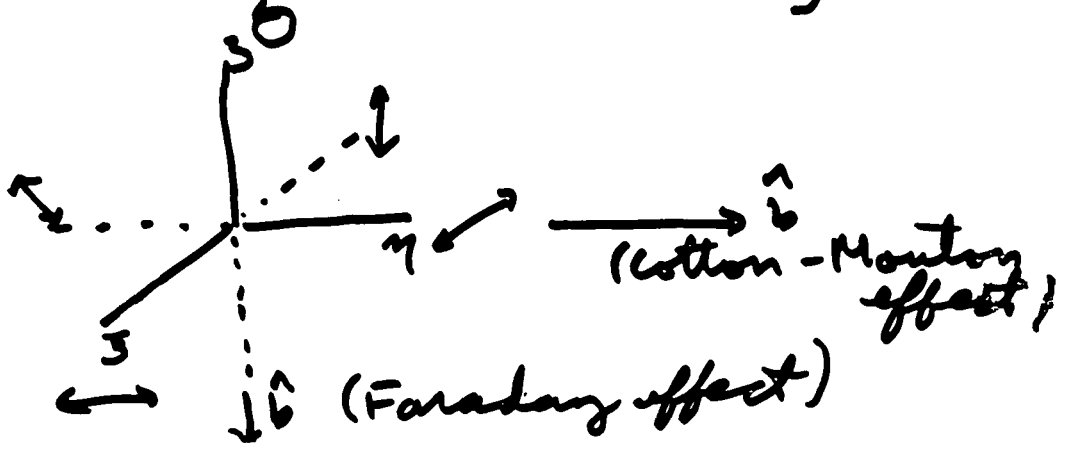

Calculation of n

$$n = 1 + \frac{2\pi}{k^2} \cdot \frac{1}{V} \bar{f}(\underline{k}\sigma \to \underline{k}\sigma')$$

---

f = forward scattering amplitude

$$\bar{f}(\underline{k}\sigma \to \underline{k}'\sigma') = \left(\frac{e^2}{mc^2}\right) \sum_a p_a \Bigg\{ \langle a | \sum_j e^{i(\underline{k}-\underline{k}')\cdot \underline{r}_j} | a \rangle \, \underline{\epsilon}'_{\sigma'} \cdot \underline{\epsilon}_\sigma$$

(charge)

$$- i \frac{\hbar\omega}{mc^2} \langle a | \sum_j e^{i(\underline{k}-\underline{k}')\cdot \underline{r}_j} \left(i \frac{\underline{K} \times \underline{p}_j}{k^2} \cdot \underline{A} + \underline{s}_j \cdot \underline{B} \right) | a \rangle$$

(magnet)

$$+ \frac{\hbar^2}{m} \sum_c \frac{\langle a | \sum_j e^{-i\underline{k}\cdot \underline{r}_j} \underline{p}_j \cdot \underline{\epsilon}'_{\sigma'} | c \rangle \langle c | \sum_i e^{i\underline{k}\cdot \underline{r}_i} \underline{p}_i \cdot \underline{\epsilon}_\sigma | a \rangle}{E_a - E_c + \hbar\omega - i\Gamma/2} \Bigg\}$$

(resonant)

$$E_a = \epsilon_a \qquad E_c = \hbar\omega_0 + \epsilon_c$$

$$\bar{f}(k\sigma \to k\sigma') = \frac{e^2}{mc^2} \Bigg\{ N \, \underline{\epsilon}'_{\sigma'} \cdot \underline{\epsilon}_\sigma$$

$$+ \frac{\hbar^2}{m} \sum_{ac} p_a \frac{\langle a | \sum_j e^{-i\underline{k}\cdot \underline{r}_j} \underline{p}_j \cdot \underline{\epsilon}'_{\sigma'} | c \rangle \langle c | \sum_i e^{i\underline{k}\cdot \underline{r}_i} \underline{p}_i \cdot \underline{\epsilon}_\sigma | a \rangle}{E_a - E_c + \hbar\omega - i\Gamma/2}$$

$$\bar{f} = \frac{e^2}{mc^2}\epsilon'^{\alpha}_{\sigma'}\epsilon^{\beta}_{\sigma}\left\{\delta^{\alpha\beta}N + m\omega_0^2\sum_{ac}P_a\frac{\langle a|\sum_j r_j^{\alpha}(1-\frac{i}{2}r_j\cdot k)|c\rangle\langle c|\sum_i r_i^{\beta}(1+\frac{i}{2}k\cdot r_i)|a\rangle}{\hbar(\omega-\omega_0)-i\frac{\Gamma}{2}}\left(1-\frac{\epsilon_a-\epsilon_c}{\omega-\omega_0-i\Gamma/2\hbar}\right)\right\}$$

Resonant Dipole term:

$$= \frac{e^2}{mc^2}\, m\omega_0^2\sum_{ac}P_a\frac{\langle a|\sum_j r_i^{\alpha}|c\rangle\langle c|\sum_i r_i^{\beta}|a\rangle}{\hbar(\omega-\omega_0)-i\frac{\Gamma}{2}}\epsilon'^{\alpha}_{\sigma'}\epsilon^{\beta}_{\sigma}$$

$$= \epsilon'^{\alpha}_{\sigma'}\epsilon^{\beta}_{\sigma}\; C^{\alpha\beta}$$

$$C^{\alpha\beta} = C_0\delta^{\alpha\beta} + C_s^{\alpha\beta} + C_a^{\alpha\beta}$$

$$C_s^{\alpha\beta} = C_s^{\beta\alpha} \qquad C_a^{\alpha\beta} = -C_a^{\beta\alpha}$$

<u>Magnetic crystal:</u>

$$C_s^{\alpha\beta} = m^{\alpha}m^{\beta} - \tfrac{1}{3}m^2\delta^{\alpha\beta}$$

$$C_a^{\alpha\beta} = i\epsilon^{\alpha\beta\gamma}m^{\gamma}$$

$$C_0 = 3\,\mathrm{tr}\,C$$

non-magnetic uniaxial crystal

$C_s^{\alpha\beta} \propto \hat{n}^\alpha \hat{n}^\beta - \frac{1}{3}\delta^{\alpha\beta}$

(Templeton scattering; EXAFS)

$C_a^{\alpha\beta} = 0$.

Magnetic and uniaxial

$$C_s^{\alpha\beta} \propto \left(\hat{n}^\alpha \hat{n}^\beta - \tfrac{1}{3}\delta^{\alpha\beta}\right)\left(a + b(\hat{n}\cdot\hat{m})^2\right)$$
$$+ \text{magnetic terms}$$
$$+ \left(n^\alpha m^\beta + n^\beta m^\alpha - \tfrac{2}{3}(\hat{n}\cdot m)\delta^{\alpha\beta}\right)(\hat{n}\cdot\hat{m})$$

$$C_a^{\alpha\beta} \propto i\varepsilon^{\alpha\beta\gamma}\hat{n}^\gamma(\hat{n}\cdot\underline{m})$$

How big are these terms?
What do we learn?

Big formula:

$$n_{\sigma'\sigma} = \delta_{\sigma\sigma'} + \epsilon_{\sigma'}^{\alpha}\epsilon_{\sigma}^{\beta}\frac{2\pi Ne^2}{m\omega^2}\Bigg\{\delta^{\alpha\beta}$$

dipole

$$+\frac{m\omega_0^2}{N}\sum_{ac}p_a\left(1-\frac{\epsilon_a-\epsilon_c}{\omega-\omega_0-i\frac{\Gamma}{2}}\right)\Bigg[\frac{\langle a|\sum_j r_j^{\alpha}|c\rangle\langle c|\sum_i r_i^{\beta}|a\rangle}{\hbar(\omega-\omega_0)-i\frac{\Gamma}{2}}$$

dipole-quadrupole (→ circular dichroism)

$$-\frac{i}{2}\frac{\langle a|\sum_j r_j^{\alpha}r_j^{\gamma}|c\rangle\langle c|\sum_i r_i^{\beta}|a\rangle}{\hbar(\omega-\omega_0)-i\frac{\Gamma}{2}}k^{\gamma}+\frac{i}{2}\frac{\langle a|\sum_i r_i^{\alpha}|c\rangle\langle c|r_j^{\beta}}{\hbar(\omega-\omega_0)-i\frac{\Gamma}{2}}$$

$$+\frac{\langle a|\sum_j r_j^{\alpha}r_j^{\gamma}|c\rangle\langle c|\sum_i r_i^{\beta}r_i^{\delta}|a\rangle}{\hbar(\omega-\omega_0)-i\frac{\Gamma}{2}}k^{\gamma}k^{\delta}\Bigg]\Bigg\}$$

quadrupole

Holmium

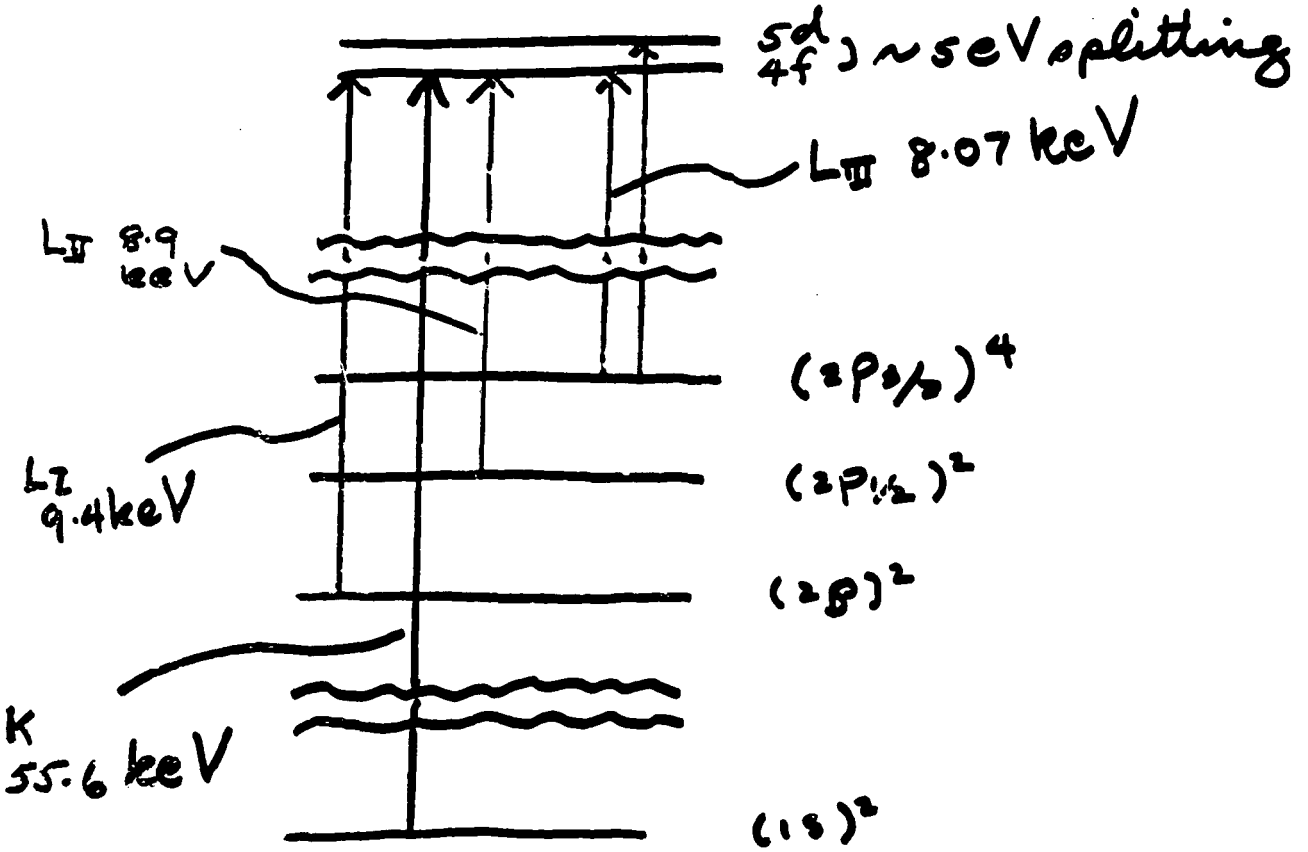
5d / 4f ~ 5eV splitting
L_{III} 8.07 keV
L_{II} 8.9 keV
$(2p_{3/2})^4$
L_I 9.4keV
$(2p_{1/2})^2$
$(2s)^2$
K 55.6 keV
$(1s)^2$

Electric Quadrupole transitions (p→f)
Calculations are more complex:
"Straightfoward but tedious – left as an exercise for the listener"
or see
Hannon, Trammell, Blume, Gibbs.

Two add'l vectors, $\underline{k}'$ and $\underline{k}$, can contribute to the scattering tensor.

Terms such as

$$(\underline{k}'\underline{k} - (\underline{k}'\cdot\hat{\underline{s}})(\underline{k}\cdot\hat{\underline{s}}))(\underline{\epsilon}'\underline{\epsilon} - (\underline{\epsilon}'\hat{\underline{s}})(\underline{\epsilon}\cdot\hat{\underline{s}})) - (k'\times k)\cdot s\,(\epsilon'\times\epsilon)\cdot s$$

$$- i\,(k'\times k)\cdot s\,(\epsilon'\epsilon - \epsilon' s(\epsilon\cdot s)) - i\,(\epsilon'\times\epsilon)\cdot s\,(k'\cdot k - k's\,k\ldots$$

⋮

etc.

Pauli principle is essential;
∴ called Resonant Exchange Scattering

Largest in E1 transitions from M levels in actinides.

X-RAY RESONANT EXCHANGE SCATTERING

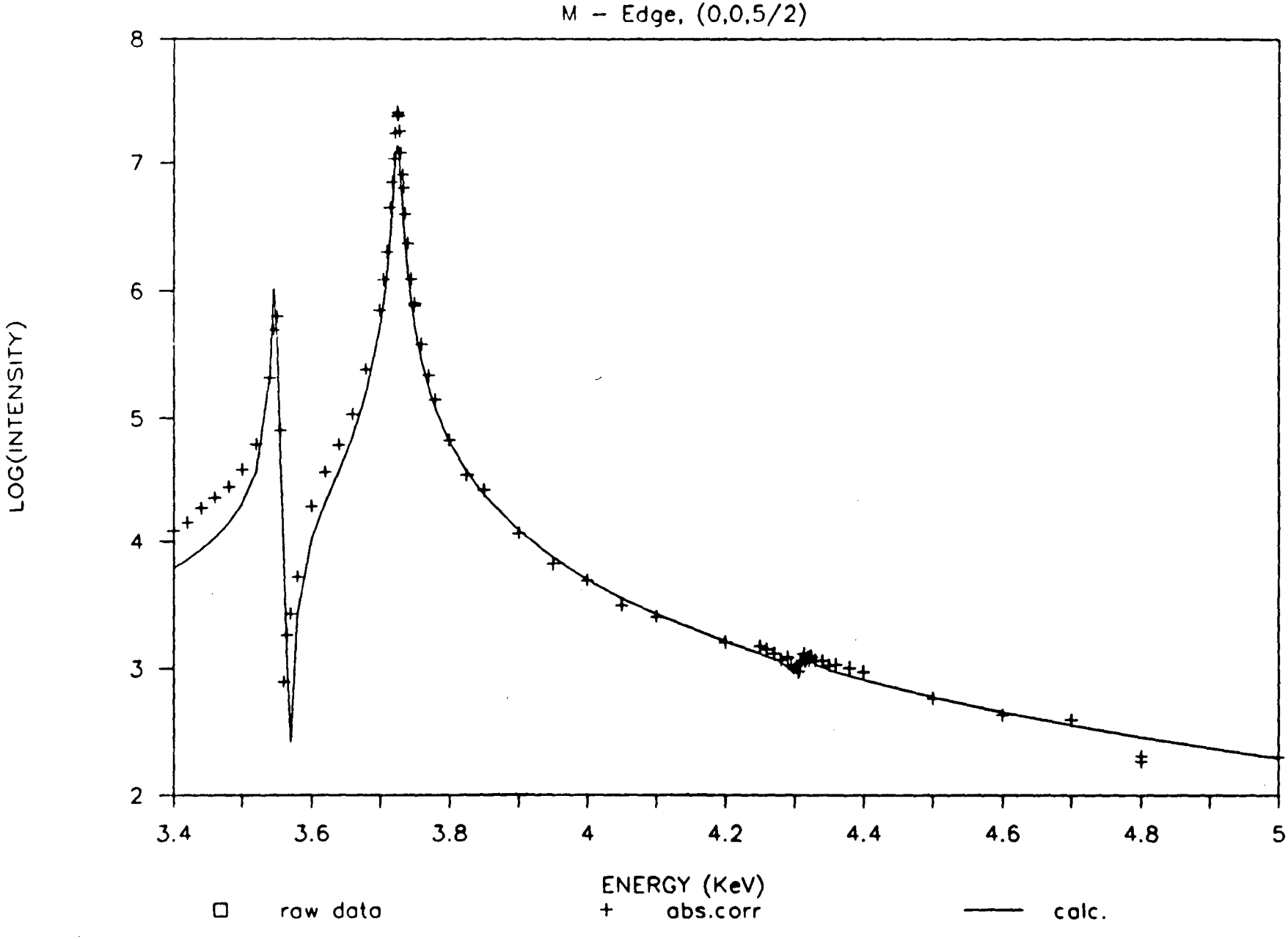

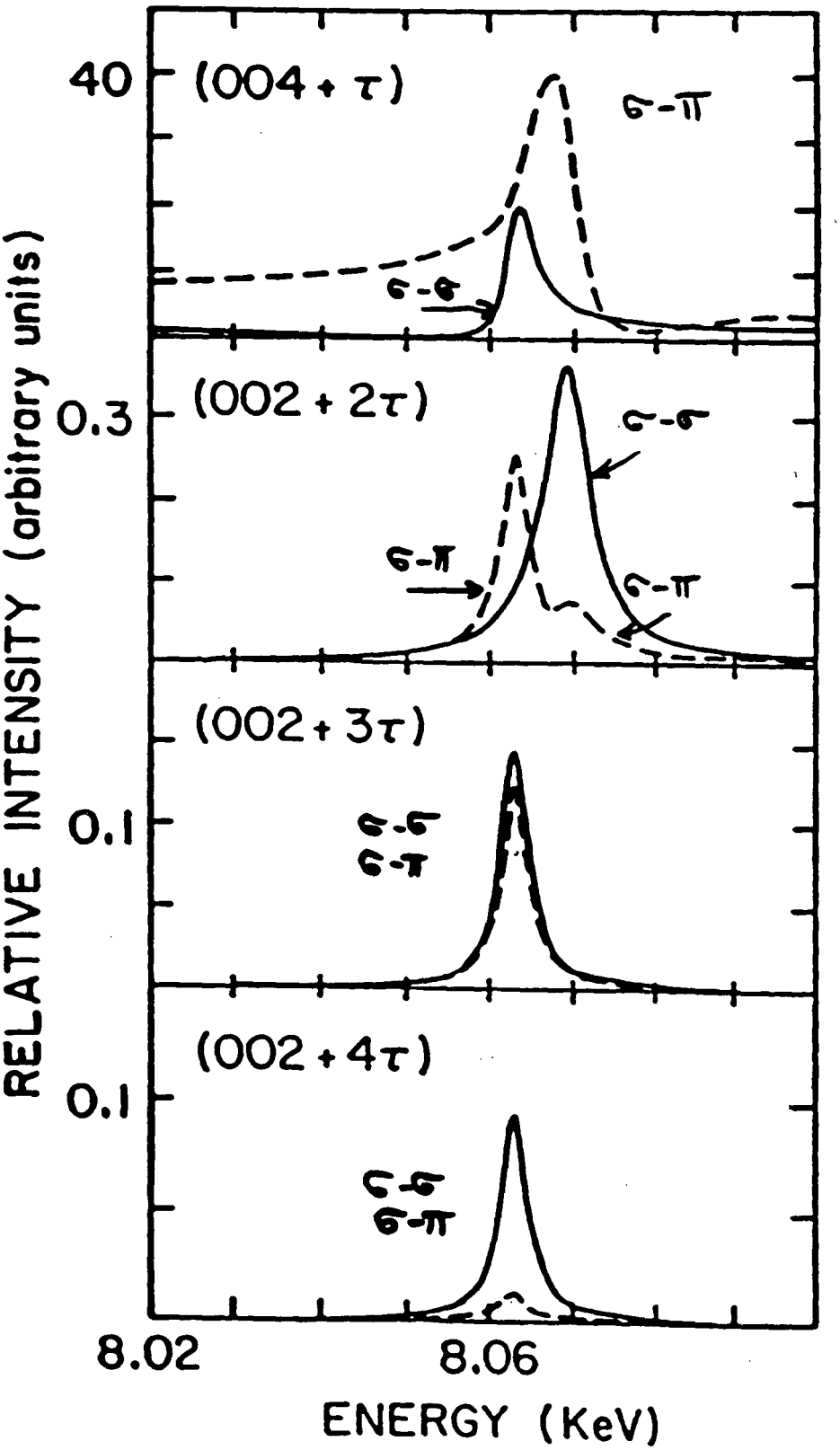

Hannon, Trammell, Blume, Gibbs, PRL 61 1245 (88).

Can ALS Photons be Used to Study Fundamental Symmetries in Atomic Physics

E.D. Commins

University of California, Berkeley

Outline of Lecture by E.D. Commins on the topic:

Can ALS Photons be used to study Fundamental Symmetries in Atomic Physics?

Many persons have asked whether circularly polarized photons in the extreme ultra-violet and soft X ray regions might usefully be employed to extend the investigation of parity non-conservation in atoms. This lecture is an attempt to provide some background information that may help the reader to answer that question.

Parity nonconservation (the breakdown of mirror symmetry) was first observed directly in nuclear beta decay and other charged weak interactions in 1957. It came as a great surprise, and was a momentous event in physics. The knowledge gained from this and other discoveries ultimately led to a great theoretical advance in the late 1960's - invention of the **Standard Model**, in which the weak and electromagnetic interactions are unified. The creators of the standard model, S. Weinberg, and independently A. Salam, proposed a class of hitherto undiscovered neutral weak interactions, as part of the new scheme.

The first neutral weak interactions were observed in 1973. During the ensuing decade a whole series of dramatic experiments were performed on neutral weak phenomena to elucidate and verify the predictions of the standard model. These culminated in direct observations of the "carriers" of the charged and neutral weak interactions: the massive intermediate vector bosons $W^{\pm}$ and Z^{o} respectively.

Among the neutral weak phenomena predicted in the standard model was parity nonconservation (PNC) in atoms. This arises from the interference between the electromagnetic interaction (photon exchange) and the neutral weak interaction (Z^{o} exchange) that couple an atomic valence electron to the nucleus. The first observations of PNC were made with optical rotation experiments in bismuth (Novosibirsk, 1978). These were followed soon therafter by other optical rotation observations in lead and eventually thallium, and by Stark interference experiments in thallium and cesium, at various laboratories in France, Britain, the USSR, and the USA. These experiments have all been done with lasers in the visible or near ultraviolet range.

The results of all this work, particularly in cesium, where atomic theory and experiment have reached the highest state of perfection, are in excellent agreement with the standard model, which in the meanwhile has been established beyond doubt as the correct description of "low-energy" neutral weak phenomena.

Although there is no longer any doubt about the standard model, there are still several good reasons for pursuing PNC experiments, provided that they can be done with sufficient precision on atoms amenable to unambiguous atomic-theoretical analysis. The

point may be made with reference to cesium, where the experimental uncertainty in the effect is 3%, and the atomic- theoretical uncertainty is 1%. If the combined uncertainty could be reduced to about .5 %, comparison with predictions of the standard model would be sensitive to radiative corrections, including several "non-standard" ones indicative of physics beyond the standard model. Furthermore, while all the first generation experiments have detected the dominant PNC effect, there are nuclear spin-dependent contributions beyond the dominant one, including that arising from a **nuclear anapole moment**, and this goal, while not of comparable importance to the first one, is certainly of considerable interest.

To detect the PNC effect, one must observe a forbidden optical transition, in practise always an M1 transition with amplitude M, which in the presence of an external electric field also acquires a Stark-induced E1 amplitude E_S. By virtue of parity violation, the initial and/or final atomic states acquire small admixtures of states of opposite parity, so that even in the absence of an external E field, there exists in addition an extremely small parity violating E1 amplitude E_{PNC}. Heavy atoms are favored for observation because E_{PNC} scales roughly as Z^3. In the cesium and thallium Stark-interference experiments one observes interference between E_S and E_{PNC} amplitudes and the experimental outcome is a determination of E_{PNC}/E_S. In other experiments, the quantity of interest is E_{PNC}/M.

Experiments have been proposed and tried in the past with hydrogen and He^+. These hydrogenic atoms have the special feature that the $2^2S_{1/2}$ and $2^2P_{1/2}$ states are nearly degenerate, being separated only by the Lamb shift. Thus, in principle, even hydrogen, with Z=1, might exhibit an observable PNC effect. The advantage is of course that hydrogenic wave-functions are known exactly- there is no atomic theoretical uncertainty. The disadvantage, so far, has been experimental: low signal, high background, fatally large and complicated systematic errors. One can imagine employing ALS circularly polarized photons to study parity violating circular dichroism in the $1^2S_{1/2}$ - $2^2S_{1/2}$ transition in hydrogenic ions. This proposal appears at first to have a number of attractive features. However, it and other proposals for the use of ALS founder because the intensity per unit bandwidth is about nine orders of magnitude less than that which can be obtained from a cw dye laser operating at the cesium transition. Therefore, at present, the answer to the question posed in the title unfortunately appears to be no.

CAN ALS PHOTONS BE USED TO STUDY FUNDAMENTAL SYMMETRIES IN ATOMS?

- PARITY NONCONSERVATION ($\not{P}$ $\not{C}$ T)
- P,T ODD EFFECTS ($\not{P}$ C $\not{T}$)
- VIOLATIONS HERE ARISE FROM BASIC LAGRANGIAN

BRIEF HISTORY:

GRAVITY
EM
STRONG
WEAK

1957 PARITY VIOLATION IN CHARGED WEAK INTERACTIONS:
NUCLEAR BETA DECAY
MUON DECAY
PION DECAY
....

1958 V-A LAW

1967-68 STANDARD ELECTROWEAK MODEL

1973 NEUTRAL WEAK CURRENTS FIRST OBSERVED

1973-83 ELUCIDATION OF STANDARD MODEL

1983 OBSERVATION OF $W^{\pm}$, Z

PARITY NONCONSERVATION IN ATOMS- THE MAIN IDEAS

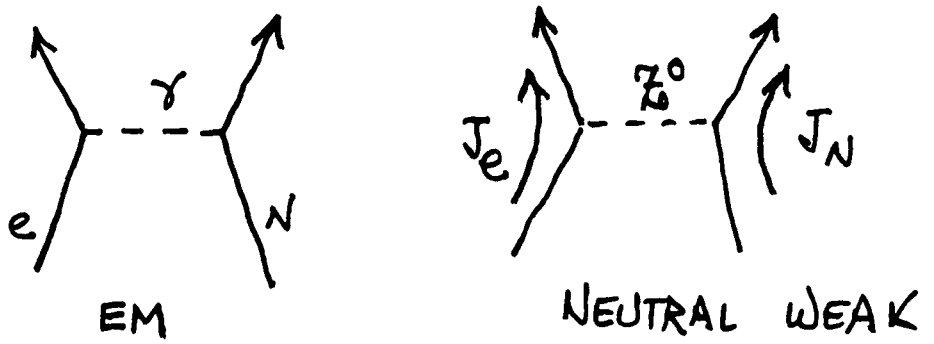

ESSENTIAL FEATURES OF NEUTRAL WEAK AMPLITUDE:

- SHORT RANGE (M_Z = 93 GEV/C^2): e^- at nucleus.

- NEUTRAL WEAK CURRENT-CURRENT INTERACTION VIOLATES PARITY:

$$J_e J_N = (V_e + A_e)(V_N + A_N) =$$

$$\underbrace{V_e V_N + A_e A_N}_{\text{Scalar}} + \underbrace{V_e A_N + A_e V_N}_{\text{Pseudoscalar}}$$

STREAMLINES OF CONSTANT j_e

$2^2p_{1/2}$, m_j= +1/2

HYDROGEN

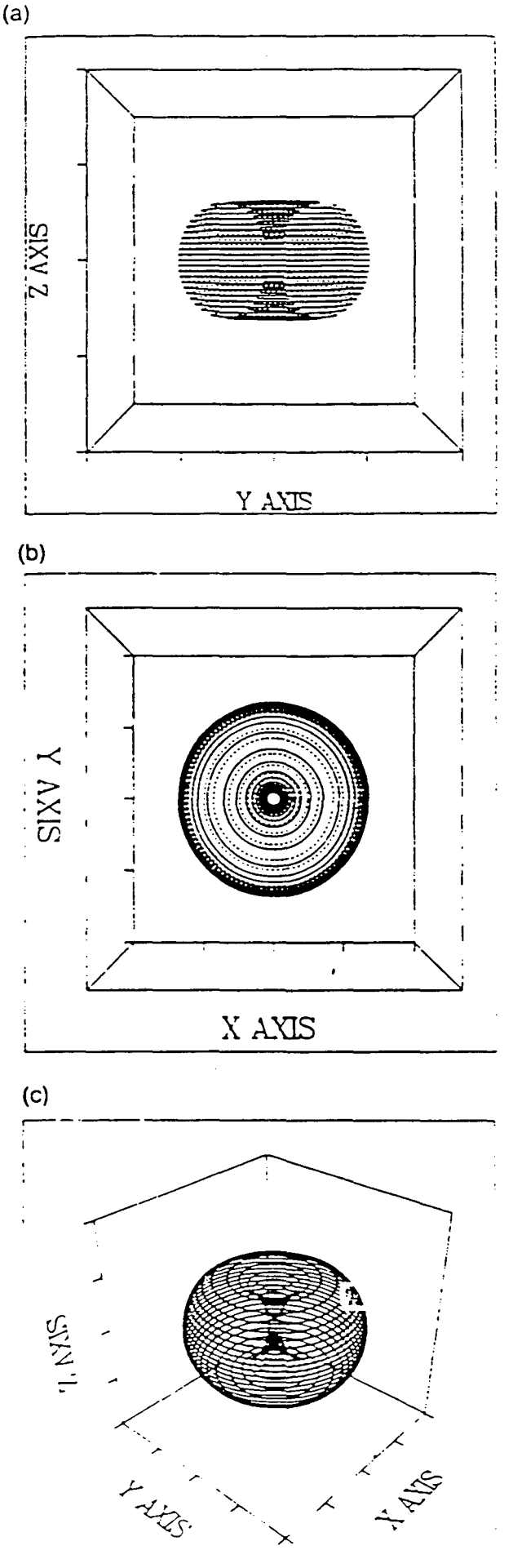

STREAMLINES OF CONSTANT j_e

$2^2p_{1/2} + i\varepsilon\, 2^2s_{1/2}$

$m_j = 1/2$

Hydrogen

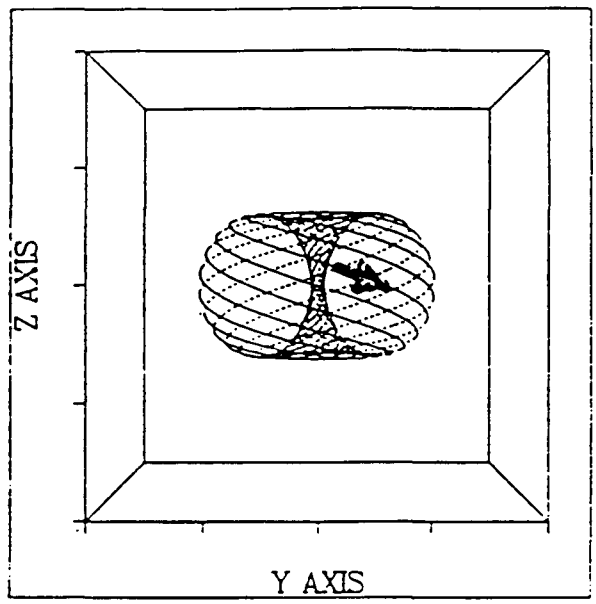

(b)

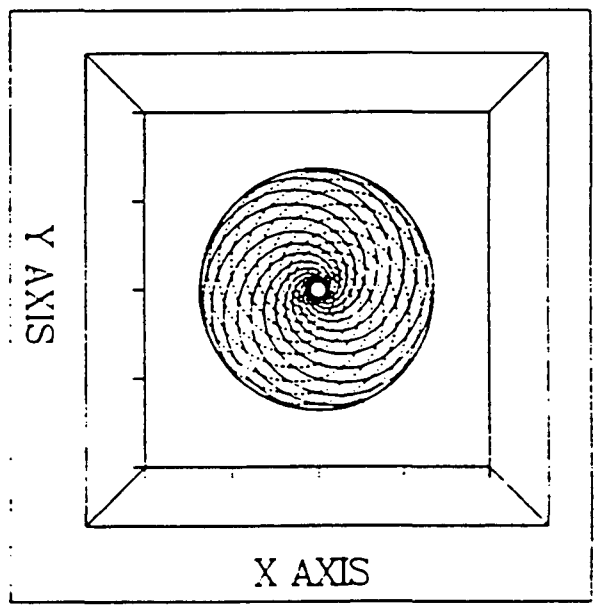

(c)

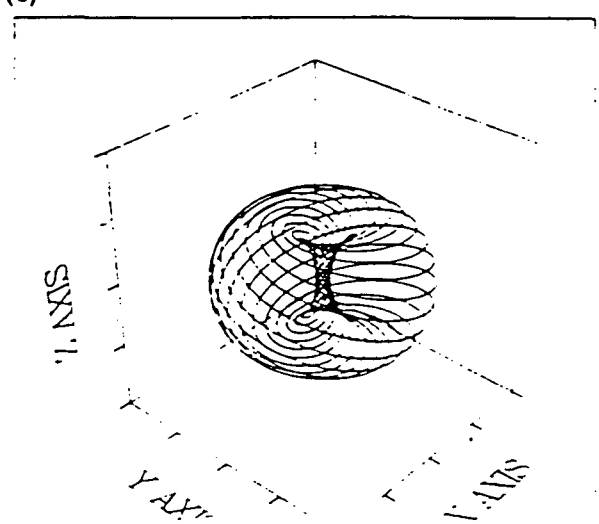

• $A_e V_N$ NUCLEONS ADD COHERENTLY

EFFECTIVE PSEUDOSCALAR HAMILTONIAN IS:

$$H_1 = \frac{G_F}{2\sqrt{2}}\left[\psi_e^{+}(\mathbf{r})\,\gamma_5\psi_e(\mathbf{r})\right]\cdot\rho_N(\mathbf{r})\cdot Q_W$$

$$Q_W = Z(1 - 4\sin^2\vartheta_W) - N$$

• MATRIX ELEMENTS OF H_1:

$$\langle S_{1/2} \mid H_1 \mid P_{1/2}\rangle \approx Z^3 \quad \text{(ROUGHLY)}$$

• $V_e A_N$ PROPORTIONAL TO (ODD) NUCLEON SPIN

EFFECTIVE PSEUDOSCALAR HAMILTONIAN H_2

$$\frac{\langle S_{1/2}| H_2 | P_{1/2}\rangle}{\langle S_{1/2}| H_1 | P_{1/2}\rangle} \approx \frac{1 - 4\sin^2\theta_W}{Z} \approx 10^{-2} \text{ to } 10^{-3}$$

$$H_2 \Rightarrow \frac{G_F}{2\sqrt{2}}\,\underset{\sim}{\sigma}_N\cdot\underset{\sim}{\sigma}_e\left\{\underset{\sim}{\sigma}_e\cdot\underset{\sim}{p}_e\,,\ \delta^3(\underset{\sim}{r})\right\}(1 - 4\sin^2\theta_W)$$

THERE EXISTS ANOTHER EFFECT WITH SAME SIGNATURE AS H_2 ..... BUT 5 TO 10 X LARGER!

PARITY VIOLATION IN NUCLEUS
(W,Z EXCHANGE BETWEEN NUCLEONS →

AXIAL VECTOR POTENTIAL GENERATED BY NUCLEUS WITH SPIN $I \neq 0$.

$$\underset{\sim}{A} = a \underset{\sim}{I}\, \delta^3(\underset{\sim}{R}) \qquad a = \text{"ANAPOLE MOMENT"}$$

$$a \underset{\sim}{I} = \text{const} \cdot \int r^2 \psi_0^* \underset{\sim}{\sigma} \psi_0 \, d\tau$$

ψ_0 = UNPERTURBED NUCLEON WAVE-FUNCTION

ATOMIC ELECTRON INTERACTS WITH **A** IN NORMAL WAY:

DIRAC EQUATION:

$$H = \underset{\sim}{\alpha} \cdot (\underset{\sim}{p} - e\underset{\sim}{A}) + m \gamma_4$$

2 COMPONENT REDUCTION → $\underset{\sim}{\sigma_n} \cdot \underset{\sim}{\sigma_e}\ \underset{\sim}{\sigma_e} \cdot \underset{\sim}{p}$

$$|\bar{\psi}\rangle = |\psi\rangle + \sum \frac{|\eta\rangle\langle\eta| H_{PNC} |\psi\rangle}{E_\psi - E_\eta}$$

$$\langle\bar{\psi}'| T_{EM} |\bar{\psi}\rangle \approx \langle\psi'| T_{EM} |\psi\rangle + \quad \leftarrow M1$$

$$\sum \frac{\langle\psi'| T_{EM}| \eta\rangle\langle\eta |H_{PNC}| \psi\rangle}{E_\psi - E_\eta} + \sum \frac{\langle\psi'| H_{PNC}| \eta\rangle\langle\eta |T_{EM}| \psi\rangle}{E_\psi - E_\eta}$$

$E1_{PNC}$

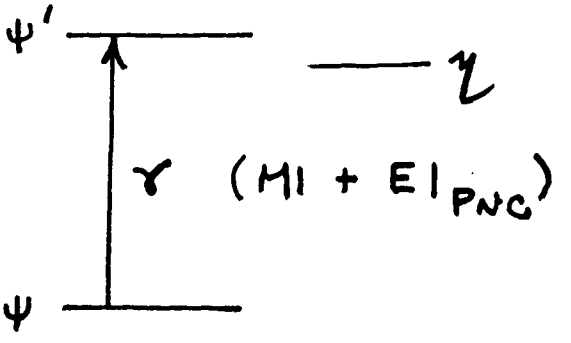

How to observe PNC!

- OPTICAL ROTATION EXPERIMENTS

BISMUTH

NOVOSIBIRSK 1978

MOSCOW

OXFORD

SEATTLE

LEAD

SEATTLE

- STARK INTERFERENCE EXPERIMENTS

CESIUM

ENS (PARIS)

JILA, BOULDER ←

THALLIUM

BERKELEY

PNC - HOW TO OBSERVE?

IN ABSENCE OF PNC $H = H_{COULOMB}$
(MIRROR SYMMETRIC)

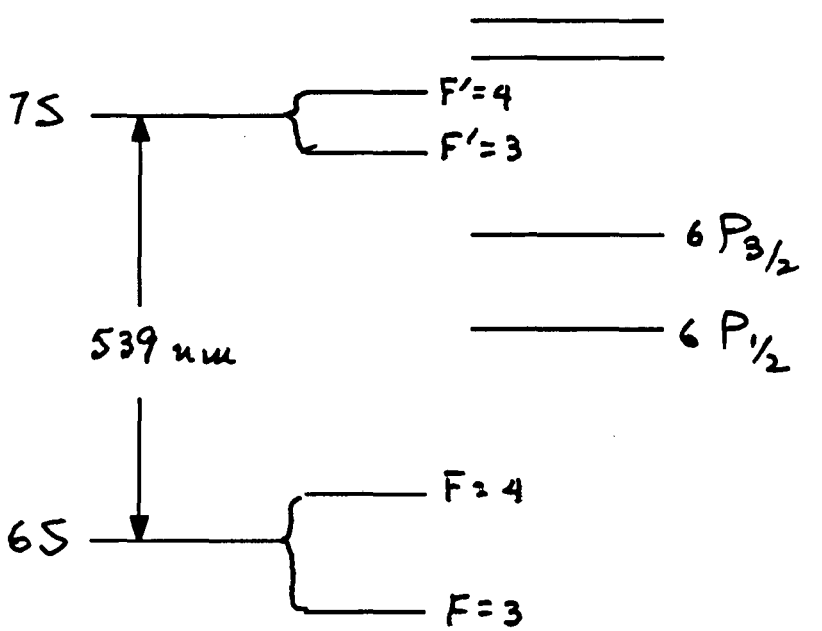

CESIUM (Z=55,N=78)

- WITHOUT PNC 539 nm TRANSITION IS PURE M1
- WITH PNC, 6S, 7S STATES HAVE SMALL ADMIXTURE OF $nP_{1/2}$
- TRANSITION AMPLITUDE (539 nm) $\rightarrow$ M1 + E_P
- IN EXTERNAL E FIELD $\rightarrow$ M1 + E_P + E_{STARK}
- OBSERVE INTERFERENCE BETWEEN E_P, E_{STARK}:
  REQUIRES SPECIAL ARRANGEMENT OF E,B FIELDS, POLARIZATION OF LIGHT

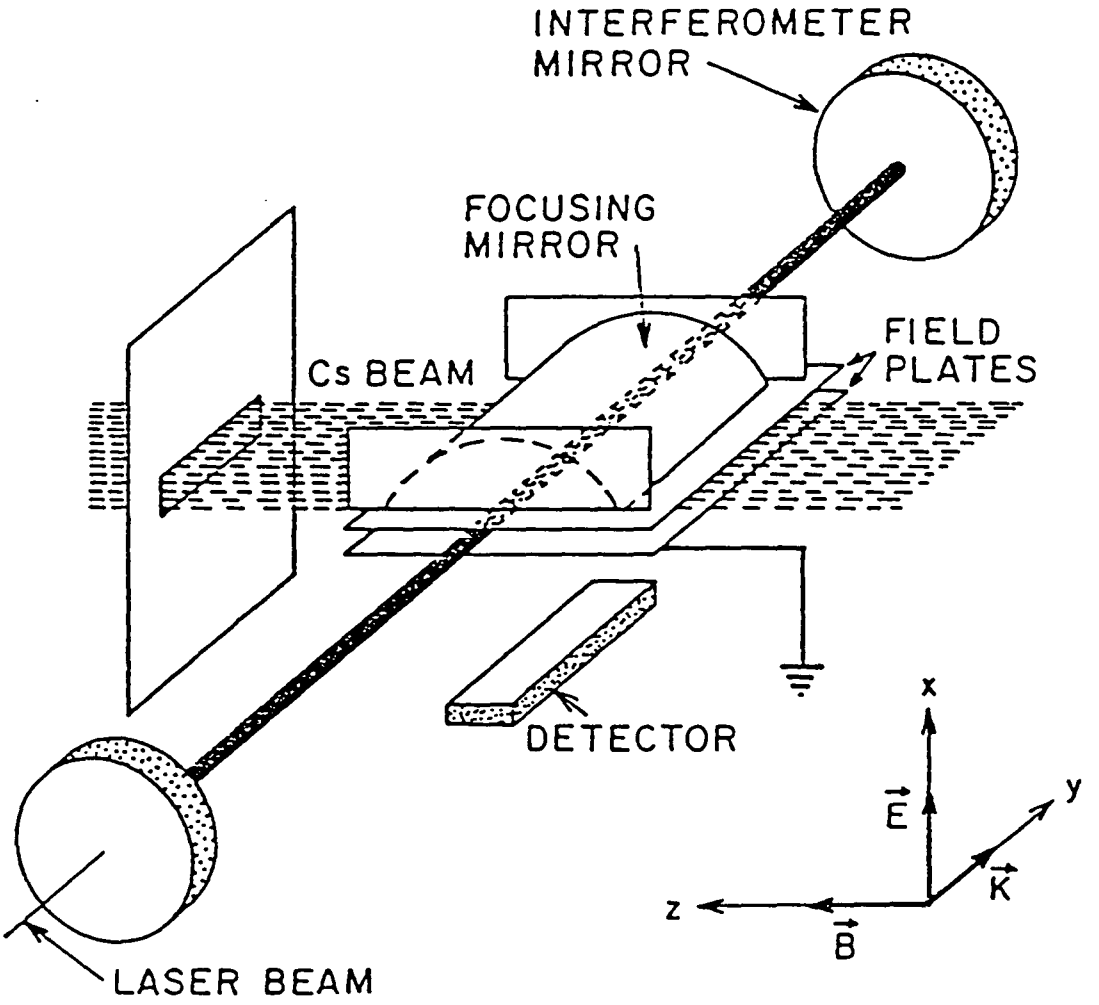
INTERFEROMETER
MIRROR
FOCUSING
MIRROR
FIELD
PLATES
Cs BEAM
DETECTOR
x
y
z
$\vec{E}$
$\vec{K}$
$\vec{B}$
LASER BEAM

STARK INTERFERENCE RESULTS CESIUM

BOULDER M.C.NOECKER ET AL PHYS REV LETT
61,310,1988

F=4 $\rightarrow$ F' = 3 Im E_P/β = -1.639(47)(08) mV/cm
F=3 $\rightarrow$ F' = 4 Im E_P/β = -1.513(49)(08) mV/cm

Av Im E_P/β = -1.576(34) mV/cm

Difference .126(68) mV/cm

THUS:

ANAPOLE + H_2 CONTRIB: K= 0.72(39)
K_{THEO} = .30 - .38

HYDROGENIC IONS ...

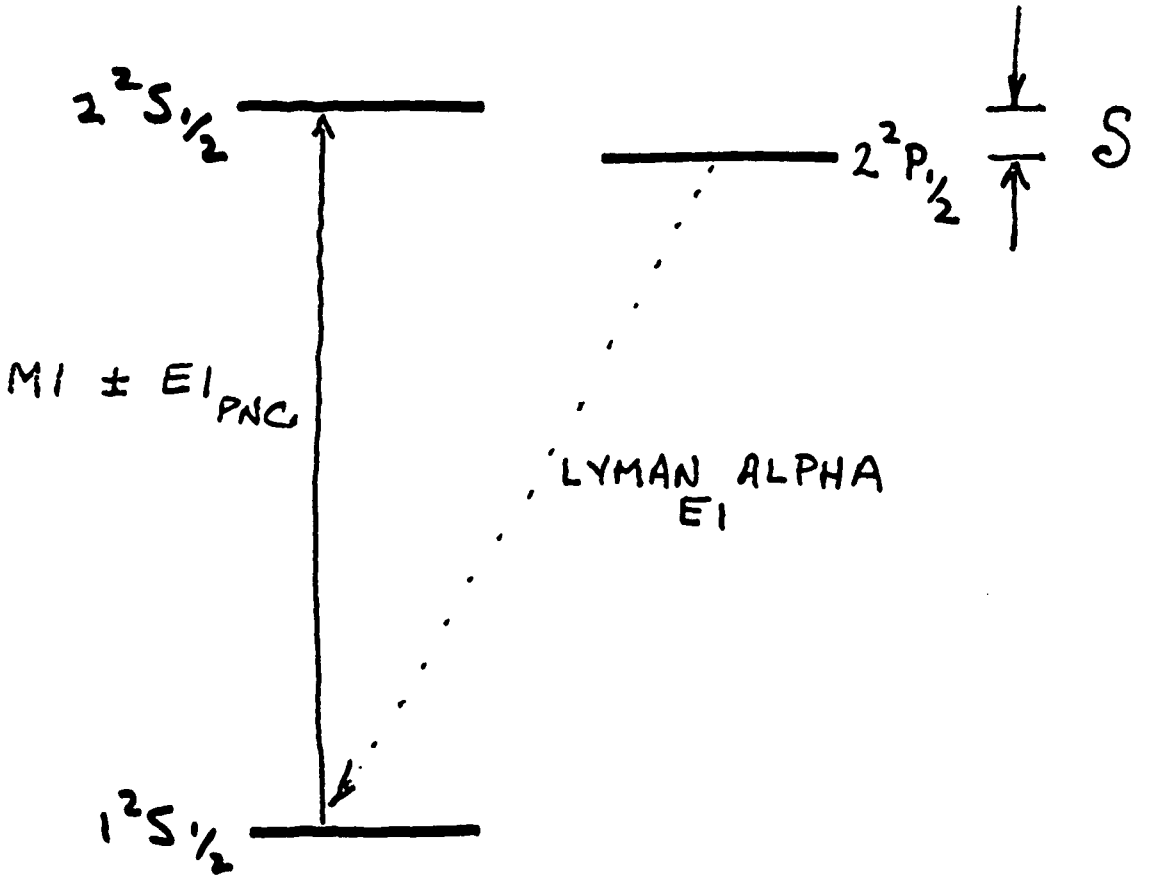

$$A_{R,L} = M1 \pm E1_{PNC} + (E1^{STRAY}_{STARK}$$

$$M1 \propto 10^{-5} \mu_0 \cdot Z^2$$

$$E1_{PNC} \propto Q_W / Z_0 \qquad Q_W \frac{Z^4}{Z^4} \cdot Z^{-1}$$

$$E1^{STRAY}_{STARK} \propto Z_0^{-1}$$

$$\Gamma(2^2P_{1/2}) \propto Z^4$$

$$\omega(1S \rightarrow 2S) \propto Z_0^2$$

n = 2 HYDROGEN

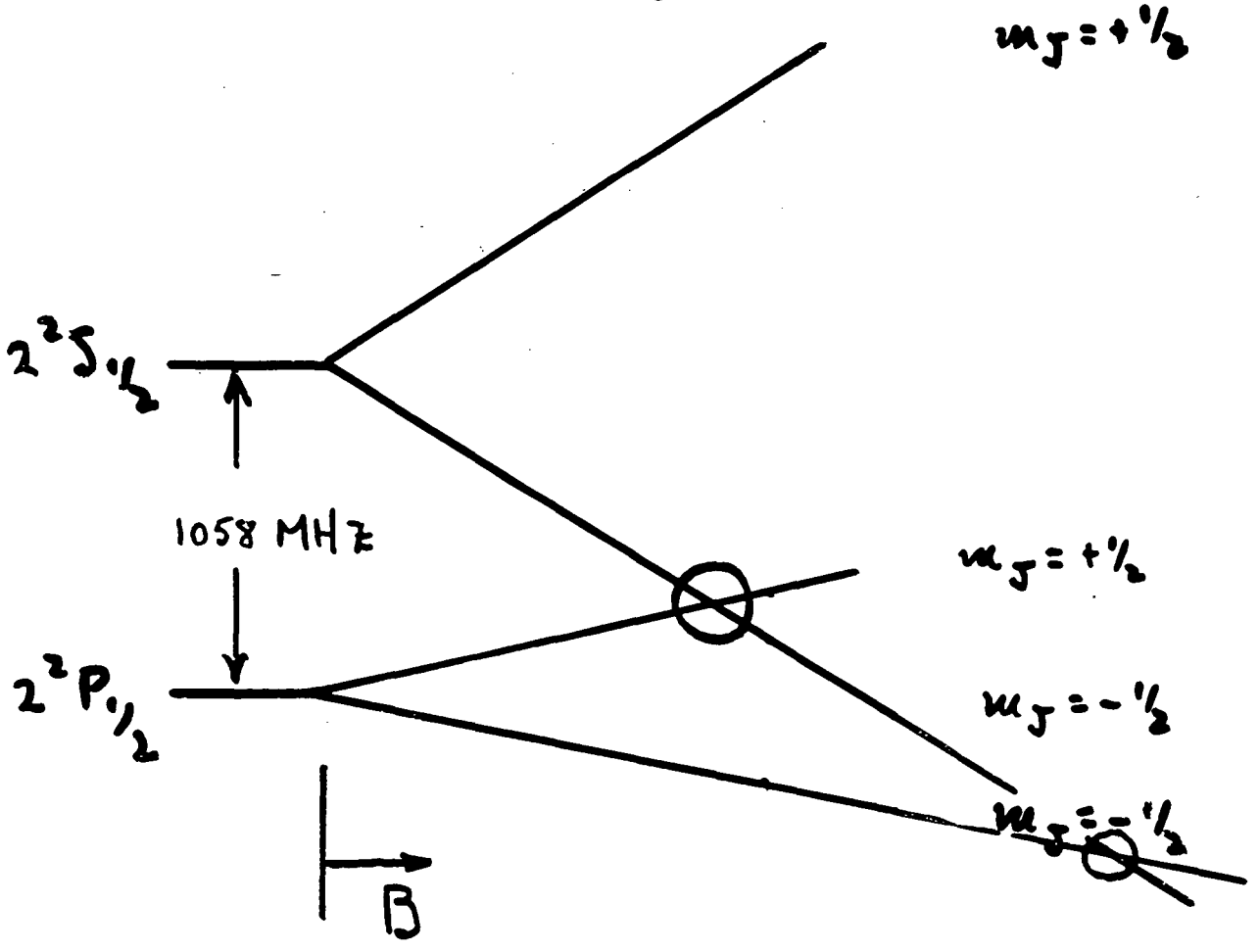

ADVANTAGES:
- HYDROGEN (EASY TO CALCULATE)
- SMALL ENERGY DENOMINATOR

DISADVANTAGES:
- SMALL Z, N
- EXPERIMENTALLY DIFFICULT
- MANY POSSIBILITIES FOR SYSTEMATIC ERROR

WHERE MIGHT WE IMAGINE THAT ALS PHOTONS COULD BE HELPFUL ?

Hg^+ $(1s^2 2s^2 \ldots 5d^{10} 6s)$

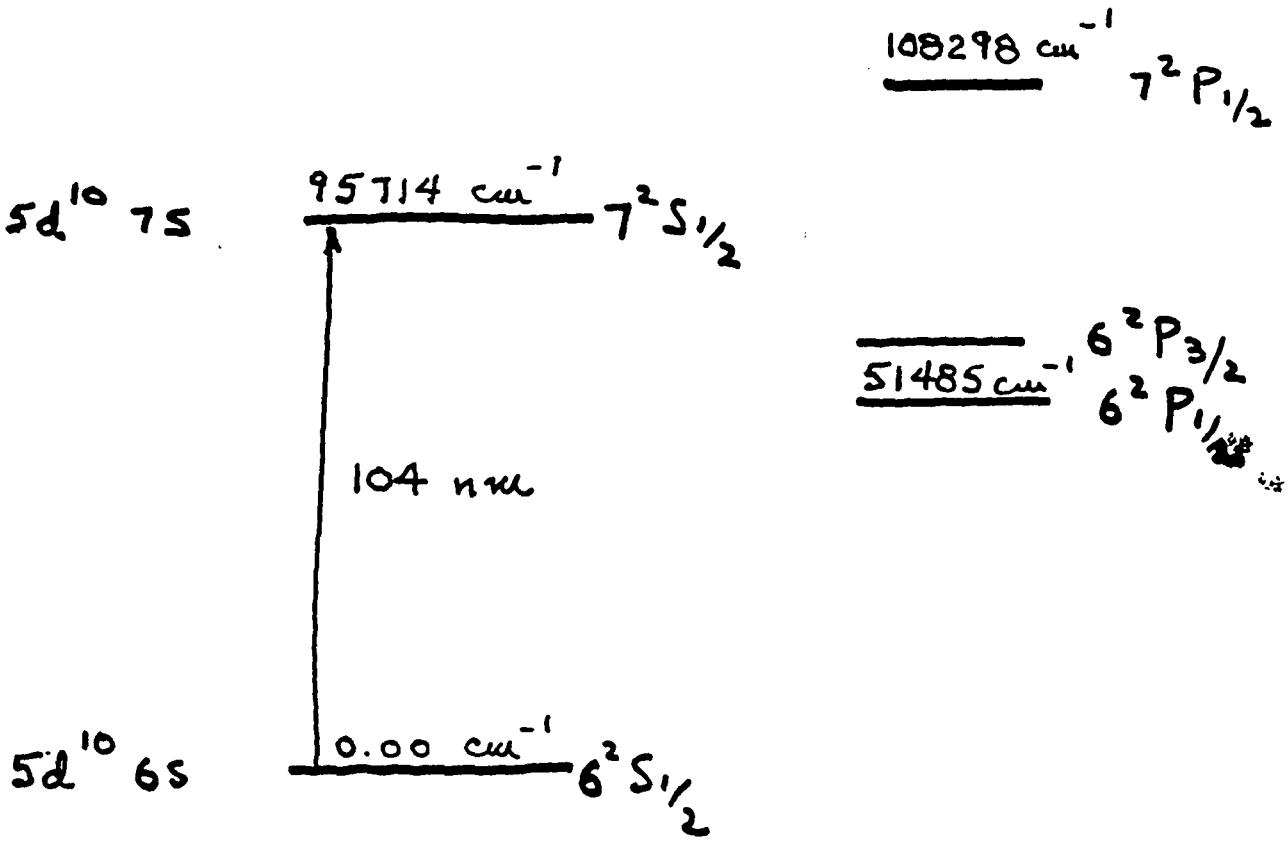

CIRC DICHROISM : $\delta = \frac{\sigma_R - \sigma_L}{\sigma_R + \sigma_L} \sim 2 \cdot 10^{-3}$

ISOTOPES :

A	%	I
198	10.0	0
199	16.8	1/2
200	23.1	0
201	13.2	3/2
202	29.8	0
204	6.9	0

HYDROGENIC IONS, ...

Z	$1S \rightarrow 2S$ PHOTON ENERGY	CIRC. DICHROISM
1	10.4 eV	$4.08 \cdot 10^{-4}$
5	260 eV	$2.63 \cdot 10^{-5}$
10	1040 eV	$8.4 \cdot 10^{-6}$
15	2340 eV	$4.5 \cdot 10^{-6}$
20	4160 eV	$2.9 \cdot 10^{-6}$
25	6500 eV	$2.1 \cdot 10^{-6}$
30	9360 eV	$1.6 \cdot 10^{-6}$

REACTION	$\sin^2\vartheta_W$	REL. WT.	q^2 (GeV/c)^2
		NOW .003	
PNC in Cs	.219 ± .007 ± .018	.06	5×10^{-6}
$\nu_\mu e \rightarrow \nu_\mu e$	.223 ± .018 ± .002	.16	4×10^{-2}
$\nu_\mu p \rightarrow \nu_\mu p$	.210 ± .033	.06	
SLAC POL e^-/D	.221 ± .015 ± .013	.08	7
μ N	.25 ± .08	.01	90
DEEP INELASTIC ν N	.233 ± .003 ±.005	1	10^2
W,Z PRODUCTION	.228 ± .007 ±.002 → NOW MUCH BETTER (LEP)	.75	10^4
ALL DATA	**.230 ± .0048**		

- **RADIATIVE CORRECTIONS MUST BE INCLUDED TO REACH PRESENT GOOD CONSISTENCY (THE STANDARD MODEL WORKS!)**
- **THE RANGE OF q^2 IS ABOUT 10^9**
- **DEEP INELASTIC ν N DATA IS STATISTICALLY MOST SIGNIFICANT**

$$\frac{\mathcal{E}_{PNC}}{\mathcal{E}_{STARK}} = \frac{G_F Q_W}{K_2 E} K_1$$

THE BOTTOM LINE:

INTENSITY OF CIRCULARLY POLARIZED PHOTONS IN BANDWIDTH OF ATOMIC TRANSITION:

$$\frac{\text{A.L.S.}}{\text{CW DYE LASER}} \approx 10^{-8} - 10^{-9}$$

Possible P,T Violations in High-T_c Superconductors

R.B. Laughlin

Stanford University

Possible P,T Violations in High-T_c Superconductors

Semionic Pairing

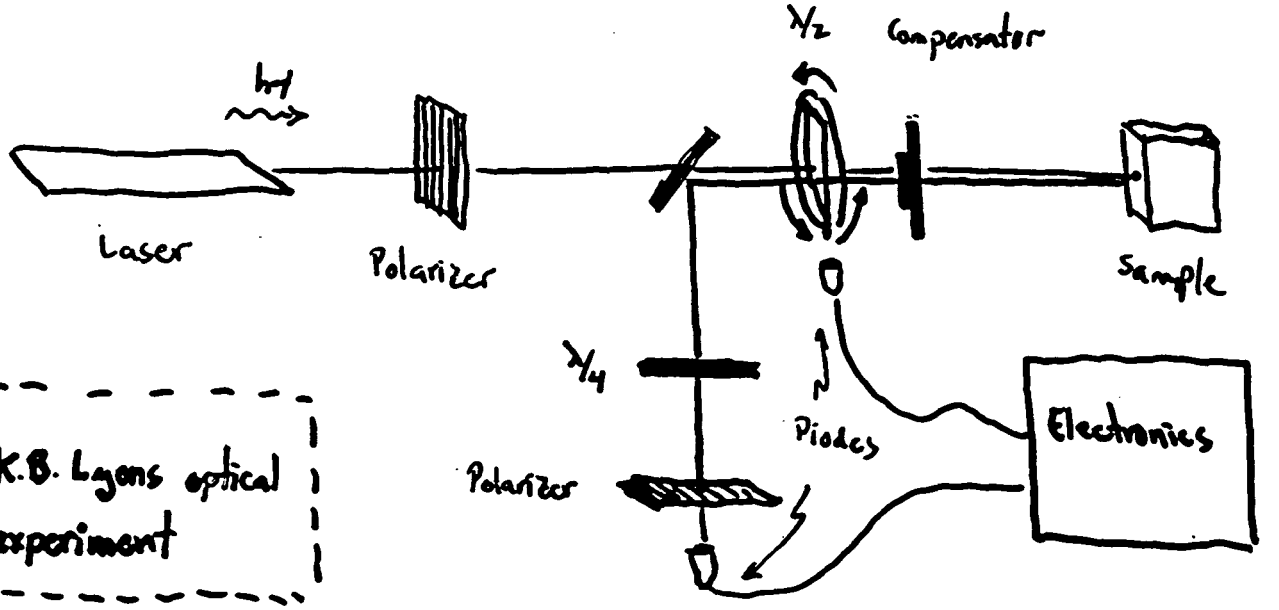

K.B. Lyons optical experiment

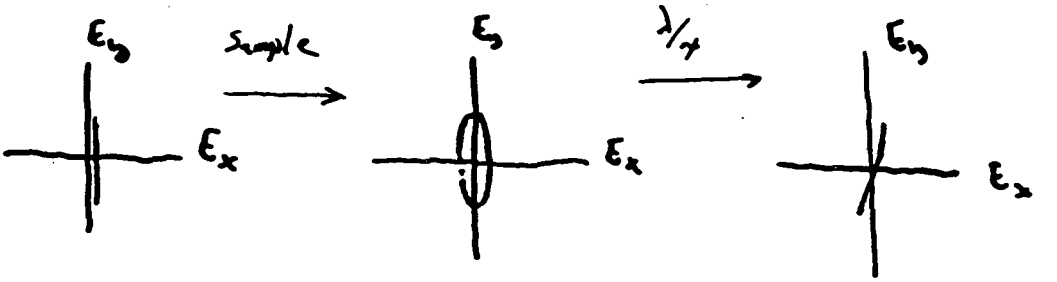

$$\frac{1}{2\pi} \ln\left[\frac{I_L - I_R}{I_L + I_R}\right] = \text{Dichroism signal in radians}$$

... H. J. Weber Experiment

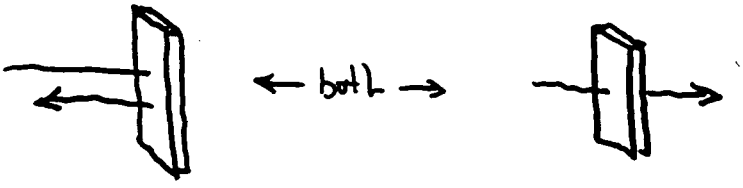

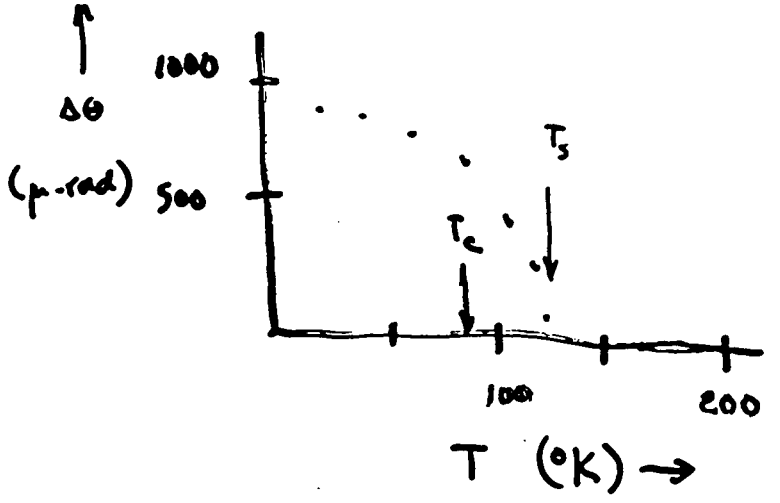

* Larger signal ... Large single X-tals
* Orients with applied B-field
  ... 100% certainty
* No signal from native thin films
  ↳ But, these can be "oriented" with 5T B-field

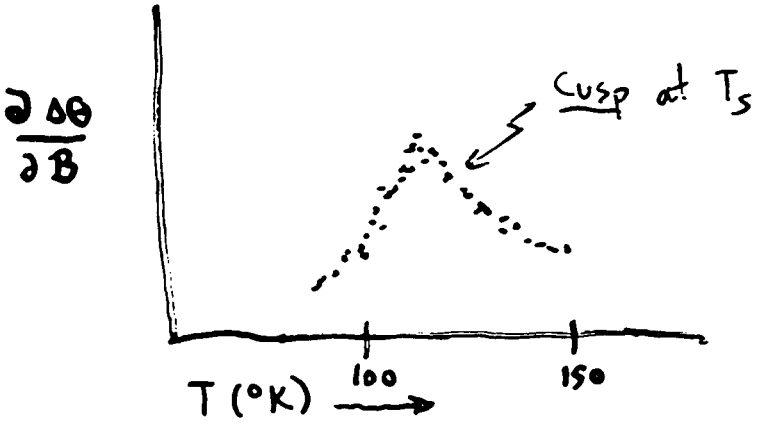

10μ

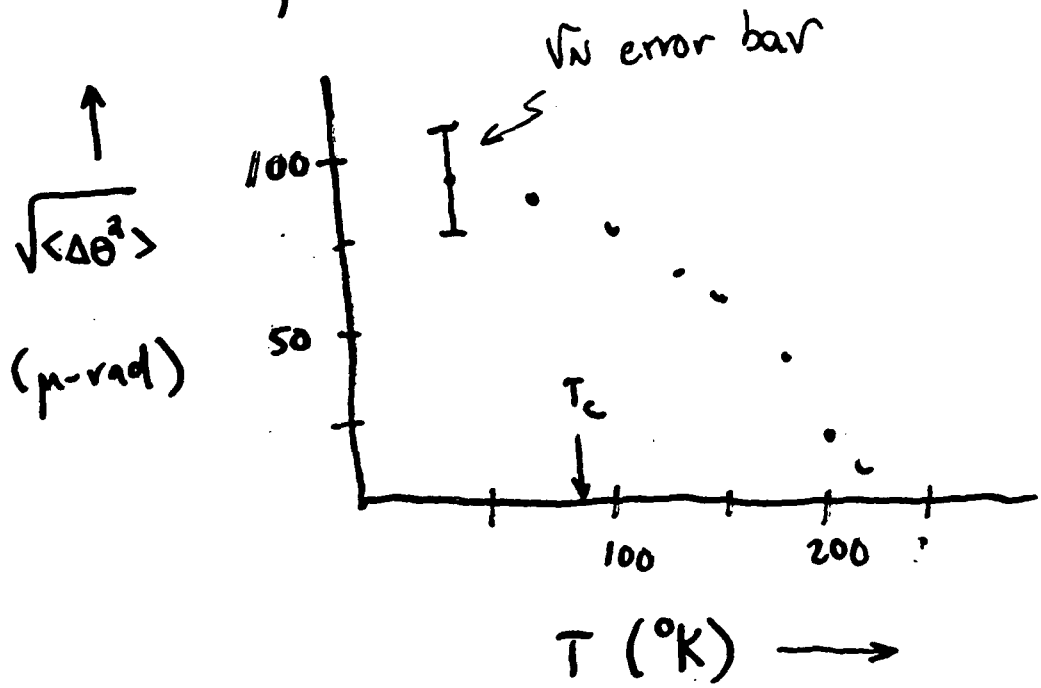

... Present only in samples that superconduct.

... Zero mean

... Seen in different kinds of samples

YBCO BSCO Single Crystals Thin films

... A. Kapitulnik experiment

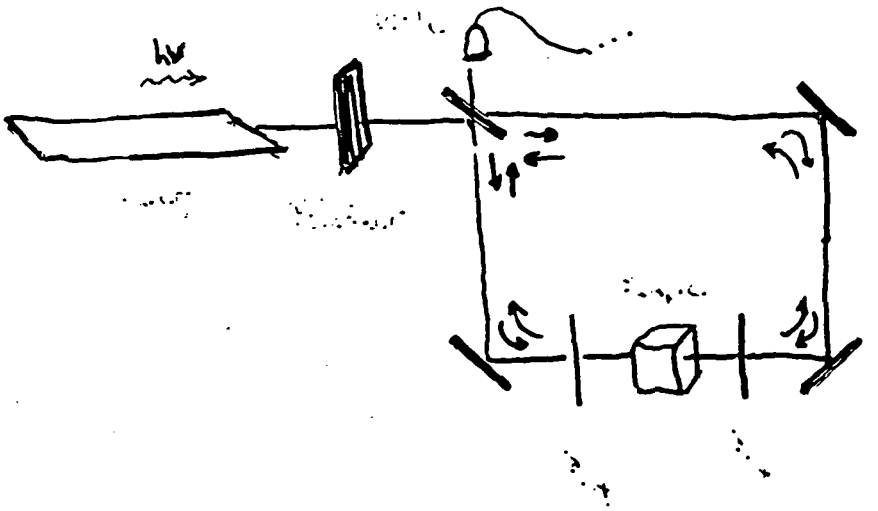

$\frac{1}{2\pi}(\Delta\phi_L - \Delta\phi_R)$ = Circular birefringence signal in radians

... No signal (less than 1 μ-rad)

... Both experimental techniques require T-violation to see signal (in principle).

(B.I. Halperin)

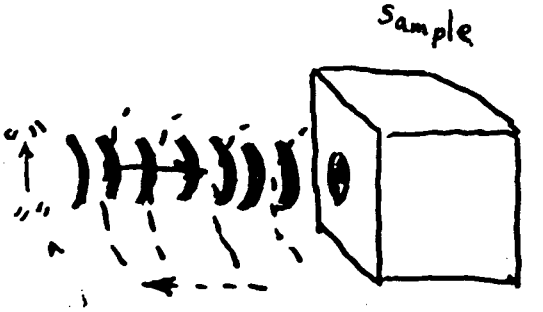

$$D_{\mu\nu}(x,y) = \frac{1}{2\pi i}\int_{-\infty}^{\infty} \langle T[A_\mu(y,t)\, A_\nu(x,0)]\rangle\, e^{i\omega t}\, dt$$

$D_{\mu\nu}(x,y)$

$= D_{\nu\mu}(y,$

... Optical activity predicted by X.-G. Wen and A. Zee

↳ R.B.L. disagrees with numbers, but not prediction itself. Breakthrough.

... No signal from μ-precession experiment. B.I. Halperin skeptical.

Anyons

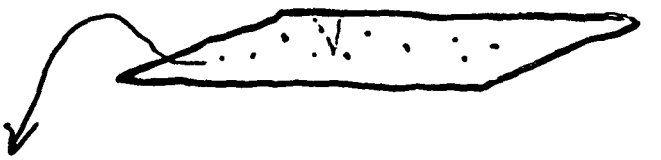

$$\mathcal{H} = \sum_j \frac{1}{2m} \left| \frac{\hbar}{i} \vec{\nabla}_j + \frac{e}{c} \vec{A}_j \right|^2$$

$$\vec{A}_j(\vec{r}_j) = \pi \frac{\hbar c}{e} \sum_{k \neq j} \frac{(\vec{r}_j - \vec{r}_k) \times \hat{z}}{|\vec{r}_j - \vec{r}_k|^2}$$

... Ground state of $\mathcal{H}$ for case of $\nu = \frac{1}{2}$ is charge-2 superconductor.

... How to make anyons

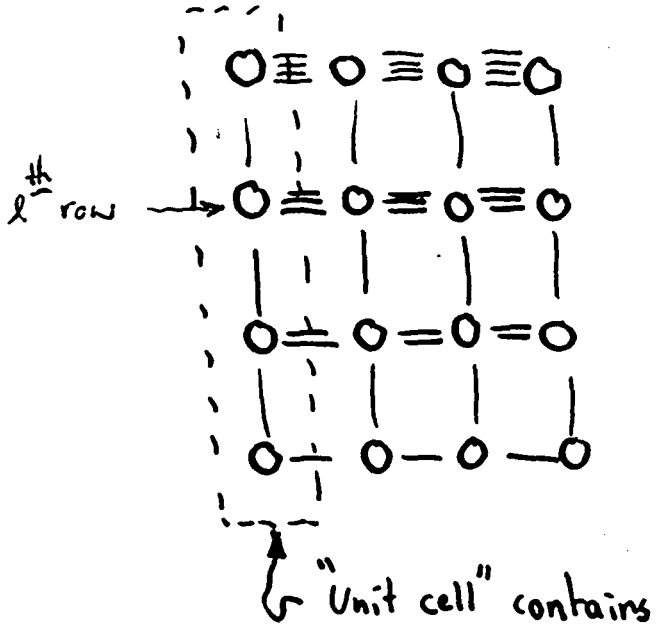

Step 1: Make fictitious "magnetic" tight-binding Hamiltonia.

$$\langle j|\mathcal{H}|k\rangle = \begin{cases} 1 & ; j \text{ and } k \text{ are } y \text{ neighbors} \\ e^{i\frac{p}{q}2\pi} & ; j \text{ and } k \text{ are } x \text{ neighbors} \\ 0 & ; \text{otherwise} \end{cases}$$

p and q are integers

Step 2: Fill "magnetic" bands with electrons.

... Expected electron density is $2\frac{p}{q}$.

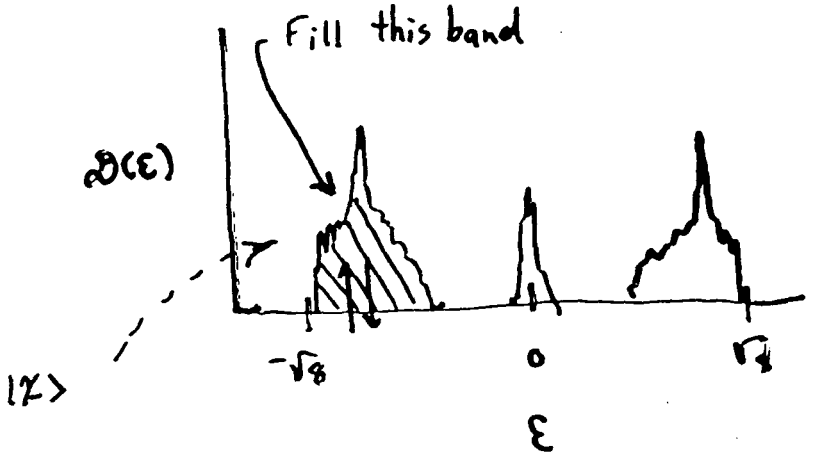

Step 3: Gutzwiller project

$$|\Psi\rangle = \prod_j (1 - n_{j\uparrow} n_{j\downarrow}) |\psi\rangle$$

Removes double-occupancy amplitudes.

Step 4: Re-interpret empty sites as "quantum numbers"

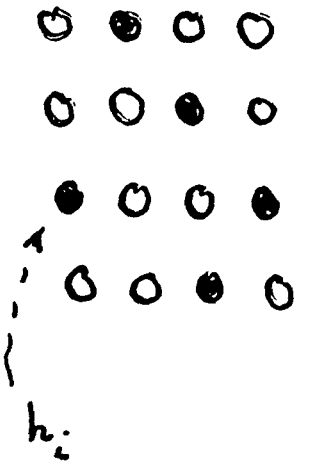

$$|h_1 \cdots h_M\rangle \equiv |\Psi\rangle$$

Step 5: Take matrix elements across actual Hamiltonian

$$\langle h_1' \cdots h_M' | \mathcal{H}_{tJ} | h_1 \cdots h_M \rangle$$

e.g.

$$\mathcal{H}_{tJ} = \sum_{\langle jk \rangle} \left\{ t \sum_\sigma c_{j\sigma}^\dagger c_{k\sigma} + \frac{J}{2} \vec{S}_j \cdot \vec{S}_k \right\}$$

Step 6: Combine to minimize energy

$$|\Psi\rangle = \sum_{h_1 \cdots h_M} a_{h_1 \cdots h_M} |h_1 \cdots h_M\rangle$$

$$\delta \left\{ \frac{\langle \Psi | \mathcal{H}_{tJ} | \Psi \rangle}{\langle \Psi | \Psi \rangle} \right\} = 0$$

... Same as anyon problem with $\nu = \frac{1}{2}$

... Correct computational tool is "gauge theory" of t-J Hamiltonian. World-wide effort to work out details.

... Circular dichroism calculations not yet reliable. But, energy scale is definitely in the infrared.

Why it matters ...

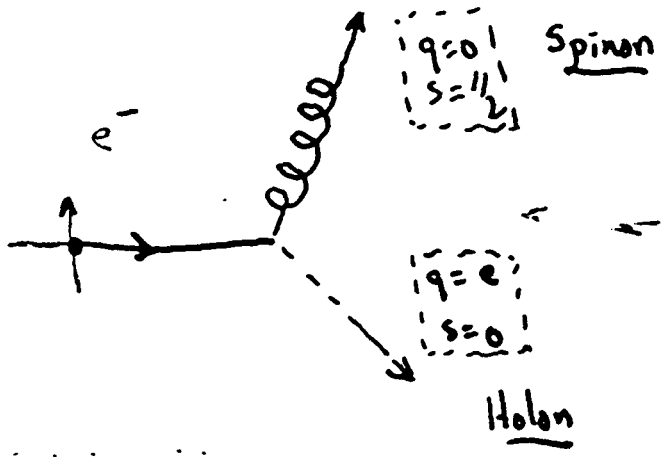

High-T_c Superconductors

Spinons and Holons

Fractional Statistics

Spontaneous P,T violation

Superfluidity

Chern-Simons cancellation

Standard Model

Quarks

Strong Force

Postulated P,T violation

Higgs Mechanism

Electroweak anomaly cancellation

Non-abelianness

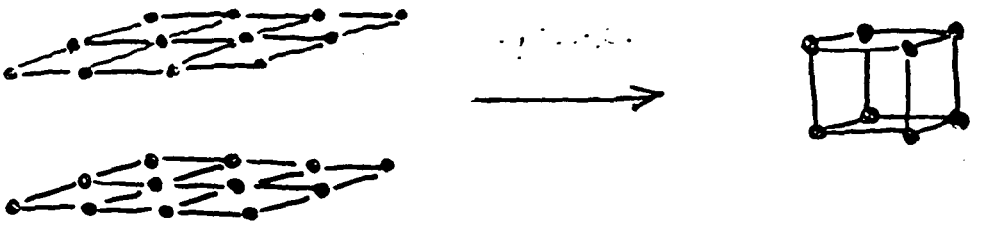

... S.B. Libby, Z. Zon, and R.B.L. studied 3-dimensional problem.

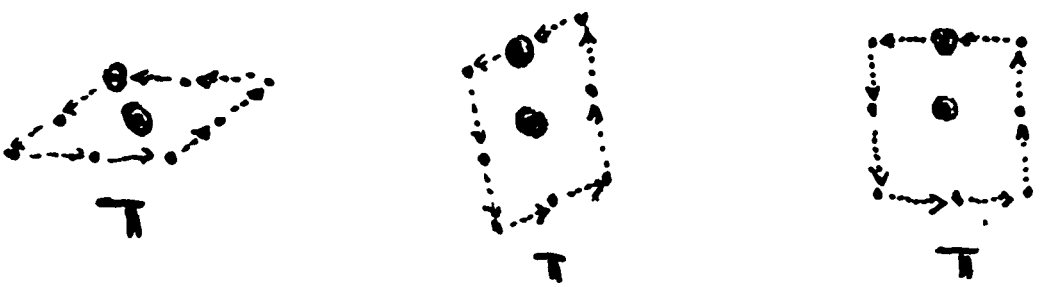

... But

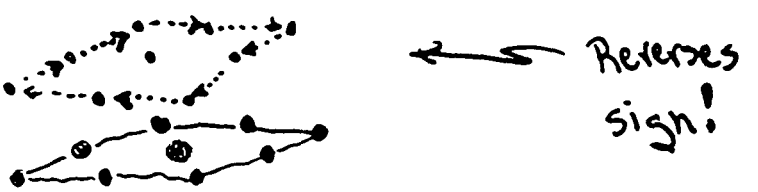

∴ we think large momentum transfer might be required. X-rays appropriate.

Magnetic Absorption and Bragg Scattering of Circularly Polarized "Hard" X-Rays in Ferro(i)magnetic Materials

G. Schütz

Technische Universität München

THE „INCLINED VIEW"-METHOD

The source of circularly pol. X-rays :

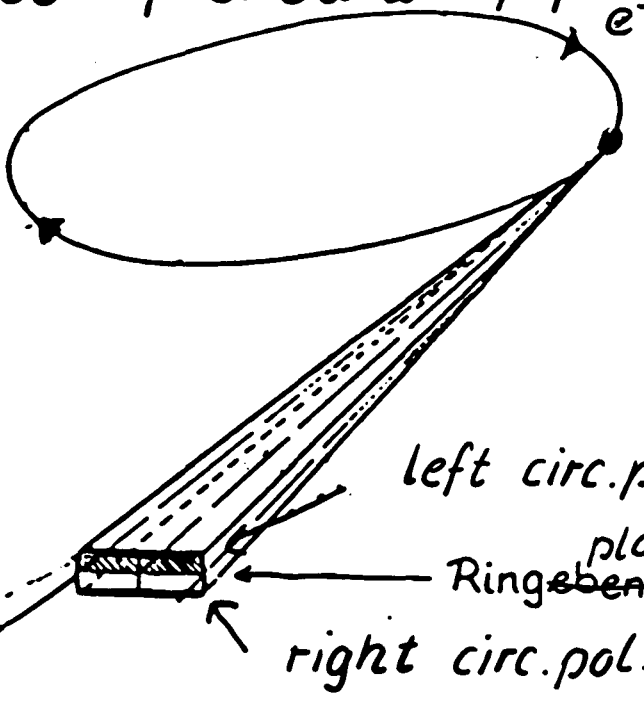

For example

DORIS II storage ring 3.5GeV, 100mA

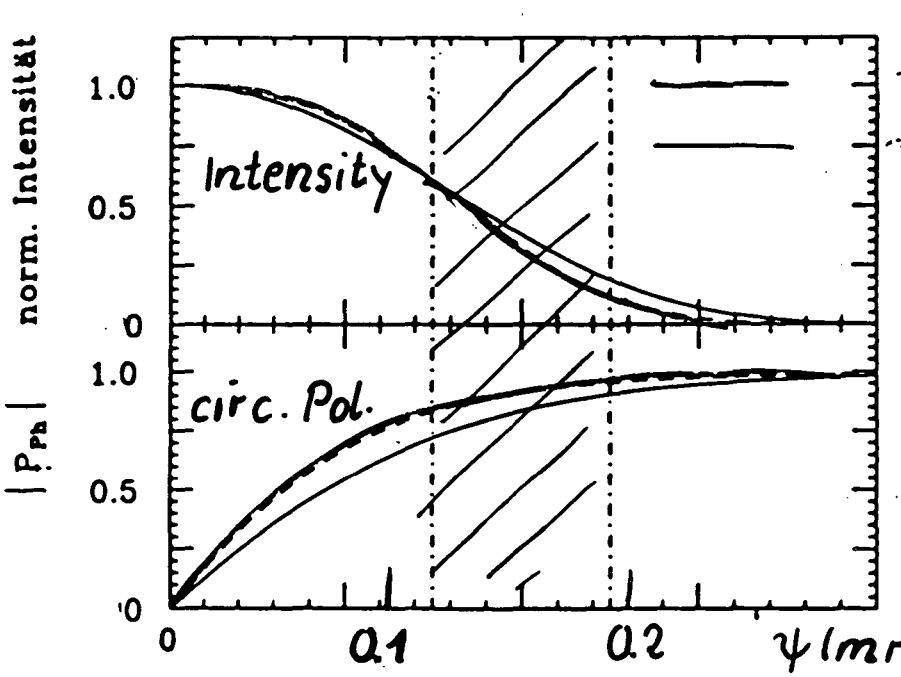

Exp. Acceptance :

$I_{ph} \sim 10^{10}$ ph/s·eV

$|P_c| \sim 0.8$ $E_\gamma \sim 8$ keV

in 25m distance from the source point

„Basic" Question:

Existence of a spin-dependent part of the photoabsorption coefficient as $\mu^{\pm} = \mu_0 \pm \mu_c$????

II. Principle of measurement [in the transmission mode]

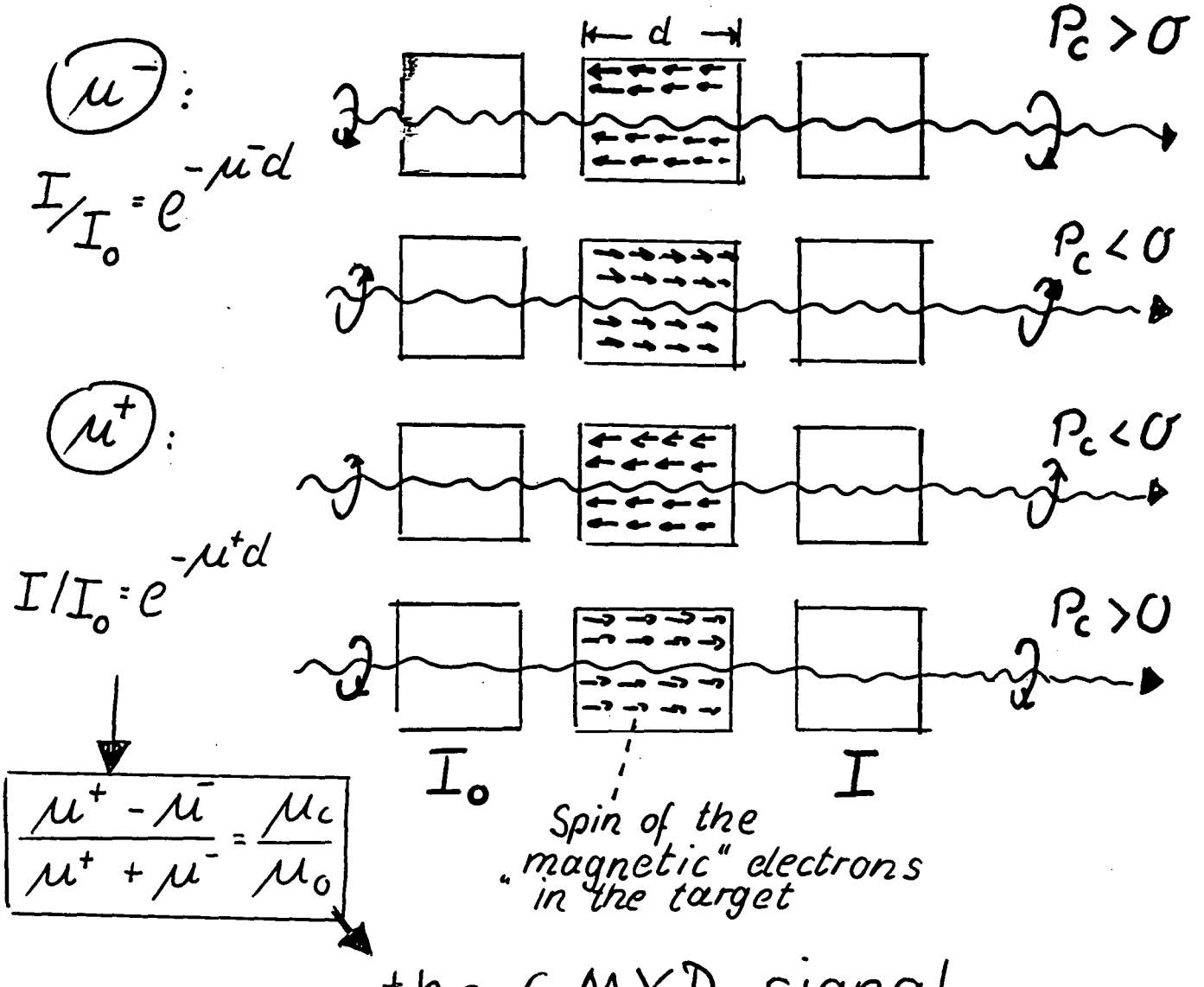

$$\frac{\mu^+ - \mu^-}{\mu^+ + \mu^-} = \frac{\mu_c}{\mu_0}$$

→ the CMXD-signal

→ „Two beam" transmission mode:

performed at HASYLAB

Ionization chambers meas. incident $[I_{0_1}, I_{0_2}]$ and transmitted intensities $[I_{0_2}, I_2]$ for two field

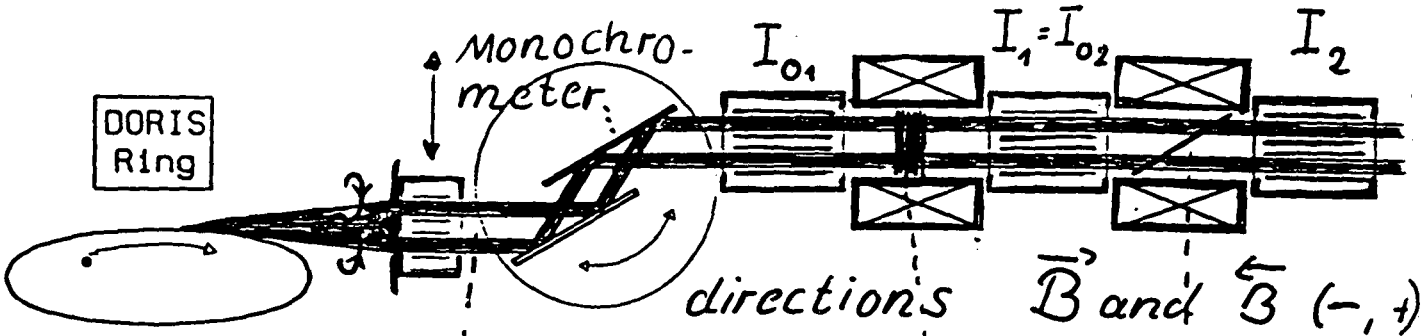

measured value:

$$\frac{\mu_c}{\mu_0} = \frac{\ln(I_0/I_1)^+ - \ln(I_0/I_1)^-}{\ln(I_0/I_1)^+ + \ln(I_0/I_1)^-} \cdot \frac{1}{P_c}$$

$P_c \sim \pm 0.8$ { degree of circ polarization

G. Schütz et al.
PRL 58, 737 (1987)

PRINCIPLES OF MEASUREMENTS

→ Fluorescence detection

performed at DARESBURY

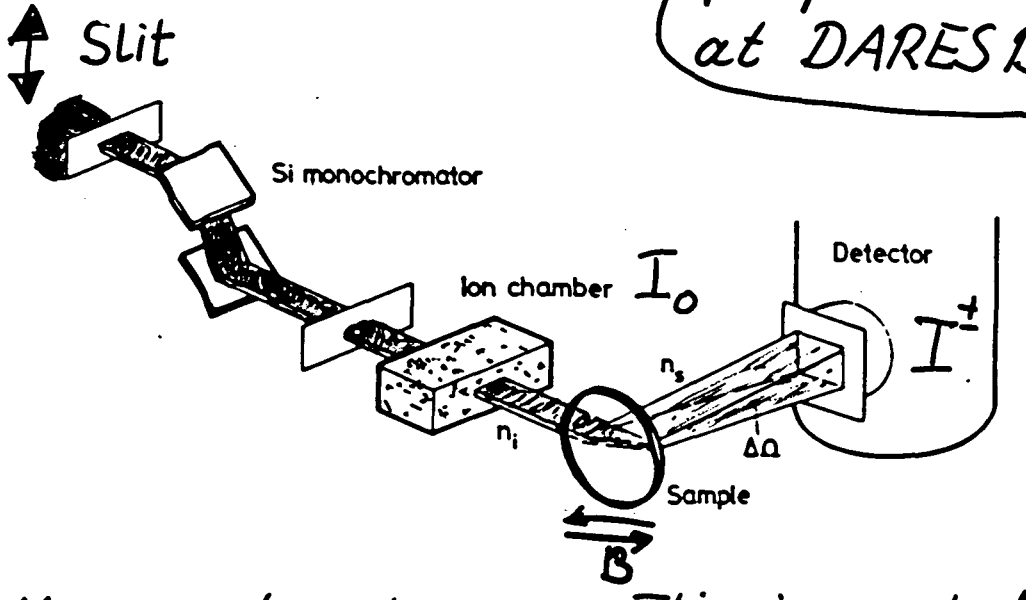

Measured value „Flipping ratio" $\overleftrightarrow{B}$ is flipped

$$\frac{I^+ - I^-}{I^+ + I^-} = \frac{\Delta\mu}{\mu} = \frac{\mu_c}{\mu_0}$$

± means parallel (+) and antiparallel orientation of photon-spin and spin of magnetic electrons in the sample

S.P. Collins et al.
J. Phys. Cond. Mat. 1, 323 (1989)

→ Transmission method in the „energy dispersive" mode:

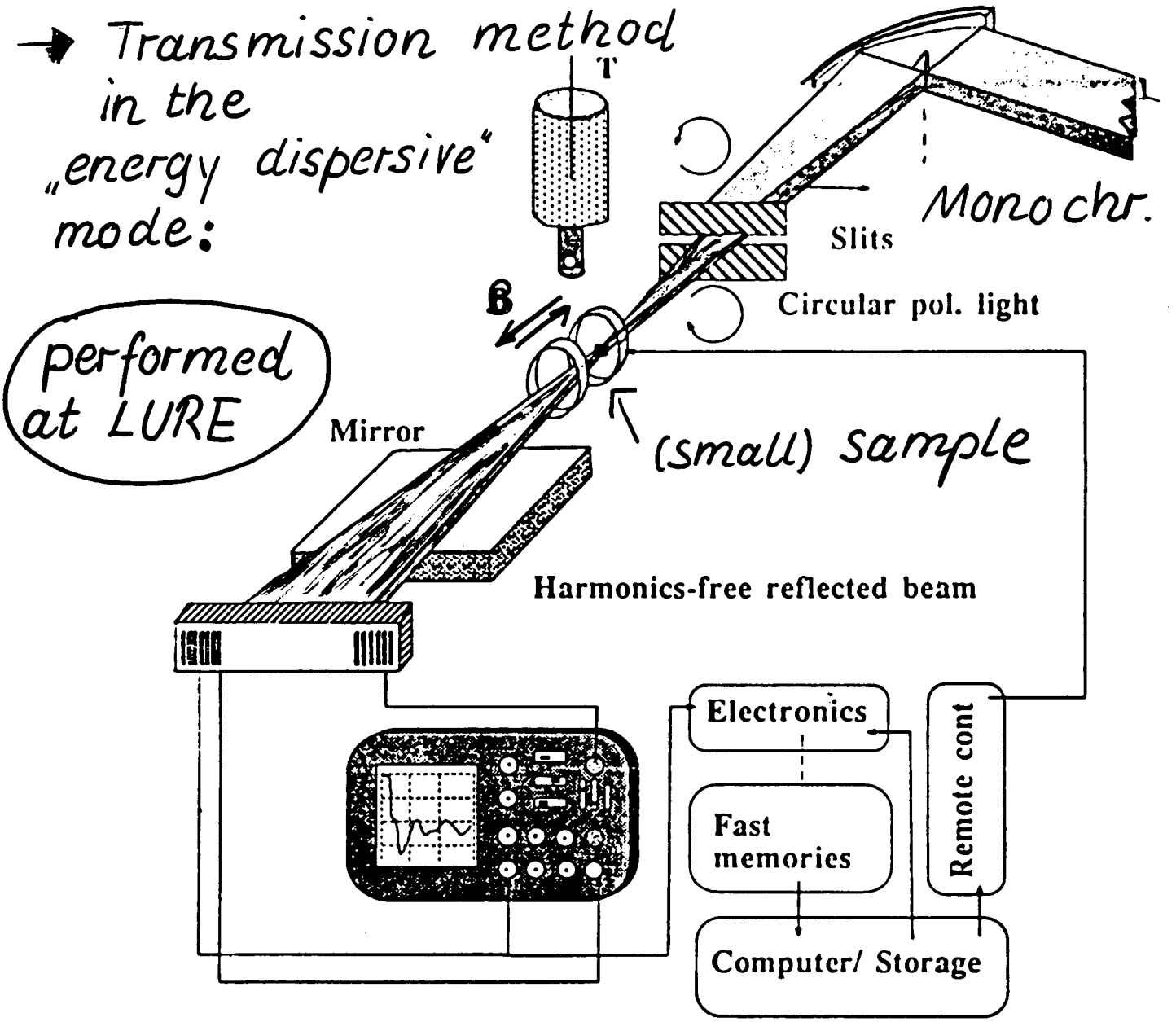

Magnetic X-ray Dichroïsm

Schematic layout of the Energy-Dispersive Spectrometer.

F. Baudelet et al. PRB, 1990 in press

Measured value $(\mu^+ - \mu^-)x$

Experiments performed at HASYLAB

circularly polarized x-ray available in an energy range $E_\gamma = 5...30$ KeV

K-edges	L-edges	M-edges
Z=21 Sc K 4.5 KeV	Z≥51 Sb L_2 4.4 KeV	Z≥82 U M_3 4.3 KeV
1. 3d-Elem.	5p-Elem.	5f-Elem.
4p-Elem.	2. 4f-Elem.	
4d-Elem.	3. 5d-Elem.	
5p-Elem.	5f-Elem.	
Z=51 Sb K 30.5 KeV		

Typical results:

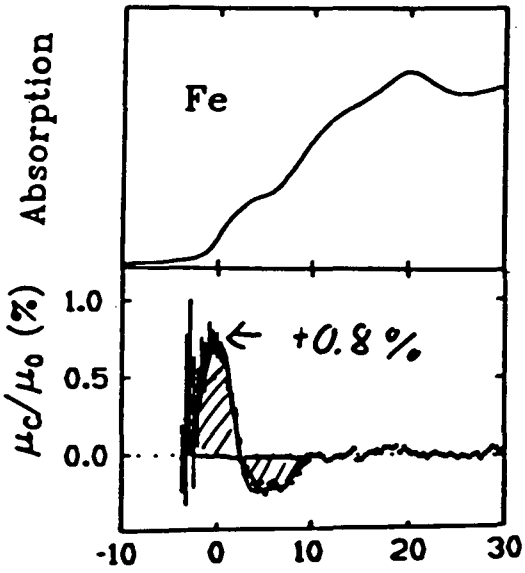

- at K-edges μ_c/μ_0 not larger than 1%

- at L-edges μ_c/μ_0 much larger

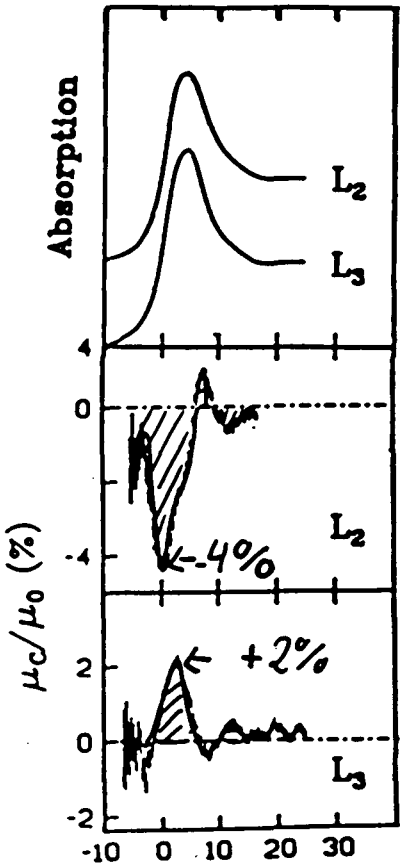

- Ratio of spindependent effects at L_2/L_3 edges often -2

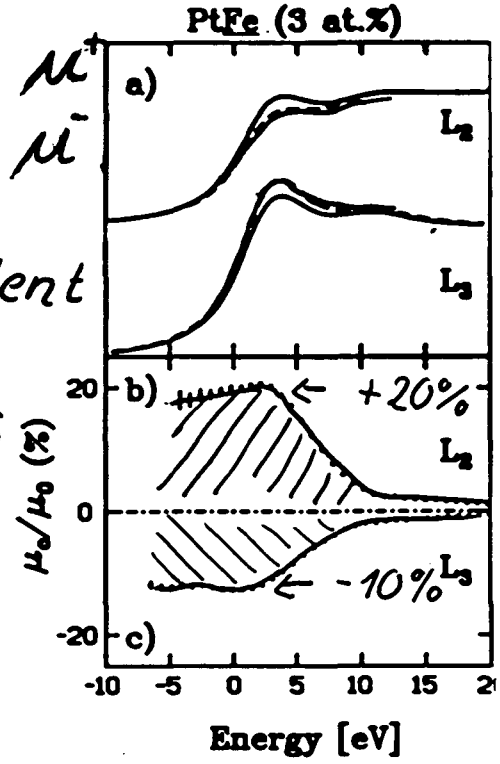

Theory of Spin-dependent absorption

- electronic structure described via KKR method → band structure
- spin-orbit coupling + magnetization are taken into account by the Dirac equation for spin-dependent potential
- connection of KKR with Green function method (for alloy, impurities ...)
- Absorption process in the single partical model

$$\mu \sim W_{fi} \sim \sum |\langle \phi_f | H' | \phi_i \rangle|^2$$

W_{fi}: representation of the final states by Greens function

$H' \sim \vec{\alpha} \cdot \vec{A}$: relativistic form of photon-electron interaction

- E2 terms included by atomic Hartree Fock-calculations with relativistic corrections

for references see:

- P.J. Durham, The el. structure of Complex System" (Plenum Press. N.Y.)
- H. Ebert et al. Z. Phys. B73, 67 (1988)
- P Strange et al. J. Phys. Cond. Matt. 2959 (1989)
- P. Carra, M. Altarelli PRL 64, 1286 (90)
- R.D. Cowan "The Theory of Atomic Spec. (Univ. of Calif. Press, Berkeley, 1981)

....in many cases well understood from theory

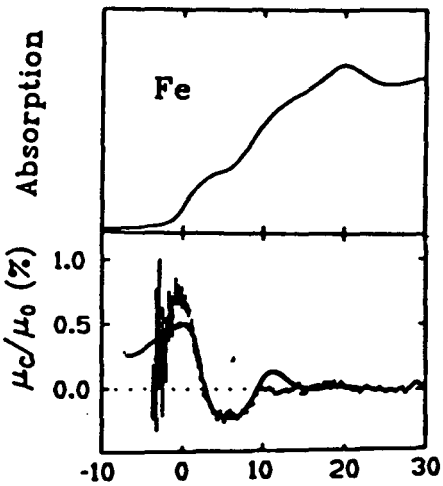

H.E. et al 1988
Z. Phys. B42, 2744

H. Ebert et al.
(voll relativistisch)

P. Carra et al.

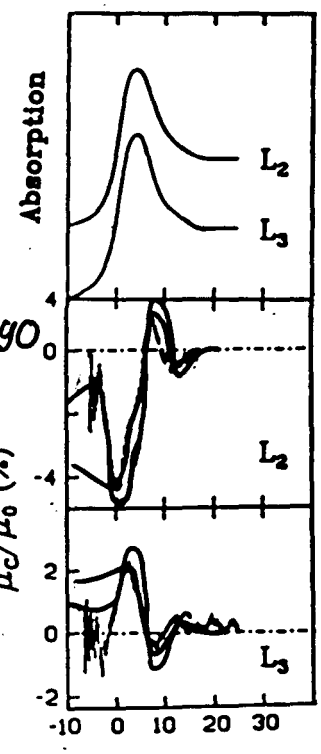

H.E. et al, 1990
Sol. St. Comm
76, 475

P. Carra
priv. Mitt.

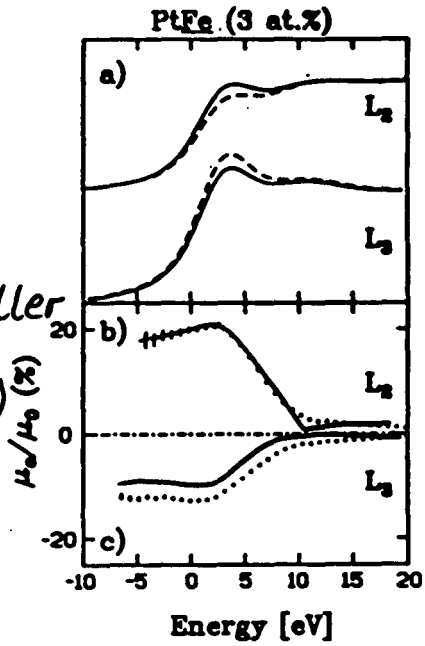

H.E. R. Zeller
PRB 42
2744 (90)

5d-impurities in Fe (3 at. %)

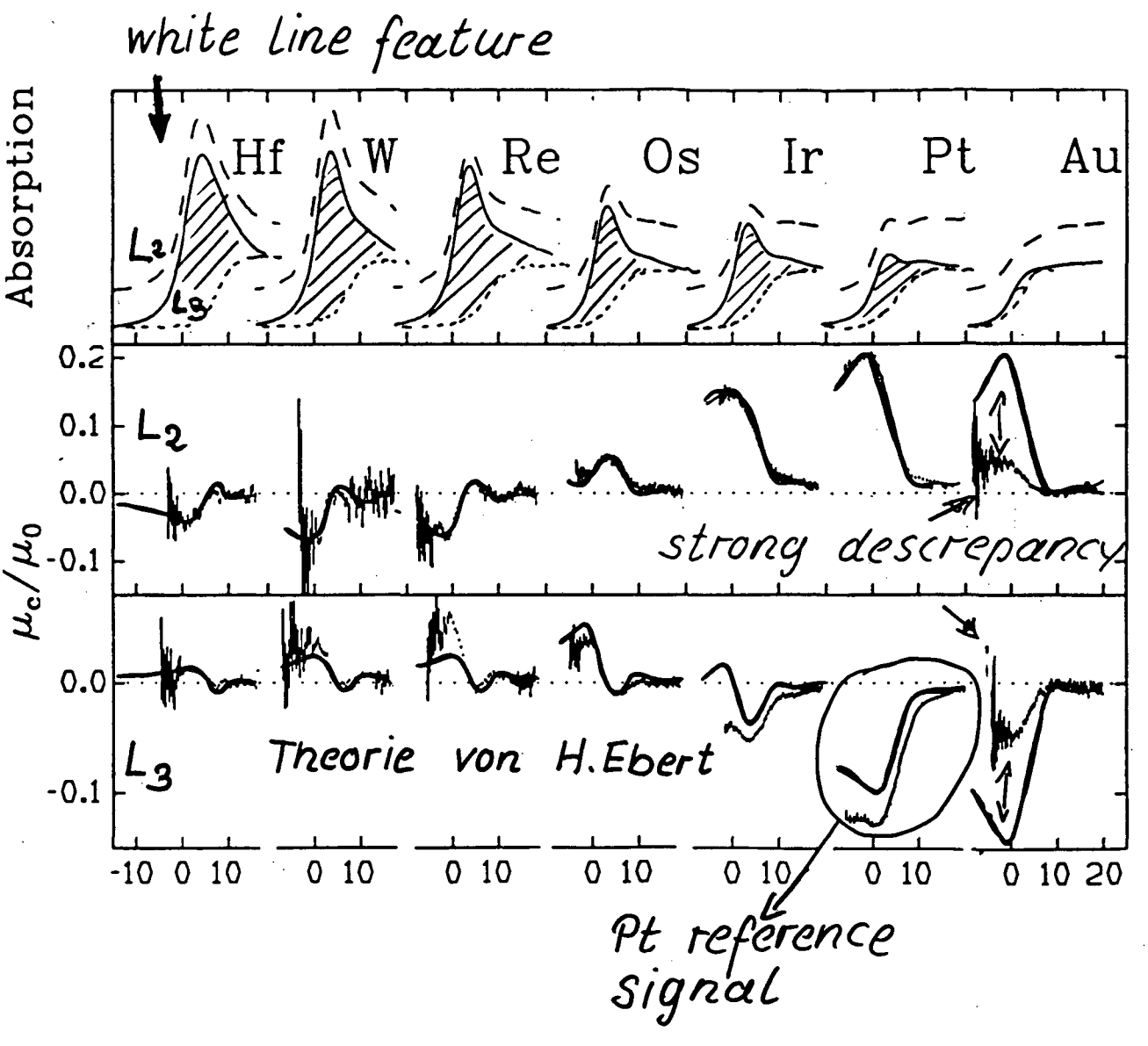

The origin of spin-dependent absorption can be understood by the ejection of a spin-polarized photoelectron after absorption of a circularly pol. photon in an unpolarized atomic core state

For a free atom the photoelectron polarization P_e can easily be calculated

Absorption edge	transition	P_e	
K	$1s \rightarrow p$	$\lesssim +0.01$	only weakly Z- and energy-dependent
L_1	$2s \rightarrow p$	$-0.1 \ldots -0.2$	
L_2	$2p_{1/2} \rightarrow d$	-0.5	
L_3	$2p_{3/2} \rightarrow d$	$+0.25$	

⇨ „Simplified" theory

Fermi's „Golden Rule"

$$\boxed{\mu \sim |M_{fi}|^2 \cdot \varrho(E)}$$

The density of the final states ϱ and the number of the photo electron n transferred to these states can be classified by their spin direction

$$\varrho = \varrho^{\uparrow} + \varrho^{\downarrow} \qquad n = n^{\uparrow} + n^{\downarrow}$$

with the definitions:

$$\boxed{\Delta\varrho = \varrho^{\uparrow} - \varrho^{\downarrow}} \quad \text{and} \quad \boxed{P_e = \frac{n^{\uparrow} - n^{\downarrow}}{n^{\uparrow} + n^{\downarrow}}}$$

and 1. Assumption: M_{fi} does not depend spin direction of the photon relative to the electron spin

$$\mu = \mu_0 + \mu_c \sim |M_{fi}|^2 (\varrho + P_e \Delta\varrho)$$

$$\boxed{\frac{\mu_c}{\mu_0} = P_e \frac{\Delta\varrho}{\varrho}}$$

CMXD at the Pt L_2 edge of Pt in PtFe

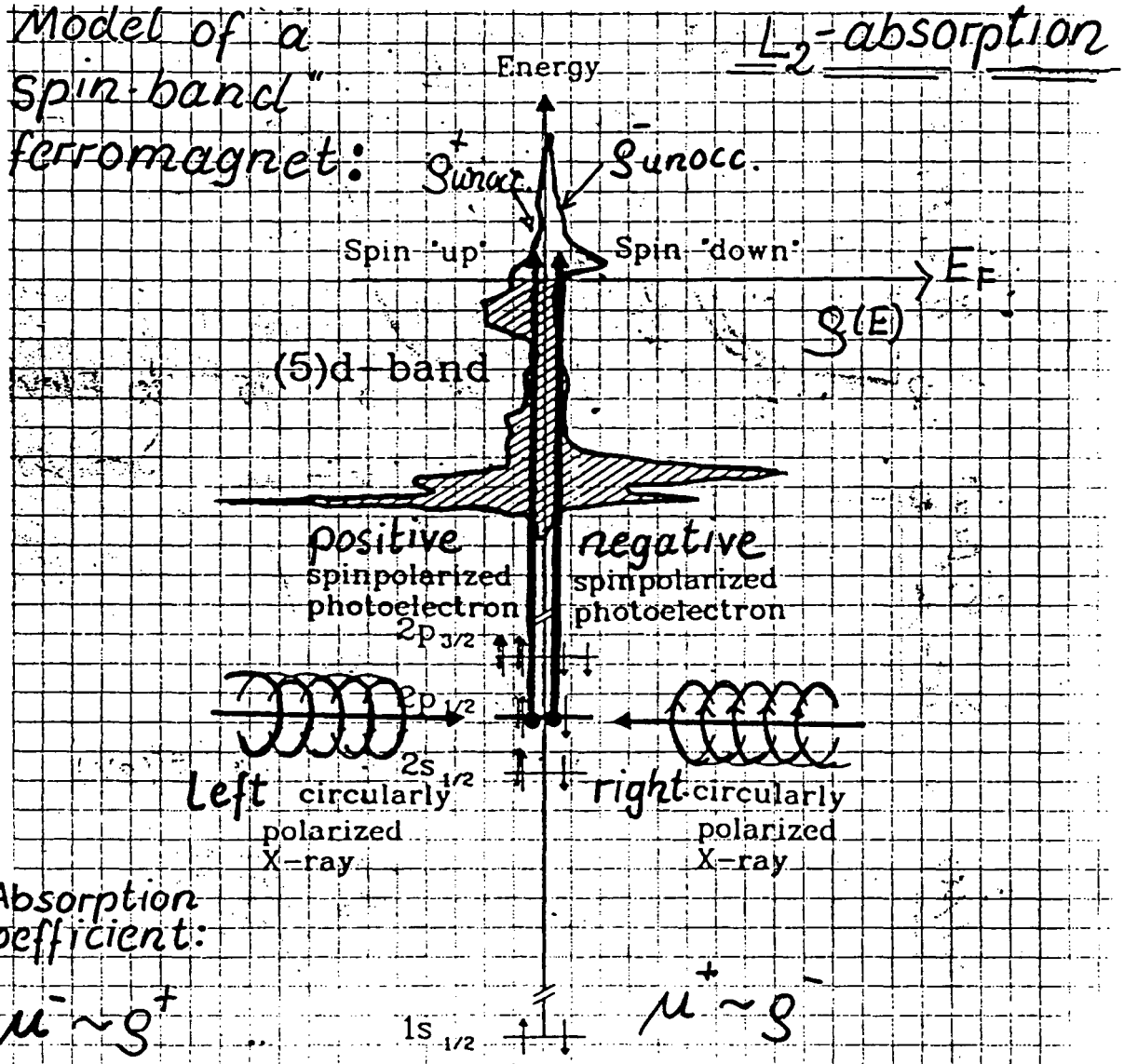

Theoretical density profile of the empty d-states :*

Measured Pt-L_3 absorption profiles

Pt Fe

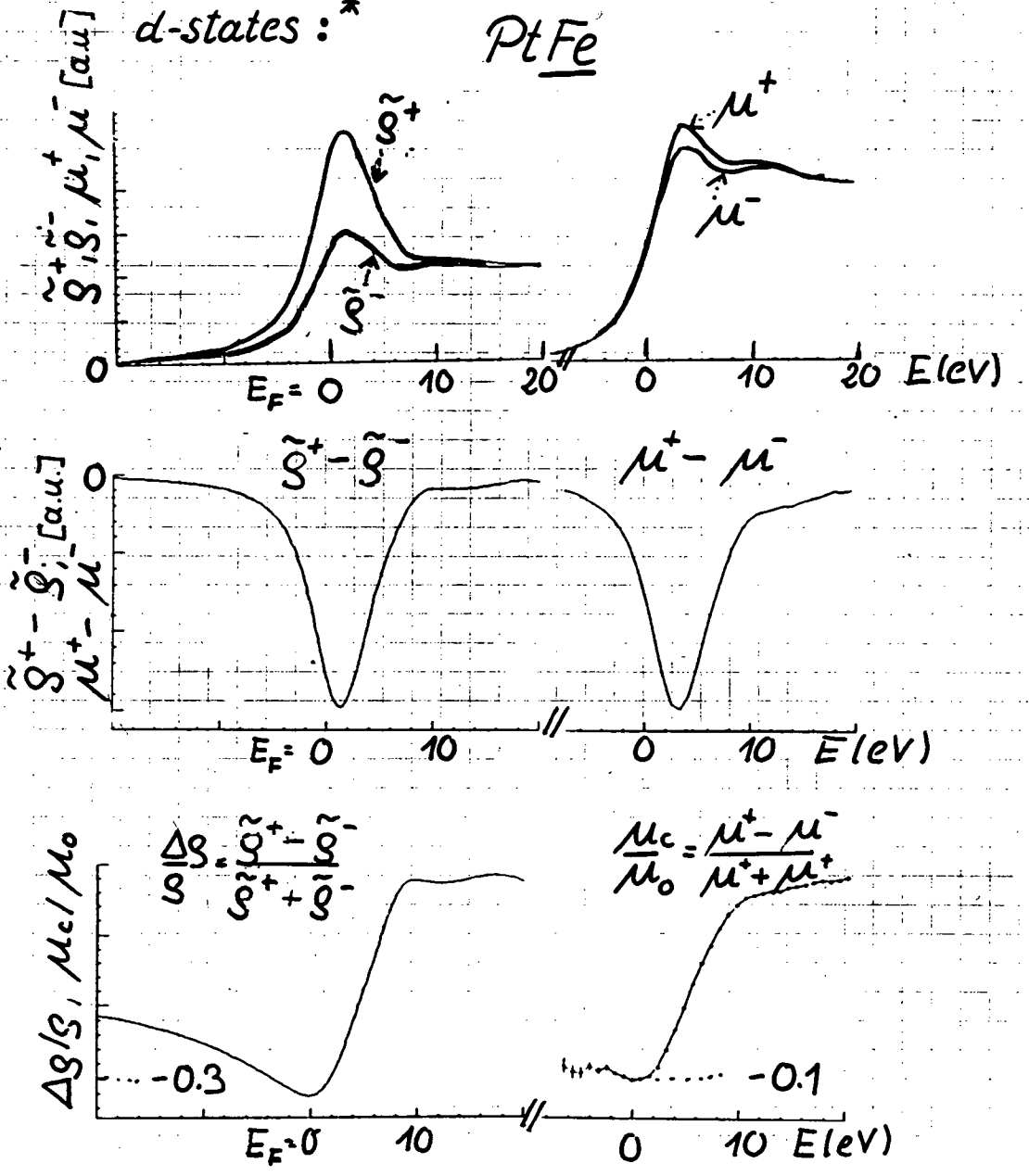

$\frac{\mu_c/\mu_0}{\Delta\varrho/\varrho} \approx 0.3$ close to the „free atom" value for $P_c = 0.25$!

$\frac{\Delta\tilde{s}}{\tilde{s}}$ deduced from $\frac{\mu_c}{\mu_o}$ via $\frac{\Delta\tilde{n}}{\tilde{n}}$ from spin-polarized band-structure calculations using „free-atom" value for P_e

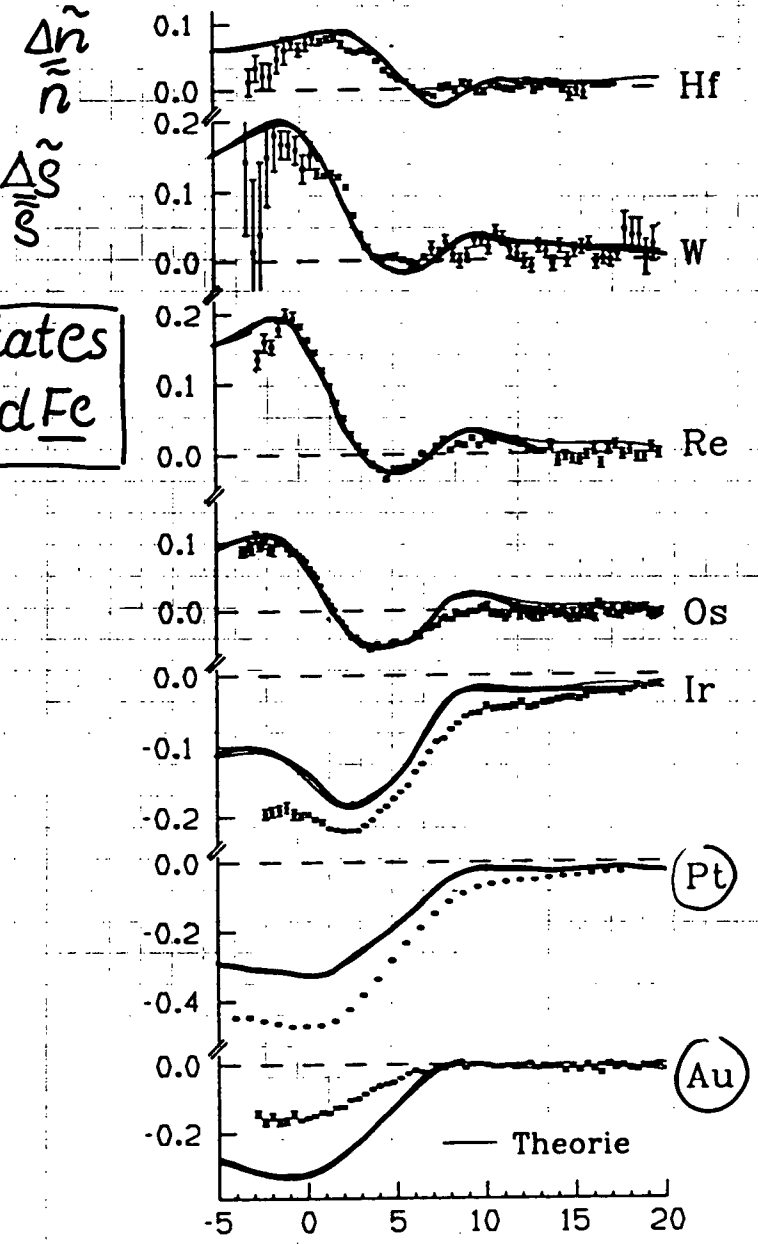

d-states of 5d Fe

only for Pt and Au disagreement in amplitude

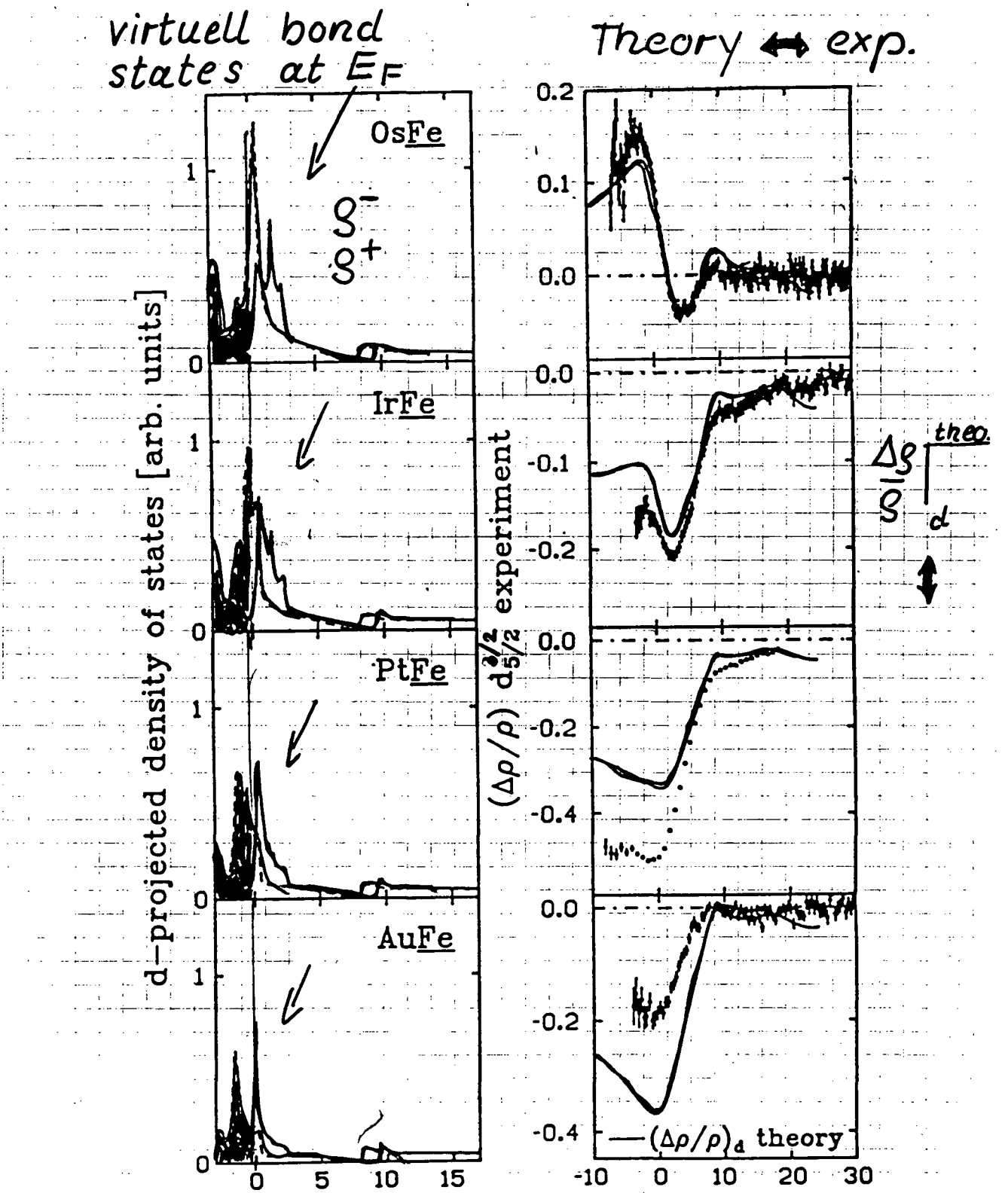
virtuell bond states at E_F
Theory ↔ exp.
OsFe
IrFe
PtFe
AuFe
g^-
g^+
d-projected density of states [arb. units]
$(\Delta\rho/\rho)\ d^{3/2}_{5/2}$ experiment
$\frac{\Delta g}{g}$ theo.
d
$(\Delta\rho/\rho)_d$ theory

CMXD → information on local moments:

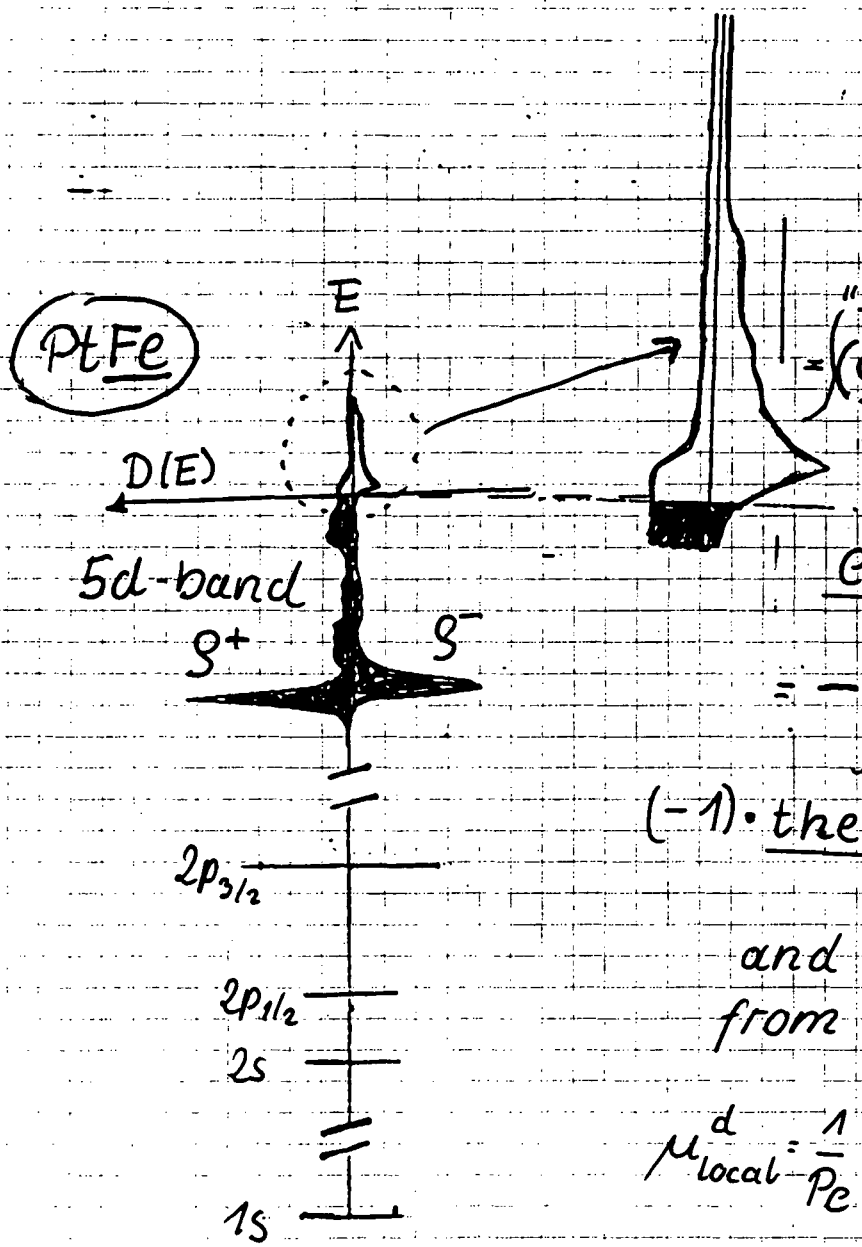

"hole" moment

$= \int (g^+_{unocc.} - g^-_{unocc.}) \mu_B$

is Δg equal to

$= -\int (g^+_{occup.} - g^-_{occup.}) \mu_B$

$(-1) \cdot$ the local d-moment

and can be deduced from the CMXD

$$\mu^d_{local} = \frac{1}{P_e} \int \frac{\mu_c}{\mu_0} g \, dE$$

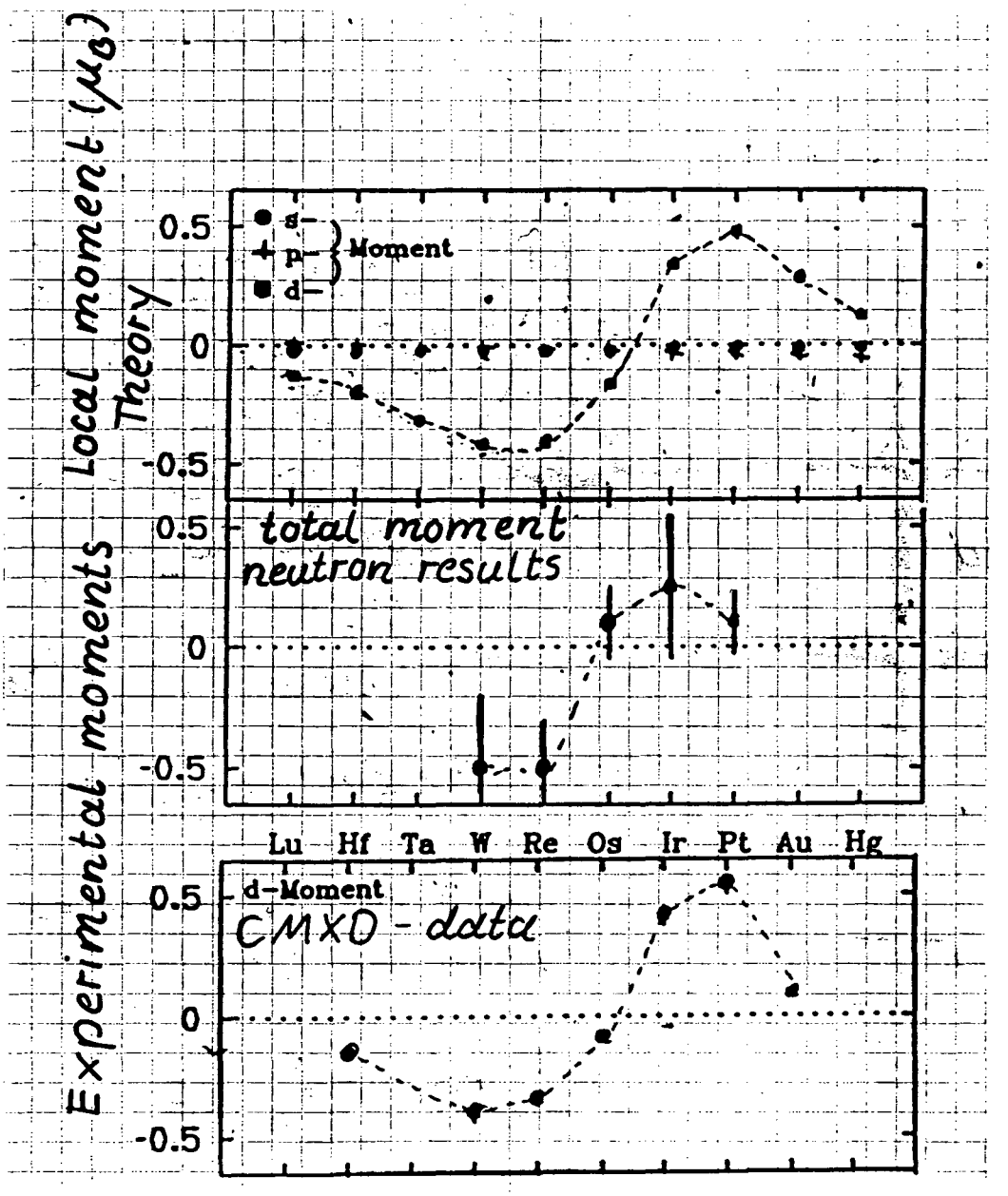
Experimental moments Local moment (μ_B)
Theory
s
p
d
Moment
0.5
0
-0.5
total moment
neutron results
Lu Hf Ta W Re Os Ir Pt Au Hg
d-Moment
CMXO - data

Spin polarization of Pt in Pt/Co multilayers studied by x-ray absorption

S. Rüegg, G. S.: Techn. Univ. Munich — Experiment

H. Ebert: Siemens AG, Erlangen — Theory

B. Zeper: Philips, Eindhoven — Sample preparation

The material investigated:

30 × (4 Å Co + x Å Pt) with x = 9, 16, 23, 30, 40

≙ (2 ML Co + x ML Pt) with x = 4, 7, 10, 13, 17

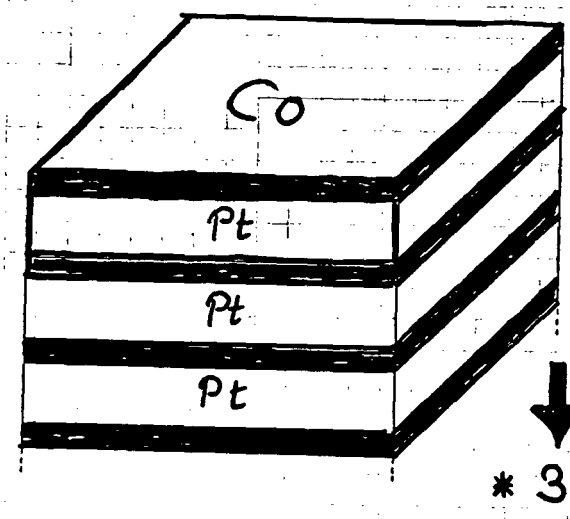

fcc

(111) texture

Pt/Co multilayer [30 × (16 Å Pt/4 Å Co)] are new candidates for magn. optical recording

B. Zeper et al.
J. Appl. Phys. 65, 4971 (1989)

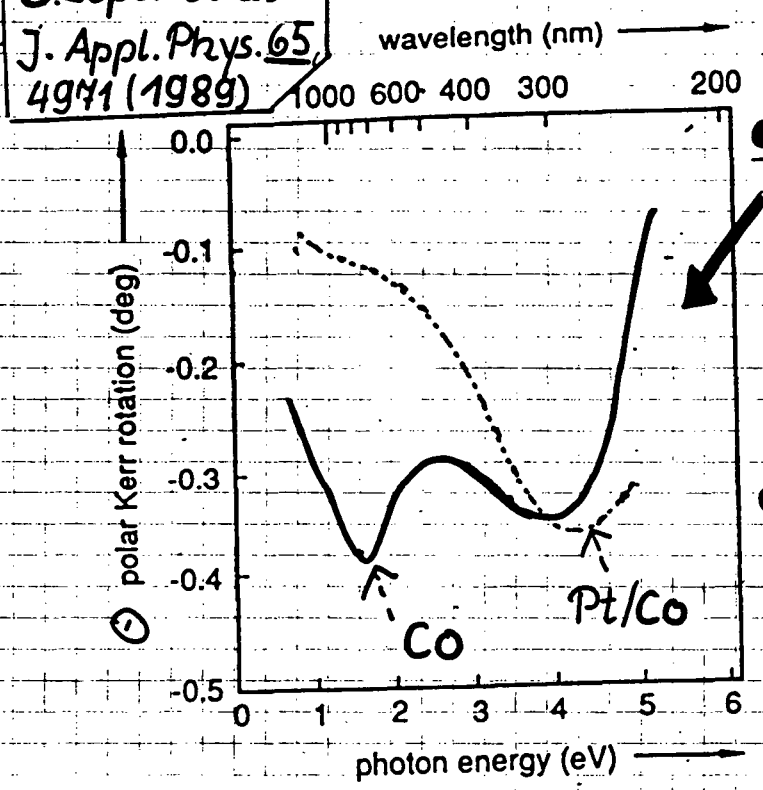

- good Kerr-rotation especially at shorter wave length
- \+
- good reflectivity R ~ 70%
- \+
- high corrosion resistence
- \+
- 100% perpendicular remanence

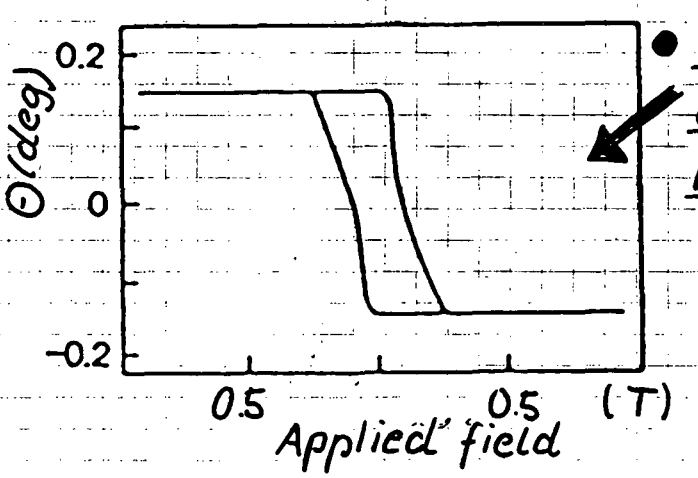

„Physically" interesting properties

Increased moment per Co atom

- T_c depending on Pt - thickness

$T_c \sim 1/d_{Pt}$

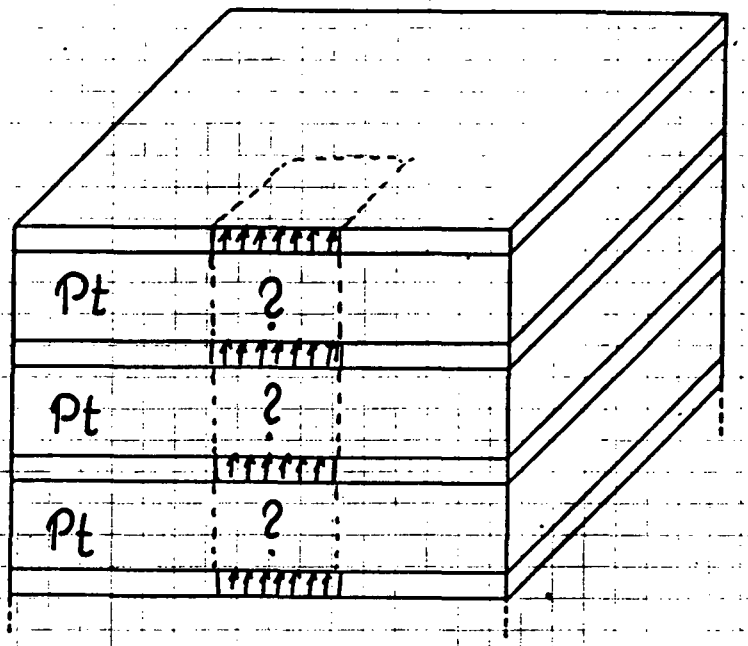

Physical Questions:

- Is Pt polarized and carries a moment?
  if it is so
- Is it a surface polarization ?
  if it is not
- How long is the exchange interaction range, is it oscillating ?

CMXD at the Pt L_3-edge in

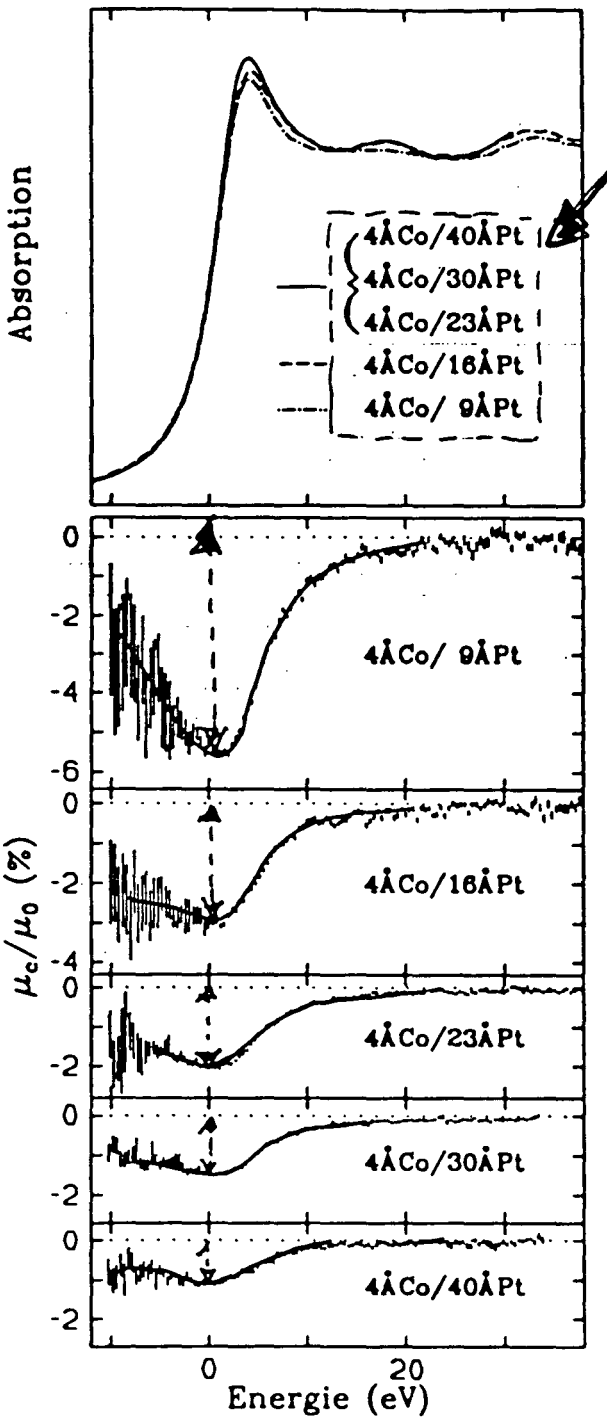

Amplitude measures the average Pt moment

Average Pt-moment in Co/Pt-multilayers

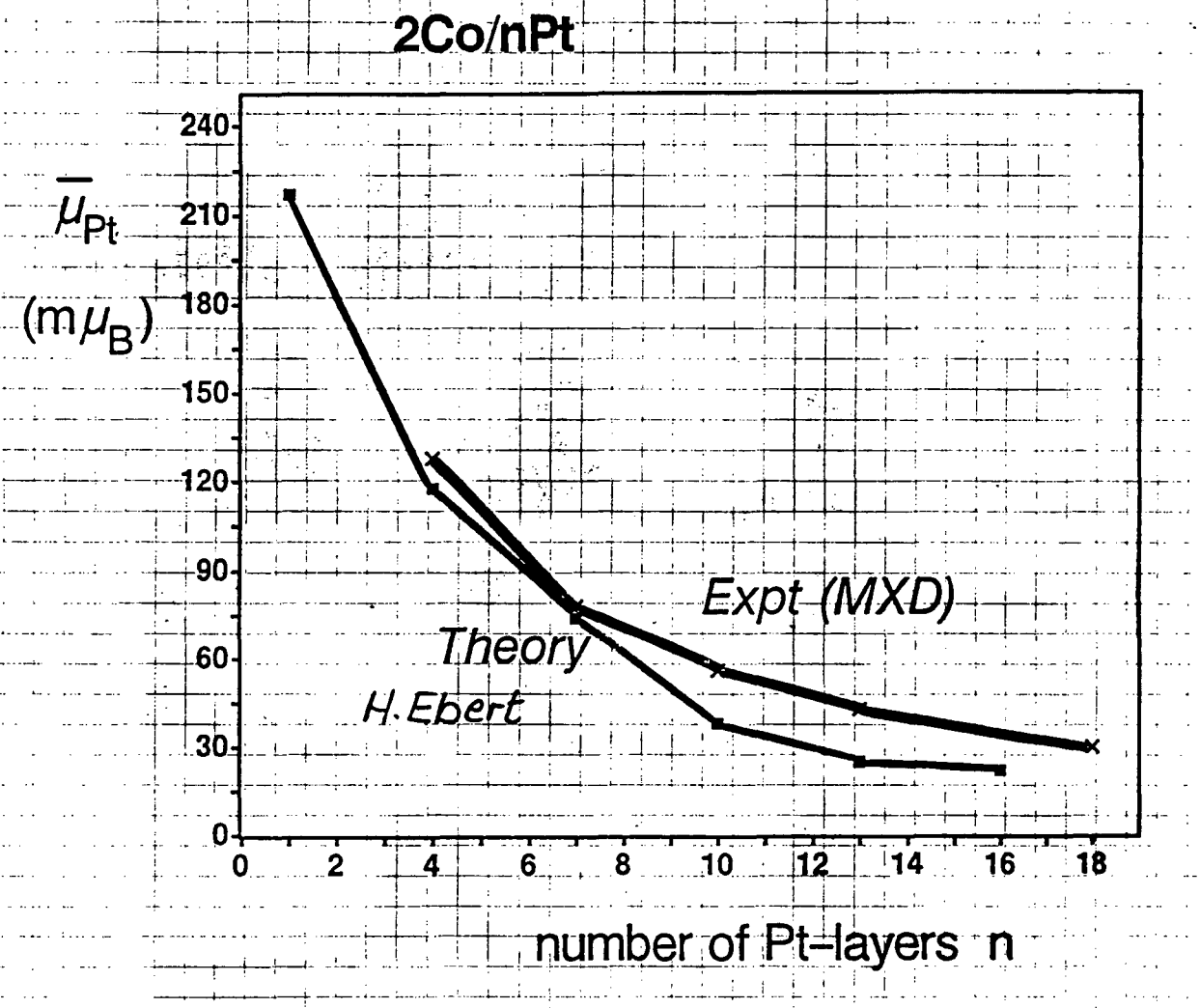

Theoretical Pt-layer moments:

H. Ebert et al

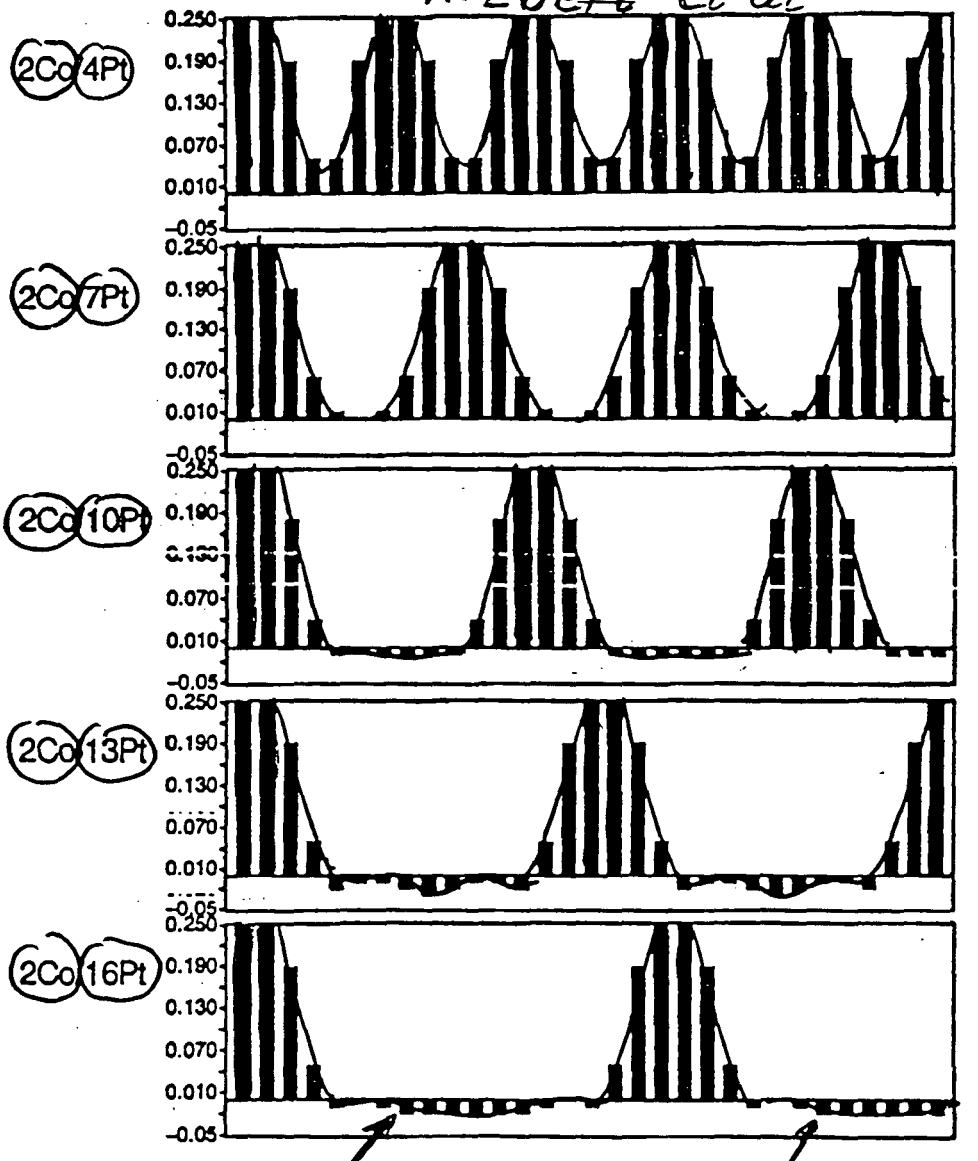

antiferromagnetic coupling regions predicted

d-Momente der gesamten Pt-Schicht
Experiment, Theorie, rel, nichtrel. von H. Ebert

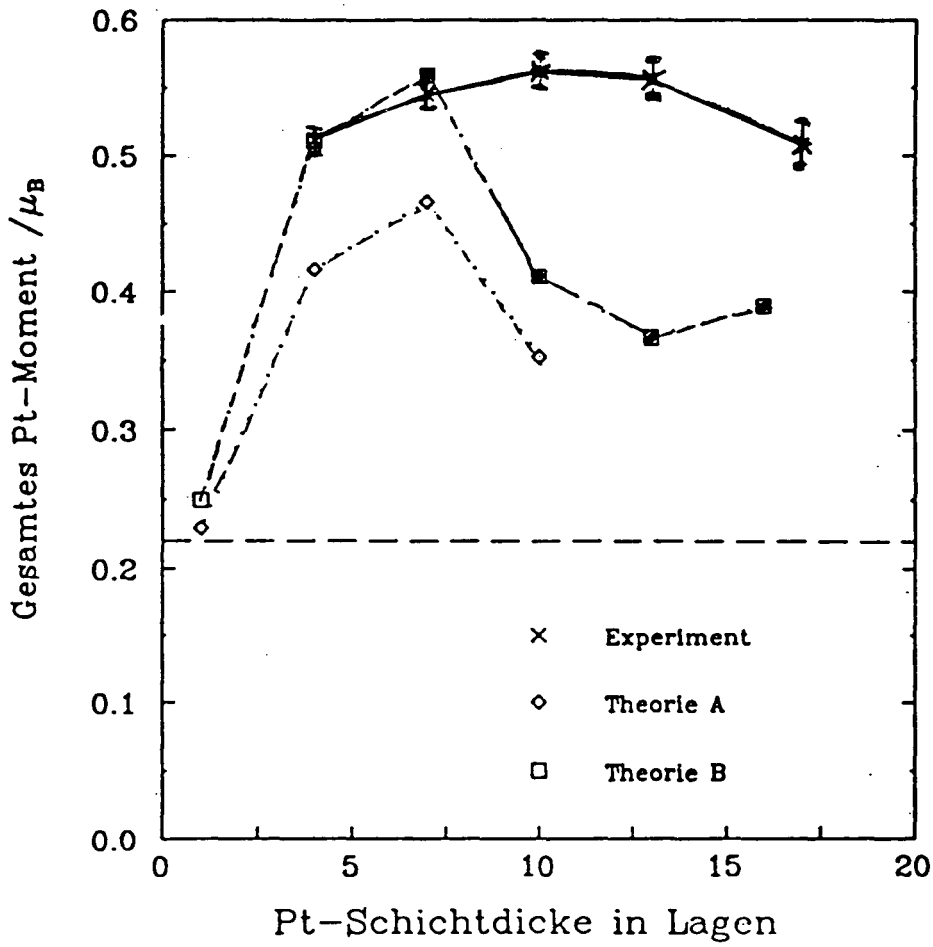

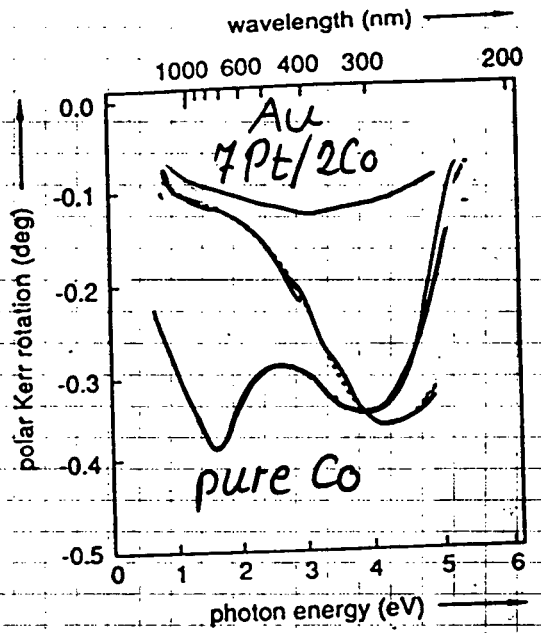

It is expected that Pt 5p-5d transitions cause enhancement of Kerr rotation

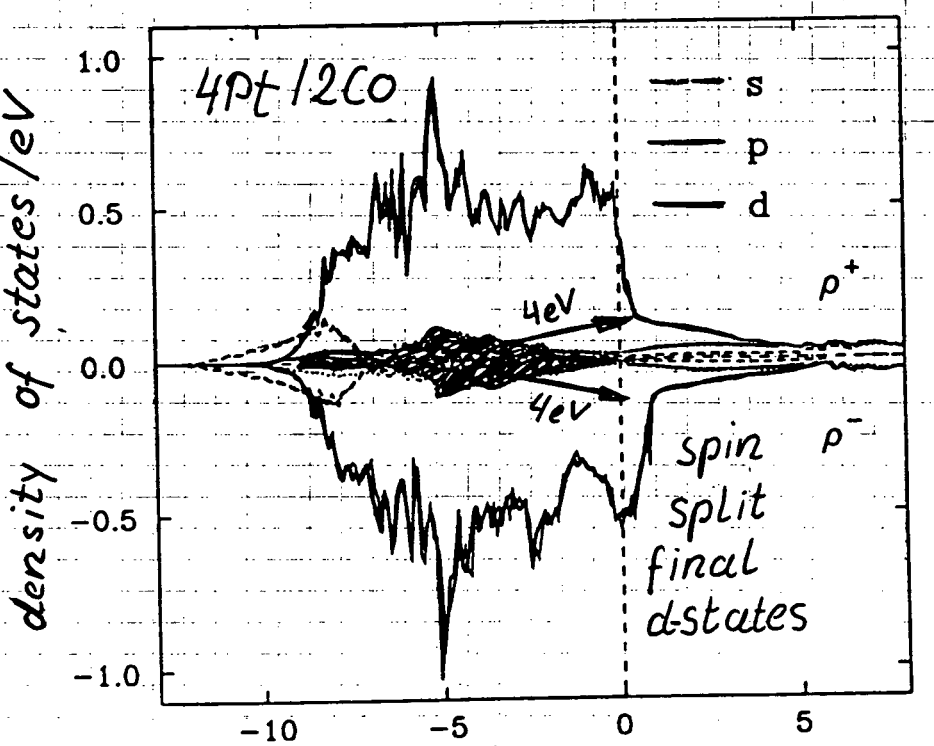

$L_{2,3}$ MXD in 4f-Elements ⇒ $(RE)_2Co_{17}$

no simple systematics observable

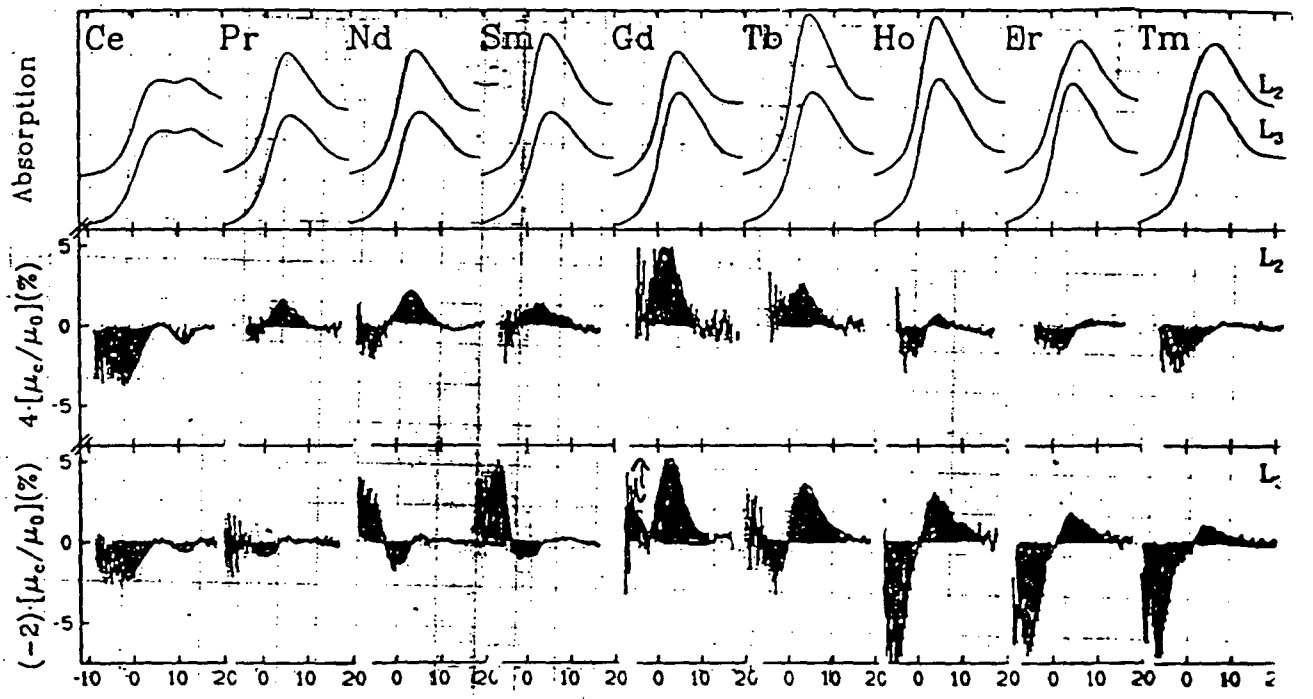

d-Like spin density ↑↑ to 4f spins

↑↓ to 4f spins

Total measurement time ~2 days

(inclusive sample changing)

If „naive" model valid for Ce ....

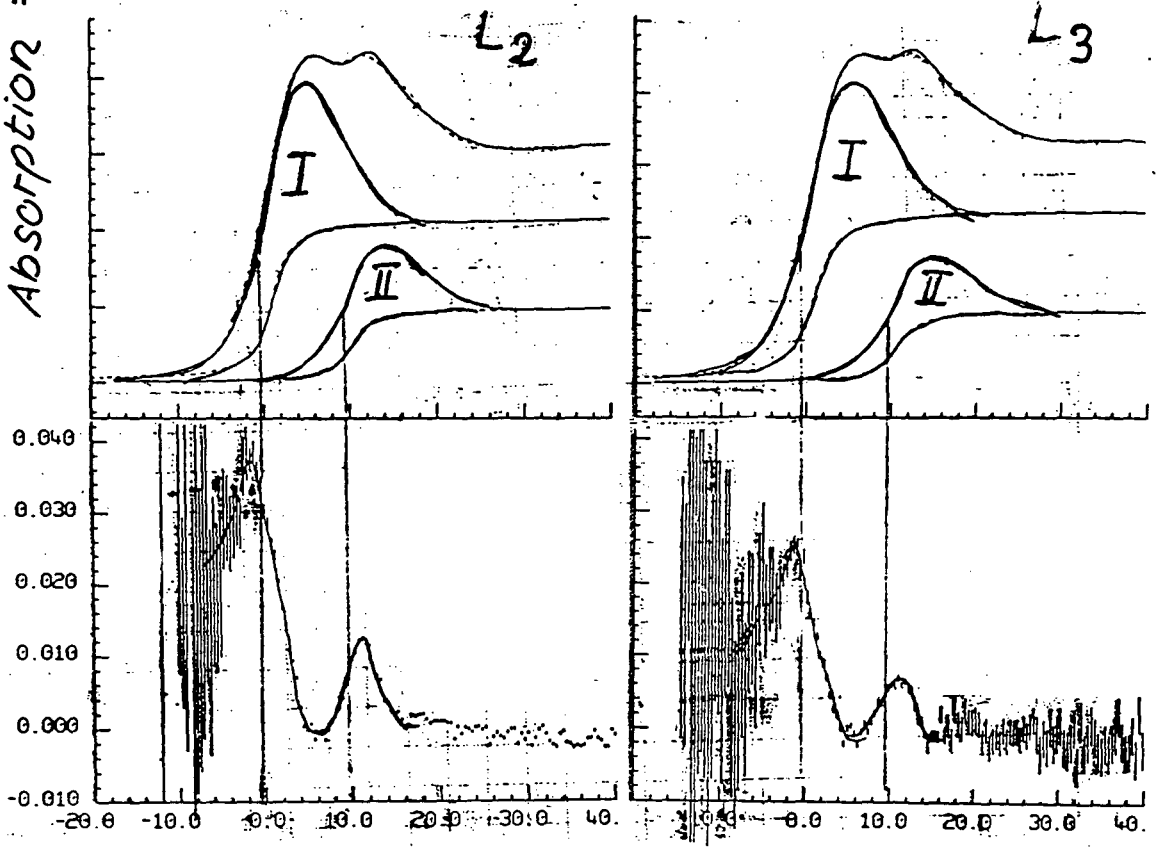

a Ce 5d-moment of $\begin{cases} \mu_d^I \sim -0.15\,\mu_B \\ \mu_d^{II} \sim -0.12\,\mu_B \end{cases}$ is estimated from MXD-results

Theory: O. Eriksson et al. PRB 41, 9111 (90) → $\mu_{5d}^{Ce}(CeCo_5) \sim -0.2\,\mu_B$

! planned to study Ce in heavy fermion systems !

Only small „chemical" influence on MXD

Gd $L_{2,3}$ MXD in different compounds:

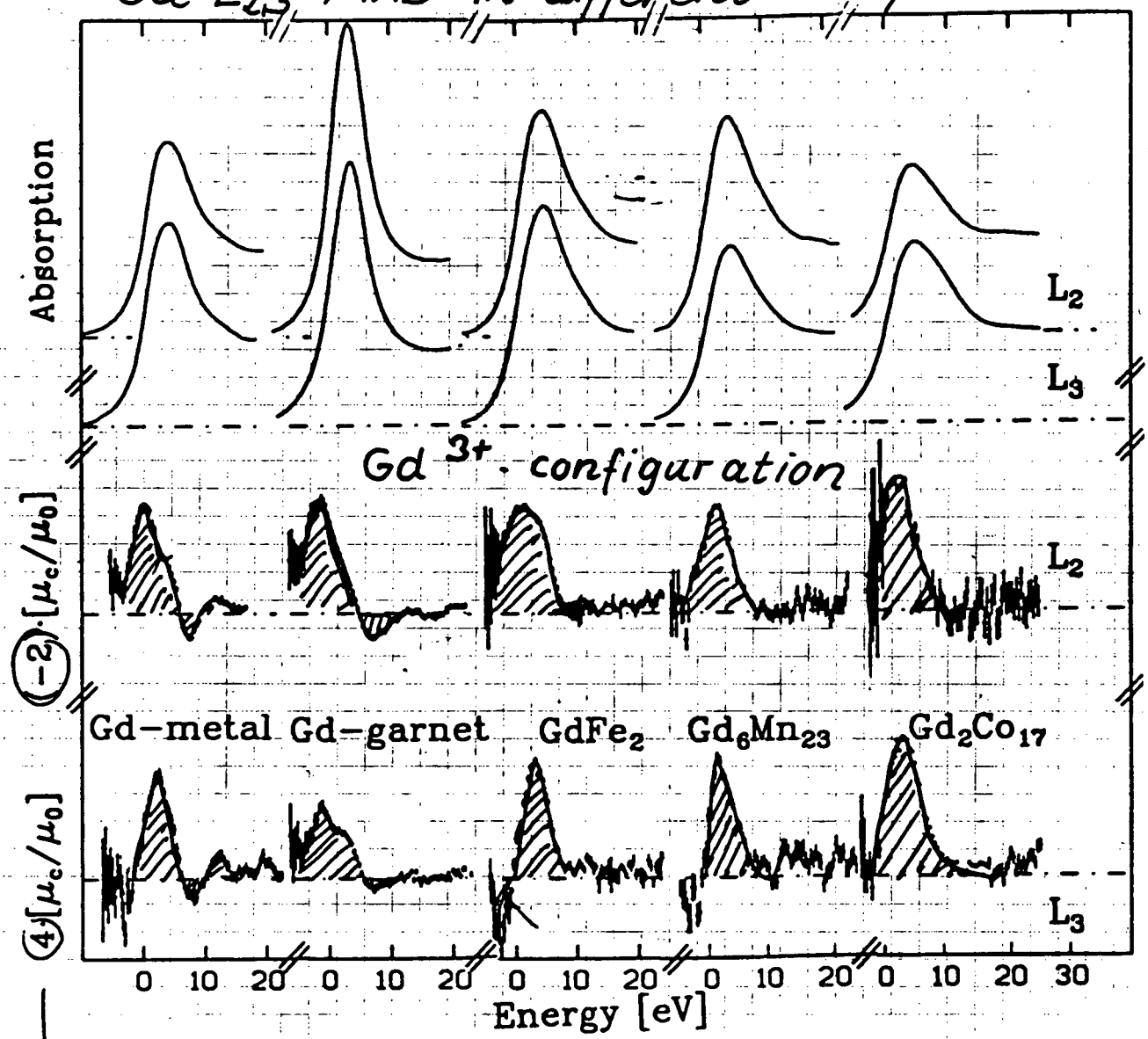

↳ MXD - recalibrated by a factor $1/p_e^{\text{free atom}}$

MXD scales with „Local" magnetization....

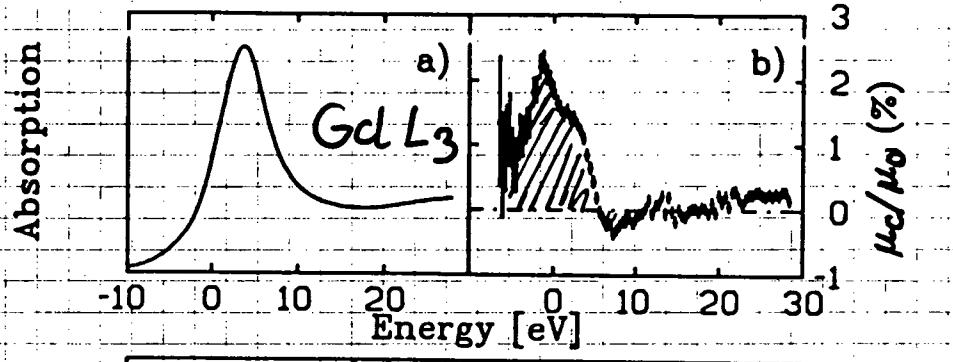

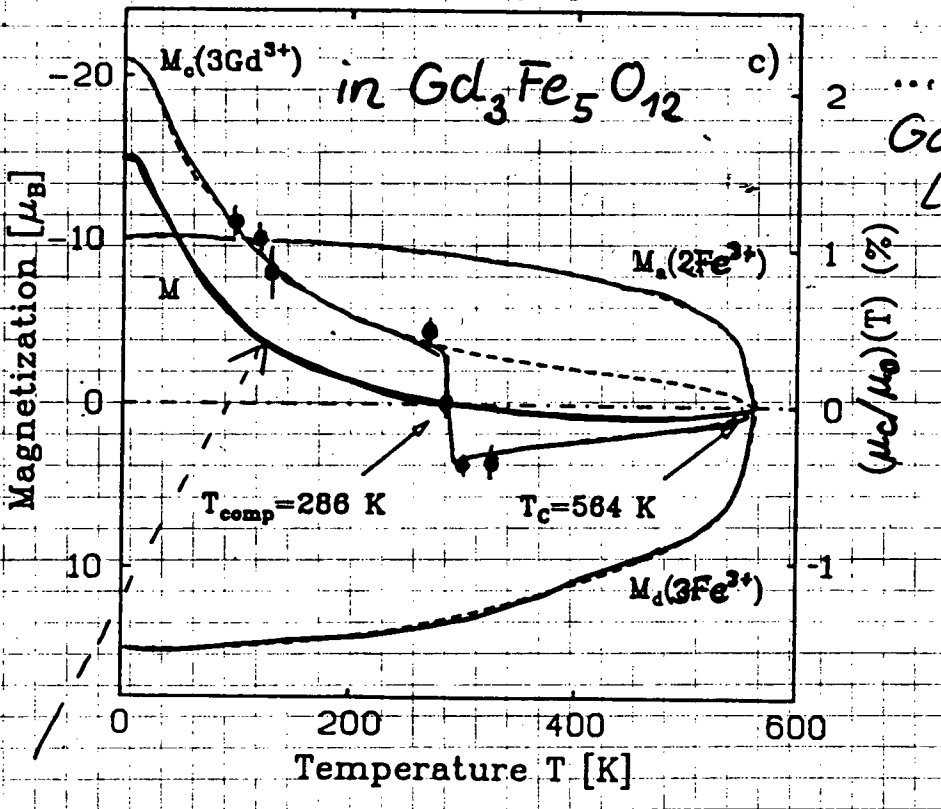

... of the Gd^{3+}-sub-lattice

and not with total magnetization

K-edge MXD

$$\frac{\mu_c}{\mu_0} = 0.01 \frac{\Delta s}{s}^{p\text{-like}}$$

$\frac{\Delta s}{s}\Big|^{p\text{-like}}$ from theory

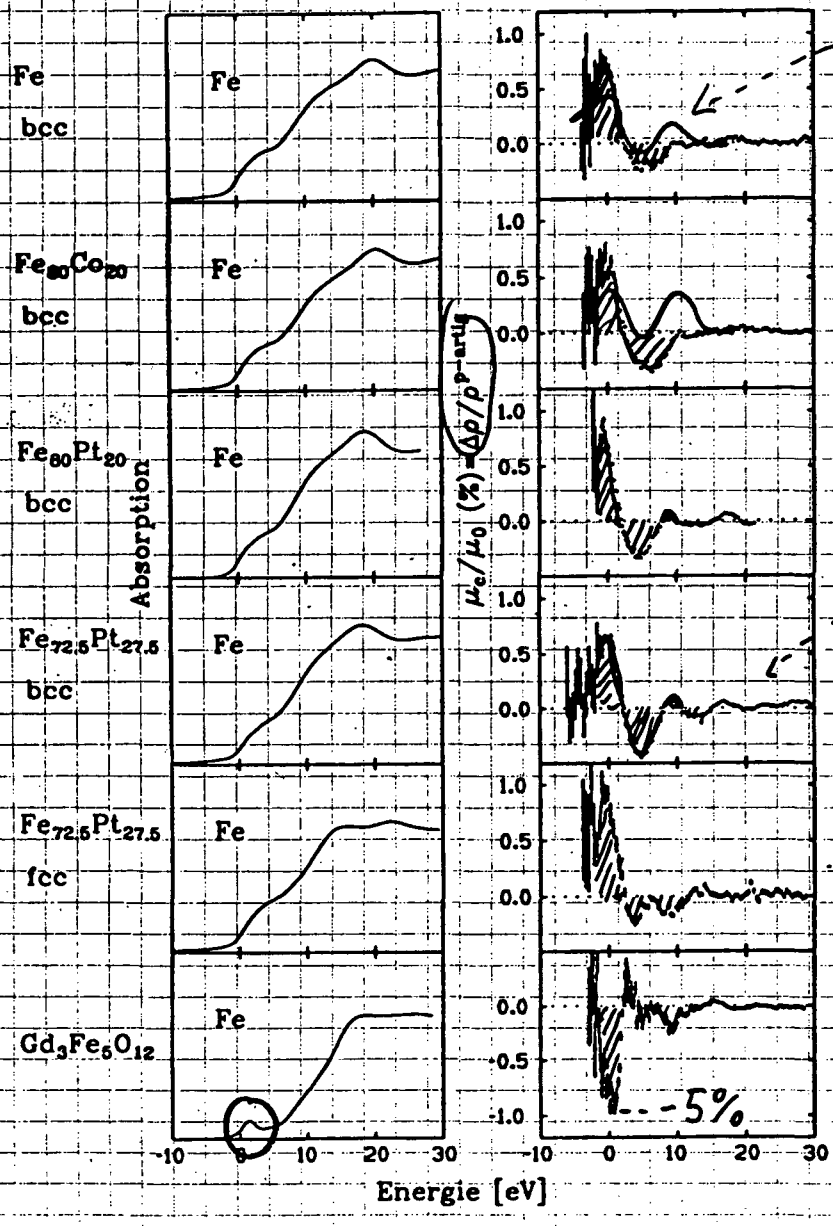

One spectra takes ~ 1-2 hou

accuracy $\sim 10^{-4}$

Prepeak due to 1s-3d E2 transition

Anwendung:

MESSUNG DER ZIRKULARPOLARISATION DER SYNCHROTRONSTRAHLUNG

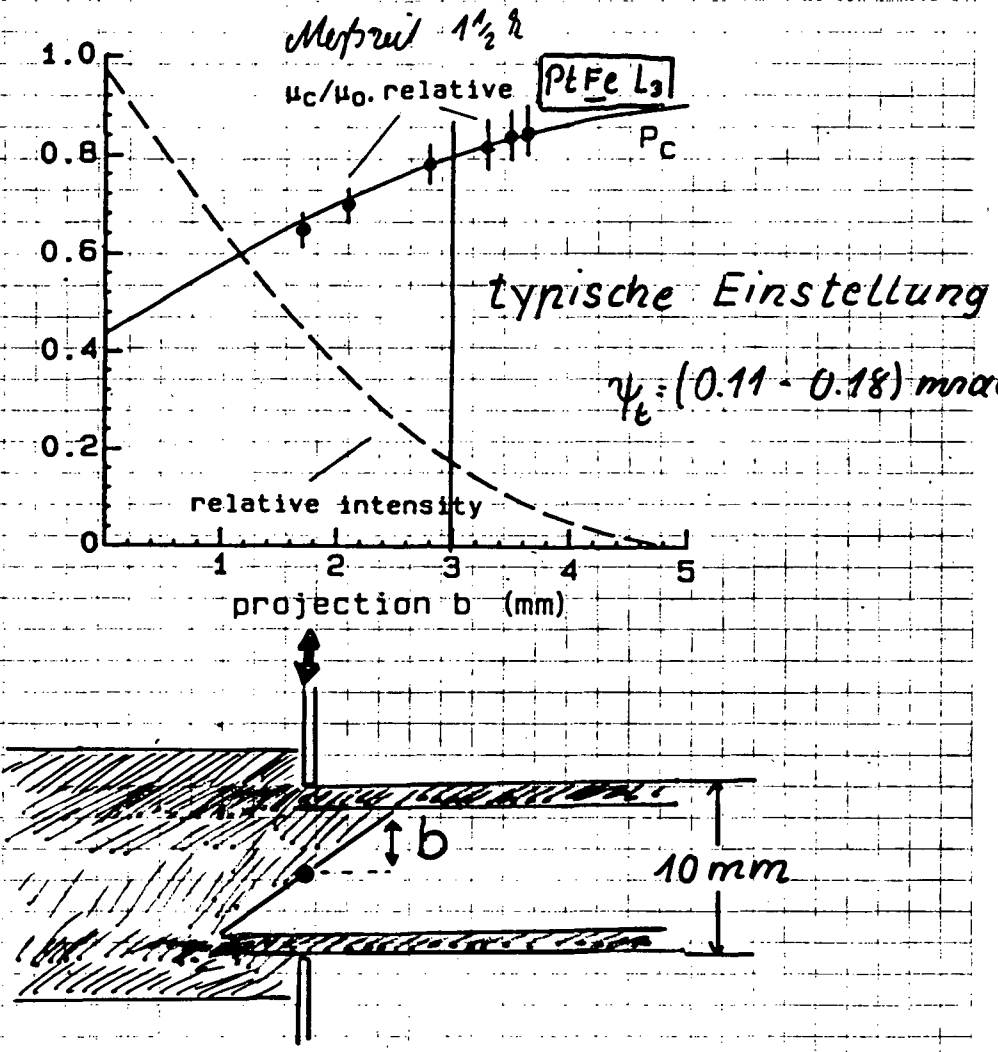

P_c depends strongly on e⁻ beam „size"

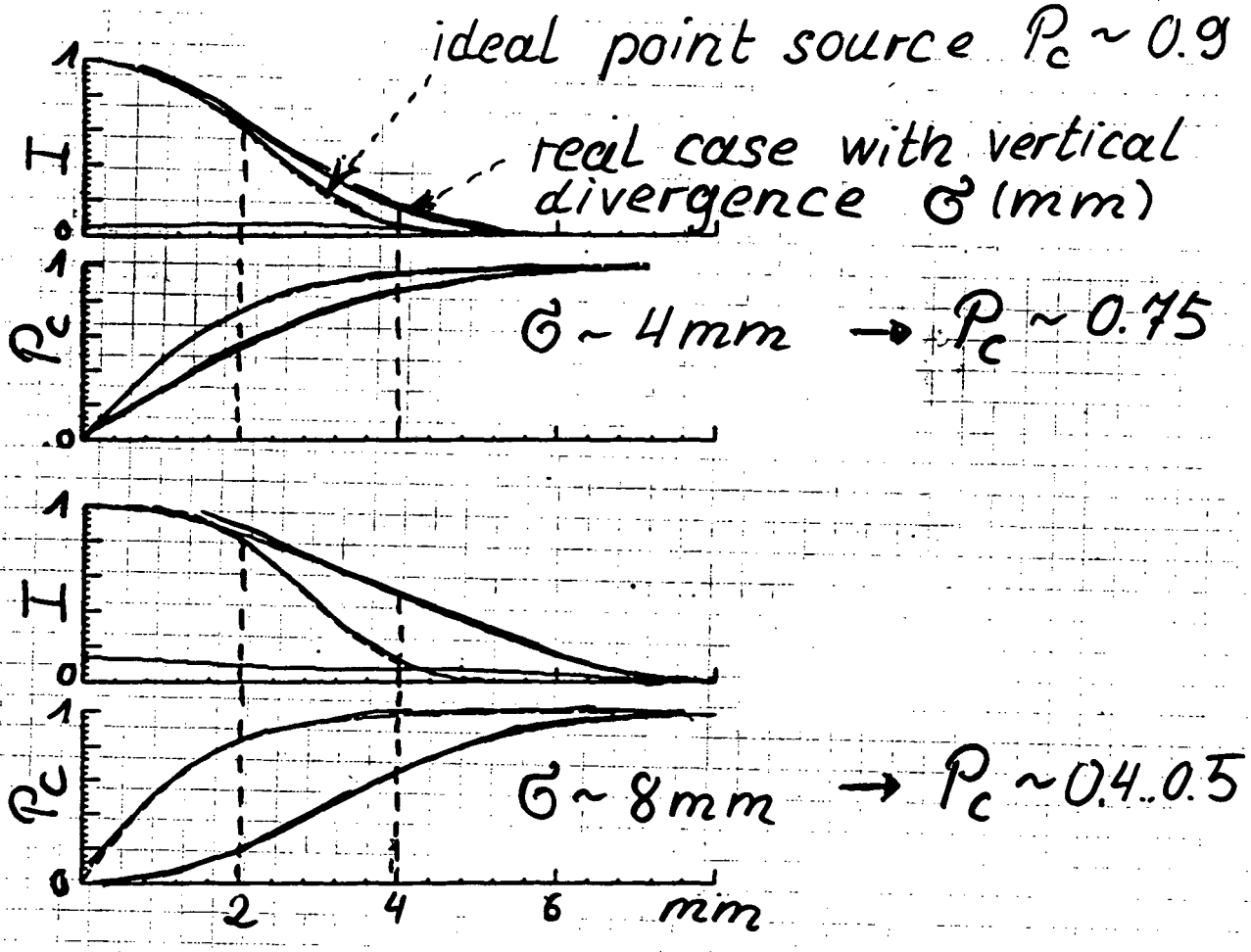

Calibration of P_c with spin-dependent absorption measurements at

E_γ	Sample	Edge	Prep.	max. μ_c/μ_0	
13.73	Au<u>Fe</u>	Au L_2	cold-rolled metallic foils	5%	
13.27	Pt<u>Fe</u>	Pt L_2		(22%)	
12.82	Ir<u>Fe</u>	Ir L_2		(14%)	
12.34	Os<u>Fe</u>	Os L_2		5%	
11.92	Au<u>Fe</u>	Au L_3		5%	
11.56	Pt<u>Fe</u>	Pt L_3		(15%)	
11.22	Ir<u>Fe</u>	Ir L_3		5%	
10.87	Os<u>Fe</u>	Os L_3		5%	
8.25	Tb	L_2		2%	80 K
7.93	Gd	L_2		4%	80 K
7.24	Gd	L_3		2%	80 K
7.11	Fe	K		0.8%	
6.17	Ce_2Co_{17}	Ce L_2	powder	1.5%	

SPIN-DEPENDENT EXAFS [SPEXAFS]

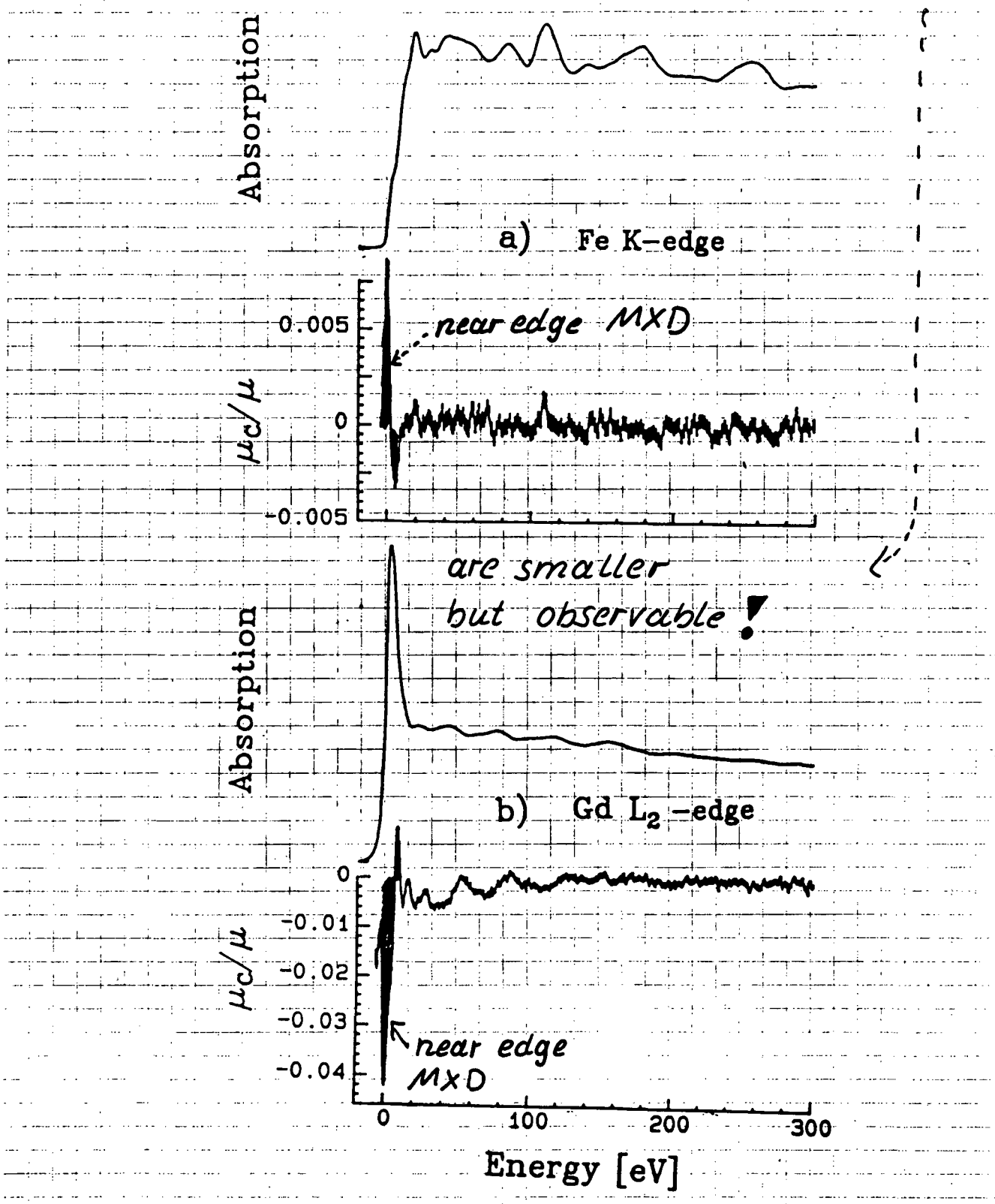

Physical Origin of SPEXAFS

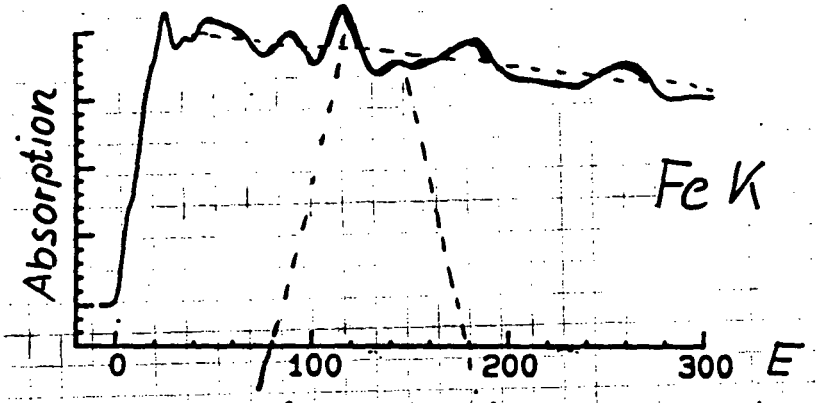

interference of outgoing and back-scattered electron wave

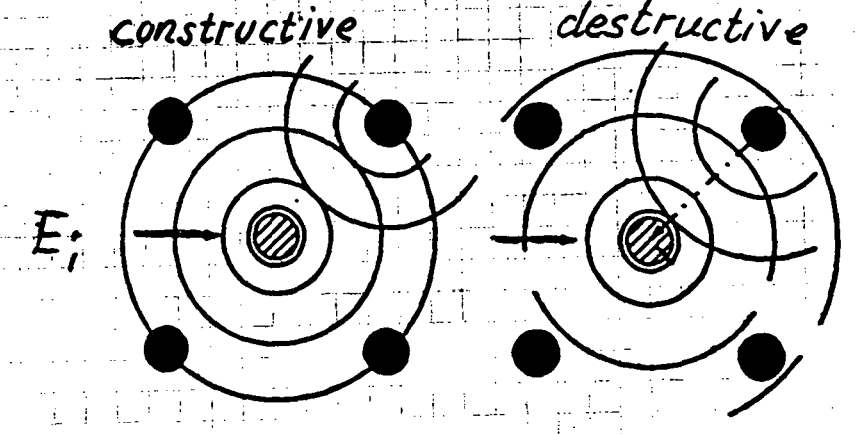

Absorption of circ. pol. x-rays in ferromagnets: The spin-pol. photoelectron is also „exchange" scattered by magnetized neighbours!

The EXAFS-Formula

$$\chi(k) = \frac{\mu(k) - \mu_{\text{free atom}}}{\mu_{\text{free atom}}}$$

$$\chi(k) = \sum_i \frac{1}{kr_i} N_i F_i e^{-2r_i/\lambda_i} D_i \sin(kr_i + \phi_i)$$

Summation $\rightarrow i$ of at r_i scattered waves

Structure parameter (spin-independent)

- N_i Number of next neighbours
- r_i Distance "
- D_i Debye-Waller-factor

Interaction parameter spin-dependent ?!

- F_i Back scattering ampl. $F = F_0 \pm F_c$
- λ_i mean free path $\lambda = \lambda_0 \pm \lambda_c$
- ϕ_i Phase shift $\phi = \phi_0 \pm \phi_c$

$$\chi = \chi^+ + \chi^-$$

$$\frac{\mu_c}{\mu_0} = \frac{\chi^+ - \chi^-}{1 + \chi^+ + \chi^-}$$

Gd $L_{2,3}$-SPEXAFS

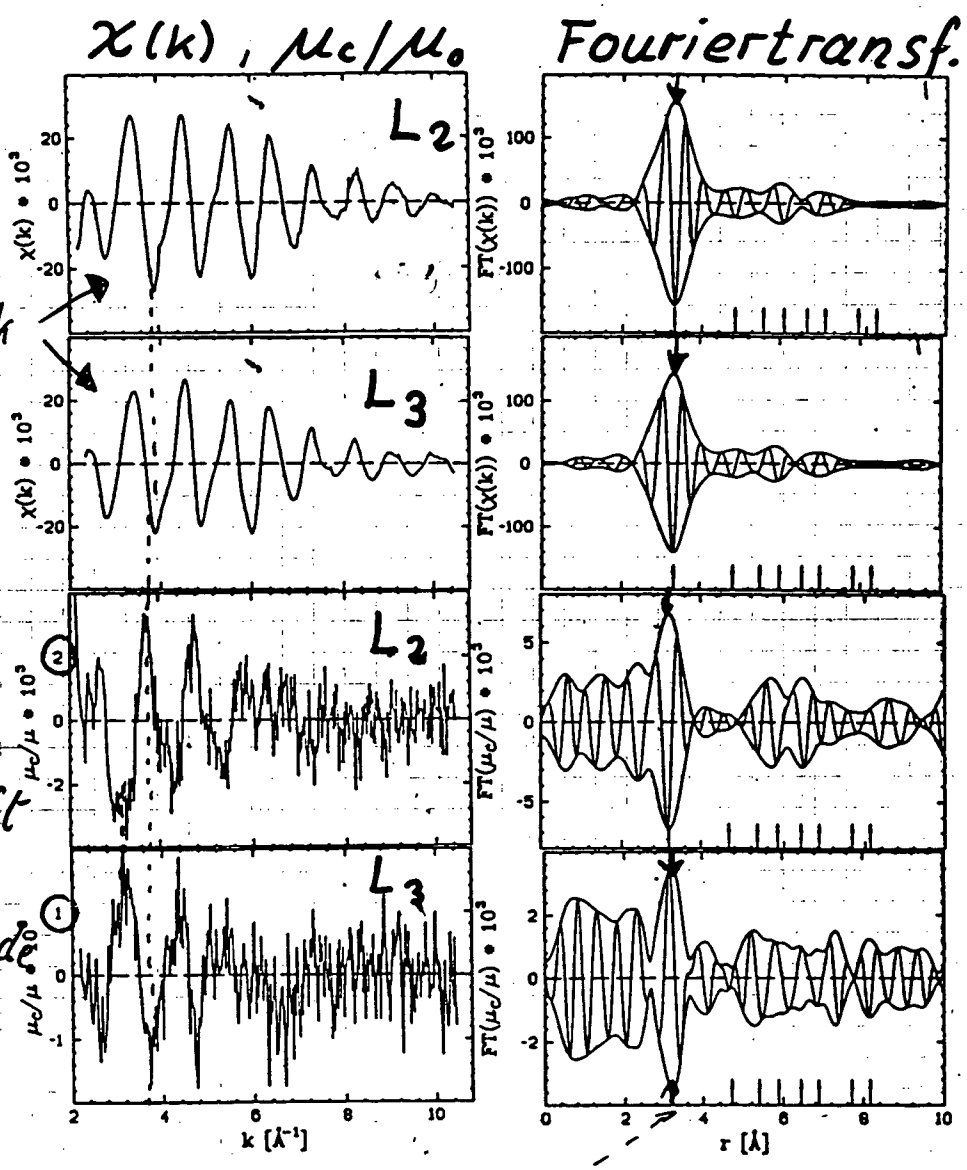

normal L_2 and L_3 EXAFS look identical

L_2 and L_3 SPEXAFS show phaseshift of π

L_3-amplitude 2× larger

next Gd neighbor

Back transformation:

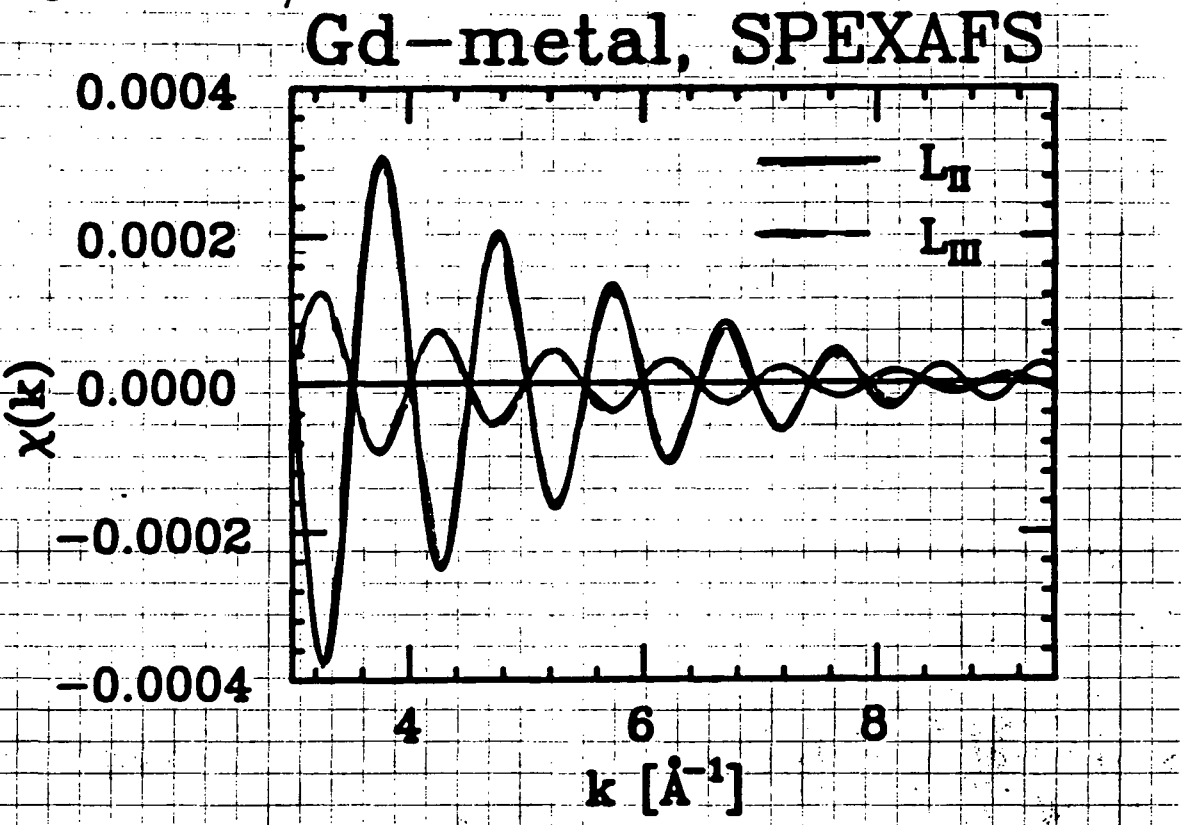

Ratio of L_2 and L_3 amplitude
" of $P_c(L_2)$ and $P_c(L_3)$ ≈ -2.5

➡ Exp. proof that for $E \gtrsim 30eV$
P_c corresponds to the free atom value

"Conventional" EXAFS:

$$\chi = \frac{\mu - \mu_{\text{free atom}}}{\mu_{\text{free atom}}}$$

Gd

Fourier transform

$FT[\chi(k)] = F(r)$

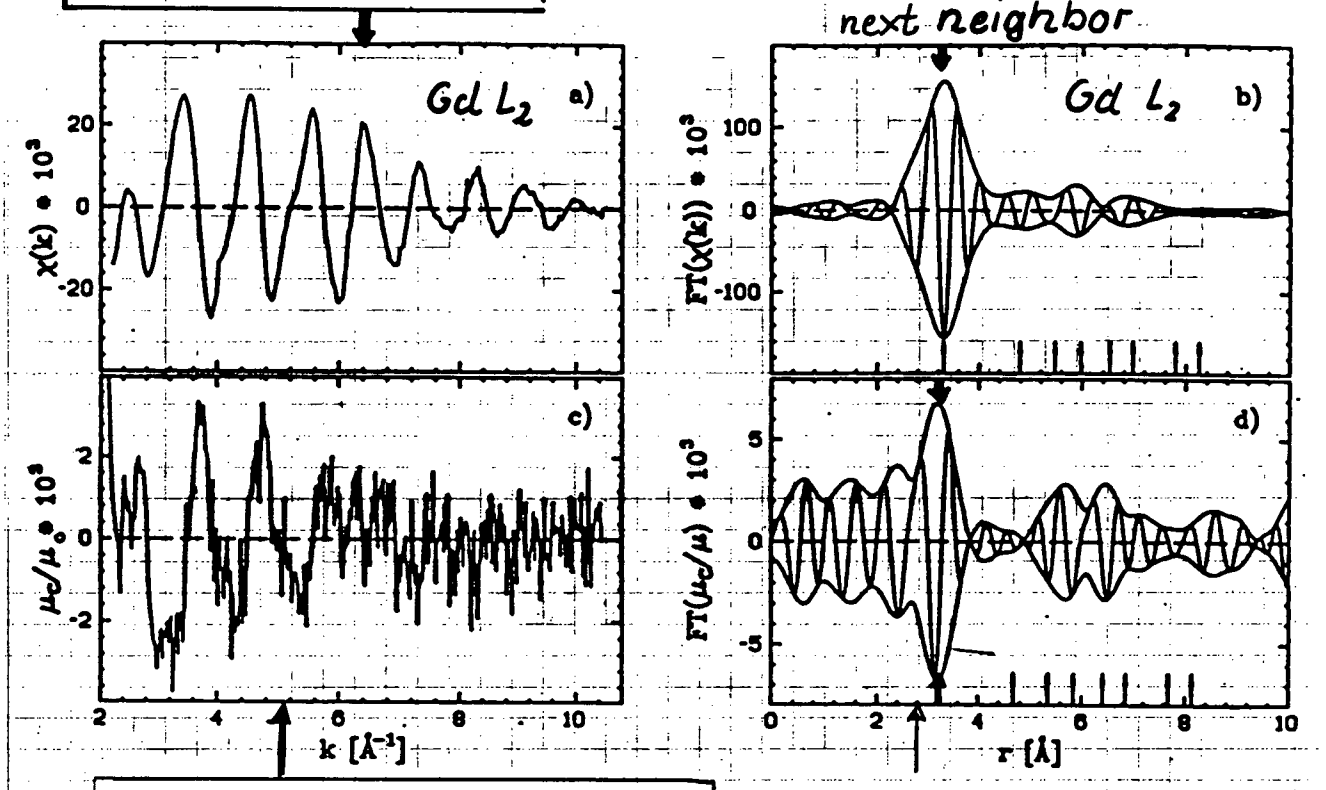

SPEXAFS $[\mu_c/\mu_0](k)$

$FT[\mu_c/\mu_0)$

From the data the spin-dependent rel. backscattering amplitude for Gd is deduced to

$$\left[F_c/F\right]_{Gd} = 0.10 \qquad \left[\mu(n_0)/2 = 0.12\right]$$

$$\left[\begin{array}{ll} \lambda_c/\lambda_0 < 0.01 & \text{estimated from} \\ \phi_c/\phi_0 < 0.05 & \text{simulation of } \mu_c/\mu_0 = \frac{\chi^+ - \chi^-}{1+\chi^+ + \chi^-} \end{array}\right]$$

SPEXAFS of $Gd_3Fe_5O_{12}$ [insulator]

$\chi(k)$ Fourier transform

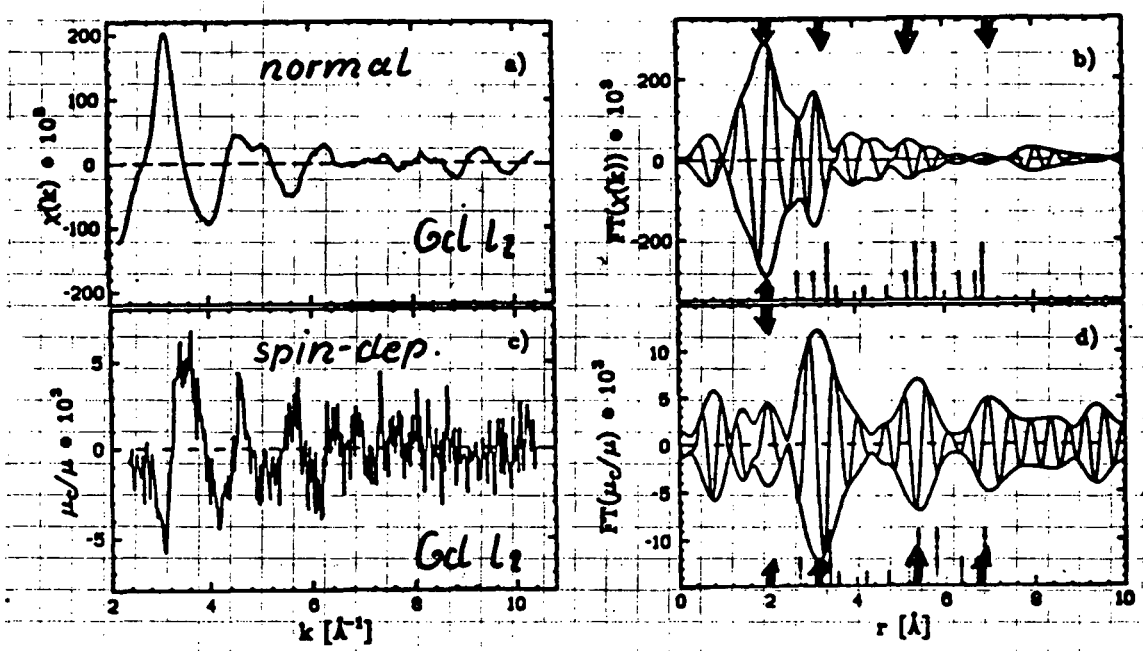

oxygen neighbors
Gd, Fe neighbors

SPEXAFS only sensitive on magnetic neighborhood

Results on $[F_c/F]_{Fe^{3+}} = 0.17$ $[\mu/l = 0.19]$

Ce L_3 SPEXAFS in $CeFe_2$

measured in energy dispersive mode

et LURE

Baudelet et al. 1990

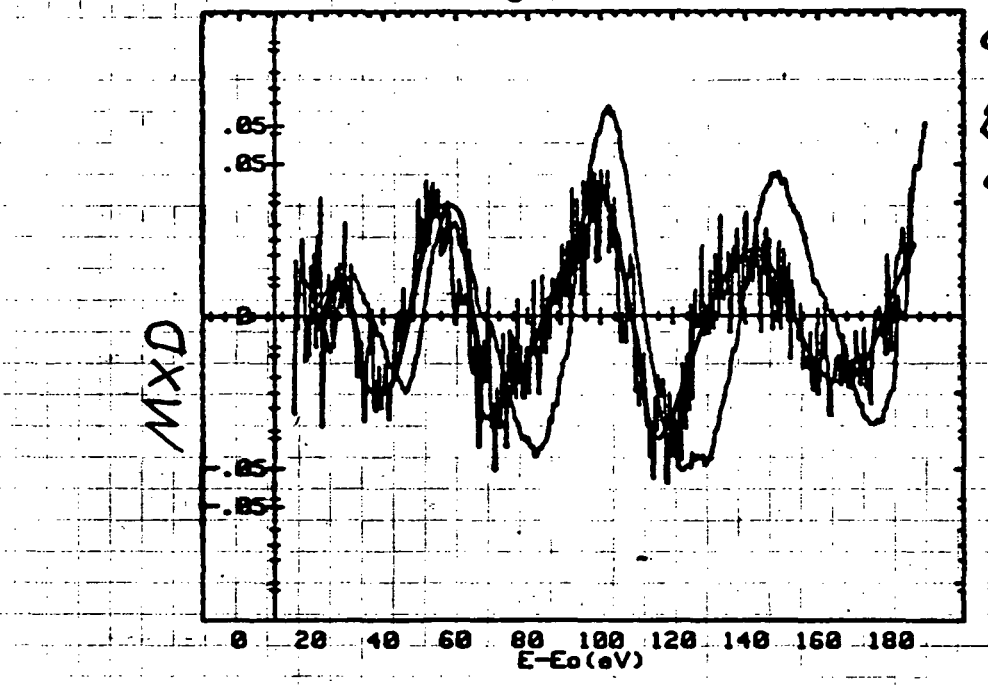

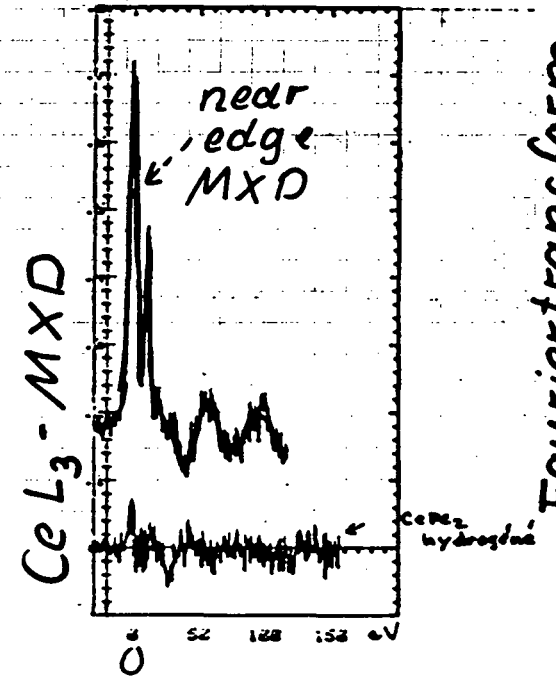

Fourier transform

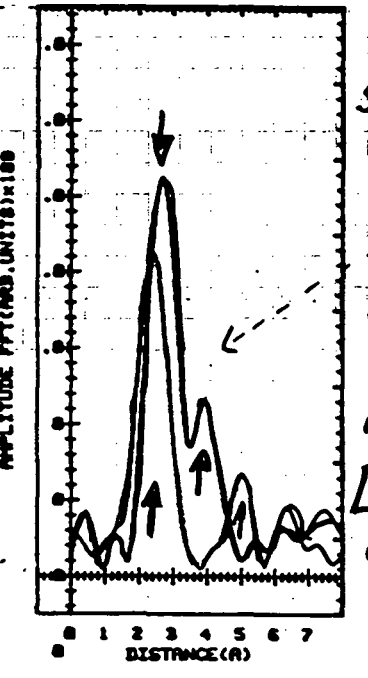

EXAFS sees Ce

SPEXAFS show only 2 iron neighbors

[Ce moment only 0.1 μ_B]

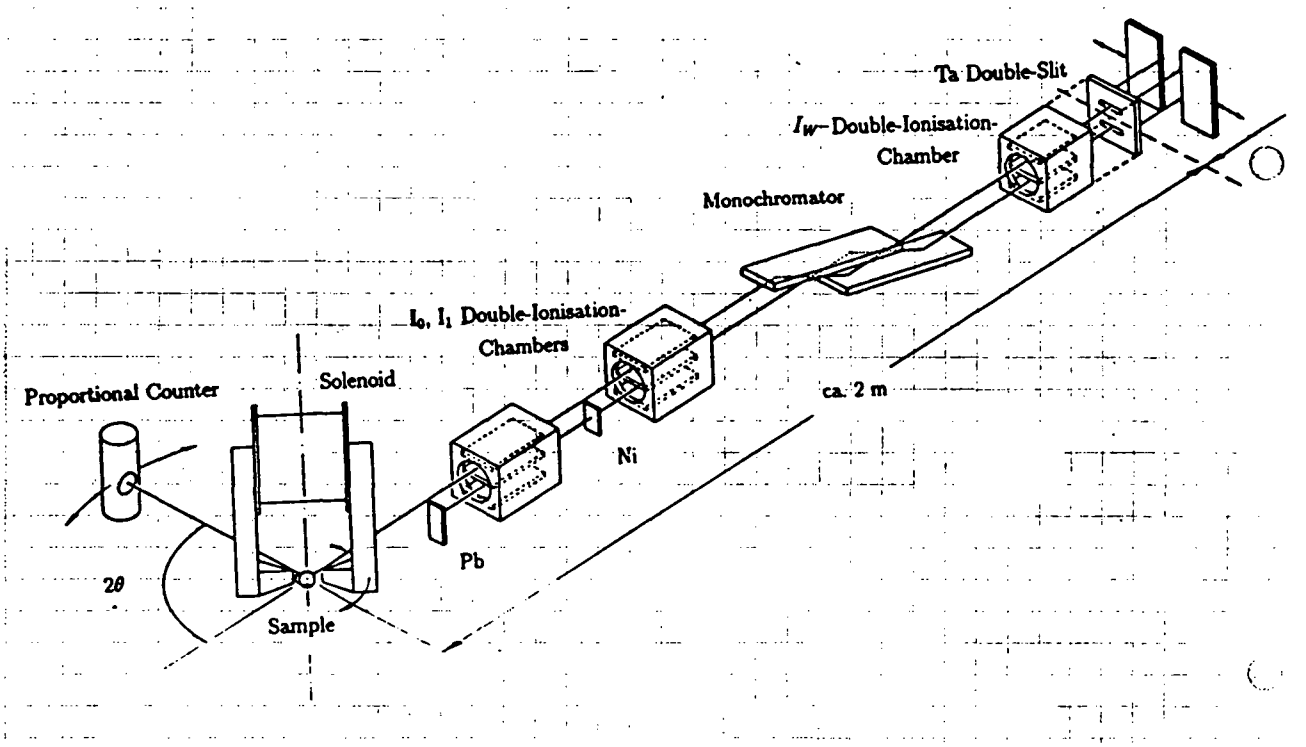
Ta Double-Slit
I_W-Double-Ionisation-Chamber
Monochromator
I_0, I_1 Double-Ionisation-Chambers
Proportional Counter
Solenoid
ca. 2 m
Ni
Pb
2θ
Sample

1. SPIN-DEPENDENT BRAGG SCATTERING

Scattering amplitude $A(k)$ faraway from resonances

$$A(k) = r_0 \left\{ T\, F(k) + i \frac{\hbar k}{mc} \left\{ \vec{S}(k) \cdot \vec{A} + \frac{1}{2} \vec{L}(k) \cdot \vec{B} \right\} \right\}$$

F, S, L, are the structure factors of charge, spin and orbital momentum

$T, \vec{A}, \vec{B}$ „polarization and scattering geometry fkt."

$$\frac{\sigma_{mag}}{\sigma_{charge}} \sim \left(\frac{\hbar\omega}{mc^2}\right)^2 \left(\frac{S}{F}\right)^2 \sim 10^{-6}$$

$$\frac{\sigma_{interference}}{\sigma_{charg}} \sim \frac{\hbar\omega}{mc^2} \frac{S}{F} \sim 10^{-3}$$

↓ observable for circularly pol. photons

SCATTERING OF CIRCULARLY POL. X-RAYS

1. $\vec{M}$ parallel to scattering plane –

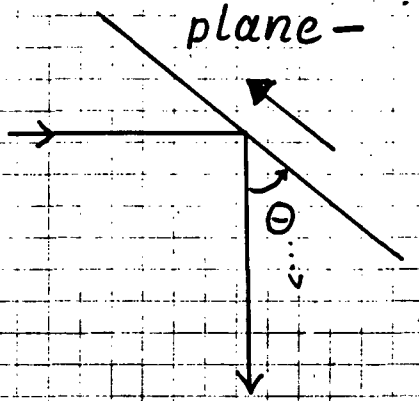

„like for neutrons"

$$\frac{\Delta I}{I} \sim \frac{h\nu}{mc^2} \frac{S+L}{F} C(\theta)$$

Spin- orbital contribution

$F \hat{=}$ charge form factor

2. $\vec{M}$ not parallel

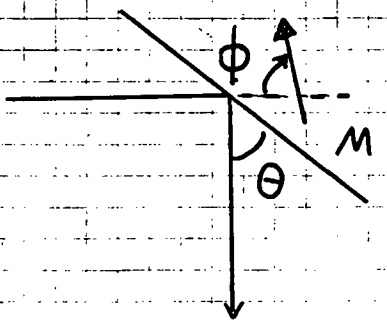

for fixed θ

$$\frac{\Delta I}{I} \sim \frac{h\nu}{mc^2} \frac{1}{F} \left(S \cdot A(\phi) + L \cdot B(\phi) \right)$$

for $\phi \neq 0$: $A(\phi) \neq B(\phi)$

Flipping-ratio $\frac{\Delta I}{I}$ contain information of $\frac{S}{L}$

SPIN-DEPENDENT BRAGG SCATTERING

W. Kaiser et al.
HASYLAB, 1989

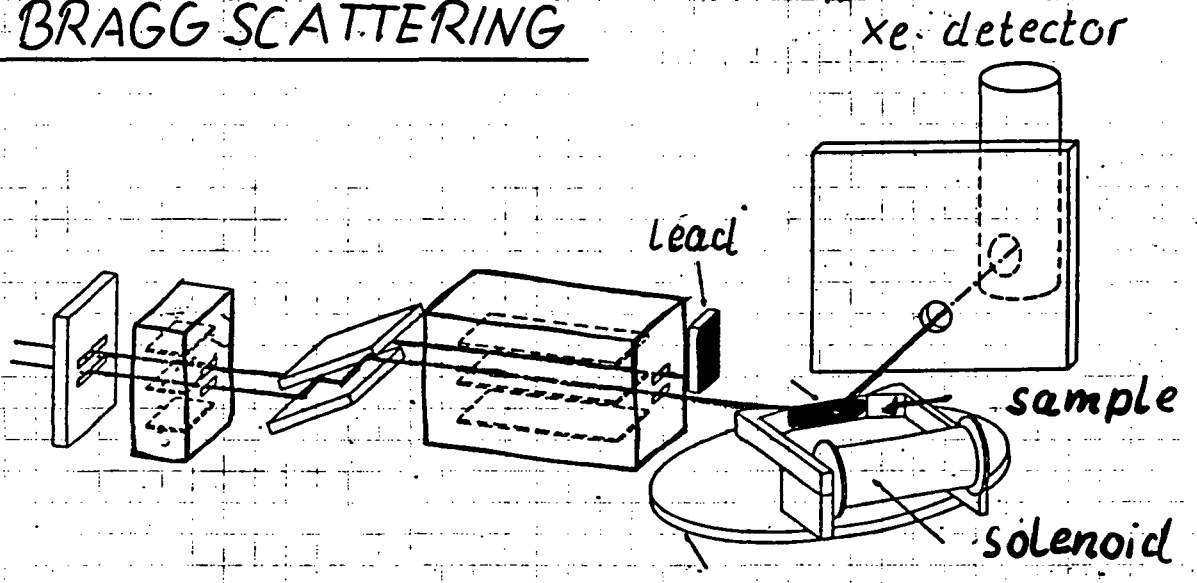

Measurements of the magn. Form factor in polycrystalline samples

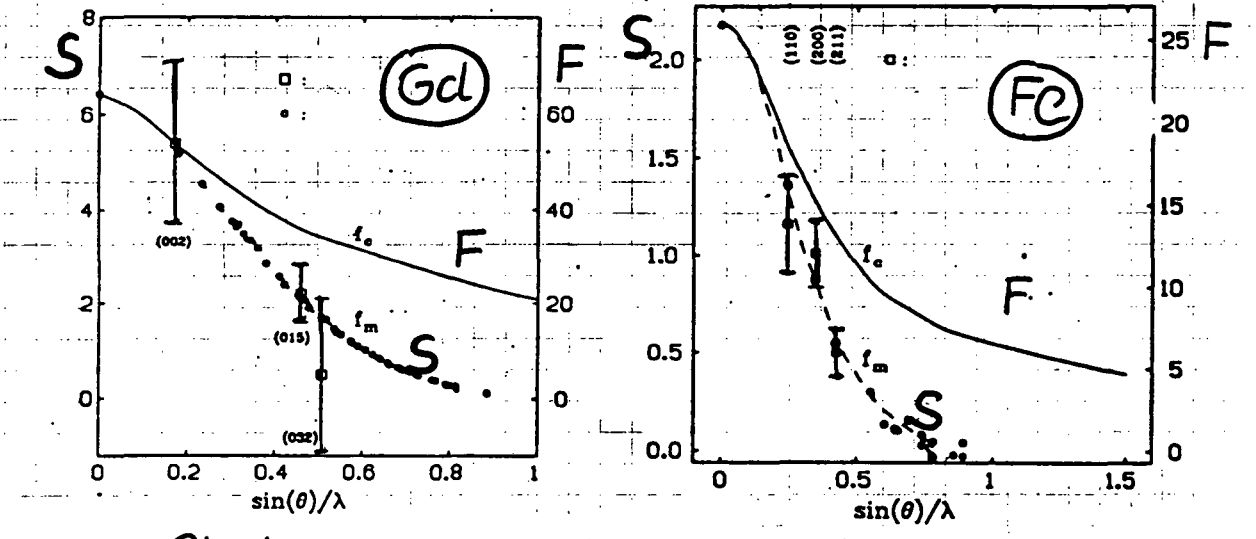

Photon data („powder" sample)
Neutron data (single crystal)

Results

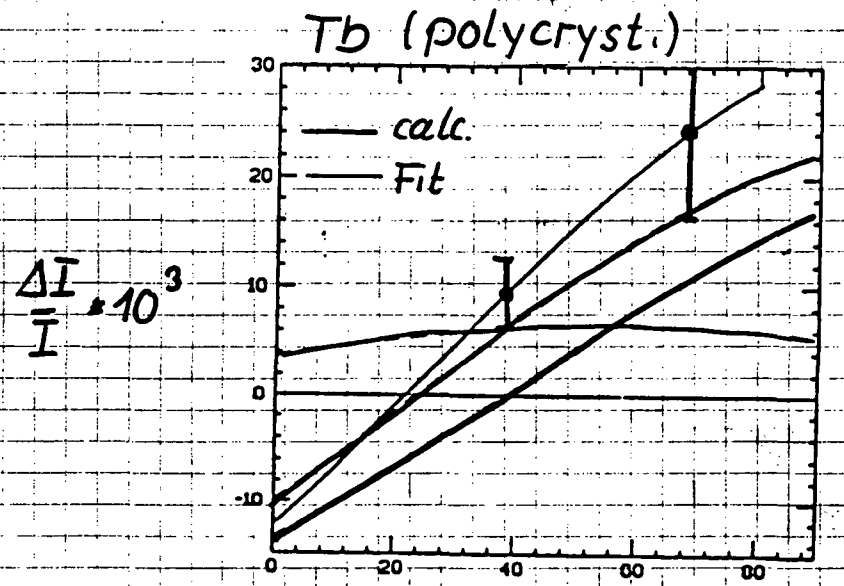

Spin-contribution $S = 3$

Orbital contribution $L = 3$

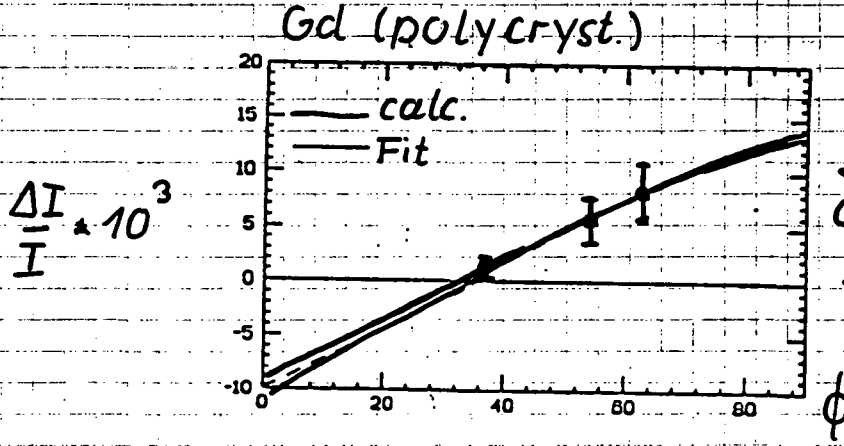

Spin contribution $S = 3.5$

Measuring time ~ 2-4 hrs per data point

MAGNETIC RESONANCE SCATTERING

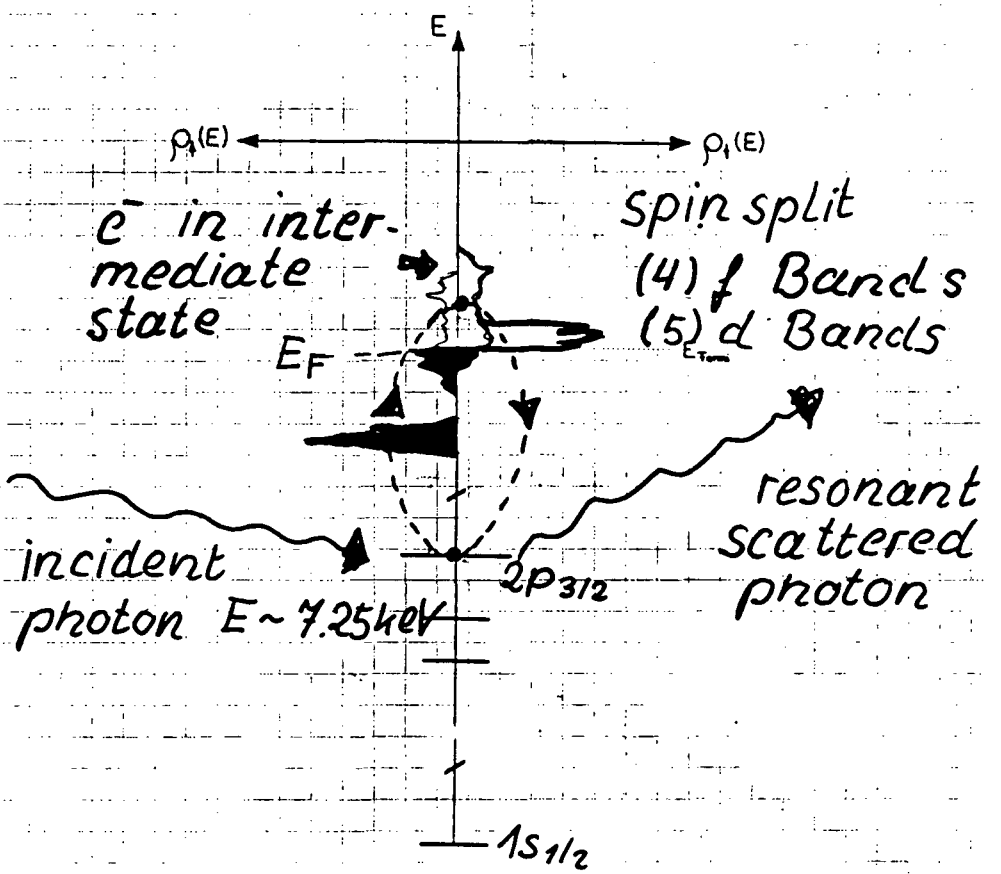

Theoretische Aspekte

Der Streuquerschnitt an einer Absorptionskante (resonante oder anormale Streuung)

near-edge scattering cross section

$$\frac{d\sigma}{d\Omega} = |f_0 + f' + if'' + if_{mag}|^2$$

f', f'' := dispersive und absorptive Korrekturterm

enthält den nicht vernachlässigbaren Interferenzterm

final state spin density

$$2f_0 f' \sim \langle 0|\sum e^{i\vec{k}\cdot\vec{r}}|0\rangle \cdot (\hat{e}' \cdot \hat{e})\, i\,|\rho^\uparrow - \rho^\downarrow| \cdot (\hat{e}'' \times \hat{e})\,\hat{z}\,|M|^2$$

Thompson f_0 term — Polarisation vectors

der im Fall eines Ferromagneten von der Spindichtedifferenz $\rho^\uparrow - \rho^\downarrow$ der unbesetzten Zwischenzustände bei E_F abhängt und bei Umkehrung der Magnetisierungsrichtung $\hat{z}$ ($\perp$ zur Streuebene) sein Vorzeichen ändert.

Magnetization direction

Dieser Effekt wird als „flipping ratio" $\frac{\Delta I}{I} = \frac{I^+ - I^-}{I^+ + I^-}$ die relative Differenz der Bragg-gestreuten Intensitäten für umbekehrte Magnetisierung des Streuers, gemessen.

Flipping ratio for linearly pol. light $\sim 2f_0 f'$ is very similar to MXD-effect

MXD for circularly pol. light

Die Differenz $\mu^+ - \mu^- \sim |\rho^\uparrow - \rho^\downarrow|\,; (\hat{e}^* \times \hat{e})\,\hat{z}\,P_e \cdot |M|^2$

hat den gleichen physikalischen Ursprung und liefert dieselbe Information über Spindichtedifferenzen

P. Hannon et al. PRL 61, 1245 (88)
" " 62, 2644 (89)
D. Gibbs et al. " 61, 1241 (88)
E.O. Isaacs et al. " 62 1671 (89)

Comarison

Circular MXD ⟷ Linear magn. Resonance

Namikawa et al., 1990
Photon Factory, Japan
t_{Mess} ?

G.S. et al. Z. f. Phys. 73
HASYLAB, 1986
t_{Mess} ~ 10 min

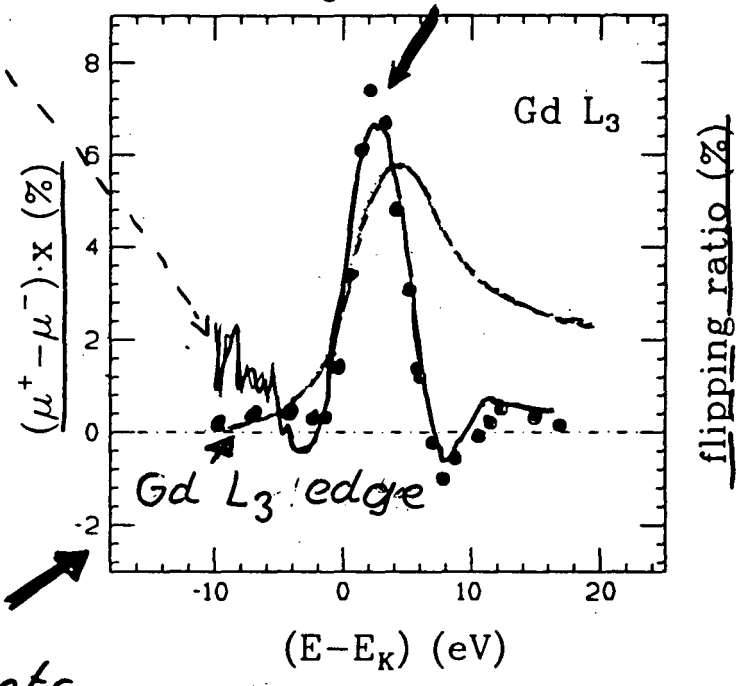

very similar magnetic effects

CIRCULAR MAGN. RESONANCE SCATTERING

due to f'fmagn. ?

enhancement of (normal) magn. scattering in the pre-edge region

magn. effect for circ. polar. x-rays ~2 * larger than for linear pol. x-rays

very similar to circ. MXD

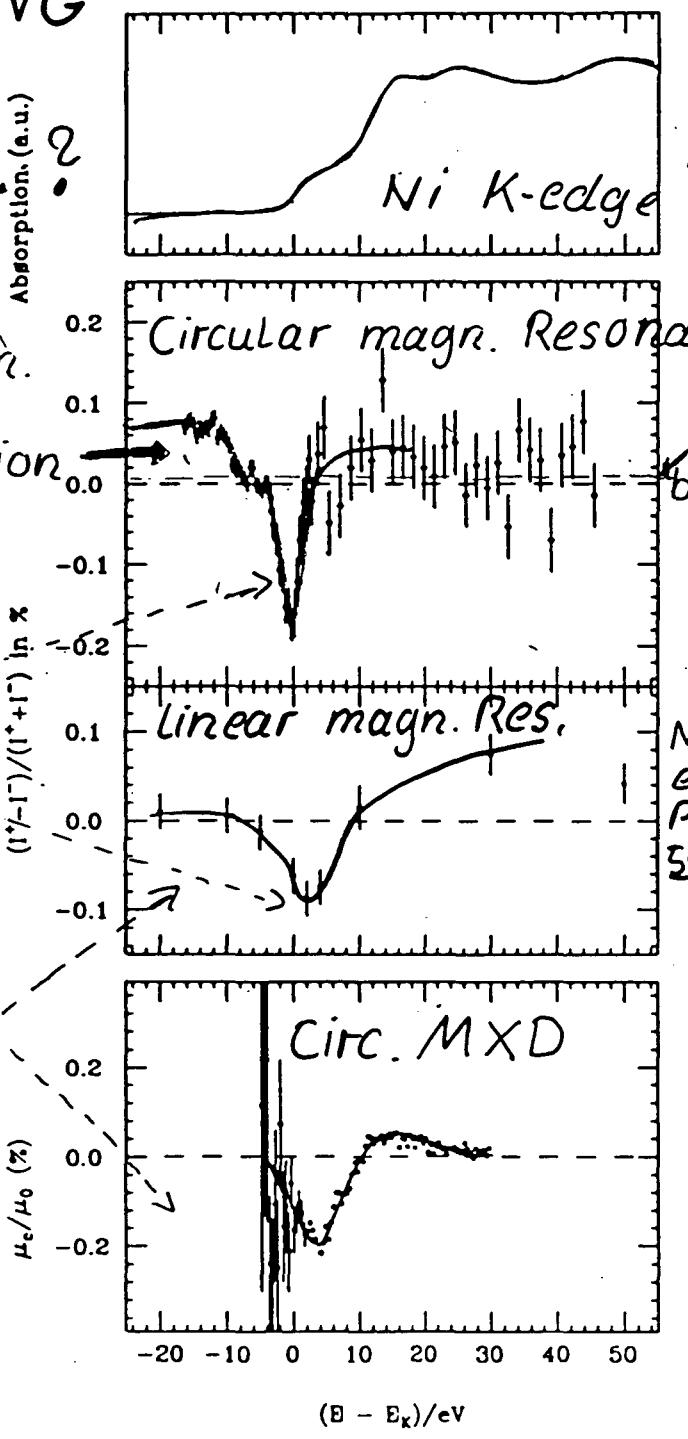

Photoemission with Circularly Polarized Synchrotron Radiation from Magnetic and Non-Magnetic Solids

J. Kirschner

Freie Universität Berlin

Spin-Resolved Electron Spectroscopy

J. Kirschner

Freie Universitat Berlin, Institut fur Experimentalphysik
Arnimallee 14
1000 Berlin 33, Germany

The information contained in the electron spin, being a vectorial quantity, strongly complements traditional electron scattering or electron emission techniques. In this talk, I will focus on angle-resolved photoemission from surfaces and thin films—both magnetic and nonmagnetic. Spin-polarized electrons from nonmagnetic materials are observed by using circularly polarized UV or soft x-ray photons, where the spin polarization comes about by spin-orbit coupling in the initial and/or final states. Examples of this effect may be found in heavy materials (e.g., Pt) as well as in light elements (e.g., Cu). The polarization analysis yields information on the relativistic symmetry properties of the wave functions in the near-surface region and their hybridization properties.

In ferromagnetic materials, the spin-polarization is determined by the exchange splitting of otherwise degenerate bands. Hence, the polarization analysis of photoelectrons provides detailed information on the spin character of the bands. As an example, we studied the magnetic properties and the electronic structure of thin epitaxial cobalt films on Cu(001).

The growth was studied by means of electron diffraction, Auger spectroscopy, and scanning tunneling microscopy. Cobalt grew in the layer-by-layer mode, with the lateral lattice constant determined by the copper substrate in the face-centered tetragonal crystal structure. The tetragonal distortion was perpendicular to the surface and amounted to a few percent as determined by LEED studies.

The electronic structure was studied by means of spin-polarized photoemission using circularly polarized synchrotron radiation. In the first few monolayers, there is a transition between two- and three-dimensional electronic structure, which is almost completely established at a thickness of 5ML. Spin-resolved bands were mapped out and compared to fully relativistic theoretical calculations. The use of circularly polarized light permits the observation of spin-orbit coupling effects in the valence band of cobalt as well as of the substrate.

The coupling of cobalt double layers with a copper intermediate layer was studied as a function of the thickness of the interlayer and the thickness of the top-layer cobalt. We observed ferromagnetic/antiferromagnetic oscillatory exchange coupling with a rather short period (3 to 4 ML Cu). These data were obtained by the magneto-optic Kerr effect as well as by a new effect, termed "magnetic dichroism in photoemission," which owes its existence to an interference between spin-orbit and exchange interaction in the occupied (or unoccupied) electronic states. The extension of these studies into the soft x-ray regime, i.e., the emission from core levels, is briefly discussed.

Why Circular Polarized Bending Magnet Radiation

1)	MCD in photoemission: (from core levels)	Determination of magnetic moments on atomic scale – element-specific – ferro -- ferri-magnets binary antiferromagnets – surface-sensitive
2)	valence bands: (non-magnetic; spin-polarization analysis)	– exp. analysis of double-group symmetries of wave functions – analysis of hybradiation of wave functions – measurement of spin-orbig interaction

3) MCD in valence band photoemission from ferromagnets:
(inteference of spin - orbit and exchange interaction)
– detailed information on spin-orbit relativistic bandstructure
– imaging of magnetic surface domains in photoemission microscope

Nonmagnetic Materials

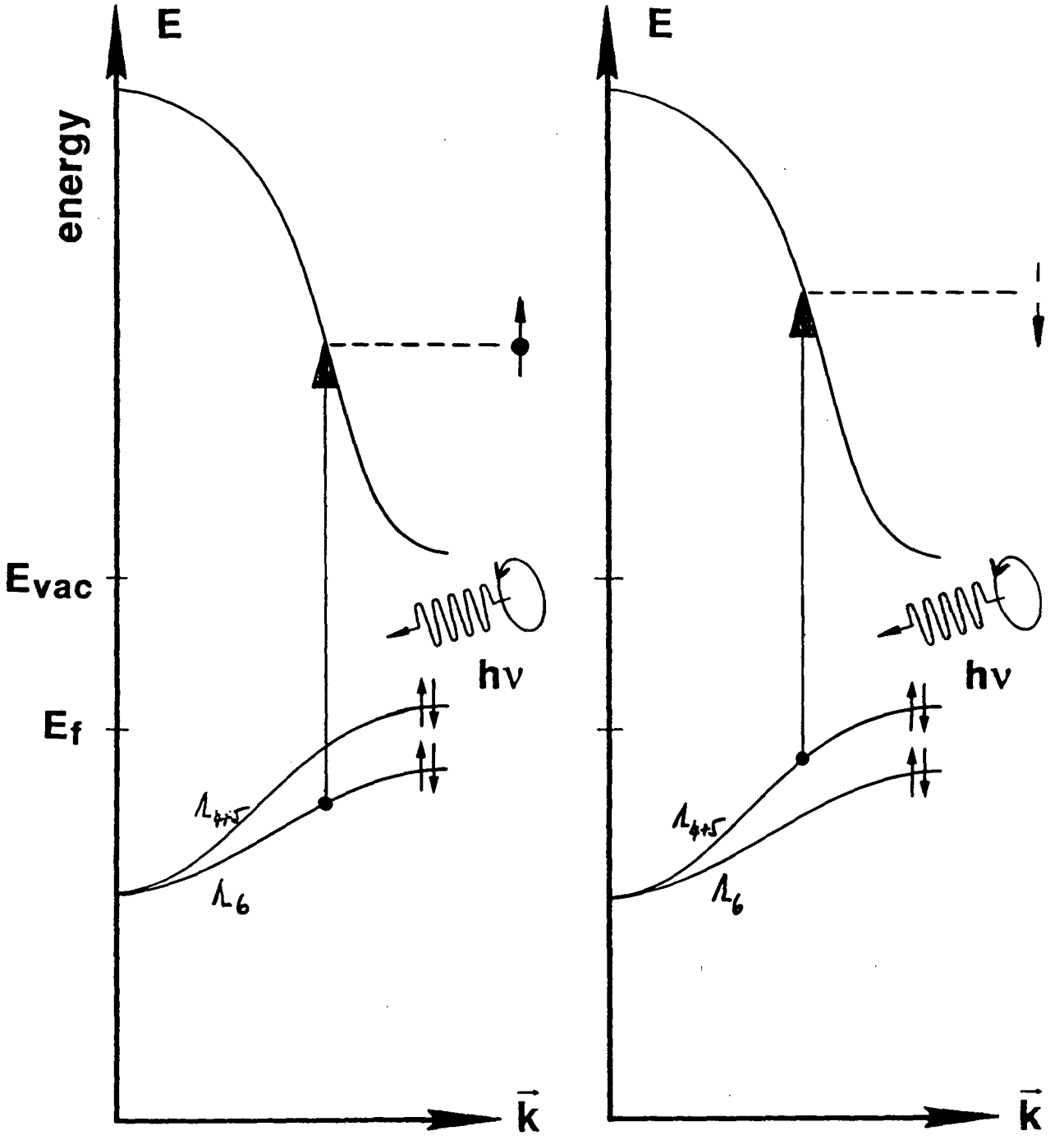

reduced wave vector

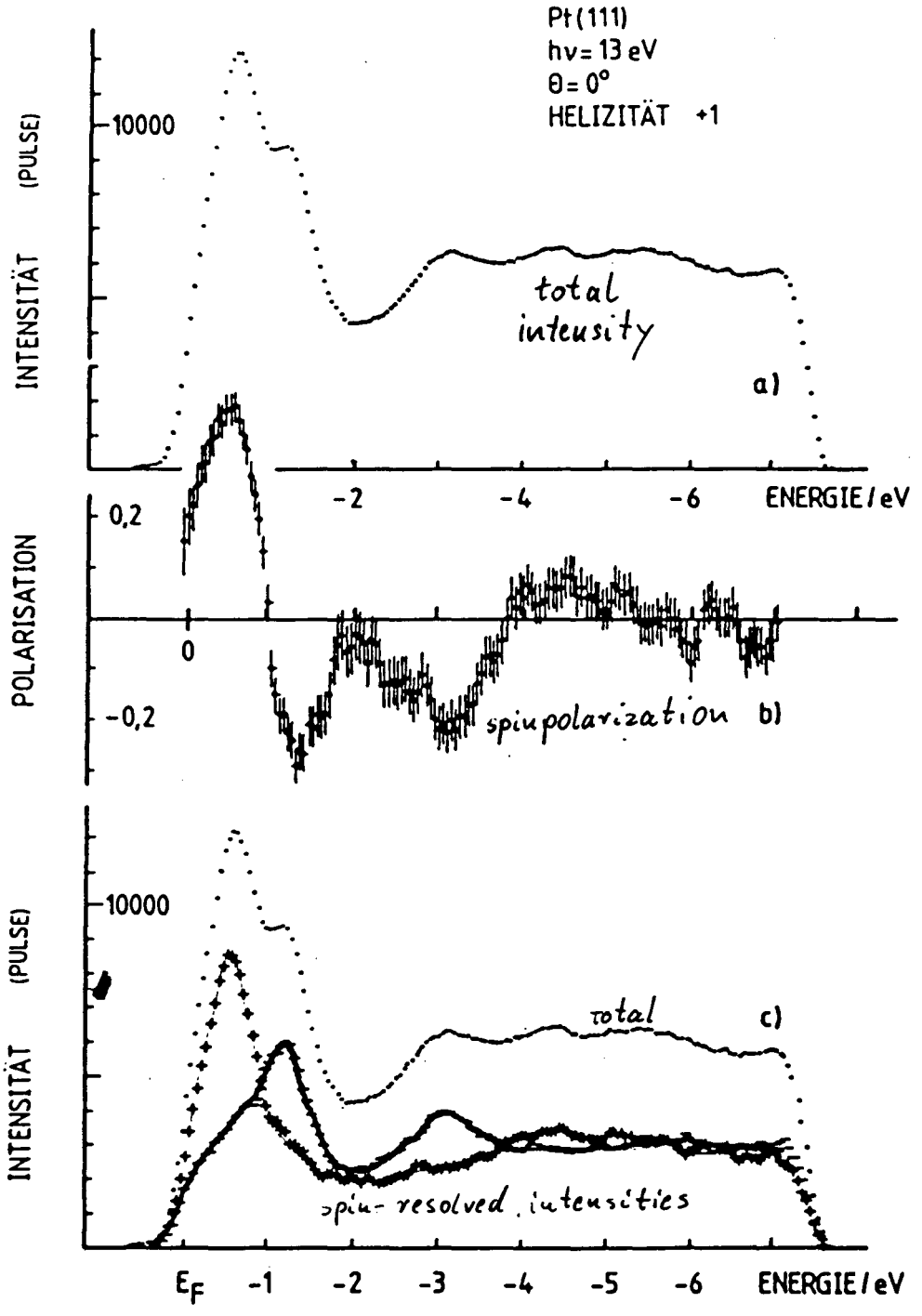
Pt(111)
hν = 13 eV
θ = 0°
HELIZITÄT +1
INTENSITÄT (PULSE)
10000
total intensity
a)
-2
-4
-6
ENERGIE / eV
POLARISATION
0,2
0
-0,2
spinpolarization
b)
INTENSITÄT (PULSE)
10000
total
c)
spin-resolved intensities
E_F
-1
-2
-3
-4
-5
-6
ENERGIE / eV

"matrix element effects" in spinpolarized photoemission

direction Δ in bcc crystals

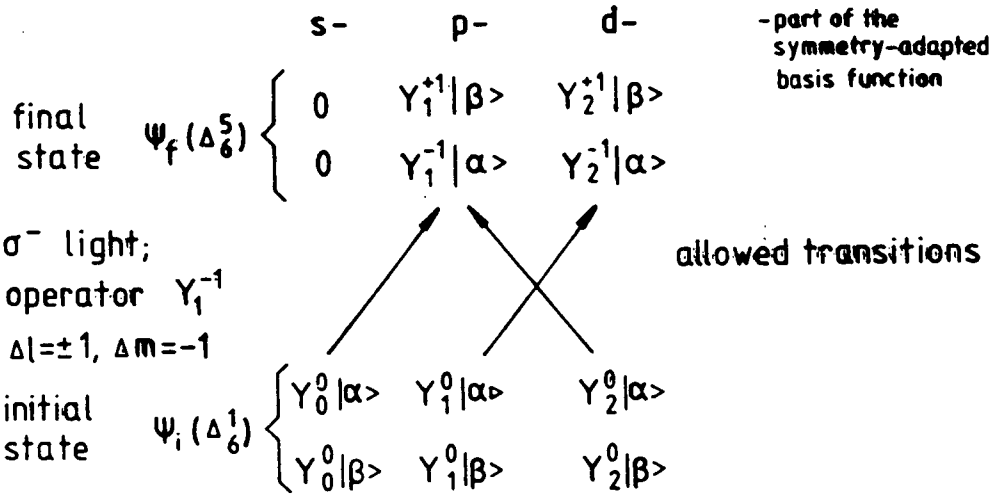

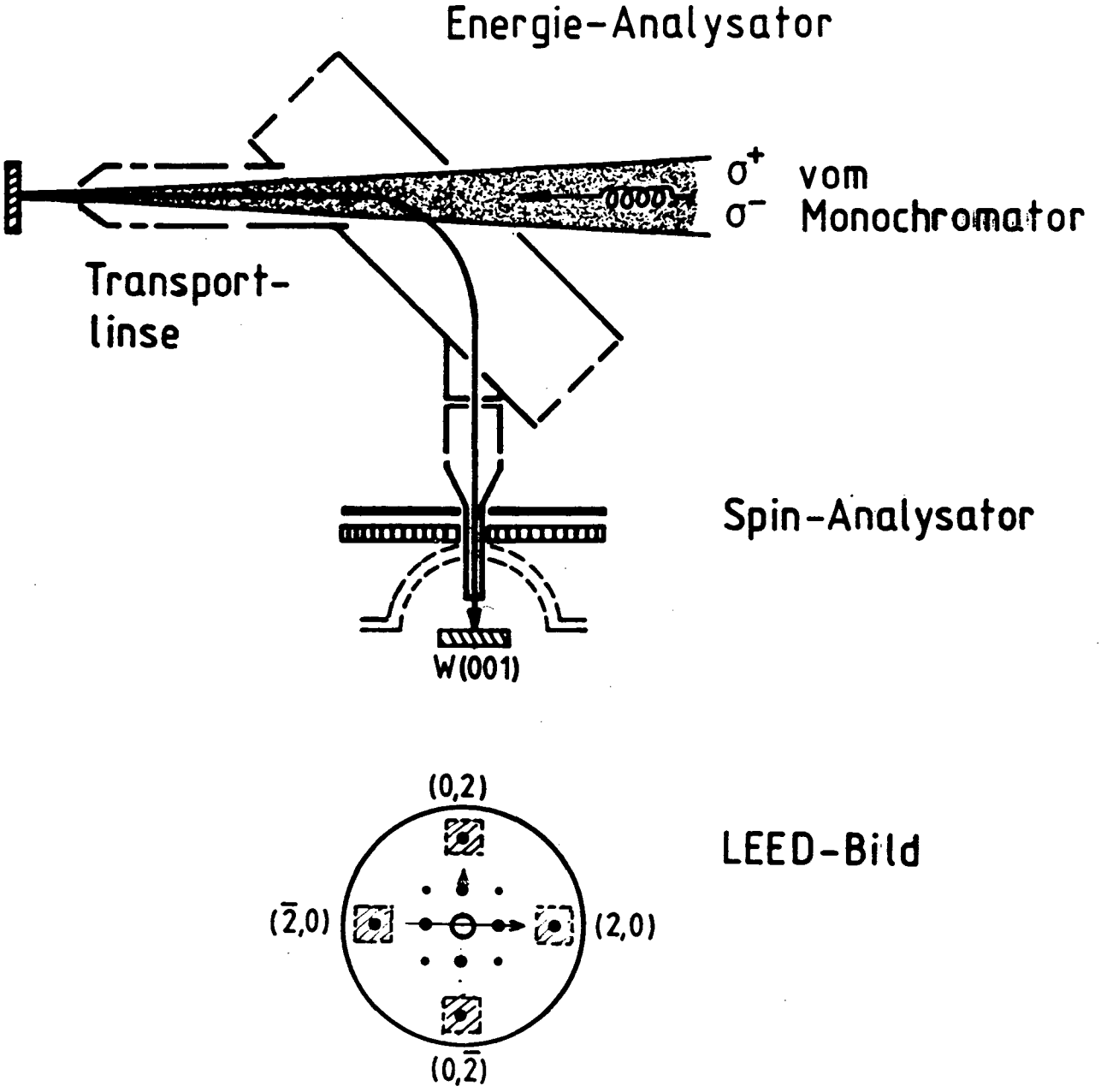
Energie-Analysator
σ^+ vom
σ^- Monochromator
Transport-
linse
Spin-Analysator
W(001)
(0,2)
($\bar{2}$,0)
(2,0)
(0,$\bar{2}$)
LEED-Bild

Pt (110) Normal Incidence/ Normal Emission

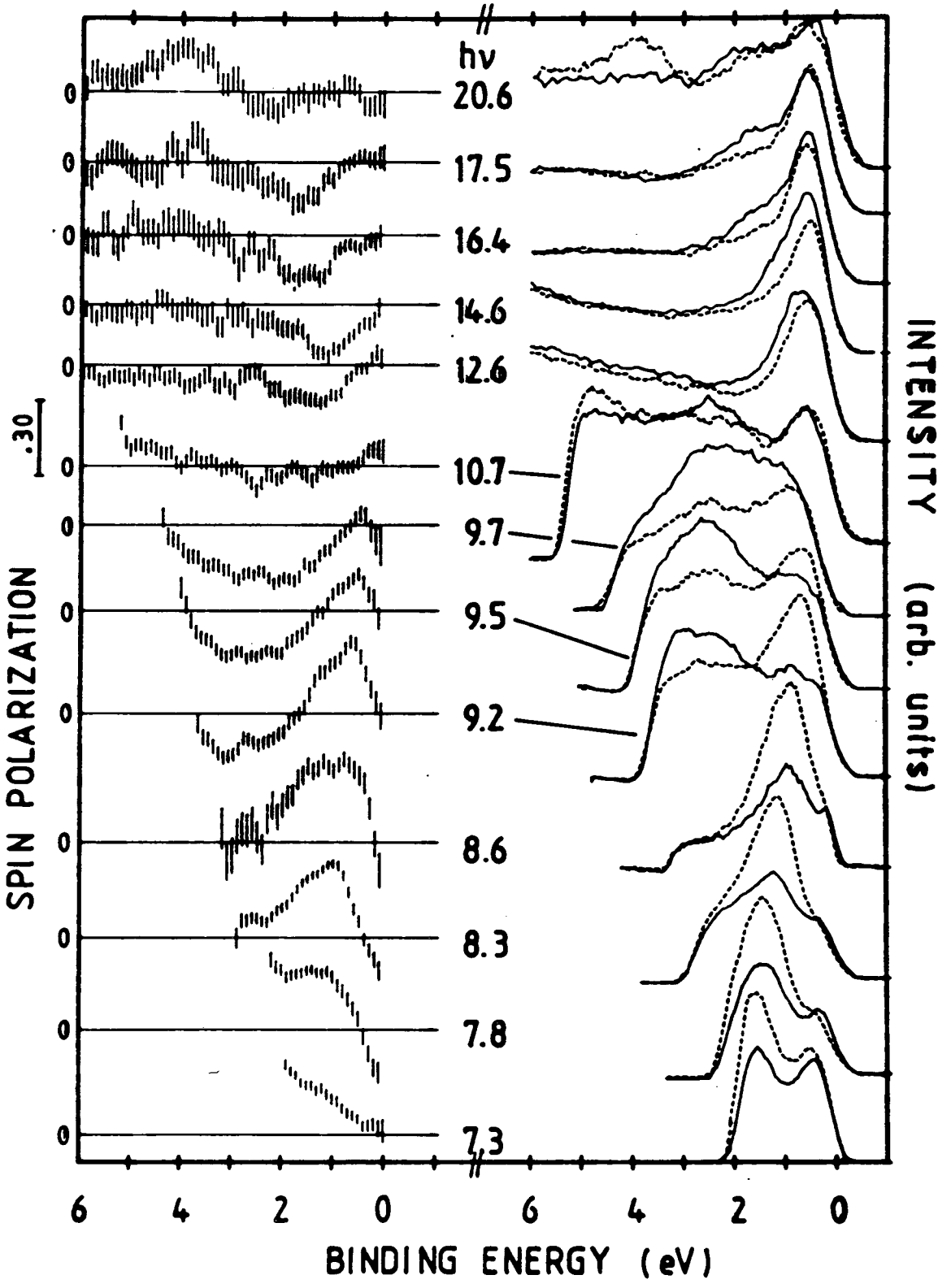

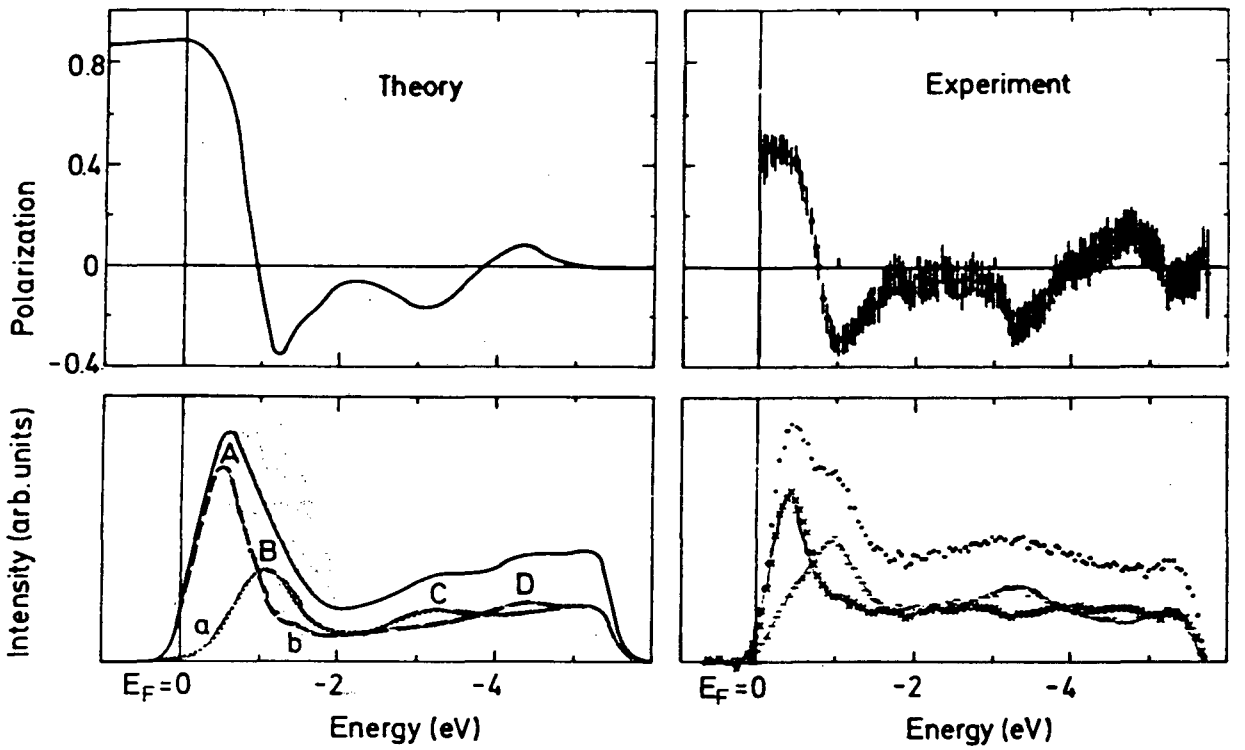
Theory
Experiment
Polarization
0.8
0.4
0
-0.4
Intensity (arb. units)
A
B
C
D
a
b
$E_F = 0$
-2
-4
Energy (eV)
$E_F = 0$
-2
-4
Energy (eV)

TaC (100)
Normal Incidence/Normal Emission

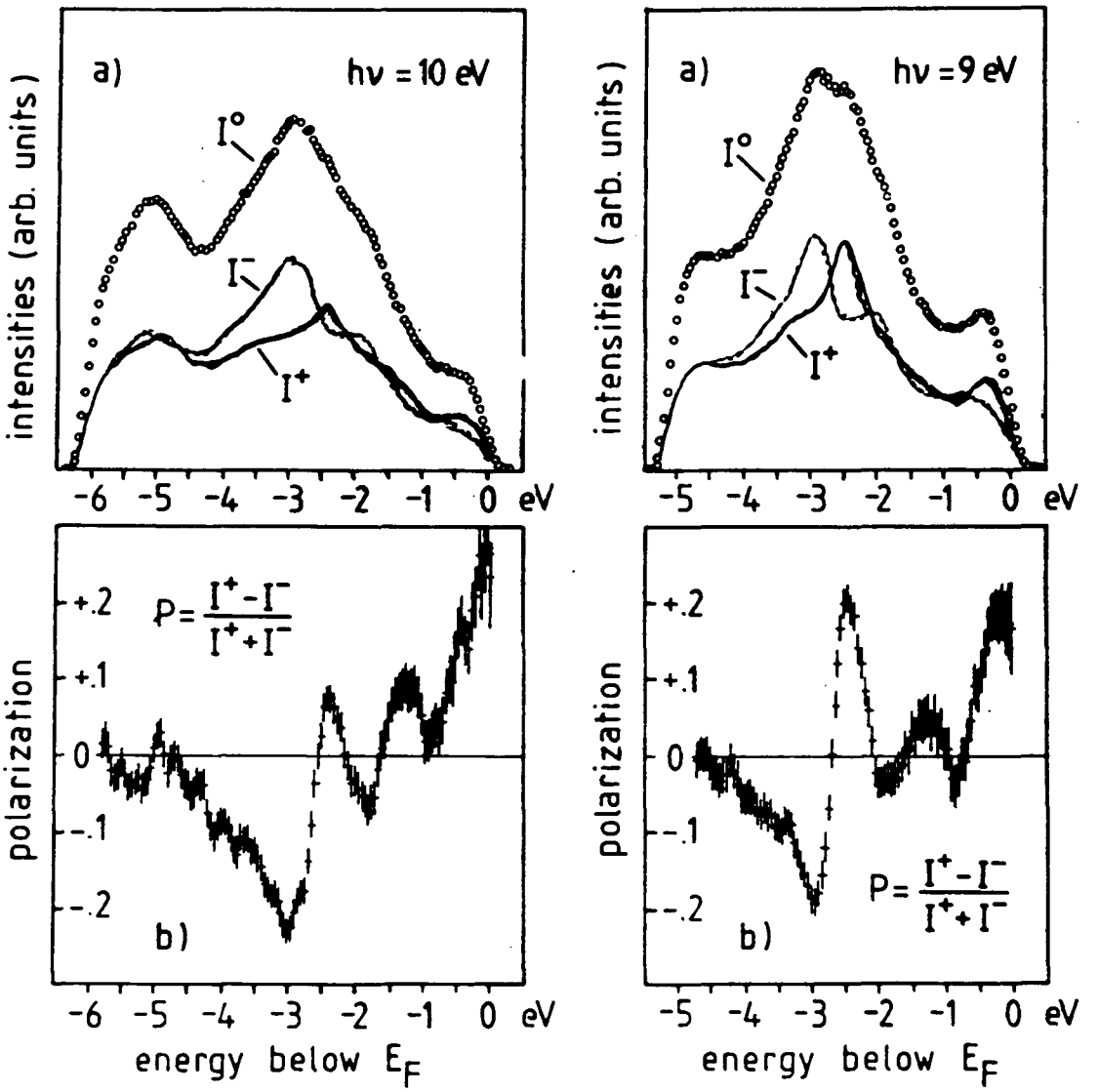

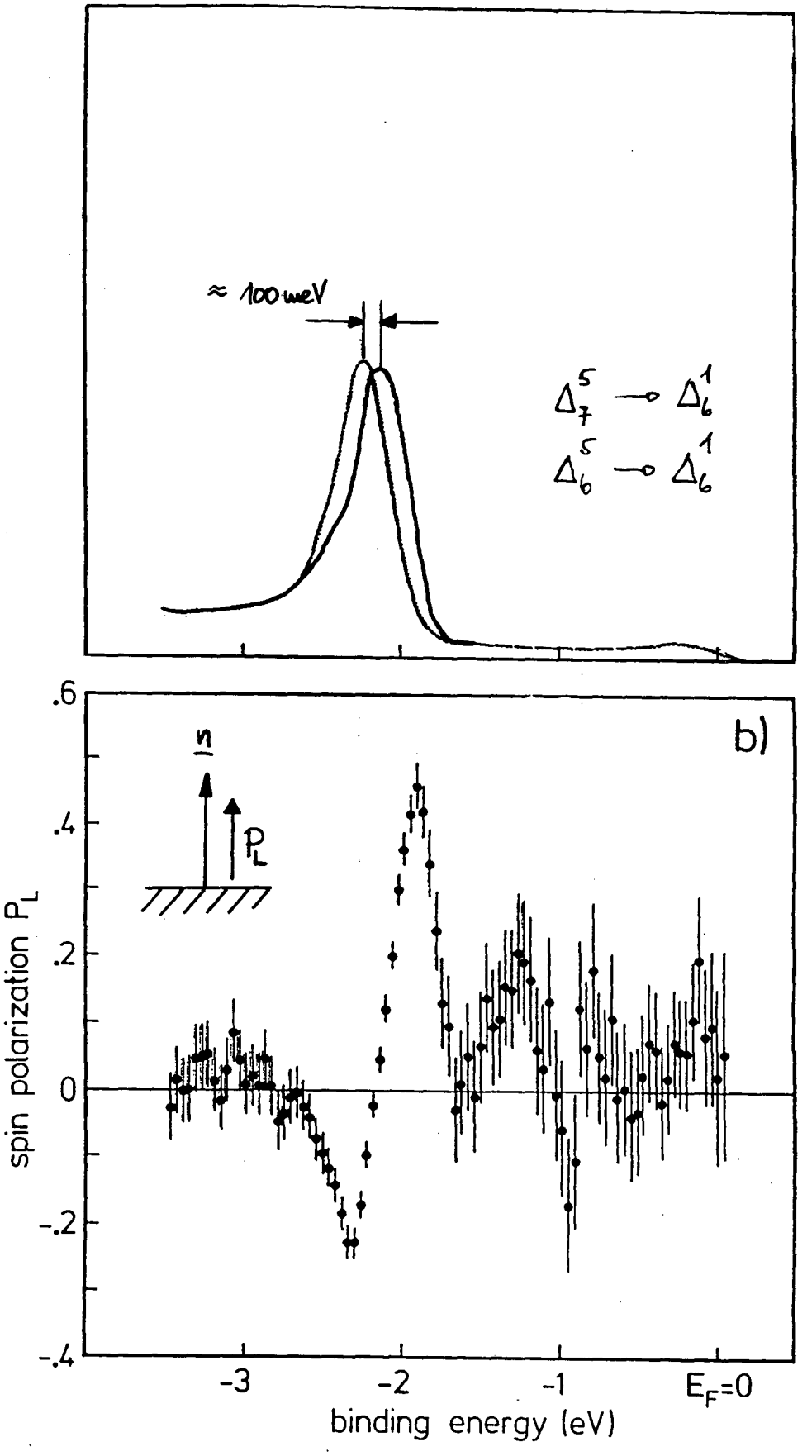
≈ 100 meV
$\Delta_7^5 \rightarrow \Delta_6^1$
$\Delta_6^5 \rightarrow \Delta_6^1$
b)
n
P_L
spin polarization P_L
.6
.4
.2
0
-.2
-.4
-3
-2
-1
E_F=0
binding energy (eV)

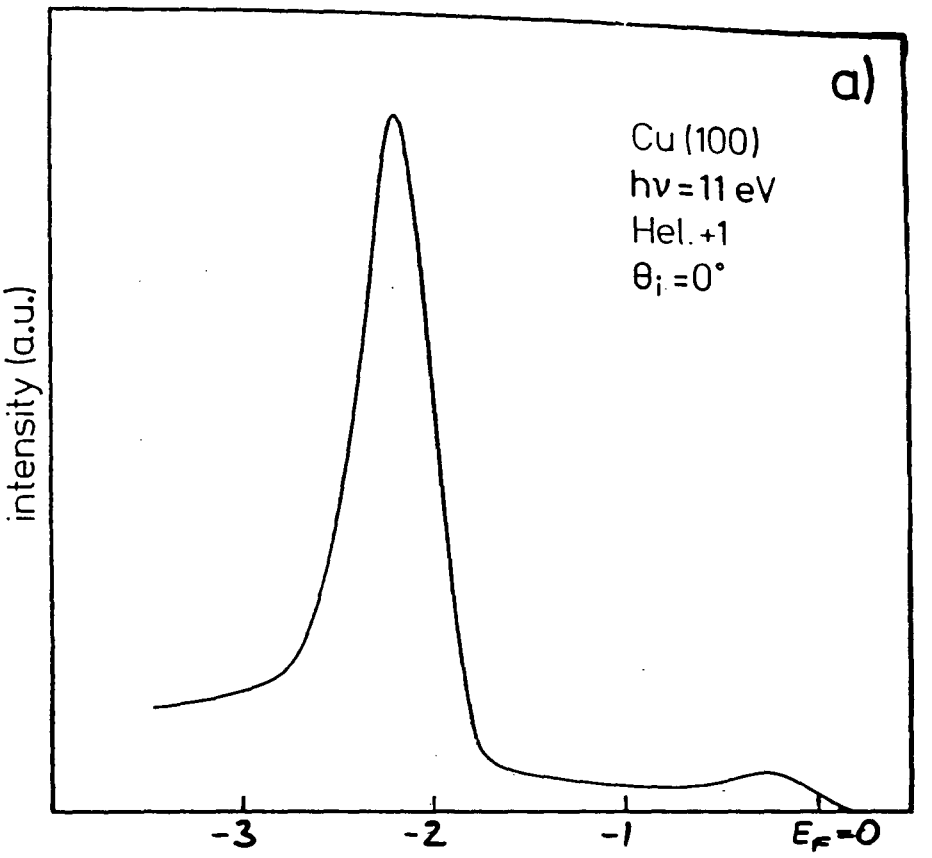
a)
Cu (100)
hν = 11 eV
Hel. +1
θi = 0°
intensity (a.u.)
-3
-2
-1
EF = 0

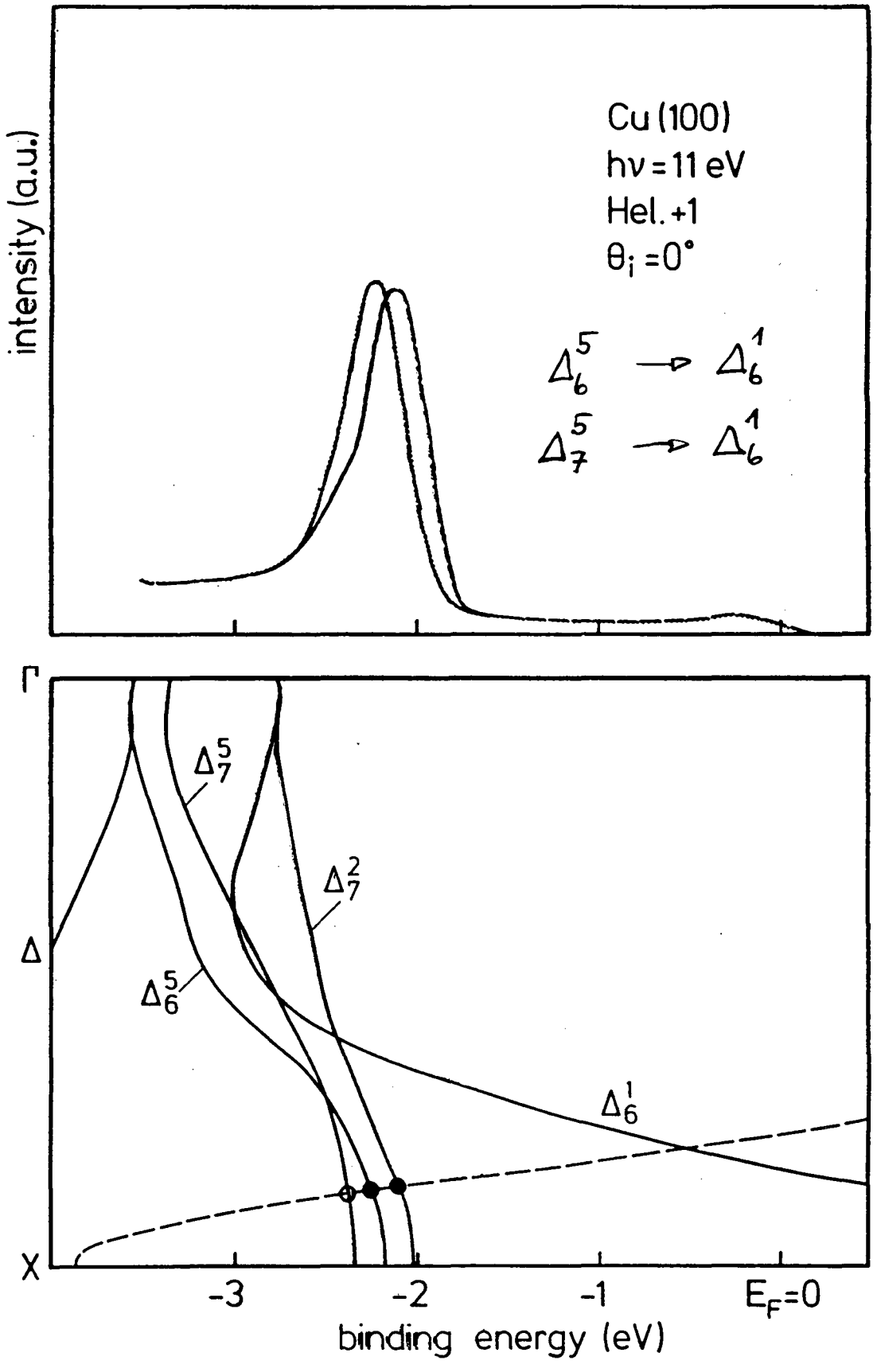
Cu (100)
hν = 11 eV
Hel. +1
θi = 0°
Δ5 6 → Δ1 6
Δ5 7 → Δ1 6
intensity (a.u.)
Γ
Δ
X
Δ5 7
Δ2 7
Δ5 6
Δ1 6
-3
-2
-1
EF=0
binding energy (eV)

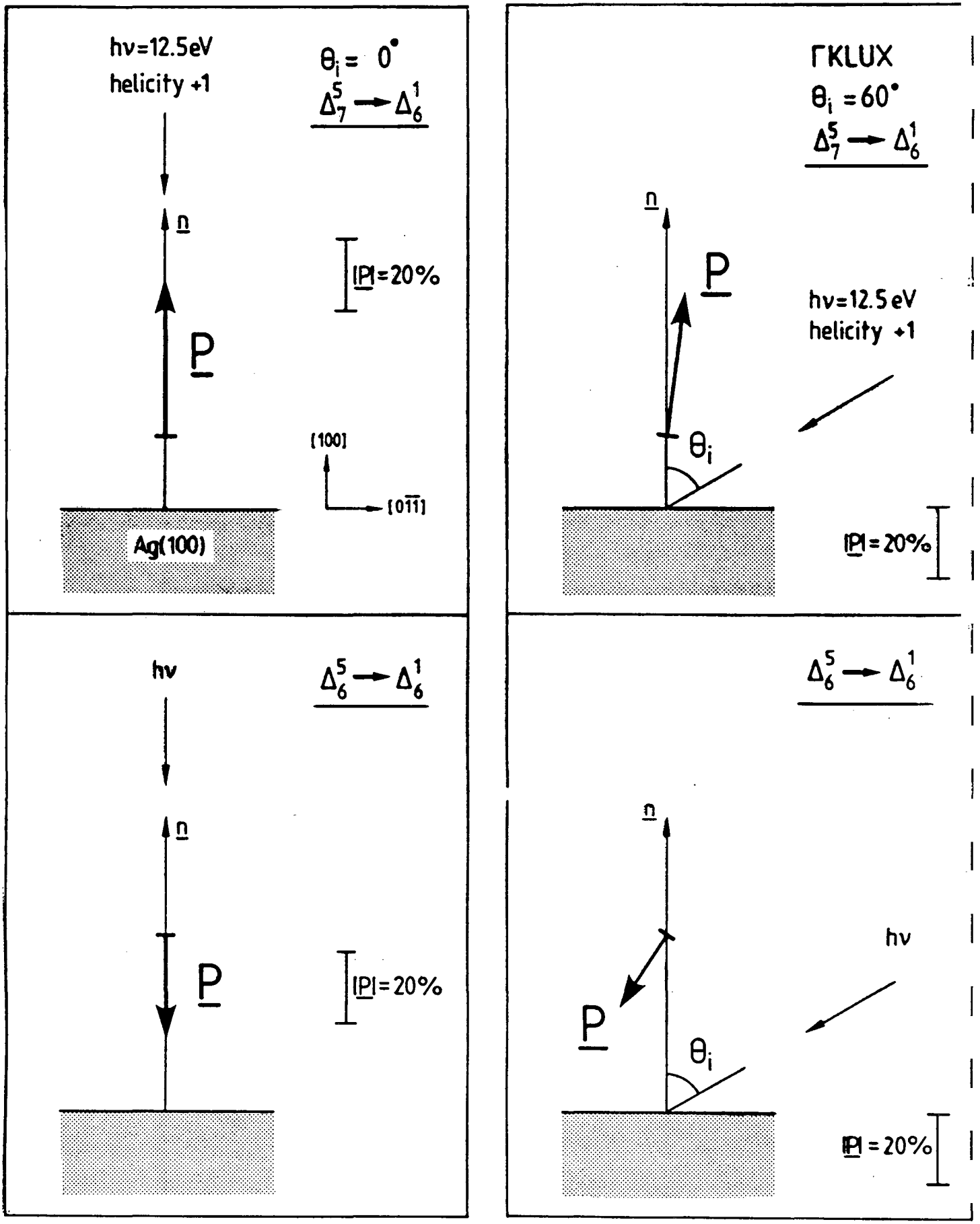
hν=12.5eV
helicity +1
θi = 0°
Δ5 7 → Δ1 6
n
P
|P|=20%
[100]
[011]
Ag(100)
ΓKLUX
θi = 60°
Δ5 7 → Δ1 6
n
P
θi
hν=12.5 eV
helicity +1
|P| = 20%
hν
Δ5 6 → Δ1 6
n
P
|P|=20%
Δ5 6 → Δ1 6
n
P
θi
hν
|P| = 20%

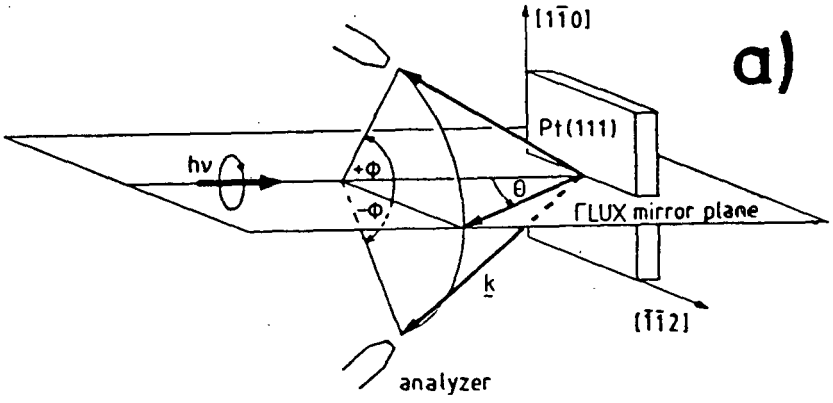

scattering geometry

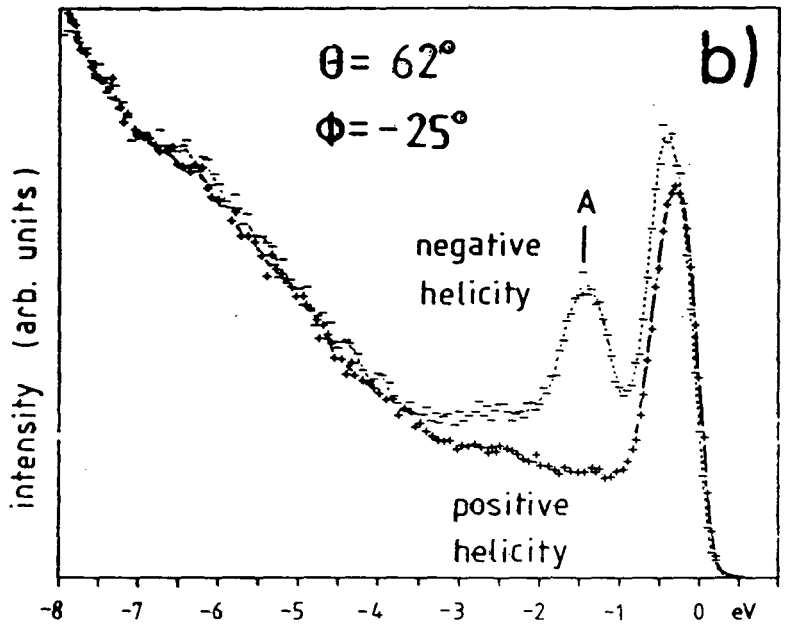

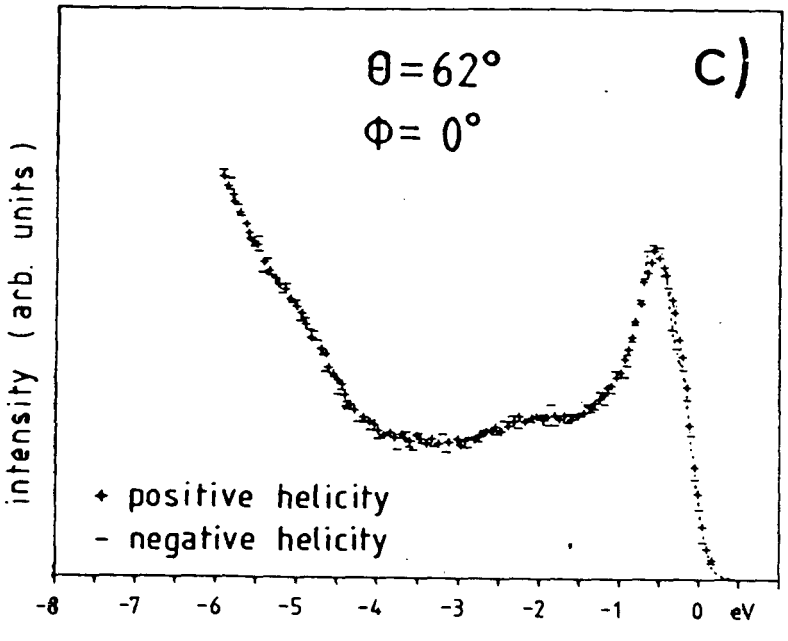

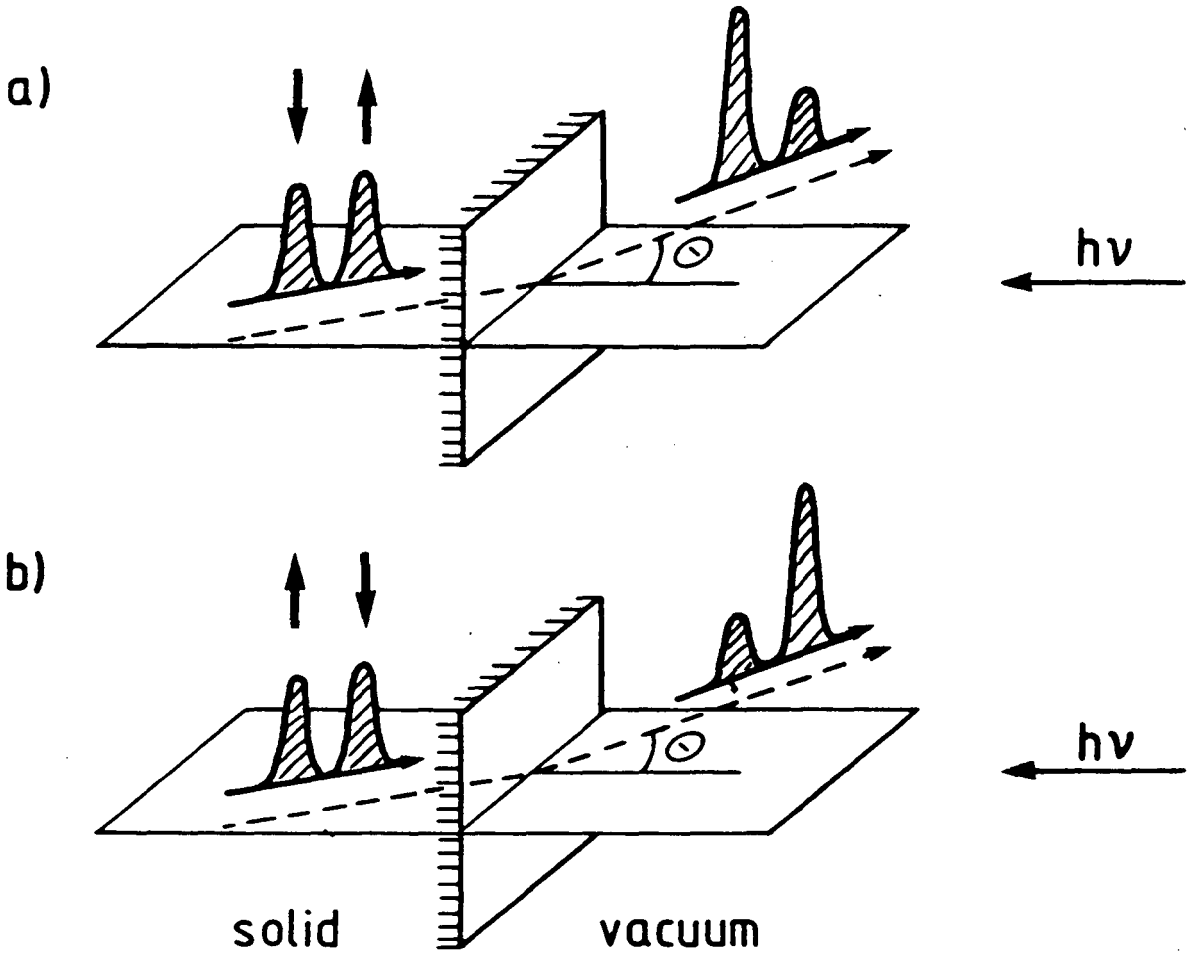

Collaborators: H.P. Oepeu, K. Hünlich, J. Garbe

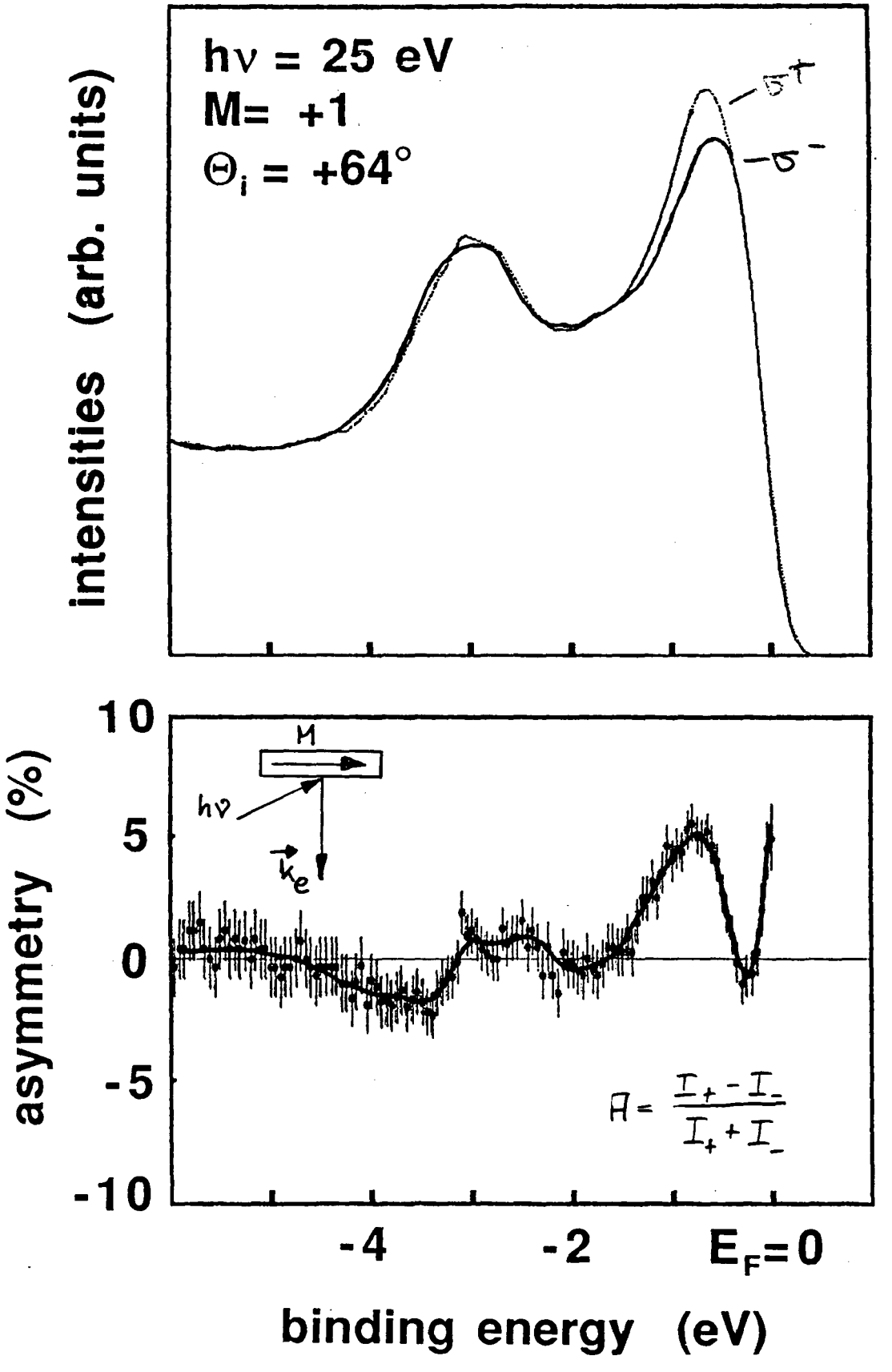
hν = 25 eV
M= +1
Θi = +64°
σ+
σ-
intensities (arb. units)
10
5
0
-5
-10
asymmetry (%)
M
hν
ke
A = (I+ - I-) / (I+ + I-)
-4
-2
EF=0
binding energy (eV)

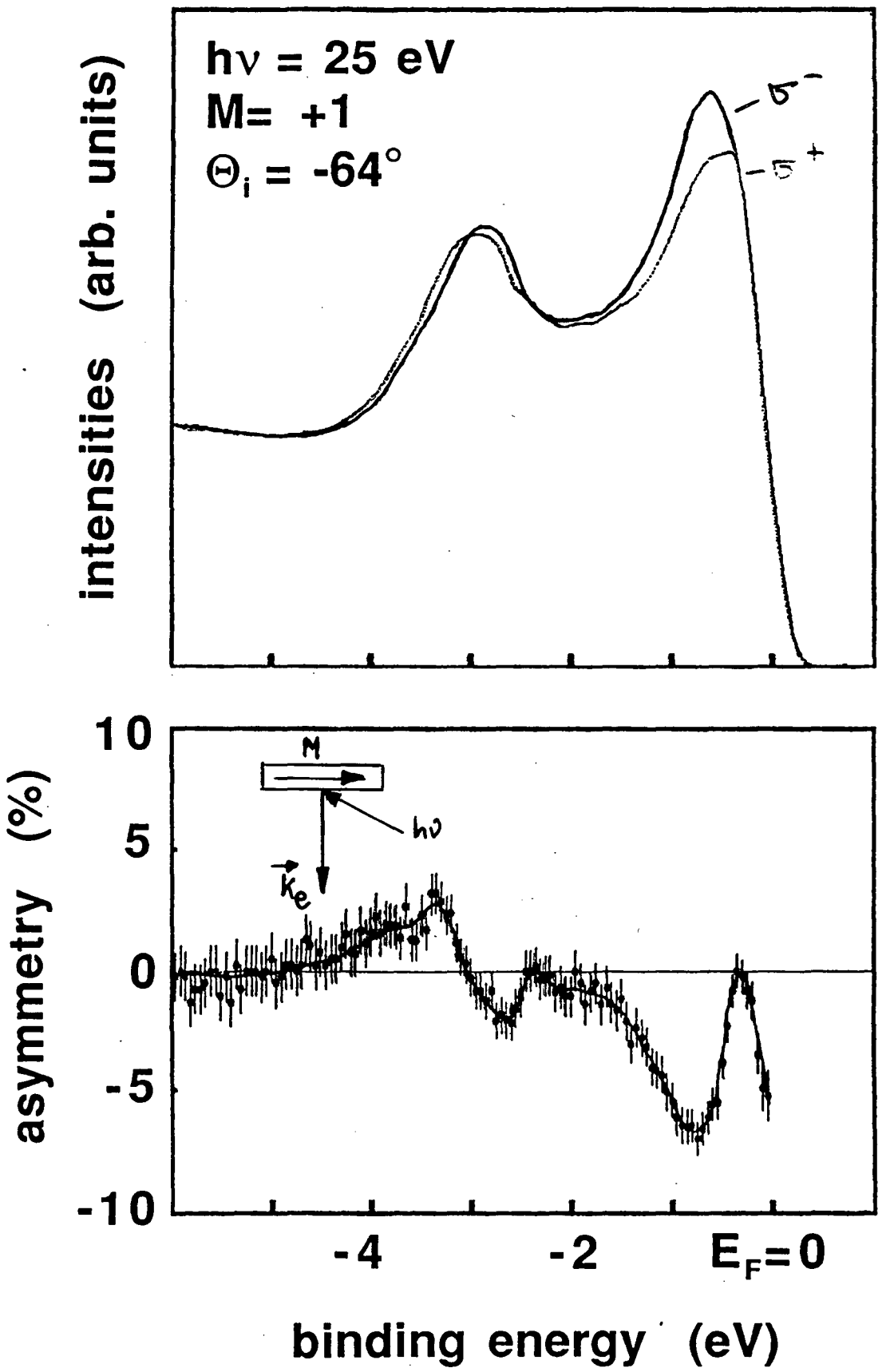
hν = 25 eV
M= +1
Θi = -64°
σ⁻
σ⁺
intensities (arb. units)
asymmetry (%)
10
5
0
-5
-10
M
hν
ke
-4
-2
EF=0
binding energy (eV)

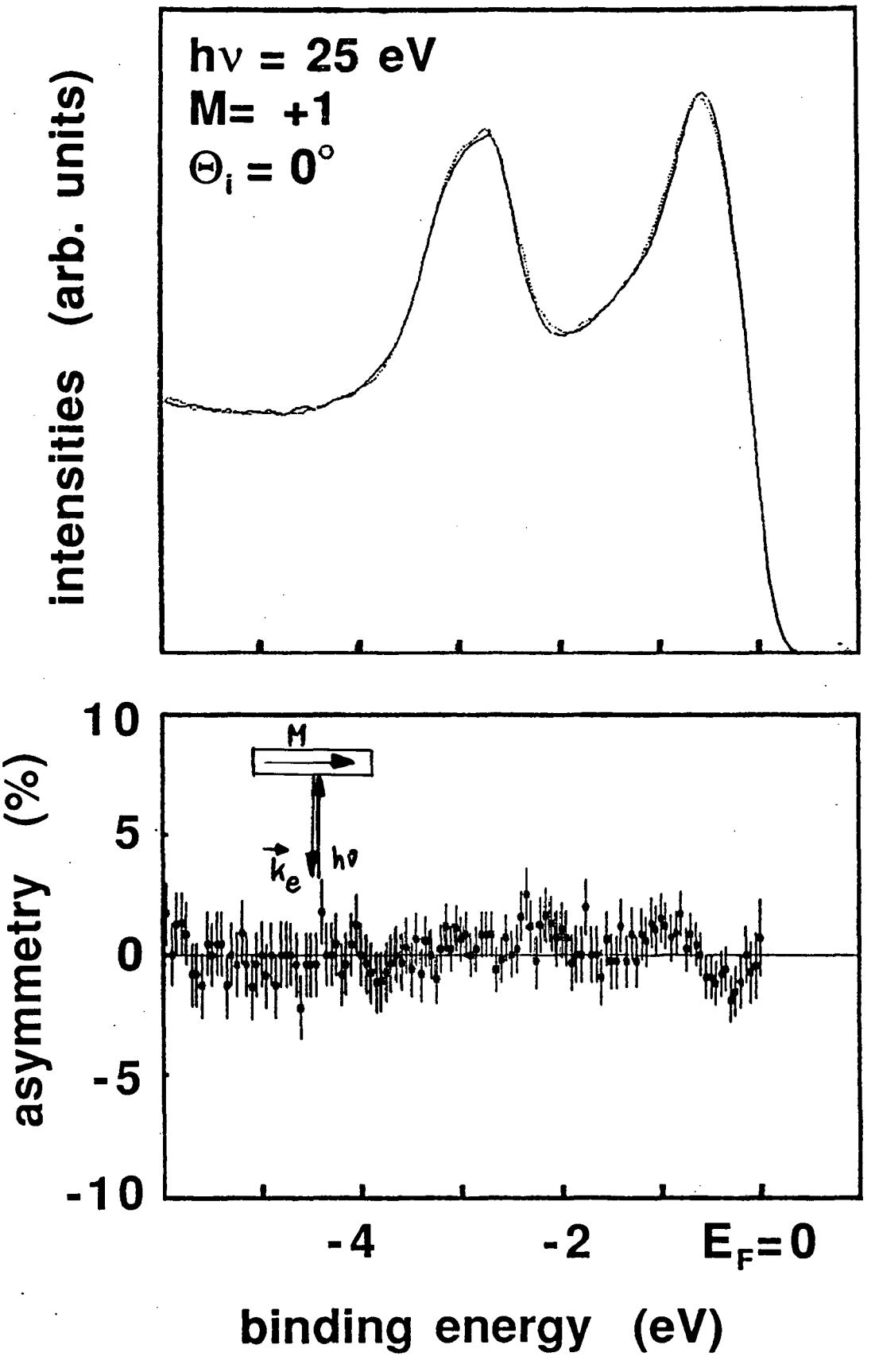
hν = 25 eV
M= +1
Θi = 0°
intensities (arb. units)
10
5
0
-5
-10
asymmetry (%)
M
ke
hν
-4
-2
EF=0
binding energy (eV)

H. Ebert, priv. comm.

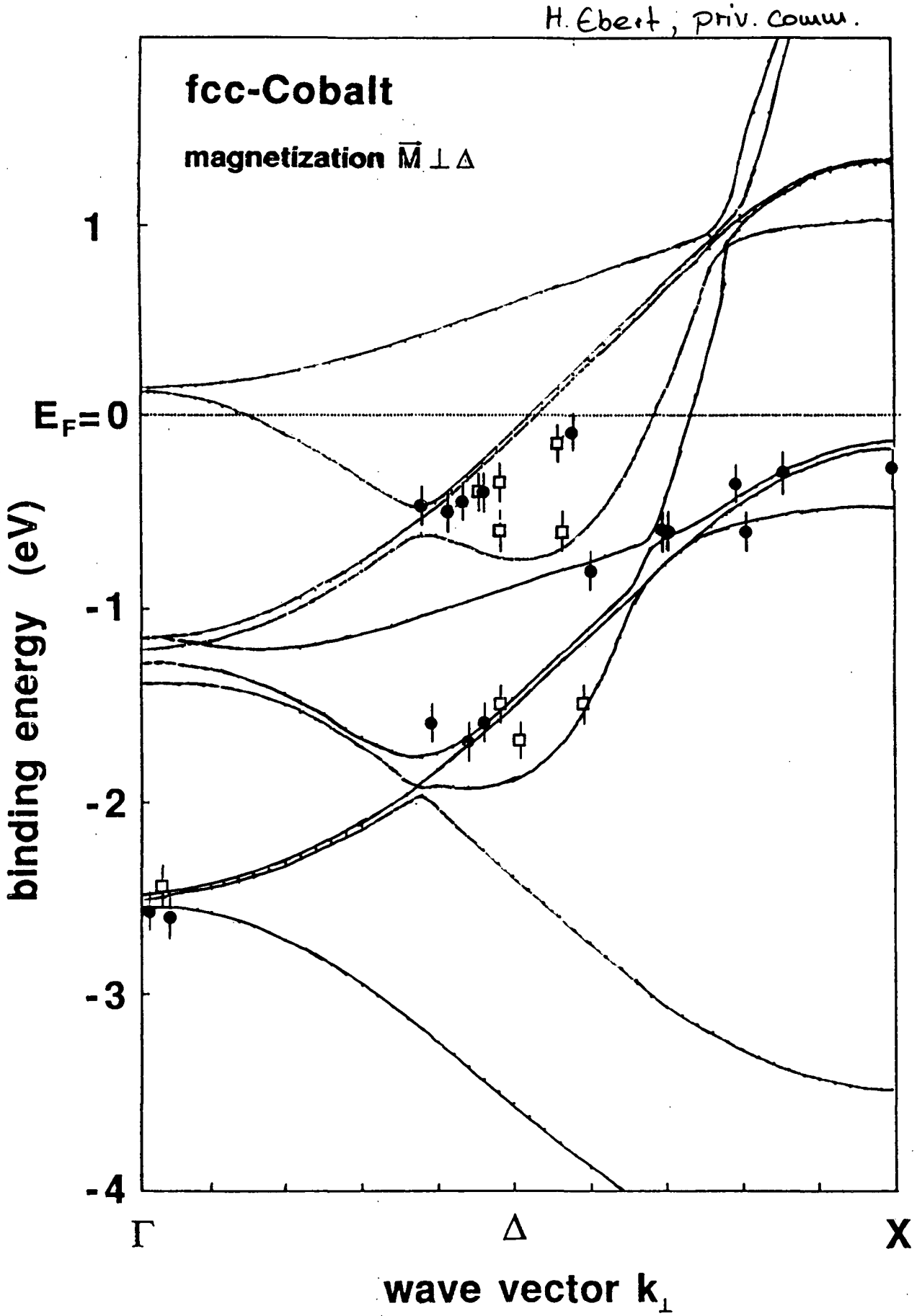

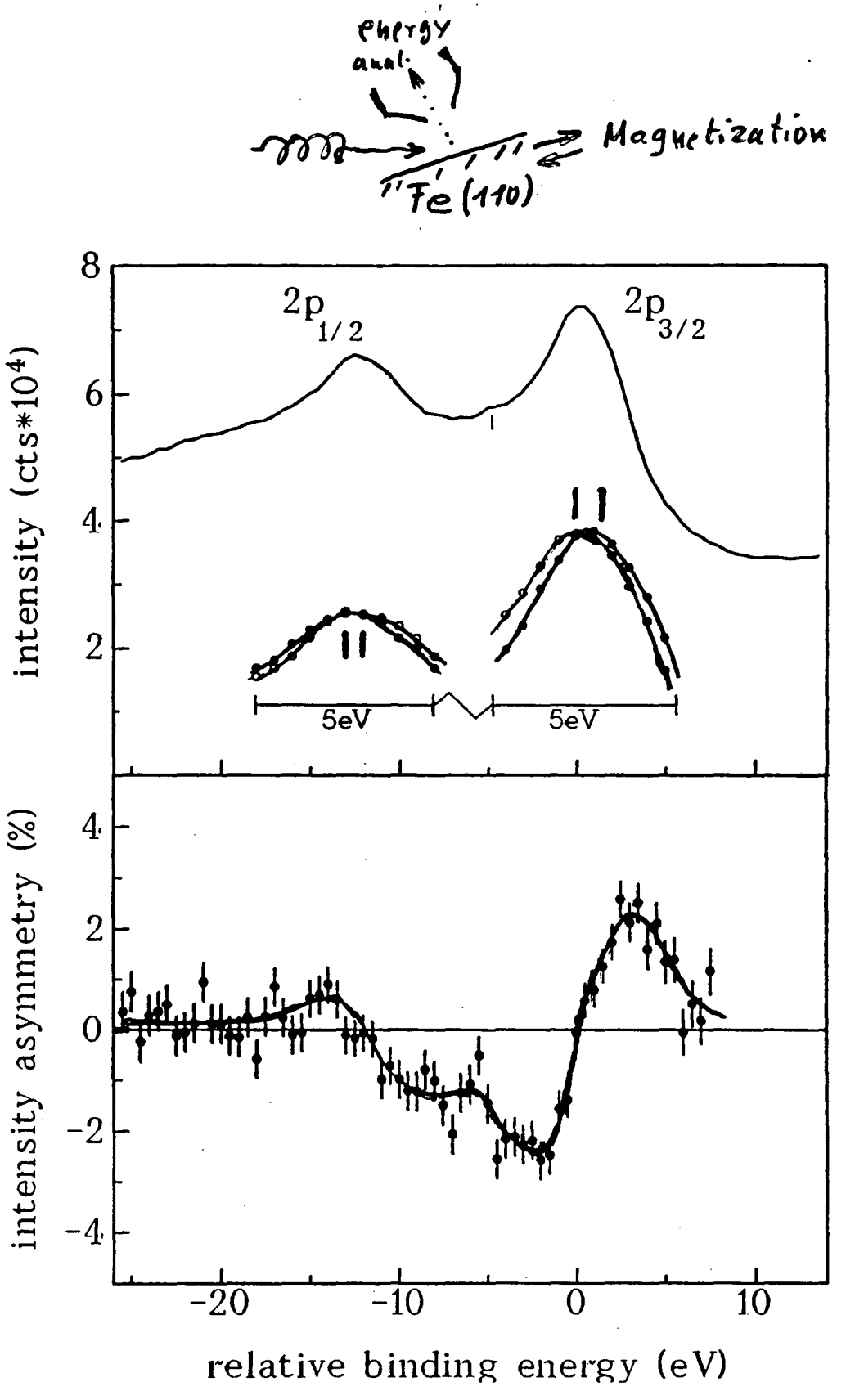
energy anal.
Magnetization
Fe(110)
8
6
4
2
intensity (cts*10⁴)
2p1/2
2p3/2
5eV
5eV
4
2
0
-2
-4
intensity asymmetry (%)
-20
-10
0
10
relative binding energy (eV)

Fe 2p

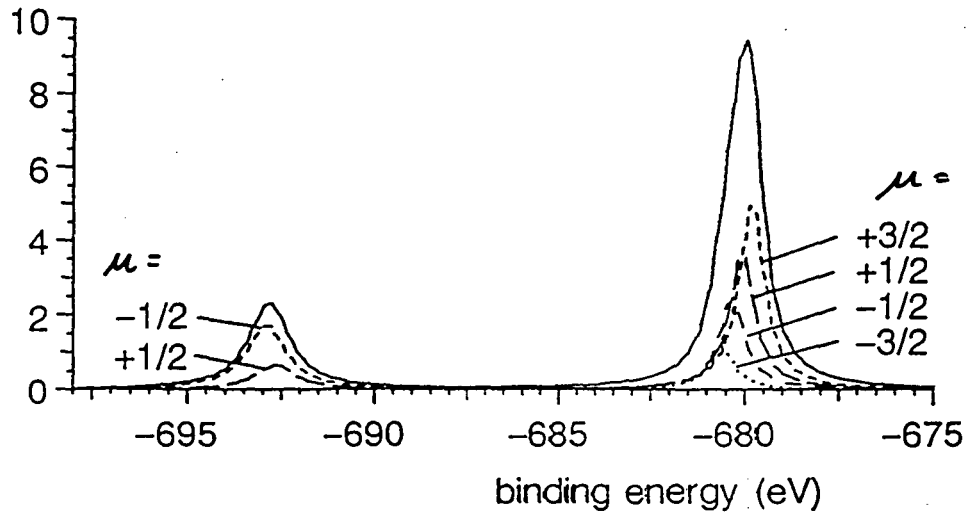

$\hbar\omega$ = 800 eV positive helicity Γ = 0.4 eV $2p_{3/2}$
0.63 eV $2p_{1/2}$

H. Ebert, L. Baumgarten, C. M. Schneider, J. Kirschner
(to be published)

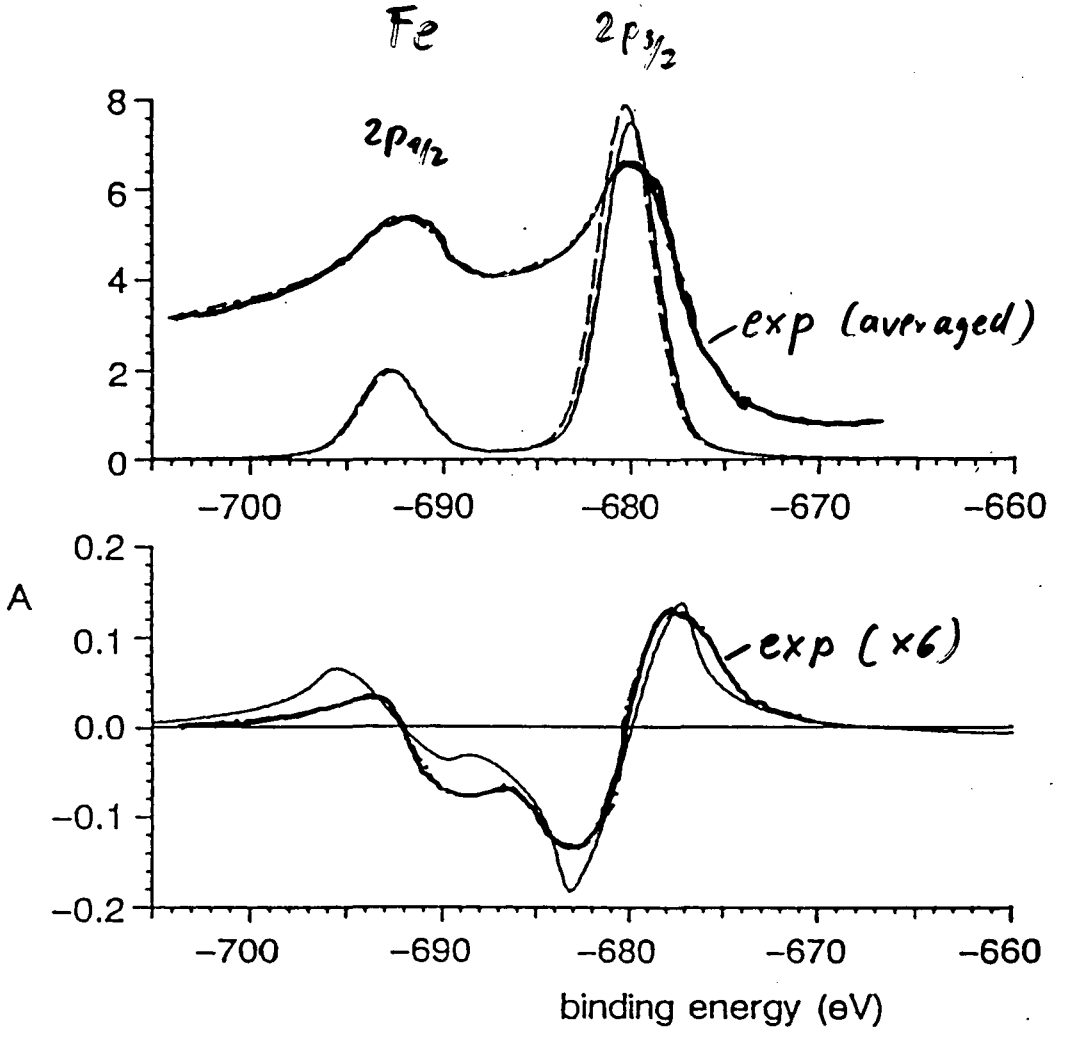

$\hbar\omega = 800\,eV$

H. Ebert, L. Baumgarten, C. M. Schneider, J. Kirschner (to be published)

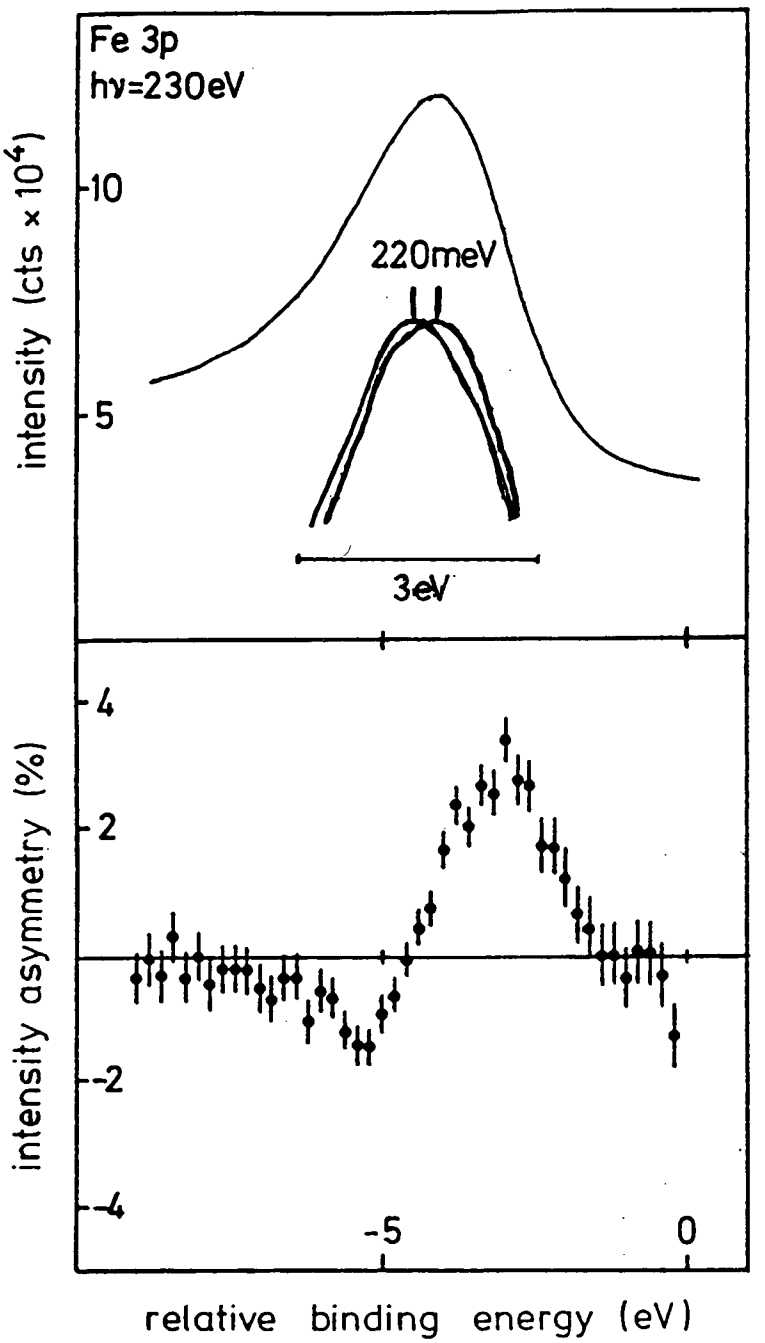
Fe 3p
hν=230eV
intensity (cts x 10⁴)
10
5
220meV
3eV
4
2
-2
-4
intensity asymmetry (%)
-5
0
relative binding energy (eV)

Applications of Polarized X-Ray Absorption to the Study of Highly Correlated Systems

G.A. Sawatzky

University of Groningen

G.A. Sawatzky
Laboratory of Applied and Solid State Physics
Materials Science Centre
University of Groningen
Nijenborgh 18
9747 AG Groningen
The Netherlands

Highly correlated systems containing transition metal (TM) and/or rare earth (RE) ions with open "core-like" valence electron states play an extremely important role in a wide variety of optical, electronic, magnetic, magneto-optical, and catalytic applications and are also important in biology. A basic understanding of the relationship between the properties and the chemical composition, electronic structure, and atomic structure is of utmost importance in the search for new materials with exceptional properties. Obviously, this understanding is far from complete since we are continually being surprised by reports of new, sometimes impossible (according to traditional knowledge) properties.

The modern developments in surface and thin-film science add a new dimension to materials preparation and modifications, which I am sure will again surprise us with discoveries of exotic properties.

Synchrotron radiation will play an even more dominating role in the study of such materials. Core-level x-ray absorption-edge structures involving the core-like open-shell valence shells can, if carried out at high resolution, provide a detailed fingerprint of the atomic and near-ground-state electronic structure. Utilizing linear and circular polarization, x-ray absorption provides direct information on the local point group symmetry, the local magnetic moment, and the crystal field splittings as well as their temperature dependence when combined with the now-available renormalized atom calculations. Of great importance is the fact that this information is site-specific and can be obtained for every TM or RE element in the material.

Actually, this is also a surprise. Who would have thought that a spectroscopic technique at an energy of KeV's and a resolution of 0.2 eV would be capable of obtaining information on a milli-electron-volt scale—for example, the temperature- and field-dependence of the local magnetic moment of an atom absorbed on a magnetic material?

X-ray absorption spectroscopy can be either bulk- or surface-sensitive, depending on the type of detection used. A coverage of 0.1 monolayer can easily be studied. New developments will make measurements at high fields and low temperatures possible and will also provide detailed information on paramagnetic systems.

The ALS source, with its high brightness, combined with state-of-the-art monochromators can play a leading role in developing this wide field of applications and answering extremely interesting basic-science questions.

Applications of Polarized Absorption to the study of highly Correlated Systems

- What kind Systems ?
- Why interesting ?
- Why XAS ?
- Examples
- Future

Valence electron states determine properties

Consider an atom (ion) in a solid

Two Extreme situations

$R \gtrsim D$	$R \ll D$
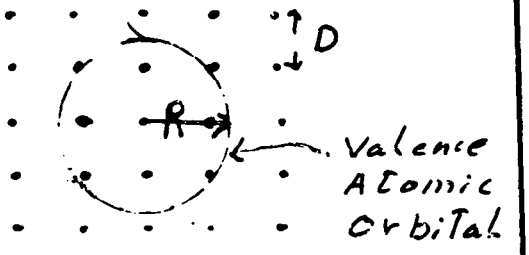	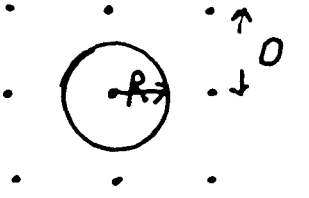
Have lost atomic identity	Remain Atomic
Broad Bands - MO theory	Narrow Bands - Conf. Int.
Small e-e interaction $U \ll W$	Large e-e interaction $U \gg W$
Low energy scale → charge fl.	Low energy scale → Spin fl.
Non Magnetic	Magnetic
Al metal MgO Cu metal [closed d shell]	Gd metal* Mn in Al* NiO CuO or High T_c
Important for XAS	
Small Interaction with core hole $Q \ll W$	Large interaction with core hole $Q \gg W$ Rare Earths 3d → 4f Transition (3d) Metal Compounds 2p → 3d

Why are R << D systems interesting

1. Applications – Wide diversity of (tunable)* physical and chemical properties.

e.g. small class of TM oxides (3d)

Metals – CrO_2 Fe_3O_4 >120k

Insulators – Cr_2O_3, V_2O_5, CoO, Co_3O_4

Semicond → Metal – VO_2, V_2O_3, Ti_4O_7

Supercond – $La_{2-x}Ba_xCuO_4$, $LiTi_2O_4$

piezo & ferroelectr. – $BaTiO_3$, $CuCl$

Catal. – Fe oxides, Co oxides, M

Ferromagnets – CrO_2

Antiferromag – MnO

Ferrimagnets – γFe_2O_3, Ferrites

Tunable T_N, T_{comp}, Anisotropy

2 Basic Research

We don't understand them!!
We are continually surprised by

Why are these interesting for XAS

For transitions core → valence ($R \ll 0$)

$2p^6 3d^n \longrightarrow 2p^5 3d^{n+1}$ (500 - 1000 eV)

$3d^{10} 4f^n \longrightarrow 3d^9 4f^{n+1}$ (800 - 2500 eV)

the core hole - valence electron interaction is so large that a local bound state is formed

The internal structure of this bound state (multiplets) can be calculated using renormalized atom or ion HF (CI) calculations.

Via dipole selection rules the relative intensities of final states are a fingerprint of the ground or initial state.

Can we learn about low energy scale in initial state (< 10 meV) with a resolution (core hole lifetime ~ 0.2 eV) of 0.2 eV?

As we ~~have seen~~ will see today the answer is YES!!

Bound state

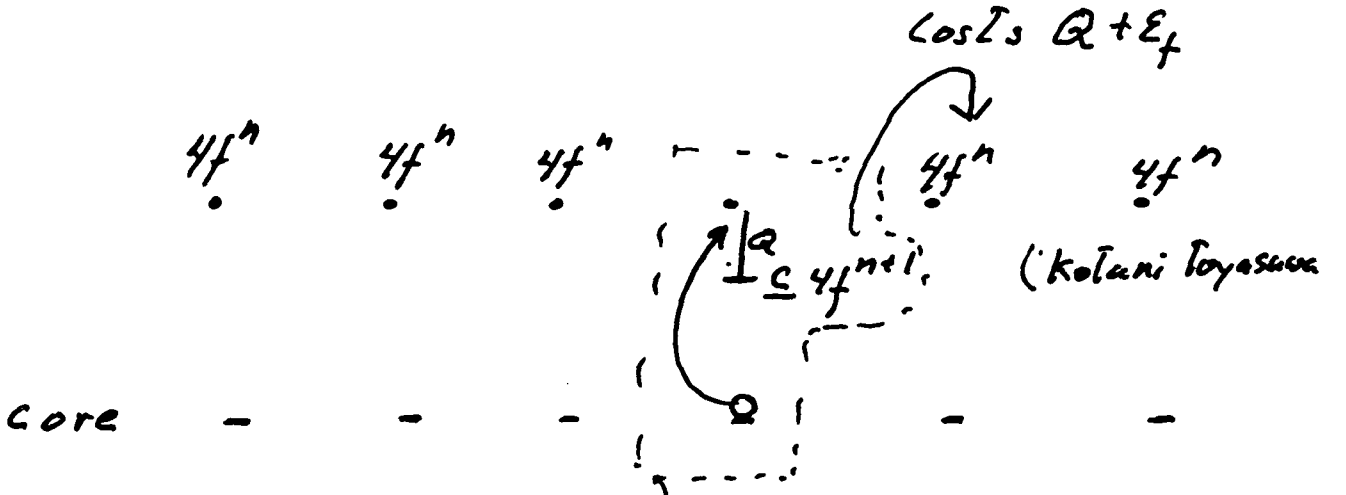
cost Q + ε_f
$4f^n$ $4f^n$ $4f^n$ $4f^n$ $4f^n$
$\underline{c}\, 4f^{n+1}$
(Kotani Toyozawa
core
the core hole on site i binds an extra f on site i And isolates this atom from the rest of the solid.

For Highly Correlated

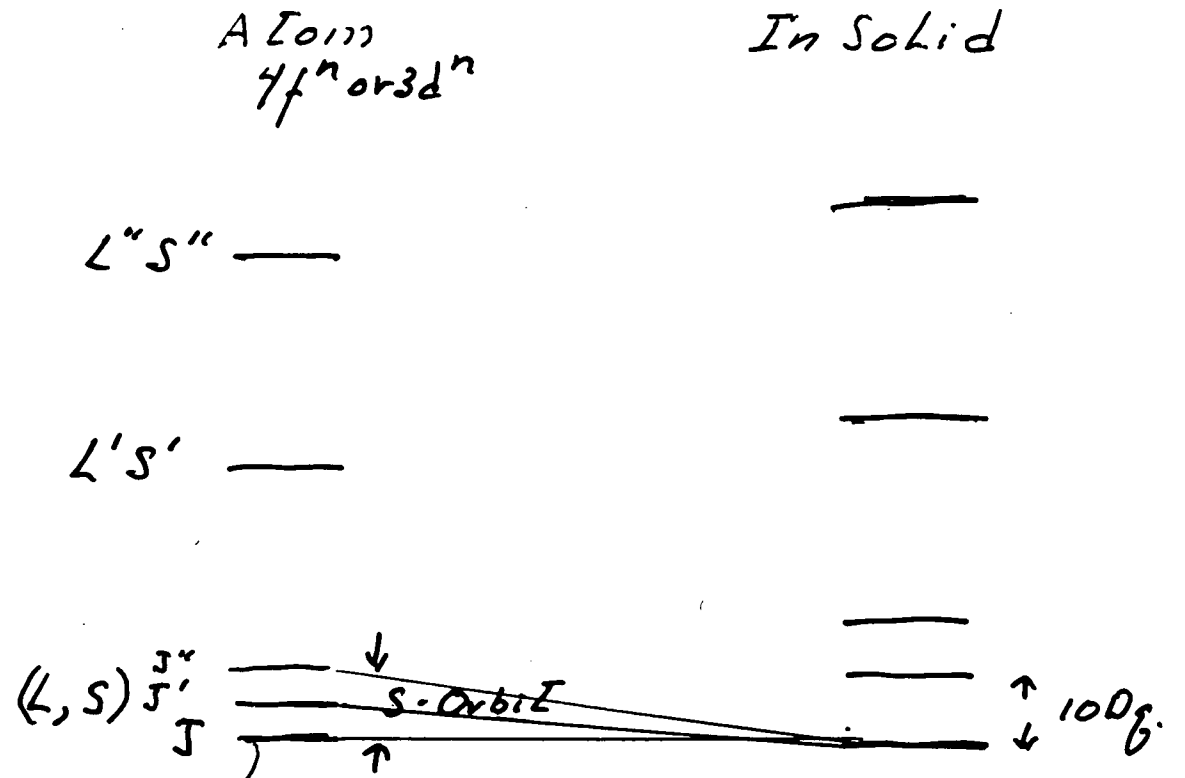

Hunds Rule
Max S, Max L.
$J = L - S$ < 1/2 full
$L + S$ > 1/2 full

For $10D_q > \partial_{S.O}$
L is quenched
Spin Only
∂_{SO} → perturbation

Transition to $\subseteq f^{n+1}(d^{n+1})$

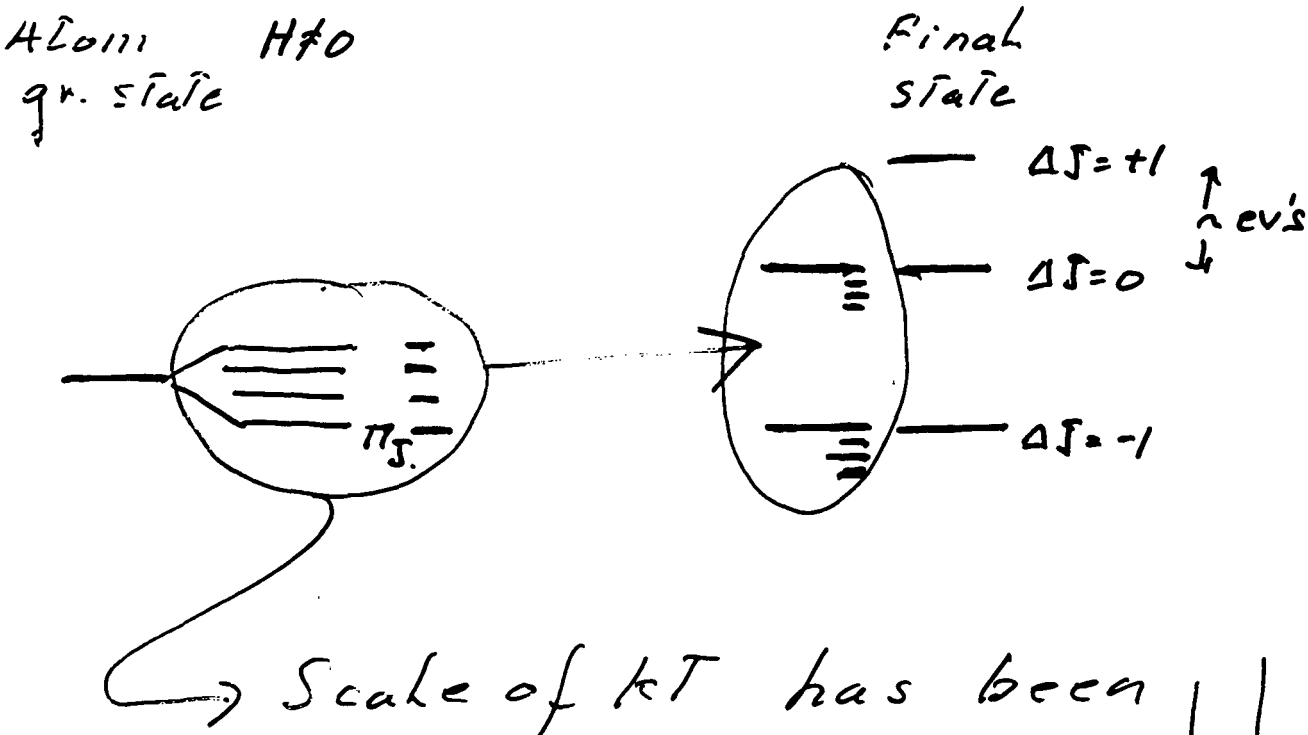

→ Scale of kT has been amplified [Suddenly J. To a scale of eV's !!

Atomic limit (neglect hybridization).

Theory (Multiplets)

Ground state - atomic

- $4f^n$ or $3d^n$
- Hunds rule ($J = L + S$)
- Wavefunction

(atomic H.F. including SO)

BOB. GOWAN

Final state

- $3d^9 4f^{n+1}$ or $2p^5 3d^{n+1}$

program calculates

- all energies (over 1000 states for Gd)
- all wavefunctions
- all optical Transition probabilities

($\Delta J = 0, \pm 1$)

Now modified (Thole) to include

Lower point group symmetries

- Crystal fields.

Synchrotron LURE.

theory Thole ↔ Cowan + Butler

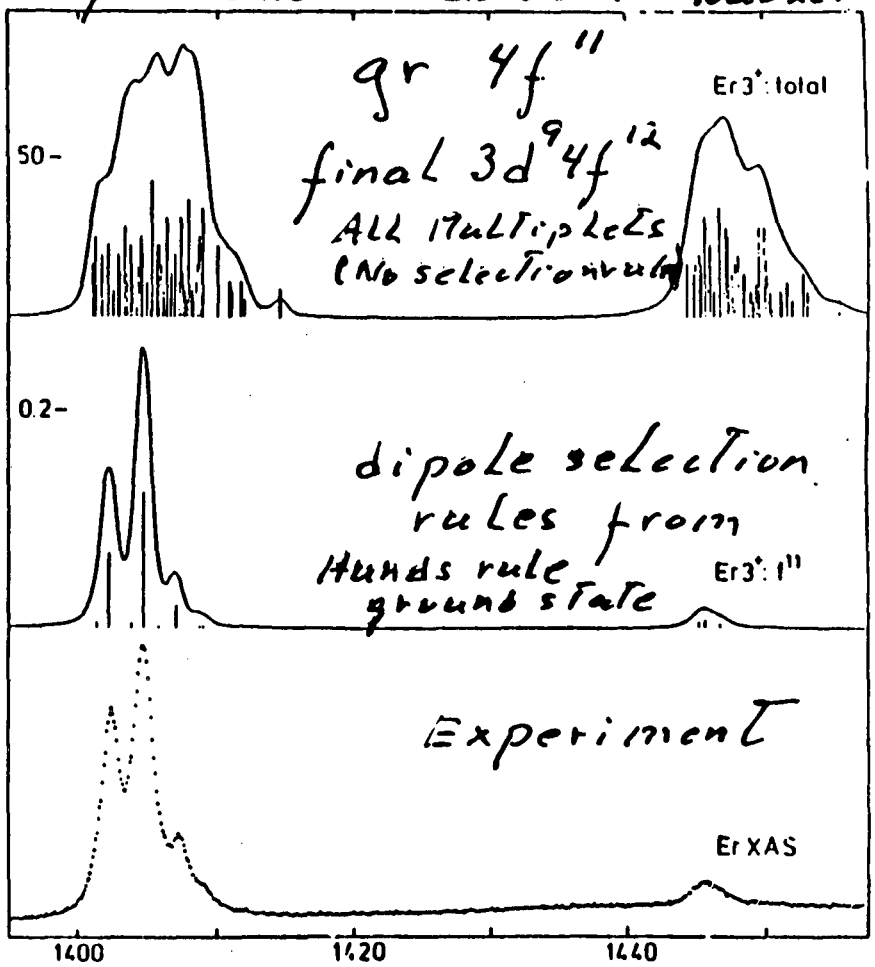

XAS Shape is a fingerprint of the L, S, J, of the ground state.

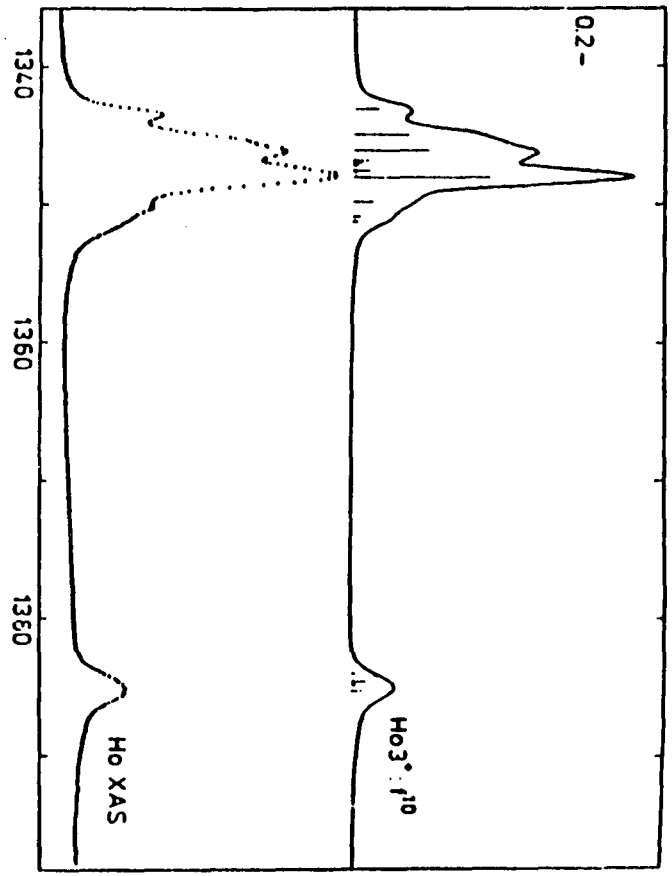

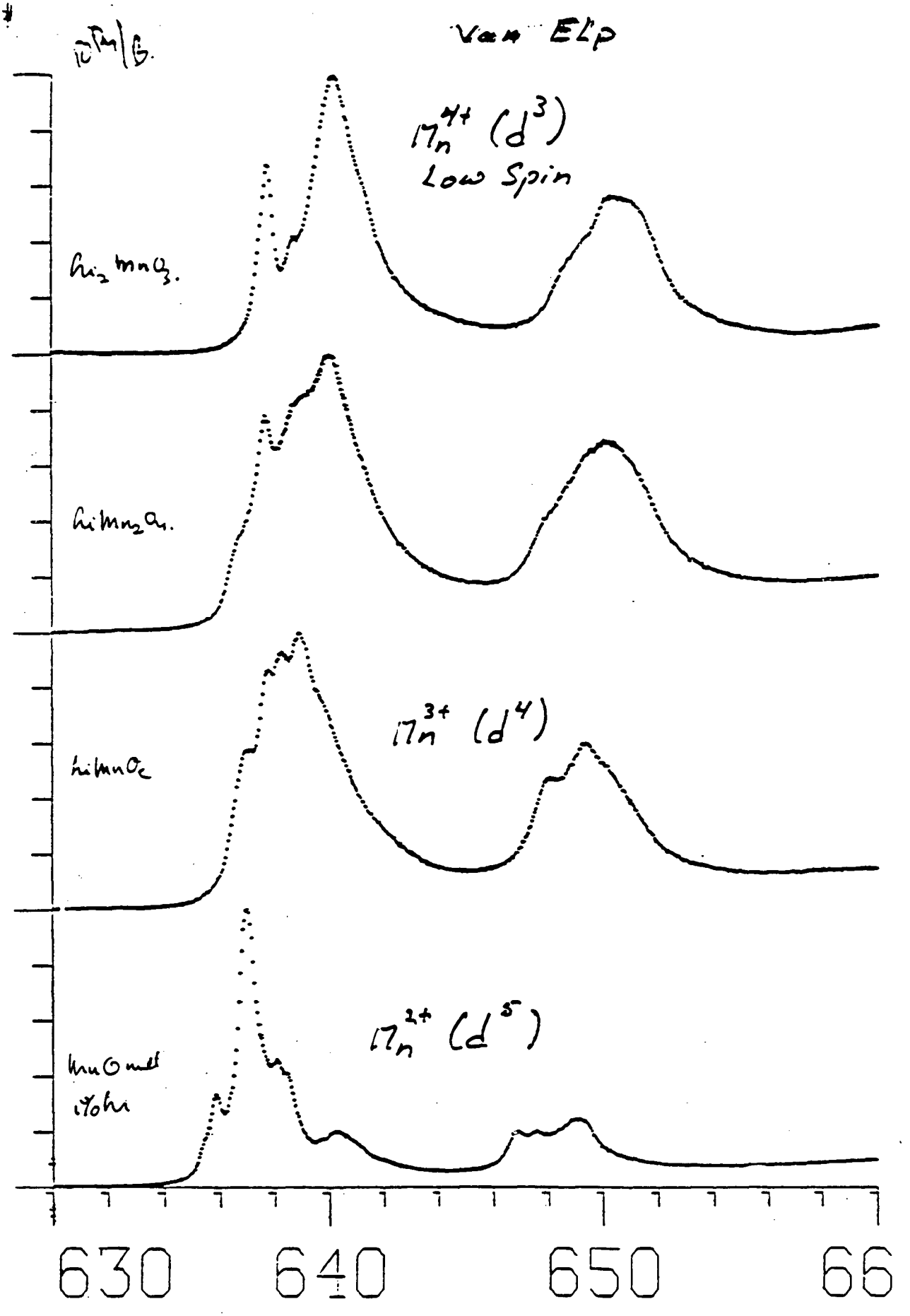
Van ELP
Mn^{4+} (d^3)
Low Spin
Li_2MnO_3.
$LiMn_2O_4$.
Mn^{3+} (d^4)
$LiMnO_2$
Mn^{2+} (d^5)
MnO mull
630
640
650
66

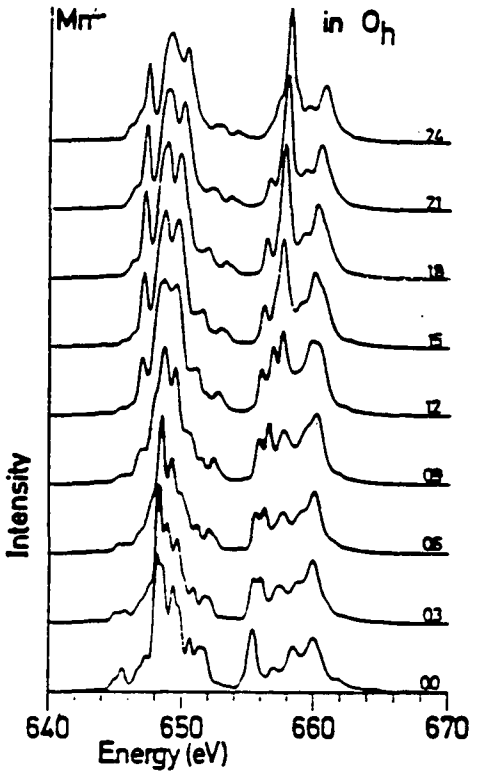

FIG. 7. Mn^{4+} $3d^3$ to $2p^53d^4$ transition in cubic crystal fields. $10Dq$ ranges from 0.0 (bottom) to 2.4 eV.

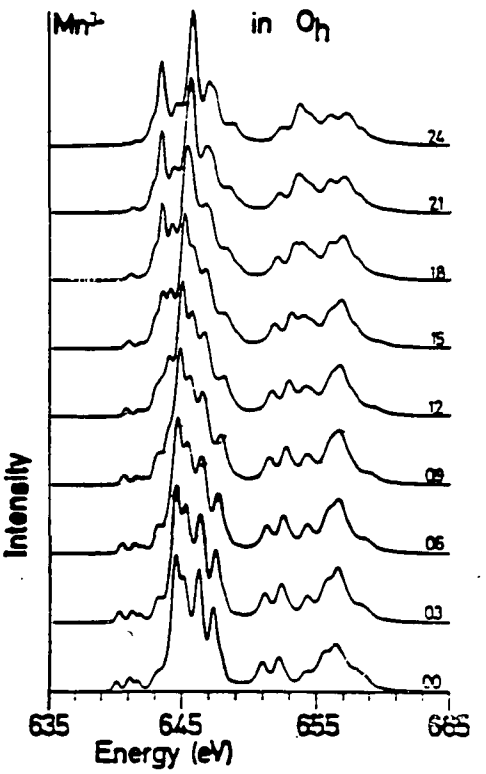

FIG. 9. Mn^{2+} $3d^4$ to $2p^53d^5$ transition in cubic crystal fields. $10Dq$ ranges from 0.0 (bottom) to 2.4 eV.

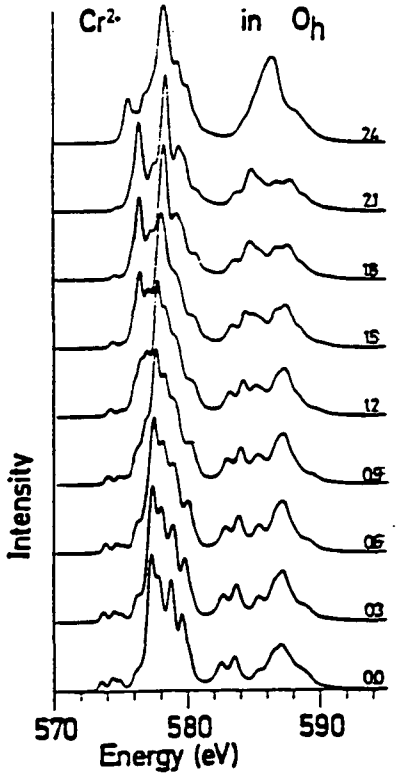

FIG. 8. Cr^{2+} $3d^4$ to $2p^53d^5$ transition in cubic crystal fields. $10Dq$ ranges from 0.0 (bottom) to 2.4 eV

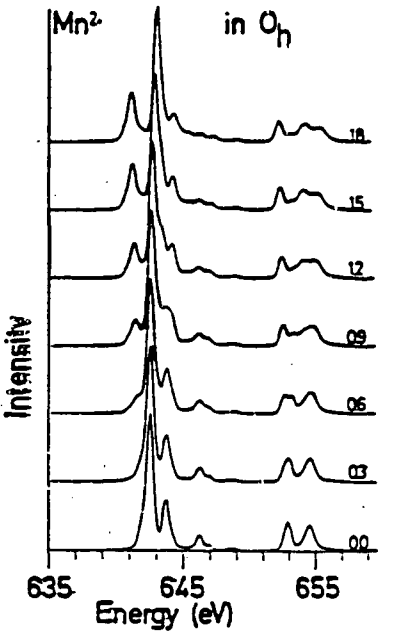

FIG. 10. Mn^{2+} $3d^5$ to $2p^53d^6$ transition in cubic crystal fields. $10Dq$ ranges from 0.0 (bottom) to 1.8 eV.

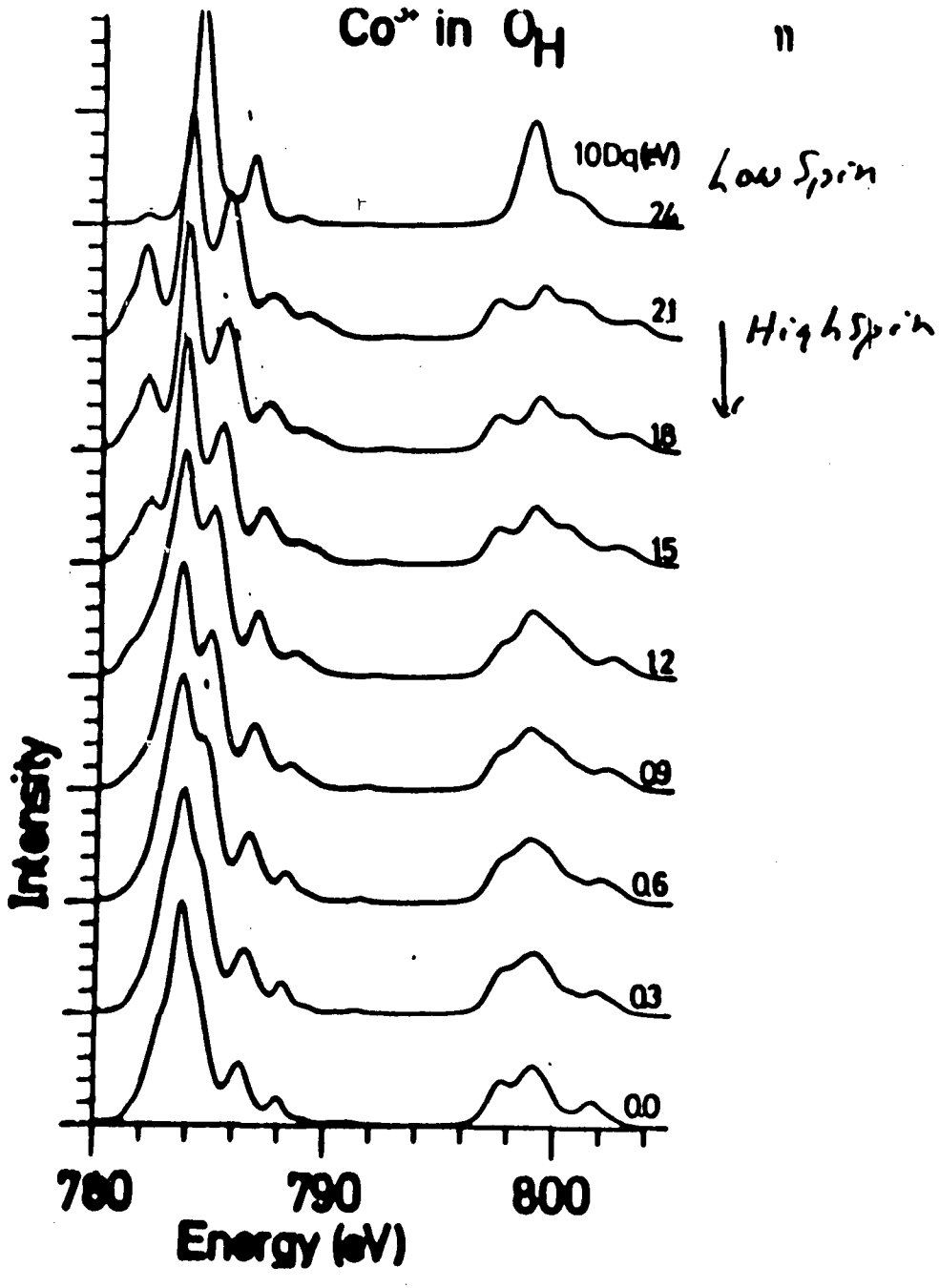
Co³⁺ in O_H
10Dq(eV)
2.4
2.1
1.8
1.5
1.2
0.9
0.6
0.3
0.0
Low Spin
High Spin
Intensity
780
790
800
Energy (eV)

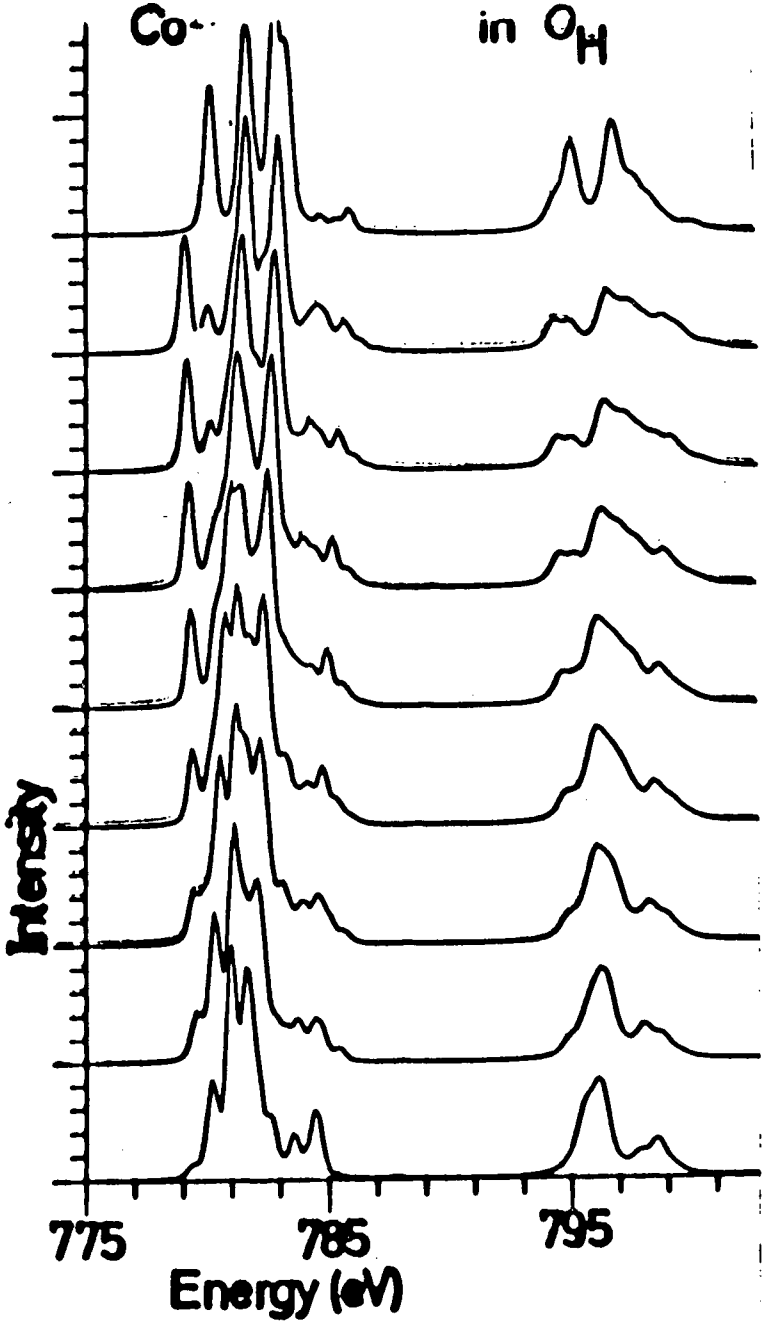
Co
in O_H
Intensity
775
785
795
Energy (eV)

de Groot et al. Fig. 7

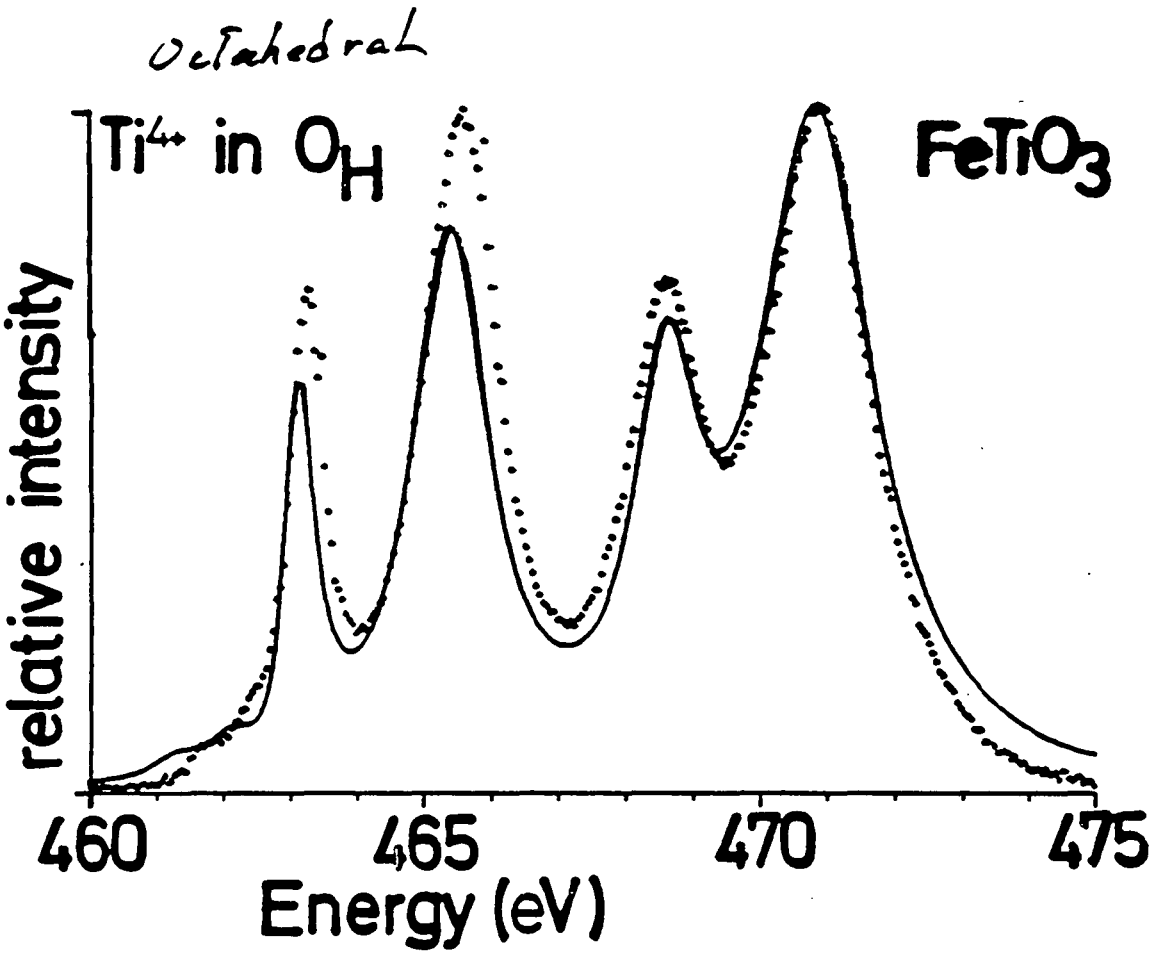

JanB | 590 | BG 4228 | de Groot | 7 | 40

de Groot et al. Fig. 9

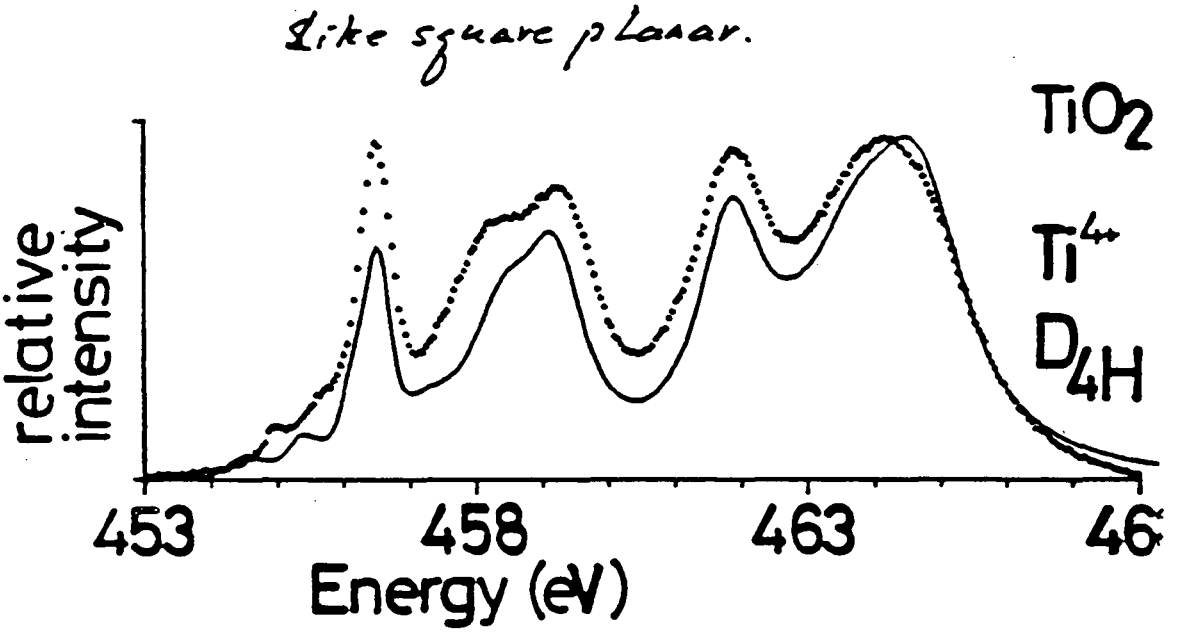

JanB | 590 | BG 4228 | de Groot | 9 | 40

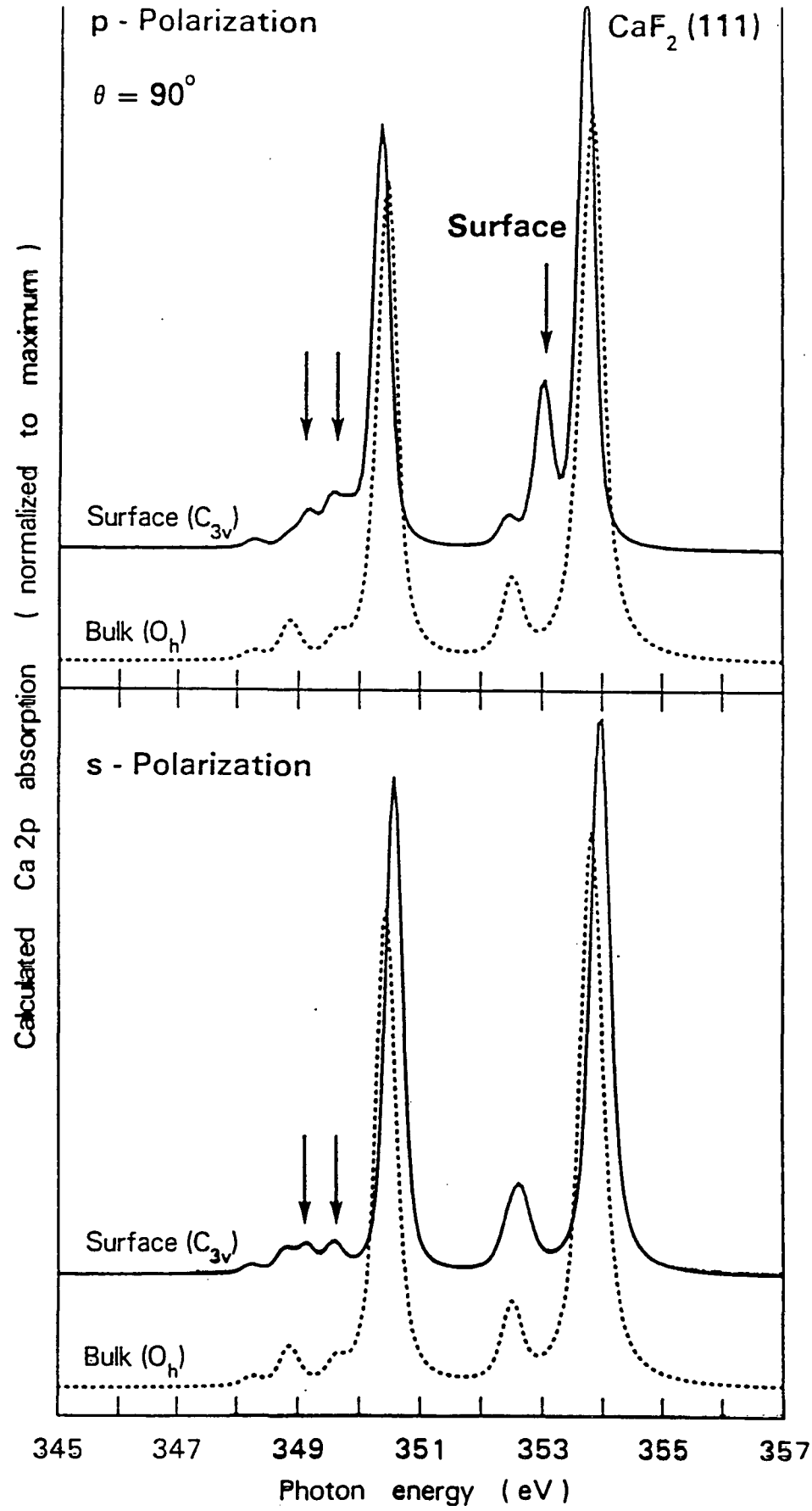

Stimpsel et al Phys. Rev 43, 6855 1991

Fig. 4a

$I_{L_3}/I_{L_2} \neq 2:1 \rightarrow$ Orbital mom. in the ground st.

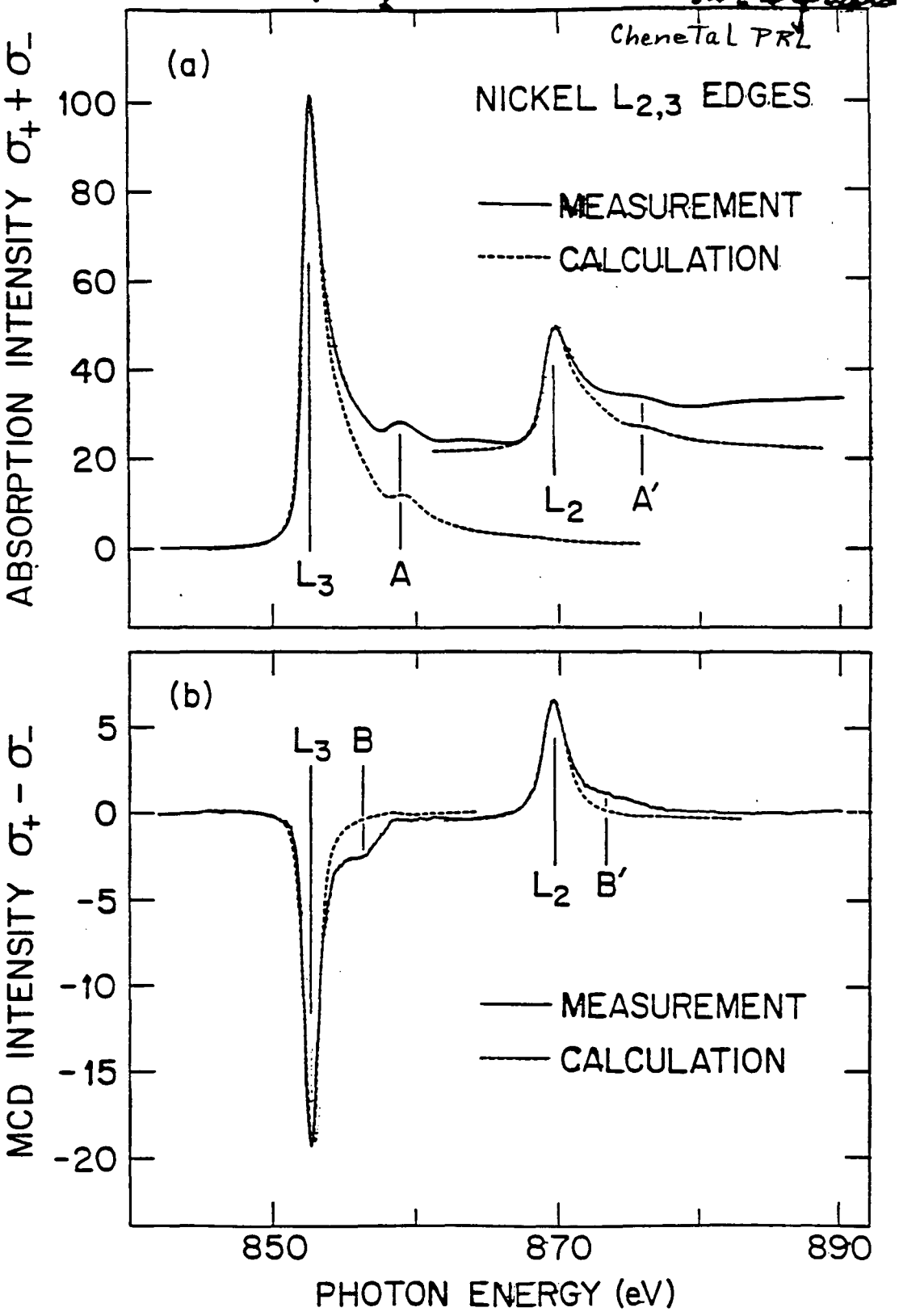

2p edge → TM, 3d edge → RE

(2p spin orbit << 10Dq; 3d spin orbit >> 10Dq)

- L, S, J of ground state (Rare earths)
- Crystal field splitting (TM) [10Dq]
- Crystal point group symmetry (roughly)
- Surface sensitive

More detail from Pol. dep.

In general: $4f^n(\alpha J) \longrightarrow 3d^9 4f^{n+1}(\alpha' J')$

many states with same J' (Lubbeisa)

$$S_{\alpha J\Pi, \alpha' J'\Pi'} = \begin{pmatrix} J & 1 & J' \\ \Pi & m & -\Pi' \end{pmatrix}^2 |\langle \alpha J \| c^{(1)} \| \alpha' J' \rangle|^2$$

polarization $\pm 1 \to x, y$; $0 \to z$

We cannot resolve various Π'

i.e splitting is $\sim kT$

$$\therefore \sum_{\Pi'}{}^{m} S_{\alpha J\Pi, \alpha' J'\Pi'} = \sum_{\Pi'} \begin{pmatrix} J & 1 & J' \\ \Pi & m & -\Pi' \end{pmatrix}^2 |\langle \; \| \; \rangle|^2$$

3j symbol: $\Pi + m - \Pi' = 0 \qquad J' - J = 0, \pm 1$

i.e for z pol $m = 0 \quad \Pi = \Pi'$

z pol.

$$\sum_{\Pi'} S = \begin{pmatrix} J & 1 & J' \\ \Pi & 0 & -\Pi \end{pmatrix}^2 |\langle \; \| \; \rangle|^2$$

in magnetic field

Boltzman factor $e^{g\mu_B H \Pi / kT} = e^{-\Pi/\theta}$

$\theta^{-1} = g\mu_B H / kT$ is reduced temp.

partition fcn $Z = \sum_{\Pi=-J}^{J} e^{-\Pi/\theta} = \dfrac{\sinh[(J+1/2)\theta]}{\sinh(1/2\theta)}$

Strong correlation between
ΔJ and ΔM_J
We can resolve ΔJ Not ΔM_J

From F. de Groot thesis Nijmegen

For $M_J = -J$ (initial state)

m / ΔJ	-1	0	$+1$
-1	(1)	0	0
0	$1/J+1$	$(J/J+1)$	0
$+1$	$\frac{1}{(2J+3)(J+1)}$	$\frac{2J+1}{(2J+3)(J+1}$	$\frac{(2J+1)(J+1)}{(2J+3)(J+1}$

○ Largest for Large J as for rare earths

Linear pol. $\propto \langle \Pi^2 \rangle$

Crystal fields of lower than cubic symmetry. [couple states Π and $-\Pi$]

Also study Antiferromagnets!

Circular pol $\propto \langle \Pi \rangle$

True Magnetic Dichroism

zero for antiferromagnet

Magnetic Dichroism

Example Yb^{3+} in ordered ($T < T_c, T_N$)

$J = 3/2$ Not allowed

$\rightarrow 4f^{13}(J = 7/2)$

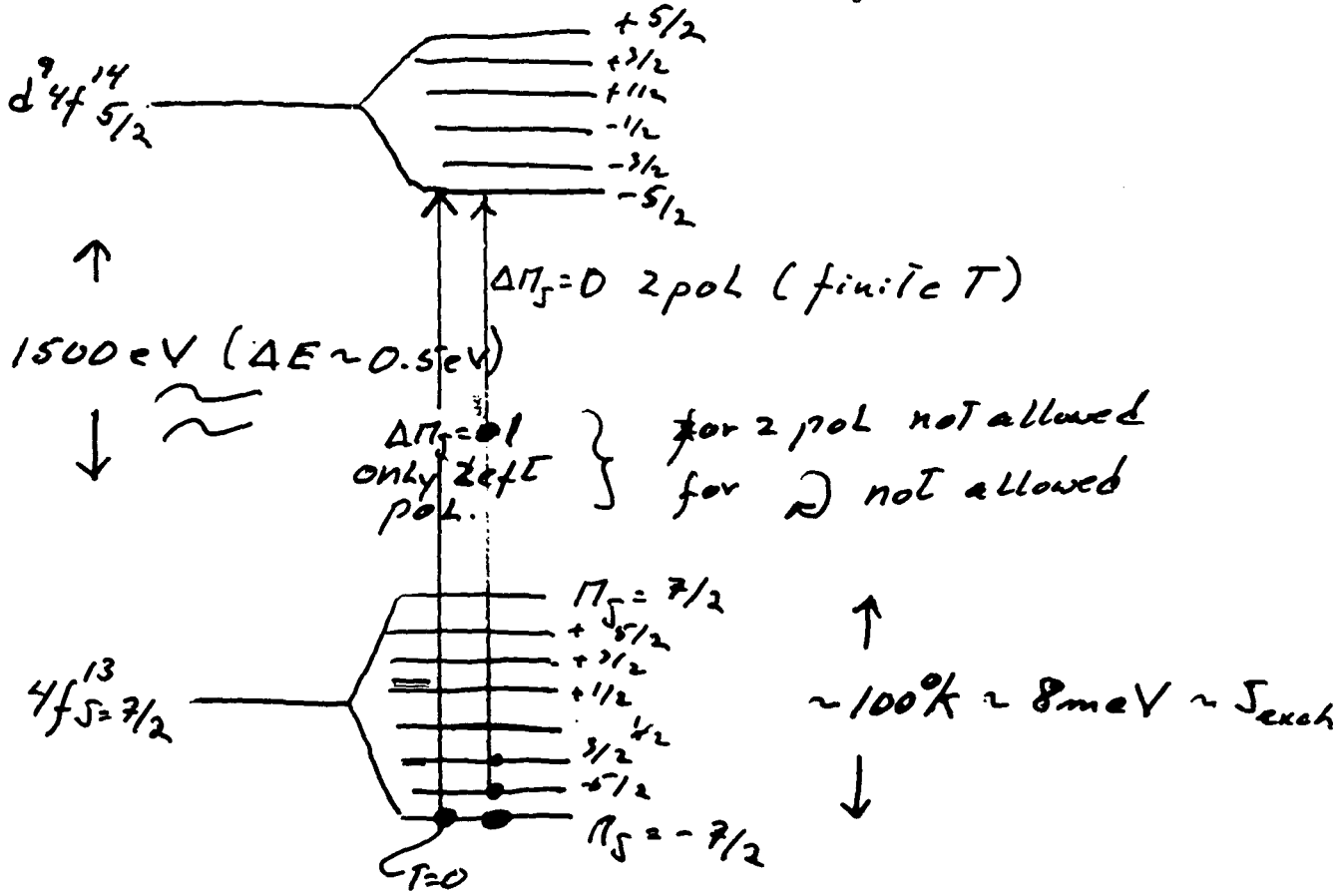

$\Delta E >> J$

Rules: tholeetal PRL 55, 2086 (1985)
Goedkoop Thesis Nijmegen (1989)
Caraetal PRL (1990)

Linear pol $I_D \sim \langle L^2 \rangle$ [antiferro]

Circular pol $I_D \sim \langle L \rangle$ [ferro or ferri]

[XAS is Surface sensitive!!].

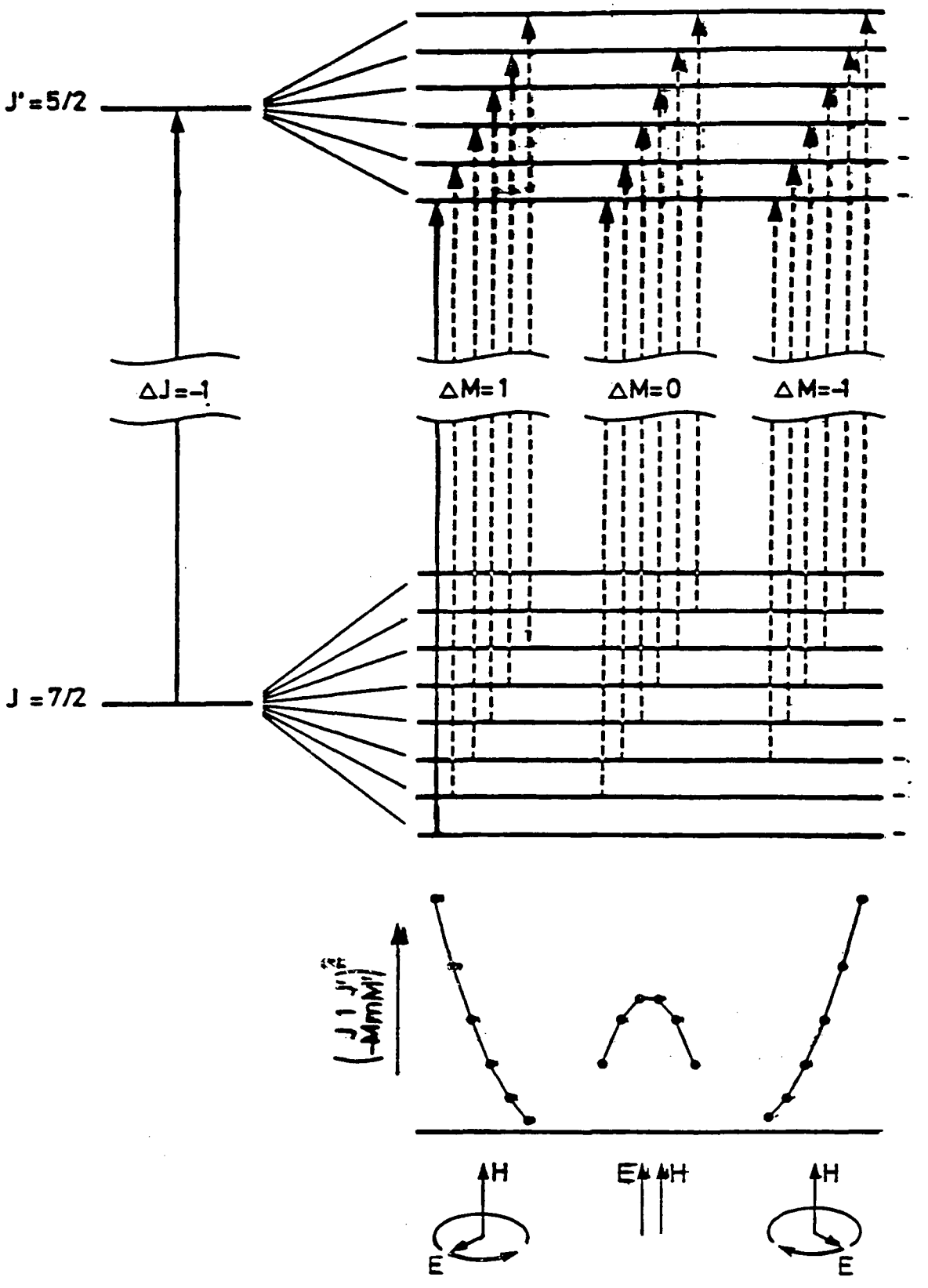
Yb3+
+ magnetic field
J' = 5/2
ΔJ = -1
J = 7/2
ΔM = 1
ΔM = 0
ΔM = -1
H
E
H
E
H
E

Sacchi et al. (LURE)

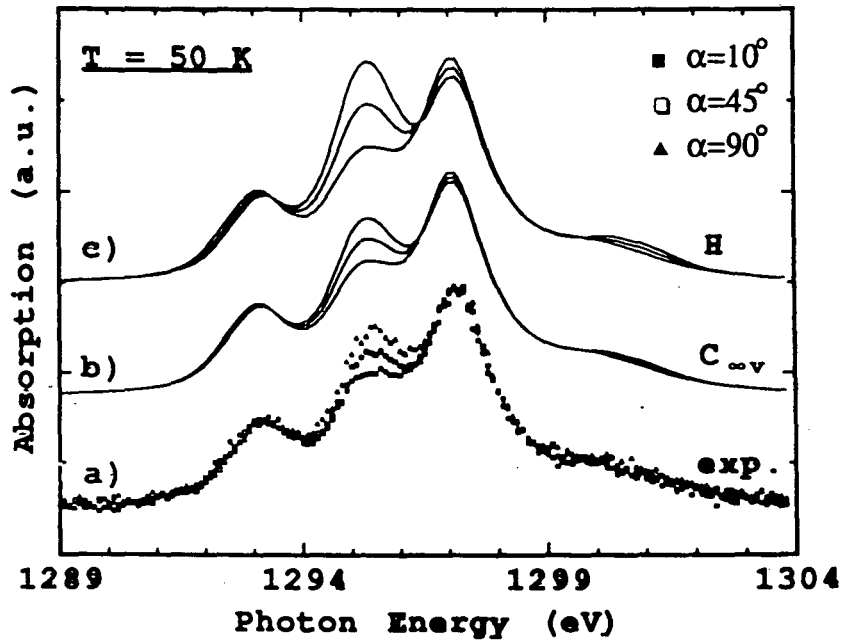

The linear polarization dependence of the M_5 edge of Dy for a 0.1 ML Dy/Si (111) interface at 50 K (a) is compared with model calculations based on the $C_{\infty v}$ (b) and magnetic (c) induced splittings. T_R is always optimized at $\alpha = 10°$.

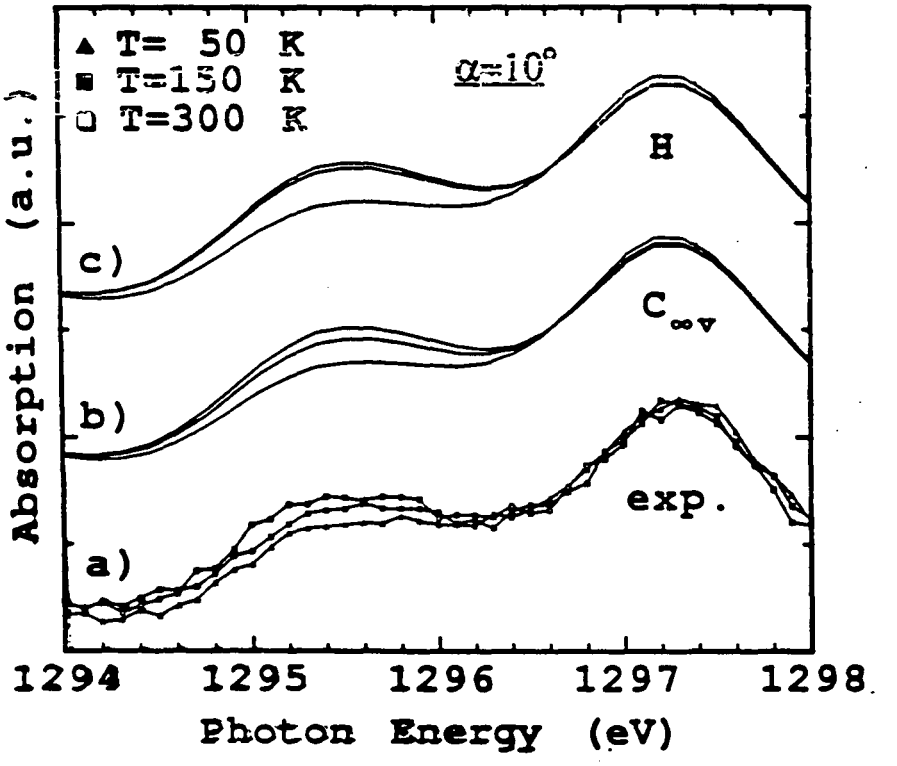

The temperature dependence of the central part of the Dy M_5 edge at $\alpha = 10°$ (a) is compared to the $C_{\infty v}$ and H model calculations.

Phys. Rev. Lett. 55, 2086 (1985)

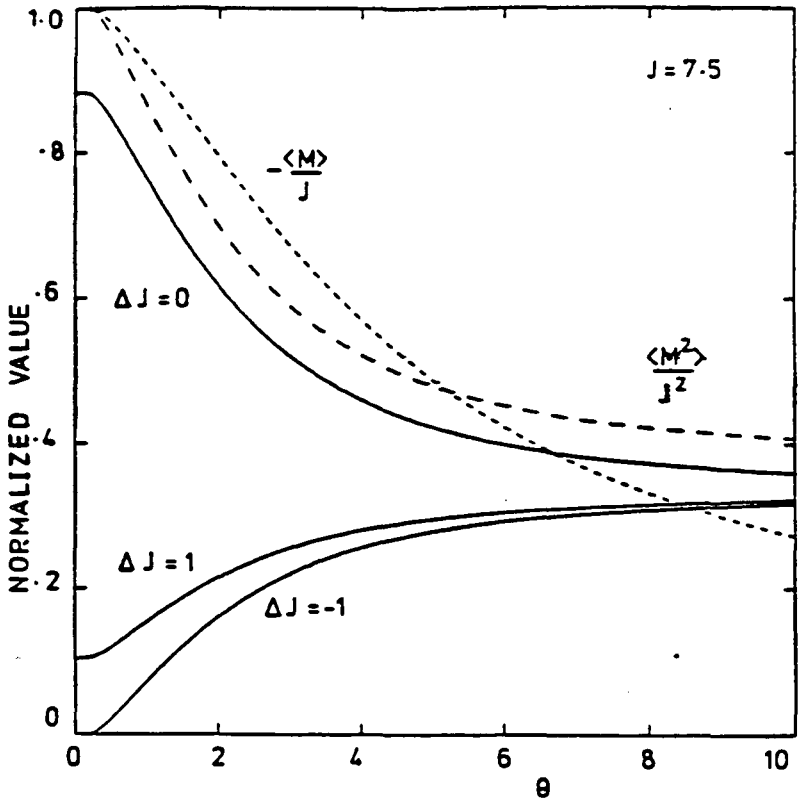

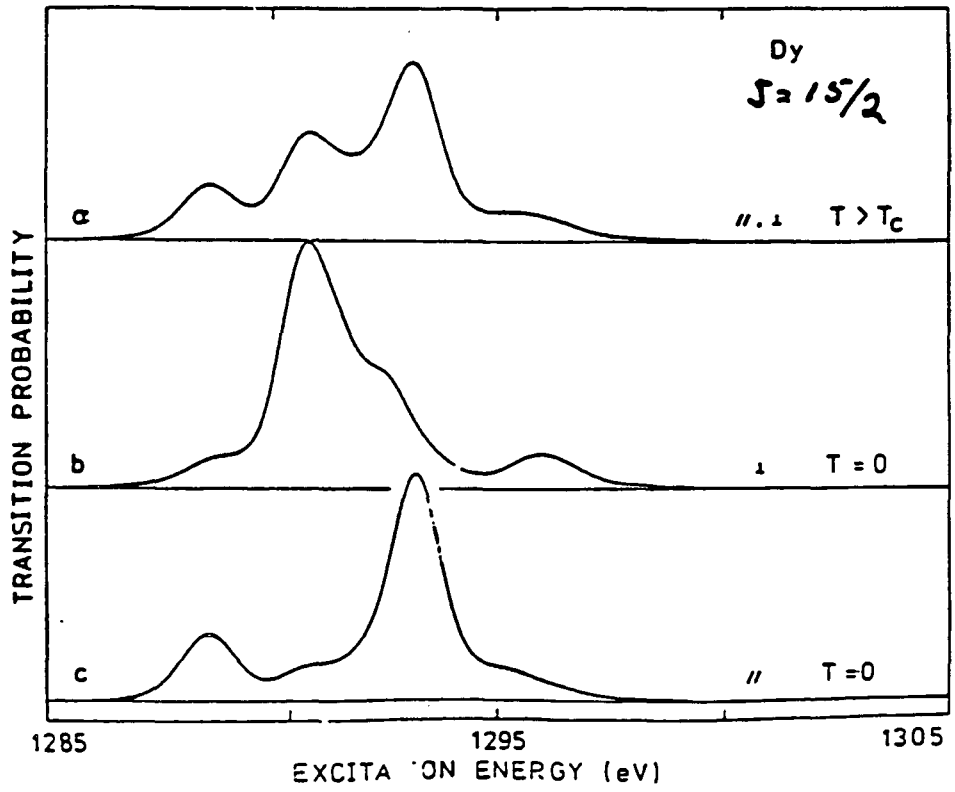

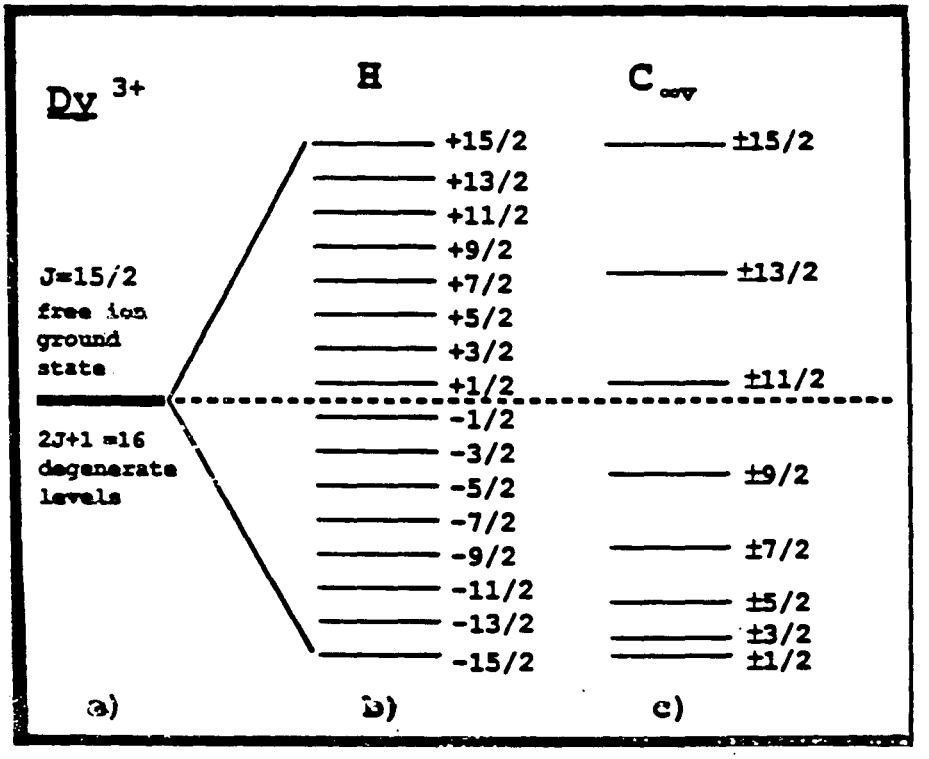

Splitting of Dy^{3+} free ion ground state (a) induced by a magnetic field (b) and by a crystal field of purely axial symmetry (c).

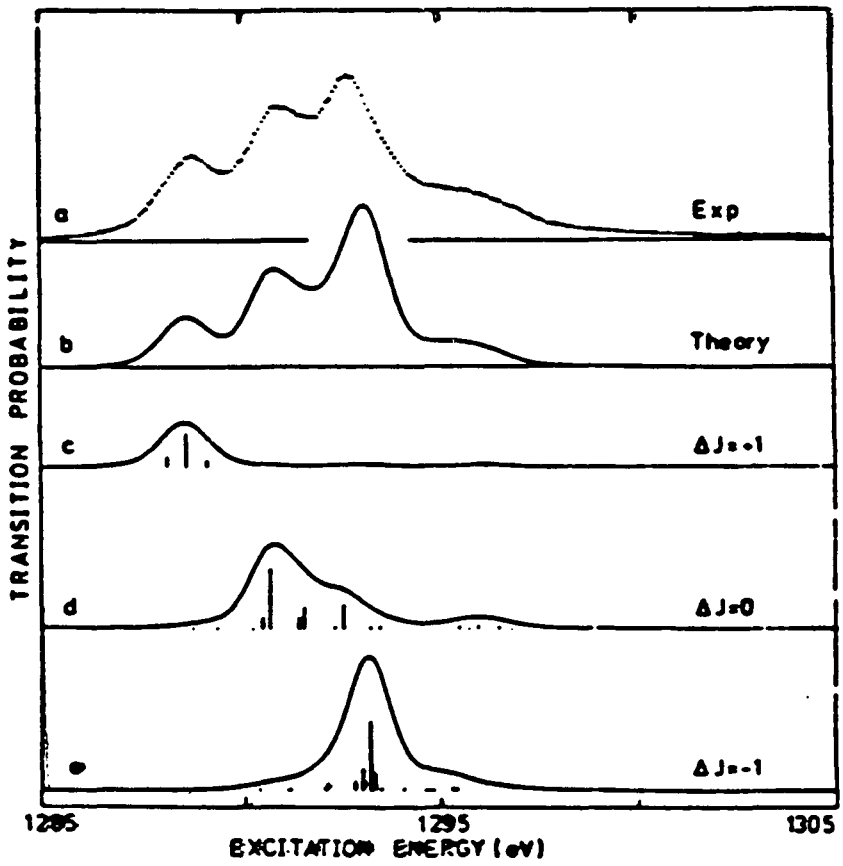

Experimental (a) and theoretical (b) M_5 XAS spectra for Dy in a non-magnetic ground-state. The separate contributions with ΔJ resolution of this spectrum are shown in (c), (d), and (e), respectively.

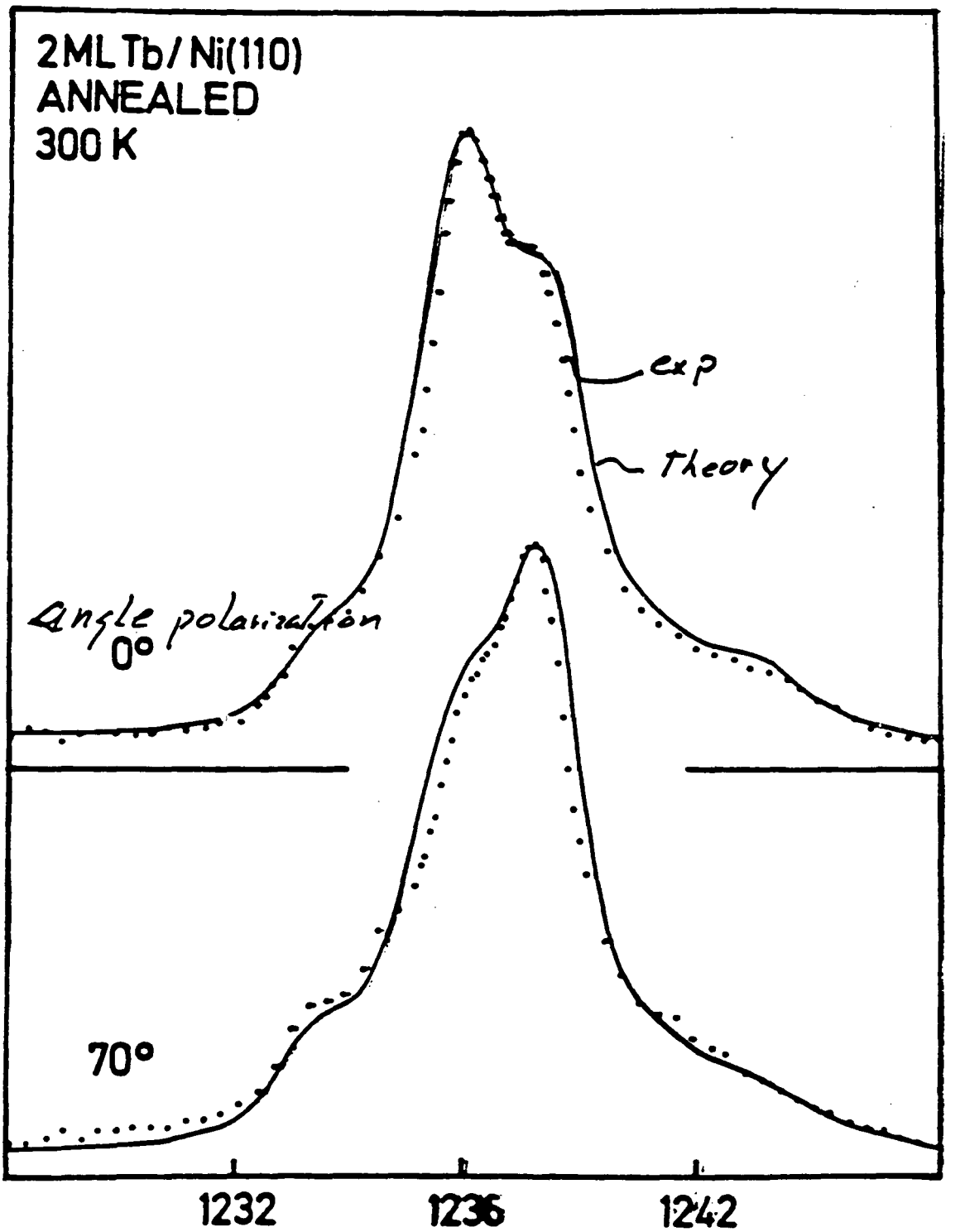
2ML Tb/ Ni(110)
ANNEALED
300 K
exp
Theory
Angle polarization
0°
70°
1232
1236
1242

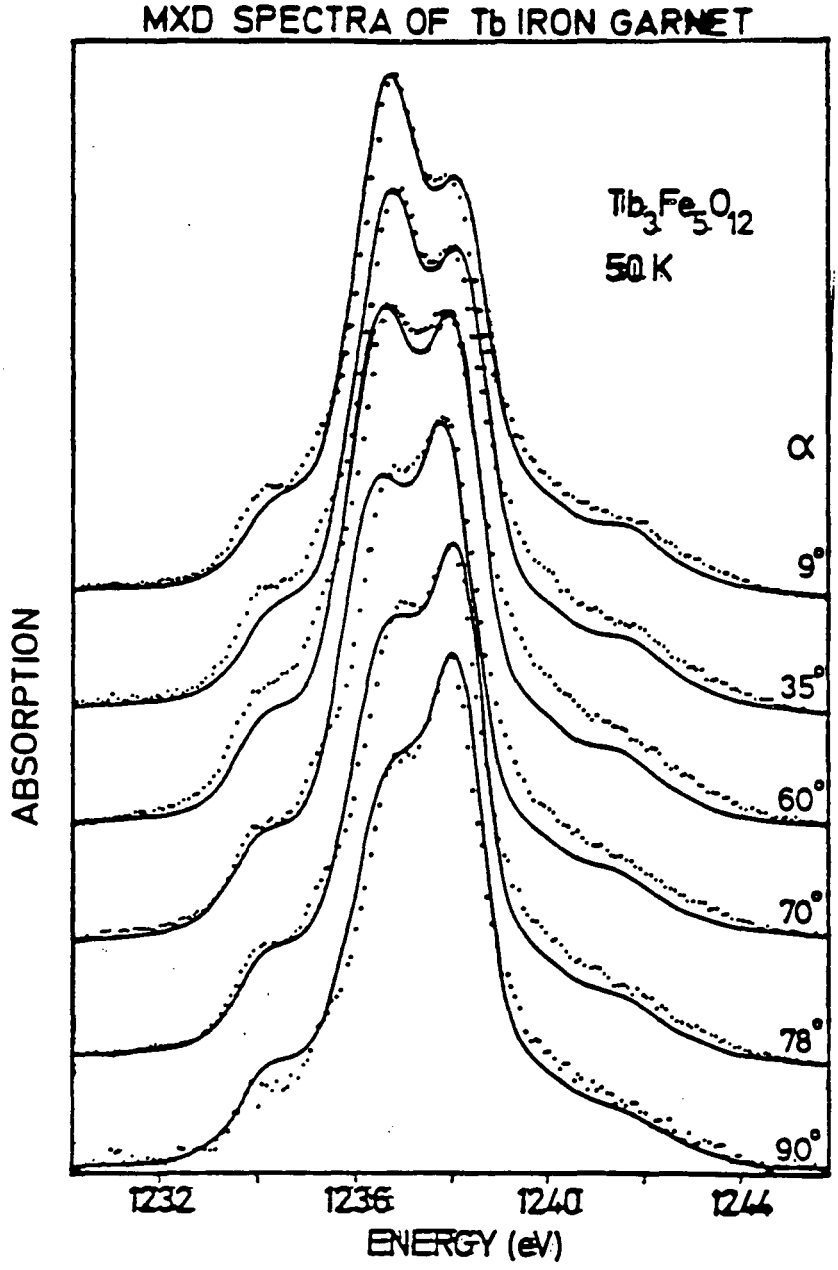

Experimental M_5 absorption spectra of $Tb_3Fe_5O_{12}$ at 50 K for various values for the angle between the x-ray polarization vector and the [111] direction of magnetization. The solid curves are theoretical fits with a 0.4–eV FWHM Gaussian and a 0.3–eV FWHM Lorentzian broadening.

Vander Laan et al.
Phys. Rev. B

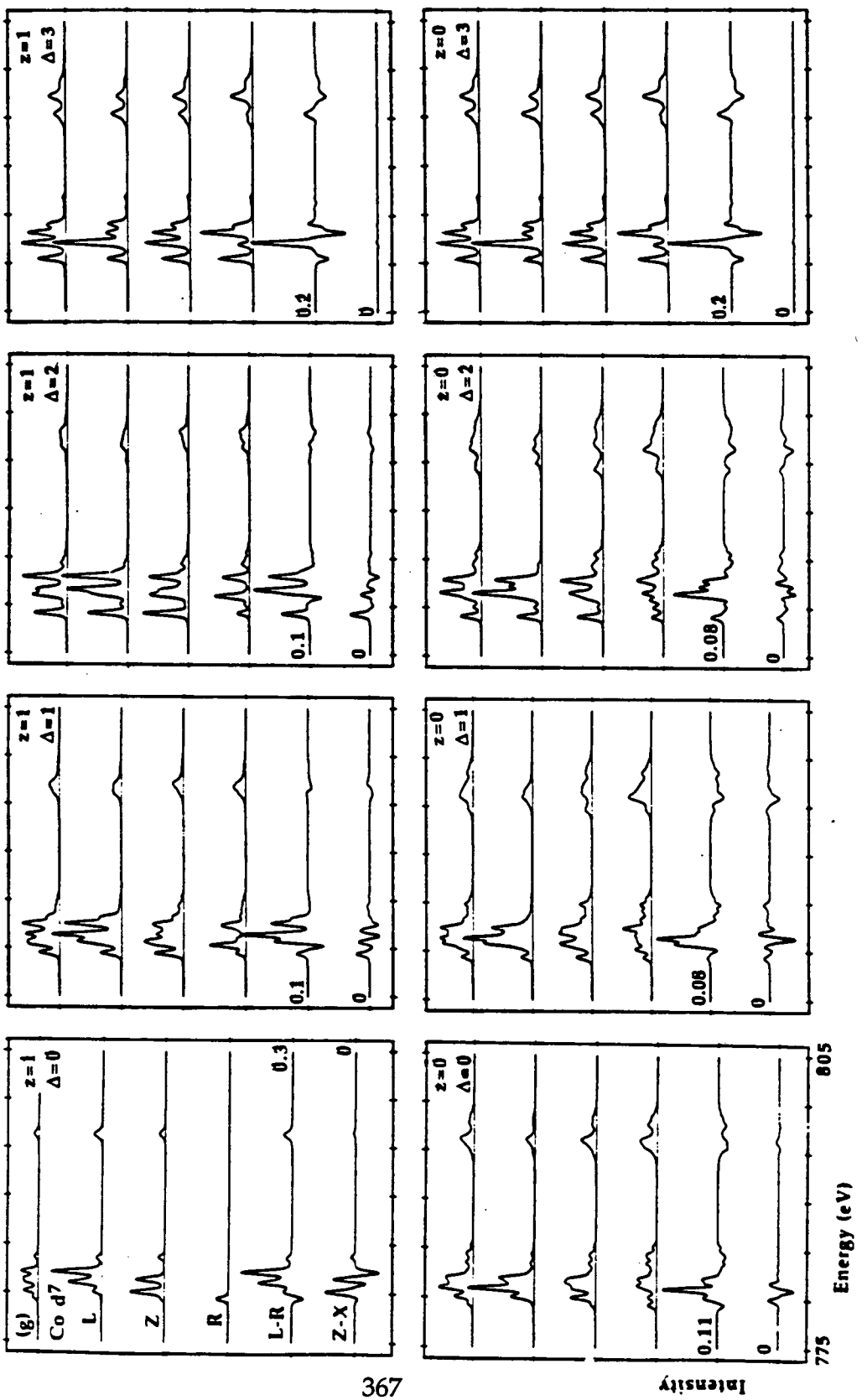

Pol. Dep.

Linear $\propto \langle m^2 \rangle$ → crystal field lower than cubic
→ Antiferromagnetism

From T dep. get crystal field or exchange splittings

circular $\propto \langle m \rangle$ → purely magnetic

Ferro - Ferri - Spiral
Antiferro for H > Spin flop field

(T dependence → J_{exch})
(Paramagnetic ions in H)

Do this separately for each element!

Surface / bulk separation
by electron, photon, ion yield!

Examples of Future interest

1) TM and Rare Earth impurities in semicond., Insl, metals – Local point group symmetry

- g factors
- Crystal field splitting
- high Spin, - low Spin
- kondo problem [what happens to local moment $T < T_K$]

(I claim MnInAu is kondo Fe in Au NoT it is heavy fermion valence fluctuation)

2) Magnetic materials

- $\langle M_i \rangle (T, H)$ for all i
- crystal fields } Anisotropy
- orbital contribution }

→ (Important for hard magnets as well as recording)

- Do high T_c's have a local magnetic moment on Cu / on O? [Can separately determine contributions to χ also the van Vleck part]

3. Surfaces - Atoms on surfaces
(for metals Magnetic Local
moment $U > W$ • free atom
always magnetic (Hunds rule)
Surface? $U_{Surf} > U_{bulk}$

$W_{Surf} < W_{bulk.}$)

- Charge Transfer gap
ionic insulators

- Multilayers

LAWRENCE BERKELEY LABORATORY
UNIVERSITY OF CALIFORNIA
TECHNICAL INFORMATION DEPARTMENT
BERKELEY, CALIFORNIA 94720